AD_____

Award Number: DAMD17-99-1-9504

TITLE: Characterization of Genetic Alterations in Ovarian Cancer

PRINCIPAL INVESTIGATOR: David I. Smith, Ph.D.

CONTRACTING ORGANIZATION: Mayo Foundation
Rochester, Minnesota 55905

REPORT DATE: October 2003

TYPE OF REPORT: Final

PREPARED FOR: U.S. Army Medical Research and Materiel Command
Fort Detrick, Maryland 21702-5012

DISTRIBUTION STATEMENT: Approved for Public Release;
Distribution Unlimited

REPORT DOCUMENTATION PAGE

Form Approved
OMB No. 074-0188

1. AGENCY USE ONLY (Leave blank)	2. REPORT DATE	3. REPORT TYPE AND DATES COVERED
	October 2003	Final (1 Oct 1999 - 30 Sep 2003)

4. TITLE AND SUBTITLE
Characterization of Genetic Alterations in Ovarian Cancer

5. FUNDING NUMBERS
DAMD17-99-1-9504

6. AUTHOR(S)
David I. Smith, Ph.D.

7. PERFORMING ORGANIZATION NAME(S) AND ADDRESS(ES)
Mayo Foundation
Rochester, Mennesota 55905

E-Mail: smith.david@mayo.edu

8. PERFORMING ORGANIZATION REPORT NUMBER

9. SPONSORING / MONITORING AGENCY NAME(S) AND ADDRESS(ES)
U.S. Army Medical Research and Materiel Command
Fort Detrick, Maryland 21702-5012

10. SPONSORING / MONITORING AGENCY REPORT NUMBER

11. SUPPLEMENTARY NOTES
Original contains color plates: All DTIC reproductions will be in black and white.

12a. DISTRIBUTION / AVAILABILITY STATEMENT
Approved for Public Release; Distribution Unlimited

12b. DISTRIBUTION CODE

13. ABSTRACT (Maximum 200 Words)
The goal of this Program Project was to utilize genetic technologies to begin to understand the important changes that underlie ovarian cancer development. Utilizing transcriptional profiling to ascertain consistently up-and down- regulated genes, we began to characterize ovarian epithelial cancer. We had three interactive projects in this Program Project. The first project, headed by Dr. Viji Shridhar, had its major aim the identification of genes that were consistently down-regulated during ovarian cancer development. Dr. Shridhar also led the efforts to transcriptionally profile the ovarian tumors and she has now identified a number of interesting and promising candidates. Dr. Fergus Couch focused on characterizing gene amplification in familial and sporadic ovarian tumors, also utilizing the database of gene expression that we obtained for the ovarian tumors. Dr. David I. Smith focused on the characterization of the highly active common fragile site, FRA6E. They also analyzed genes consistently down-regulated in ovarian tumors that were derived from chromosomal regions containing common fragile sites. They were able to identify a number of previously uncloned common fragile sites and identify important genes in those regions. We have begun to unravel the complex genetic changes that underlie the development of this aggressive cancer.

14. SUBJECT TERMS
No Subject Terms Provided.

15. NUMBER OF PAGES
170

16. PRICE CODE

17. SECURITY CLASSIFICATION OF REPORT	18. SECURITY CLASSIFICATION OF THIS PAGE	19. SECURITY CLASSIFICATION OF ABSTRACT	20. LIMITATION OF ABSTRACT
Unclassified	Unclassified	Unclassified	Unlimited

Table of Contents

INTRODUCTION

The members of the Ovarian Cancer Program of the Mayo Clinic Cancer Center are eternally grateful to the Department of Defense Ovarian Program for their support over the past four years. Although he Ovarian Cancer Program officially started in 1991 with Drs. Lynn Hartmann and Robert Jenkins, it was not until the awarding of the Program Project grant from the Department of Defense that this Program was officially recognized by the Mayo Clinic Cancer Center. Although the funds provided only support for some of projects underway within the Ovarian Cancer Program, the Core facilities supported by the Program Project grant provided a strong focal point for the entire Program. The number of members who are a part of this Program has grown and we have incorporated new expertises into the Program including genetic epidemiology, high throughput proteomics, and viral approaches for cancer treatment. The Ovarian Cancer Program submitted a Specialized Program of Research Excellence (SPORE) Grant in Ovarian Cancer in February 2003. We built this SPORE Program on the very successful Program Project grant model and incorporated five projects: (1) Therapeutic targeting of Hsp90-dependent signaling by Drs. Larry Karnitz and Charles Erlichman; (2) Targeted measles virotherapy for ovarian cancer by Drs. Kah-Whye Peng and Eva Galanis; (3) SNPs in steroid hormone metabolism: etiology and outcome by Drs. Richard Weinshilboum and Thomas Sellers; (4) Ovarian cancer screening using comprehensive proteomics by Drs. David Muddiman and William Cliby; and (5) a project that came out of Project #1 from this Program Project- H-Sulf-1, apoptosis and drug resistance in ovarian cancer by Drs. Viji Shridhar and Scott Kaufmann. Directly as a result of the Department of Defense Program Project grant we had a much larger group of investigators to draw potential translational projects from to submit with the SPORE application.

There were 10 SPORE applications submitted for the February 1, 2003 Ovarian SPORE. Four of the applications were deemed non-competitive and were not scored. Three of the SPOREs, including two previously funded Ovarian SPORE groups received scores less than 200 (160, 176 and 196). Two of the previously funded SPOREs received scores greater than 200 (210 and 214) and the Mayo Ovarian Cancer SPORE received a score of 219. The possibility of the Mayo group receiving SPORE funding from this competition is quite slim, although the National Cancer Institute SPORE staff is currently considering this. However, in the interim, two of the projects that were part of this SPORE, Project #1 (Hsp90-dependent signaling) and Project #4- High throughput Proteomics, were submitted separately and both have been funded with outstanding priority scores. Thus, even if the submitted SPORE application is not funded we have additional members of the SPORE Program with funding for research in ovarian cancer. In addition several other members of the Program have grants in ovarian cancer that are currently under review. We will thus be poised for all future Ovarian SPORE competitions by virtue of having a sufficient base of funded investigators working in and with ovarian cancer.

One of the greatest benefits to having received funding for this Program Project was that it enabled us to build the infrastructure of the Ovarian Cancer Program. This began within the Administrative Core of this Program Project Grant and with the help of Dr. Kimberly Kalli we were able to organize our ovarian tissue resources into a resource of over 1,200 fresh-frozen ovarian samples that have been characterized for histology and tumor content and that are linked to a relational database containing significant information on each patient and the clinical course of their disease. Detailed descriptions of the current tissue repository and the database will be included in the section on the Tissue Procurement Core.

Once we received recognition from the Department of Defense we also received financial support from the Mayo Clinic Cancer Center to help us continue to grow and develop the Program. We provided funds to assist both the Administrative Core and the Tissue Procurement Core and also were able to provide seed money to several young investigators. This led to additional work in ovarian cancer and

has now translated into additional extramural funding for members of our Program. We were quite pleased to recently find that two of the Department of Defense Ovarian Idea Awards were awarded to Drs. Viji Shridhar and David I Smith based upon work that they initiated as part of this Program Project grant. In addition, Dr. Kah-Whye Peng was able to develop her measles virotherapy approach for the treatment of ovarian cancer which resulted in an outstanding publication in *Nature Medicine* and an NCI supported clinical trial. In addition, as mentioned above, our Proteomics effort (led by Drs. David Muddiman and William Cliby) has received funding from the R33 mechanism.

Hence, as a direct result of Department of Defense funding we have been able to develop into a strong extramurally funded program that is just beginning to get national recognition. Our long term goal is to continue to grow and develop our Program, while at the same time continue to develop collaborations with the other funded Ovarian Programs, as we have so successfully done in the past four years.

We will now describe the body of the work conducted in this Program Project in each of the three projects. We will then describe efforts by each of the Cores and how they have supported both the Program Project grant and the entire Mayo Clinic Ovarian Cancer Program.

****

PROJECT #1: DOWN-REGULATED GENES IN OVARIAN CANCER.
DR. VIJI SHRIDHAR, P.I.

INTRODUCTION

The specific goal of this project is to identify genes that are down regulated during the development of ovarian cancer with an expression based strategy. The two main strategies are 1) In collaboration with Millennium Predictive Medicine (MPMx, Cambridge, MA), use their 25K cDNA gene expression arrays to screen for changes in expression of primary ovarian tumors and cell lines; and 2) Generate suppression subtraction cDNA libraries between ovarian tumors from patients with different stages of the disease and normal ovarian epithelial cells. In addition to the above two expression-based strategies, we also did differential display PCR (DD-PCR) of short term ovarian epithelial cells in culture versus seven ovarian cancer cell lines, five of which were established at Mayo Foundation.

Genes identified from this preliminary screening will be characterized in the following ways:

(A) The expression profiles of down regulated genes will be confirmed by Northern and semi-quantitative RT-PCR analysis in primary tumors and cell lines.

(B) The down-regulated genes from (A) will be analyzed on a corresponding Southern blot of DNA from primary ovarian tumors and cell lines to identify any altered bands at the genomic level.

(C) Identify corresponding BAC clones and map it to specific chromosomal regions either by FISH or by radiation hybrid mapping panel.

(D) Test candidate genes for mutations using high throughput capabilities of denaturing high performance liquid chromatography (DHPLC).

(E) The final specific aim of this project is to correlate the expression of down regulated genes in a significant proportion of a large panel of primary ovarian tumors from patients for whom we have extensive outcome data. This will allow us to determine the clinical significance of alterations in these genes.

KEY RESEARCH ACCOMPLISHMENTS

- Differential Display PCR was performed on short-term cultures of ovarian epithelial cells (OSE) and seven ovarian cancer cell lines with three downstream primers and 24 upstream primers. Several differentially expressed transcripts were identified. One of the down-regulated transcript was characterized in greater detail. The gene, which mapped to 13q14.1, has partial homology in the DNAJ domain to a number of proteins with a similar domain and was designated as methylation-

controlled J protein (MCJ). MCJ has the highest similarity to a functionally undefined protein from Caenorhabditis elegans. MCJ is expressed as a 1.2-kb transcript in several adult tissues, with testis showing the highest level of expression. Expression of MCJ was absent in three of seven ovarian cancer cell lines. Similarly, expression analysis using semiquantitative reverse transcription-PCR indicated that 12 of 18 primary ovarian tumors examined had either a complete absence or lower levels of expression of this gene. 5-Aza-2'-deoxycytidine treatment of the OV202 cell line induced MCJ expression in a dose-dependent manner, implicating methylation in this induction. Loss of heterozygosity and methylation-specific PCR analysis revealed that the loss of MCJ expression in primary tumors and cell lines was attributable to deletion of one allele and methylation of the other. To assess the potential functional significance of MCJ down-regulation, the sensitivity of parental (MCJ-nonexpressing) and MCJ-transfected OV167 cells to antineoplastic agents was evaluated. MCJ expression was associated with enhanced sensitivity to paclitaxel, topotecan, and cisplatin, suggesting that MCJ loss may play a role in de novo chemoresistance in ovarian carcinoma. These observations raise the possibility that MCJ loss may: (a) have potential prognostic significance in ovarian cancer; and (b) contribute to the malignant phenotype by conferring resistance to the most commonly used chemotherapeutic agents for ovarian cancer. **The manuscript describing these results is published in Cancer Research (MS #1: Shridhar et al., 2001, 61:4258-65) is included in the appendix.**

- Other differentially expressed transcripts that mapped to Fragile Sites were characterized as part of Project #3, Common Fragile Sites and Ovarian Cancer. **The manuscript describing one of these genes, PAPPA, was published in Oncogene (Callahan et al., 2003, 22:590-601).** In addition, we analyzed ten genes that were consistently down-regulated in ovarian tumors that were derived from chromosomal bands known to contain common fragile sites. This analysis revealed that 9 of these 10 genes were indeed present within common fragile sites. **This work was published in *Genes, Chromosomes and Cancer* (Denison et al., 2003, 34: 406-415).** See report on Project #3 for details.
- In an attempt to understand early events in ovarian carcinogenesis, and to explore steps in its progression, we have applied multiple molecular genetic techniques to the analysis of twenty-one early stage (stage I/II) and seventeen-advanced stage (stage III/IV) ovarian tumors. These techniques included expression profiling seven each of early and late stage tumors with cDNA micro-arrays containing approximately 18,000 expressed sequences, and comparative genomic hybridization to address the chromosomal locations of copy number gains as well as losses. *Results from the analysis indicate that "early stage" ovarian cancers exhibit profound alterations in gene expression, many of which are similar to those identified in late stage tumors. However, differences observed at the genomic level suggest differences between the early and late stage tumors, and provide support for a progression model for ovarian cancer development.* **The manuscript describing these results is published in Cancer Research (MS #2: Shridhar et al., 2001, 61:5895-5904) is included in the appendix.**
- In order to identify novel tumor suppressor genes involved in ovarian carcinogenesis, we generated four down regulated suppression subtraction cDNA libraries from two early stage (Stage I/II) and two late stage (Stage III) primary ovarian tumors each subtracted against cDNAs derived from normal ovarian epithelial cell brushings. Approximately 600-700 distinct clones were sequenced from each library. Comparison of down regulated clones obtained from early and late stage tumors revealed genes that were unique to each library suggesting tumor specific differences. We found 45 down regulated genes that were common in all four libraries. We also identified several genes whose role in tumor development has yet to be elucidated, in addition to several under expressed genes whose potential role in carcinogenesis has previously been described. The differential expression of a subset of these genes was confirmed by semi-quantitative RT-PCR using GAPDH as control in a panel of 15 Stage I and 15 Stage III tumors of mixed histological subtypes. Chromosomal sorting of library sequences revealed that several of the genes mapped to known regions of deletion in ovarian cancer. Loss of heterozygosity analysis revealed multiple genomic regions with a high frequency of loss in both early and late stage tumors. In order to determine if loss

of expression of some of the genes corresponds to loss of an allele by LOH, we utilized a microsatellite marker for one of the novel genes on 8q and have shown that loss of expression of this novel gene correlates with loss of an allele by LOH. In conclusion, our analysis has identified down regulated genes, which map to known as well as novel regions of deletions and may represent potential candidate tumor suppressor genes involved in ovarian cancer. *While some of the genes identified from these libraries were also identified as down regulated genes by transcriptional profiling of the same tumor, we identified several known and unknown genes of very low abundance only in the SSH libraries. The data from the SSH library analysis also revealed that there were many genes which were differentially expressed in both early and late stage tumors.* **The manuscript describing these results is published in Cancer Research (MS #3: Shridhar et al, 2002, 62:262-270) is included in the appendix.**

REPORTABLE OUTCOMES

The expression of the down regulated genes were characterized in the following ways:

(A) By ***Northern, Semi-Quantitative RT-PCR and Light Cycler analysis*** –See **figures** in attached manuscripts for details (MS #1-5).

Several differentially expressed transcripts were tested for expression analysis both in cell lines and primary ovarian tumors by semiquantitative RT-PCR and northern based analysis. Over 100 transcripts from all three screens were tested by semiqunatitative RT-PCR analysis with gene specific primers in a panel of ovarian cancer cell lines. Table 1 on the following page is a partial list of the genes that showed either a complete loss or lower levels of expression compared to short term cultures of normal ovarian epithelial cells in at least one or more of the seven cell lines tested (Manuscripts #2 & #3).

Based on the results presented above, we selected a subset of genes for further analysis based on the following criteria.

- Using the UCSC genome database (www.genome.ucsc.edu), chromosomal locations of genes were determined to check if any of the down regulated genes mapped to known regions of deletions in ovarian cancer
- Novel down regulated genes that mapped known regions of deletions were further characterized in detail. In addition, we determined novel regions of deletions for some of these down regulated genes [examples include MCJ (MS#1), HSulf-1 (MS #4) and HtrA1 (MS#5)].
- After generating the ORF for genes of interest (for both known and novel genes), using NCBI's Conserved Domain Database, we determined protein domains that could potentially be involved in inducing apoptosis and domains that could modulate signal transduction pathways. These genes were selected for more detailed functional characterization.

Table1: Expression levels of selected genes in ovarian cell line panel by Semiquantitative RT-PCR

GENES	OSE	OV 167	OV 177	OV 202	OV 207	OV 266	OVCAR 5	SKOV 3	Chromosomal location
HSD3B1	+	-	-	-	-	-	-	-	1p13
CTSK	++	weak	weak	Weak	++	+	weak	+	1q21
IGFBP5	+	-	-	+	-	-	ND	ND	2q33-36
AREG	+	+	++	-	ND	++	+	-	4q13-21
Hevin	+	-	-	-	-	-	-	-	4q22.1
SEPP1	+	+	+	-	-	+	+	+	5q31
TCEB1L	+	-	+	+	+	+	+	+	5q31
SPARC	+	-	-	Weak	-	-	-	-	5q31
FGF1	+	-	-	-	+	-	-	+	5q31
Testican	+	-	+	+	+	-	+	-	5q31
CDC23	++	weak	weak	++	weak	weak	weak	+	5q31.2
Nesprin-1	+	-	-	+	-	-	-	+	6q25
THBS2	++	weak	-	-	-	-	-	-	6q27
PAI1	++	+	-	-	weak	weak	weak	+	7q21
STAR	+	-	-	+	-	weak	-	-	8p11.2
HSulf-1	+	+	-	+	-	-	-	-	8q13
GAS1	++	+	+	+	-	-	weak	-	9q21.3
HtrA1	++	-	-	+	-	-	+	+	10q25
Cyclin D2	+	-	-	+	-	-	-	-	12p13
EGR1	+	weak	weak	Weak	weak	+	weak	++	12q13.3
Decorin	++	-	-	++	-	-	-	-	12q21.3
FGF7	+		-	+	-	-	-	-	15q15-21.1
PEG 3	+	-	++	++	-	-	-	-	19q13.4
ITM2A	++	-	-	-	+	-	-	-	Xq13.3-21.1
PAPX	+	-	-	-	-	-	-	-	Xq22

(B) ***Southern Blot Analysis***. We tested the following genes at the southern level.

1. **HtrA1:** A serine protease with a high degree of similarity to HtrA2/ Omi, a member of the serine protease family with PDZ domain and IGFBP domains. HtrA2 is a proapoptotic mitochondrial protein.
2. **PAPX:** A novel transcriptional regulatory protein whose expression by RT-PCR and northern analysis is lost in 90% of cell lines and primary ovarian tumors. PAPX maps to Xq22, a region of X chromosome inactivation.
3. **SYNE1:** A huge protein (>300KD) with several spectrin repeats mapping to 6q25 with loss of expression in 60% of cell lines and primary ovarian tumors. One of 21 primary ovarian tumors, OV#13 showed an altered band at the Southern level. Experiments are ongoing to map the site of this alteration in this tumor. We have seen loss of an allele by LOH within this gene in >60% of primary ovarian tumors (Manuscript under preparation). On treatment with the methylase inhibitor 5-aza-2'-deoxycytidine, a dose dependant increase in the transcription of SYNE1 was observed in cell lines (with loss of SYNE1 expression), implicating methylation as a mechanism for loss of expression.
4. **HSulf-1:** A novel sulfatase domain containing protein mapping to 8q13, a region which we have shown is lost in 50% of both early and late stage tumors (MS#3).
5. **PEG3:** Paternally expressed gene 3 maps to 19q13. Expression of PEG3 is lost in 50% of cell lines and primary ovarian tumors.

Except for SYNE1, we did not detect any altered bands at the genomic level with the down-regulated genes tested.

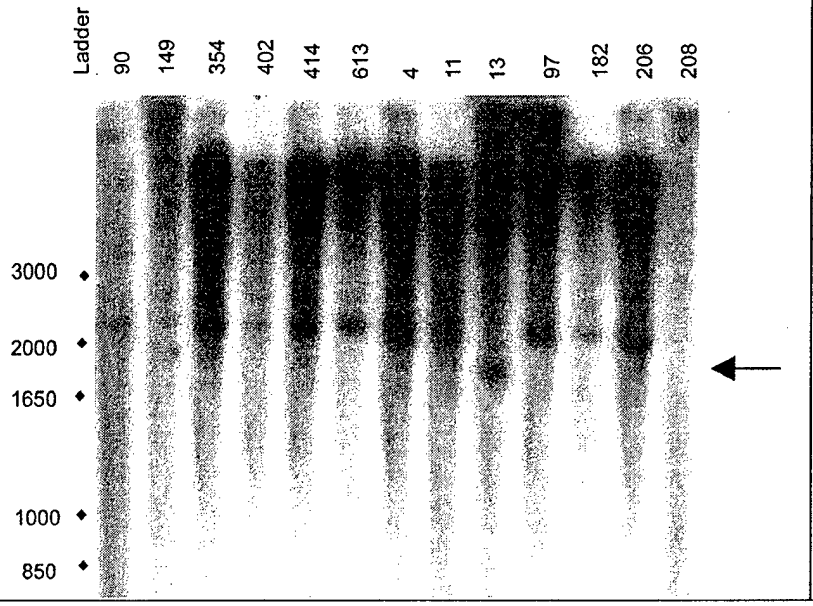

Figure: 3' end probe of SYNE1 was hybridized to PstI digested DNA from primary ovarian tumors and analyzed by southern blot. The arrow points to the altered band in OV13. The numbers on top of the gel panel are specific ovarian tumor samples.

(C) ***Chromosomal mapping*** of corresponding BACS was not performed due to the extensive chromosomally assigned sequences available as a result of the human genome project. For most of the genes identified from these screens, chromosomal positions are known.

(D) ***Mutation screening using DHPLC*** for selected genes.
For the genes tested, primers within introns, flanking the exons were synthesized and 96 tumors including 8 ovarian cell lines were amplified. Mutational analysis was performed on the following genes by DHPLC.

1. MCJ
2. PAPX
3. HtrA1
4. HSulf-1-ongoing.

No tumor specific mutations were seen in the first three genes. Preliminary anlysis of HSulf-1 indicates homozygous deletions of specific exons in couple of primary tumors. Experiments are ongoing to determine if these can be validated at the southern level.

(E) Studies of the clinical significance of alterations in these genes are ongoing.
However, we have preliminary data to suggest that the presence of HtrA1 and HSulf-1 confers chemosensitivity. Based on this preliminary data we have generated polyclonal antibodies to both HtrA1 and HSulf-1. The conditions for immunohistochemistry on paraffin embedded tissues have been established for both HtrA1 and HSulf-1.

Rationale for testing anti-HtrA1 on patient cohorts classified as good and bad responders - ONGOING EXPERIMENTS

Our laboratory has identified a pro-apoptotic serine protease, HtrA1, as a down regulated gene in ovarian cancer [Chien, 2003 (MS#5); Shridhar, 2002 (MS#3)]. Our preliminary results indicate that **1)** HtrA1 expression is markedly reduced or lost in majority of ovarian cell lines and tumors. **2)** More importantly relevant to this proposal we have shown that HtrA1 expression is affected by exposure to cisplatin. Cisplatin upregulates HtrA1 expression in immortalized normal cells within 2 hours of

exposure. 3) Forced expression of HtrA1 in ovarian cancer cells leads to auto-catalytic processing of HtrA1, activation of potent serine protease, destruction of microtubules, severe cytoplasmic reduction, cell rounding, and apoptosis [Chien et al., Manuscript in preparation]. These results suggest the possibility that HtrA1 may modulate cisplatin sensitivity by mediating cisplatin-induced apoptosis. Consistent with this possibility, additional experiments have demonstrated that forced expression of HtrA1 confers cisplatin chemosensitivity (Chien et al., Manuscript in preparation).

Preliminary Results: Within two hours of exposure to indicated stress, HtrA1 is upregulated by cisplatin (CDDP), prostaglandin A_2 (PGA_2) and phorbol ester (PMA) (Figure 1A). Consistent with this observation, OV167 containing higher levels of HtrA1 is more sensitive to cisplatin compared to isogenic vector transfected cell line (1B) as determined by a clonogenic assay (3).

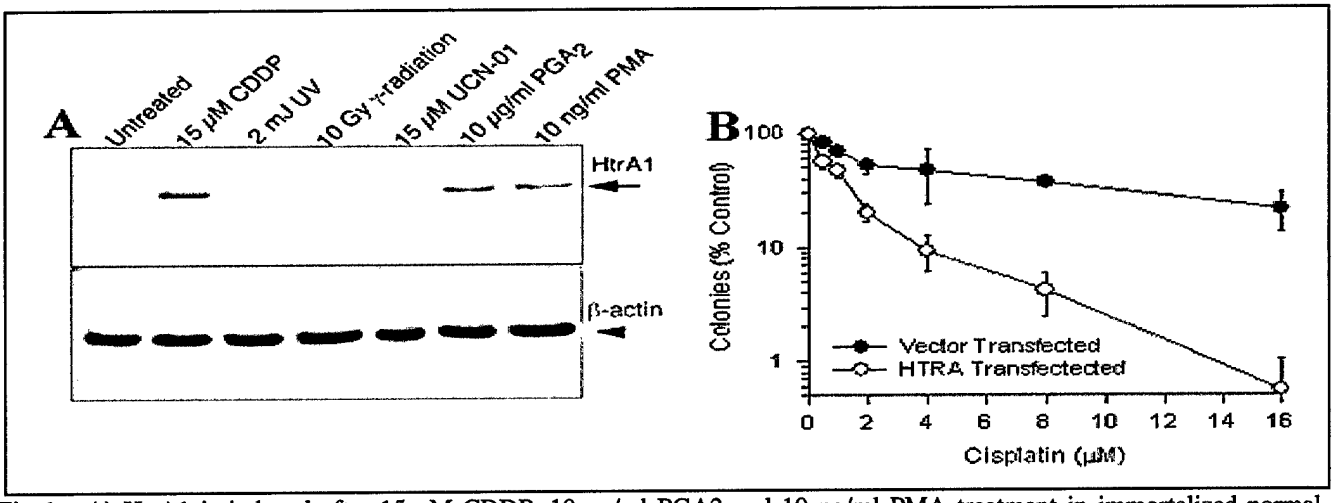

Fig 1 **A)** HtrA1 is induced after 15 μM CDDP, 10 μg/ml PGA2 and 10 ng/ml PMA treatment in immortalized normal ovarian cells in culture (**Upper panel**: Lanes 2, 6 and 7 respectively). **Lower panel:** The blot was stripped and probed with actin to show equal loading. **B)** Vector and HtrA1 transfected stable clones were exposed to various concentrations of cisplatin for 24 h, washed, and incubated in drug-free medium for 12-14 days to allow colonies to form. Each data point represents the mean colony count from triplicate plates. Error bars, ±1SD. Results are each representative of four independent experiments with CDDP.

Based on these novel observations, **we propose that loss of expression of HtrA1 promotes the survival of cancer cells under cisplatin treatment, and this represents another mechanism of platinum resistance in ovarian cancer.**

We have identified a set of patients with stage III ovarian cancer (serous, endometrioid or mixed serous/endometrioid) whose clinical responses represent the two ends of the spectrum. At one end of the spectrum are patients in the good outcome group, with a median time to recurrence (time from surgery to start of second-line treatment) of 35.5 months. At the other end of the spectrum is the poor outcome cohort, with a median time to recurrence of 8.7 months. All patients were treated with paclitaxel-platinum. Tissue blocks from all of these patients were obtained at the time of initial surgery, snap frozen, and stored in liquid nitrogen.

Our overall approach will be to quantitate HtrA1 mRNA by quantitative RT-PCR and determine whether down-regulation is more common in one group than the other. We are in the process of extracting RNA and generating cDNAs from these sample sets. An alternative approach would be to evaluate protein expression using anti-HtrA1 antibody. Staining will be graded into 0 (no reactivity), 1+ (weakly reactive), 2+ (moderate reactivity), 3+ (strongly positive). To explore the relationship of the staining with clinical outcome, we will dichotomize the four possible outcomes for staining (0, 1+, 2+, and 3+) into two groups, high (2+ and 3+) vs. low (0, 1+) or negative (0) vs. positive (1+, 2+, 3+). Fisher's Exact test will be used to detect any significant relationships between these dichotomous vari-

ables and treatment response. With a sample size of 80 patients, 40% with >30 month disease-free survival and 60% with shorter disease-free survival, there will be 87% power to detect a difference in incidence of HtrA1 down-regulation of 85% in the poor outcome group vs. 55% in the good outcome group.

Rationale for testing anti-HSulf-1 on patient cohorts classified as good and bad responders- ONGOING EXPERIMENTS-

Rationale: Preliminary data presented indicate that HSulf-1 resistance to cisplatin-induced apoptosis accompanies HSulf-1 downregulation (MS#4).
We hypothesize that HSulf-1 downregulation serves as a marker for patients with particularly resistant disease. *We propose to test the hypothesis that patients who do poorly have tumors with diminished HSulf-1 expression.* For these experiments, we will use the same set of patient cohorts as described for HtrA1.

We recently generated a polyclonal rabbit serum against HSulf-1 (4647) and tested its specificity on western blot and paraffin embedded normal and malignant ovarian specimens. Figure 2 shows that the serum recognizes HSulf-1 protein expressed in baculovirus system. Figure 3 shows that this antibody also recognizes HSulf-1 protein expressed on normal ovarian epithelial cells. Antibody preincubated with antigenic peptide attenuated the signal generated by anti-HSulf serum 4647, demonstrating that the serum is specific to this antigen. In contrast, tumor samples show reduced expression compared to adjacent normal ovarian surface epithelial cells from the same samples. Although ongoing experiments are designed to identify optimal conditions for using this reagent, these preliminary results demonstrate that the anti-HSulf-1 antiserum we have generated is specific for HSulf-1 and is applicable in immunoblot and immunohistochemical analyses.

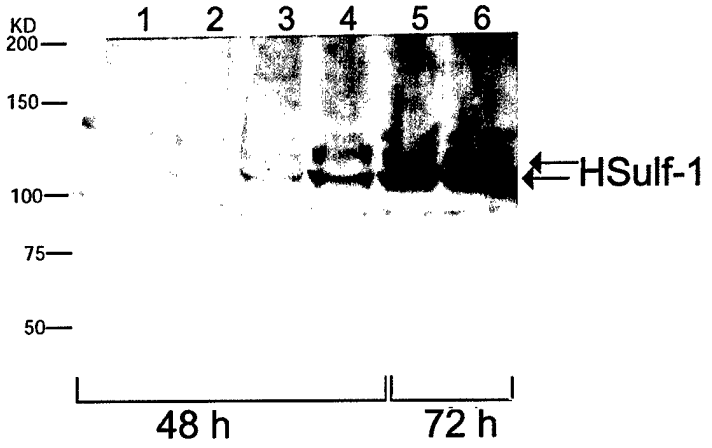

1. Uninfected Sf9 insect cells
2. Wild type baculovirus
3. HSulf-1 baculovirus ($1x10^7$ pfu)
4. HSulf-1 baculovirus ($1x10^8$ pfu)
5. HSulf-1 baculovirus ($1x10^7$ pfu)
6. HSulf-1 baculovirus ($1x10^8$ pfu)

Fig. 2: Rabbit polyclonal antiserum raised against HSulf-1 peptides recognizes HSulf-1 protein expressed in a baculovirus expression system. Uninfected Sf9 insect cells and cells transfected with either wild-type or HSulf-1 expressing baculovirus at different levels of infectivity (1×10^7 or 1×10^8 plaque forming units per 2.5×10^6 cells in a 60 mm plate) were incubated for 24, 48, or 72 h. The cell extracts were resolved on a SDS polyacrylamide gel and probed using rabbit polyclonal antiserum raised against a mixture of two KLH-conjugated HSulf-1 peptides. Two HSulf-1 protein bands were identified at 130 kDa and 110 kDa. HSulf-1 protein expression increased with increasing amounts of baculovirus and also with increasing time after viral infection

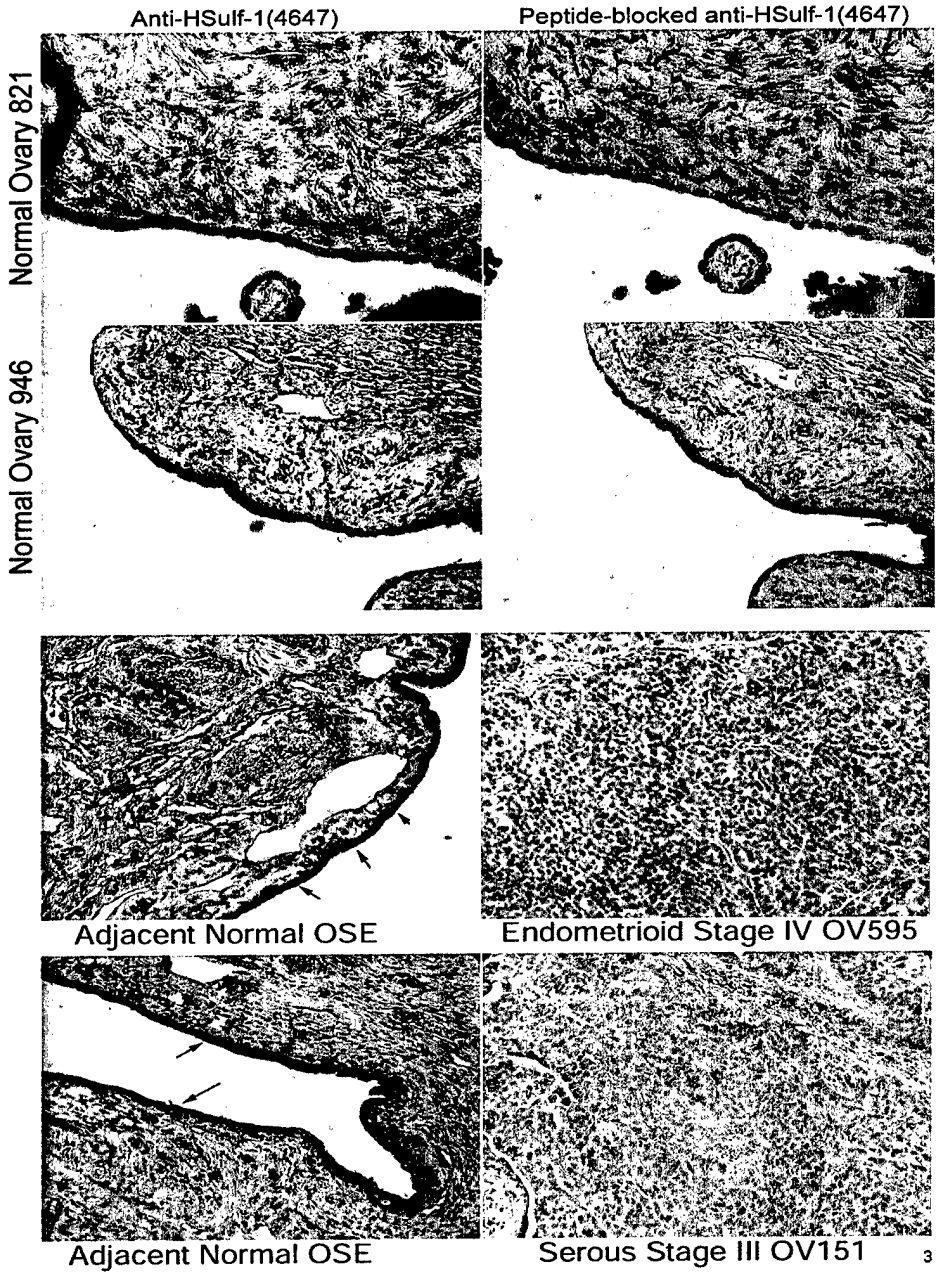

Fig. 3: Rabbit polyclonal antiserum raised against HSulf-1 peptides specifically recognizes HSulf-1 protein expressed on normal ovarian epithelial cells in tumor samples and shows reduced expression in adjacent tumor tissues from the same samples. Immunohistochemical detection of HSulf-1 with anti-HSulf-1 antibody 4647 (1:1500 dilution) in normal ovaries from patients without cancer and in ovarian tumors OV595, OV151. The sections were lightly counterstained with hematoxylin. Top two left panels, intense staining of surface epithelial cells with anti-HSulf-1 antibody of normal ovaries 821 and 946 (1:1500 dilution). Top two right panels, immunostaining (at 1:750 dilution) of normal ovaries 821 and 946 with anti-HSulf-1 4647 preblocked for 1 h with 3.5 μg/ml of HSulf-1 peptide at a ratio of 1:1 (peptide: antibody) used to immunize the rabbits. Notice less to no immunostaining with peptide preblocked with anti-HSulf-1 4647 in these panels, indicating the specificity of anti HSulf-1 4647. Bottom two left panels adjacent normal ovarian epithelial cells in OV595 and OV151 tumor tissues showing intense staining with anti HSulf-1 polyclonal antibody 4647. Bottom two right panels, neoplastic OV595 and OV151 cells on the same slide show much less immunostaing with anti- HSulf-1 antibody 4647 compared to adjacent normal cells from the same slide.

Attached Manuscripts

1. **Shridhar V*,** Bible KC, Staub J, Avula R, Lee YK, Kalli K, Huang H, Hartmann LC, Kaufmann SH, Smith DI. Loss of expression of a new member of the DNAJ protein family confers resistance to chemotherapeutic agents used in the treatment of ovarian cancer *Cancer Research* 2001; 61:4258-4265. (MS #1)
2. **Shridhar V**, Lee J, Pandita A, Iturria S, Avula R, Staub J, Calhoun E, Sen A, James CD, Kalli K, Keeney G, Roche P, Mills G, Bast R, Cliby W, Couch F, Hartmann LC, Lillie J, Smith DI. Genetic analysis of early versus late stage ovarian tumors. *Cancer Research* 61:5895-5904, 2001. (MS #2)
3. **Shridhar V***, Sen A, Chien J, Staub J, Avula R, Kovats S, Lee J, Lillie J, Smith DI. Identification of under-expressed genes in early and late stage primary ovarian tumors by suppression subtraction hybridization. *Cancer Res* 2002; 62: 262-270. (MS #3)
4. Lai J, Chien J, Staub J, Avula R, Greene EL, Matthews T, Smith DI, Kaufmann S, Roberts LR and **Shridhar V***. Loss of HSulf-1 upregulates heparin binding growth factor signaling in cancer *J. Biol Chem.* 2003; 278:23107-17. (MS #4)
5. Chien J, Staub J, Hu Shou-Ih, Erickson-Johnson MR, Couch FJ, Smith DI, Crowl RM, Kaufmann SH and **Shridhar V*.** A Candidate Tumor Suppressor HtrA1 is Downregulated in Ovarian Cancer (IN PRESS-ONCOGENE). (MS #5)

****

PROJECT #2: Characterization of the Role of Amplified Oncogenes in the Development of Familial and Sporadic Ovarian Cancer. Fergus Couch, Ph.D.

INTRODUCTION:

The specific goal of this project was to identify genes that are amplified and over-expressed during the development of ovarian cancer. The goal was to also use these genes to test the hypotheses 1) that gene amplification contributes significantly to the development and progression of ovarian cancer, and 2) that familial and sporadic ovarian tumors have different progression pathways.

To achieve this goal, we proposed the following four major aims:

Specific Aim #1: Assembly of collections of frozen familial and sporadic ovarian tumors.
Specific Aim #2: Assessment of the extent of gene amplification in familial and sporadic tumors.
Specific Aim #3: Identification of novel amplicons and amplified genes in familial and sporadic ovarian tumors.
Specific Aim #4: Characterization of the oncogenic activity of candidate oncogenes.

BODY:

Specific Aim #1/Task 1: Assembly of collections of frozen familial and sporadic ovarian tumors.

The Mayo Clinic Ovarian tumor Database was screened in order to identify tumors from patients with a family history of breast and ovarian cancer. We identified 50 ovarian tumors from patients with family history and an additional 25 high grade serous ovarian tumors for mutation screening of the BRCA1 and BRCA2 genes. These tumors were screened for mutations in the BRCA1 and BRCA2 genes using a combination of conformation sensitive gel electrophoresis (CSGE) and dHPLC mutation detection techniques. Briefly, all exons and splice junctions of the BRCA1 and BRCA2 genes from each tumor were PCR amplified using 82 different PCR primer pairs and the PCR products were subjected to CSGE or dHPLC associated heteroduplex analysis. Nine BRCA1 mutations and four BRCA2 mutations were found. Subsequent sequencing revealed 8 frameshifts, one splice site mutation, 2 in-frame deletions, and 2 missense mutations. Nine of these were found in tumors from individuals with a family history of breast and/or ovarian cancer. As expected 6 of the 12 or 50% of individuals with significant family history of cancer (3 or more cases of breast and/or ovarian cancer) had mutations. Germline DNA was only available for 4 of these individuals, but was used to show that 3 or the 4 individuals carried the

BRCA1 or BRCA2 mutations in their germline DNA. Loss of heterozygosity (LOH) studies were not performed to enrich for tumors with loss of the BRCA1 and BRCA2 loci because of the number with mutations identified during the mutation screen.

Specific Aim #2/Task 2: Assessment of the extent of gene amplification in familial and sporadic tumors.

Our goal in this section was to determine the extent of gene amplification in ovarian tumors using cytogenetic approaches. We performed comparative genome hybridization (CGH) analysis on a series of 25 early and late stage ovarian tumors. Results from this work showed that amplification is generally restricted to late stage ovarian tumors (Shridhar et al., 2001). Amplification of known oncogenes such as Cyclin D1 on 11q13, c-Myc on 8q24, AIB-1 on 20q12, ZNF217 on 20q13.2, Cyclin E and AKT2 on 19q12, and PI3KCA on 3q26.3 was detected at a frequency of greater than 10% and validated by Southern blot. A number of other amplified regions including 1p, 1q, 8p, 11p, 12p, 16p, and 19p were also identified. Oncogenes associated with ovarian cancer have not previously been identified in these regions.

AmpliOnc array studies of the tumors aimed at studying copy number of a series of 164 different elements including 58 known amplification targets in the human genome were not carried out because the array reader available at the Mayo Clinic was not capable of scanning the new generation of AmpliOnc arrays produced by Vysis Inc. However, the success of the CGH technique indicated that the AmpliOnc Array analysis was not necessary.

We did not pursue CGH studies of BRCA1 and BRCA2 mutant tumors because three other groups were already known to be conducting this work with large numbers of tumors (Israeli et al., 2003; Hedenfalk et al., 2003; Ramus et al., 2003). Interestingly, BRCA1 and BRCA2 tumors tend to contain several regions of amplification that are much less frequently detected in sporadic ovarian tumors. These include chromosome 5q and 10q that have more frequent amplification in BRCA2 tumors, 9p which has more frequent amplification in BRCA1 tumors, and 6p, 11q, and 13q that are found more frequently amplified in both BRCA1 and BRCA2 tumors. In contrast only 3p and 22q are significantly more frequently amplified in sporadic tumors relative to BRCA1 and BRCA2 tumors. Thus, the candidate oncogenes that we examined, as described above, would not have shown any difference in frequency of amplification between BRCA1/BRCA2 tumors and sporadic tumors.

Specific Aim #3/Task 3: Identification of novel amplicons and amplified genes in familial and sporadic ovarian tumors.

Our goal in this section was to identify novel amplified and over-expressed genes in ovarian tumors. To achieve this goal we profiled a total of 78 stage II and III ovarian tumors and 5 normal ovarian epithelial cell samples on a 30,000 gene expression array in collaboration with Millennium Predictive Medicine (MPMx). These tumors were part of a study aimed at identifying genes that mediated tumor recurrence in patients treated with cisplatinum/carboplatinum and paclitaxel. All tumors were surgically removed prior to chemotherapy. Half of the tumors were derived from women who suffered recurrence of disease within 18 months and half from women who did not suffer a recurrence for at least 18 months. We used bioinformatics analysis of the gene expression array data from these tumors to generate moving median profiles of each tumor by plotting the median expression level of sequential 50 gene sets along each chromosome. Randomized datasets were used to generate confidence intervals and to identify gene windows that are likely upregulated by more than chance alone. Our hypothesis was that the 50 gene windows represent areas of amplification. This hypothesis is based on the knowledge that it is very unusual to find multiple genes within a defined genomic region commonly upregulated. By identifying peaks on the moving window plot we selected 15 candidate regions of amplification. In Table 1 we identify the candidate oncogenes that are located within these areas.

It is important to note that this type of analysis only detects aberrant regions and does not accurately define regional boundaries of amplified regions. Therefore, the regions of actual amplification could be larger or smaller than the regions defined in Table 1. In addition, we noted that the candidate regions identified in this process did not coincide well with the regions of amplification identified during our CGH studies and those of others. To verify that this approach actually identified regions of amplification we performed Fluorescent *In Situ* Hybridization (FISH) studies. Tissue Microarrays containing 3 X 0.6mm cores from 48 of the 78 tumors were generated and representative Bacterial Artificial Chromosome (BAC) probes from four of the candidate regions were selected. These BAC probes were hybridized to the Tissue Microarrays along with relevant centromeric probes (Vysis Inc.) and a ratio of BAC probe signals to centromeric signals in 60 nuclei from each core were calculated to determine if amplification is present. If one of the three cores from a sample was positive then the tumor was considered amplified. This approach accounts for heterogeneity of amplification in tumors. These micorarray FISH studies of the 12p (K-Ras), 3q (MCM2), 19q (AKT2), and 20q11.2 (E2F1) candidate regions of amplification found 15%, 5%, 10%, and 5% amplification respectively. We considered 5% as equivalent to background levels of amplification. These data suggested that 1) the moving median technique identifies a large number of false positives and is not useful for selecting regions of amplification; or 2) the BAC clones chosen for each region may not represent the peak of amplification within that region. Because of the low levels of amplification of the four chosen candidates we attempted to verify that these tumors did contain some regions of amplification and that our FISH technique was detecting regions of amplification. To accomplish this we used probes for CCND1 and c-Myc to show that these genes were amplified in 20% of the tumors. As these levels are in keeping with previous studies the suggestion is that there are no technical problems in the experiment. We also showed that the N-Myc (2p24.1) was not amplified in these tumors.

Unfortunately the outcome of the study was that the Moving Median approach did not identify many regions of amplification and did not identify regions of amplification that discriminated between tumors associated with short and long time to disease recurrence.

Array CGH: Because of the high false positive rate for the Moving Median approach, we took a different approach to identifying amplified regions and genes in ovarian tumors. In collaboration with Dr. Barbara Weber from the University of Pennsylvania, we profiled 26 of the same group of ovarian tumors on CGH arrays. These arrays contain 4,000 BAC clones spotted in duplicate on glass slides. DNA from tumors was fluorescently labeled with cy3 dye by nick translation and mixed in equal proportion with cy5 labeled normal genomic DNA. The complex probe was then hybridized to the array and the intensity of fluorescent signal at both the cy3 and cy5 fluorescent ratios for each spot was measured with an Axon scanner. The fluorescence intensity was normalized to the median intensity value for each array and the cy3/cy5 ratio was calculated. The $\log_2$ (intensity ratio) for each BAC was plotted against the position of the BAC in the genome. Careful analysis of control samples with known levels of amplification of certain genes determined that the lower boundary for amplification (5 gene copies) using this technique was 0.75, while the boundary for loss of heterozygosity (LOH) or deletion was -0.75. The Log_2 (intensity ratio) was used to produce a more uniform spread of the intensity data. The Weber group has developed CGH browser software to facilitate this process. An example of a plot is shown in Figure 1. Selected BACs on these plots can be directly linked to the BAC ID and to FISH mapping data from the Human Genome Project.

Table 1.		
Cytoband Location of Amplification	Amplified Region - Radiation Hybrid Map Location (GeneMap'99)*	Significant genes with respect to cancer
Resistance		
1p34	110-118 cR3000	AK2 adenylate kinase 2 MYCL1 v-myc oncogene homolog 1
1q	740-777 cR3000	
2q	312-340 cR3000	
2q22	502-515 cR3000	ARHE ras homolog member E NMI N-myc (and STAT) interactor
3q	429-451 cR3000	RAB7 RAS oncogene homolog MCM2 minichromosome maintenance deficient (S. cerevisiae) 2 (mitotin)
3q	487-542 cR3000	
4q	332-419 cR3000	KIT v-kit GRO2 oncogene
12p	84-137 cR3000	KRAS2 v-Ki-ras2 Kirsten rat sarcoma 2 viral oncogene homolog
14q	231-269 cR3000	AKT1 v-akt oncogene homolog CCNK cyclin K
16p	23-59 cR3000	
19q13.1	218.315-238.63 cR3000	Hs.200816 AKT2 oncogene
19p	269-285 cR3000	
20q11.2	198.18-207.61 cR3000	E2F1 transcription factor Hs.112594 hepatocellular carcinoma-associated antigen 58
20q13.1	225-267 cR3000	AIB1 regulator of ER MYBL2 v-myb oncogene homolog-like 2 TOP1 topoisomerase (DNA) I CSEIL/CAS chromosome segregation 1
20q13.1-13.2	278-336 cR3000	STK15/BTAK serine/threonine kinase 15 BCAS1 breast carcinoma amplified sequence 1 **ZABC1/ZNF217 transcription factor** PTPN1 protein tyrosine phosphatase, non-receptor type 1

Using this approach we visually identified a number of regions of amplification and loss throughout the genome of each tumor. Specifically, we identified 44 independent regions of amplification in this set of tumors. However, the majority of these amplification events were found in less than 10% of the tumors. A total of 9 regions were identified in greater than 10% of the tumors. These include 8q11, 8q21, 8q24, 18p11, 18q12, 19p12, 19q13.2, 19q13.4, and 20q13. Of particular interest was the c-myc gene in the 8q24 region that was amplified in 40% of the tumors. It was of some concern that none of the well known tragets of amplification in ovarian cancer were found to be amplified by this approach. In checking with the Weber group, it was discovered that many of these genes were not represented on the array. Subsequently, an additional 500 BACs have been added to the arrays to fill large gaps in the genome and to include important cancer associated genes.

For the purposes of identifying specific genes, we focused our efforts on the 19q13.2 region of amplification that had been identified in 18% of the tumors. Literature review suggested that this

amplicon included the AKT2, c-AXL, and XRCC1 candidate oncogenes. FISH analysis demonstrated that only the AKT2 gene was amplified in >10% of the tumors on the tissue microarrays. However, we had identified several different amplified BACs from this region of 19q suggesting that there are targets of amplification other than AKT2 in this area in ovarian tumors. We postulated that the CLG gene encoding a G-protein coupled receptor activating protein might be one of these targets because this gene is over-expressed in 30% of ovarian tumors and has oncogenic capacity (personal communication – Daniel Billadeau). CLG is located 2 Mb distal to AKT2 and 1 Mb proximal to c-AXL. However, southern blotting of this gene using DNA from10 ovarian cancer cell lines and 25 ovarian tumors did not detect any amplification. Thus, to date we have not discovered any new targets of amplification in this region.

This region remains of significant interest and even though this grant is now concluded, we will pursue our interests here by Southern blotting ovarian tumors and cell lines with 40 different Southern blot probes derived from genes in this 19q13.2 region in an effort to identify the targets of amplification. Subsequent molecular studies will be needed to verify if any genes from this region contribute to ovarian oncogenesis and to the process of tumor recurrence.

CBP: During these array studies we noted that a region on chromosome 16q had LOH in several tumors. Analysis of the literature determined that this region contained the CBP gene that encodes a transcriptional co-activator and modulator of p53 activity. CBP has primarily been implicated in cancer as a target of translocations resulting in hyper-activated fusion proteins. However, the CBP gene is not known to be a mutational target in ovarian cancer. Because of the LOH we decided to evaluate whether CBP is mutated in ovarian tumors. To undertake this study we obtained 80 frozen ovarian tumor specimens from the Tumor Bank of the Ovarian Research Program of the Mayo Clinic. Each tumor specimen was defined by H+E analysis as containing at least 30% tumor cells. A total of 20 X 10 μm sections were cut from each tumor by the Tissue Acquisition and Processing Core of the Mayo Clinic Cancer Center and genomic DNA was prepared by standard techniques. Each genomic DNA sample was PCR amplified using 35 independent PCR primer sets that covered the entire coding region and splice sites of the CBP gene (Coupry et al., 2002). PCR products were heteroduplexed. Samples were subjected to dHPLC analysis (Wavemaker, Transgenomics, Inc.) using optimal melting conditions that had been established for each PCR product. Samples with altered peak structure were re-amplified from the original genomic DNA and sequenced in the Molecular Biology Core of the Mayo Clinic to identify the specific sequence alterations.

A total of four mutations were detected in ovarian tumors, two of which resulted in truncated CBP proteins (Table 2). Of considerable interest is the finding that the four mutations detected in ovarian tumors were found in 4 histologically different forms of the disease (Table 3). This suggests that CBP mutations are not restricted to specific histological subtypes and are relevant to all forms of ovarian cancer. Immunohistochemistry analysis of sections from these four tumors with antibodies detecting the N and C-termini of CBP revealed that the tumors containing the deletion mutations had no full length CBP protein in tumor cells but did express a truncated form of CBP while normal stromal cells showed normal expression of CBP. This confirms that the tumors with mutations also had LOH of the normal allele and strongly suggests that CBP is a mutational target in up to 5% of ovarian tumors.

Table 2. Mutations in the CBP gene in breast and ovarian tumors

MUTATION TYPE	TUMOR SAMPLE	LOCATION	PROTEIN DOMAIN	AMINO ACID CHANGE
Frameshift/Truncation				
765delC	ov623	Exon 2	N-Terminal TAD	L297X
4675delA	ov519A	Exon 27	HATD	L1548X
Missense				
1597G>A	ov519A	Exon 6	Cys/His-Rich Region 1 and CREB-Binding Domain	A467T
2876C>T	BT0167	Exon 14		S893L
3409G>A	OVCAR5	Exon 16		A1081T
4259C>T	ov51	Exon 24	HATD and Trithorax Consensus Finger	A1354V
6130A>G	ov735	Exon 31	Gln-Rich Region and C-Terminal TAD	N1978D
6130A>G	B110	Exon 31	Gln-Rich Region and C-Terminal TAD	N1978D
Silent				
2151T>C	B73, B143, ov519A, B103, and ov141	Exon 10	CREB-Binding Domain and KIX Domain	Y651Y (polymorphism)
2755C>T	BT0167	Exon 14		L852L
3171C>T	B73 and ov323	Exon 15		D1049D
5250C>T	B78	Exon 30	HATD	S1741S
5634C>G	B93	Exon 31		T1812T
5651G>A	ov542, ov985, ov177, and OV177 (cell line)	Exon 31	HATD	V1818V (polymorphism)
7047C>T	MDA463	Exon 31		S2283S
7410A>G	ov182	Exon 31		E2404E
3'-UTR				
7552insC	B61	Exon 31	3'-UTR	--
7549T>C	UACC812	Exon 31	3'-UTR	--
7610C>A	B113	Exon 31	3'-UTR	--
7631G>A	B92	Exon 31	3'-UTR	--
Intronic				
IVS2-31A>G	B80 and B101	Intron 2		--
IVS5-33G>T	B81	Intron 5		--
IVS8-39delA	B92 and ov69	Intron 8		--
IVS9-24A>G	MDA468	Intron 9		--
IVS17-16delTTT	ov647	Intron 17		--
IVS21-8C>T	B81, B96, and UACC812	Intron 21		--
IVS27+37A>C	ov742	Intron 27		--
IVS27+46G>A	ov742	Intron 27		--
IVS28-15C>T	B80	Intron 28		--
IVS28-14G>C	ov990	Intron 28		--
IVS28-14G>C	MDA361	Intron 28		--
IVS28-12C>G	ov526	Intron 28		--

Protein domain/function based on: Giles et al 1997 and Vendel & Lumb 2003

HATD = histone acetyltransferase domain
TAD = transactivation domain
KIX = KID-interacting domain

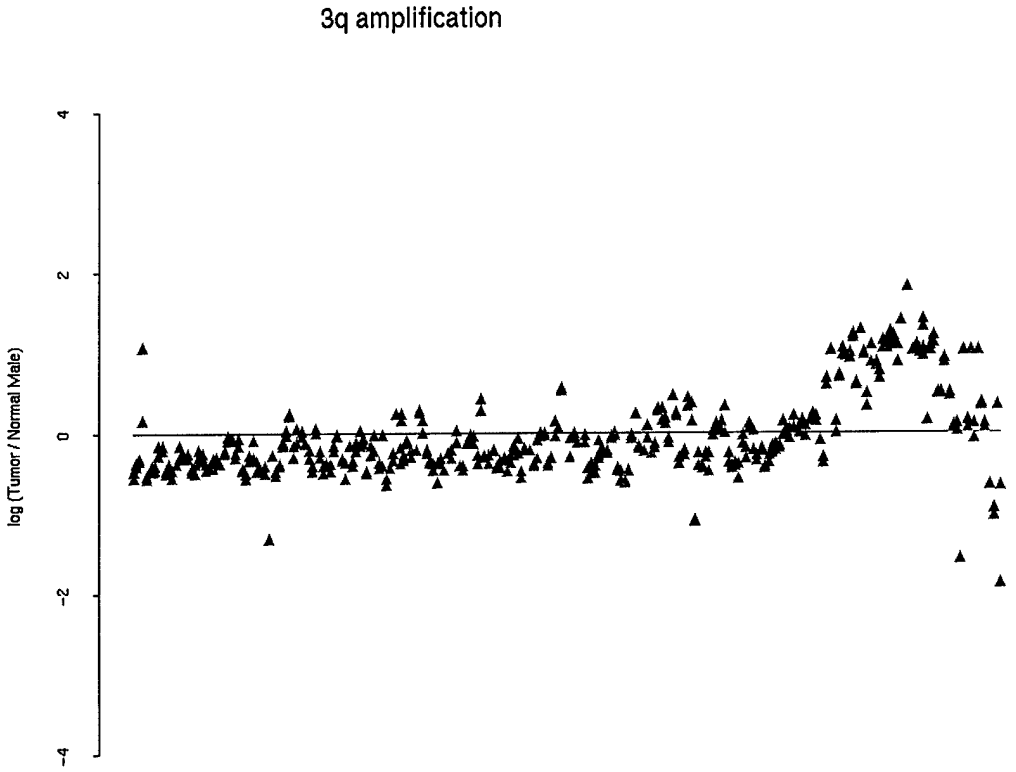

Figure 1. Amplification on chromosome 3q in an ovarian tumor as detected by gCGH. The $\log_2$ (intensity ratio) for each BAC on chromosome 3 was plotted against the relative chromosomal position of the BAC. Duplicate intensity values for each BAC are plotted. Points of greater than 0.75 on the y-axis are considered amplified.

Table 3. Pathological characteristics of CBP mutant ovarian tumors

Tumor	CBP Mutation	Stage	Grade	Histology
Ov51	A1354V	1C	2	Endometrioid
Ov519	4675delA	1C	1	Transitional Cell
Ov623	765delC	3C	3	Clear Cell
Ov735	N1978D	3C	3	Serous

Specific Aim #4/Task 4: Characterization of the oncogenic activity of candidate oncogenes.

The goal of this work was to establish the oncogenic activity of amplified genes in ovarian cancer. As described above, none of our cytogenetic and amplification studies resulted in identification of novel genes that are amplified at high frequency in familial or sporadic ovarian cancer, although this work is continuing. However, we did identify the ID-4 gene as a candidate oncogene using our microarray studies. Basically, supervised clustering of the gene expression array data from the 78 ovarian tumors with different responses to cisplatinum/carboplatinum and paclitaxel therapy revealed a set of 12 genes that predicted long time to recurrence of disease within 18 months of surgery (unpublished data). This may equate with sensitivity to these chemotherapeutic agents within the tumors. We selected the ID-4 gene from this set of 12 because of its role as a transcriptional repressor. Stable expression of ID-4 was established in NIH3T3 mouse fibroblast cells and Ov202 ovarian cancer cells and was verified by western blot. Initial growth rate studies using the MTS assay (Clontech) established that over-expression

of ID-4 enhances cell growth and proliferation (data not shown). We postulate that ID-4 is a novel oncogene that confers sensitivity to combined cisplatinum/carboplatinum and paclitaxel therapy upon cancer cells.

While we have now reached the end of this grant, we aim to continue this work by 1) establishing the oncogenic properties of the gene using anchorage independence soft agar transformation assays, focus formation transformation assays, and tumorigenesis assays in nude mice; 2) establishing the role of ID4 in confering sensitivity to cisplatinum/carboplatinum and paclitaxel treatment using *in vitro* clonogenic survival assays. It is our hope that ID-4 may prove useful as a novel therapy for ovarian cancer through its putative ability to establish sensitivity to chemotherapeutic agents in tumor cells.

Reportable Outcomes:

Manuscript in Preparation

Ward R, Johnson M, Kalli K, Shridhar V, van Deursen J, Couch, FJ. CBP is an ovarian cancer tumor suppressor gene.

References

Shridhar V, Lee J, Pandita A, Iturria S, Avula R, Staub J, Morrissey M, Calhoun E, Sen A, Kalli K, Keeney G, Roche P, Cliby W, Lu K, Schmandt R, Mills GB, Bast RC Jr, James CD, Couch FJ, Hartmann LC, Lillie J, Smith DI. Genetic analysis of early- versus late-stage ovarian tumors. Cancer Res. 2001;61(15):5895-904.

Israeli O, Gotlieb WH, Friedman E, Goldman B, Ben-Baruch G, Aviram-Goldring A, Rienstein S. Familial vs sporadic ovarian tumors: characteristic genomic alterations analyzed by CGH. Gynecol Oncol. 2003;90(3):629-36.

Hedenfalk I, Ringner M, Ben-Dor A, Yakhini Z, Chen Y, Chebil G, Ach R, Loman N, Olsson H, Meltzer P, Borg A, Trent J. Molecular classification of familial non-BRCA1/BRCA2 breast cancer. Proc Natl Acad Sci U S A. 2003;100(5):2532-7.

Ramus SJ, Pharoah PD, Harrington P, Pye C, Werness B, Bobrow L, Ayhan A, Wells D, Fishman A, Gore M, DiCioccio RA, Piver MS, Whittemore AS, Ponder BA, Gayther SA. BRCA1/2 mutation status influences somatic genetic progression in inherited and sporadic epithelial ovarian cancer cases. Cancer Res. 2003;63(2):417-23.

Coupry I, Roudaut C, Stef M, Delrue MA, Marche M, Burgelin I, Taine L, Cruaud C, Lacombe D, Arveiler B. (2002). Molecular analysis of the CBP gene in 60 patients with Rubinstein-Taybi syndrome. J Med Genet. 39(6):415-21.

****

Project #3: Common Fragile Sites and Ovarian Cancer- David I Smith, Ph.D.

There were four specific aims to this research proposal. **Specific Aim #1**: The cloning and characterization of FRA6F (6q21) and FRA6E (6q26) as these two common fragile sites are derived from chromosomal regions that are frequently deleted during the development of ovarian cancer. **Specific Aim #2**: The isolation of genes from the FRA6E and FRA6F regions, followed by examining each of them as potential tumor suppressor genes or sensors of genomic damage. **Specific Aim #3:** To perform clinical correlative studies in ovarian cancer with our impressive resource of fresh frozen ovarian tumors with full clinical follow-up. **Specific Aim #4:** To characterize aberrantly expressed genes derived from chromosomal bands containing common fragile sites, and to determine if these genes do actually reside within the common fragile sites in those bands.

Specific Aim #1: Characterization of FRA6F (6q21) and FRA6E (6q26). Our first goal was to analyze the two chromosomal regions on chromosome 6 that are frequently deleted in ovarian tumors and that contain two of the common fragile sites, FRA6F (6q21) and FRA6E (6q26). We entered into a collaboration with the group of Dr. Barbanti-Brodano (University of Ferrara, Italy) as their group was already working on the FRA6F cloning. We participated in the characterization of the 6q21 region surrounding FRA6F which eventually determined that instability in 6q21 extended for at least 1200 Kb. Contained within this region are a number of small genes, including REV3L, DIF13, FYN, and LAMA4. A comparison between the sequence within FRA6F and the published sequences for FRA6E, FRA16D and FRA3B revealed that there were two regions within FRA6F that had multiple helix flexibility peaks as determined by the FlexStab Program (1). Molecular markers within the FRA6F common fragile sites showed the highest loss of heterozygosity in ovarian tumors. Finally, a replicative senescence gene was localized within the FRA6F region, and a gene associated with hereditary schizophrenia. All of this work was published in *Oncogene* (Morelli C et al., Cloning and characterization of the common fragile site FRA6F harboring a replicative senescence gene and frequently deleted in human tumors. *Oncogene* 2002; 21:7266-7276).

We apologize to the reviewers of this proposal but we are going to list the Specific Aims from this point on slightly out of order. Our rationale for doing this is that we actually performed Specific Aim #4 right after Dr. Shridhar obtained the transcriptional profiling data at Millennium. It was the identification of a number of consistently down-regulated genes that mapped within 6q26 and the FRA6E region that really got us started on the characterization of this common fragile site and the very interesting Parkin gene. We will therefore describe first Specific Aim #4 which then got us into finishing up Specific Aim #1 and then going on to Specific Aims #2 and #3. We will therefore rearrange the Specific Aims accordingly.

Specific Aim #4: Characterize aberrantly expressed genes derived from chromosomal bands containing common fragile sites.

Transcriptional Profiling of Ovarian Tumors

We collaborated with researchers at Millennium (Cambridge, MA) to gain access to their technology platform for transcriptional profiling in exchange for supplying clinical samples. The purpose of this collaboration was to form an academic-industry partnership to gain insights into the pathogenesis of ovarian epithelial cancer. The Millennium platform utilizes cDNA inserts "spotted" at high density onto nylon-backed membranes. These membranes, which contained 25,000 (and then later 30,000 independent cDNA clones) are hybridized with ^{33}P-labeled cDNA isolated from various tissues, and the expression of the various cDNAs is assessed.

Our laboratory has been especially interested in the characterization of genes that are expressed in normal ovarian epithelium, but whose expression is lost during ovarian cancer development. We were also interested in comparisons between the expression profiles of early-stage versus late stage ovarian tumors to determine if gene expression analysis could give insights into the dramatic differences in survival between early and late-stage tumors. We compared transcriptional profiles of 7 early stage (stage I/II) and 7 late stage (stage III/IV) tumors with HOSE to find that both early and late-stage disease are characterized by more down-regulated than up-regulated genes. Unexpectedly, however, aberrantly regulated genes in late stage disease were similarly dysregulated in early stage disease. We have also analyzed the same tumors that were transcriptionally profiled using comparative genomic hybridization. This analysis confirmed the results of profiling. The only major difference observed was that gene amplification was infrequent in early stage disease. This may be very important as instability within the common fragile sites has been shown to mediate gene amplification events (2).

The transcriptional profiling analysis of 14 primary ovarian tumors identified approximately 12,000 genes that were at least 2-fold decreased in expression in one or more sampled tumors (3). Among genes at least 2-fold downregulated were several that have been mapped to common fragile sites, including FHIT and caveolin-1 (WWOX was not present on the 25,000 gene cDNA arrays utilized by Millennium). *We were, therefore, very interested in whether other CFS genes might also be consistently down-regulated in ovarian cancers.* We selected a subset of genes to determine if they localized within CFS regions. We found that there were 262 genes that were down-regulated at least 2-fold in 13 of the 14 tumors profiled. We selected 10 of these genes based on the following criteria: (A) They were localized to a chromosomal band known to contain a CFS; (B) There were documented aberrations within that chromosomal region in at least one malignancy; and (C) The feasibility of scoring breakage at that specific CFS. FISH analysis was performed on BAC clones encompassing portions of these genes to determine the positions of these genes relative to their corresponding CFSs. *Nine of the ten genes were determined to localize within seven previously uncloned CFSs.* As a result of this work, BACs have been identified that cross a portion of the previously uncloned CFSs mapping to 1p31 (FRA1C), 4q12 (FRA4B), 5q11 (4), 6q26 (FRA6E), 10q22 (FRA10D), 11p15.1 (FRA11C) and 15q22 (FRA15A). Three of the nine genes identified by this work as localized within CFSs (NOEY2, IGF2R, and TSG101) have already been determined to be putative tumor suppressor genes (5-11).

Specific Aim #1: Characterization of FRA6E. Three of the ten genes chosen were derived from chromosomal band 6q26. All three of these genes, LPA, PLG and IGF2R, were found to map within the FRA6E CFS. This CFS is derived from a region that is consistently deleted in multiple tumor types including ovarian cancer (12-15). As mentioned above IGF2R is a putative tumor suppressor gene (6,7). The BAC which spanned IGF2R was mapped to the proximal end of FRA6E. A BAC spanning LPA also mapped to the proximal end of FRA6E, but the frequency of hybridization of this BAC distal to the region of decondensation/breakage suggested that LPA was located closer to the middle of the FRA6E region than IGF2R. We decided to characterize the FRA6E CFS further by assembling a contig of overlapping BAC clones electronically and then using these BAC clones for a FISH-based analysis of fragility within chromosomal band 6q26. When we had completed this analysis for the FRA6E region, we found that the entire region where aphidicolin-induced decondensation/breakage occurred was 3.5Mb in size. This is, therefore, another large CFS region.

This 3.5 Mb region contains a number of interesting genes, including all the genes from 6q26 that we identified as having consistent loss of expression in ovarian tumors using transcriptional profiling. In addition, there were several other small genes present on the centromeric end of FRA6E that did not show loss of expression in ovarian tumors. The "center" of FRA6E is spanned by a single very large gene, which is 1.5 Mb in size. This gene, PARK2, was identified as being mutated in patients with autosomal recessive juvenile Parkinsonism (ARJP) (16-17). Interestingly, there are frequent large mutations in PARK2 observed in some ARJP patients. These deletions occur around exons 3 and 4 of the PARK2 gene, which are also in the "center" of the FRA6E region (16,17). The Figure below shows the entire FRA6E region and the BACs that define it. Also included on this Figure are the various genes found to map within FRA6E. Finally, we have also included the results of the FISH analysis of aphidicolin induced decondensation/breakage within this region (showing the number of times that individual BAC clones hybridize proximal, distal or crossing to the region of breakage).

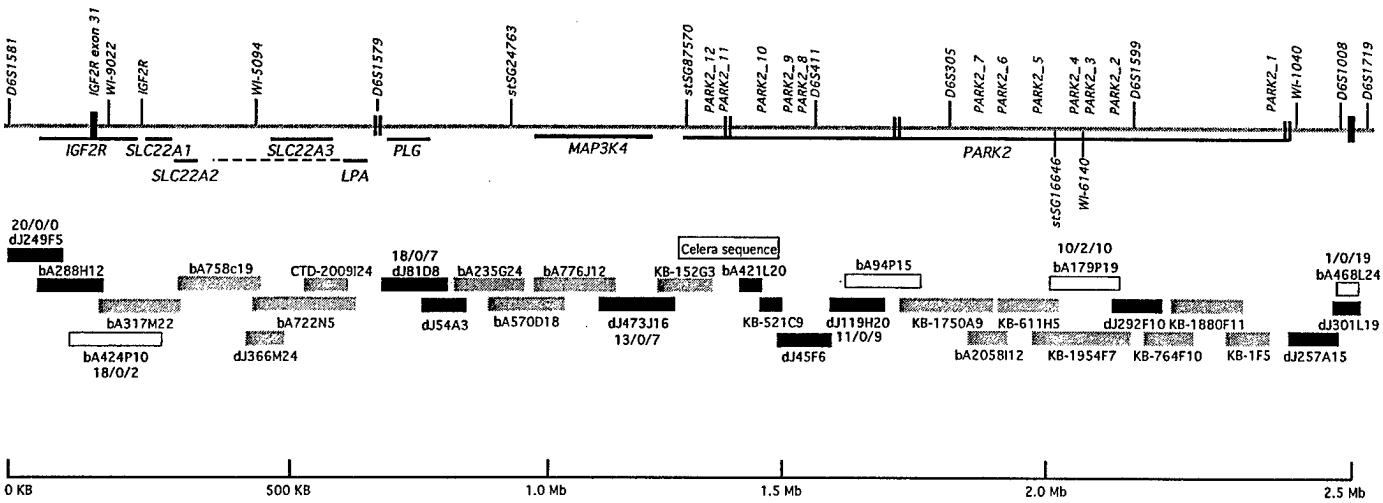

LOH at the IGF2R locus (located in the 3' UTR of the IGF2R gene) has been documented in both invasive and in situ breast cancers, hepatocellular tumors, and squamous cell carcinomas of the lung (18-19). In addition to the IGF2R locus, microsatellite markers mapping to 6q26 have been associated with a high frequency of LOH in a variety of different tumor types, including ovarian cancer (12-14). Therefore, we took microsatellite markers from throughout the FRA6E region and analyzed LOH in primary ovarian tumors. Percent LOH observed across the eight markers mapping to the FRA6E region ranged from 30% (D6S1581) to 72% (D6S1599). LOH analysis of these eight markers identified a significantly high frequency of LOH at D6S1599 (72.7%) and D6S305 (61.1%) (Figure below). These markers localize to introns 2 and 6, respectively, of the PARK2 gene suggesting that PARK2 was in fact the target of the instability.

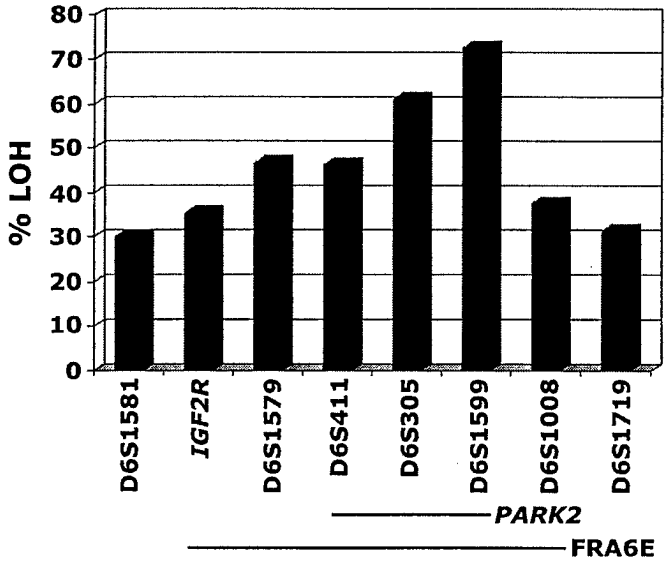

Specific Aim #2 The isolation and characterization of genes from the FRA6E region.

We next performed semi-quantitative RT-PCR analysis of all 8 genes localizing to the FRA6E region to determine if PARK2 exhibited the highest loss of expression (LOE) of all the genes in the region. Contrary to what would be expected for a gene targeted by instability, LOE analysis of these genes identified SLC22A3 as the gene with the highest LOE (87%) when compared to that of NOSE. Though PARK2 was not the gene with the highest LOE, it was down regulated in 39% of the ovarian cell line and primary tumors analyzed. *Additionally, LOE analysis of PARK2 using primers encompassing exons 2 to 6 revealed the presence of alternative transcripts in both ovarian cell lines and primary ovarian tumors.*

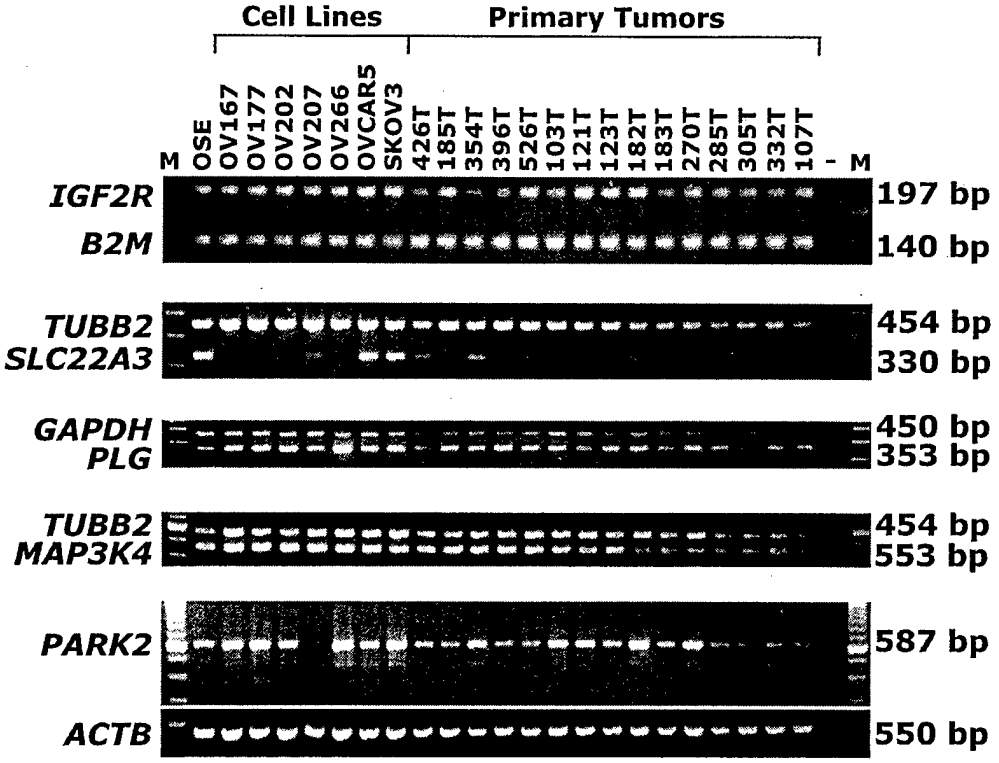

Parkinson's disease is the second most prevalent neurodegenerative disorder with autosomal recessive juvenile Parkinson's disease (ARJP), caused by mutations in the *PARK2* gene, being characterized by an early onset of Parkinsonism (before the age of 40) (16). Various intragenic homozygous and heterozygous deletions/duplications and point mutations have been identified in patients with ARJP and result in either protein truncation or an amino acid substitution (16,17). The figure below identifies the documented deletions and duplications that have been identified in ARJP patients.

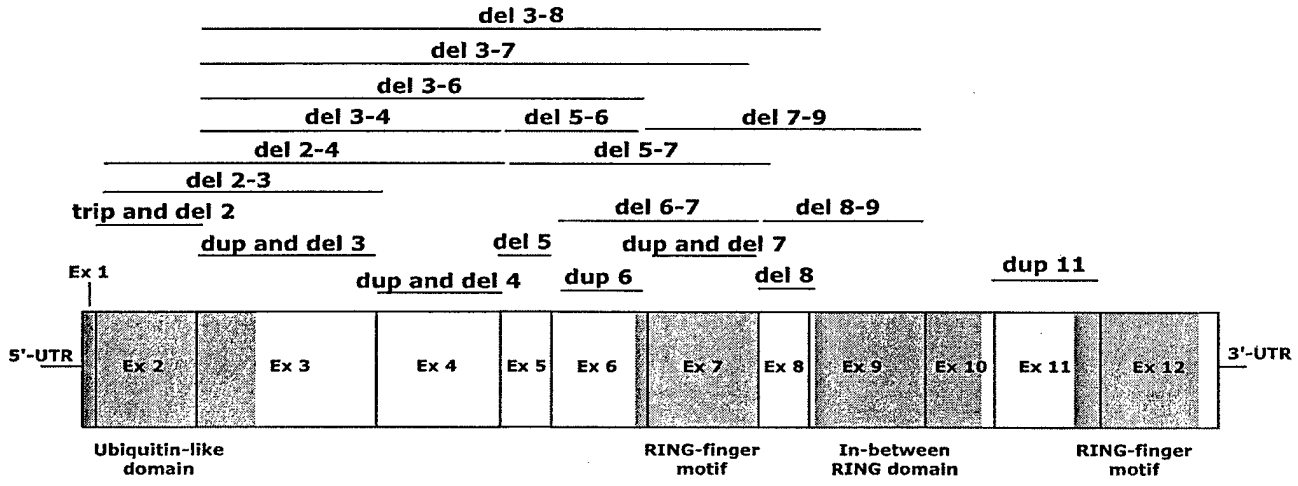

In particular, variable deletions and duplications have been documented throughout exons 3-8 of PARK2. Exons 2-8 of PARK2 span the "center" (most unstable region) of FRA6E suggesting that the fragility at FRA6E plays a role in ARJP and that PARK2 may play a role in the development of ovarian cancer. As exons 3-8 is considered to be the "hot spot" for PARK2 mutations, we designed RT-primers which produced a product encompassing exons 2-8 of PARK2 to analyze 7 ovarian cell lines and 22 primary ovarian tumors for alternative PARK2 transcripts. Previous alternative transcript analysis of FHIT and WWOX was performed by nested PCR analysis of cell lines and primary tumors. Because we observed alternative transcripts using conventional single round (28 cycle) PCR, we opted to merely increase the number of PCR cycles to 35 rather than perform nested PCR. PCR analysis of the cell

line/primary tumor panel identified numerous alternative transcripts in both the cell lines and primary tumors analyzed.

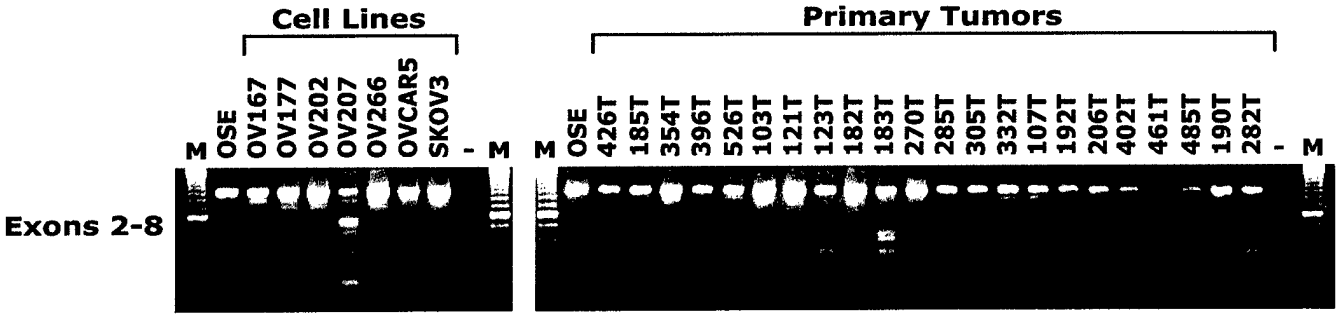

The most important question is expression of the Parkin protein. We used a commercially available

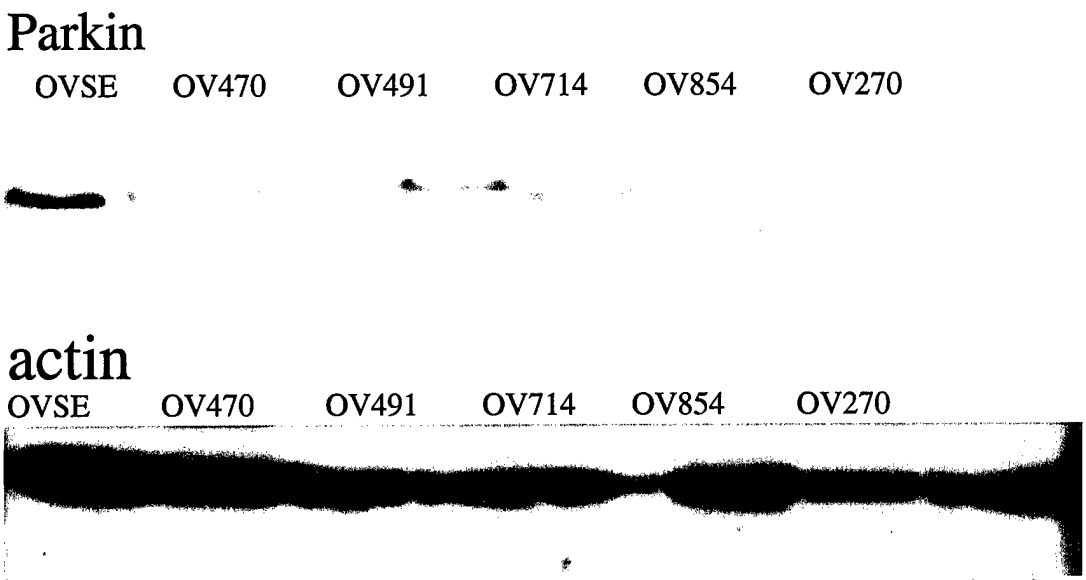

Parkin antibody to measure Parkin expression in several primary ovarian tumors vs. normal ovarian surface epithelium.

We also performed mutational studies to determine if we could identify any mutations in ovarian tumor samples. We did observe a few polymorphisms in certain individuals but no bona fide mutations. We next made primers for each of the Parkin exons and tested a panel of 50 cancer-derived cell lines, including cell lines derived from ovarian cancers, breast, prostate and pancreatic cancers and hepatocellular carcinoma. Only a single hepatocellular carcinoma cell line, pLC5, had a homozgyous deletion of a Parkin exon. Based upon this, we did analyze hepatocellular carcinoma cell lines and found the complete absense of Parkin protein in any of them.

We used two hepatocellular carcinoma cell lines, pLC5 and Hep3B, to begin to analyze the role that loss of Parkin expression had on those cells. We generated stable Parkin and Parkin-myc transfectants in the HCC cell lines and then tested the growth characteristics of cells expressing and not expressing Parkin. This analysis (shown below) reveals that cells expressing Parkin grew slightly slower than cells that did not.

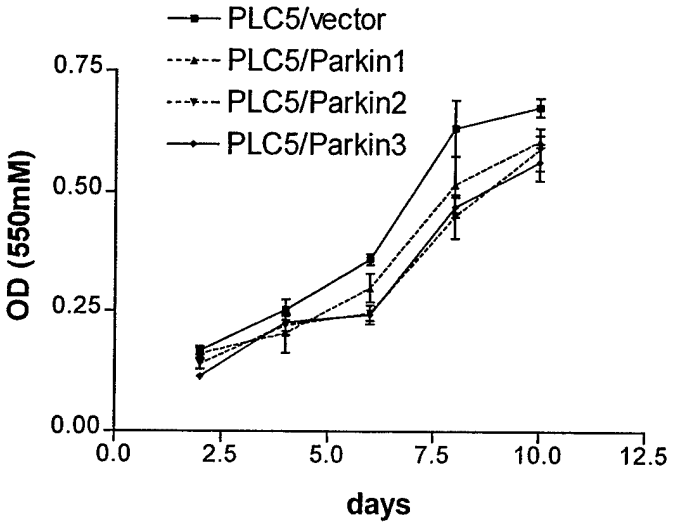

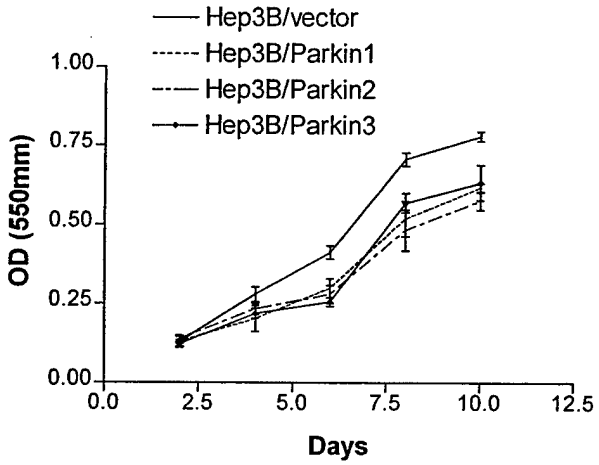

We also tested the sensitivity of the various cells to different apoptosis-inducing agents. This analysis revealed that expression of Parkin did result in greater sensitivity to specific apoptotic inducers as is shown below.

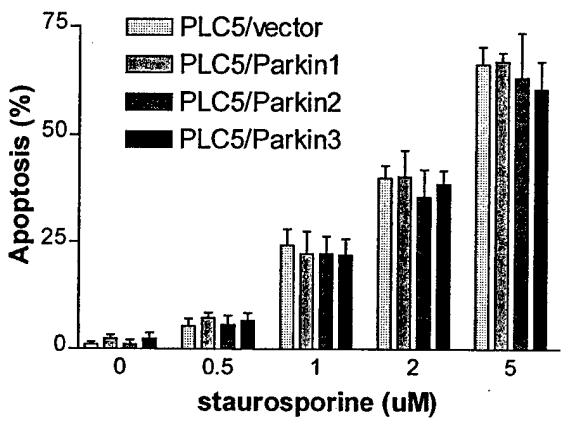

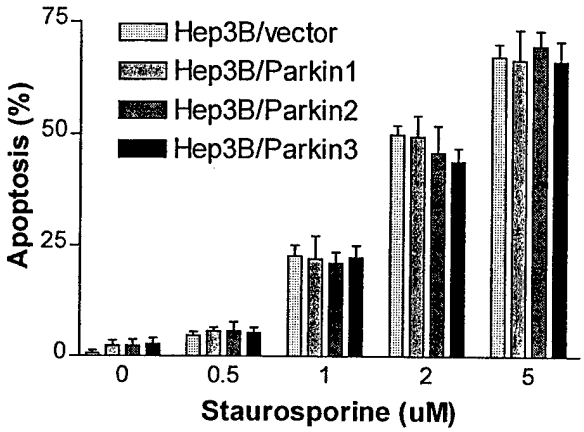

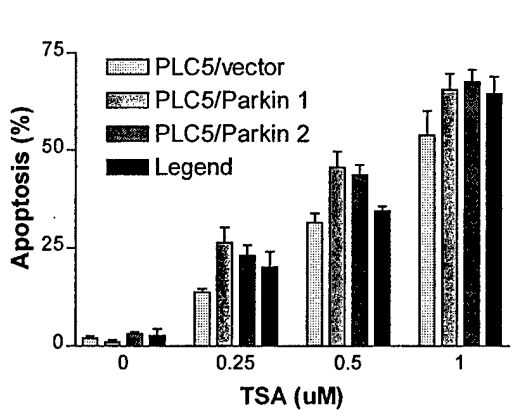

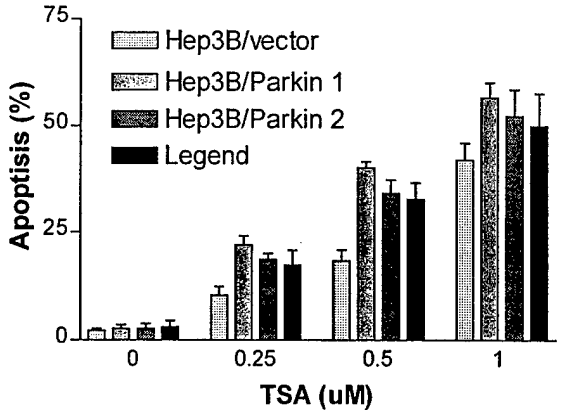

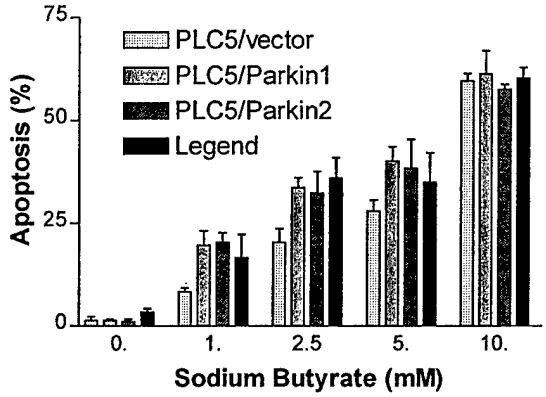

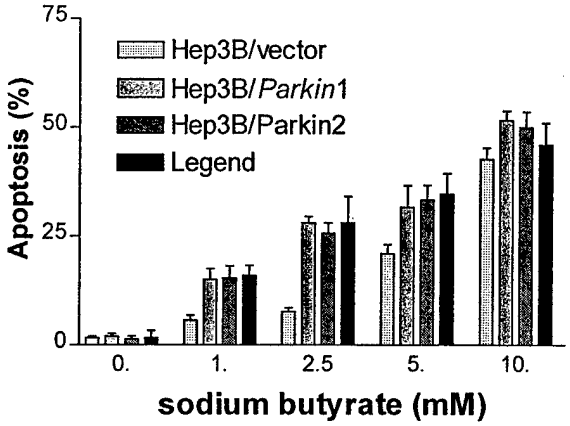

Our next steps, although not part of the original proposal was to begin to characterize Parkin in greater detail to determine functionally its' role in the normal cell and how its' absence might contribute to the development of ovarian cancer. We utilized the Parkin-myc stable transfectants to immunoprecipitate other proteins that might interact with Parkin. There is now a great deal of information available on Parkin substrates in neural cells based upon its association with autosomal recessive juvenile Parkinsonism, but little information about Parkin substrates in epithelial cells. Parkin is an ubiquitin E3 ligase that ubiquitinylates a number of different substrates. We took the Parkin-myc stable transfectants and immunoprecipitated proteins that bound to Parkin in the pLC5 cells. This analysis revealed that cytokeratin 18 was tightly bound to Parkin. Cytokeratin 18 is a key component of the cytoskeleton (in conjunction with CK8), so we used immunofluoresence to examine the co-localization of Parkin and the CK8/CK18 present within the cytoskeleton. This analysis revealed that Parkin was indeed co-localized with the cytoskeleton. Our current theory is that Parkin may be involved in "sensing" cytoskeletal stress which may be observed by an increase in misfolded cytokeratins. We are again thankful to the Department of Defense for their continued support of our work in this area and we hope to demonstrate that Parkin (and indeed the group of common fragile site genes) works as a stress-sensing network within normal cells.

Specific Aim #3: Clinical correlative studies.

The goal of the third Specific Aim is to perform clinical correlative studies in ovarian cancer with our impressive resource of primary ovarian tumors. What we did not specify previously was how we were going to monitor Parkin expression to correlate that with clinical survival. We very quickly realized that measuring Parkin mRNA levels was not the most effective means of performing this analysis and that we should directly measure Parkin protein levels utilizing antibodies. We therefore obtained two commerical Parkin antibodies and used them to measure Parkin protein expression in a panel of primary ovarian cancers. Although many ovarian cancer specimens had reduced or absent Parkin expression we

did not observe any significant clinical correlations between level of Parkin expression and the resulting clinical phenotype. Our current hypothesis for this observation is that perhaps cancer involves the inactivation of multiple common fragile site genes. Thus, we might not expect to see a significant difference between cells that do and don't express Parkin. What we are just beginning to do (hence this work is not complete and we don't yet have an answer to this question) is to measure the expression levels of multiple common fragile sites together to determine if together they are correlated with overall clinical survival and response to chemotherapeutic agents.

Key Research Accomplishments

- Participated in the cloning and characterization of FRA6F (6q21). Resulted in a publication in *Oncogene* 2002; 21: 7266-7276.
- Cloned and characterized FRA6E, a 3.5 megabase region of instability. Resulted in a publication in *Genes, Chromosomes and Cancer* 2003; 38: 40-52 .
- Identified Parkin, as a large common fragile site gene that is frequently not expressed in ovarian tumors and in other cancers. Resulted in a publication in *Oncogene* that is currently In Press.
- Found that a number of consistently down-regulated genes in ovarian tumors are actually derived from within the common fragile sites. This led to the cloning of a number of previously uncloned common fragiles sites and increased the growing list of common fragile site genes.
- Placing Parkin back into cell lines that do not express it results in slight growth inhibition.
- Parkin expression is associated with greater sensitivity to specific apoptosis-inducing agents.
- Identified cytokeratin 8 and 18 as proteins that bind to and localize with Parkin. Parkin may therefore have an important role in the cytoskeleton.

Reportable Outcomes

Publications

Shridhar V, Bible KC, Staub J, Avula R, Lee YK, Kalli K, Huang H, Hartmann LC, Kaufmann SH, **Smith DI**. Loss of expression of a new member of the DNAJ protein family confers resistance to chemotherapeutic agents used in the treatment of ovarian cancer. Cancer Res 2001; 61:4258-4265. (MS #1)

Shridhar V, Lee J, Pandita A, Iturria S, Avula R, Staub J, Morrissey M, Calhoun E, Sen A, Kalli K, Keeney G, Roche P, Cliby W, Lu K, Schmandt R, Mills GB, Bast RC Jr., James CD, Couch FJ, Hartmann LC, Lillie J, **Smith DI**. Genetic analysis of early- versus late-stage ovarian tumors. *Cancer Res.* 2001; 61: 4258-4265. (MS #2)

Lai J, Chien J, Staub J, Avula R, Greene EL, Matthews TA, **Smith DI**, Kaufmann SH, Roberts LR, Shridhar V. Loss of HSulf-1 up-regulates heparin-binding growth factor signaling in cancer. J Biol Chem 2003; 278:23107-23117. (MS #4)

Chien J, Staub J, Hu S-I, Erickson-Johnson MR, Couch FJ, **Smith DI**, Crowl RM, Kaufmann SH, Shridhar V. A candidate tumor suppressor HtrA1 is downregulated in ovarian cancer. Oncogene 2003; in press. (MS #5)

Acquatai F, Morelli C, Cinquetti R, Bianchi MG, Porrini D, Varesco L, Gismondi V, Rocchetti R, Talevi S, Possati L, Magnanini C, Tibiletti MG, Bernasconi B, Daidone MG, Shridhar V, **Smith DI**, Negrini M, Barbanti-Brodano G, Taramelli R. Cloning and characterization of a senesence inducing and class II tumor suppressor gene in ovarian carcinoma at chromosomal region 6q27. *Oncogene* 2001; 20: 980-988. (MS #6)

Smith DI. Transcriptional profiling develops molecular signatures for ovarian tumors. *Cytometry* 2002; 47: 60-62. (MS #7)

Hellman A, Zlotorynski E, Scherere SW, Cheung J, Vincent JB, **Smith DI**, Trakhtenbrot L, Kerem B. A role for common fragile site induction in amplification of human oncogenes. *Cancer Cell* 2002; 1: 89-97. (MS #8)

Denison SR, Becker NA, Ferber MJ, Phillips LA, Kalli KR, Lee J, Lee J, **Smith DI**, Shridhar V. Transcriptional profiling reveals that several common fragile sites genes are down-regulated in ovarian cancer. *Genes, Chromosomes Cancer* 2002; 34: 406-415. (MS #9)

Morelli C, Karayianni E, Magnanini C, Mungall AJ, Thorland E, Negrini M, **Smith DI**, Barbanti-Brodano G. Cloning and characterization of the common fragile site FRA6F harboring a replicative senesence gene and frequently deleted in human tumors. *Oncogene* 21: 7266-7276. (MS #10)

Becker N, Thorland E, Denison S, Phillips LA, **Smith DI**. Evidence that instability within the Fra3B region extends four megabases. *Oncogene* 2002; 21: 8713-8722. (MS #11)

Callahan G, Denison SR, Phillips LA, Shridhar V, **Smith DI**. Characterization of the common fragile site FRA9E and its potential role in ovarian cancer. *Oncogene* 2003; 22: 590-601. (MS #12)

Denison SR. Callahan G, Becker NA, Phillips LA, **Smith DI**. Characterization of FRA6E and its potential role in autosomal recessive juvenile parkinsonism and ovarian cancer. *Genes Chromosomes Cancer* 2003; 38: 40-52. (MS #13)

Denison SR, Wang F, Becker NA, Mueller B, Kock N, Phillips LA, Klein C, **Smith DI.** Alterations in the common fragile site gene Parkin in ovarian & other cancers. *Oncogene* 2003, In Press. (MS#14)

Abstracts

Shridhar V, Staub J, Huang H, Callahan G, Bright RK, Yokomizo A, Wang L, Pass HI, Hartmann L, **Smith DI.** Loss of expression by deletion and hypermethylation of a new member of the DNAJ protein family on 13q14.1 in ovarian cancer. *Amer. J. Hum. Genet.* 65:A1817, 1999.

Smith DI, Thorland E, Krummel K, Kawakami M, Myers S., Roberts L. Role of the common fragile sites in cancer development. *Cancer Genetics and Epigenetics: Gordon Research Conference*, Feb. 20-25, 2000.

Smith DI, Thorland E, Krummel K, Kawakami M, Myers S., Roberts LR. Role of the common fragile sites in cancer development. Miami Nature Biotechnology Winter Symposium: DNA, RNA, and Cancer. Miami Beach, FL, Feb. 2000.

Shridhar V, Callahan G, Staub J, Avula R, Hartmann LC, **Smith DI**. Identification of novel genes not expressed in primary ovarian tumors and cell lines. *Cancer Res.* 41:A1983, 2000.

Callahan G, Shridhar V, Bale LK, Kalli KR, Hartmann LC, Conover C, **Smith DI**. Loss of PAPP-A expression in ovarian epithelial carcinoma. *Cancer Res.* 41:A2214, 2000.

Callahan G, Shridhar V, Bale LK, Kalli KR, Hartmann LC, Conover CA, Smith DI. Loss of PAPP-A expression in ovarian epithelial carcinoma. Cancer Res 2000; 41:A349.

Asaf H, Scherer SW, Skaug J, Rahat A, **Smith DI**, Kerem B. DNA replication pattern along a broad region that contains FRA7G, a common fragile site on human chromosome 7. Amer. J. Hum. Genet, 67:A176, 2000.

Denison SR, Shridhar V, Ferber MJ, Becker NA, Callahan G, Lee J, Lillie J, **Smith DI**. Cloning and characterization of FRA6E. Amer. J. Hum. Genet. 67:A110, 2000.

Ferber MJ, Denison SR, Becker NA, Lee J, Lillie J, Hartmann LC, Shridhar V, **Smith DI.** Genes within the common fragile sites are down-regulated in ovarian cancer. Amer. J. Hum. Genet. 67:A447, 2000.

Smith DI, Sen A, Avula R, Staub J, Lee J, Hartmann L, Lillie J, Shridhar V. Identification of differentially expressed genes in early and late stage primary ovarian tumors by the construction of subtraction suppression hybridization cDNA libraries. Amer. J. Hum. Genet. 67:A505, 2000.

Shridhar V, Callahan G, Staub J, Avula R, Hartmann LC, Smith DI. Identification of novel genes not expressed in primary ovarian tumors and cell lines. Cancer Res 2000; 41:A1983.

Shridhar V, Pandita A, Lee J, Iturria S, Staub J, Avula R, Sen A, Calhoun R, Couch F, James CD, Hartmann L, Lillie J, **Smith DI**. Comprehensive analysis of genetic alterations in ovarian cancer. Oncogenomics meeting in Tucson, Arizona, January 25-27, 2001.

Callahan G, Denison S, Shridhar V, **Smith DI**. Cloning and characterization of FRA9E. Amer. Assoc. for Cancer Research 42:A338, 2001.

Denison SR, Phillips LA, Shridhar V, **Smith DI**. FRA6E (6q26), a 1 MB gene-rich common fragile site. Amer. Assoc. for Cancer Research 42:A346, 2001.

Chien J, Staub J, Avula R, **Smith DI**. Aberrant expression of perlecan in ovarian cancer. Amer. Assoc. for Cancer Research 42:A1723, 2001.

Avula R, Stuab U, Sen A, Lee J, Hartmann L, Lillie J, **Smith DI**, Shridhar V. Identification of differentially expressed genes in early and late stage primary ovarian tumors by suppression subtaction hybridization. Amer. Assoc. for Cancer Research 42:A1729, 2001.

Shridhar V, Pandita A, Lee J, Iturria S, Staub J, Avula R, Sen A, Calhoun E, Couch F, James CD, Hartmann L, Lillie J, **Smith DI**. Comprehensive analysis of genetic alterations in ovarian cancer. Amer. Assoc. for Cancer Research 42:A2307, 2001

Becker N, Denison S, Callahan G, Thorland E, Ferber M, Phillips L, **Smith DI**. Expression of common fragile site genes in cancer-derived cell lines. Amer. Association for Cancer Research, 2002.

Chien J, Staub J, Avula R, Kaufmann SH, Bible KC, Lee YK, **Smith DI**, Hu S-I, Crowl RM, Shridhar V. Human HtrA, identified as a differentially expressed gene product in ovarian cancer, is involved in stress response. AACR Meeting on Apoptosis, 2002.

Chien J, Avula R, Staub J, Hartmann LC, **Smith DI**, Kaufmann SH, Shridhar V. A novel proapototic protein is down-regulated in ovarian cancer by hypermethylation. AACR Meeting on Apoptosis, 2002.

Aderca I, Krajnik KL, Kolbert CP, Montoya DP, Nagorney DM, Burgart LJ, **Smith**

Lai J-P, Staub J, Avula R, Chien J, **Smith DI**, Roberts LR, Shridhar V. A novel sulfatase domain-containing gene, hSULF, promotes apoptosis in ovarian carcinoma. AACR Meeting on Apoptosis, 2002.

Lai J-P, Avula R, Montoya D, **Smith DI**, Shridhar V, Roberts LR. A novel sulfatase domain containing protein, hSULF, promotes apoptosis of hepatocellular carcinoma cells. Amer. Assoc. for Cancer Research, 2002.

Lai J-P, Staub J, Avula R, Chien J, **Smith DI**, Roberts LR, Shridhar V. Characterization of a novel sulfatase domain-containing gene hSULF in ovarian carcinoma. Amer. Assoc. for Cancer Research, 2002.

Smith DI, Denison S, Callahan aG, Ferber M, Becker N, Phillips L. Common Fragile Site Regions May Contain Many Important Tumor Suppressor Genes. Cancer Genetics and Tumor Suppressor Cold Spring Harbor Meeting, 2002.

Smith DI, Denison S, Becker N, Callahan G, Ferber M, Shridhar V, Bast R. Common Fragile Site Genes are Not Frequently Expressed in Ovarian Tumors and are Mutational Targets in Ovarian and Other Cancers.

Lu KH, Patterson A, Atkinson EN, Baggerly K, Marquez R, Liu J, **Smith DI**, Hartmann L, Fishman D, Berchuck A, Whitakeer R, Bast RC Jr. Selection of potential markers for epithelial ovarian cancer with gene expression array and recursive descent partition analysis. AACR 2003.

Marquez R, Baggerly K, Patterson A, Frumovitz M, Atkinson EN, Liu J, **Smith DI**, Hartmann L, Fishman D, Berchuck A, Whitaker R, Bast RC Jr, Lu KH. Gene expression array analysis distinguishes different histotypes of epithelial ovarian cancer and suggests a distinct transcriptional program for mucinous cancers. AACR 2003.

PRESENTATIONS:

The role of the common fragile sites in cancer. Presented at Albert Einstein College of Medicine to the Department of Molecular Pharmacology, May 17, 1999.

Common fragile sites and cancer. Presented to the Frontiers in Clinical Genetics at George Washington University, Sept. 16, 1999.

Role of the Common Fragile Sites in Cancer Development. Presented at the Miami Winter Symposium on DNA, RNA and Cancer, February 6, 2000.

The Ovarian Cancer Research Program of the Mayo Clinic Cancer Center. Presented at Virginia Medical College, Richmond, Virginia, March 6, 2000.

The Genetics of Ovarian Cancer in the Post-Genomics Era, Presented as the Distinguished Lecturer for the Women's Cancer Program at M.D. Anderson Cancer Center, Houston, Texas, June 7, 2000.

Transcriptional Profiling to Understand the Underlying Biology of the Development of Ovarian Cancer, Presented as the Distinguished Lecturer for the Women's Cancer Program at M.D. Anderson Cancer Center, Houston, Texas, June 7, 2000.

Transcriptional Profiling to Understand the Underlying Biology of the Development of Ovarian Cancer. Presented at Henry Ford Hospital, July 14, 2000.

Common Fragile Sites and Cancer. Presented at the Common Fragile Sites, Gene Amplification and Cancer Meeting, Held at Mayo Foundation, August 25-26, 2000.

Common Fragile Sites and Cancer. Presented at the University of Nebraska in Omaha, Sept. 11, 2000.

Common fragile sites and the development of cancer. Presented to graduate students at Mayo, September 27, 2000.

Transcriptional Profiling of Ovarian Tumors. Presented at Eli Lilly, Indianapolis, IN, November 13, 2000.

Transcriptional Profiling of Ovarian Tumors- Presented at the Department of Defense Annual Meeting on Ovarian Cancer, Dulles Hilton, Maryland, November 30, 2000.

Generation of a Molecular Profile for Ovarian Cancer- Presented at the Huntsman Cancer Center, Salt Lake City, Utah, December 15, 2000.

Common Fragile Sites and Cancer- Presented at Case Western Reserve, Cleveland, Ohio, January 19, 2001.

The Ovarian Cancer Program of the Mayo Clinic Cancer Center - Presented at the University of Minnesota, April 13, 2001.

Common fragile sites and Cancer- Presented to the Department of Microbiology and Molecular Genetics, SUNY Stonybrook, Nov. 19, 2001.

Large common fragile site genes are mutational targets in ovarian cancer. Fox Chase Cancer Center, Philadelphia, PA, April 16, 2002.

Large common fragile site genes are mutational targets in ovarian cancer. University of Michigan Cancer Center, Ann Arbor, MI, April 19, 2002.

Using expression profiling to study the biology of ovarian cancer. Presented at Shaw College of the Chinese University of Hong Kong. September 27, 2002.

Common fragile site genes: a stress response network within cells? Presented at the Helene Harris Memorial Trust (HHMT) bi-annual meeting in Stratford Upon Avon, March 25, 2003.

Parkin, a large common fragile site gene, involved in cancer development. Presented at Johns Hopkins University to the laboratory of Dr. Ted Dawson, August 18, 2003.

Large common fragile site genes and cancer. Presented at the Guthrie Research Institute in Sayre, Pennsylvania, October 17, 2003.

Funding applied for based upon work supported by this award.

National Cancer Institute- A large common fragile site gene, Parkin, and ovarian cancer. We repeatedly tried to obtain funding for this work from the National Cancer Institute, but could never convince reviewers that Parkin was indeed an important cancer-related gene. CA-095187.

Department of Defense Ovarian Program- OC030016. PARK2, a large common fragile site gene, is part of a stress response network in normal cells that is disrupted during the development of ovarian cancer. We recently received word that this grant will be funded by the Department of Defense.

Minnesota Ovarian Cancer Alliance- PARK2, a mutational target in ovarian cancer. Applied to MOCA and received a $50,000 one year grant to study Parkin and its role in the development of ovarian cancer.

National Cancer Institute- Specialized Program in Research Excellence (SPORE) in Ovarian Cancer from the Mayo Clinic Cancer Center. David I Smith, Ph.D. was the P.I. on this SPORE application. Our SPORE was competitive but will probably not receive funding.

CONCLUSIONS

We have now identified the third very large common fragile site gene, Parkin. Parkin and the FRA6E region surrounding it have many similarities to two other large gene/active common fragile site regions, FHIT/FRA3B and WWOX/FRA16D. As more detail becomes available about the functions of each of these very large, highly conserved genes, it is becoming more and more clear that these genes do indeed play an important role in cancer development. What we have done is to demonstrate that many of the alterations observed in FHIT and WWOX in ovarian and many other cancers are indeed observed in Parkin. These genes are not typical tumor suppressors, as one rarely detects point mutations in these genes in cancer. However, the instrinsic instability within the common fragile site regions may predispose these very large genes to heterogeneous deletions and duplications that result in no functional protein being produced. Although these genes do not have the mutational spectrum of the typical tumor suppressor what they may share (and this has been demonstrated for FHIT) is that they can functionally suppress tumor formation. An important point to consider is that there may be a large number of these large common fragile site genes distributed throughout the genome and each of these may have frequent deletions and alterations in developing cancer cells. The net effect is that genomic instability within the common fragile site regions could result in the inactivation of a whole cadre of important cancer-related genes. Another very important point to consider is that all of our focus has been on the role of the common fragile sites and the genes contained within them in cancer development. What has not been examined is the role of this potential "system" in the normal cells. Our hypothesis is that the entire group of common fragile sites and their genes work to sense cellular stress (at many levels) and so that they cells can appropriately respond. Our analysis of cancer cells is simply examining this system after it has broken down. Again, we are very grateful for continued Department of Defense support so that we can pursue this completely unexplored area of research.

PERSONNEL RECEIVING SUPPORT

Viji Shridhar, PhD personnel

Jeremy Chien, PhD
Wanguo Liu, PhD
David I Smith, PhD
Heyu Zhang, MD, PhD
Rajeswari Avula
Julie Staub

Fergus Couch, PhD personnel

Shannon Hinson, PhD
Shubhashish Sarkar, PhD
Tieling Wang, PhD
Jianmin Wu, PhD

David I Smith, PhD personnel

Casey Hall
Leslie Phillips
Fang Wang, PhD

REFERENCES

1) Mishmar D, Rahat A, Scherer SW, Nyakatura G, Hinzmann B, Kohwi Y, Mandel-Gutfroind Y, Lee JR, Drescher B, Sas DE, Margalit H, Platzer M, Weiss A, Tsui LC, Rosenthal A, Kerem B. Molecular characterization of a common fragile site (FRA7H) on human chromosome 7 by the cloning of a simian virus 40 integration site. *Proc Natl Acad Sci USA* 1998; 95: 8141-8146.
2) Hellman A, Zlotorynski E, Scherer SW, Cheung J, Vincent JB, Smith DI, Trakhtenbrot L, Kerem B. A role for common fragile site induction in amplification of human oncogenes. *Cancer Cell* 2002: 1: 89-97.
3) Shridhar V, Lee J, Pandita A, Iturria S, Avulaa R, Staub J, Morrissey M, Calhoun E, Sen A, Kalli K, Kenney G, Roche P, Cliby W, Lu K, Schmandt R, Mills GB, Bast RC, James CD, Couch FJ, Hartmann LC, Lillie J, Smith Di. Genetic analysis of early- versus late-stage ovarian tumors. *Cancer Res* 2001: 61: 5895-5904.
4) Hecht F, Tajara EH, Lockwood D, Sandberg AA, Hecht BK. New common fragile sites. *Cancer Genet Cytogenet* 1988 33: 1-9.
5) De Souza AT, Hankins GR, Washington MK, Orton TC, Jirtle RL. M6P-IGF2R gene is mutated in hepatocellular carcinomas with a loss of heterozygosity. *Nat Genet* 1995;11:447-9.
6) Li L, Li X, Francke U, Cohen SN. The tsg101 tumor susceptibility gene is located in chromosome 11 band p15 and is mutated in human breast cancer. *Cell* 1997: 88: 143-154.
7) Sun Z, Pan J, Bubley G, Balk SP. Frequent abnormalities in tsg101 transcripts in human prostate cancer. *Oncogene* 1997: 15: 3121-3125.
8) Oates AJ, Schumaker LM, Jenkins SB, Pearce AA, DaCosta SA, Arun B, Ellis MJ. The mannose 6-phospate/insulin like growth factor receptor (M6P/IGF2R), a putative breast tumor suppressor gene. *Breast Cancer Res Treat* 1998: 47: 268-281.
9) Yu Y, Xu F, Peng H, Fang X, Zhao S, Li Y, Cuevas B, Kuo WL, Gray JW, Siciliano M, Mills GB, Bast RC. NOEY2 (ARH1) an imprinted putative tumor suppressor gene in ovarian and breast carcinomas. *Proc Natl Acad Sci USA* 1999: 96: 214-219.
10) Kong FM, Anscher MS, Washington MK, Killina JK, Jirtle RL. M6P/IGR2R is mutated in squamous cell carcinoma of the lung. *Oncogene* 2000: 19: 1572-1578.
11) Luo RZ, Peng H, Xu F, Bao J, Pang Y, Pershad R, Issa JP, Liao WS, Bast RC, Yu Y. Genomic strucutre and promoter characterization of an imprinted tumor suppressor gene, ARH1. *Biochem Biophys Acta* 2001: 1519: 216-222.
12) Chappell SA, Walsh T, Walker RA, Shaw JA. Loss of heterozygosity at the mannose 6-phosphate insulin-like growth factor 2 receptor gene correlates with poor differentiation in early breast carcinomas. *Br J Cancer* 1997: 76: 1581-1561.
13) Oates AJ, Schumaker LM, Jenkins SB, Pearce AA, DaCosta SA, Arun B, Ellis MJ. The mannose 6-phospate/insulin like growth factor receptor (M6P/IGF2R), a putative breast tumor suppressor gene. *Breast Cancer Res Treat* 1998: 47: 268-281.
14) Bando K, Matsumoto S, Onda M, Akiyama F, Sakamaoto G, Yoshimoto M, Emi M, Jordan VC. Frequent allele loss at 6q26-27 in breast carcinomass of the solid-tubular histologic type. *Breast Cancer* 1998: 5: 127-130.
15) Hauptschein RS, Gamberi B, Rao PH, Frigeri F, Scotto L, Venkatraj VS, Gaidano G, Rutner T, Edwads YH, Chaganti RS. Dalla-Favera R. Cloning and mapping of human chromosome 6q26-q27 deleted in B-cell non-Hodgkin lymphoma and multiple tumor types. *Genomics* 1998: 50: 170-186.
16) Giasson BI. Lee VM. Parkin and the molecular pathways of Parkinson's disease. *Neuron* 2001: 31: 885-888.
17) Mizuno Y, Hattori N, Mori H, Suzuki T, Tanaka K. Parkin and parkinson's disease. *Curr Opin Neurol* 2001: 14: 477-482.
18) Kishismoto Y, Morisawa T, Kitano M, Shiota G, Horie Y, Suou T, Ito H, Kawasaki H, Hasegawa J. Loss of heterozygosity of the mannose 6-phosphate/insulin-like growth II receptor and p53 genes in human hepatocellular carcinoma. *Hepatol Res* 20012: 20: 68-83.
19) DaCosta SA, Schumaker LM, Ellis MJ. Mannose 6-phosphate/insulin-like growth factor 2 receptor, a bona fide tumor suppressor gene or just a promising candidate? *J Mammary Gland Biol Neoplasia* 2000: 5: 85-94.

ACCOMPLISHMENTS OF THE CORES

Administrative Core

Background. The premise of our entire program project grant is that ovarian cancer develops upon a background of significant genetic alterations and that we can combine several powerful strategies, based upon a rich tissue repository, to clone many of the genes involved in ovarian cancer development.

Objective. The overall purpose of the Administration Core is to support and oversee the work done by all three projects and the other three Cores. In addition, the Administration Core functioned to begin to coordinate all the efforts within the Ovarian Cancer Program of the Mayo Clinic Cancer Center.

Relevance to Ovarian Cancer. There is ample data that frequent genetic alterations underlie the development of epithelial ovarian cancer. This is the premise underlying our entire program project grant. The Administration Core integrates all our efforts to (1) determine which of the many genetic abnormalities are relevant and (2) identify the biologic function of the relevant alterations.

Support Provided to Research Projects by Administration Core. The Administration Core performs these functions:

1) Provides access to the tissue repository
2) Provides clinical and follow-up data for tissue specimens
3) Links tissue and clinical data via a relational database
4) Provides statistical support to all projects and cores
5) Oversees all projects and cores including budgets
6) Manage all human subject issues
7) Organize meetings of investigators and external advisors
8) Maintain a liaison with educational and outreach specialists within the Mayo Women's Cancer Program and the Mayo Clinic Cancer Center
9) Formalize a partnership with representatives of the advocacy community including the Minnesota Ovarian Cancer Alliance (MOCA).

In addition, the Administration Core was set up as if we were actually a Specialized Program of Research Excellence (SPORE) in Ovarian Cancer. Our rationale for this was that this would position us better to be competitive for SPORE funding from the National Cancer Institute. Thus, our Administration Core not only coordinated the efforts of the three projects and three Cores, but we utilized funds from the Mayo Clinic Cancer Center to support other people at Mayo to get them involved in working on ovarian cancer.

Tissue Acquisition Core

Tissue repository: The Ovarian Program has stored specimens of a variety of ovarian tumors since 1991. At the present time we have 1,516 ovarian specimens in a fresh, frozen state. This is consistent with our predicted accrual of 100–125 new ovarian tumor specimens annually. Over 85% of the patients with epithelial ovarian cancer who entered the study during the funding period have donated a blood specimen. Dr. Gary Keeney, a pathologist specializing in gynecologic malignancies, has performed tumor grade and morphology review on the majority of epithelial tumor specimens. The fresh tissues have been used to prepare RNA and DNA supporting the three projects in this program project grant, as well as several other IRB-approved studies. In addition, tissue microarrays have been constructed from paraffin-embedded tumor material maintained by the Mayo Clinic Tissue registry. These arrays have been used for a variety of immunohistochemical analyses in collaboration with the Mayo Clinic Tissue Acquisition Shared Resource. This Mayo Clinic Cancer Center facility recently purchased a new digital imaging system, the Bacus Laboratories Inc. Slide Scanner (BLISS, Lombard IL), and computer servers that allow more efficient visualization and analysis of stained microarrays. For example, the pathologist can enter staining results directly on the screen while observing a specific core on the computer monitor.

These data are downloaded directly into a spreadsheet suitable for use by the biostatisticians who correlate the data with clinical parameters. The servers connected to the imaging system will allow long-term archiving of the images for future review and publication.

Relational database: We have completed our transition from a SAS-based patient registry to a Mayo Intranet-based secure clinical database stored on an Ingres database server. All previously abstracted charts were downloaded directly into the new database and extensively audited to ensure data quality. New charts are now entered directly into the new database using a platform-independent data entry system written in Java. This application is made to be portable, allowing the authenticated user to enter data on virtually any computer from within Mayo Rochester. The new database uses entry forms that provide multiple benefits over the old system. For example, the categories of data are grouped more closely based on what would be found proximally in the patient medical record, allowing more efficient retrieval and entry of data. Data entry forms utilize pull-down menus whenever possible, thereby reducing the chances of typographical errors. In addition, "impossible" or absent values are immediately highlighted on the entry page, allowing efficient recognition of the error and timely resolution of the problem. 879 charts have been abstracted into this database, generally within 1-6 months of the time the patient has completed chemotherapy after their diagnostic surgery. The study coordinator performs regular and ad hoc reviews of the medical records of patients in post-treatment follow-up to determine changes in disease or treatment status, and updates the new database to reflect the new information and date of review.

In addition to the clinical database, a real-time patient registry database has been constructed that allows tracking of patients as they enter the system. For example, this registry is used to document whether the patients have completed their risk factor questionnaire while in the hospital, or if they have requested to complete it after their hospitalization by phone interview or by mail. It identifies the level of consent provided by each individual (i.e., permission to utilize their donated biological specimens at Mayo only, for ovarian cancer research only or also for other health problems). This system has provided an effective way to track the status of the patients and to prevent study coordinators from asking redundant questions. In addition, the suitability of a specific patient for any of the IRB-approved studies open at the time can be checked off at the time of patient entry. This simplifies the process of selecting sample sets. Finally, checking the registry before approaching patients allows the study coordinators to refrain from visiting those who have previously declined to participate in the ovarian cancer research opportunities at Mayo.

Individual users of these registries are authenticated only to the level of access that they require so that they can perform their job functions (i.e. data entry only vs. permission for data retrieval and viewing). Both the clinical database and the new patient registry are password-protected, secure systems that are backed up daily using established Mayo systems and procedures.

Molecular Cytogenetics Core

We were very fortunate to have Dr. Robert Jenkins directing our Molecular Cytogenetics Core Facility. Dr. Jenkins was responsible for originally starting the Ovarian Cancer Program with Dr. Hartmann in 1991. His group was responsible for much of the work on the characterization of many of the early-collected ovarian tumor specimens. As previously mentioned we did not request funding from the Department of Defense to support the Molecular Cytogenetics Core. Instead, this Core is supported by the Mayo Clinic Cancer Center. However, we still expected the Core to provide support for routine cytogenetic and molecular cytogenetic services to members of the Ovarian Cancer Program.

The Molecular Cytogenetics Core provided help and assistance to each of the Projects in this program project. Dr. Viji Shridhar had already performed transcriptional profiling of a number of early-stage and late-stage ovarian tumors and we were quite surprised that most of the aberrantly regulated genes in the late stage tumors were also aberrantly regulated in the early stage tumors. We therefore decided to perform comparative genomic hybridization of the ovarian tumors in the Cytogenetics Core. Dr. Jenkins was instrumental in providing help and assistance for this work, and as a result of this analysis we found that there was one key difference between early- and late-stage tumors. This was that gene amplification was much more frequently observed in the late stage tumors. This work became part of the seminal paper that we published on a comprehensive genetic analysis of ovarian cancer.

The Molecular Cytogenetics Core was also utilized by the second project where they began to utilize CGH to compare genetic and sporadic ovarian tumors. However, Dr. Couch quickly decided to switch to genomic CGH studies with Dr. Barbara Weber, hence he stopped utilizing our Cytogenetics Core.

The third project, by Dr. Smith's laboratory relied upon the Cytogenetics Core throughout the entire program project grant. Each of the common fragile site regions that were characterized (which includes the entire FRA6E region) were analyzed in the Cytogenetics Core using the outstanding equipment available there.

Biological Function Core

There are two main functions to the Biological Function Core. The first is to provide ovarian cancer cell lines and short term cultures of normal ovarian surface epithelium to members of the Ovarian Cancer Program. This is essential as we need a resource of normal cells to compare to the various cell lines and primary tumors, especially when we are assaying mRNA or protein levels. The second function is to provide support for research characterizing the functions of some of the consistently aberrantly regulated genes that we identify.

Hypothesis: The Functional studies are undertaken to determine whether the genetic alterations detected in ovarian cancer cells alter the proliferative rate, apoptotic threshold, and/or drug sensitivity of the tumor cells *in vitro* and *in vivo*.

Relevance to ovarian cancer: These activities are designed to (1) provide additional sample and models that can be used to study the biology of ovarian cancer versus normal ovarian surface epithelium; (2) to demonstrate how individual genetic alterations contribute to the cancer phenotype and (3) to potentially identify new gene products that can be investigated as possible therapeutic targets.

Core Facility Support Provided to Research Projects. The Biological Function Core provided normal ovarian surface epithelial cells and the ovarian cancer cell lines to all three Projects as well as many other members of the Ovarian Cancer Program. In addition, two of the Projects (Projects #1 and #3) relied very heavily on the Biological Function Core to assist in the biological characterization of interesting genes identified by Dr. Shridhar.

The initial studies in the Biological Function Core were on a gene identified by Dr. Shridhar which was a DNA-J homolog, MCJ. Subsequently each of the genes identified by Dr. Shridhar (and described in detail in her section) were also analyzed in collaboration with the Biological Function Core.

Dr. Smith also worked closely with this Core to begin to study the role of Parkin and its loss of expression on the development of ovarian cancer.

CONCLUSIONS

The members of the Ovarian Cancer Program of the Mayo Clinic Cancer Center are eternally grateful to the Department of Defense Ovarian Cancer Program for providing us with the resources to kick-start our program. Although the entire focus of this program project was on the genetic characterization of ovarian cancer, because of support provided by the Mayo Clinic Cancer Center, we were able to recruit many more people into working on this poorly understood disease of women. We feel that we have made significant contributions into understanding the genetics of ovarian cancer development, but we now also have researchers examining new therapeutic strategies for the treatment of this disease using measles virus (Dr. Kah-Whye Peng) and a group performing high resolution mass spectrometry analysis to identify markers for the early detection of this disease (Dr. David Muddiman).

The major scientific accomplishments of this Program Project Grant include the comprehensive analysis of early- versus late-stage ovarian cancers where we observed that most of the genes that are aberrantly regulated in late stage disease are similarly dysregulated in early-stage disease. The key difference observed was that gene amplification (and the corresponding greater genomic instability) is more frequently observed in late-stage disease. This is highly relevant to the studies on the common fragile sites, as they have been shown to mediate a number of key processes in developing cancer cells including gene amplification.

One of the problems with our collaboration with Millennium was that we were not free to share our expression profiling data with other investigators at other institutions. We therefore entered into a collaboration with several other funded ovarian cancer groups (including the Ovarian Cancer SPORE at M.D. Anderson and the early detection ovarian cancer program at Northwestern University) to develop a database of gene expression in ovarian cancer that could be freely shared with other investigators. We utilized the Affymetrix GeneChip Platform and performed all the analyses within the Microarray Core of the Mayo Clinic Cancer Center. This data is currently being analyzed by a number of different ovarian cancer groups as we had originally planned.

Dr. Viji Shridhar has done an outstanding job of fishing through the large number of genes that were consistently down-regulated in ovarian tumors. She has demonstrated that several of the genes that she is interested in do play an important role in key processes within the cell and that their loss of expression could be very important in ovarian cancer development and in the development of chemoresistance in ovarian tumors.

Dr. Couch has been less successful with his work to compare genetic to sporadic ovarian tumors due to a number of technical problems. In spite of this, he has identified several genes that are amplified in ovarian tumors and several of these may prove to be suitable targets for therapeutic intervention.

Dr. Smith and his group have found a number of important common fragile site genes that are consistently down-regulated during the development of ovarian cancer. The strategy of finding down-regulated genes derived from chromosomal bands known to contain common fragile sites has proven very successful and a number of interesting genes have now been shown to map to common fragile sites. This includes a number of putative tumor suppressors including IGF2R and tsg101. In addition, the identification of the large Parkin gene as a common fragile site gene that has frequent alterations in ovarian tumors demonstrates that many common fragile sites have extremely large genes contained within them. Dr. Smith's group has gone on to show that loss of Parkin does result in increased growth rates and greater resistance to apoptotic induction by certain apoptosis-inducing agents. Finally, his group has demonstrated that the cytokeratins are substrates of Parkin and that Parkin may play a role in the cytoskeleton in epithelial cells. As more information is obtained about the three large common

fragile site genes, FHIT, WWOX and Parkin, it is indeed becoming clear that the genes within the common fragile sites might indeed be functioning as some sort of stress response network within normal cells. We are therefore extremely thankful to the Department of Defense for their willingness to support Dr. Smith's Idea Grant to characterize Parkin in greater detail and to determine if Parkin is indeed part of a stress response network in normal cells.

We feel that we have been very successful in completing most of our stated goals when we first wrote this program project grant. In addition, to having a better understanding of the complex genetics involved in the development of ovarian cancer. Most importantly, we have really evolved into a full program mostly due to support from the Department of Defense. Our goal over the next few years is to really impact upon this disease by first developing markers for the early detection of ovarian cancer and then to develop better strategies for the treatment of this disease based upon knowledge obtained from understanding the biology of the development of ovarian cancer.

MS#1

[CANCER RESEARCH 61, 4258–4265, May 15, 2001]

Loss of Expression of a New Member of the DNAJ Protein Family Confers Resistance to Chemotherapeutic Agents Used in the Treatment of Ovarian Cancer[1]

Viji Shridhar,[2] Keith C. Bible, Julie Staub, Rajeswari Avula, Yean Kit Lee, Kimberly Kalli, Haojie Huang, Lynn C. Hartmann, Scott H. Kaufmann, and David I. Smith

Division of Experimental Pathology, Department of Laboratory Medicine and Pathology [V. S., J. S., R. A., H. H., D. I. S.], Division of Medical Oncology and Oncology Research [K. C. B., L. C. H.], Departments of Oncology [K. C. B., Y. K. L., S. H. K.] and Molecular Pharmacology [K. C. B., S. H. K.], and Endocrine Research Unit [K. K.], Mayo Clinic/Foundation, Rochester, Minnesota 55905

ABSTRACT

Differential display-PCR between ovarian tumor cell lines and short-term cultures of normal ovarian epithelial cell brushings was used to isolate a differentially expressed transcript and its corresponding gene. The gene, which mapped to 13q14.1, has partial homology in the DNAJ domain to a number of proteins with a similar domain and was designated as *methylation-controlled J protein* (*MCJ*). MCJ has the highest similarity to a functionally undefined protein from *Caenorhabditis elegans*. *MCJ* is expressed as a 1.2-kb transcript in several adult tissues, with testis showing the highest level of expression. Expression of *MCJ* was absent in three of seven ovarian cancer cell lines. Similarly, expression analysis using semiquantitative reverse transcription-PCR indicated that 12 of 18 primary ovarian tumors examined had either a complete absence or lower levels of expression of this gene. 5-Aza-2′-deoxycytidine treatment of the OV202 cell line induced *MCJ* expression in a dose-dependent manner, implicating methylation in this induction. Loss of heterozygosity and methylation-specific PCR analysis revealed that the loss of *MCJ* expression in primary tumors and cell lines was attributable to deletion of one allele and methylation of the other. To assess the potential functional significance of *MCJ* down-regulation, the sensitivity of parental (*MCJ*-nonexpressing) and MCJ-transfected OV167 cells to antineoplastic agents was evaluated. *MCJ* expression was associated with enhanced sensitivity to paclitaxel, topotecan, and cisplatin, suggesting that *MCJ* loss may play a role in *de novo* chemoresistance in ovarian carcinoma. These observations raise the possibility that *MCJ* loss may: (*a*) have potential prognostic significance in ovarian cancer; and (*b*) contribute to the malignant phenotype by conferring resistance to the most commonly used chemotherapeutic agents for ovarian cancer.

INTRODUCTION

The DNAJ proteins are a highly conserved family of proteins with the *Escherichia coli* heat shock protein, DNAJ (the human HSP40[3] orthologue), as its founding member (1). The defining feature of the HSP40 family is a highly conserved 70-amino acid residue, termed the DNAJ domain, that includes a signature tripeptide, HPD, that is critical for the function of the DNAJ domain (2). DNAJ proteins belonging to the HSP40 family contain four distinct domains including the DNAJ domain, whereas other proteins from this superfamily only possess the DNAJ domain (2). J-domains are present in diverse proteins and participate in complex biological processes. For example, HSP40 family J-domain proteins serve as cochaperones by recruiting HSP70 and accelerating ATP hydrolysis (3, 4). The DNAJ proteins participate in processes such as protein folding and translocation (5), cell cycle control by DNA tumor viruses (6–12), and regulation of protein kinases (13).

In this report, we describe the molecular cloning of a new member of the DNAJ domain protein family designated as MCJ. Collectively, our studies demonstrate that MCJ loss is common in human ovarian cancer, results from the deletion of one allele (LOH) and the silencing of the other by hypermethylation, and confers resistance to the three drugs most commonly used in the treatment of ovarian cancer. Here we show that stable transfectants expressing *MCJ* in OV167 are more sensitive to cisplatin, paclitaxel, and topotecan than parental and vector-transfected controls, implicating *MCJ* down-regulation in processes leading to decreased drug sensitivity.

MATERIALS AND METHODS

Cell Culture. Five of eight ovarian carcinoma cell lines (OV167, OV177, OV202, OV207, and OV266) were low-passage primary lines established at the Mayo Clinic (14), whereas OVCAR-5, SKOV-3, and the PC3 prostate cancer cell line were purchased from American Type Culture Collection (Manassas, VA). All cells were grown according to the provider's recommendations.

Assessment of Methylation Control. The OV202 cell line was treated with varying concentrations of 5-aza-2′-dC, ranging from 1 to 5 μM the day after plating. After a 48-h exposure to 5-aza-2′-dC, the cells were harvested in Trizol (Life Technologies, Inc., Rockville, MD) for RNA extraction.

mRNA Differential Display. DD-PCR was performed on the short-term cultures of normal OCEs and tumor cell lines as described by Liang and Pardee (15). Total RNA was extracted from the cell lines using Trizol and treated with RNase-free DNase I to eliminate genomic DNA contamination. Differential display of the expressed transcripts was performed using the RNA Image kit (GenHunter Corp., Nashville, TN) according to the manufacturer's instructions. Of the several bands identified that were differentially expressed, band 13 was absent in the tumor lane. This band was excised from the gel, reamplified with T11G and AP6 primers, and sequenced using dye terminator technology by the Molecular Biology Shared Resource of the Mayo Foundation.

Strategy for Cloning the Gene. BLAST search of the isolated sequence identified several homologous ESTs in the database EST. The homologous ESTs were assembled into a contig with the use of Sequencher 3 (Gene Codes Corp., Ann Arbor, MI) software. The integrity of the full-length cDNA obtained by this electronic walking was confirmed by PCR analysis using PCR primers flanking each junction between EST clones. The entire cDNA contig was sequenced twice with overlapping primers.

MS-PCR. The methylation state of *MCJ* was determined using the recently described technique of MS-PCR (17). DNA was modified with sodium bisulfite according to Herman *et al.* (17) with the following modifications. DNA (1–1.5 μg) was digested with *Eco*RI in a 50-μl reaction overnight. The digested DNA was extracted once with phenol:chloroform:isoamyl alcohol (25:24:1) and precipitated with 0.1 volume of 5 M ammonium acetate and

Received 11/28/00; accepted 3/16/01.

The costs of publication of this article were defrayed in part by the payment of page charges. This article must therefore be hereby marked *advertisement* in accordance with 18 U.S.C. Section 1734 solely to indicate this fact.

[1] Supported by NIH Grant CA48031, Department of Defense Grant DAMD17-98-1-8522 (both to D. I. S.), Department of Defense Grant DAMD17-99-1-9504 (to V. S., D. I. S., and S. H. K.), and by the Mayo Foundation.

[2] To whom requests for reprints should be addressed, at Mayo Clinic/Foundation, Division of Experimental Pathology, 200 First Street SW, Rochester, MN 55905. Phone: (507) 266-2775; Fax: (507) 266-5193; E-mail: shridhar.viji@mayo.edu.

[3] The abbreviations used are: HSP40, heat shock protein 40; DD-PCR, differential display-PCR; RT-PCR, reverse transcription-PCR; LOH, loss of heterozygosity; MS-PCR, methylation-specific PCR; RACE, rapid amplification of cDNA ends; 5-aza-2′-dC, 5-aza-2′-deoxycytidine; EST, expressed sequence tag; ORF, open reading frame; BAC, bacterial artificial chromosome; FISH, fluorescence *in situ* hybridization; GAPDH, glyceraldehyde-3-phosphate dehydrogenase; OCE, ovarian epithelial cell; FACS, fluorescence-activated cell sorting; MCJ, methylation-controlled J-protein.

100% ethanol in the presence of 1 μl of 20 mg/ml glycogen (Boehringer Mannheim, Indianapolis, IN). The DNA pellet was washed twice with 70% ethanol, and the DNA was taken up in 90 μl of 10 mM Tris (pH 7.5) containing 1 mM EDTA (TE buffer). Ten μl of freshly prepared 3 M NaOH were added to each sample, and the DNA was denatured at 42°C for 30 min. After the addition of 10 μl of distilled water, 1020 μl of 3.0 M sodium bisulfite (pH 5.0), and 60 μl of 10 mM hydroquinone, the samples were incubated in the dark at 55°C overnight (16–20 h). Modified DNA was purified using the Wizard purification system (Promega Corp., Madison, WI) according to the manufacturer's instructions, followed by denaturation with 0.3 M NaOH for 15 min at 37°C. The DNA was eluted in 50–100 μl of TE and stored at −20°C in the dark.

We sequenced portions of BAC 251N23 and obtained an additional 361 bp 5′ of the reported cDNA sequence (GenBank accession no. AF126473). Restriction site analysis of this additional sequence revealed the presence of a *Sma*I site 75 bases upstream of the reported cDNA sequence. A pair of primers, MCJ-WTF (5′-CGTGAGCCACCGCACCGGC-3′) at 108 bp upstream of the *Sma*I site and MCJ-WTR (5′-CTTTCCTGACCCCCTTCCG-3′) at 86 bp downstream of the *Sma*I site, were used to detect unmodified DNA. Nucleotide sequences of primers specific for methylation-mediated, modified DNA were MCJ-MF (5′-CGTGAGTTATCGTATTCGGT-3′) and MCJ-MR (5′-CTTTC-CTAACCCCCTTCCG-3′), which yielded a product of 195 bp. Primers used for the analysis of unmethylated sequences in the modified DNA were MCJ-UF (5′-GTTTTTAAAGTGTTGGGAT-3′) at 101 bp upstream of the *Sma*I site and MCJ-UR (5′-TAAACTTACCTAAACTTTCC-3′) at 100 bp downstream of the *Sma*I site, which yielded a product of 234 bp. The primers for amplifying unmethylated sequences were specifically chosen not to contain any CpG-rich sequences at the 3′ end of the primer. PCR was performed by the "hot-start" method (Taq gold; Perkin-Elmer) with an initial denaturation of 10 min, followed by 30 cycles of amplification at 56°C, annealing with primers amplifying methylated sequences and 50°C, and annealing for amplifying nonmethylated/modified DNA with UF/UR primers. Controls without DNA and positive controls with unmodified DNA were performed for each set of reactions.

5′ RACE. To obtain the missing 5′ end sequences, 5′ RACE was performed with poly(A)$^+$ RNA isolated from PC3 cells. Adaptor ligation and PCR were performed according to the instructions provided in the Marathon Ready cDNA amplification kit (Clontech, Palo Alto, CA). Primers used for 5′ RACE were 5′-GCAAGTACTCAGCGTAGCGC-3′ and MCJ-nested 5′-CCGTAGGGACAAACTAGTTACGC-3′.

Northern Blot Analysis. Fifteen μg of total RNA were fractionated on 1.2% formaldehyde agarose gels and blotted in 1× SPC buffer (20 mM Na_2HPO_4, 2 mM CDTA pH 6.8) onto Hybond-N membranes (Amersham, Piscataway, NJ). The probes were labeled using the random primer labeling system (Life Technologies, Inc.) and purified using spin columns (100 TE) from Clontech. Filters were hybridized at 68°C with radioactive probes in a microhybridization incubator (Model 2000; Robbins Scientific, Sunnyvale, CA) for 1–3 h in Express Hybridization solution (Clontech) and washed according to the manufacturer's guidelines.

Semiquantitative RT-PCR. Fifty-100 ng of reverse transcribed cDNA were used in a multiplex reaction with the forward MCJ-4 (5′-GCGC-TACGCTGAGTACTTGC-3′) and reverse primer MCJ-5 (5′-AGATAA-GACTGTGGTCAATC-3′) to yield a 595-bp product and *GAPDH* forward (5′-ACCACAGTCCATGCCATCAC-3′) and reverse (5′-TCCACCACCCT-GTTGCTTGTA-3′) primers to yield a 450-bp product. The PCR reaction mixes contained 50 mM KCl, 10 mM Tris-HCl (pH 8.3), 1.5 mM $MgCl_2$, 400 μM concentration of each primer for *MCJ* and 50 μM for the *GAPDH* primers, and 0.5 unit of Taq polymerase (Promega) in a 12.5-μl reaction volume. The conditions for amplification were 94°C for 3 min and then 29 cycles of 94°C for 30 s, 58°C for 30 s, and 72°C for 30 s in a Perkin-Elmer-Cetus 9600 Gene-Amp PCR system. The products of the reaction were resolved on a 1.6% agarose gel. Band intensities were quantified using the Gel Doc 1000 photo documentation system (Bio-Rad, Hercules, CA) and its associated software.

BAC Library Screening and FISH. MCJ primers (5′-AAGCTCCCT-GAGGGTCCGCGTTG-3′ with 5′-GGGTAACGTGTCCCGTGCAAG-3′ and 5′-GCGCTACGCTGAGTACTTGC-3′ with 5′-GCGTAGCGACCTGCA-AAT-3′) were used for the isolation of two BACs (420G23 and 251N23) by screening a BAC library from Research Genetics, Inc. (Huntsville, AL) according to the manufacturer's instructions. BAC DNA was extracted from an overnight 500-ml culture with TIP500 from Qiagen (Valencia, CA) according to the protocol provided by the manufacturer. The 251N23 BAC was labeled with biotin-16-dUTP using the Nick Translation kit (Boehringer Mannheim). FISH analysis was then performed with this labeled BAC clone. Primers used to determine the exon/intron junctions in the genomic BAC clone by direct sequencing of the BAC DNA are shown in Table 3.

LOH Analysis of Primary Ovarian Tumors. We used eight pairs of microsatellite markers on chromosome 13q obtained from Research Genetics in addition to the *MCJ*-associated microsatellite (MCJ3′NF, 5′-GATTGAC-CACAGTCTTATCT and MCJ18, 5′-TAAGAGGTCTACTCATTGCTCAC). The markers used in this study are listed in Table 1 along with their chromosomal locations. The PCR reaction mix contained 50 ng of genomic DNA, 50 mM KCl, 10 mM Tris-HCl (pH 8.3), 1.5 mM $MgCl_2$, a 200 μM concentration of each primer, 0.05 μl of [^{32}P]CTP (10 μCi/μl), and 0.5 unit of Taq polymerase (Promega) in a 10-μl reaction volume. The conditions for amplification were 94°C for 2 min and then 30 cycles of 94°C for 30 s, 52°C-57°C for 30 s, and 72°C for 30 s in a Perkin-Elmer-Cetus 9600 Gene-Amp PCR system in a 96-well plate. The PCR products were denatured and run on 6% polyacrylamide sequencing gels containing 8 M urea. The gels were dried and autoradiographed for 16–24 h and scored for LOH. Multiple exposures were used before scoring for LOH. Allelic imbalance indicative of LOH was scored when there was >50% loss of intensity of one allele in the tumor sample with respect to the matched allele from normal tissue. The evaluation of the intensity of the signal between the different alleles was determined by visual examination by two independent viewers (V. S. and J. S.).

Establishment of MCJ Stable Transfectants. On the basis of the cDNA sequence of MCJ, two primers were synthesized to amplify a 536-bp fragment of MCJ from base 367-903 containing the entire ORF. A *Hin*dIII site was introduced into the forward primer 5′-CCTGAAGCTTACTAGTTTGTC-CCT-3′ and a *Bam*HI site into the reverse primer 5′GCGGGATCCTTCCT-TCAGTGTG-3′ (restriction sites are underlined in the sequences). The PCR product was digested with both *Hin*dIII and *Bam*HI, gel purified, subcloned into the cloning sites of the mammalian expression vector pcDNA3.1(+) (Invitrogen, Carlsbad, CA), and transformed into *Escherichia coli* DH5α (Life Technologies, Inc.) cells. Mini-preparations of the ampicillin-resistant colonies were sequenced and verified. Exponentially growing cells of OV167 in 100-mm dishes were washed with serum-free medium and treated with a mixture of 5 μg of plasmid, 30 μl of LipofectAMINE, and 20 μl of Plus reagent. After a 3-h incubation, complete medium with serum was added. Beginning 24 h after the start of transfection, G418 was added to select the transfectants. Two stable clonal transfectants, MCJ 6 and MCJ 13, were subsequently generated. For controls, cells were similarly transfected with vector [pcDNA3.1(+) only] and selected.

Tissue Culture and Colony-forming Assays. Topotecan was kindly provided by the Pharmaceutical Resources Branch of the National Cancer Institute. Paclitaxel and cisplatin were purchased from Sigma Chemical Co. (St. Louis, MO). All other reagents were obtained as described previously (16, 18, 19). Stock (1000-fold concentrated) solutions of paclitaxel and topotecan were prepared in DMSO and stored at −20°C prior to use. Cisplatin was prepared immediately before use as a 1000-fold concentrated solution in DMSO.

OV167 cell lines were cultured in MEM with Earle's salts and nonessential amino acids containing 20% (v/v) heat-inactivated fetal bovine serum, 100 units/ml penicillin G, 100 μg/ml streptomycin, and 2 mM glutamine (medium A). Cells were passaged once weekly and maintained at 37°C in an atmosphere containing 95% air/5% CO_2 (v/v). To determine population doubling times, 1×10^5 cells were seeded in triplicate 100-mm tissue culture plates, incubated for intervals between 24 and 240 h, trypsinized, and counted on a hemacytometer. Colony-forming assays were performed as described previously (16).

Table 1 *Results of LOH analysis in primary ovarian tumors*

Marker	13q	% LOH (no. of cases with LOH/no. of informative cases)
898	14.1	0% (0/10)
325	14.1	35% (6/17)
263	14.1	48% (12/25)
MCJ	14.1	48% (10/21)
1272	14.2	8% (2/25)
887	14.2	25% (2/8)
328	14.3	35% (6/17)
168	14.3	44% (7/16)

In brief, subconfluent cells were released with trypsin, plated at a density of 4000 cells/plate in multiple 35-mm dishes containing 2 ml of medium A, and incubated for 14–16 h at 37°C to allow cells to attach. Graded concentrations of each drug or equivalent volumes of DMSO (0.1%) were then added to triplicate plates. After a 24-h treatment, plates were washed twice with serum-free MEM and incubated in drug-free medium A for an additional 14 days. The resulting colonies were stained with Coomassie Blue and counted manually. Diluent-treated control plates typically contained 75–200 colonies and served as a basis for estimates of colony-forming efficiency for the four lines.

Flow Cytometry. Flow cytometry for cell cycle analysis was performed as reported previously (18). Briefly, cells were grown to 30–40% confluence in 100-mm tissue culture dishes, released by trypsinization, and sedimented at 200 × *g* for 5 min. All additional steps were performed at 4°C unless otherwise indicated. Samples were fixed in 50% ethanol, treated with RNase A, stained with propidium iodide, and analyzed by flow cytometry on a Becton Dickinson FACScan (San Jose, CA) using an excitation wavelength of 488 nm and an emission wavelength of 585 nm as described (19). Histograms were analyzed using ModFit software (Verity Software House, Topsham, ME). Cellular accumulation of topotecan was assessed by FACS analysis as described previously (20). Briefly, cells grown to 50–60% confluence in 100-mm dishes were incubated for 1 h in the presence of 20 μM topotecan, trypsinized in the continued presence of topotecan, and examined by FACS using an excitation wavelength of 488 nm and an emission wavelength of 585 nm.

Assessment of Cell Viability. To directly assess cell viability, cells were grown to 30% confluence in 100-mm dishes, treated with 100 nM paclitaxel for 24 h, harvested at the indicated time points, and assessed for either their ability to exclude trypan blue or apoptotic morphology by staining with Hoescht 33258, as described previously (16, 18). Floating and adherent cells from each dish were combined prior to evaluation with trypan blue or Hoescht staining.

Statistics. Reliabilities of differences in sample means (statistical significances) were calculated using the *t* distribution (two-sided) and pooled estimates of sample variances.

RESULTS

Isolation and Characterization of a Novel cDNA Containing the DNAJ Domain. We performed DD-PCR with primers HT11G and AP6 from the RNA Image kit (GenHunter Corp.) against low-passage cell lines established from primary ovarian tumors and short-term cultures of normal OCEs. Several fragments were isolated. One fragment (13) was expressed exclusively in the normal cell line and absent in three of seven tumor cell lanes. This band was isolated from the gel by standard procedures, reamplified with the same set of primers, and sequenced. Comparative sequence analysis of this fragment using the BLAST alignment revealed that the 150-bp fragment showed considerable homology to several ESTs. Computer-based walking with the available ESTs (National Center for Biotechnology Information/BLAST) using Sequencher 3 software generated a contig of 720 bp of sequence.

```
MCJ:          LIAVGLGVAALAFAGRYAFR----IWKPLEQVITETAKKISTPSFSSYYKGGFEQKMSRR 95
              LI  GLG+AA+ F  RY  R    I K +E +       ++  +FS+YY+GGF+QKMSR
C. elegans:   LIVAGLGLAAVGFGARYVLRNQALIKKGMEAI------PVAGGAFSNYYRGGFDQKMSRA 58

MCJ:          EAGLILGVSPSAGKAKIRTAHRRVMILNHPDKGGSPYVAAKINEAKDLLETTKH 149
              EA  ILGV+PSA  AKI+ AH++VMI+NHPD+GGSPY+AAKINEAKDL+E++
C. elegans:   EAAKILGVAPSAKPAKIKEAHKKVMIVNHPDRGGSPYLAAKINEAKDLMESS 110
```

Fig. 2. GAP-BLASTP alignment of MCJ (residues 40–149) with a DNAJ-like protein from *C. elegans* (GenBank accession no. U80438; cDNA CEESD64F). *Double underline,* J-domain. *Underline,* predicted transmembrane domain. +, a conservative substitution.

Analysis of this sequence for the presence of an ORF with the National Center for Biotechnology Information ORF search revealed a protein with a predicted ORF of 150 amino acids (Fig. 1). A BLAST search of protein sequences (GAP-BLASTP; Ref. 21) revealed that this putative protein had the highest homology to a *C. elegans* DNAJ containing M_r 16,500 protein of unknown function (GenBank accession no. U80438 and cDNA CEESD64F), and this homology extended beyond the DNAJ domain. The alignment of the putative protein encoded by the isolated sequences and CEESD64F (Fig. 2) showed 56% (63 of 112) identity and 73% (83 of 112) overall similarity. These two proteins are similar in two respects. In contrast to the majority of DNAJ-containing proteins, both MCJ and CEESD64F contain their DNAJ domains in the COOH-terminal half of the protein. In addition, both have a potential membrane-spanning domain (between residues 36–58 in MCJ and residues 5–23 in CEESD64F) at the NH_2 terminus of each respective protein (Fig. 2).

Expression of MCJ in Ovarian Tumor Cell Lines and Normal Tissues. Primers MCJ1 (5′-TAACTAGTTTGTCCCTA-3′) and MCJ2 (5′-CAGTGTGGTCCTTAAGC-3′) were synthesized based on the 720-bp sequence flanking the ORF. RT-PCR was performed on short-term cultures of normal OCEs and epithelial cell brushings from patients without cancer (Fig. 3*A*) and seven ovarian tumor cell lines including OV167, OV177, OV202, OV207, OV266, OVCAR5, and SKOV3. With the exception of OV167, OV202, and OV266, all other cell lines amplified the expected 540-bp fragment (Fig. 3*B*). Northern blot analysis confirmed the results obtained with RT-PCR (Fig. 3*C*). The probe used for Northern analysis was the full-length ORF probe generated by RT-PCR in the normal cell line. Expression analysis with the multiple-tissue Northern blot revealed that MCJ is expressed as ~1.2-kb message in all tissues examined (data not shown). Testis showed the highest level of expression, whereas expression in other normal tissues, including adrenal gland, total brain, fetal brain, kidney, lung, pancreas, prostate, and uterus, was much lower.

```
                                                GGTCAGGAAAGCTCAGGCAAGCCCACCCTCAGGCATTACAGCTAGACTCCGAGCTTACTGGGCAGTCATCTGATTC  75
GACCAACATCAGTTCGCAGGGCTTAAGCCCAGTCCCTTACGGCGGCTGGGGAGGGACCAGGCCCAAGTATATAAAGCTCCCTGAGGGTCC 164
GCGTTGGCTTTGCGCCTGTGAGTGTGATTCAAGAACGTCCCAGTGCCCTTGGCTCCTTTCGGAGTGTGACCCCGTGCTTGCACGGGACAC 253
GTTACCCAGCTCGGGTGAGAAGGGTATCTTCCGGGAACCTCGCCTTTAATAGCACAACGAGCGCACGGCCCCCTGGATCTGCGAGAAGGA 342
TCTGCGAGAAGAAACCGCGCTAACTAGTTTGTCCCTACGGCCGCCTCGTAGTCACTGCCGCGGCGCCTTGAGTCTCCGGGCCGCCTTGCC 431
ATGGCTGCCCGTGGTGTCATCGCTCCAGTTGGCGAGAGTTTGCGCTACGCTGAGTACTTGCAGCCCTCGGCCAAACGGCCAGACGCCGAC 520
 M  A  A  R  G  V  I  A  P  V  G  E  S  L  R  Y  A  E  Y  L  Q  P  S  A  K  A  P  D  A  D  30
GTCGACCAGCAGGGACTGGTAAGAAGTTTGATAGCTGTAGGACTGGGTGTTGCAGCTCTTGCATTTGCAGGTCGCTACGCATTTCGGATC 609
 V  D  Q  Q  G  L  V  R  S  L  I  A  V  G  L  G  V  A  A  L  A  F  A  G  R  Y  A  F  R  I  60
TGGAAACCTCTAGAACAAGTTATCACAGAAACTGCAAAGAAGATTTCAACTCCTAGCTTTTCATCCTACTATAAAGGAGGATTTGAACAG 698
 W  K  P  L  E  Q  V  I  T  E  T  A  K  K  I  S  T  P  S  F  S  S  Y  Y  K  G  G  F  E  Q  90
AAAATGAGTAGGCGAGAAGCTGGTCTTATTTTAGGTGTAAGCCCATCTGCTGGCAAGGCTAAGATTAGAACAGCTCATAGGAGAGTCATG 787
 K  M  S  R  R  E  A  G  L  I  L  G  V  S  P  S  A  G  K  A  K  I  R  T  A  H  R  R  V  M 120
ATTTTGAATCACCCAGATAAAGGTGGATCTCCTTACGTAGCAGCCAAAATAAATGAAGCAAAAGACTTGCTAGAAACAACCACCAAACAT 876
 I  L  N  [redacted]  K  G  G  S  P  Y  V  A  A  K  I  N  E  A  K  D  L  L  E  T  T  T  K  H 150
TGATGCTTAAGGACCACACTGAAGGAAAAAAAAAAGAGGGGACTTCGAAAAAAAAAAAAAGCCCTGCAAAATATTCTAAAACATGGTCTTCT 965
 *
TAATTTTCTATATGGATTGACCACAGTCTTATCTTCCACCATTAAGCTGTATAACAATAAAATGTTAATAGTCTTGCTTTTTATTATCTT 1054
TTAAAGATCTCCTTAAATTCT 1076
```

Fig. 1. cDNA nucleotide sequence and the putative protein sequence of MCJ. *Highlighted,* transmembrane domain at the NH_2 terminus and DNAJ domain at the COOH terminus of the protein. *Boxed,* signature tripeptide (*HPD*). *Underlined,* polyadenylation signal. *Small arrowheads,* positions of the introns.

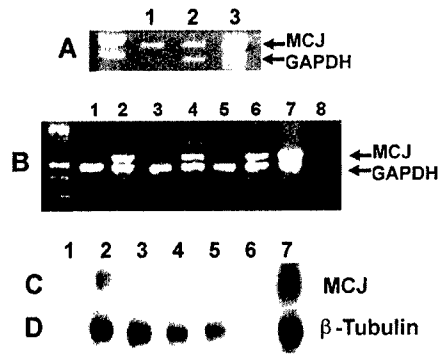

Fig. 3. *A*, agarose gel showing the products of the MCJ ORF region. *Lanes 1* and *2*, normal epithelial cell brushings from patients without cancer. *Lane 3*, short-term cultures of normal OCEs. *B*, agarose gel showing the products of the MCJ ORF region by semiquantitative RT-PCR in the ovarian cell lines. *Lane 1*, OV167; *Lane 2*, OV177; *Lane 3*, OV202; *Lane 4*, OV207; *Lane 5*, OV266; *Lane 6*, OVCAR5; *Lane 7*, SKOV3; *Lane 8*, water control. The *lane* to the *left* of *Lane 1* is a marker. *C*, autoradiograph showing the Northern hybridization results in the same cell lines (with MCJ ORF as probe) as in *A*. *Lane 1*, OV167; *Lane 2*, OV177; *Lane 3*, OV202; *Lane 4*, OV207; *Lane 5*, OV266; *Lane 6*, OVCAR5; *Lane 7*, SKOV3. *D*, tubulin hybridization of the corresponding samples.

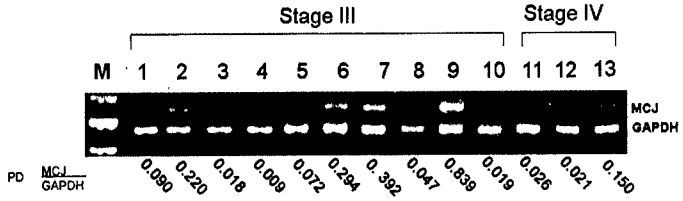

Fig. 4. Agarose gel showing the products of semiquantitative RT-PCR resolved on a 1.6% agarose gel. Sample numbers are indicated at the *top* of the figure, and the staging information for these tumors is indicated *above* the tumor numbers. *M*, 100-bp ladder. *Top band*, product of amplification with MCJ-4 and MCJ-5 primers. *Bottom band*, product of amplification with *GAPDH* primers F and R. Ratio of the band intensities of MCJ: GAPDH in pixel density are shown *below* each lane.

Cloning the Full-Length cDNA by 5′ RACE. The cDNA generated by EST-based walking was 720 bp in length. This cDNA contained a polyadenylation signal, AATAAA. However, the size of the transcript estimated by Northern analysis was 1.2 kb. To generate the missing 5′ end of this cDNA, 5′ RACE was performed with the Marathon Ready cDNA kit using RNA isolated from PC3 cells under conditions recommended by the manufacturer. We obtained an additional 354 bp of sequences with 5′ RACE. Reanalysis of the 5′ RACE sequences revealed that the ORF generated from the original 740-bp sequence was not changed (GenBank accession no. AF126743). In addition, the putative initiation codon occurs within a strong Kozak context (22) and is preceded by a stop codon (Fig. 1).

Expression Analysis of MCJ in Primary Ovarian Tumors. To determine whether MCJ was expressed in primary ovarian serous adenocarcinomas, we analyzed the expression of MCJ in 18 stage III and 3 stage IV serous ovarian carcinomas by a semiquantitative RT-PCR analysis using MCJ primers MCJ-4 (5′-GCGCTACGCTGAGTACTTGC-3′) and MCJ-5 (5′-AGATAAGACTGTGGTCAATC-3′; expected product size of 595 bp). GAPDH primers served as controls. We found that there was complete loss of MCJ expression in 5 of 15 stage III tumors and in 2 of 3 stage IV tumors. Also, 4 of 15 stage III and 1 of 3 stage IV tumors showed lower levels of MCJ expression (representative examples are shown in Fig. 4). Taken together, two-thirds (12 of 18) of the primary ovarian tumors showed either loss or diminished levels of expression by semiquantitative RT-PCR analysis.

LOH Analysis MCJ in Primary Ovarian Tumors. Sequencing a portion of the 420G23 BAC revealed a dinucleotide repeat consisting of 14 CA repeats ~80 bases downstream of the 3′ end of MCJ. We made primers (MCJ3′NF and MCJ18) flanking this repeat and found that this sequence was polymorphic in humans. We then performed LOH analysis with this new microsatellite in the primary ovarian tumor samples that showed lower levels or absence of expression of MCJ. In the tumors tested, this marker was 75% informative. None of the benign tumors but 48% of the high-stage tumors showed loss of this marker (Fig. 5).

To further delineate the region of loss, we analyzed seven other markers (*D13S263, D13S325, D13S898, D13S1272, D13S887, D13S328,* and *D13S168*) for LOH in these tumors (see Table 1 for band location and LOH data). According to the LDB database (Genetic Location database at Southampton, United Kingdom), markers *D13S1272* and *D13S887* map to 13q14.2, whereas *D13S328* and *D13S168* are in 13q14.3. The closest marker to the MCJ marker is *D13S263* (in 13q14.1), which is 100-kb distal to MCJ (23). The next highest frequency of loss was seen with the markers *D13S328* and *D13S168* in 13q14.3, which are in close proximity to the *esterase D* locus. These two markers are 10 cM away from *D13S263*.

Transcriptional Induction in the OV202 Cell Line by 5-aza-2′-dC Treatment. Because there was an absence of expression of *MCJ* mRNA in the OV202 cell line by both RT-PCR and Northern analysis, we were interested in whether methylation of this gene resulted in absence of its expression in this cell line. Therefore, we treated the OV202 cell line with the methyltransferase inhibitor 2′-deoxy-5-azacytidine to determine its effect on the transcription of the *MCJ* gene. After 2-day exposure to concentrations of 5-aza-2′-dC ranging from 1 to 5 μM, RNA was extracted from control and subjected to RT-PCR to assess *MCJ* mRNA expression. There was a dose-dependent increase in the expression of this message after treatment with 5-aza-2′-dC (Fig. 6), which is an inhibitor of DNA methyltransferases (24, 25). Because the reexpression of this message seems to be linked to the methylation status of this gene or to some other regulatory gene controlling the expression of this gene, we named this gene *MCJ*.

MS-PCR of MCJ in Cell Lines and Primary Tumors. On the basis of the results obtained with 5-aza-2′-dC, we tested cell lines lacking MCJ expression for CpG island methylation using MS-PCR (17). To distinguish unmodified from modified DNA, primers that encompassed regions containing multiple cytosines were chosen. In addition, restriction site analysis revealed the presence of rare restriction sites, such as *Sac*II and *Eag*I, in these regions. Thus, CpG pairs

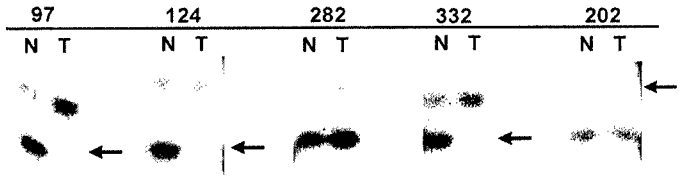

Fig. 5. Autoradiograph of LOH results of selected tumor samples with the MCJ-associated marker. For each panel, the tumor number is shown *above* the rule. *N*, normal DNA; *T*, tumor DNA. *Arrow*, loss of allele in the tumor.

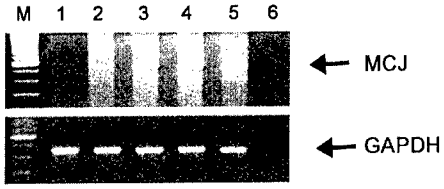

Fig. 6. Agarose gel electrophoresis of RT-PCR amplification product of *GAPDH* and *MCJ* ORF region in OV202 cell line after 5-aza-2′-dC treatment. *Lane 1*, control untreated OV202; *Lanes 2–5*, 0.1, 0.5, 1.0, and 5.0 μM 5-aza-2′-dC, respectively; *Lane 6*, water control.

near the 3′ end of the primers could provide maximum discrimination between methylated *versus* unmethylated sequences. Primers (wild-type, methyl-specific, and primers that would amplify unmethylated sequences) were synthesized flanking these restriction sites at nucleotide position 331 and at nucleotide position 484 of the MCJ cDNA sequence to amplify a 154-bp product. PCR amplification of bisulfite-modified DNA with these methyl-specific primers yielded a product both in matched normal (WBC) and tumor DNA. Sequencing of these products revealed no differences in the methylation status of either the *Sac*II, *Eag*I, or other CpG sites within this sequence between the normal and tumor samples. This indicated clearly to us that the methylation site specific for lower levels of expression was probably present 5′ to this sequence.

To check for other potential CpG sites, we sequenced the BAC 251N23 and obtained an additional 361 bp of sequences. Restriction site analysis of this additional sequence revealed the presence of a *Sma*I site 75 bases upstream of the reported cDNA sequence. Primers were designed to amplify the methylated and unmethylated sequences at this position, as described in "Materials and Methods." Using this set of primers, we amplified methylation-specific products both in normal and tumor DNA (data not shown). However, sequencing these products with the reverse primer revealed that the *Sma*I site showed the presence of both methylated unconverted Cs as well as Ts (Gs and As, respectively, in the sequence Fig. 7, *A* and *D*) in all of the normal blood DNA samples. In tumor samples expressing MCJ (tumors 183 and 270), only the unmethylated fully converted Ts (A in the opposite strand) are seen. Panels *B* and *C* in Fig. 7 show the sequence of the MS-PCR product amplified with methyl-specific primers in the blood and tumor DNA, respectively, of patient 183. In tumor samples with complete loss of MCJ expression (tumors 202, 220, 332, 485, 97, and 107), only the nonconverted methylated Cs (G as seen in Fig. 7*E*) were visible at the *Sma*I site. The sequence of the MS-PCR product amplified with methyl-specific primers in the blood and tumor DNA, respectively, of patient 485 is shown in Fig. 7, *D* and *E*. In addition, in tumor samples with complete loss of MCJ expression, we saw the loss of the other allele by LOH (Fig. 7*E, inset,* for tumor 485). Table 2 lists the results of the RT-PCR expression analysis, along with the MSP-PCR results and LOH status, in 18 high-stage tumors with and without the loss of expression of MCJ. In tumors 202, 220, 332, 485, and 107 (which have all lost MCJ expression), there is a loss of one allele (LOH analysis) and loss of expression of the other allele, attributable to methylation in the same tumor. In tumors with lower levels of expression (tumors 121, 124, 323, and 282) or normal MCJ expression (tumors 183, 417, and 531), we did not see LOH of the *MCJ* allele (Fig. 7*C, inset*). This marker, however, was uninformative in some of the samples. In tumors 183 and 270, the presence of a clear RT-PCR product also corresponded with the presence of only unmethylated alleles at this site (Fig. 7*C*). In samples with lower levels of expression and no LOH, the presence of both methylated and unmethylated alleles was seen at this site (Table 2).

Genomic Organization and FISH Mapping of MCJ. We isolated two different BACs by screening the Research Genetics BAC pools. Sequencing of these two BACs with cDNA-specific primers revealed that the coding region of *MCJ* is interrupted by introns. We assembled the exonic sequences to the sequence of the BAC 335G18 that was available on the HTGS database. *MCJ* spans ~83 kb of genomic DNA and is interrupted by five introns. The primers spanning the intron/exon sequences are listed in Table 3. The 3′ end BAC 421G23 was used to map *MCJ* to chromosome 13q14.1 by FISH analysis (data not shown). This mapping reconfirmed the EST-based mapping of one of the ESTs (AA812596) used to build the cDNA contig.

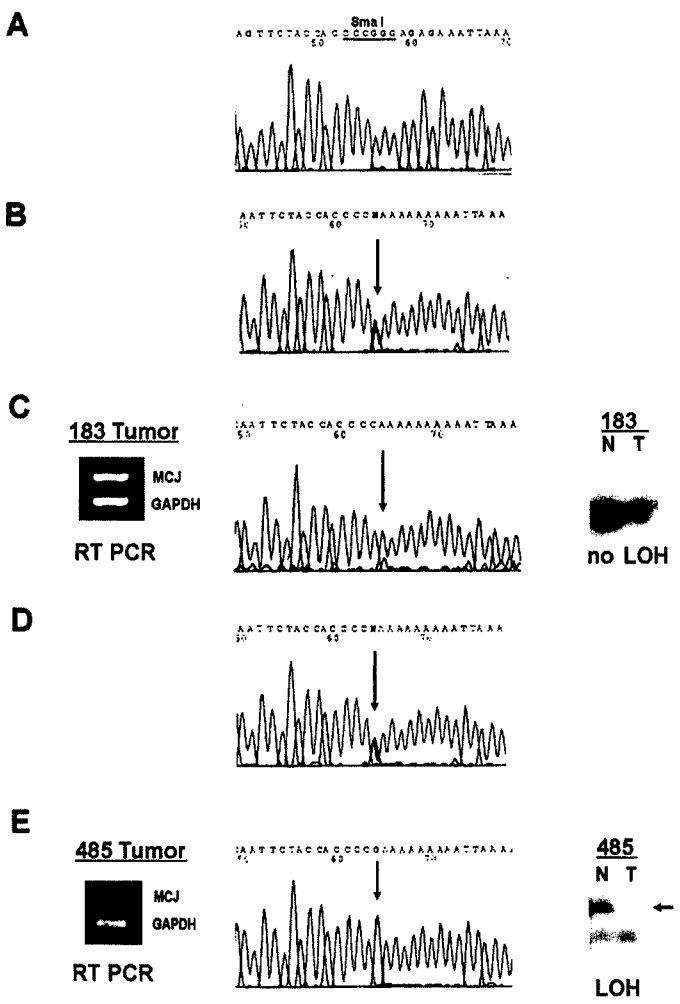

Fig. 7. *A*, 5′ end sequence of MCJ. *Underlined, Sma*I site. *B–E,* sequence of the MS-PCR product amplified with methylation-specific primers (*B* and *D*, in the blood of patient 183 and 485, respectively). *Arrow,* presence of both methylated and unmethylated alleles at the *Sma*I site. *C*, tumor of patient 183. *Arrow,* presence of only unmethylated alleles at the *Sma*I site. *Left inset,* result of semiquantitative RT-PCR of *MCJ* and *GAPDH*. Notice the expression of *MCJ* in the tumor. *Right inset,* result of LOH analysis of this marker in this tumor. *E,* tumor of patient of 485. *Arrow,* presence of only the methylated allele at the *Sma*I site. *Left inset,* result of semiquantitative RT-PCR of *MCJ* and *GAPDH*. Notice the absence of expression of *MCJ* in the tumor. *Right inset,* result of the LOH analysis of this marker in this tumor. Notice that there is LOH of this marker in this tumor. Because the products of the MS-PCR were sequenced with the reverse primer only, the observed Gs and As correspond to Cs and Ts in the opposite strand.

Mutational Analysis of MCJ in Primary Tumors. Primers (Table 3) were synthesized from intronic sequences flanking individual exons. Individual exons were amplified from matching blood and tumor DNA from several patients and sequenced directly to check for mutations within the coding sequences. Whereas several sequence polymorphisms were seen, no tumor-specific mutations were detected in any of the exons.

Functional Analysis of MCJ in OV167. A parental MCJ-nonexpressing primary ovarian carcinoma cell line (OV167), vector transfected control, and two stable MCJ clones (6 and 13) were tested for the expression of MCJ by semiquantitative RT-PCR. Only the two MCJ transfectants expressed the MCJ transcript (Fig. 8*A*). Examination of the four OV167 lines demonstrated no consistent differences between MCJ-high (clones 6 and 13) and MCJ-nonexpressing (OV167 and empty vector transfectant) lines with respect to doubling time (*i.e.,* proliferation rate). In particular, doubling times for the parental OV167 and the vector control were 5.0 and 3.0 days, respectively, whereas doubling times for the two MCJ transfectants (clones

Table 2 *Results of RT-PCR, LOH, and MSP analysis in high-stage tumors*

Sample	Stage	RT-PCR	LOH	MSP *Sma*I site
98	III	+[a]	−	NT[b]
183	III	+	−	UNM
209	III	+	UI	NT
270	III	+	UI	UNM
417	III	+	−	M/UNM
531	III	+	−	NT
121	III	L	−	M/UNM
124	III	L	+[c]	NT
285	III	L	UI	M/UNM
305	III	L	UI	M/UNM
323	III	L	UI	M
282	IV	L	−	M/UNM
202	III	−	+	M
220	III	−	+	M
332	III	−	+	M
485	III	−	+	M
97	IV	−	+	M
107	IV	−	+	M

[a] NT, not tested; L, lower levels of expression; UI, uninformative; M, methylated *Sma*I site; UNM, unmethylated *Sma*I site; M/UNM, presence of both methylated and unmethylated allele at the *Sma*I site.
[b] +, the presence of a product in RT-PCR.
[c] +, LOH.

6 and 13) were 3.0 ± 1.0 and 3.5 ± 0.5 days, respectively (not significant). Colony-forming efficiencies were also similar in the MCJ-nonexpressing (OV167, 5.33 ± 1.1%; vector control, 2.95 ± 0.83%) and MCJ-high (clone 6, 0.95 ± 0.62%; clone 13, 2.55 ± 0.84%) lines (not significant), although transfection tended to somewhat reduce colony-forming ability of the parental line.

Despite the above similarities, the four lines displayed clear differences in their sensitivities to paclitaxel, topotecan, and cisplatin, as assessed by colony-forming assays. The two MCJ-nonexpressing lines displayed IC_{50}s that were 3.5-fold higher for paclitaxel ($P < 0.005$; Fig. 8*B*), 2.2-fold higher for topotecan ($P < 0.0005$; Fig. 8*C*), and 2-fold higher for cisplatin ($P < 0.005$; data not shown) than the IC_{50}s of the MCJ-expressing lines (clones 6 and 13).

To confirm that the observed differences in colony formation were reflective of differences in cell killing, we also examined the sensitivities of the lines to paclitaxel by directly assessing cell death (using trypan blue staining) and apoptosis (using Hoescht 33258 staining). Trypan blue staining confirmed that the two MCJ-expressing clones were more sensitive to paclitaxel-induced cytotoxicity (data not shown). Hoescht staining showed that the MCJ-expressing lines were similarly more sensitive to paclitaxel-induced apoptosis (Fig. 8*D*).

Although the MCJ-high and MCJ-nonexpressing lines did not vary significantly with respect to doubling time, we had some concern that the observed resistance of the MCJ-deficient lines to the cell cycle-dependent agents paclitaxel and topotecan might be attributable to differences in cell cycle distributions. To evaluate this possibility, we examined cell cycle distribution in all four lines. As shown in Fig. 8*E*, the cell cycle distributions of the four lines were similar and could not, therefore, explain the observed differences in drug sensitivity.

In an effort to determine whether differential drug accumulation

Table 3 *Intron/exon primer sequences*

Lowercase letters are intronic sequences, and uppercase letters represent exon sequences. Splice donor and acceptor sites, in lowercase letters, are underlined. The polyadenylation (AATAAA) sequence in 3′ untranslated region is underlined.

Intron	Exon #	Exon Size	Intron	Size (bp)
	1	531	GCAGAGACTG<u>gt</u>gatccctgcca	41963
ttttcttcca<u>ag</u>GTAAGAAGTT	2	54	GCATTTGCAG<u>gt</u>aagataaagaat	3189
cttttactatt<u>ag</u>GTCGCTACGC	3	72	TCAACTCCAT<u>gt</u>aagttaaacgtgg	9609
ctttcctata<u>ag</u>AGCTTTTCATC	4	77	TAGGTGTAAG<u>gt</u>aggtgtgcaataa	7078
atttctttta<u>ag</u>CCCATCTGCTG	5	73	CCAGATAAAG<u>gt</u>aggtagaattcct	21336
tttgttctctcc<u>ag</u>GTGGATCTCCTT	6	267	TAAC<u>AATAAA</u>ATGTTAATA	
			GTCTTGCTTTTTATTATCTTT	
			TAAAGATCTCCTTAAATTCT+polyA	

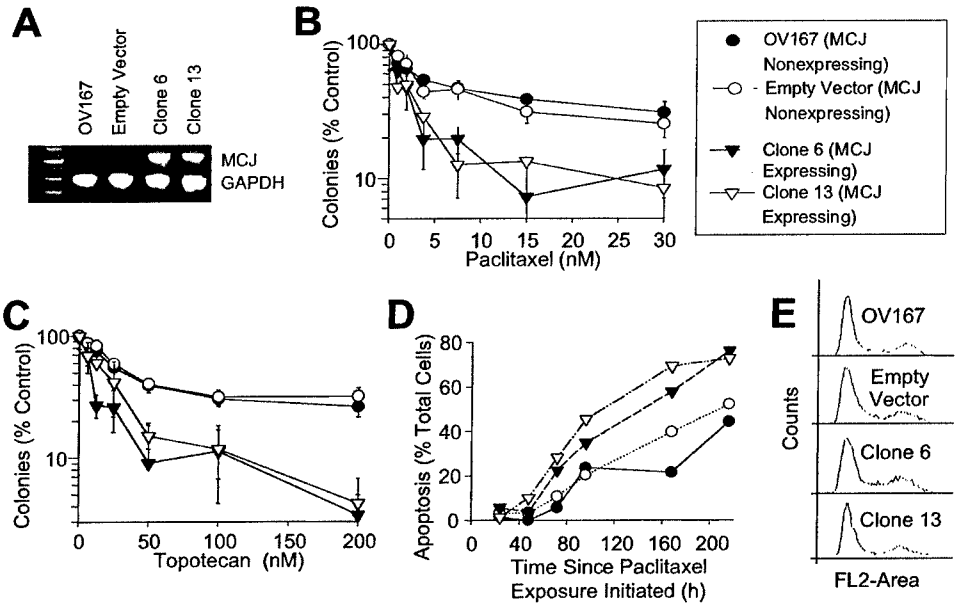

Fig. 8. Effects of paclitaxel and topotecan in MCJ-nonexpressing and MCJ high-expressing ovarian cell lines. *A*, agarose gel electrophoresis of RT-PCR amplification product of GAPDH and MCJ. The *lane* to the *left* of *Lane 1* is the marker. *Lane 1*, parental OV167; *Lane 2*, vector transfected OV167; *Lanes 3* and *4*, stable MCJ clones 6 and 13. *B* and *C*, effects of paclitaxel (*B*) or topotecan (*C*) on colony formation in OV167 cell lines. Cells were exposed to the indicated drug for 24 h, followed by incubation in drug-free medium for 12–14 days to allow colonies to form. Each *data point* represents the mean colony count from triplicate plates. *B* and *C*, $P < 0.005$ and $P < 0.0005$, respectively, as indicated in the text. The results are each representative of four independent experiments; *bars*, ±1 SD. *D*, effects of paclitaxel on induction of apoptosis in OV167 cell lines. Cells were exposed to paclitaxel for 24 h and incubated in drug-free medium. After combining floating and adherent cells from each plate, apoptosis was assessed by Hoescht 33258 staining. Data shown are representative of duplicate experiments. *E*, cell cycle distributions of subconfluent OV167 cell lines. Cells were grown to 30% confluence, harvested, fixed, stained with propidium iodide, and examined using FACS as described in the text.

might be responsible for the observed differences in drug sensitivities of MCJ-high and MCJ-low lines, we also examined topotecan accumulation in the four lines by FACS analysis (20). These studies showed no significant difference between the lines (data not shown), eliminating the possibility that differential drug accumulation was responsible for the observed differences in drug sensitivities.

DISCUSSION

In the United States, ovarian cancer is the fourth most common cause of cancer-related deaths among women. Approximately 23,000 women are diagnosed with and ~14,000 women die from ovarian cancer annually in the United States (26). Although women with low-stage ovarian cancer have a good prognosis, most women are diagnosed with late-stage disease and eventually succumb to their cancer (27). Much progress, therefore, remains to be made in the early diagnosis and treatment of ovarian cancer. A major concern in treating ovarian cancer patients is the frequent development of resistance to chemotherapy. Whereas most patients initially respond to the commonly used chemotherapeutic drugs, resistance to these drugs usually develops, and the patients eventually succumb to the disease. Many mechanisms have been postulated to explain this resistance (28–33), but these remain to be tested in clinical materials. Accordingly, there is considerable interest in identifying genes that could differentiate between chemosensitive and chemoresistant ovarian tumors.

Similar to cancers of other tissues, multiple genetic alterations are common in ovarian carcinomas. Alterations in tumor suppressor genes such as *p53* (34), *pRB* (35), and *NOEY2* (36) have been implicated in ovarian carcinogenesis. Chromosomal regions of loss have frequently identified new tumor suppressor genes involved in either the initiation, progression, or metastasis of cancer-related genes. In the present study, we report the discovery of a novel gene (*MCJ*) that we identified using DD-PCR between ovarian tumor cell lines and short-term cultures of normal OSEs. Expression of this gene was either absent or reduced in a majority of primary ovarian tumors and ovarian carcinoma cell lines. In specimens lacking *MCJ* expression, one allele was lost and the other silenced by methylation. Interestingly, a comparison of the *MCJ*-expressing and *MCJ*-nonexpressing low-passage primary ovarian carcinoma cell lines implicates *MCJ* loss in conferring resistance to the three drugs most commonly used in the treatment of ovarian cancer. These findings have potentially important implications for ovarian cancer development and treatment.

After *MCJ* was identified by DD-PCR, analysis of the ORF revealed that *MCJ* is a new member of the DNAJ family of proteins with sequence identity between MCJ and other DNAJ domain-containing proteins ranging from 30 to 50%. The major difference between MCJ and most other DNAJ-like proteins is the location of the DNAJ domain. Expression analysis of MCJ on a multiple-tissue Northern blot showed that this gene was highly expressed in testis. In this respect, it is similar to the *Drosophila melanogaster* DNAJ protein, DNAJ60 (37). Iliopoulos *et al.* (37) have shown that DNAJ60 encodes a putative protein of 217 amino acids with a molecular mass of 27.7 kDa and a pI of 10.5 that may play an important function during spermatogenesis and/or in the male genital tract. Whereas we have no evidence at present about a testis-specific function of MCJ, it is interesting to note that both MCJ and DNAJ60 are extremely basic proteins with similar pIs of 10.35. Another member of the DNAJ family of proteins with testis-specific expression is MSJ-1 (38). However, sequence analysis of MCJ revealed that it had no significant homology to MSJ-1.

We have shown that the absence of expression of *MCJ* is related directly to the methylation status of this gene. In the OV202 cell line, induction of *MCJ* is observed after 5-aza-2′-dC treatment. This is the first report linking methylation to the absence of expression of a DNAJ-like protein. The cell lines with loss of expression of *MCJ* were all cell lines derived from primary tumors harvested at the time of surgery, and therefore, the methylation pattern seen in these cell lines is a *de novo* effect and not the result of following exposure to chemotherapeutic agents *in vivo*. LOH analysis on 13q14.1 identifies this as a new region of LOH in ovarian cancer in the region of *MCJ*. We have shown LOH of the marker identified only 80 bases downstream of the 3′ end of the *MCJ* gene and that there is loss of an *MCJ* allele in some of the tumors not expressing *MCJ*. Whereas we have not found any tumor-specific mutations in the *MCJ* coding region, we have seen loss of expression of this gene both by LOH and hypermethylation in the same tumor. Although there are no reports of a DNAJ domain protein acting as a tumor suppressor, our data clearly indicate the mechanism for loss of function of this gene is probably attributable to loss of DNA sequences by deletion (LOH) and to hypermethylation. In this regard, this gene fits the criteria as a class II tumor suppressor.

To examine the effects of differences in *MCJ* expression, we evaluated the cytotoxic effects of cisplatin, paclitaxel, and topotecan in cells lacking or expressing *MCJ*. Cisplatin/carboplatin and Taxol are the most effective drugs in the treatment of ovarian cancer, and the combination of carboplatin/paclitaxel has been widely accepted as standard treatment for advanced ovarian cancer (28). Several lines of evidence support the idea that there is a direct correlation between the induction of apoptosis and drug sensitivity. For example, inactivation of the *p53* gene could confer resistance to cisplatin and DNA-damaging agents as measured by both the induction of apoptosis and resulting antiproliferative effects (33, 34). It is clear from several studies that there may be multiple mechanisms involved in determining drug resistance (30, 31). Our preliminary studies suggest that loss of *MCJ* in ovarian carcinoma may be of potential functional significance. In particular, *MCJ* loss appears to be associated with *de novo* resistance to the antineoplastic agents paclitaxel, topotecan, and cisplatin in the OV167 cell line. On the other hand, it is important to note that the magnitude of resistance (2–3.5-fold) conferred by *MCJ* loss is less than resistance conferred by some other means. For example, overexpression of P-glycoprotein can confer a much greater level of resistance to paclitaxel (16, 39). On the other hand, the 2–3.5-fold resistance to these agents might be significant in the clinical setting, particularly when combined with other resistance-inducing changes. We speculate, therefore, that MCJ loss may have potential prognostic significance in ovarian cancer. The impact of MCJ loss within the context of the full spectrum of genetic alterations in ovarian cancer, however, remains to be more fully elucidated. It would be very informative to look at sequential tumor specimens derived from patients undergoing multiple surgeries to try to correlate the *in vitro* and *in vivo* chemoresistance characteristics.

ACKNOWLEDGMENTS

We thank Gwen Callahan for providing ovarian samples for analysis.

REFERENCES

1. Pellecchia, M., Szyperski, T., Wall, D., Georgopoulos, C., and Wuthrich, K. NMR structure of the J-domain and the Gly/Phe-rich region of the *Escherichia coli* DnaJ chaperone. J. Mol. Biol., *260:* 236–250, 1996.
2. Kelley, W. L. The J-domain family and the recruitment of chaperone power. Trends Biochem. Sci., *23:* 222–227, 1998.
3. Greene, M. K., Maskos, K., and Landry, S. J. Role of the J-domain in the cooperation of Hsp40 with Hsp70. Proc. Natl. Acad. Sci. USA, *95:* 6108–6113, 1998.
4. Suh, W. C., Burkholder, W. F., Lu, C. Z., Zhao, X., Gottesman, M. E., and Gross, C. A. Interaction of the Hsp70 molecular chaperone, DnaK, with its cochaperone DnaJ. Proc. Natl. Acad. Sci. USA, *95:* 15223–15228, 1998.

5. Hendrick, J. P., Langer, T., Davis, T. A., Hartl, F. U., and Wiedmann, M. Control of folding and membrane translocation by binding of the chaperone DnaJ to nascent polypeptides. Proc. Natl. Acad. Sci. USA, *90:* 10216–10220, 1993.
6. Wall, D., Zylicz, M., and Georgopoulos, C. The conserved G/F motif of the DnaJ chaperone is necessary for the activation of the substrate binding properties of the DnaK chaperone. J. Biol. Chem., *269:* 5446–5451, 1994.
7. Sheng, Q., Denis, D., Ratnofsky, M., Roberts, T. M., DeCaprio, J. A., and Schaffhausen, B. The DnaJ domain of polyomavirus large T antigen is required to regulate Rb family tumor suppressor function. J. Virol., *71:* 9410–9416, 1997.
8. Campbell, K. S., Mullane, K. P., Aksoy, I. A., Stubdal, H., Zalvide, J., Pipas, J. M., Silver, P. A., Roberts, T. M., Schaffhausen, B. S., and DeCaprio, J. A. DnaJ/hsp40 chaperone domain of SV40 large T antigen promotes efficient viral DNA replication. Genes Dev., *11:* 1098–1110, 1997.
9. Zalvide, J., Stubdal, H., and DeCaprio, J. A. The J domain of simian virus 40 large T antigen is required to functionally inactivate RB family proteins. Mol. Cell. Biol., *3:* 1408–1415, 1998.
10. Pipas, J. M. Molecular chaperone function of the SV40 large T antigen. Dev. Biol., *94:* 313–319, 1998.
11. Schilling, B., De-Medina, T., Syken, J., Vidal, M., and Munger, K. A novel human DnaJ protein, hTid-1, a homolog of the Drosophila tumor suppressor protein Tid56, can interact with the human papillomavirus type 16 E7 oncoprotein. Virology, *247:* 74–85, 1998.
12. Yaglom, J. A., Goldberg, A. L., Finley, D., and Sherman, M. Y. The molecular chaperone Ydj1 is required for the p34CDC28-dependent phosphorylation of the cyclin Cln3 that signals its degradation. Mol. Cell. Biol., *16:* 3679–3684, 1996.
13. Caplan, A. J., Langley, E., Wilson, E. M., and Vidal, J. Hormone-dependent transactivation by the human androgen receptor is regulated by a DnaJ protein. J. Biol. Chem., *270:* 5251–5257, 1995.
14. Conover, C. A., Hartmann, L. C., Bradley, S., Stalboerger, P., Klee, G. G., Kalli, K. R., and Jenkins, R. B. Biological characterization of human epithelial ovarian carcinoma cells in primary culture: the insulin-like growth factor system. Exp. Cell Res., *238:* 439–449, 1998.
15. Liang, P., and Pardee, A. B. Differential display of eukaryotic messenger RNA by means of the polymerase chain reaction. Science (Wash. DC), *257:* 967–971, 1992.
16 Bible, K. C., Boerner, S. A., Kirkland, K., Anderl, K. L., Bartelt, D., Jr., Svingen, P. A., Kottke, T. J., Lee, Y. K., Eckdahl, S., Stalboerger, P. G., Jenkins, R. B., and Kaufmann, S. H. Characterization of an ovarian carcinoma cell line resistant to cisplatin and flavopiridol. Clin. Cancer Res., *6:* 661–670, 2000.
17 Herman, J. G., Graff, J. R., Myohanen, S., Nelkin, B. D., and Baylin, S. B. Methylation-specific PCR: a novel PCR assay for methylation status of CpG islands. Proc. Natl. Acad. Sci. USA, *93:* 9821–9826, 1993.
18 Bible, K. C., and Kaufmann, S. H. Flavopiridol (NSC 649890, L86–8275): a cytotoxic flavone that induces death in noncycling A549 human lung carcinoma cells. Cancer Res., *56:* 4856–4861, 1996.
19 Bible, K. C., and Kaufmann, S. H. Cytotoxic synergy between flavopiridol (NSC 649890, L86–8275) and various antineoplastic agents: the importance of sequence of administration. Cancer Res., *57:* 3375–3380, 1997.
20. Hendricks, C. B., Rowinsky, E. K., Grochow, L. B., Donehower, R. C., and Kaufmann, S. H. Effect of P-glycoprotein expression on the accumulation and cytotoxicity of topotecan (SK&F 104864), a new camptothecin analogue. Cancer Res., *52:* 2268–2278, 1992.
21. Atschul, S. F., Madden, T. L., Schaffer, A. A., Zhang, J., Zhang, Z., Miller, W., and Lipman, D. J. Gapped BLAST and PSI-BLAST: a new generation of protein database search programs. Nucleic Acids Res., *25:* 3389–3402, 1997.
22. Kozak, M. An analysis of 5′-noncoding sequences from 699 vertebrate messenger RNAs. Nucleic Acids Res., *15:* 8125–8148, 1987.
23. Deloukas, P., Schuler, G. D., Gyapaym, G., Beasley, E. M., Soderlund, C., Rodriguez-Tome, P., Hui, L., Matise, T. C., McKusick, K. B., Beckmann, J. S., Bentolila, S., Bihoreau, M., Birren, B. B., Browne, J., Butler, A., Castle, A. B., Chiannilkulchai, N., Clee, C., Day, P. J., Dehejia, A., Dibling, T., Drouot, N., Duprat, S., Fizames, C., Bentley, D. R., *et al.* A physical map of 30,000 human genes. Science (Wash. DC), *282:* 744–746, 1998.
24. Saitoh, F., Hiraishi, K., Adachi, M., and Hozumi, M. Induction by 5-aza-2′-deoxycytidine, an inhibitor of DNA methylation, of Le(y) antigen, apoptosis, and differentiation in human lung cancer cells. Anticancer Res., *15:* 2137–2143, 1995.
25. Persengiev, S. P., and Kilpatrick, D. L. The DNA methyltransferase inhibitor 5-azacytidine specifically alters the expression of helix-loop-helix proteins Id1, Id2, and Id3 during neuronal differentiation. Neuroreport, *8:* 2091–2095, 1997.
26. Landis, S. H., Murray, T., Bolden, S., and Wingo, P. I. Cancer Statistics 1999. CA Cancer J. Clin., *49:* 8–31, 1999.
27. Micahel, F. L. Prognostic factors in ovarian cancer. Semin. Oncol., *25:* 305–311, 1998.
28. Neijt, J. P., Engelholm, S. A., Tuxen, M. K., Sorensen, P. G., Hansen, M., Sessa, C., de Swart, C. A., Hirsch, F. R., Lund, B., and van Houwelingen, H. C. Exploratory Phase III study of paclitaxel and cisplatin *versus* paclitaxel and carboplatin in advanced ovarian cancer. J Clin. Oncol., *18:* 3084–3092, 2000.
29. Godwin, A. K., Meister, A., O'Dwyer, P. J., Huang, C. S., Hamilton, T. C., and Anderson, M. E. High resistance to cisplatin in human ovarian cancer cell lines is associated with marked increase of glutathione synthesis. Proc. Natl. Acad. Sci. USA, *89:* 3070–3074, 1992.
30. Schroder, C. P., Godwin, A. K., O'Dwyer, P. J., Tew, K. D., Hamilton, T. C., and Ozols, R. F. Glutathione and drug resistance. Cancer Investig., *14:* 158–168, 1996.
31. Andrews, P. A., and Howell, S. B. Cellular pharmacology of cisplatin: perspectives on mechanisms of acquired resistance. Cancer Cells (Cold Spring Harbor), *2:* 35–43, 1990.
32. Ohie, S., Udagawa, Y., Kozu, A., Komuro, Y., Aoki, D., Nozawa, S., Moossa, A. R., and Hoffman, R. M. Cisplatin sensitivity of ovarian cancer in the histoculture drug response assay correlates to clinical response to combination chemotherapy with cisplatin, doxorubicin, and cyclophosphamide. Anticancer Res., *20:* 2049–2054, 2000.
33. Holford, J., Beale, P. J., Boxall, F. E., Sharp, S. Y., and Kelland, L. R. Mechanisms of drug resistance to the platinum complex ZD0473 in ovarian cancer cell lines. Eur. J. Cancer, *36:* 1984–1990, 2000.
34. Murphy, M., McManus, D. T., Toner, P. G., and Russell, S. E. TP53 mutation in ovarian carcinoma. Eur. J. Cancer, *33:* 1281–1283, 1997.
35. Liu, Y., Heyman, M., Wang, Y., Falkmer, U., Hising, C., Szekely, L., and Einhorn, S. Molecular analysis of the retinoblastoma gene in primary ovarian cancer cells. Int. J. Cancer, *58:* 663–667, 1994.
36. Yu, Y., Xu, F., Peng, H., Fang, X., Zhao, S., Li, Y., Cuevas, B., Kuo, W. L., Gray, J. W., Siciliano, M., Mills, G. B., and Bast, R. C., Jr. NOEY2 (ARHI), an imprinted putative tumor suppressor gene in ovarian and breast carcinomas. Proc. Natl. Acad. Sci. USA, *96:* 214–219, 1999.
37. Iliopoulos, I., Torok, I., and Mechler, B. M. The *DnaJ60* gene of *Drosophila melanogaster* encodes a new member of the DnaJ family of proteins. Biol. Chem., *378:* 1177–1178, 1997.
38. Berruti, G., Perego, L., Borgonovo, B., and Martegani, E. MSJ-1, a new member of the DNAJ family of proteins, is a male germ cell specific gene product. Exp. Cell Res., *2392:* 430–441, 1998.
39. Ford, J. M., Yang, J. M., and Hait, W. N. P-Glycoprotein-mediated multidrug resistance: experimental and clinical strategies for its reversal. Cancer Treat. Res., *87:* 3–38, 1996.

MS#2

[CANCER RESEARCH 61, 5895–5904, August 1, 2001]

Genetic Analysis of Early- *versus* Late-Stage Ovarian Tumors[1]

Viji Shridhar, John Lee, Ajay Pandita, Steve Iturria, Rajeswari Avula, Julie Staub, Mike Morrissey, Eric Calhoun, Ami Sen, Kimberly Kalli, Gary Keeney, Patrick Roche, William Cliby, Karen Lu, Rosemarie Schmandt, Gordon B. Mills, Robert C. Bast, Jr., C. David James, Fergus J. Couch, Lynn C. Hartmann, Jim Lillie, and David I. Smith[2]

Departments of Experimental Pathology, Division of Laboratory Medicine [V. S., A. P., R. A., J. S., E. C., P. R., C. D. J., F. J. C., D. I. S.], Health Sciences Research, Division of Biostatistics [S. I.], Molecular Pharmacology and Endocrine Research [K. K.], Gynecologic Surgery, Division of Anatomic Pathology [G. K.], and Oncology, Section of Gynecologic Surgery [W. C., L. C. H.], The Mayo Clinic, Rochester, Minnesota 55905; Millennium Predictive Medicine, Cambridge, Massachusetts [J. Le., M. M., A. S., J. Li.]; and Departments of Gynaecologic Oncology [K. L., R. S.], Molecular Therapeutics [G. B. M.], and Experimental Therapeutics [R. C. B.], University of Texas M. D. Anderson Cancer Center, Houston, Texas, 77030

ABSTRACT

In the United States, ovarian cancer is the fourth most common cause of cancer-related deaths among women. The most important prognostic factor for this cancer is tumor stage, or extent of disease at diagnosis. Although women with low-stage tumors have a relatively good prognosis, most women diagnosed with late-stage disease eventually succumb to their cancer. In an attempt to understand early events in ovarian carcinogenesis, and to explore steps in its progression, we have applied multiple molecular genetic techniques to the analysis of 21 early-stage (stage I/II) and 17 advanced-stage (stage III/IV) ovarian tumors. These techniques included expression profiling with cDNA microarrays containing approximately 18,000 expressed sequences, and comparative genomic hybridization to address the chromosomal locations of copy number gains as well as losses. Results from the analysis indicate that early-stage ovarian cancers exhibit profound alterations in gene expression, many of which are similar to those identified in late-stage tumors. However, differences observed at the genomic level suggest differences between the early- and late-stage tumors and provide support for a progression model for ovarian cancer development.

INTRODUCTION

Of the cancers unique to women, ovarian cancer has the highest mortality rate. Over 26,000 women are diagnosed with this disease in the United States annually, and 60% of those diagnosed will die of the disease (1). There has been little change in ovarian cancer incidence and mortality over the past 5 decades and unfortunately there are a number of significant barriers to progress in its treatment. These include poor understanding of the underlying biology of this disease, inadequate screening tools as well as few early warning signs. The 5-year survival for patients with stage I disease can exceed 90%, but it is less than 25% for advanced-stage disease (2). These statistics underscore the need for better tools for the screening and staging of ovarian cancer.

Like other solid tumors, ovarian cancer is thought to result from an accumulation of genetic alterations. These events lead to changes in expression of many genes. Alterations in tumor suppressor genes such as *p53* (3, 4), *pRB* (3, 5), *NOEY2* (6), *BRCA1* (7), and oncogenes such as *K-ras* (8), *c-myc* (9) and *c-erbB-2* (10) have been shown to play an important role in ovarian carcinogenesis. There is very little information, however, on the sequence of genetic changes that are associated with progression of disease from early to advanced stage.

Examining tumors for alterations in gene expression is a potentially useful approach to identifying molecular differences between early- and late-stage ovarian carcinomas. Although there are several approaches to investigate differential gene expression in tumors, here we have used cDNA microarrays to develop expression profiles of early- and late-stage ovarian cancer (11–13). To extend our understanding of any stepwise genetic alterations that may underlie the assumed clinical progression from early- to late-stage ovarian cancer, CGH[3] (14) was used to identify regions of genome loss and gain in the same series of tumors.

MATERIALS AND METHODS

Tissue Processing and Tumor Selection. Surgically removed ovarian tumors were snap-frozen in the surgical pathology unit of the Mayo Clinic. The tumor content of the specimens was assessed by H&E-stained sections. Only high-grade specimens containing more than 75% tumor were used for these experiments. Twenty normal OSEs from patients without cancer were used as normal controls. The epithelial nature of these brushings was verified by cytokeratin staining. The majority of these patients were between 45 and 65 years old, undergoing incidental oophorectomy at the time of pelvic surgery for other indications. All of the ovaries were examined pathologically and found to be benign or they were excluded. RNA from five such pooled brushings were profiled on cDNA microarrays along with five stage I, two stage II, and seven stage III ovarian tumors. The histology, grade, and stage of each tumor used in cDNA microarray, semiquantitative RT-PCR, and CGH studies are listed in Tables 1 and 5, respectively. Tumors were staged according to International Federation of Gynecology and Obstetrics criteria.

Ovarian Cell Lines. Five of seven ovarian-carcinoma cell lines (OV 167, OV 177, OV 202, OV 207, and OV 266) were low-passage primary lines established at the Mayo Clinic (15). OVCAR-5 is a NIH cell line (16) and SKOV-3 was purchased from American Type Culture Collection (Manassas, VA). All of the cells were grown according to the provider's recommendations.

cDNA Microarrays. The cDNA microarray consisted of 25,000 elements from the Unigene set from Research Genetics Inc. (Huntsville, AL), which included 10,000 known genes; 13,000 ESTs; and 2,000 elements made up of control genes, dyes, bacterial genes, and water controls. After consolidating genes or ESTs belonging to the same Unigene clusters, we estimated that there were a total of 18,304 unique genes or ESTs. All of the genes and ESTs on the array were sequence verified before being arrayed on a high-precision robotics platform. Each 3- × 5-inch membrane contained up to 6,000 elements and each probe was hybridized to five sets of membranes in duplicate.

Total RNA Isolation and Labeling. Total RNA was extracted from specific tumor samples using Trizol (Life Technologies, Inc., Rockville, MD) as recommended by the manufacturer after estimating the tumor content by standard histological methods. The integrity of the RNA was assessed by ethidium bromide staining after agarose gel electrophoresis. Total RNA was labeled with [α-^{33}P]CTP after reverse transcription with oligo(dT)$_{30}$. Fifteen μg of total RNA was annealed to 3 μg of oligo-dT$_{30}$ primer in 13 μl of total volume and incubated at 70°C for 2 min in a PCR machine and held at 4°C.

Received 2/12/01; accepted 5/24/01.

The costs of publication of this article were defrayed in part by the payment of page charges. This article must therefore be hereby marked *advertisement* in accordance with 18 U.S.C. Section 1734 solely to indicate this fact.

[1] Supported by NIH Grant CA48031 (to D. I. S.) and Department of Defense Grant DAMD 17-99-1-9504 (to D. I. S. and V. S.), and by the Mayo Foundation.

[2] To whom requests for reprints should be addressed, at Division of Experimental Pathology, Mayo Clinic/Foundation, 200 First Street, SW, Rochester, MN 55905. Phone: (507) 266-0309; Fax: (507) 266-5193; E-mail: smith.david@mayo.edu.

[3] The abbreviations used are: CGH, comparative genomic hybridization; OSE, ovarian epithelial cell brushing; EST, expressed sequence tag; RT-PCR, reverse transcription-PCR; GAPDH, glyceraldehyde-3-phosphate dehydrogenase.

Table 1 *Tumor cohort*

Histology	Stage	Grade	cDNA microarray	RT-PCR
Cl cell OV 106	I	3	+[b]	+
Cl cell OV 267	I	3		+
Cl cell OV 496	I	3	+	+
Endo OV 51	I	3		+
Endo OV 78	I	3		+
Endo OV 88	I	3		+
Endo OV 105	I	3		+
Endo OV 338	I	3		+
Endo OV 647	I	3	+	+
Serous OV 6	I	3		+
Serous OV 17	I	3	+	+
Serous OV 20	I	3		+
Serous OV 90	I	3		+
Serous OV 234	I	3		+
Serous OV 363	I	3		+
Serous OV 526	I	3	+	+
Cl cell OV 102	II	3		+
Endo OV 296	II	3		+
Serous OV 149	II	3		+
Serous OV 354	II	3		+
Serous OV 401	II	3	+	+
Serous OV 402	II	3	+	+
Serous OV 414	II	3		+
Cl cell OV 176	III	3		+
Endo OV 93	III	3		+
Endo OV 110	III	3		+
Endo OV 259	III	3		+
Serous OV 4	III	3	+	+
Serous OV 11	III	3	+	+
Serous OV 13	III	3	+	+
Serous OV 16	III	3	+	+
Serous OV 29	III	3	+	+
Serous OV 150	III	3	+	+
Serous OV 167	III	3		+
Serous OV 206	III	3		+
Serous OV 208	III	3		+
Serous OV 461	III	3		+
Serous OV 472	III	3	+	+
Serous OV 97	IV	3		+

[a] Cl, clear; OV, ovarian; Endo, endometrioid.
[b] +, the tumors used in each analysis.

Reverse transcription of this annealed template was carried out in a final volume of 50 μl, 1× first strand buffer (DTT, 40 units of Rnase inhibitor, 400 units of Superscript II reverse transcriptase, 2 μl of 10 mM dNTP mix with dCTP at 0.1 mM concentration, 100 μCi of [α-^{33}P] dCTP at 42°C for 60 min. The reaction was stopped by consecutive addition of the following reagents: 4 μl of 50 mM EDTA, 4 μl of 0.5 M NaOH, and 2 μl of diethylpyrocarbonate water. Heating at 65°C for 10 min degrades the RNA template in the reaction. Unincorporated nucleotides were removed from the labeled probe using a Clontech (Palo Alto, CA) Chroma Spin TE-30 spin column. The labeled probe with an estimated specific activity of 1×10^6 cpm/μl was preannealed to 100 mg of COT1 DNA to block repetitive sequences in a final volume of 100 μl. The blocked probe was heated for 5 min at 95°C followed by 65°C for 20 min and then added to the duplicate filters along with 5 μg/ml of denatured salmon sperm DNA. The filters were hybridized overnight at 65°C in a Hybaid hybridization oven. Each probe was hybridized to duplicate filters. The next day, the filters were washed for 15 min at 65°C with 4% SDS solution in 20 mM sodium phosphate (pH 7.2) with 1 mM EDTA followed by 1% SDS solution in the same buffer with three changes at 65°C. After the wash, the filters were dried between whatman papers and baked at 80°C for 1 h. The filters were imaged on a storm 840 phosphoimager after 24–48 h exposure.

Image Analysis and Data Recovery. The ArrayVision program (Imaging Research Inc., St. Catharines, ON, Canada) was used to quantify the spot intensities of the scanned images for each membrane. For each membrane, the spot intensities were normalized by the median intensity for the entire array, resulting in a new median intensity of 1.0. Spots that were <0.1 after normalization were thresholded to 0.1 to account for the level of background noise. After normalization and thresholding, spot intensities were averaged across the duplicate filters for each tissue sample. Fold-regulation for each tumor, at each gene, was determined by calculating the ratio of tumor expression:average expression for the five (pooled) control normal OSEs.

Semiquantitative RT-PCR. Reverse transcribed cDNAs (50–100 ng) were used in a multiplex reaction with gene-specific primers and GAPDH, forward primer (5′-ACCACAGTCCATGCCATCAC-3′) and reverse primer (5′-TCCACCACCCTGTTGCTTGTA-3′) yielding a 450-bp product. The PCR reaction mixtures consist of 50 mM Tris-HCl (pH 8.3), 1.5 mM $MgCl_2$, 400 μM concentration of each primer for the specific gene to be analyzed (50 μM for the GAPDH primers), and 0.5 units of Taq polymerase (Promega, Madison, WI), in a 12.5-μl reaction volume. The conditions for amplification were as follows: 94°C for 3 min, then 29 cycles of 94°C for 30 s, 50–62°C for

Table 2 *Differential gene expression in ovarian tumors: number of sequences with expression changes >2-fold, 5-fold, 10-fold, and 20-fold*

No. of tumors	Down-regulated				Up-regulated			
	2-fold	5-fold	10-fold	20-fold	2-fold	5-fold	10-fold	20-fold
14	148	24	9	2	11	1	0	0
13	262	48	16	6	30	6	1	0
12	409	56	19	6	43	9	2	1
11	565	68	21	7	67	11	5	1
10	719	87	24	8	108	12	5	1
9	945	108	27	11	168	15	6	1
8	1261	135	34	12	265	25	8	1
7	1750	179	46	12	435	36	12	3
6	2346	248	56	18	794	51	18	5
5	3115	409	115	42	1417	72	27	7
4	4159	565	144	52	2510	116	32	12
3	5718	781	187	65	4303	198	51	25
2	8245	1159	279	81	7051	388	105	42
1	12106	2940	1044	414	11178	1552	480	183

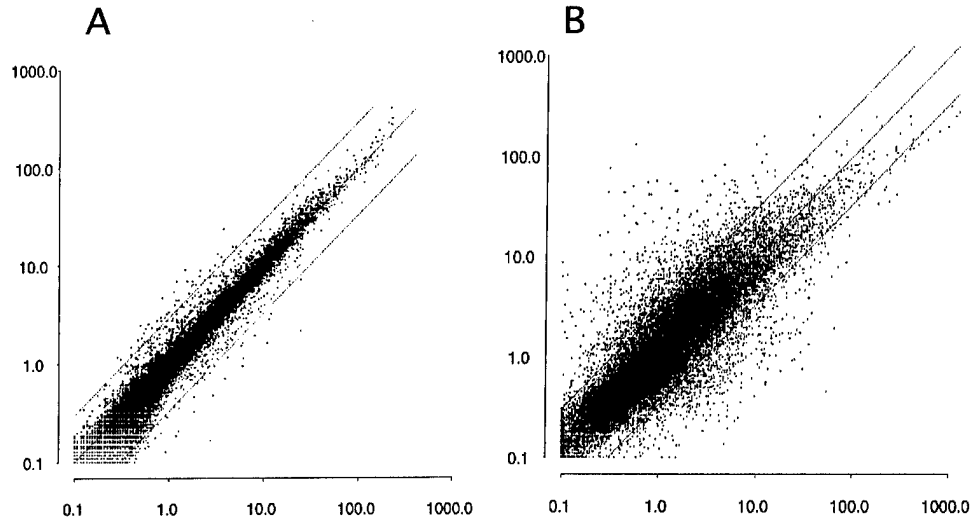

Fig. 1. Representative scatter plots of cDNA microarray analysis. *A*, duplicate filters of OV 106 hybridization (Pearson correlation, 0.97). *B*, scatter plot of an early-stage tumor (OV106) *versus* one of the pooled normal epithelial brushings (Pearson correlation coefficient, 0.76). The *lines*, 2-fold differences in expression levels between samples.

Table 3 *Differential gene expression as a function of tumor stage*

	Stage I/II down				Stage III/IV down				Stage I/II up				Stage III/IV up			
No. of tumors	2-fold	5-fold	10-fold	20-fold	2-fold	5-fold	10-fold	20-fold	2-fold	5-fold	10-fold	20-fold	2-fold	5-fold	10-fold	20-fold
7	200	35	11	2	406	56	18	6	19	2	0	0	48	10	3	0
6	413	62	19	6	739	91	22	9	64	8	2	1	99	12	4	1
5	759	86	26	8	1393	154	36	11	185	19	7	1	239	16	5	1
4	1322	152	38	13	2360	321	99	42	498	39	15	3	714	27	8	2
3	2500	275	65	16	3365	508	127	47	1311	92	36	9	1615	65	17	8

30 s depending on the gene-specific primers being tested, and 72°C for 30 s in a Perkin-Elmer-Cetus (Norwalk, CT) 9600 Gene-Amp PCR system. The products of the reactions were resolved on a 1.6% agarose gel. Band intensities were quantified using the Gel Doc 1000 photo-documentation system (Bio-Rad, Hercules, CA) and its associated software. Gene specific primers were as follows: for *Gas 1*, forward, CGC GCC TCG TCT CCT TTC CC, and reverse, GGC GCG TGG GCT AAA AGA GC; for *PAI1*, forward AAT CGC AAG GCA CCT CTG AG, and reverse, GAT CTG GTT TAC CAT CTT TT; for *StAR*, forward, GAC CCC ACC ACT GCC ACA TT, and reverse, GAT CTT AGA CTT GCA GGC TT; for *AREG*, forward, CCG CTG CGA AGG ACC AAT GA, reverse, CTA TGA CTT GGC AGT CAG TC; for *FGF7*, forward, TAA TGC ACA AAT GGA TAC, and reverse, ATT GCC ATA GGA AGA AAG; for *HPR6*, forward, TGC CTA GCG CGG CCC AAC, and reverse, CAG ACT GGA CTG TTA CAA ATG; for *ITM2A*, forward, CGC AGC CCG AAG ATT CAC TAT G, and reverse, R-CTT ATT ACC AAG GAC ACT CTA TCT; and for *decorin*, forward, CCT GGT TGT GAA AAT ACA TGA, and reverse, TGA CAT TAA CAA GAT TTT GCC.

CGH. Metaphase spreads from normal human lymphocytes were prepared using standard protocols (17). The slides were aged for 2–3 days prior to denaturation at 70°C by 70% formamide in 2× SSC, followed by dehydration in a series of ethanol-water mixtures. The slides were treated with proteinase K, at a concentration of 0.1 μg/ml in 20 mM Tris (pH 7.5)-2 mM $CaCl_2$, prior to hybridization. The CGH procedure was similar to published standard protocols (14, 17). Twenty images were captured using a Nikon Labophot-2

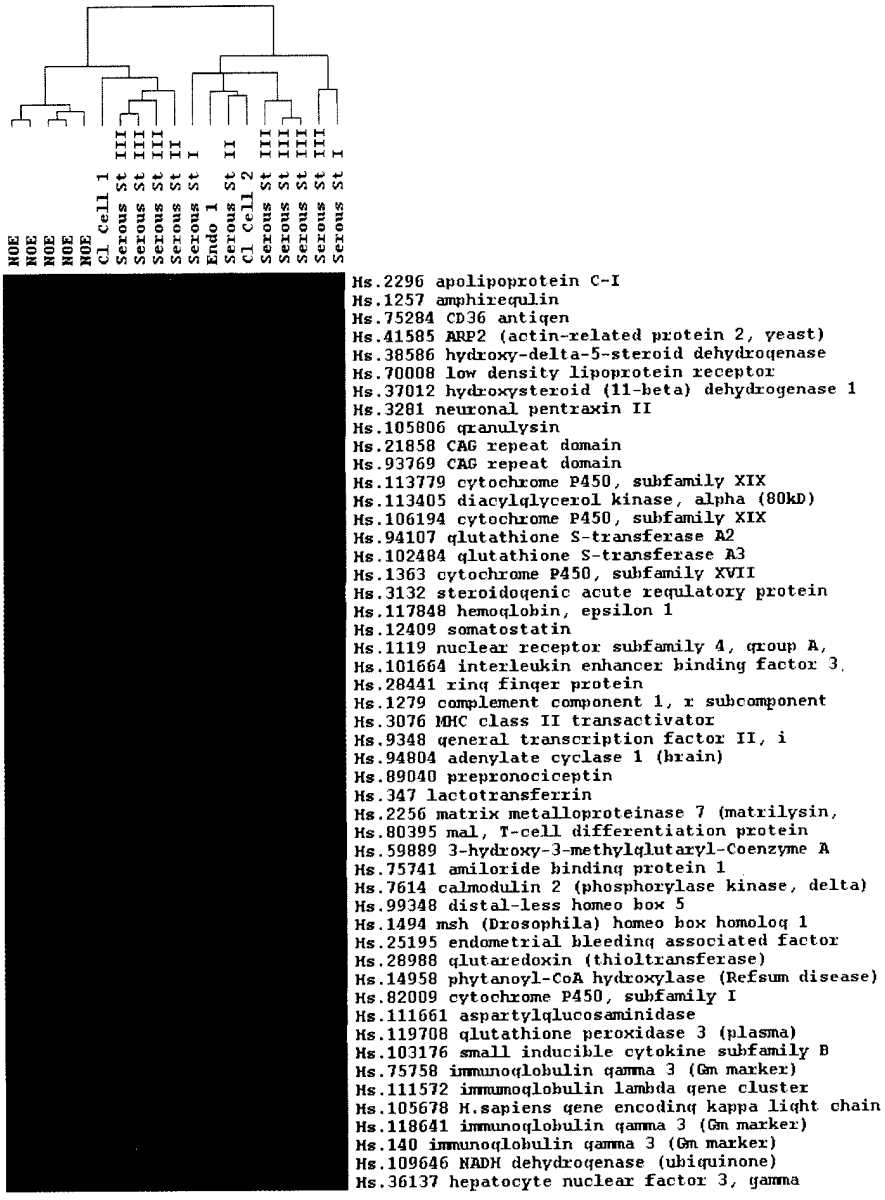

Fig. 2. Hierarchical clustering of 19 ovarian epithelial samples, using Eisen's Stanford clustering package. Eighteen thousand expressed sequences were profiled against five normal ovarian epithelial (NOE), two early-stage clear cell, one early-stage endometrioid, four early-stage serous, and seven late-stage (stage-III) serous samples. The 50 annotated clones with maximal normalized expression variance (SD divided by mean of expression) are shown. Data were log-transformed after addition of a baseline noise compensation term and were clustered using centered Pearson correlation. Whereas the normal samples neatly cluster together, separation between early- and late-stage samples is less compelling.

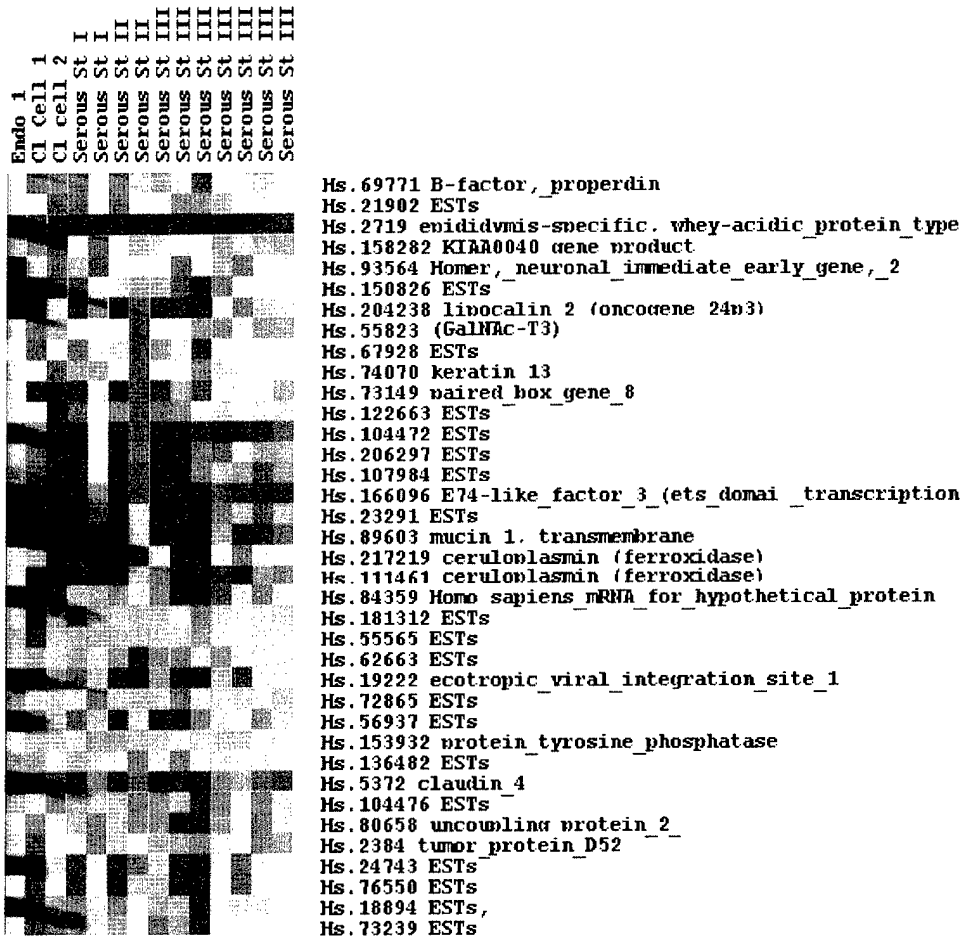

Fig. 3. Hierarchical clustering of 14 ovarian tumor samples, using Eisen's Stanford clustering package. Data were log-transformed and clustered by centered Pearson correlation. Cluster tree analysis of five times or more up-regulated genes in early- and late-stage tumors. *Red*, fold up-regulation of five times or more. *Green boxes*, fold regulation between 1 and 2. *Different shades of green*, values above 2 but less than 3.

microscope equipped with an automatic filter wheel and an 83,000 filter set (Chroma, Brattleboro, VT) with single band pass exciter filters for UV/FITC (490 nm), 4′,6-diamidino-2-phenylindole (360 nm), and rhodamine (570 nm), and were analyzed using the QUIPS CGH software version 3.12 (Vysis Inc., IL). Using this software, the ratio of rhodamine:FITC signal is expressed as a red:green ratio, with deviations from a 1:1 ratio indicative of gain or loss of chromosome material. The lower and upper limits for gain and loss were established by performing control CGH experiments with a well-characterized tumor cell line, IMR32 (18), and DNA derived from male or female normal tissue. On the basis of these findings, a 95% confidence interval for gain and loss was set at 1.20 and 0.80, respectively, with gene amplification defined as gain >1.5.

Cluster Analyses. Hierarchical cluster analyses were performed using the Cluster software package (19). Genes were clustered using the Pearson correlation coefficient as the distance metric, and clusters were agglomerated using the average linkage criterion. Graphical displays of our cluster analyses were obtained using the TreeView program (19).

RESULTS

Gene Expression Patterns of Early-Stage (I/II) and Late-Stage (III/IV) Tumors. We examined gene expression in seven early- and seven late-stage ovarian tumors (Table 1) using cDNA microarray filters containing approximately 25,000 members of the Unigene set and control probes. Each tumor was examined in duplicate, with results indicating excellent reproducibility (Pearson correlation, >0.97 in all cases). The overall degree of similarity in gene expression between duplicate microarray experiments and among different tissue specimens was assessed using scatter plots. A representative scatter plot for two duplicate filters is shown in Fig. 1*A* (Pearson correlation, 0.97), and Fig. 1*B* displays the scatter plot of an early-stage tumor (OV106) *versus* one of the pooled normal epithelial brushings (Pearson correlation coefficient, 0.76).

Analysis of the Differential Expression in Early- and Late-Stage Ovarian Tumors. Table 2 displays the number of genes for which we found varying levels of differential expression relative to normal ovarian epithelial cell brushings. Generally speaking, more genes were determined to be down-regulated than up-regulated. For example, 46 genes are at least 10-fold down-regulated in at least seven of the tumors that were expression-profiled. The number of genes that are 10-fold up-regulated in at least seven tumors is only 12. A similar trend was evident when the tumors were grouped by stage (Table 3). Heirarchical clustering for a set of genes selected for maximal variance (without prejudice toward differential expression) are shown in Fig. 2. The dendrogram in Fig. 2 shows the tight clustering of normal samples, whereas separation between early- and late-stage samples is far less compelling. Figs. 3 and 4 display heirarchical clustering for a set of genes that are $\geq$5-fold up- and down-regulated in a significant number of early- and late-stage tumors, respectively, relative to the pooled epithelial cell brushings. It is evident from these analyses that several of the genes are aberrantly regulated to the same extent in both early- and late-stage tumors.

To assess the extent to which genes in specific functional categories are differentially expressed in both early- and late-stage tumors, expressed sequences showing five times the expression changes in a majority of early-and late-stage tumors were grouped in one of four categories: cell-cell interactions; intermediate filament markers; cell cycle and growth regulators; and genes involved in invasion and metastasis (Fig. 5). This analysis revealed that genes involved in cell-cell interactions such as *cadherin 11* (20), *cadherin 2* (21), and

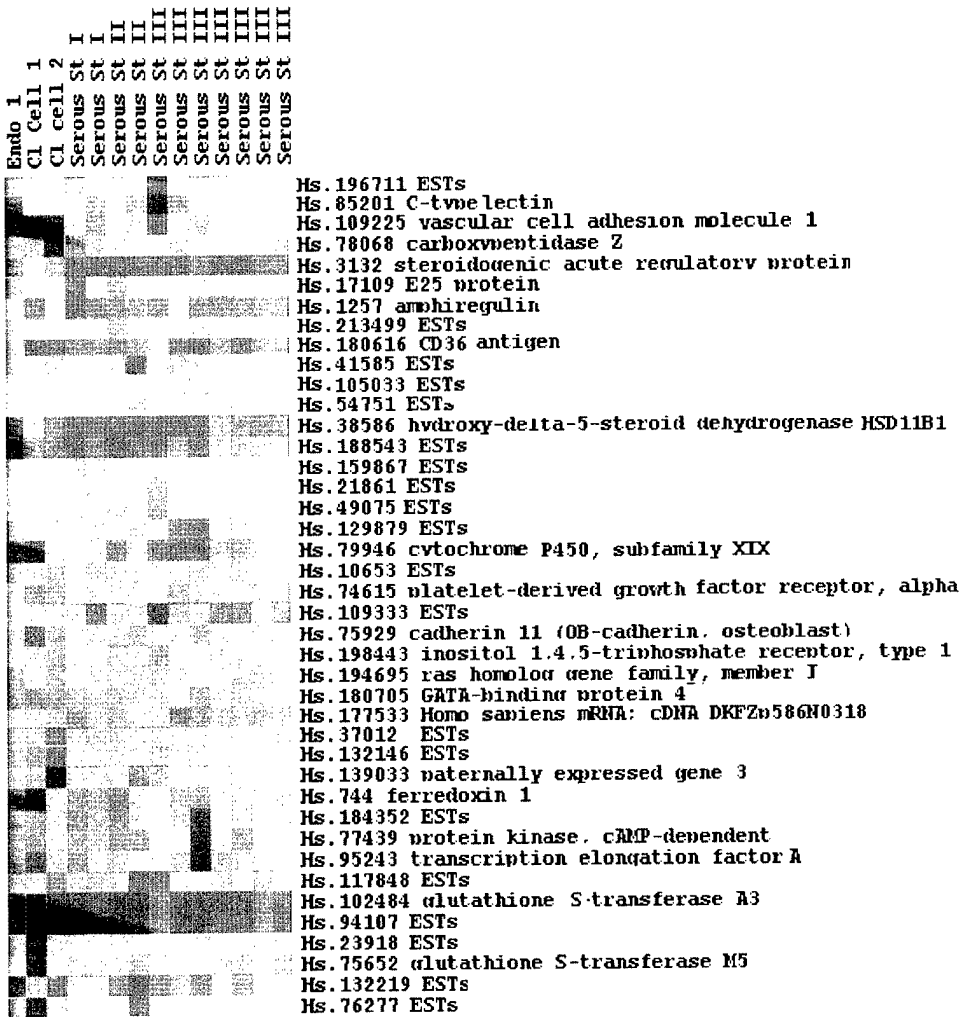

Fig. 4. Hierarchical clustering of 14 ovarian tumor samples, using Eisen's Stanford clustering package. Data were log-transformed and clustered by centered Pearson correlation. Cluster tree analysis of five times or more down-regulated genes in early- and late-stage tumors. *Green boxes*, fold down-regulation of five times or more. *Red boxes*, fold regulation between 1 and 2. *Different shades of red*, values above 2 but less than 3.

Fig. 5. Cluster tree analysis of gene categories, five times or more differentially regulated genes in early- and late-stage tumors. *Green boxes*, fold down-regulation of five times or more. *Red boxes*, fold up-regulation. *A*, intermediate filament genes; *B*, cell-cell interactions; *C*, cell invasion and metastasis; and *D*, cell cycle and growth regulators.

Table 4 *Genes with expression level changes >10-fold in both early- and late-stage tumors*

Cluster identification	Cluster title
10-fold down-regulated genes in early- and late-stage tumors	
Hs.[a]38586	*Hydroxy-δ-5-steroid dehydrogenase, 3 β- and steroid δ-isomerase 1*
Hs.213499	*ESTs*
Hs.49075	*Human DNA sequence from clone 22D12 on chromosome Xq21.1-21.33*
Hs.188543	*ESTs*
Hs.129879	*ESTs*
Hs.79946	*Cytochrome P-450, subfamily XIX (aromatization of androgens)*
Hs.180616	*CD36 antigen (collagen type I receptor, thrombospondin receptor)-like 1*
Hs.159867	*ESTs*
Hs.1275	*Amphiregulin (schwannoma-derived growth factor)*
Hs.41585	*ESTs*
Hs.94107	*ESTs*
Hs.3132	*Steroidogenic acute regulatory protein*
Hs.105033	*ESTs*
Hs.109333	*ESTs*
Hs.117848	*ESTs*
Hs.102488	*Glutathione S-transferase A3*
Hs.54751	*ESTs*
Hs.17109	*Integral membrane protein 2A*
Hs.21858	*CAG repeat containing (glia-derived nexin I α)*
Hs.54751	*ESTs*
Hs.9914	*Follistatin*
Hs.139033	*Paternally expressed gene 3*
Hs.105806	*Granulysin*
Hs.169228	*δ (Drosophila)-like 1*
Hs.37012	*Homo sapiens DNA sequence from PAC 434O14 on chromosome 1q32.3-41*
Hs.148493	*Cathepsin B*
10-fold up-regulated genes in early and late stage tumors	
Hs.5372	*Claudin 4*
Hs.2719	*Epididymis-specific, whey-acidic protein type, HE 4*
Hs.16696	*E74-like factor 3 (ets domain transcription factor)*
Hs.19222	*Ecotropic viral integration site 1*
Hs.896603	*Mucin 1, transmembrane*
Hs.24743	*ESTs*
Hs.111461	*Ceruloplasmin (ferroxidase)*
Hs.206297	*ESTs*
Hs.104472	*ESTs*
Hs.23291	*ESTs*
Hs.73149	*Paired box gene 8*
Hs.2256	*Matrix metalloproteinase 7 (matrilysin, uterine)*
Hs.204238	*Lipocalin 2 (oncogene 24p3)*
Hs.76550	*ESTs*
Hs.36451	*Glutamate receptor, ionotropic, N-methyl D-aspartate 2C*
Hs.155097	*Carbonic anhydrase II*

[a] Hs., unigene cluster IDs.

nidogen (*enactin*; Ref. 22) were all down-regulated in a majority of tumors, whereas genes involved in invasion and metastasis, including *matrilysin* (*MMP 7*; Refs. 23, 24), *gelatinase* (*MMP 9*; Ref. 25), *matrix metalloproteinase 10* and *12* (Ref. 23) were up-regulated in a majority of tumors. Genes belonging to the intermediate filament category, such as *vimentin* (26) and *keratin 10* (27) were down-regulated in both early- and late-stage tumors, whereas *keratins 8* (28), *13* (29), and *18* (28) were up-regulated in both stages. For the cell cycle/growth regulators, *cyclin D2* (30, 31), *cyclin dependent kinase 5*, *growth arrest-specific 1* (32), and the *E2F*-related transcription factor *DP1* (33) were all down-regulated. Other genes in this category, such as *cyclin E2* (34), proliferating cell nuclear antigen (35), and transcription factor *E2F5* (36), were up-regulated in both early and late-stage tumors.

The genes with an average-fold change of at least 10-fold change across all tumors are listed in Table 4. Several of these genes, such as *mucin 1* (37), *ceruloplasmin ferroxidase* (38), *claudin 4*, and *HE4* (39, 40) have been previously identified as up-regulated in ovarian tumors.

Validation of Microarray Results by Semiquantitative RT-PCR. To validate the expression levels of genes from the profiling analysis, we performed semiquantitative RT-PCR, with GAPDH as a control in seven ovarian tumor cell lines, on 20 early (I/II)- and 16 late (III/IV)-stage tumors (Table 1) with a set of genes that showed 5-fold differential regulation in at least 50% of the tumors. Fig. 6*A* shows the expression levels of a subset of the genes in ovarian tumor cell lines compared with short-term cultures of ovarian epithelial cells. Fig. 6*B* shows the expression levels of four of these genes in primary ovarian tumors compared with normal epithelial cell brushings. Among the genes with the most striking difference in expression in tumors relative to normal epithelial cell brushings, *FGF7* showed complete loss of expression in all of both early- and late-stage serous tumors and in six of the seven ovarian tumor cell lines. *Decorin*, a small proteoglycan involved in the activation of *EGFR* (41) pathway showed lower levels of expression in 22 of 31 tumors and in five of seven cell lines. The expression of plasminogen activator inhibitor 1 (*PAI1*; Ref. 42), a well-characterized serine protease inhibitor, was also lost in most (25 of 36) of the tumors tested. Among the genes showing frequent up-regulation by microarray analysis, *PUMP-1* (24, 43) and *HE4*, an epididymis-specific whey acidic protein (40), showed overexpression in almost all of the tumors tested (data not shown).

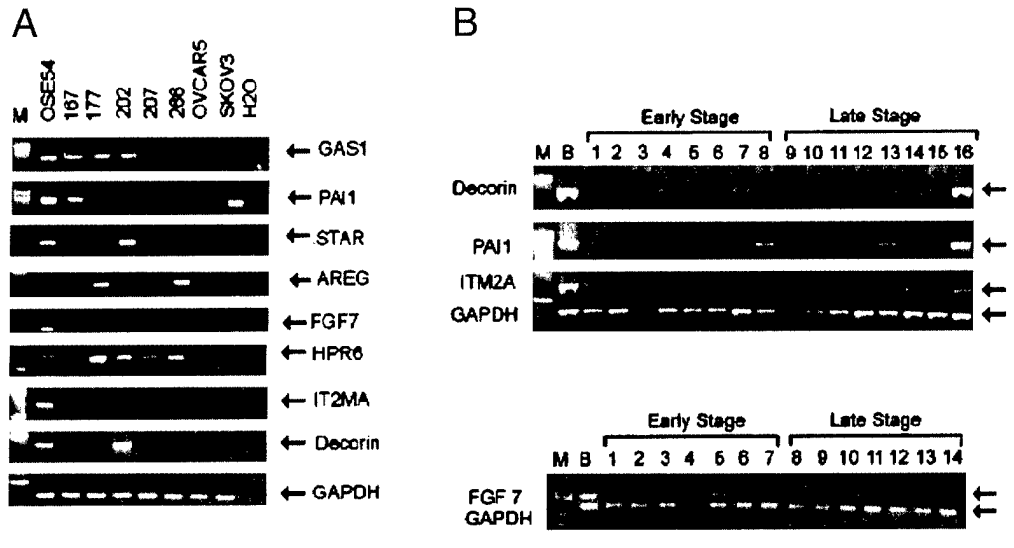

Fig. 6. *A*, agarose gel showing the products of semiquantitative RT-PCR in the ovarian cell lines. *M*, 100-bp ladder; *Lane 1*, short-term cultures of normal ovarian epithelial cells (*OSE54*); *Lane 2*, OV 167; *Lane 3*, OV 177; *Lane 4*, OV 202; *Lane 5*, OV 207; *Lane 6*, OV 266; *Lane 7*, OVCAR 5; *Lane 8*, SKOV; *Lane 9*, water control (*H2O*). Probes: *panel 1*, growth arrest-specific gene 1 (*GAS1*); *panel 2*, plasminogen activator inhibitor 1 (*PAI1*); *panel 3*, steroidogenic acute regulatory protein (*STAR*); *panel 4*, amphiregulin (*AREG*); *panel 5*, fibroblast growth factor 7 (*FGF 7*); *panel 6*, human progesterone binding protein (*HPR6*); *panel 7*, integral membrane protein 2A (*ITM2A*), *panel 8*, decorin; *panel 9*, GAPDH. *B*, agarose gel showing the products of the result of semiquantitative RT-PCR resolved on a 1.6% agarose gel. *On top of the figure*, sample numbers; *on top of the tumor numbers*, the staging information for these tumors. *M*, 100-bp ladder; *Lane 1*, normal epithelial cell brushings (*B*). *Panel 1*, decorin; *panel 2*, plasminogen activator inhibitor 1 (*PAI1*); *panel 3*, integral membrane protein 2A (*ITM2A*); *panel 4*, fibroblast growth factor 7 (*FGF 7*) and GAPDH.

Table 5 *CGH results*

Patient no. (histology; stage)	CGH changes
OV106 (Clear Cell; I)	−1p32-pter;+1q;+**3q22-26**[a];−4q;−6q24-27;+8q;+12p;−13q21-qter;−18q12-21;−Xq21-23
OV496 (Clear Cell; I)	+1p32-pter;−2q21-qter;−3;−4q12-28;+5p;−5q;−6;−12q;−13q21-33;+16;+18;+19;−Xq
OV51 (Endo; I)	NAD
OV105 (Endo; I)	+1q31-42;−2q22-24;−4q13-24;−5q12-23;−6q21-23;+11q22-24;+12q23-qter;−13q21-31;−15q21-24;+16p12-13;+19;+20q;−21
OV338 (Endo; I)	+1q21-qter;+6;+8;−9p;−21q
OV647 (Endo; I)	−4q;−5q;+6q24-27;−7q21-31;+16p12-13.2;+17;−18q;+20
OV6 (Serous; I)	+1p35-qter;−1p21-31;−2q23-32;−4q21-31.3;−5q14-32;+8q;−13q13-33;+19;+20q;+22q;−Xq21-qter
OV90 (Serous; I)	−1q24-31;+3q24-qter;−4q13-25;−5q21-23;−6;+8q23-qter;−9p13-23;+12p11.2-qter;−13q21-qter;−15q21;+17q24-25;−18q12-21; +20q12-qter;+22q
OV234 (Serous; I)	−1p33-35;+2q22;−4q22-31;−5q14-21;−6q14-16;−10p;+12p12-13;+17q;+20q
OV102 (Clear Cell; II)	−1p12-31;+1q31-42;−2q34-36;**+3q24-26**;−17p
OV401 (Serous; II)	+3q;**+3q24**;**+3q26**;−4q;+5p;−5q;−6;−7p;**+8q24**;**+11q23-24**;−18q21-22;+20;−Xq21-qters
OV402 (Serous; II)	+1q41-44;−2q24-32;+3q24-27;−5q21-23;−6q21-23;+11q13;−13q21-31;−18q12-22;+19;+20q;−Xq
OV176 (Clear Cell; III)	**+3q25-26**;+8q;+17q;**+20q12-13**
OV453 (Clear Cell; III)	+3q24-26.3;+17q24-25
OV522 (Clear Cell; III)	**+2p24-25**
OV623 (Clear Cell; III)	+8q
OV78 (Endo; III)	+1q21-41;−2p14-16;+3q13.1-13.3;−4q;+5p;+8q21.1-24;+9p21-23;+11q12-13;+17q23-25;−18q21-22;+20q;−X
OV93 (Endo; III)	+1q32-44;+2p24-25;+2q23-24;+3q13.3-qter;+3q24-26;−4q;−5;−6q22-qter;−8p;+8q;+9p22-23;+12p12-13;−13q31-34;−18q12-23;+20q13
OV110 (Endo; III)	+1p36;−4q13-32;−5q13-22;+8q24;+10;+11q24-25;+12p12-13;−14q23-24;+16q21-23;+19q;+20q
OV259 (Endo; III)	−1p13-22;+1q;+2q35-37;+**3q13**;+**3q25-27**;−4q23-qter;+5p;−5q14-qter;−6q;−7p;−11;+**12p12-13**;−13q;+19q;+**20q12-13**;+**22q12.2-12.3**;−Xq
OV4 (Serous III)	−2q;+**3q26.1-26.3**;−4q22-24;−5q13-23;−6q16.3-25;+**7q33-35**;+**8q23-24**;+**11q13-14**;+**12p11-13**;−18q12.3-22;+20q12-13.2
OV11 (Serous III)	−4q;−5q13.3-23.2;+**8q23-24**;+**11q23-24**;+12p12-13;−Xq21-qter
OV16 (Serous III)	+1q;−18q22;+22;−Xq23-25
OV29 (Serous III)	**+1q21-22**;−2q22-24;−5q;+8q;+**8q23-24**;+**11q12-13**;−18q12-qter;+**18p11.2-11.3**;+20q;−Xq
OV72 (Serous III)	+1p32-36.3;+1q31-32;−2q22-34;+5p13-15;−5q;+6p21.1-pter;+**7p21**;+8;+**8q23-24**;−9p;+**11q12-13**;+**12p12-13**;−18q12-qter;+19;+20;−Xq
OV150 (Serous III)	+**1q21-24**;+**2p24**;−3p;+**3q26-1-26.3**;−4p;+**5p14-15**;−6q13-21;+**8q24**;−9p24;+**11q13**;+**12p12-13**;−13q21-22;16p12-13.2;−18q;+20q12-13;−Xq
OV392 (Serous III)	+3q26;−4q221;−5q12-21;−6q24-27;+7q32-qter;+8q24.1-24.3;+12p13;−13q14-22;+20q;−X
OV448 (Serous III)	+**1p36**;−2q31-34;−5q14-23.3;+**17q24-25**;+19;+**20q12-13.2**;−X
OV319 (Endo; IV)	−1p31;+1q;+**2p24**;+2q24;+**3q21-26**;−4q32-qter;+**8q11.2-21.2**;+**8q23-24**;−9p23;−13q31;−15q21-qter;−18q;+**20q13**;−X

[a] Boldface denotes amplification.

CGH Analysis. To investigate whether any of the results from the gene expression analysis could be associated with genomic alterations, we performed CGH on a set of 29 ovarian tumors. The overall trend suggested similar changes in both early- and late-stage tumors (Table 5; Fig. 7). There were, however, conspicuous differences between the two tumor groups. For instance, the CGH results indicated that losses are more common than gains in the early-stage tumors. Consistent losses were observed at chromosomal regions of 2q (5 of 12), 4q (8 of 12), 5q (8 of 12), 6q (6 of 12), 13q (6 of 12), 18q (3 of 14), and Xq (5 of 12). Additional losses were also observed on chromosomes 7, 9, and 15 (2 cases); and 3, 12, 17, and 21 (1 case each). Gains involving chromosomes 20 (7 of 12); 1 (6 of 12); 3 and 8 (5 of 14); 19 (4 of 12); 11, 12, 16, 17, and 22 (3 of 14); 2, 5, 6, and 18 (1 of 12) were also observed. The chromosomal arms that showed frequent loss in the late-stage tumors were nearly identical to those observed in the early-stage tumors, and included 2q (5 of 17), 4q (9 of 17), 5q (9 of 17), 6q and 13q (5 of 17), 18q (6 of 13), and Xq (10 of 17). Less frequent losses were seen on chromosomes 9 (3 cases); 1p (2 cases); and 3, 7, 8, 11, 14, and 15 (1 case each). Gains on chromosomes 8 (76%), 20 (70%), 1 and 3 (58%), 12 (52%), 11 (41%), and 2 (35%) were evident in at least six of the late-stage tumors. Less frequent gains were observed on chromosomes 19 and 17 (4 of 17); 5 and 7 (3 of 17); 9, 16, and 22 (2 of 13); and 6 and 10 (1 case each).

Amplifications were mainly confined to the late-stage ovarian tumors. These involved regions at 8q23–24 (8 cases); 20q12–13 (6 cases); 3q24–26, 11q12–13, and 12p11–13 (5 cases each); 2p24–25 (3cases); 1p36, 9p21–23, 11q24–25, and 17q24–25 (2 cases each); and 1 case each on 1q32–44, 2q23–24, 3q13, 5p14–15, 7p21, 7q35, 8q11–21, and 22q12. In contrast, amplifications in the early-stage cancers were observed in just six instances: three times at chromosome 3q24–26 and one case each on 3q23, 8q23–24, and 11q24–25.

DISCUSSION

This report represents the first communication of an investigation involving the genome-wide examination of changes in gene expression and chromosomal regions for early- and late-stage ovarian cancer. In our cDNA microarray analysis, we identified several differentially expressed genes the potential role of which in carcinogenesis have been described previously. However, this analysis also identified several genes, both of known and unknown function, the role of which in tumor development has yet to be elucidated.

We validated the differential expression of several of the genes identified through microarray analysis by semiquantitative RT-PCR of RNA from both ovarian tumor cell lines and primary tumors. The down-regulation (at least 5-fold) of genes such as hydroxy-δ-5 steroid dehydrogenase, 3β (*HSD3B1*; Ref. 44), steroidogenic acute regulatory protein (*StAR*; Ref. 45, 46), *amphiregulin* (47), *glutathione S-transferase A3* (48), paternally expressed *gene 3* (49), and *integral membrane protein 2A* (50) have not previously been associated with ovarian cancer. Other genes such as *decorin* (41, 51), *platelet-derived growth factor receptor* α (52), *cadherin 11* (21), *cyclin D2* (53), *E2F*-related transcription factor *DP1* (33), *NOEY2* (6), and secreted frizzled related protein (*SFRP*; Ref. 54), have functions that can be or have been linked with carcinogenesis. Our expression analysis further revealed the consistent up-regulation of several genes, including *HE4* (40), *matrilysin* (*MMP 7*), *ceruloplasmin ferroxidase* (38), *claudin 4* (39), *cyclin D1* (55), *mucin 1* (56) *protease serine 8* (57), *keratins 7* (58) and *8* (28), as well as several ESTs. We have also validated the expression levels of *HE4*, *MMP7*, *ITM2A*, *HSD3B1*, and *PEG3* by real time RT-PCR in a smaller panel of primary tumors, and the results were similar to the semiquantitative RT-PCR analysis (data not shown).

To address the issue of whether the changes that we observed at the expression level were present at the genomic level, CGH analysis was performed on 12 early- and 17 late-stage tumors. Chromosomes 2, 4, 5, 6, 13, and 18 showed regions of loss in both stages at a similar frequency (59–61). Previous genomic sequence copy number screenings of ovarian tumors by conventional and molecular cytogenetics have reported similar findings (62). High copy number gains or amplifications were mainly observed in the late-stage tumors (62).

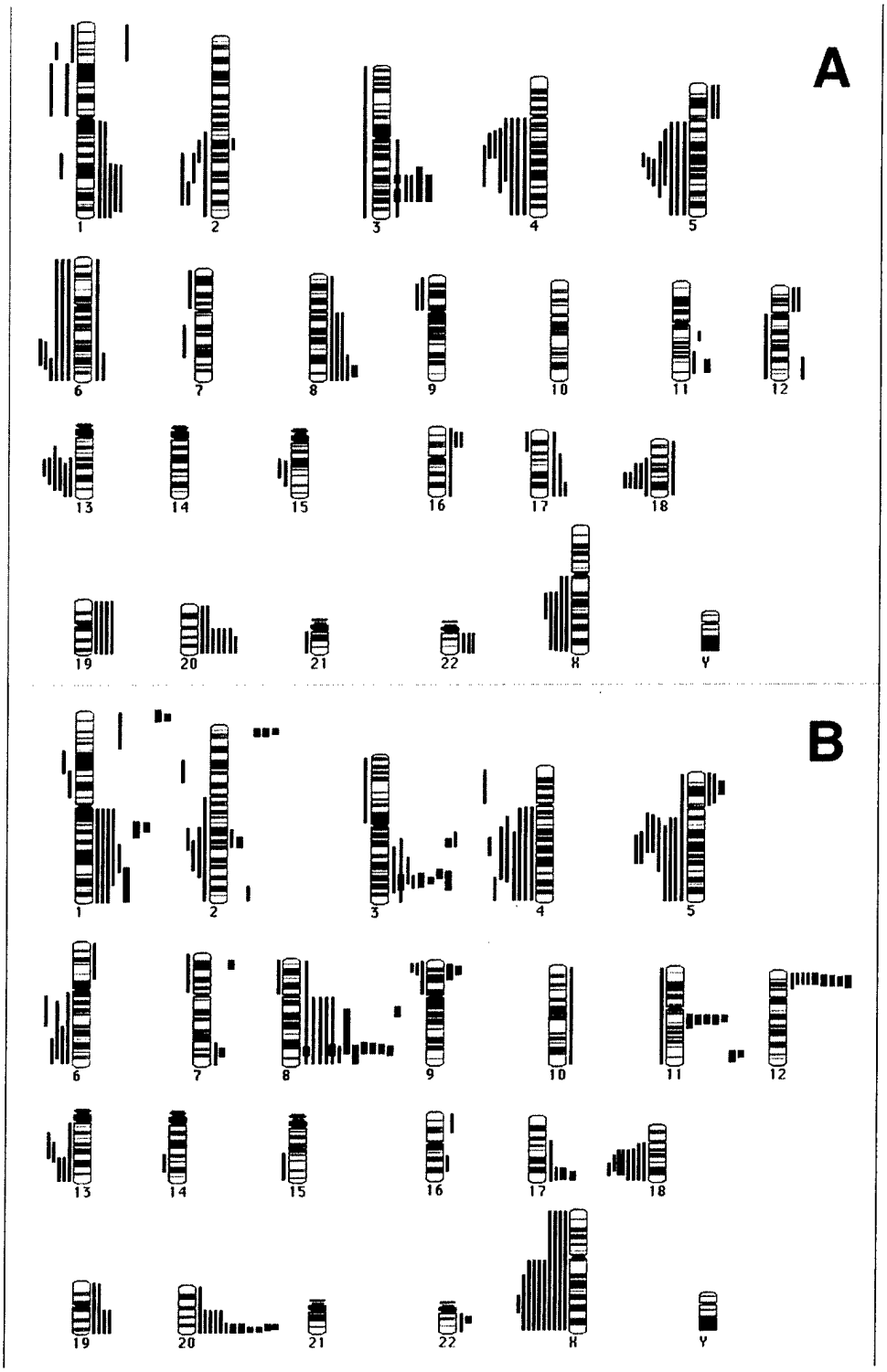

Fig. 7. Ideograms of the results of CGH analysis of 29 ovarian tumors. *Vertical lines to the right of schematic chromosomes*, gains; *vertical lines to the left*, losses. *Thicker line to the right*, the presence of high copy gain/amplification. *A*, CGH analysis of early-stage (I/II) tumors. Copy number changes of 12 tumors indicate a pattern of losses. In particular, loss of chromosomes 2, 4, 5, 6, 13, and 18 are frequent. Gains were less frequent, mainly involving chromosomes 1, 3, 6, 8 11, 19, and 20. *B*, CGH analysis of late-stage (III/IV) tumors. Copy number changes of 17 tumors indicate a pattern of losses and gene amplification; *thicker lines*, high level gains/amplifications (~>5 copy number). In contrast to the early-stage ovarian carcinomas, there are more chromosomal gains, and more tumors with localized gene amplification, predominantly involving the 3q24–26, 8q23–24, 11q12–13, 12p12–13, and 20q12–13 region. Other amplifications were detected on chromosomal arms 1p, 1q, 2p, 2q, 5p, 7q, 9p, 11q, 16p, 17q, and 18p. Losses were common on chromosomes 2, 4, 5,6, 13, and 18.

Chromosomal regions involved in amplification were 3q24–26 (63), 8q23–24 (64), 11q12–13 (55), 12p11–12 (65), 17q24–25 (66), and 20q12–13 (67).

Inspection of the data generated by CGH and expression profiling allows one to speculate on a mechanistic basis for the differential expression of at least some of the genes. For example, CGH results indicated high-level gains of 8q24 and 11q13 in multiple tumors (Fig. 8), and the microarray analysis of the same tumors indicated an increase in expression of genes/ESTs from these same regions: *i.e., cyclin D1 (PRAD1), uncoupling protein 2, folate receptor, and matrix metalloproteinase 7*, from 11q13; and *MYCC* (68), *PTK2 protein tyrosine kinase 2* (69), *RAD21* homologue (70), and several ESTs from 8q24 (data not shown), respectively. From the combined results, it seems reasonable to consider that the overexpression of these genes may be the result of gene amplification. Similarly, loss of genomic sequences from chromosomal region 4q could be responsible for the low expression of *LIM* (71), *Hevin* (72), *MAP kinase 10* and several ESTs detected by the expression profiling from the same region.

The data from the microarray analysis revealed that the majority of genes that were differentially expressed in ovarian cancer showed

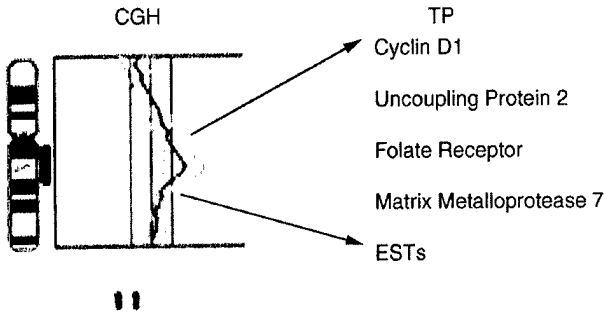

Fig. 8. CGH profile of an ovarian tumor illustrating a high copy gain/amplification in the 11q12–13 region of chromosome 11. The transcription profile of the same tumor by cDNA microarray analysis exhibited overexpression of cyclin D1, uncoupling protein 2, folate receptor, metalloproteinase 7, and some ESTs from this region.

aberrant transcript levels in both early- and late-stage tumors. At initial consideration, such results seem contrary to the genetic dogma associated with solid-tumor evolution that holds that gene alterations, and presumably, therefore, gene expression changes, become more prevalent as tumors become increasingly malignant. Interestingly, the CGH data indicate some differences between early- and late-stage tumors, especially the more common finding of regional gain and/or amplification in the late-stage tumors. Consequently, the CGH data provide some support for the genetic evolution of this solid tumor.

The inconsistency observed between the expression profiling and the CGH data could potentially be attributable to epigenetic changes such as methylation. Inactivation of genes attributable to CpG island methylation is very well documented (73). Evidence seems to indicate that these changes are probably very early events in carcinogenesis (74, 75). This may partially explain why the majority of genes are aberrantly regulated in early-stage tumors. It is also well documented that amplification events in carcinogenesis are late events (76–78) and is consistent with what is observed from the CGH data. Abnormal expression of genes is not attributable only to gene amplification or gains. Other genomic changes like rearrangements (translocations) are also responsible for alteration in gene expression. CGH can only aid in detecting net chromosomal losses or gains in tumor cells and does not account for rearrangements, thus overlooking changes that could be responsible for abnormal expression detected by microarray analysis.

An aspect of our finding that may be especially important to the clinical treatment of ovarian cancer is the determination of extensive, aberrant gene expression in early-stage tumors. One of the assumptions of most screening strategies is that a significant fraction of stage III/IV disease metastasizes from stage I lesions. These data are consistent with that possibility. In addition, poorly differentiated stage I cancers have been treated with cytotoxic chemotherapy. These data suggest that early-stage lesions have most of the genetic changes required for metastatic spread, consistent with a need for aggressive therapy. Further study of the genes that show consistent, high-level expression changes may result in the identification of markers useful for early cancer detection and may further point to potential therapeutic targets.

REFERENCES

1. Landis, S. H., Murray, T., Bolden, S., and Wingo, P. A. Cancer statistics, 1999. CA Cancer J. Clin., *49:* 8–31, 1999.
2. Friedlander, M. L. Prognostic factors in ovarian cancer. Semin. Oncol., *25:* 305–314, 1998.
3. Dong, Y., Walsh, M. D., McGuckin, M. A., Cummings, M. C., Gabrielli, B. G., Wright, G. R., Hurst, T., Khoo, S. K., and Parsons, P. G. Reduced expression of retinoblastoma gene product (pRB) and high expression of p53 are associated with poor prognosis in ovarian cancer. Int. J. Cancer, *74:* 407–415, 1997.
4. Gershenson, D. M., Deavers, M., Diaz, S., Tortolero-Luna, G., Miller, B. E., Bast, R. C., Jr., Mills, G. B., and Silva, E. G. Prognostic significance of p53 expression in advanced-stage ovarian serous borderline tumors. Clin. Cancer Res., *5:* 4053–4058, 1999.
5. Aprelikova, O. N., Fang, B. S., Meissner, E. G., Cotter, S., Campbell, M., Kuthiala, A., Bessho, M., Jensen, R. A., and Liu, E. T. BRCA1-associated growth arrest is RB-dependent. Proc. Natl. Acad. Sci. USA, *96:* 11866–11871, 1999.
6. Yu, Y., Xu, F., Peng, H., Fang, X., Zhao, S., Li, Y., Cuevas, B., Kuo, W. L., Gray, J. W., Siciliano, M., Mills, G. B., and Bast, R. C., Jr. NOEY2 (*ARHI*), an imprinted putative tumor suppressor gene in ovarian and breast carcinomas. Proc. Natl. Acad. Sci. USA, *96:* 214–219, 1999.
7. Catteau, A., Harris, W. H., Xu, C. F., and Solomon, E. Methylation of the BRCA1 promoter region in sporadic breast and ovarian cancer: correlation with disease characteristics. Oncogene, *18:* 1957–1965, 1999.
8. Scambia, G., Masciullo, V., Benedetti Panici, P., Marone, M., Ferrandina, G., Todaro, N., Bellacosa, A., Jain, S. K., Neri, G., Piffanelli, A., and Mancuso, S. Prognostic significance of ras/p21 alterations in human ovarian cancer. Br. J. Cancer, *75:* 1547–1553, 1997.
9. Tanner, B., Hengstler, J. G., Luch, A., Meinert, R., Kreutz, E., Arand, M., Wilkens, C., Hofmann, M., Oesch, F., Knapstein, P. G., and Becker, R. C-myc mRNA expression in epithelial ovarian carcinomas in relation to estrogen receptor status, metastatic spread, survival time. FIGO stage, and histologic grade and type. Int. J. Gynecol. Pathol., *17:* 66–74, 1998.
10. Bourguignon, L. Y., Zhu, H., Chu, A., Iida, N., Zhang, L., and Hung, M. C. Interaction between the adhesion receptor, CD44, and the oncogene product, p185HER2, promotes human ovarian tumor cell activation. J. Biol. Chem., *272:* 27913–27918, 1997.
11. Wang, K., Gan, L., Jeffery, E., Gayle, M., Gown, A. M., Skelly, M., Nelson, P. S., Ng, W. V., Schummer, M., Hood, L., and Mulligan, J. Monitoring gene expression profile changes in ovarian carcinomas using cDNA microarray. Gene (Amst.), *229:* 101–108, 1999.
12. Alaiya, A. A., Franzen, B., Hagman, A., Silfversward, C., Moberger, B., Linder, S., and Auer, G. Classification of human ovarian tumors using multivariate data analysis of polypeptide expression patterns. Int. J. Cancer, *86:* 731–736, 2000.
13. Schena, M., Shalon, D., Davis, R. W., and Brown, P. O. Quantitative monitoring of gene expression patterns with a complementary DNA microarray. Science (Wash. DC), *270:* 467–470, 1995.
14. Kallioniemi, A., Kallioniemi, O. P., Sudar, D., Rutovitz, D., Gray, J. W., Waldman, F., and Pinkel, D. Comparative genomic hybridization for molecular cytogenetic analysis of solid tumors. Science (Wash. DC), *258:* 818–821, 1992.
15. Conover, C. A., Hartmann, L. C., Bradley, S., Stalboerger, P., Klee, G. G., Kalli, K. R., and Jenkins, R. B. Biological characterization of human epithelial ovarian carcinoma cells in primary culture: the insulin-like growth factor system. Exp. Cell Res., *238:* 439–449, 1998.
16. Hamilton, T. C., Young, R. C., and Ozols, R. F. Experimental model systems of ovarian cancer: applications to the design and evaluation of new treatment approaches. Semin. Oncol., *11:* 285–298, 1984.
17. Dracopoli, N. C. Current Protocols in Human Genetics. New York: John Wiley & Sons, Inc., 1999.
18. Tumilowicz, J. J., Nichols, W. W., Cholon, J. J., and Greene, A. E. Definition of a continuous human cell line derived from neuroblastoma. Cancer Res., *30:* 2110–2118, 1970.
19. Eisen, M. B., Spellman, P. T., Brown, P. O., and Botstein, D. Cluster analysis and display of genome-wide expression patterns. Proc. Natl. Acad. Sci. USA, *95:* 14863–14868, 1998.
20. Kremmidiotis, G., Baker, E., Crawford, J., Eyre, H. J., Nahmias, J., and Callen, D. F. Localization of human cadherin genes to chromosome regions exhibiting cancer-related loss of heterozygosity. Genomics, *49:* 467–471, 1998.
21. Peralta Soler, A., Knudsen, K. A., Tecson-Miguel, A., McBrearty, F. X., Han, A. C., and Salazar, H. Expression of E-cadherin and N-cadherin in surface epithelial-stromal tumors of the ovary distinguishes mucinous from serous and endometrioid tumors. Hum. Pathol., *28:* 734–739, 1997.
22. Zedlacher, M., Schmoll, M., Zimmermann, K., Horstkorte, O., and Nischt, R. Differential regulation of the human nidogen gene promoter region by a novel cell-type-specific silencer element. Biochem. J., *338:* 343–350, 1999.
23. Moser, T. L., Young, T. N., Rodriguez, G. C., Pizzo, S. V., Bast, R. C., Jr., and Stack, M. S. Secretion of extracellular matrix-degrading proteinases is increased in epithelial ovarian carcinoma. Int. J. Cancer, *56:* 552–559, 1994.
24. Tanimoto, H., Underwood, L. J., Shigemasa, K., Parmley, T. H., Wang, Y., Yan, Y., Clarke, J., and O'Brien, T. J. The matrix metalloprotease pump-1 (MMP-7. Matrilysin): a candidate marker/target for ovarian cancer detection and treatment. Tumor Biol., *20:* 88–98, 1999.
25. Shibata, K., Kikkawa, F., Nawa, A., Tamakoshi, K., Suganuma, N., and Tomoda, Y. Increased matrix metalloproteinase-9 activity in human ovarian cancer cells cultured with conditioned medium from human peritoneal tissue. Clin. Exp. Metastasis, *15:* 612–619, 1997.
26. Ferrari, S., Battini, R., Kaczmarek, L., Rittling, S., Calabretta, B., de Riel, J. K., Philiponis, V., Wei, J. F., and Baserga, R. Coding sequence and growth regulation of the human vimentin gene. Mol. Cell. Biol., *6:* 3614–3620, 1986.
27. Rogaev, E. I., Rogaeva, E. A., Ginter, E. K., Korovaitseva, G. I., Farrer, L., Shlenskii, A. B., Prytkov, A. N., St. George-Hyslop, P., and Mordovtsev, V. N. Mapping the gene for palmoplantar hyperkeratosis (thylosis) to chromosome 17 in the 17q12–q24 region. Genetica (Dordr.), *30:* 326–329, 1994.
28. Waseem, A., Gough, A. C., Spurr, N. K., and Lane, E. B. Localization of the gene for human simple epithelial keratin 18 to chromosome 12 using polymerase chain reaction. Genomics, *7:* 188–194, 1990.

29. Waseem, A., Alam, Y., Dogan, B., White, K. N., Leigh, I. M., and Waseem, N. H. Isolation, sequence and expression of the gene encoding human keratin 13 [published erratum appears in Gene, *221:* 287, 1998]. Gene, *215:* 269–279, 1998.
30. Palmero, I., Holder, A., Sinclair, A. J., Dickson, C., and Peters, G. Cyclins D1 and D2 are differentially expressed in human B-lymphoid cell lines. Oncogene, *8:* 1049–1054, 1993.
31. Palmero, I., and Peters, G. Perturbation of cell cycle regulators in human cancer. Cancer Surv., *27:* 351–367, 1996.
32. Ruaro, M. E., Stebel, M., Vatta, P., Marzinotto, S., and Schneider, C. Analysis of the domain requirement in Gas1 growth suppressing activity. FEBS Lett., *481:* 159–163, 2000.
33. Johnson, D. G., Cress, W. D., Jakoi, L., and Nevins, J. R. Oncogenic capacity of the *E2F1* gene. Proc. Natl. Acad. Sci. USA, *91:* 12823–12827, 1994.
34. Gudas, J. M., Payton, M., Thukral, S., Chen, E., Bass, M., Robinson, M. O., and Coats, S. Cyclin E2, a novel G1 cyclin that binds Cdk2 and is aberrantly expressed in human cancers. Mol. Cell. Biol., *19:* 612–622, 1999.
35. Liu, F. S., Chen, J. T., Liu, S. C., Shih, A., Shih, R. T., and Ho, E. S. Expression and prognostic significance of proliferating cell nuclear antigen and Ki-67 in malignant ovarian germ cell tumors. Chung Hua I Hsueh Tsa Chih (Taipei), *62:* 695–702, 1999.
36. Polanowska, J., Le Cam, L., Orsetti, B., Valles, H., Fabbrizio, E., Fajas, L., Taviaux, S., Theillet, C., and Sardet, C. Human *E2F5* gene is oncogenic in primary rodent cells and is amplified in human breast tumors. Zhonghua Yi Xue Za Zhi, *28:* 126–130, 2000.
37. Giuntoli, R. L., II, Rodriguez, G. C., Whitaker, R. S., Dodge, R., and Voynow, J. A. *Mucin* gene expression in ovarian cancers. Cancer Res., *58:* 5546–5550, 1998.
38. Senra Varela, A., Lopez Saez, J. J., and Quintela Senra, D. Serum ceruloplasmin as a diagnostic marker of cancer. Cancer Lett., *121:* 139–145, 1997.
39. Hough, C. D., Sherman-Baust, C. A., Pizer, E. S., Montz, F. J., Im, D. D., Rosenshein, N. B., Cho, K. R., Riggins, G. J., and Morin, P. J. Large-scale serial analysis of gene expression reveals genes differentially expressed in ovarian cancer. Cancer Res., *60:* 6281–6287, 2000.
40. Schummer, M., Ng, W. V., Bumgarner, R. E., Nelson, P. S., Schummer, B., Bednarski, D. W., Hassell, L., Baldwin, R. L., Karlan, B. Y., and Hood, L. Comparative hybridization of an array of 21,500 ovarian cDNAs for the discovery of genes overexpressed in ovarian carcinomas. Gene (Amst.), *238:* 375–385, 1999.
41. Nash, M. A., Loercher, A. E., and Freedman, R. S. *In vitro* growth inhibition of ovarian cancer cells by decorin: synergism of action between decorin and carboplatin. Cancer Res., *59:* 6192–6196, 1999.
42. Pujade-Lauraine, E., Lu, H., Mirshahi, S., Soria, J., Soria, C., Bernadou, A., Kruithof, E. K., Lijnen, H. R., and Burtin, P. The plasminogen-activation system in ovarian tumors. Int. J. Cancer, *55:* 27–31, 1993.
43. Shigemasa, K., Tanimoto, H., Sakata, K., Nagai, N., Parmley, T. H., Ohama, K., and O'Brien, T. J. Induction of matrix metalloprotease-7 is common in mucinous ovarian tumors including early stage disease. Med. Oncol., *17:* 52–58, 2000.
44. Milewich, L., Shaw, C. E., Mason, J. I., Carr, B. R., Blomquist, C. H., and Thomas, J. L. 3β-hydroxysteroid dehydrogenase activity in tissues of the human fetus determined with 5α-androstane-3β,17 β-diol and dehydroepiandrosterone as substrates. J. Steroid Biochem. Mol. Biol., *45:* 525–537, 1993.
45. Lee, H. K., Yoo, M. S., Choi, H. S., Kwon, H. B., and Soh, J. Retinoic acids up-regulate steroidogenic acute regulatory protein gene. Mol. Cell. Endocrinol., *148:* 1–10, 1999.
46. Brand, C., Souchelnytskiy, S., Chambaz, E. M., Feige, J. J., and Bailly, S. Smad3 is involved in the intracellular signaling pathways that mediate the inhibitory effects of transforming growth factor-β on StAR expression. Biochem. Biophys. Res. Commun., *253:* 780–785, 1998.
47. Funatomi, H., Itakura, J., Ishiwata, T., Pastan, I., Thompson, S. A., Johnson, G. R., and Korc, M. Amphiregulin antisense oligonucleotide inhibits the growth of T3M4 human pancreatic cancer cells and sensitizes the cells to EGF receptor-targeted therapy. Int. J. Cancer, *72:* 512–517, 1997.
48. Letourneau, S., Palerme, J. S., Delisle, J. S., Beausejour, C. M., Momparler, R. L., and Cournoyer, D. Coexpression of rat glutathione *S*-transferase A3 and human cytidine deaminase by a bicistronic retroviral vector confers *in vitro* resistance to nitrogen mustards and 1-β-D-arabinofuranosylcytosine in murine fibroblasts. Cancer Gene Ther., *7:* 757–765, 2000.
49. Li, L. L., Szeto, I. Y., Cattanach, B. M., Ishino, F., and Surani, M. A. Organization and parent-of-origin-specific methylation of imprinted *Peg3* gene on mouse proximal chromosome 7. Genomics, *63:* 333–340, 2000.
50. Tuckermann, J. P., Pittois, K., Partridge, N. C., Merregaert, J., and Angel, P. Collagenase-3 (*MMP-13*) and integral membrane protein 2a (*Itm2a*) are marker genes of chondrogenic/osteoblastic cells in bone formation: sequential temporal, and spatial expression of Itm2a, alkaline phosphatase, MMP-13, and osteocalcin in the mouse. J. Bone Miner. Res., *15:* 1257–1265, 2000.
51. Iozzo, R. V., Moscatello, D. K., McQuillan, D. J., and Eichstetter, I. Decorin is a biological ligand for the epidermal growth factor receptor. J. Biol. Chem., *274:* 4489–4492, 1999.
52. Shawver, L. K., Schwartz, D. P., Mann, E., Chen, H., Tsai, J., Chu, L., Taylorson, L., Longhi, M., Meredith, S., Germain, L., Jacobs, J. S., Tang, C., Ullrich, A., Berens, M. E., Hersh, E., McMahon, G., Hirth, K. P., and Powell, T. J. Inhibition of platelet-derived growth factor-mediated signal transduction and tumor growth by *N*-[4-(trifluoromethyl)-phenyl]5- methylisoxazole-4-carboxamide. Clin. Cancer Res., *3:* 1167–1177, 1997.
53. Sicinski, P., Donaher, J. L., Geng, Y., Parker, S. B., Gardner, H., Park, M. Y., Robker, R. L., Richards, J. S., McGinnis, L. K., Biggers, J. D., Eppig, J. J., Bronson, R. T., Elledge, S. J., and Weinberg, R. A. *Cyclin D2* is an FSH-responsive gene involved in gonadal cell proliferation and oncogenesis. Nature (Lond.), *384:* 470–474, 1996.
54. Roth, W., Wild-Bode, C., Platten, M., Grimmel, C., Melkonyan, H. S., Dichgans, J., and Weller, M. Secreted frizzled-related proteins inhibit motility and promote growth of human malignant glioma cells. Oncogene, *19:* 4210–4220, 2000.
55. Shigemasa, K., Tanimoto, H., Parham, G. P., Parmley, T. H., Ohama, K., and O'Brien, T. J. Cyclin D1 overexpression and p53 mutation status in epithelial ovarian cancer. J. Soc. Gynecol. Investig., *6:* 102–108, 1999.
56. Dong, Y., Walsh, M. D., Cummings, M. C., Wright, R. G., Khoo, S. K., Parsons, P. G., and McGuckin, M. A. Expression of MUC1 and MUC2 mucins in epithelial ovarian tumours. J. Pathol., *183:* 311–317, 1997.
57. Yu, J. X., Chao, L., Ward, D. C., and Chao, J. Structure and chromosomal localization of the human prostasin (*PRSS8*) gene. Genomics, *32:* 334–340, 1996.
58. Sack, M. J., and Roberts, S. A. Cytokeratins 20 and 7 in the differential diagnosis of metastatic carcinoma in cytologic specimens. Diagn. Cytopathol., *16:* 132–136, 1997.
59. Takakura, S., Okamoto, A., Saito, M., Yasuhara, T., Shinozaki, H., Isonishi, S., Yoshimura, T., Ohtake, Y., Ochiai, K., and Tanaka, T. Allelic imbalance in chromosome band 18q21 and SMAD4 mutations in ovarian cancers. Genes Chromosomes Cancer, *24:* 264–271, 1999.
60. Allan, G. J., Cottrell, S., Trowsdale, J., and Foulkes, W. D. Loss of heterozygosity on chromosome 5 in sporadic ovarian carcinoma is a late event and is not associated with mutations in APC at 5q21–22. Hum. Mutat., *3:* 283–291, 1994.
61. Watson, R. H., Roy, W. J., Jr., Davis, M., Hitchcock, A., and Campbell, I. G. Loss of heterozygosity at the α-inhibin locus on chromosome 2q is not a feature of human granulosa cell tumors. Gynecol. Oncol., *65:* 387–390, 1997.
62. Wasenius, V. M., Jekunen, A., Monni, O., Joensuu, H., Aebi, S., Howell, S. B., and Knuutila, S. Comparative genomic hybridization analysis of chromosomal changes occurring during development of acquired resistance to cisplatin in human ovarian carcinoma cells. Genes Chromosomes Cancer, *18:* 286–291, 1997.
63. Hu, L., Zaloudek, C., Mills, G. B., Gray, J., and Jaffe, R. B. *In vivo* and *in vitro* ovarian carcinoma growth inhibition by a phosphatidylinositol 3-kinase inhibitor (LY294002). Clin. Cancer Res., *6:* 880–886, 2000.
64. Baker, V. V., Borst, M. P., Dixon, D., Hatch, K. D., Shingleton, H. M., and Miller, D. c-myc amplification in ovarian cancer. Gynecol. Oncol., *38:* 340–342, 1990.
65. Fukumoto, M., Estensen, R. D., Sha, L., Oakley, G. J., Twiggs, L. B., Adcock, L. L., Carson, L. F., and Roninson, I. B. Association of Ki-ras with amplified DNA sequences, detected in human ovarian carcinomas by a modified in-gel renaturation assay. Cancer Res., *49:* 1693–1697, 1989.
66. Gogusev, J., de Joliniere, J. B., Telvi, L., Doussau, M., du Manoir, S., Stojkoski, A., and Levardon, M. Genetic abnormalities detected by comparative genomic hybridization in a human endometriosis-derived cell line. Mol. Hum. Reprod., *6:* 821–827, 2000.
67. Courjal, F., Cuny, M., Rodriguez, C., Louason, G., Speiser, P., Katsaros, D., Tanner, M. M., Zeillinger, R., and Theillet, C. DNA amplifications at 20q13 and MDM2 define distinct subsets of evolved breast and ovarian tumours. Br. J. Cancer, *74:* 1984–1989, 1996.
68. Schraml, P., Kononen, J., Bubendorf, L., Moch, H., Bissig, H., Nocito, A., Mihatsch, M. J., Kallioniemi, O. P., and Sauter, G. Tissue microarrays for gene amplification surveys in many different tumor types. Clin. Cancer Res., *5:* 1966–1975, 1999.
69. Agochiya, M., Brunton, V. G., Owens, D. W., Parkinson, E. K., Paraskeva, C., Keith, W. N., and Frame, M. C. Increased dosage and amplification of the focal adhesion kinase gene in human cancer cells. Oncogene, *18:* 5646–5653, 1999.
70. Hoque, M. T., and Ishikawa, F. Human chromatid cohesin component hRad21 Is phosphorylated in M phase and associated with metaphase centromeres. J. Biol. Chem., *276:* 5059–5067, 2001.
71. Bouju, S., Pietu, G., Le Cunff, M., Cros, N., Malzac, P., Pellissier, J. F., Pons, F., Leger, J. J., Auffray, C., and Dechesne, C. A. Exclusion of muscle specific actinin-associated LIM protein (*ALP*) gene from 4q35 facioscapulohumeral muscular dystrophy (*FSHD*) candidate genes. Neuromuscul. Disord., *9:* 3–10, 1999.
72. Nelson, P. S., Plymate, S. R., Wang, K., True, L. D., Ware, J. L., Gan, L., Liu, A. Y., and Hood, L. Hevin, an antiadhesive extracellular matrix protein, is down-regulated in metastatic prostate adenocarcinoma. Cancer Res., *58:* 232–236, 1998.
73. Robertson, K. D., and Jones, P. A. DNA methylation: past, present and future directions. Carcinogenesis (Lond.), *21:* 461–467, 2000.
74. Cheng, P., Schmutte, C., Cofer, K. F., Felix, J. C., Yu, M. C., and Dubeau, L. Alterations in DNA methylation are early, but not initial, events in ovarian tumorigenesis. Br. J. Cancer, *75:* 396–402, 1997.
75. Rideout, W. M., III, Eversole-Cire, P., Spruck, C. H., III, Hustad, C. M., Coetzee, G. A., Gonzales, F. A., and Jones, P. A. Progressive increases in the methylation status and heterochromatinization of the myoD CpG island during oncogenic transformation. Mol. Cell. Biol., *14:* 6143–6152, 1994.
76. Calugi, A., Eleuteri, P., Cavallo, D., Naso, G., Albonici, L., Lombardi, M. P., Manzari, V., Romanini, C., and DeVita, R. Detection of cellular heterogeneity by DNA ploidy, 17 chromosome, and *p53* gene in primary carcinoma and metastasis in a case of ovarian cancer. Int. J. Gynecol Pathol., *15:* 77–81, 1996.
77. Anderson, M. W., Reynolds, S. H., You, M., and Maronpot, R. M. Role of proto-oncogene activation in carcinogenesis. Environ. Health Perspect., *98:* 13–24, 1992.
78. Ranzani, G. N., Pellegata, N. S., Previdere, C., Saragoni, A., Vio, A., Maltoni, M., and Amadori, D. Heterogeneous protooncogene amplification correlates with tumor progression and presence of metastases in gastric cancer patients. Cancer Res., *50:* 7811–7814, 1990.

MS #3

[CANCER RESEARCH 62, 262–270, January 1, 2002]

Identification of Underexpressed Genes in Early- and Late-Stage Primary Ovarian Tumors by Suppression Subtraction Hybridization[1]

Viji Shridhar,[2] Ami Sen, Jeremy Chien, Julie Staub, Rajeswari Avula, Steve Kovats, John Lee, Jim Lillie, and David I. Smith

Department of Experimental Pathology, Division of Laboratory Medicine, Mayo Clinic, Rochester, Minnesota 55905 [V. S., J. C., J. S., R. A., D. I. S.]; Millennium Predictive Medicine, Cambridge, Massachusetts 02139 [A. S., S. K., J. Li.]; and Corning, Acton, Massachusetts 01720 [J. Le.]

ABSTRACT

To identify novel tumor suppressor genes involved in ovarian carcinogenesis, we generated four down-regulated suppression subtraction cDNA libraries from two early-stage (stage I/II) and two late-stage (stage III) primary ovarian tumors, each subtracted against cDNAs derived from normal ovarian epithelial cell brushings. Approximately 600–700 distinct clones were sequenced from each library. Comparison of down-regulated clones obtained from early- and late-stage tumors revealed genes that were unique to each library which suggested tumor-specific differences. We found 45 down-regulated genes that were common in all four libraries. We also identified several genes, the role of which in tumor development has yet to be elucidated, in addition to several under expressed genes, the potential role of which in carcinogenesis has been described previously (Bagnoli *et al.*, Oncogene, *19:* 4754–4763, 2000; Yu *et al.*, Proc. Natl. Acad. Sci. USA, *96:* 214–219, 1999; Mok *et al.*, Oncogene, *12:* 1895–1901, 1996). The differential expression of a subset of these genes was confirmed by semiquantitative reverse transcription-PCR using glyceraldehyde-3-phosphate dehydrogenase (GAPDH) as control in a panel of 15 stage I and 15 stage III tumors of mixed histological subtypes. Chromosomal sorting of library sequences revealed that several of the genes mapped to known regions of deletion in ovarian cancer. Loss of heterozygosity (LOH) analysis revealed multiple genomic regions with a high frequency of loss in both early- and late-stage tumors. To determine whether loss of expression of some of the genes corresponds to loss of an allele by LOH, we used a microsatellite marker for one of the novel genes on 8q and have shown that loss of expression of this novel gene correlates with loss of an allele by LOH. In conclusion, our analysis has identified down-regulated genes, which map to known as well as novel regions of deletions and may represent potential candidate tumor suppressor genes involved in ovarian cancer.

INTRODUCTION

Each year approximately 16,000 American women succumb to ovarian cancer, the deadliest of all gynecological malignancies (1). Because ovarian cancer is frequently asymptomatic in its early stages, 75% of patients have advanced-stage disease at the time of diagnosis. However, if the disease is caught in an early stage, the five-year survival rate jumps to 92%, whereas the anticipated 5-year survival for patients with advanced stage disease is less than 20%. If stage I disease is a precursor of late-stage ovarian cancer, as is the case with many other tumor types, identifying molecular alterations in early-stage tumors should provide insights into developing strategies for early detection.

There are several PCR-based approaches to analysis of gene expression changes including mRNA DD-PCR[3] (2, 3), RNA fingerprinting by arbitrary primed-PCR (4, 5), and RDA (6–8). In RDA, several rounds of subtractions are needed. In addition, RDA does not resolve the problem of the wide differences in abundance of individual RNA species. Whereas DD-PCR and arbitrary primed-PCR are potentially faster methods of identifying expression differences between two populations, both of these methods have high levels of false positives and are biased for high-copy-number mRNAs. SSH (9–11) has the distinct advantage over other PCR-based techniques in that SSH is used to selectively amplify target cDNA fragments (differentially expressed) while simultaneously suppressing nontarget DNA amplification and generating a library of differentially expressed sequences. The normalization step equalizes the abundant cDNAs within a target population, and the subtraction step excludes the common sequences between the driver and tester populations.

In this study, we report on down-regulated genes identified from two early- and two late-stage primary ovarian tumors subtracted against normal ovarian epithelial cell brushings. Collectively our studies demonstrate that (*a*) several genes, identified in the SSH libraries as down-regulated genes, map to known regions of deletions in ovarian cancer; and (*b*) LOH analysis revealed novel regions of deletions not previously identified in early-stage tumors.

MATERIALS AND METHODS

Tissue Processing. All of the specimens were snap-frozen in the surgical pathology unit at the Mayo Clinic. The tumor content of the specimens was assessed by H&E-stained sections. Only specimens with >75% tumor content were used for all of the experiments. Twenty normal ovarian epithelial cell brushings from patients without cancer were pooled, and the epithelial nature of these brushings was verified by cytokeratin staining. Only brushings that contained >90% epithelial cell content were used. A majority of patients providing normal ovaries were between 45 and 65 years old and were undergoing incidental oophorectomy at the time of pelvic surgery for other indications. All of the ovaries were examined pathologically and found to be benign. The histology, grade, and stage of each tumor used in SSH library construction, semiquantitative RT-PCR, and LOH studies are listed in Table 1. Tumors were staged according to the criteria proposed by International Federation of Gynecology and Obstetrics.

Cell Culture. Five of seven ovarian-carcinoma cell lines (OV 167, OV 177, OV 202, OV 207, and OV 266) were low-passage primary lines established at the Mayo Clinic (12); SKOV-3 was purchased from American Type Culture Collection (Manassas, VA); OVCAR 5 is a NIH human ovarian cancer cell line (13). All cells were grown according to the supplier's recommendations.

Suppression Subtraction Libraries. Four down-regulated libraries were generated from individual tumors. OV 338 (stage I endometrioid), OV 402 (stage II serous), and two stage III serous tumors (OV 4 and OV 13) were all subtracted against normal ovarian epithelial cell brushings.

Tester and Driver Preparations. Total cellular RNA from primary ovarian tumors (driver) and from 20 pooled normal ovarian epithelial cell brushings (tester) was prepared using Trizol reagent (Life Technologies, Inc., Rockville, MD) followed by purification by RNAeasy kit (Qiagen Inc, Valencia, CA). The integrity of the RNA was assessed by agarose gel electrophoresis. One μg

Received 6/26/01; accepted 11/01/01.

The costs of publication of this article were defrayed in part by the payment of page charges. This article must therefore be hereby marked *advertisement* in accordance with 18 U.S.C. Section 1734 solely to indicate this fact.

[1] Supported by Department of Defense Grant DAMD 17-99-1-9504 (to V. S. and D. I. S.) and by the Mayo Foundation.

[2] To whom requests for reprints should be addressed, at Division of Experimental Pathology, Mayo Clinic/Foundation, 200 First Street SW, Rochester, MN 55905. Phone: (507) 266-2775; Fax: (507) 266-5193; E-mail: shridv@exrch.mayo.edu.

[3] The abbreviations used are: DD-PCR, differential display-PCR; RDA, representational difference analysis; SSH, suppression subtraction hybridization; LOH, loss of heterozygosity; RT-PCR, reverse transcription-PCR; GAPDH, glyceraldehyde-3-phosphate dehydrogenase; HSD3B1, hydroxy-δ-5-steroid dehydrogenase 3β-steroid δ-isomerase 1; EGR1, early growth response 1; EST, expressed sequence tag; NP, nested primer; OSE, ovarian surface epithelial cells.

Table 1 *Tumor cohort*

Histology	Stage	Grade	LOH	Northern	RT-PCR	SSH
Cl Cell[a] OV 106	I	3	−	−	+	−
Cl Cell OV 267	I	3	+	−	+	−
Cl Cell OV 496	I	3	+	−	+	−
Endo OV 51	I	3	+	−	+	−
Endo OV 78	I	3	+	−	+	−
Endo OV 88	I	3	−	−	+	−
Endo OV 105	I	3	+	−	+	−
Endo OV 338	I	3	+	+	+	+
Endo OV 647	I	3	+	+	+	−
Endo OV 684	I	3	+	−	−	−
Serous OV 6	I	3	−	−	+	−
Serous OV 17	I	3	−	−	+	−
Serous OV 20	I	3	−	+	+	−
Serous OV 90	I	3	+	−	+	−
Serous OV 234	I	3	+	−	+	−
Serous OV 363	I	3	−	−	+	−
Serous OV 526	I	3	−	−	+	−
Cl Cell OV 102	II	3	+	−	+	−
Endo OV 296	II	3	+	−	+	−
Serous OV 149	II	3	+	+	+	−
Serous OV 354	II	3	+	−	+	−
Serous OV 401	II	3	−	−	+	−
Serous OV 402	II	3	+	−	+	+
Serous OV 414	II	3	+	−	+	−
Cl Cell OV 176	III	3	+	−	+	−
Cl Cell OV 453	III	3	+	−	−	−
Cl Cell OV 623	III	3	+	−	−	−
Endo OV 93	III	3	+	+	+	−
Endo OV 110	III	3	+	−	+	−
Endo OV 259	III	3	+	−	+	−
Serous OV 4	III	3	+	+	+	+
Serous OV 11	III	3	+		+	−
Serous OV 13	III	3	+	+	+	+
Serous OV 16	III	3	+	−	+	−
Serous OV 29	III	3	+	−	+	−
Serous OV 150	III	3	+	−	+	−
Serous OV 167	III	3	+	−	+	−
Serous OV 182	III	3	+	−	+	−
Serous OV 206	III	3	+	−	+	−
Serous OV 208	III	3	+	−	+	−
Serous OV 461	III	3	+	−	+	−
Serous OV 472	III	3	−	−	+	−
Serous OV 97	IV	3	+	−	+	−

[a] Cl Cell, clear cell; +, tumors in which the specific analysis was performed; Endo, endometrioid.

of total RNA was then used for first- and second-strand cDNA synthesis in a 10-μl reaction volume using Smart II oligonucleotides and cDNA synthesis (CDS) primer (Clontech, Palo Alto, CA) following the manufacturer's instructions. The concentration of reverse-transcribed cDNA was adjusted to 25 ng/μl. The resulting cDNAs were amplified, and the cycle number was optimized for each sample after amplification with PCR primer (5′-AAGCAGTGGTAACAACGCAGAGT-3′). For cycle optimization, aliquots of the PCR reactions were removed after 15, 18, 21, and 24 cycles of amplifications. The resulting products were resolved on a 1.5% agarose gel, and optimum cycle number was chosen after southern hybridization with GAPDH and transferrin receptor genes as probes. For most samples, the optimum cycle numbers were between 17 and 19 cycles of amplification. The reaction was scaled up to generate 3 μg of double stranded cDNAs. The resulting cDNA was precipitated, washed with 70% ethanol, dissolved in 40 μl of deionized water, and digested with *Rsa*I in a 50-μl reaction mixture containing 100 units of enzyme (Boeringher Mannheim, Indianopolis, IN) for 3 h. The blunt-ended cDNAs were then purified using PCR purification columns (Promega, Madison, WI). The driver cDNAs from primary tumors were adjusted to 300 ng/μl in a final 7-μl volume. Fifty ng of digested double-stranded tester (normal ovarian epithelial cell brushings) cDNA was ligated in two separate reactions with 2 μl of adapter 1 (10 μM) and adapter 2 (10 μM; provided in the kit), respectively, and 1.0 unit of T4 DNA ligase (Life Technologies, Inc.) in a 10-μl total volume with buffer supplied by the manufacturer. After ligation, 1 μl of 0.2 M EDTA was added and the samples were heated at 75°C for 5 min to inactivate the ligase and stored at −20°C.

Subtractive Hybridization. SSH was performed between tester and driver mRNA populations using the PCR-select cDNA subtraction kit (Clontech) according to the manufacturer's recommendations. Two μl of driver double-stranded cDNA (150–200 ng/μl) was added to each of two tubes containing one μl of adapter-1 and adapter-2 ligated tester cDNA (10 ng) with 1× hybridization buffer in a total volume of 4 μl. The solution was overlaid with 10 μl of mineral oil and the cDNAs were denatured (1.5 min, 98°C) and allowed to anneal for 8–9 h at 68°C. After the first hybridization, the two samples were combined and an additional heat-denatured driver (300 ng) in 1× hybridization buffer was added. The sample was allowed to hybridize for another 16 h at 68°C. The final hybridization reaction was diluted with 200 μl of dilution buffer provided by the manufacturer, heated at 68°C for 7 min, and stored at −20°C.

PCR Amplification. For each subtraction, two PCR amplifications were performed. The primary PCR reaction in 25 μl contained 1 μl of subtracted cDNA, 1 μl of PCR primer1 (10 μM, 5′-CTAATACGACTCACTATGGGC-3′), and 0.5 μl each of 50× Advantage cDNA polymerase mix (Clontech) and 10 mM dNTP mix. The cycling parameters were 75°C for 7 min, followed by 27 cycles at 94°C for 30 s, 68°C for 30 s, and 72°C for 2 min. The amplified products were diluted 10-fold with deionized water and 2 μl were used in the secondary PCR reactions with NP1 and NP2 primers (provided in the kit). The cycling conditions were the same as in the primary PCR amplification, except the reactions were in a 50-μl volume for 11 cycles only, with a final extension cycle for 7 min at 68°C. The subtraction efficiency was determined by both PCR and-Southern based methods as instructed by the manufacturer.

Cloning and Analysis of the Subtracted cDNAs. Products from the secondary PCRs were inserted into PCR2.1-TOPO TA cloning kit (Invitrogen, Carlsbad, CA) following manufacturer's instructions. Prior to ligation, the subtracted cDNA mix was incubated for 1 h at 72°C with dATP and AmpliTaq DNA polymerase (Perkin-Elmer Cetus, Foster City, CA) to ensure that most of the cDNA fragments contained "A" overhangs. Approximately 100 ng of PCR-amplified cDNA were ligated into 50 ng of vector without further purification. Two μl of ligated products (10 ng of vector and 50 ng of cDNAs ligated in 10-μl volume) were transformed into 40 μl of DH10B cells by electroporation (Bio-Rad, Hercules, CA). Routinely, 50- and 200-μl aliquots of the transformed cells (grown in 1 ml of medium) were plated onto 150-mm Luria-Bertani/agar plates containing 100 μg/ml of ampicillin, with 100 μM isopropyl-1-thio-β-D-galactopyranoside (IPTG) and 50 μg/ml 5-bromo-4-chloro-3-indolyl-β-D-galactopyranoside (X-Gal) to discriminate white from blue colonies. The transformation efficiency was 2–4 × 10^6 colonies/μg of DNA.

Hybridization and Screening for Differentially Expressed Transcripts. The differential hybridization was performed initially on 96 randomly picked clones to determine subtraction efficiency. The inserts in the plasmid were amplified using NP-1 and NP-2 primers provided in the kit. The PCR conditions were 94°C for 4 min followed by 30 cycles of 94°C for 30 s, 60°C for 30 s, and 72°C for 2 min, followed by a final extension at 72°C for 5 min. The products of the PCR reactions were resolved on a 2% agarose gel run in duplicate. After Southern blotting of the amplified inserts onto Hybond N membranes (Amersham, Piscataway, NJ). The membranes were stained with methylene blue in 0.2× SSC and visualized to ensure complete transfer of all of the products. The blots were then hybridized with *Rsa*I-digested cDNA probes (reverse Northern). Fifty ng of *Rsa*I-digested tester and driver cDNAs were labeled using random primer labeling kit (Stratagene, LA Jolla, CA) with 50 μCi of [^{33}P]dCTP following manufacturer's instructions. Equal counts (1–2 × 10^7 cpm/μl) of the cDNA probes from normal and tumor tissues were heat-denatured and used to probe duplicate blots. Hybridization was performed at stringent conditions in 0.5 M Na_2PO_4 (pH 7.2), 7% SDS at 65°C. The next day, the filters were washed twice in 2× SSC, 0.5% SDS at 68°C, then once in 0.1% SSC, 0.1% SDS at 68°C, and exposed to phosphorimager screens overnight. The signal intensity of each spot in the membranes was compared between tester and driver hybridized duplicates. cDNA fragments displaying differential expression levels of >1.8-fold or higher were selected to estimate the efficiency of the differential hybridization.

Approximately 600–700 unique clones from each of the four libraries were successfully sequenced with M13 forward primer using an ABI Prism dye terminator cycle sequencing in the sequencing core at Millennium Predictive Medicine, Cambridge, MA. Sequences were compared with the National Center for Biotechnology Information sequence database using the BLAST program.

Semiquantitative RT-PCR. Fifty to 100 ng of reverse-transcribed cDNAs were used in a multiplex reaction with a pair of gene-specific primers and GAPDH forward (5′-ACCACAGTCCATGCCATCAC-3′) and reverse prim-

ers (5′-TCCACCACCCTGTTGCTTGTA-3′), which yield a 450-bp product. The PCR reaction mixes contained 50 mM Tris-HCl (pH 8.3), 1.5 mM $MgCl_2$, 400 μM gene-specific primers, 50 μM each of the GAPDH primers, and 0.5 units of Taq polymerase (Promega, Madison, WI), in a 12.5-μl reaction volume. The conditions for amplification were as follows: 94°C for three min, then 29 cycles of 94°C for 30 s, 50–62°C for 30 s depending on the gene-specific primers being tested, and 72°C for 30 s in a Perkin-Elmer-Cetus 9600 Gene-Amp PCR system. The products of the reactions were resolved on a 1.6% agarose gel. Band intensities were quantified using the Gel Doc 1000 photo-documentation system (Bio-Rad, Hercules, CA) and its associated software.

The following gene-specific primers were used: for CTSK, (forward) F-GGA GAT ACT GGA CAAC CCA CTG and (reverse) R-CCA ACT CCC TTC CAA AGT GC; for PAI1, F-AAT CGC AAG GCA CCT CTG AG and R-GAT CTG GTT TAC CAT CTT TT; for cyclin D2, F-AGC TGC TGT GCC ACG AGG T and R-ACT GGC ATC CTC ACA GGT C; for FGF7, F-TAA TGC ACA AAT GGA TAC and R-ATT GCC ATA GGA AGA AAG; for EGR1, F-GAC ACC AGC TCT CCA GCC TGC and R-GGA AGG GCT TCT GGT CTG GGG; for SPARC, F-CCA CTG AGG GTT CCC AGC AC and R-GGA AAC ACG AAG GGG AGG GT; for decorin, F-CCT GGT TGT GAA AAT ACA TGA and R-TGA CAT TAA CAA GAT TTT GCC; for THBS2, F-TGG TCA CCA GGA CAA AGA CAC and R-ATC CTG CCA GCA AGC TGA CA; for ITM2A, F-CGC AGC CCG AAG ATT CAC TAT G and R-CTT ATT ACC AAG GAC ACT CTA TCT; for PEG3, F-CGG AGA ACT GTG AGA AGC TCG TC and R-GGT GGG GCT AGG CTA GAA GG.

Northern Blot Analysis. Fifteen μg of total RNA was fractionated on 1.2% formaldehyde agarose gels and blotted in 1× SPC buffer [10 mM sodium phosphate (pH 6.8), 1 mM CDTA (Sigma Chemical Co., St. Louis, MO)] onto Hybond N membranes (Amersham, Piscataway, NJ). The control small ribosomal protein S9, (*RPS9*) and gene-specific probes were labeled using the random primer labeling system (Life Technologies, Inc., Gaithersburg, MD) and purified using spin columns (TE-100) from Clontech. Filters were hybridized at 68°C with radioactive probes in a microhybridization incubator (Model 2000, Robbins Scientific, Sunnyvale, CA) for 1–3 h in Express hybridization solution (Clontech, Palo Alto, CA) and washed according to the supplier's guidelines. The primers, F-GCA ACA TGC CAG TGG CCC GG and R-ATC CTC CTC CTC GTC GTC TC for RPS9 yield a 586-bp cDNA fragment, and the conditions for amplification are similar to the semiquantitative RT-PCR conditions described above.

LOH Analysis. Fifteen early- and 18 late-stage tumors of differing histologies (Table 1) were analyzed. The 15 early-stage tumors included 3 clear-cell, and 6 each of endometrioid and serous tumors. The 18 late-stage tumors included 3 clear- cell, 4 endometrioid, and 12 serous tumors. The markers (Research Genetics, Huntsville, AL) used in this study are listed in Table 1 along with their chromosomal locations. Two new microsatellite markers, one near Methylation Controlled J protein on 13q14.1 (14) and another marker within BAC CIT-B-470f8 on 19q14.3 (AC006115) are: *MCJ*-NF-5′-GATTGACCACAGTCTTATCT-3′ and *MCJ*-18–5′-TAA-GAGGTCTACTCATTGCTCAC-3′, and 19-F-5′-GCACCTGGCCCA-ACTGTAAC-3′ and 19R-5′-CCAGCTGCTGGCTCACCTT-3′, respectively. The individual oligonucleotides were synthesized in the Mayo Molecular Technology Core at the Mayo Clinic, Rochester, MN. The PCR reaction mix contained: 50 ng of genomic DNA, 50 mM KCl, 10 mM Tris-HCl (pH 8.3), 1.5 mM $MgCl_2$, 200 μM concentration of each primer, 0.05 μl of [^{32}P]dCTP (10 μCi/μl), and 0.5 units of Taq polymerase (Promega, Madison, WI) in a 10-μl reaction volume. The conditions for amplification were: 94°C for two min, then 30 cycles of 94°C for 30 s, 52–57°C for 30 s, and 72°C for 30 s in a Perkin-Elmer-Cetus 9600 Gene-Amp PCR system in a 96-well plate. PCR products were denatured and run on 6% polyacrylamide sequencing gels containing 8 M urea. The gels were dried and autoradiographed for 16–24 h and scored for LOH. Multiple exposures were used before scoring for LOH. Allelic imbalance indicative of LOH was scored when there was more than 50% loss of intensity of one allele in the tumor sample with respect to the matched allele from normal tissue. The evaluation of the intensity of the signal between the different alleles was determined by visual examination by two independent viewers (V. S. and J. S.).

RESULTS

In an attempt to identify novel tumor suppressor genes in ovarian cancer, we generated down-regulated cDNA libraries from two early-stage (stages I and II; OV 338 and OV 402) and two late-stage (stage III; OV 4 and OV 13) tumors subtracted against normal ovarian epithelial cell brushings. The libraries were monitored at each stage of library construction to ensure that the clones generated from each of the four libraries truly reflected differentially expressed sequences. The subtraction efficiency was determined by both Southern- and PCR-based protocols. Fig. 1, *A* and *B* show the subtraction efficiency of libraries OV 402 (*panel 1*) and OV 4 (*panel 2*) by Southern- and PCR-based methods (Fig. 1*B*), respectively. We estimated a 60- to 70-fold enrichment of the differentially expressed genes in all four libraries. This was confirmed with the Southern-based analysis, in which we saw a complete subtraction of GAPDH in the subtracted cDNAs (Fig. 1*A*).

We evaluated the differential expression of genes in each of the libraries by hybridizing tester and driver cDNAs to randomly amplify 96 cloned inserts by colony PCR. PCR products were resolved in duplicate. Care was taken to ensure equal loading of the PCR products onto 2% agarose gels to allow direct comparison of hybridization signal intensities (Fig. 2*A*). After transfer of the PCR products onto nylon membranes, we performed reverse Northern analyses to identify differentially expressed transcripts. The cDNA probes used for hybridization were restricted with *Rsa*I to minimize background hybridization. Faint signals representing rare transcripts could easily be distinguished with this approach (Fig. 2*B*). After densitometric analysis of each of the corresponding bands hybridized with tester and driver cDNAs, the percentage of these clones that showed the expected differential hybridization was 70–80%.

We sequenced ~2000 randomly picked clones from each of the four libraries. After consolidating for clones that appeared more than once in the libraries, we estimated that there were ~600 distinct clones sequenced from each of the four libraries.

Analysis of SSH Library Genes. To discern the differences in gene expression in early- *versus* late-stage tumors, we compared the genes in each of the libraries to one another to verify how many of the

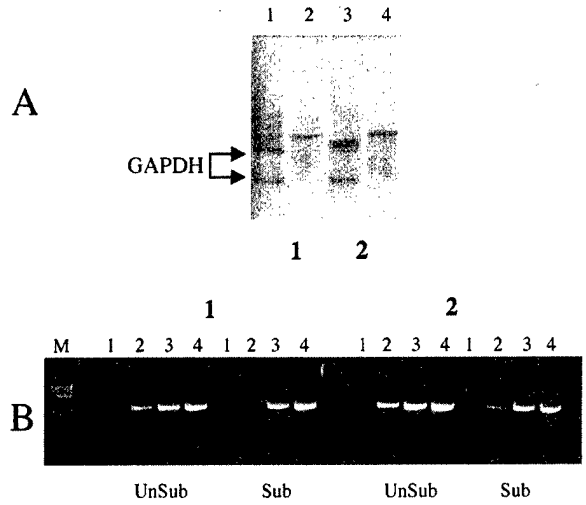

Fig. 1. *A*, Southern analysis: equal amounts of unsubtracted and subtracted cDNAs were fractionated on 2% agarose gel, blotted, and hybridized with [^{33}P]dCTP-labeled GAPDH. *Along bottom of image*: *1*, OV 402 library; 2, OV 4 library. *Lanes 1* and *3*, unsubtracted cDNAs; *Lanes 2* and *4*, subtracted cDNAs. *B*, PCR-based analysis: 10 ng of unsubtracted (*Unsub*) and subtracted (*Sub*) cDNAs were amplified with GAPDH primers as described in "Materials and Methods." *Uppermost numbers*, *1*, OV 402 library; 2, OV 4 library. *Lanes 1–4*, products after 18, 23, 28, and 32 cycles of GAPDH amplification; *M*, 100-bp ladder.

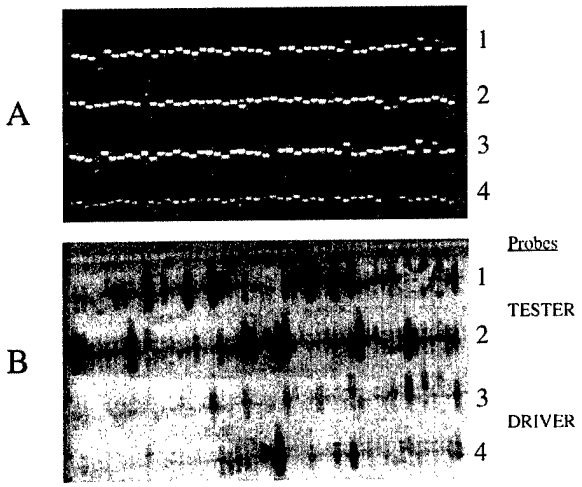

Fig. 2. *A*, products of colony PCR resolved on a 2% agarose gel. The gels were stained with ethidium bromide and photographed to ensure equal loading. Rows 1 and 3 and 2 and 4 are duplicates. *B*, duplicate filters hybridized with double-stranded P^{33}-tester (*rows 1* and *2*) and -driver (*rows 3* and *4*) cDNAs of equal specificity under the same conditions as described in "Materials and Methods."

differentially expressed genes were in common among these four libraries. Of the 600 or so distinct clones in each library, 45 genes were common to all four libraries (Table 2). These potentially represent genes that may consistently be down-regulated in both early- and late-stage ovarian tumors. Similar comparison of genes that were isolated from any three of four libraries revealed 80 common genes. There were 130 common genes in the two early-stage tumors. Sixty of these 130 genes were also present in one of the two late-stage tumors. A similar kind of analysis comparing sequences in the two late-stage libraries revealed that there were 210 genes that were common between them. Only 55 of 210 genes were also identified in either one of the two libraries generated from early-stage tumors.

Because we had randomly picked the clones for sequencing, we validated the differential expression of 20 genes ranging from clones that were highly represented to those that were infrequently occurring in the libraries to ensure that the sequences generated truly represented differentially expressed genes between normal and tumor cells. Initially, seven ovarian tumor cell lines were used for validation by semiquantitative RT-PCR with GAPDH as control. The expression profile of these genes in tumor cell lines was compared with short-term cultures of normal ovarian epithelial cells. Several of these genes showed complete loss of expression in a number of cell lines (Fig. 3*A*; Table 3). For example, *HSD3B1* (15), which was represented by only two clones in each of the four libraries, showed complete loss of expression in all of the seven tested cell lines (Table 4). However, *PAI1* (16), which appeared several times (100–140) in each of the two late-stage libraries, showed complete loss of expression in only two of seven cell lines. We also tested the differential expression of these genes in 20 early (I/II)-stage and 16 late (III/IV)-stage primary tumors of mixed histological subtypes by semiquantitative RT-PCR comparing them with normal epithelial cell brushings. The 20 early-stage tumors included 5 clear cell, 6 endometrioid, and 9 serous tumors. The late-stage tumors included 1 clear cell, 4 endometrioid, and 11 serous tumors (Table 1). Fig. 3*B* shows the results of this analysis for *PAI1* (16), *ITM2A* (17), *FGF7* (18), *PEG3* (19), and a novel gene on 8q.

In addition we tested the expression of *HSD3B1* and *PRSS11*, a serine protease with an insulin-like growth-factor-binding domain (20), in cell lines and primary tumors by Northern analysis (Fig. 4, *A* and *B*). *HSD3B1* showed complete loss of expression in all of the cell lines and the primary tumors. *PRSS11* showed complete loss of expression in four of seven cell lines in three of eight primary tumors. Lower levels of *PRSS11* expression was also detected in four of eight primary tumors. Control probe *RPS9* was hybridized to the cell line and primary tumor blots to indicate equal loading of RNA.

Chromosomal Sorting of SSH Genes. Genes from each of the four libraries were sorted based on their chromosomal positions. Several of the common genes identified in three or all four libraries mapped to known regions of deletions in ovarian cancer (21–24). For example, *ARHI* (*NOEY2*), a well-characterized imprinted tumor suppressor gene, with a reported LOH in 40–50% of ovarian cancer cases maps to 1p31 (25). In addition, *caveolin 1* (26), on 7q31.1–31.2, was identified in all four libraries that maps to a known region of deletion in ovarian cancer (27). Table 4 lists additional genes mapping to specific chromosomal regions of deletions in ovarian cancer. Of interest are chromosomal bands 5q31–32, 10q11, and 10q25.3–26.2, because several of the down-regulated genes, isolated from these bands, were common to three, or were in all four, of the libraries. The 5q31–32 genes are *catenin* (28), *FGF1* (29), *HDAC3* (30), *selenoprotein P, plasma1* (*SEPP1*; Ref. 31), testican (*SPOCK*; 32), *transcription elongation factor B* (*SIII*) *polypeptide-like* (*TCEB1L*; Ref. 33), *transforming growth factor*, β-induced, M_r 68,000 (*TGFβ1*); Ref. 34), *CDC23*, (35) *EGR1* (36), and *osteonectin* (*SPARC*; Ref. 37). Down-regulated genes from chromosomal band 10q11.2 and 10q25.3–26.2

Table 2 *Common down-regulated genes in all four libraries*
The unigene cluster identifications (IDs) and gene descriptions are included.

Cluster ID	Cluster title
Hs. 195851	Actin, α 2, smooth muscle
Hs. 180952	Actin, γ 1
Hs. 75442	Albumin
Hs. 4	Alcohol dehydrogenase 2, β polypeptide
Hs. 87268	Annexin, A8
Hs. 182183	Caldesmon
Hs. 83942	Cathepsin K
Hs. 74034	Caveolin 1
Hs. 169756	Complement component, 1 s subcomponent
Hs. 78065	Complement component 7
Hs. 76053	DEAD/H box polypeptide 5 (RNA helicase, M_r 68,000)
Hs. 76152	Decorin
Hs. 58419	DKFZP586L2024 protein
Hs. 181165	Eukaryotic translation elongation factor 1, α 1
Hs. 2186	Eukaryotic translation elongation factor 1, γ 1
Hs. 62954	Ferritin, heavy polypeptide 1
Hs. 89552	Glutathione *S*-transferase A2
Hs. 5662	G protein, β polypeptide 2-like 1
Hs. 83381	Guanine nucleotide binding protein 11
Hs. 3297	H. sapiens Uba80, mRNA for ubiquitin
Hs. 180532	Heat shock, M_r 90,000 protein 1, α
Hs. 158675	Heat shock factor binding protein 1
Hs. 155376	Hemoglobin, β
Hs. 75445	Hevin
Hs. 103391	IGFBP5
Hs. 38586	HSD3B1
Hs. 825	HSD3B2
Hs. 182187	IGF2
Hs. 107169	Insulin-like growth factor binding protein 5
Hs. 17109	Integral membrane protein 2A
Hs. 184914	KIAA0471-myosin heavy chain
Hs. 181357	Laminin receptor 1 (M_r 67,000, ribosomal protein SA)
Hs. 173714	MORF-related gene X
Hs. 153837	Myeloid cell nuclear differentiation antigen
Hs. 1255	Nuclear receptor subfamily 2, group F, member 2
Hs. 74615	PDGF, α polypeptide
Hs. 75111	PRSS11
Hs. 194695	Ras homolog gene family, member 1 (NOEY2)
Hs. 184108	Ribosomal protein L21
Hs. 180946	Ribosomal protein L5
Hs. 217493	Ribosomal protein S6
Hs. 151604	Ribosomal protein S8
Hs. 82448	Selectin L
Hs. 3314	Selenoprotein P, plasma, 1-histidine rich
Hs. 56306	Small proline-rich protein A
Hs. 46158	ESTs
Hs. 182643	Transcription factor B (SIII), polypeptide 1-like
Hs. 2064	Vimentin

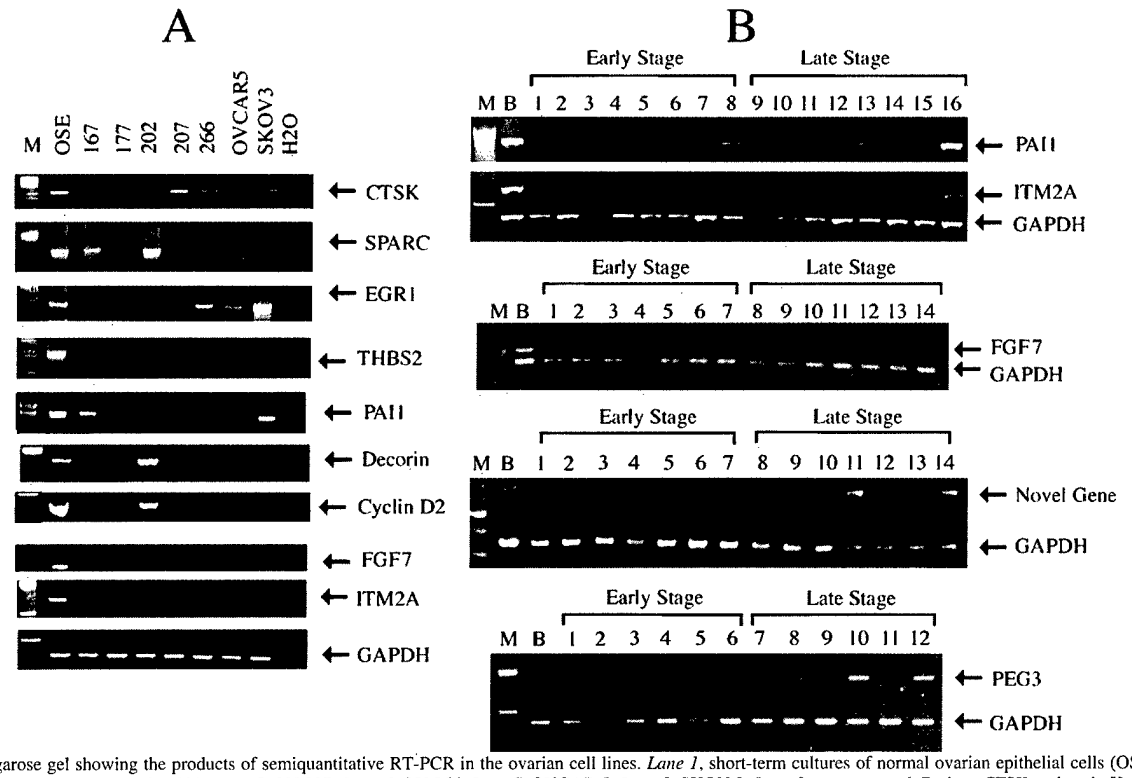

Fig. 3. *A*, agarose gel showing the products of semiquantitative RT-PCR in the ovarian cell lines. *Lane 1*, short-term cultures of normal ovarian epithelial cells (OSE 54); *Lane 2*, OV 167; *Lane 3*, OV 177; *Lane 4*, OV 202; *Lane 5*, OV 207; *Lane 6*, OV 266; *Lane 7*, OVCAR 5; *Lane 8*, SKOV 3; *Lane 9*, water control. Probes: *CTSK*, cathepsin K; *SPARC*; *EGR1*; *THBS2*, thrombospondin 2; *PAI1*, plasminogen activator inhibitor 1; *decorin*; *cyclin D2*; *FGF7*, fibroblast growth factor 7; *ITM2A*, integral membrane protein 2A; and *GAPDH*. *B*, agarose gel showing the products of the result of semiquantitative RT-PCR resolved on a 1.6% agarose gel. *Along top of the figure*, tumor sample numbers; *above top of the tumor numbers*, the staging information for these tumors. *Lane M*, 100-bp ladder; *Lane B*, normal epithelial cell brushings. *Panel 1*, *PAI1*, plasminogen activator inhibitor 1; *Panel 2*, *ITM2A*, integral membrane protein 2A; *Panel 3*, *FGF 7*, fibroblast growth factor 7; *Panel 4*, A novel gene; *Panel 5*, PEG3 and GAPDH .

that were identified from all four libraries were *annexin A8* (*ANXA8*; Ref. 38) and *PRSS11* (39), respectively. Other genes such as *nuclear receptor coactivator 4* (*ELE1*, 10q11.2; Ref. 40), *proteoglycan, secretory granule* (*PRG1*, 10q22.1; Ref. 41), *vinculin* (*VCL*, 10q22.1–23; Ref. 42), *lipase A* (*LIPA*, 10q23.3; Ref. 43), and *protein phosphatase regulatory (inhibitor) subunit 5* (*PPP1R5*, 10q23–24; Ref. 44) were identified only from the two late-stage libraries, OV 4 and OV 13.

LOH Analysis of Chromosomal Regions 1p, 6q, 7q, 8p, 9p, 10q, 13q, 17p, and 19q in Stage I/II and Stage III/IV tumors. Because many of the genes identified from the SSH libraries mapped to known regions of deletions in ovarian cancer, we analyzed a set of early- and late-stage tumors for LOH in regions of the genome to which some of the down-regulated genes mapped. The chromosomal locations of the markers and the potential down-regulated genes (identified in the SSH libraries) mapping to these regions are listed in Table 5. Fig. 5 shows the overall LOH profile obtained. Down-regulated genes mapping to chromosomal regions of loss identified from the libraries are *HSD3B1*, *EGR1*, *serum glucocorticoid kinase* (*SGK*; Ref. 45), and *forkhead* (*Drosophila*) *homologue 1* (*rhabdomyosarcoma*; *FRKH*; Ref. 46) mapping to 1p12–13, 5q31.1–31.2, 6q23.3, and 13q14.1, respectively. The approximate positions of these genes in relation to the markers of their respective chromosomes are also shown (Fig. 5). The chromosome 1p11–13 and 6q 23.3 markers showed a higher frequency of loss in late stage-tumors compared with early-stage tumors. Other markers on chromosomes 8, 9, and 10 also showed more losses in high-stage tumors. However, two markers on 5q31 and 13q14.1 and a marker within the BAC CIT-B-470f8 100-kb distal to the *PEG3* locus on 19q13.4 had a higher frequency of LOH in early- compared with late-stage tumors. Markers *D1S440*, *D1S534*, *D6S377*, and *D19S572* showed no LOH in early-stage tumors. To test whether loss, and/or lower levels, of expression of a gene corresponded to a region of loss, we used a microsatellite repeat present within intron 2 of a novel gene on 8q that was identified in this study to determine the frequency of LOH in these tumors. This marker showed 50% loss both in low- and high-stage tumors (Table 5; Fig. 5). Fig. 6 shows the pattern of LOH of this marker in ovarian tumors with the loss of expression of this gene. For example, as shown in Fig. 6, there was a direct correlation between lower levels of expression of this gene and loss of an allele by LOH (tumor numbers 684 and 208). In tumor with complete loss of expression and deletion of one of the alleles by LOH (tumor number 182), the remaining allele could be inactivated either by hypermethylation or by transcriptional inactivation as a result of other mechanisms. Tumors without LOH (tumors numbers 13 and 234) showed no loss of expression, as evidenced by semiquantitative RT-PCR.

Thus our LOH analysis revealed known and novel regions of loss to which down-regulated genes identified from the SSH libraries map, lending support to the strength of the SSH technique to identify genes with low levels of expression in tumors. Some of these genes could potentially represent candidate tumor suppressor genes involved in ovarian carcinogenesis.

DISCUSSION

This is the first report of down-regulated genes in SSH libraries generated from primary ovarian tumors. The concept of identifying differentially expressed genes has been used before in techniques such as DD-PCR and RDA. The strength of the SSH library is in the technique's ability to identify low-abundance transcripts. Although some of the genes identified from these libraries were also identified as down-regulated genes by transcriptional profiling of the same

Table 3 *Chromosomal localization of down-regulated genes from SSH libraries*

Chromosome	Down-regulated genes
1p12-13	*Hydroxy-δ-5-steroid dehydrogenase, 3 β- and steroid δ-isomerase 2*
1p12-13	Hydroxy-δ-5-steroid dehydrogenase, 3 β- and steroid δ-isomerase 1
1p31	Ras homolog gene family, member I
1q21	Cathepsin K (pycnodysostosis)
1q21-q22	Small proline-rich protein 2A
2q33-36	Insulin-like growth factor binding protein 5
2q33	Aldehyde oxidase 1
3p21.3	Ras homolog gene family, member A
4q12	Insulin-like growth factor binding protein 7
4q21.2	Alcohol dehydrogenase 2 (class I), β polypeptide
5q31	Selenoprotein P, plasma, 1
5q31	Early growth response 1
5q31	Secreted protein, acidic, cysteine-rich (osteonectin)
6p12.2	Glutathione S-transferase A2
6q23.3	Serum/glucocorticoid regulated kinase
6q27	Thrombospondin 2
7p15-13	Inhibin, β A (activin A, activin AB α polypeptide)
7q21.3-22	Plasminogen activator inhibitor, type I
7q31.1-31.2	Caveolin 1, caveolae protein, M_r 22,000
8p22-p21.3	Platelet-derived growth factor receptor-like
8q21	Novel gene
9p21	Ribosomal protein S6
9q11-q22	Annexin A1
10q24.3	Cytochrome P450, subfamily XVII (steroid 17-α-hydroxylase)
10q25.3-q26.2	Protease, serine, 11 (IGF binding)
11p15.5	Hemoglobin, β
11p15.5	Insulin-like growth factor 2 (somatomedin A)
12p13	Cyclin D2
12q23	Decorin
13q14.1	Forkhead (Drosophila) homolog 1 (rhabdomyosarcoma)
13q14.3	Integral membrane protein 2B
14q32.1	Protease inhibitor 1 (anti-elastase), α-1-antitrypsin
14q22-q24	Butyrate response factor 1 (EGF-response factor 1)
15q15-q21.1	Fibroblast growth factor 7 (keratinocyte growth factor)
15q15	Thrombospondin 1
16q13-q21	Matrix metalloproteinase 2 (gelatinase A, M_r 72,000)
16q24.2-q24.3	Cadherin 13, H-cadherin (heart)
17	ESTs
19q13.4	Paternally expressed gene 3
22q12.3	Tissue inhibitor of metalloproteinase 3
Xq13.3-Xq21.2	Integral membrane protein 2A
Xq21.1	ESTs

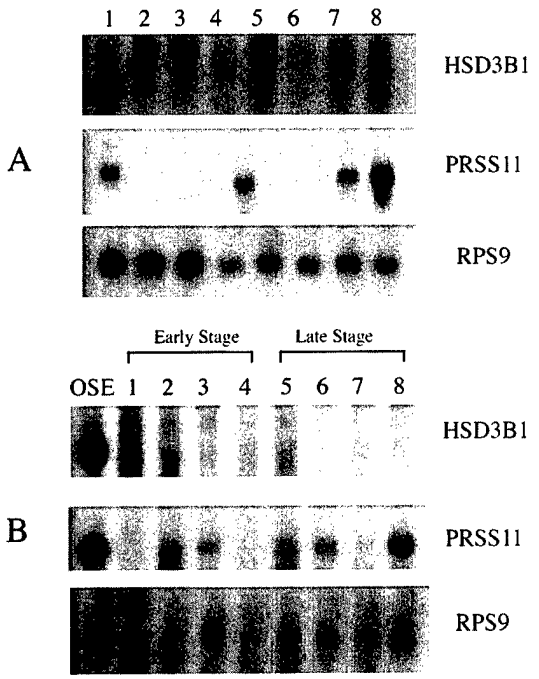

Fig. 4. Autoradiograph showing the Northern hybridization results with probes *HSD3B1* and *PRSS11*. *RPS9*, ribosomal protein S9. *A*, *cell lines*: OSE; *Lane 1*, OV167; *Lane 2*, OV 177; *Lane 3*, OV 202; *Lane 4*, OV 207; *Lane 5*, OV 266; *Lane 6*, OVCAR 5; *Lane 7*, SKOV3. *B*, primary tumors: *Lanes 1–4*, early-stage tumors; *Lanes 5–8*, late-stage tumors. The staging information for the primary tumors is listed in Table 1.

tumors (47), we identified several known and unknown genes of very low abundance only in the SSH libraries.

Analysis of the differentially expressed sequences from early and late tumors allowed us to compare the library sequences to one another. In the four SSH libraries, we identified several genes the function of which in carcinogenesis is known and others with no known roles in cancer. Some of the common genes, such as *tissue plasminogen activator inhibitor 1*, *SPARC*, *caveolin1*, and *NOEY2* have been demonstrated by others (16, 25, 26) to be differentially regulated in tumors. The potential tumor-associated function of genes such as *aldehyde oxidase*, *HSD3B1* and 2, *ITM2A*, *alcohol dehydrogenase 2* (48), *PRSS11*, and *PEG3* have not previously been linked with ovarian cancer. In addition, the function of several novel ESTs and genes identified from these libraries remain to be determined.

Table 4 *Results of semiquantitative RT-PCR analysis of down-regulated genes in ovarian cancer cell lines*

Genes	OSE	OV 167	OV 177	OV 202	OV 207	OV 266	OVCAR 5	SKOV 3	Chromosomal location
HSD3B1	+	−	−	−	−	−	−	−	1p13
CTSK	++	weak	−	−	−	−	−	−	1q21
IGFBP5	+	−	−	+	−	−	ND	ND	2q33-36
Hevin	+	−	−	−	−	−	−	−	4
SEPP1	+	+	+	−	−	+	+	+	5q31
TCEB1L	+	−	+	+	+	+	+	+	5q31
EGR1	+	weak	−	−	weak	+	weak	++	5q31
SPARC	+	−	−	weak	−	−	−	−	5q31
FGF1	+	−	−	−	+	−	−	+	5q31
Testican	+	−	+	+	+	−	+	−	5q31
THBS2	++	weak	−	−	−	−	−	−	6q27
PAI1	++	+	−	−	weak	weak	weak	+	7q21
Novel gene	+	+	−	+	−	−	−	−	8q21
PRSS11	++	−	−	+	−	−	+	+	10q25
Cyclin D2	+	−	−	+	−	−	−	−	12p13
Decorin	++	−	−	++	−	−	−	−	12q21.3
FGF7	+	−	−	+	−	−	−	−	15q15-21.1
PEG3	+		++	++	−	−	−	−	19q13.4
ITM2A	++	−	−	−	+	−	−	−	Xq13.3-21.1
Novel gene	+	−	−	−	−	−	−	−	Xq22

[a] +, presence of a product; −, Absence of a product; weak, presence of a weak product; ND, not determined.

Table 5 *Markers used for LOH analysis and % LOH in early- and late-stage tumors*

The numbers in parentheses are the number of tumors with LOH/total number of informative tumors.

Markers	% LOH in early-stage tumors	% LOH in late-stage tumors	Cytogenetic band location	Down-regulated genes from SSH libraries
D1S189	27 (4/15)	26 (5/17)	1p13.1	
D1S440	0 (0/13)	19 (3/16)	1p12	
D1S453	14 (2/14)	29 (5/17)	1p12	
D1S2863	27 (3/11)	29 (5/17)	1p12	*HSD3B1*
D1S534	0 (0/10)	22 (4/18)	1p11.2	
D1S514	14 (2/14)	33 (6/18)	1p11.2	
D5S396	50 (6/12)	50 (8/16)	5q31.1	*EGR1, SPARC*
D5S500	50 (5/10)	38 (5/13)	5q31.2	
D5S476	28 (2/7)	50 (6/12)	5q31.2	
D5S2119	30 (3/10)	25 (2/8)	5q31.2	
D6S311	0 (0/8)	54 (6/11)	6q23.1	*SGK*
D6S977	18 (2/11)	46 (6/13)	6q23.3	
D6S1008	10 (1/10)	37.5 (6/16)	6q25	
D7S1805	25 (2/8)	64 (7/11)	7q36	
D8S258	18 (2/11)	37.5 (6/16)	8p21	*PDGFRL 8q Novel Gene*
8q NG	50 (6/12)	50 (4/8)	8q	
D9S259	36 (5/14)	44 (8/18)	9p21	
D10S215	9 (1/11)	20 (3/15)	10q23.1	*LIPA, Actin α 2 smooth muscle (ACTA2)*
D10S574	21 (3/15)	17 (3/18)	10q23.3	
D17S1868	50 (4/8)	23 (3/13)	17q21.1	
D13S263	67 (6/9)	50 (9/18)	13q14.1	
MCJ[a]	62 (5/8)	46 (8/15)	13q14.1	*FKHR*
D19S180	17 (2/12)	28 (5/18)	19q13.3	
D19S572	0 (0/15)	14 (2/17)	19q13.3	
PEG3[a]	33 (4/12)	19 (3/16)	19q13.4	*PEG3*
D19S254	42 (5/12)	53 (9/17)	19q13.4	
D19S926	23 (3/13)	50 (8/16)	19q13.4	

[a] Primers are listed in the "Materials and Methods" section.

Some of these same genes have been identified as down-regulated genes by other techniques such as cDNA microarray analysis (47, 49) and DD-PCR (25).

It is a well-accepted concept that functional inactivation of both the alleles is a prerequisite for a tumor suppressor gene to be defined as such. The loss of expression of a gene could be caused by the deletion of both alleles (homozygous deletions), or deletion of one of the alleles and inactivation of the other allele either by inactivating mutations or by hypermethylation (50, 51) and/or by altered activity of a transcriptional repressor (52).

However, chromosomal sorting of ~600 genes and ESTs from each of the libraries revealed some interesting trends. Many of the genes identified from the SSH libraries were already mapped to known regions of deletions in ovarian cancer (21–24, 53, 54). We wanted to determine whether some of the known and novel genes identified from this screen would also map to regions of loss in ovarian cancer.

As evidenced in the LOH analysis, several of these coincided with regions of deletions observed in ovarian cancer. We identified several genes mapping to 5q31–32 in the SSH libraries. Of interest is *EGR1*, which has recently been identified as a down-regulated gene in ovarian cancer by cDNA microarray analysis (49). Two markers in the region, *D5S396* and *D5S500*, showed a high frequency of LOH in early-stage tumors not previously seen. *SPARC*, an acidic, cysteine-rich component of the extracellular matrix, is directly regulated by progesterone and dexamethasone and indirectly by cytokines (55). Mok *et al.* transfected the full length *SPARC* into SKOV3 cells and

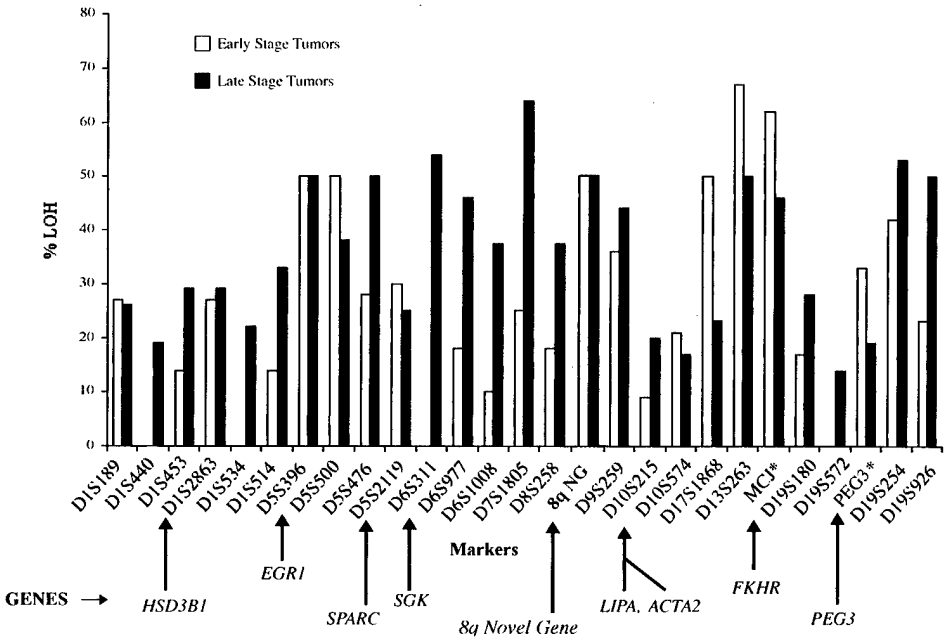

Fig. 5. Histogram of the results of LOH with the markers tested. □, early stage; ■, late stage. *% LOH* (on Y axis), frequency of LOH with specific markers. *Arrows*, approximate positions of these genes in relation to the markers on their respective chromosomes.

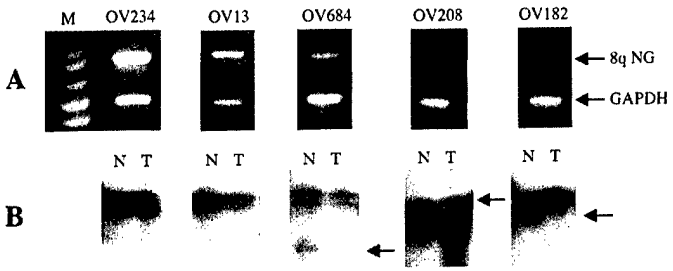

Fig. 6. *On top of the figure* for both *A* and *B*, tumor sample numbers. *A*, agarose gel showing the products of semiquantitative RT-PCR resolved on a 1.6% agarose gel. *M*, 1-kb-plus ladder; the top band is the product of amplification with novel gene (*8q NG*) primers. Bottom band is the product of amplification with GAPDH primers F (forward) and R (reverse). *B*, autoradiograph of LOH results of corresponding tumor samples with intron 2-associated microsatellite marker. *N*, normal DNA; *T*, tumor DNA; *arrow*, loss of the allele in the tumor.

showed both a reduced growth rate in cells expressing SPARC and a reduced ability of these cells to form tumors in nude mice, which lent support to *SPARC* as a tumor suppressor. *SPARC* was identified as a down-regulated gene in all four libraries from 5q31. Serum glucocorticoid kinase on 6q23.3, another region of deletion (23), was recently shown by Brunet *et al.* (56) to act in concert with Akt in phosphorylating forkhead transcription factor, *FKHRL1*. This phosphorylation event leads to the activation of the phosphatidylinositol 3-kinase cascade. Bagnoli *et al.* (52) have shown a reciprocal negative regulation of α folate receptor (αFR) and caveolin 1 (Cav-1, on 7q31.1) proteins providing evidence for a new mechanism of *Cav-1* silencing in ovarian cancer. As indicated above, comparison of some of the down-regulated genes identified from the libraries corresponded with chromosomal regions of loss identified from the LOH studies. A marker 100 kb distal to paternally expressed gene 3 on 19q13.4 that was identified in all four libraries showed a higher frequency of deletion in low-stage compared with high-stage tumors. This is the first report of such a high frequency of deletion (33%) in early-stage tumors in this region. Combining genomic with expression-based analysis, we were able to identify novel regions of loss in ovarian cancer. We have identified several known and novel genes, including ESTs, whose functions in cancer have yet to be discerned. These genes could potentially lead to the identification of candidate tumor suppressor genes involved in ovarian cancer.

However, not all of the down-regulated genes in these libraries could potentially represent tumor suppressor genes. This is essentially true for ribosomal genes. Other investigators also have reported the loss of expression of several ribosomal genes (Cancer Genome Anatomy Project-Digital Differential Display) in cancer and yet the functional consequence of loss of expression of these genes have not been directly linked to tumor suppression. Although some of the genes such as *ARHI, caveolin 1*, and *SPARC* that map to regions of deletions in ovarian cancer have known tumor-suppressing functions, for other genes, neither the mechanistic basis for the loss nor the functional consequence of such a loss is known. One of the novel genes identified in this screen showed 50% LOH in both early- and late-stage tumors. Using a microsatellite marker associated with this gene, we were able to correlate the loss and/or lower levels of expression of this gene with the loss of an allele by LOH.

The data from the SSH library analysis revealed that there were many genes that were differentially expressed in both early- and late-stage tumors. Genes identified in only one library could potentially indicate tumor-specific differences. We do not yet know what changes are critical in an early-stage tumor to progress to a more malignant tumor. The genes identified from the SSH libraries are all based on expression differences. This technique cannot detect gross genomic changes, including chromosomal rearrangements or the mutator phenotype (57), unless they result in concomitant changes in transcript levels of genes. However, one very important epigenetic phenomenon, namely, methylation (58, 59), has been associated with changes in the levels of gene expression. Evidence seems to indicate that methylation changes are early events in carcinogenesis leading to the possibility that the majority of the genes inactivated in early-stage tumors could be hypermethylated. Some of the genes isolated in this screen have been reported by others to be inactivated by hypermethylation in ovarian cancer (60, 61). For example, two of the down-regulated genes identified from chromosomal band 12p13 from the library sequences such as cyclin D2 (62) and complement component 1 subcomponent (63) do not map to known regions of deletion in ovarian cancer. These genes could be inactivated by methylation. The inactivation of cyclin D2 by methylation in Burkitt's lymphoma (62) and breast cancer (64) has previously been reported. Transcriptional inactivation can also result because of aberrant regulation of factors.

In conclusion, we have identified several known and several novel genes that are down-regulated both in early- and in late-stage tumors. Several of these genes were later mapped to the regions of loss by LOH analysis. However, we do not rule out the possibility that loss of expression of some of these genes could also be attributable to decreased transcriptional inactivation or through promoter hypermethylation. Thus, combining expression- and genomic-based analyses has provided us with novel regions of alterations in ovarian cancer not previously reported. We are currently pursuing the cloning and characterization of some of the novel genes identified from these libraries to address the functional roles of these genes in ovarian cancer.

ACKNOWLEDGMENTS

We acknowledge Dr. Kimberly Kalli, Mayo Clinic, Rochester, MN, for providing the cells from the short-term cultures of OSEs.

REFERENCES

1. Landis, S. H., Murray, T., Bolden, S., and Wingo, P. A. Cancer statistics, 1999. CA Cancer J. Clin., *49:* 8–31, 1999.
2. Liang, P., and Pardee, A. B. Differential display of eukaryotic messenger RNA by means of the polymerase chain reaction. Science (Wash. DC), *257:* 967–971, 1992.
3. Liang, X., Zhuang, G., and Fang, Q. The secretion and receptor gene of insulin-like growth factor-I quantitative expression in ovarian stroma in polycystic ovarian syndrome patients. Chung Hua Fu Chan Ko Tsa Chih, *32:* 582–585, 1997.
4. Rothschild, C. B., Brewer, C. S., and Offden, D. W. DD/AP-PCR: combination of differential display and arbitrarily primed PCR of oligo(dT) cDNA. Anal. Biochem., *245:* 48–54, 1997.
5. Peinado, M. A., Malkhosyan, S., Velazquez, A., and Perucho, M. Isolation and characterization of allelic losses and gains in colorectal tumors by arbitrarily primed polymerase chain reaction. Proc. Natl. Acad. Sci. USA, *89:* 10065–10069, 1992.
6. Lin, H., Pizer, E. S., and Morin, P. J. A frequent deletion polymorphism on chromosome 22q13 identified by representational difference analysis of ovarian cancer. Genomics, *69:* 391–394, 2000.
7. Yuan, L., Shan, J., De Risi, D., Broome, J., Lovecchio, J., Gal, D., Vinciguerra, V., and Xu, H. P. Isolation of a novel gene, *TSP50*, by a hypomethylated DNA fragment in human breast cancer. Cancer Res., *59:* 3215–3221, 1999.
8. Watson, J. E., Gabra, H., Taylor, K. J., Rabiasz, G. J., Morrison, H., Perry, P., Smyth, J. F., and Porteous, D. J. Identification and characterization of a homozygous deletion found in ovarian ascites by representational difference analysis. Genome Res., *9:* 226–233, 1999.
9. Ye, Z., and Connor, J. R. Identification of iron responsive genes by screening cDNA libraries from suppression subtractive hybridization with antisense probes from three iron conditions. Nucleic Acids Res., *28:* 1802–1807, 2000.
10. Diatchenko, L., Lau, Y. F., Campbell, A. P., Chenchik, A., Moqadam, F., Huang, B., Lukyanov, S., Lukyanov, K., Gurskaya, N., Sverdlov, E. D., and Siebert, P. D. Suppression subtractive hybridization: a method for generating differentially regulated or tissue-specific cDNA probes and libraries. Proc. Natl. Acad. Sci. USA, *93:* 6025–6030, 1996.
11. Diatchenko, L., Lukyanov, S., Lau, Y. F., and Siebert, P. D. Suppression subtractive hybridization: a versatile method for identifying differentially expressed genes. Methods Enzymol., *303:* 349–380, 1999.
12. Conover, C. A., Hartmann, L. C., Bradley, S., Stalboerger, P., Klee, G. G., Kalli, K. R., and Jenkins, R. B. Biological characterization of human epithelial ovarian

carcinoma cells in primary culture: the insulin-like growth factor system. Exp. Cell Res., *238:* 439–449, 1998.
13. Hamilton, T. C., Young, R. C., and Ozols, R. F. Experimental model systems of ovarian cancer: applications to the design and evaluation of new treatment approaches. Semin. Oncol., *11:* 285–298, 1984.
14. Shridhar, V., Bible, K. C., Staub, J., Avula, R., Lee, Y. K., Kalli, K., Huang, H., Hartmann, L. C., Kaufmann, S. H., and Smith, D. I. Loss of expression of a new member of the DNAJ protein family confers resistance to chemotherapeutic agents used in the treatment of ovarian cancer. Cancer Res., *61:* 4258–4265, 2001.
15. Morissette, J., Rheaume, E., Leblanc, J. F., Luu-The, V., Labrie, F., and Simard, J. Genetic linkage mapping of HSD3B1 and HSD3B2 encoding human types I and II 3 β-hydroxysteroid dehydrogenase/δ5-δ4-isomerase close to D1S514 and the centromeric D1Z5 locus. Cytogenet. Cell Genet., *69:* 59–62, 1995.
16. Bajou, K., Noel, A., Gerard, R. D., Masson, V., Brunner, N., Holst-Hansen, C., Skobe, M., Fusenig, N. E., Carmeliet, P., Collen, D., and Foidart, J. M. Absence of host plasminogen activator inhibitor 1 prevents cancer invasion and vascularization. Nat. Med., *4:* 923–928, 1998.
17. Kirchner, J., and Bevan, M. J. ITM2A is induced during thymocyte selection and T cell activation and causes down-regulation of CD8 when overexpressed in CD4(+)CD8(+) double positive thymocytes. J. Exp. Med., *190:* 217–228, 1999.
18. Jacquemier, J., Sun, Z. Z., Penault-Llorca, F., Geneix, J., Devilard, E., Adelaide, J., and Birnbaum, D. FGF7 protein expression in human breast carcinomas. J. Pathol., *186:* 269–274, 1998.
19. Kim, J., Bergmann, A., and Stubbs, L. Exon sharing of a novel human zinc-finger gene, *ZIM2*, and paternally expressed gene 3 (*PEG3*). Genomics, *64:* 114–118, 2000.
20. Zumbrunn, J., and Trueb, B. Localization of the gene for a serine protease with IGF-binding domain (PRSS11) to human chromosome 10q25.3-q26.2. Genomics, *45:* 461–462, 1997.
21. Allan, G. J., Cottrell, S., Trowsdale, J., and Foulkes, W. D. Loss of heterozygosity on chromosome 5 in sporadic ovarian carcinoma is a late event and is not associated with mutations in APC at 5q21–22. Hum. Mutat., *3:* 283–291, 1994.
22. Cliby, W., Ritland, S., Hartmann, L., Dodson, M., Halling, K. C., Keeney, G., Podratz, K. C., and Jenkins, R. B. Human epithelial ovarian cancer allelotype. Cancer Res., *53:* 2393–2398, 1993.
23. Shridhar, V., Staub, J., Huntley, B., Cliby, W., Jenkins, R., Pass, H. I., Hartmann, L., and Smith, D. I. A novel region of deletion on chromosome 6q23.3 spanning less than 500 Kb in high-grade invasive epithelial ovarian cancer. Oncogene, *18:* 3913–3918, 1999.
24. Bicher, A., Ault, K., Kimmelman, A., Gershenson, D., Reed, E., and Liang, B. Loss of heterozygosity in human ovarian cancer on chromosome 19q. Gynecol. Oncol., *66:* 36–40, 1997.
25. Yu, Y., Xu, F., Peng, H., Fang, X., Zhao, S., Li, Y., Cuevas, B., Kuo, W. L., Gray, J. W., Siciliano, M., Mills, G. B., and Bast, R. C., Jr. NOEY2 (*ARHI*), an imprinted putative tumor suppressor gene in ovarian and breast carcinomas. Proc. Natl. Acad. Sci. USA, *96:* 214–219, 1999.
26. Engelman, J. A., Zhang, X. L., and Lisanti, M. P. Genes encoding human caveolin-1 and -2 are co-localized to the *D7S522* locus (7q31.1), a known fragile site (FRA7G) that is frequently deleted in human cancers. FEBS Lett., *436:* 403–410, 1998.
27. Huang, H., Reed, C. P., Mordi, A., Lomberk, G., Wang, L., Shridhar, V., Hartmann, L., Jenkins, R., and Smith, D. I. Frequent deletions within FRA7G at 7q31.2 in invasive epithelial ovarian cancer. Genes Chromosomes Cancer, *24:* 48–55, 1999.
28. Bugert, P., Von Knobloch, R., and Kovacs, G. Duplication of two distinct regions on chromosome 5q in non-papillary renal-cell carcinomas. Int. J. Cancer, *76:* 337–340, 1998.
29. Crickard, K., Gross, J. L., Crickard, U., Yoonessi, M., Lele, S., Herblin, W. F., and Eidsvoog, K. Basic fibroblast growth factor and receptor expression in human ovarian cancer. Gynecol. Oncol., *55:* 277–284, 1994.
30. Wen, Y. D., Perissi, V., Staszewski, L. M., Yang, W. M., Krones, A., Glass, C. K., Rosenfeld, M. G., and Seto, E. The histone deacetylase-3 complex contains nuclear receptor corepressors. Proc. Natl. Acad. Sci. USA, *97:* 7202–7207, 2000.
31. Holben, D. H., and Smith, A. M. The diverse role of selenium within selenoproteins: a review. J. Am. Diet. Assoc., *99:* 836–843, 1999.
32. Charbonnier, F., Perin, J. P., Mattei, M. G., Camuzat, A., Bonnet, F., Gressin, L., and Alliel, P. M. Genomic organization of the human *SPOCK* gene and its chromosomal localization to 5q31. Genomics, *48:* 377–380, 1998.
33. Conaway, J. W., Bradsher, J. N., Tan, S., and Conaway, R. C. Transcription factor SIII: a novel component of the RNA polymerase II elongation complex. Cell. Mol. Biol. Res., *39:* 323–329, 1993.
34. Cardillo, M. R., Yap, E., and Castagna, G. Molecular genetic analysis of TGF-β1 in ovarian neoplasia. J. Exp. Clin. Cancer Res., *16:* 49–56, 1997.
35. Zhao, N., Lai, F., Fernald, A. A., Eisenbart, J. D., Espinosa, R., Wang, P. W., and Le Beau, M. M. Human *CDC23*: cDNA cloning, mapping to 5q31, genomic structure, and evaluation as a candidate tumor suppressor gene in myeloid leukemias. Genomics, *53:* 184–190, 1998.
36. Du, B., Fu, C., Kent, K. C., Bush, H., Jr., Schulick, A. H., Kreiger, K., Collins, T., and McCaffrey, T. A. Elevated egr-1 in human atherosclerotic cells transcriptionally represses the transforming growth factor-β type II receptor. J. Biol. Chem., *275:* 39039–39047, 2000.
37. Brown, T. J., Shaw, P. A., Karp, X., Huynh, M. H., Begley, H., and Ringuette, M. J. Activation of SPARC expression in reactive stroma associated with human epithelial ovarian cancer. Gynecol. Oncol., *75:* 25–33, 1999.
38. Liu, D., Rudland, P. S., Sibson, D. R., Platt-Higgins, A., and Barraclough, R. Expression of calcium-binding protein S100A2 in breast lesions. Br. J. Cancer, *83:* 1473–1479, 2000.
39. Hu, S. I., Carozza, M., Klein, M., Nantermet, P., Luk, D., and Crowl, R. M. Human HtrA, an evolutionarily conserved serine protease identified as a differentially expressed gene product in osteoarthritic cartilage. J. Biol. Chem., *273:* 34406–34412, 1998.
40. Klugbauer, S., Demidchik, E. P., Lengfelder, E., and Rabes, H. M. Molecular analysis of new subtypes of ELE/RET rearrangements, their reciprocal transcripts and breakpoints in papillary thyroid carcinomas of children after Chernobyl. Oncogene, *16:* 671–675, 1998.
41. Mattei, M. G., Perin, J. P., Alliel, P. M., Bonnet, F., Maillet, P., Passage, E., Mattei, J. F., and Jolles, P. Localization of human platelet proteoglycan gene to chromosome 10, band q22.1, by *in situ* hybridization. Hum. Genet., *82:* 87–88, 1989.
42. Mulligan, L. M., Gardner, E., Telenius, H., and Ponder, B. A. Complementary physical and genetic techniques map the vinculin (*VCL*) gene on chromosome 10q. Genomics, *13:* 1347–1349, 1992.
43. Anderson, R. A., and Sando, G. N. Cloning and expression of cDNA encoding human lysosomal acid lipase/cholesteryl ester hydrolase. Similarities to gastric and lingual lipases. J. Biol. Chem., *266:* 22479–22484, 1991.
44. Permana, P. A., Luczy-Bachman, G., and Bogardus, C. Protein targeting to glycogen/PPP1R5: screening of coding and flanking genomic regions for polymorphisms and association analysis with insulin action in Pima Indians. Biochem. Biophys. Res. Commun., *258:* 184–186, 1999.
45. Brennan, F. E., and Fuller, P. J. Rapid upregulation of serum and glucocorticoid-regulated kinase (*sgk*) gene expression by corticosteroids *in vivo*. Mol. Cell. Endocrinol., *166:* 129–136, 2000.
46. Davis, R. J., Bennicelli, J. L., Macina, R. A., Nycum, L. M., Biegel, J. A., and Barr, F. G. Structural characterization of the *FKHR* gene and its rearrangement in alveolar rhabdomyosarcoma. Hum. Mol. Genet., *4:* 2355–2362, 1995.
47. Shridhar, V., Lee, J., Pandita, A., Iturria, S., Avula, R., Staub, J., Morrissey, M., Calhoun, E., Sen, A., Kalli, K., Keeney, G., Roche, P., Cliby, W., Lu, K., Schmandt, R., Mills, G. B., Bast, R. C., Jr., James, C. D., Couch, F. J., Hartmann, L. C., Lillie, J., and Smith, D. I. Genetic analysis of early- *versus* late-stage ovarian tumors. Cancer Res., *61:* 5895–5904, 2001.
48. Yokoyama, A., Muramatsu, T., Omori, T., Yokoyama, T., Matsushita, S., Higuchi, S., Maruyama, K., and Ishii, H. Alcohol and aldehyde dehydrogenase gene polymorphisms and oropharyngolaryngeal, esophageal and stomach cancers in Japanese alcoholics. Carcinogenesis (Lond.), *22:* 433–439, 2001.
49. Welsh, J. B., Zarrinkar, P. P., Sapinoso, L. M., Kern, S. G., Behling, C. A., Monk, B. J., Lockhart, D. J., Burger, R. A., and Hampton, G. M. Analysis of gene expression profiles in normal and neoplastic ovarian tissue samples identifies candidate molecular markers of epithelial ovarian cancer. Proc. Natl. Acad. Sci. USA, *98:* 1176–1181, 2001.
50. Yakicier, M. C., Legoix, P., Vaury, C., Gressin, L., Tubacher, E., Capron, F., Bayer, J., Degott, C., Balabaud, C., and Zucman-Rossi, J. Identification of homozygous deletions at chromosome 16q23 in Aflatoxin B1 exposed hepatocellular carcinoma. Oncogene, *20:* 5232–5238, 2001.
51. Watanabe, T., Nakamura, M., Yonekawa, Y., Kleihues, P., and Ohgaki, H. Promoter hypermethylation and homozygous deletion of the *p14ARF* and *p16INK4a* genes in oligodendrogliomas. Acta Neuropathol., *101:* 185–189, 2001.
52. Bagnoli, M., Tomassetti, A., Figini, M., Flati, S., Dolo, V., Canevari, S., and Miotti, S. Downmodulation of caveolin-1 expression in human ovarian carcinoma is directly related to α-folate receptor overexpression. Oncogene, *19:* 4754–4763, 2000.
53. Sato, N., Tsunoda, H., Nishida, M., Morishita, Y., Takimoto, Y., Kubo, T., and Noguchi, M. Loss of heterozygosity on 10q23.3 and mutation of the tumor suppressor gene *PTEN* in benign endometrial cyst of the ovary: possible sequence progression from benign endometrial cyst to endometrioid carcinoma and clear cell carcinoma of the ovary. Cancer Res., *60:* 7052–7056, 2000.
54. Watson, R. H., Neville, P. J., Roy, W. J., Jr., Hitchcock, A., and Campbell, I. G. Loss of heterozygosity on chromosomes 7p, 7q, 9p and 11q is an early event in ovarian tumorigenesis. Oncogene, *17:* 207–212, 1998.
55. Mok, S. C., Chan, W. Y., Wong, K. K., Muto, M. G., and Berkowitz, R. S. SPARC, an extracellular matrix protein with tumor-suppressing activity in human ovarian epithelial cells. Oncogene, *12:* 1895–1901, 1996.
56. Brunet, A., Park, J., Tran, H., Hu, L. S., Hemmings, B. A., and Greenberg, M. E. Protein kinase SGK mediates survival signals by phosphorylating the forkhead transcription factor FKHRL1 (FOXO3a). Mol. Cell. Biol., *21:* 952–965, 2001.
57. Loeb, K. R., and Loeb, L. A. Significance of multiple mutations in cancer. Carcinogenesis (Lond.), *21:* 379–385, 2000.
58. Jones, P. A., and Laird, P. W. Cancer epigenetics comes of age. Nat. Genet., *21:* 163–167, 1999.
59. Robertson, K. D., and Jones, P. A. DNA methylation: past, present and future directions. Carcinogenesis (Lond.), *21:* 461–467, 2000.
60. Luo, R. Z., Peng, H., Xu, F., Bao, J., Pang, Y., Pershad, R., Issa, J. P., Liao, W. S., Bast, R. C., Jr., and Yu, Y. Genomic structure and promoter characterization of an imprinted tumor suppressor gene *ARHI*. Biochim. Biophys. Acta, *1519:* 216–222, 2001.
61. Kawakami, M., Staub, J., Cliby, W., Hartmann, L., Smith, D. I., and Shridhar, V. Involvement of H-cadherin (CDH13) on 16q in the region of frequent deletion in ovarian cancer. Int. J. Oncol., *15:* 715–720, 1999.
62. Sinclair, A. J., Palmero, I., Holder, A., Peters, G., and Farrell, P. J. Expression of cyclin D2 in Epstein-Barr virus-positive Burkitt's lymphoma cell lines is related to methylation status of the gene. J. Virol., *69:* 1292–1295, 1995.
63. Leytus, S. P., Kurachi, K., Sakariassen, K. S., and Davie, E. W. Nucleotide sequence of the cDNA coding for human complement C1r. Biochemistry, *25:* 4855–4863, 1986.
64. Evron, E., Umbricht, C. B., Korz, D., Raman, V., Loeb, D. M., Niranjan, B., Buluwela, L., Weitzman, S. A., Marks, J., and Sukumar, S. Loss of cyclin D2 expression in the majority of breast cancers is associated with promoter hypermethylation. Cancer Res., *61:* 2782–2787, 2001.

MS#4

THE JOURNAL OF BIOLOGICAL CHEMISTRY
Vol. 278, No. 25, Issue of June 20, pp. 23107–23117, 2003
Printed in U.S.A.

Loss of HSulf-1 Up-regulates Heparin-binding Growth Factor Signaling in Cancer*

Received for publication, March 3, 2003, and in revised form, April 8, 2003
Published, JBC Papers in Press, April 9, 2003, DOI 10.1074/jbc.M302203200

Jinping Lai‡, Jeremy Chien§, Julie Staub§, Rajeswari Avula§, Eddie L. Greene¶, Tori A. Matthews¶, David I. Smith§, Scott H. Kaufmann‖, Lewis R. Roberts‡**, and Viji Shridhar§**‡‡**

From the ‡Mayo Clinic Cancer Center and Divisions of Gastroenterology and Hepatology, §Experimental Pathology, ¶Nephrology, and ‖Oncology Research, Mayo Clinic and Foundation, Rochester, Minnesota 55905

Emerging data suggest that signaling by heparin-binding growth factors is influenced by the sulfation state of *N*-acetylglucosamine residues of heparan sulfate proteoglycans (HSPGs). Here we report that the recently identified protein HSulf-1, a heparin-degrading endosulfatase, encodes a cell surface-associated enzyme that diminishes sulfation of cell surface HSPGs. The message encoding this enzyme is readily detectable in a variety of normal tissues, including normal ovarian surface epithelial cells, but is undetectable in 5 of 7 ovarian carcinoma cell lines and markedly diminished or undetectable in ~75% of ovarian cancers. Similar down-regulation is also observed in breast, pancreatic, renal cells, and hepatocellular carcinoma lines. Re-expression of HSulf-1 in ovarian cancer cell lines resulted in diminished HSPG sulfation, diminished phosphorylation of receptor tyrosine kinases that require sulfated HSPGs as co-receptors for their cognate ligands, and diminished downstream signaling through the extracellular signal-regulated kinase pathway after treatment with fibroblast growth factor-2 or heparin-binding epidermal growth factor. Consistent with these changes, HSulf-1 re-expression resulted in reduced proliferation as well as sensitivity to induction of apoptosis by the broad spectrum kinase inhibitor staurosporine and the chemotherapeutic agent cisplatin. Collectively, these observations provide evidence that HSulf-1 modulates signaling by heparin-binding growth factors, and HSulf-1 down-regulation represents a novel mechanism by which cancer cells can enhance growth factor signaling.

HSPGs[1] are major constituents of the extracellular matrix, where they act as important mediators of adhesion as well as modulators of growth factor signaling and proteolysis (1, 2). These biological effects result, in part, from the binding of polypeptides to the highly sulfated glycosaminoglycan chains of HSPGs. In some cases, this binding requires sulfation of specific sites on the glycosaminoglycan chains. Previous work, for example, has suggested that specific sulfate groups play critical roles in the interactions between heparin, FGF, and the FGF receptor (3, 4). In particular, the *N*- and 2-*O*-sulfate groups of heparin are essential for its binding to FGF-2, whereas the 6-*O*-sulfate groups are required for stimulation of FGFR-1 (5, 6).

The sulfation state of HSPGs is classically thought to reflect the activity of sulfotransferases that are active during HSPG biosynthesis. Dhoot *et al.* (7), however, previously identified the quail sulfatase QSulf-1 as a developmentally regulated protein that modulates Wnt signaling by altering HSPG sulfation. Unlike many other sulfatases, which are lysosomal enzymes, QSulf-1 was localized on the cell surface (7). These observations raise the possibility that signaling by other HB-GFs might be modulated by cell surface sulfatase expression.

Morimoto-Tomita *et al.* (8) recently utilized the EST KIAA1077 to identify HSulf-1 as a human homolog of QSulf-1. Upon expression in Chinese hamster ovary cells, HSulf-1 reportedly is released into the medium, where it catalyzes endoglucosamine-6-sulfatase activity (8). Further analysis by PCR demonstrated that HSulf-1 mRNA was expressed in a variety of tissues, including ovary, although the size of the transcripts and the possibility of alternative splice forms was not investigated (8).

In a recent study, we performed suppression subtraction hybridization analyses of two early and late stage tumors subtracted against normal ovarian epithelial brushings, and we demonstrated that the mRNA corresponding to KIAA1077 is down-regulated (9). In view of the report of Dhoot *et al.* (7) identifying Qsulf-1 as a modulator of Wnt signaling, this observation raised the possibility that KIAA1077 down-regulation might alter growth factor signaling in ovarian cancer. Current understanding suggests that generation of the neoplastic phenotype requires multiple genetic or epigenetic changes that increase proliferation, inhibit apoptosis, and enhance cell invasiveness (10). Of interest in the present context is the observation that enhanced signaling by certain "growth factors" can simultaneously stimulate proliferation and inhibit apoptosis (11–13). Elevated expression of and signaling by growth factors that activate the mitogen-activated kinase path-

* This work was supported by Department of Defense Grant DAMD17-99-1-9504 (to V. S., D. I. S, and S. H. K.), a John W. Anderson Foundation grant (to V. S.), and the Mayo Foundation. The costs of publication of this article were defrayed in part by the payment of page charges. This article must therefore be hereby marked "*advertisement*" in accordance with 18 U.S.C. Section 1734 solely to indicate this fact.

** These senior authors contributed equally to this work.

‡‡ To whom correspondence should be addressed: Division of Experimental Pathology, Mayo Foundation, 200 First St. SW, Rochester, MN 55905. Tel.: 507-266-2775; Fax: 507-266-5193; E-mail: shridv@exrch.mayo.edu.

[1] The abbreviations used are: HSPGs, heparan sulfate proteoglycans; DAPI, 4′,6-diamidino-2-phenylindole dihydrochloride; EGFR, epidermal growth factor receptor; ERK, extracellular signal-regulated kinase; EST, expressed sequence tag; FITC, fluorescein isothiocyanate; GFP, green fluorescent protein; HB-GFs, heparin-binding growth factors; 4-MUS, 4-methylumbelliferyl sulfate; PBS, phosphate-buffered saline; UTR, untranslated region; RT, reverse transcriptase; GAPDH, glyceraldehyde-3-phosphate dehydrogenase; HMEC, human mammary epithelial cells; HS-GAG, heparan sulfate glycosaminoglycan; FGF, fibroblast growth factor; FGFR, FGF receptor; CDTA, 1,2-cyclohexylenedinitrilotetraacetic acid; TRITC, tetramethylrhodamine isothiocyanate; LOH, loss of heterozygosity.

TABLE I
Primers used in LOH analysis

Sequences	Location within the gene	Product size	% LOH (no. samples with LOH/ no. informative samples)
		bp	
CA1F-5′ CATCTCCATGTCTGAACTTC 3′ CA1R-5′ ACCTCTTCCTTCAACCTCTG 3′	5′ UTR 13 CA repeats	379	46% (4/9)
CA2F-5′ GTCCCTTGTAATGATAATAAG 3′ CA2R-5′ GAAGACCAAAGTGGCATC 3′	Intron 1 21 CA repeats	275	47% (7/15)
CA3F-5′ GAGTAAGAAGAGATATTGGAG 3′ CA3R-5′ CCTAGCTGTGTGGATCATTGC 3′	Intron 2 11 CA repeats	247	53% (9/17)
CA4F-5′ CGAACTCCTGACCTCAAGTG 3′ CA4R-5′ CAGAGGGTGGGTGCAGAGTC 3′	Intron 3-1 24 CA repeats	212	50% (4/7)
CA5F-5′ TAGAATACCTGCACTTCACTG 3′ CA5R-5′ GAAGACCAAAGTGGCATC 3′	Intron 3-2 10 GAAG repeats	193	50% (10/20)

way, including FGF and HB-EGF, have been seen frequently in ovarian cancers and other solid tumors (14–20). Moreover, activation of the ERK pathway has been implicated in enhanced proliferation as well as resistance to apoptosis (21, 22). As a result, there is considerable interest in understanding the factors that contribute to activation of this pathway as well as mechanisms that can reverse this activation.

In this report, we describe the widespread down-regulation of HSulf-1 in cancer cell lines and ovarian cancer specimens. To examine the functional consequences of this down-regulation, we re-expressed HSulf-1 in two ovarian cancer cell lines that lack this message. Results of this analysis suggest that HSulf-1 is a cell surface sulfatase that diminishes HSPG sulfation, thereby modulating signaling by HB-GFs. Consistent with this conclusion, we demonstrate diminished ERK pathway activation after treatment with FGF-2 and HB-EGF, diminished proliferation, and enhanced drug-induced apoptosis in ovarian cancer cell lines in which HSulf-1 is re-expressed. These observations not only provide new insight into the function of HSufl-1, but also suggest that its down-regulation is a previously unidentified mechanism by which cancer cells enhance growth factor signaling.

MATERIALS AND METHODS

Cell Culture—OV167, OV177, OV202, OV207, and OV266 ovarian cancer cell lines and the short term cultures of the normal ovarian epithelium were established at the Mayo Clinic (23). The ovarian cancer cell lines OVCAR-5 and SKOV-3, as well as breast (BT474, MCF-7, MCF-10A, MDA-MB-157, MDA-MB-361, MDA-MB-435, UACC812, and UACC893), pancreas (AsPc1, BxPc3, CAPAN 1, CAPAN 2, CFPAC-1, and Mia), kidney (HTB45, HTB49, and CRL 1633), and hepatocellular carcinomas (Hep3B, HepG2, HUH7, HSNU182, SNU387, SNU423, SNU449, SNU475, SKHep1 and PLC5) were from American Type Culture Collection (Manassas, VA). Normal human mammary epithelial Cells (HMEC) were from Clonetics Corp. (San Diego). All cells were grown according to the providers' recommendations.

Drugs and Reagents—Staurosporine (Sigma) and UCN-01 (Drug Synthesis Branch, NCI, National Institutes of Health) were dissolved in Me_2SO at a concentration of 1 mM, stored at −20 °C, and subsequently diluted with serum-free medium before use. In all experiments the concentration of Me_2SO did not exceed 0.1%. Cisplatin (Sigma) was prepared immediately before use as a 1000-fold concentrated solution in Me_2SO. Fibroblast growth factor, heparin-stabilized FGF, and heparin-binding epidermal growth factors (Sigma) were dissolved in water.

Cloning of HSulf-1 cDNA and Gene—BLAST search of the isolated sequence from SSH libraries of early and late stage tumors identified ESTs homologous to KIAA1077 in the dbEST. The homologous ESTs were assembled into a contig with the use of Sequencher 3 software (Gene Codes Corp, Ann Arbor, MI). Additional 5′ sequences not present in KIAA1077 were obtained with electronic walking by assembling overlapping EST sequences in the genome BLAST server. The integrity of the full-length cDNA obtained by this electronic walking was confirmed by PCR analysis using PCR primers flanking each junction between EST clones.

For expression of truncation mutants of HSulf-1, the N-terminal portion of HSulf-1 (N-Sulf) containing only the sulfatase domain was amplified using primers NF (5′-ATTGGACCAAATACAATGAAG-3′) and NRFlg (ttaagccttgtcatcgtccttgtagtcGAATGTATCACGCCAAAT), where the lowercase letters encode the FLAG epitope. The C-terminal portion of HSulf-1 (C-Sulf) was amplified using primers CF (5′-CGTGATACATTCCTAGTGG) and CRFlg (ttaagccttgtcatcgtccttgtagtcACCTTCCCATCCATCCCA) with a stop codon introduced after the epitope tag. The full-length HSulf-1 was amplified using primers NF and CRFlg using Expand™ Long Template PCR system (Roche Applied Science). All three products were cloned into GFP Fusion TOPO® TA Expression plasmid (Invitrogen). For generating a full-length HSulf-1/GFP fusion construct, the stop codon of CRFlg was not included. cDNAs generated from short term cultures of normal ovarian surface epithelial cells were used as a template for generating PCR products for cloning. The products of each PCR were resolved on a 1.6% agarose gel and purified using a gel extraction kit (Qiagen, Valencia, CA) for cloning into expression vectors.

Establishment of Stable Transfectants—Exponentially growing SKOV3 cells in 100-mm dishes were washed with serum-free medium and treated with a mixture containing 4 μg of plasmid, 30 μl of LipofectAMINE, and 20 μl of Plus reagent. After 3 h of incubation, complete medium with serum was added. G418 (400 μg/ml) was added 24 h later to select transfectants. Individual colonies were subsequently cloned using cloning cylinders. For controls, cells were similarly transfected with vector (pcDNA3.1 GFP-CT); and stable clones were selected.

Semi-quantitative RT-PCR—Total RNA was extracted from 7 ovarian cancer cell lines and 30 primary ovarian tumors using the RNeasy mini kit (Qiagen). cDNA synthesis was performed as described (9). 50–100 ng of reverse-transcribed cDNA was used in a multiplex reaction with three different primer pairs Sulf-1F (5′-CCACCTTCATCAATGCCTT-3′) and Sulf-1R (5′-CCTTGACCAGTCCAAACCTGC-3′), Sulf-2F (5′-CATCATTTACACCGCCGACC) and Sulf-2R (5′-CTGCCGTCTCTTCTCCTTC-3′), Sulf-3F (5′-GAGCCATCTTCACCCATTCAA-3′) and Sulf-3R (5′-TTCCCAACCTTATGCCTTGGGT-3′), and GAPDH-F (5′-ACCACAGTCCATGCCATCAC-3′) and GAPDH-R (5′-TCCACCACCCTGTTGCTTGTA-3′) in separate reactions to yield 760-, 1260-, and 825-bp products, respectively. The PCR mixes contained 50 mM KCl, 10 mM Tris-HCl (pH 8.3), 1.5 mM $MgCl_2$, 400 μM concentration of each primer for HSulf-1 and 50 μM for the GAPDH primers, and 0.5 units of *Taq* polymerase (Promega) in a 12.5-μl reaction volume. The conditions for amplification are as follows: 94 °C for 3 min followed by 29 cycles of 94 °C for 30 s, 58 °C for 30 s, and 72 °C for 30 s in a PerkinElmer Life Sciences 9600 Gene-Amp PCR system. The products of the reaction were resolved on a 1.6% agarose gel and photographed using the Gel Doc 1000 photo documentation system.

LOH Analysis—The 5 pairs of microsatellite markers within the *HSulf-1* gene used in this study are listed in Table I along with their locations within the *HSulf-1* gene. Amplifications were performed as described (9) except that annealing was performed at 52–57 °C, and reactions were run in a 96-well plate. After denaturation, PCR products were run on 6% polyacrylamide sequencing gels containing 8 M urea. Gels were dried, subjected to autoradiography using multiple exposure

times, and scored for LOH. Allelic imbalance indicative of LOH was scored, and a >50% loss of intensity of one allele in the tumor sample with respect to the matched allele from normal tissue was observed.

Northern Blot—Total RNA (15 μg) was fractionated on 1.2% formaldehyde agarose gels and blotted in 1× SPC buffer (20 mM Na_2HPO_4, 2 mM CDTA (pH 6.8)) onto Hybond-N membranes (Amersham Biosciences). The probes were labeled using the random primer labeling system (Invitrogen) and purified using spin columns (100 TE) from Clontech. Filters were hybridized at 68 °C with radioactive probes in a hybridization incubator and washed according to the manufacturer's guidelines.

Analysis of Apoptosis—Apoptosis was quantitated by assessing the number of cells containing nuclear changes indicative of apoptosis (chromatin condensation and nuclear fragmentation) after staining with DAPI. HSulf-1-transfected SKOV3 cells were seeded in 35-mm plates at a density of 2×10^5 cells/well. After incubation at 37 °C for 24 h, the plates were washed and changed to serum-free medium. Staurosporine was added to a final concentration of 1 μM for 5 h. DAPI was then added to each well at a final concentration of 5 μg/ml. After a 20-min incubation in the dark at 20 °C, cells were examined by fluorescence microscopy (Nikon Eclipse TE200; Nikon Corp., Tokyo, Japan) using excitation and emission filters of 380 and 430 nm. An individual blinded to the experimental conditions counted at least 300 cells in six different high power fields for each treatment. Each treatment was repeated at least three times, performed in triplicate each time. To inhibit apoptosis, the cells were pretreated with 40 μM *N*-(*N*$^{\alpha}$-benzyloxycarbonylvalinylalanyl) aspartic acid (*O*-methyl ester) fluoromethyl ketone for 1 h before the addition of staurosporine. The significance of differences between experimental variables was determined using the Student's *t* test.

Proliferation Assays—SKOV3 parental cells and cells stably transfected with empty vector were plated at 100,000 cells/10-cm disk in triplicate in complete medium. After trypsinization, the total number of trypan blue-excluding cells was determined daily for 5 days.

Treatment with FGF-2, HB-EGF, and EGF—To assess the role of HSulf-1 in HB-GF-mediated signaling, vector-transfected and HSulf-1 clones 7 and 8 were serum-starved for 8–12 h, treated with diluent, 10 ng/ml FGF-2, 100 ng/ml HB-EGF (Sigma), or 10 ng/ml EGF for the times indicated in individual figures. Following treatment, cells were rinsed with ice-cold PBS, scraped from the dishes, and lysed at 4 °C in SDS sample buffer without bromphenol blue. Protein concentrations were determined with bicinchoninic acid (Pierce).

Immunoblotting—Equal amounts of protein (20 μg/lane) were separated by electrophoresis on an SDS gel containing a 4–12% acrylamide gradient and electrophoretically transferred to nitrocellulose. Blots were washed once with TBS, 0.2% Tween 20 (TBST) and blocked with TBST containing 5% non-fat dry milk for 1 h at 20 °C. The blocking solution was replaced with a fresh solution containing a 1:500 dilution of rabbit anti-phospho-ERK (Cell Signaling Inc., Beverly, MA). After overnight incubation at 4 °C, the blots were washed three times for 10 min each in TBS, 0.1% (w/v) Tween 20 and incubated with horseradish peroxidase-conjugated secondary antibody in 5% milk/TBST at 20 °C for 1 h. After washing 3 times in TBST, the proteins were visualized using enhanced chemiluminescence (Amersham Biosciences). The blots were stripped and reprobed with antisera that recognize total ERK, EGFR phosphorylated on Tyr^{1068} and/or Tyr^{992}, total EGFR (all from Cell Signaling Inc., Beverly, MA), or mouse monoclonal anti-actin (Sigma).

Sulfatase Assay—Confluent flasks of stable transfectants were washed in ice-cold PBS and lysed in SIE buffer (250 mM sucrose, 3 mM imidazole (pH 7.4), 1% ethanol) containing 1% (w/v) Nonidet P-40 and protease inhibitor mixture (Roche Applied Science). After cells were sheared by passage through a 20-gauge needle, protein concentration was determined using the Bradford assay. 100 μg of total cellular protein was preincubated with 10 μM estrone 3-*O*-sulfamate (Sigma) at 37 °C for 1 h to inhibit steroid sulfatases. 4-MUS was then added to a final concentration of 10 mM in the presence of 10 mM lead acetate in a total volume of 200 μl. After incubation for 24 h at 37 °C, the reaction was terminated by addition of 1 ml of 0.5 M Na_2CO_3/$NaHCO_3$ (pH 10.7). The fluorescence of the liberated 4-methylumbelliferone was measured using excitation and emission wavelengths of 360 and 460 nm, respectively. To assess the effects of transient transfection, SKOV3 cell lysates prepared 48 h after transfection with empty vector, full-length HSulf-1 cDNA, or mutant N-Sulf were assayed as described above except that the incubation was shortened to 3.5 h.

HSulf-1 Localization—SKOV3 cells seeded on glass coverslips were allowed to adhere overnight and then transfected with empty vector or cDNA encoding full-length HSulf-1 fused at its C terminus to GFP. 24 h after transfection, cells were fixed in 4% paraformaldehyde, permeabilized with 0.2% Triton X-100, and mounted with Vectorshield® mounting medium containing DAPI. The GFP fusion protein was visualized using a Zeiss LS510 laser scanning confocal microscope. Alternatively, SKOV3 cells were transfected with 4 μg of plasmid encoding FLAG-tagged HSulf-1, incubated for 24 h, washed with PBS, fixed for 10 min in PBS containing 3.7% formaldehyde and 1% sucrose, washed with 0.1 M glycine in PBS, permeabilized with PBS containing 0.4% Triton X-100 and 2% bovine serum albumin for 20 min, and washed three times in washing buffer (PBS containing 0.2% bovine serum albumin and 0.1% Triton X-100). After incubation for 1 h at 20 °C with anti-EGFR antibody, cells were washed four times with washing buffer, incubated with 1:200 TRITC-conjugated anti-rabbit IgG and 1:200 FITC-conjugated anti-FLAG monoclonal antibody (Sigma) in the dark, washed twice in washing buffer, stained with 0.5 μg/ml DAPI for 5 min, washed twice in PBS, and viewed with an Axiovert 35 epifluorescence microscope (Carl Zeiss, Thornwood, NY) equipped with a 100-watt mercury lamp or a Zeiss LSM510 confocal microscope.

HSulf-1 Distribution—48 h after transfection of cDNA encoding GFP-tagged HSulf-1 into SKOV3 parental cells, cells and medium were collected separately. The cells were washed in ice-cold PBS, scraped, and lysed at 4 °C in SDS buffer without bromphenol blue. Protein concentrations were determined with bicinchoninic acid (Pierce). Conditioned medium was concentrated in a Centricon 10 microconcentrator (Millipore Corp). The cell lysate and 50× concentrated medium were resolved on 7.5% SDS-polyacrylamide gels under reducing conditions. Immunoblotting was performed as described above using anti-GFP antibody (Santa Cruz Biotechnology).

Sulfation State of Cell Surface HS-GAGs—Cells growing on coverslips for 24 h were fixed in methanol for 10 min at −20 °C, washed with PBS, and incubated for 1 h at 20 °C with 1:30 dilution of mouse 10E4 antibody, which recognizes an epitope that includes the *N*-sulfated glucosamine residue (Seikagaku America, Falmouth, MA). After washing, cells were stained with FITC-conjugated anti-mouse IgG and examined by laser scanning confocal microscopy as described above. As a control, cells were stained with antibody 3G10, which recognizes nonglycosylated glycosaminoglycans. In brief, cells grown on coverslips for 24 h were fixed in 4% paraformaldehyde at 37 °C for 20 min, washed, preincubated in buffer containing 50 mM sodium acetate (pH 7.0), 100 mM NaCl, and 3.3 mM $CaCl_2$ at 37 °C for 1 h, and followed by incubation with 20 milliunits/ml of heparitinase I (Sigma) for 1.5 h at 37 °C. After thorough washing, cells were incubated with a 1:250 dilution of 3G10 monoclonal antibody (Seikagaku America) for 2 h at 37 °C followed by FITC-conjugated anti-mouse IgG and examined as described above.

RESULTS

Characterization of the HSulf-1 cDNA and Gene—Differential screening of suppression subtraction cDNA libraries generated from primary ovarian tumors subtracted against normal ovarian epithelial cells previously identified an EST homologous to KIAA1077 (9) as a transcript that is down-regulated in ovarian cancer. In order to study the function of the corresponding polypeptide, the cDNA and gene were cloned as described under "Materials and Methods."

After HSulf-1 was assembled into a contig using Sequencher 3 software, a 5696-bp cDNA containing a single open reading frame encoding an 871-amino acid polypeptide was isolated (GenBank™ accession number AF545571). The predicted amino acid sequence is identical to that recently reported for HSulf-1 (8). Based on the computer algorithm Signal P version 1.1 at the Centre for Biological Sequence Analysis website (24), a 22-amino acid signal peptide (MKYSCCALVLAVLGTELLGSLC ↓ ST) is found at the N terminus, with the most likely cleavage site indicated by ↓. The transmembrane prediction program TMPRED (25) predicts two additional membrane-spanning domains at amino acids 69–88 and 754–779. The cDNA contains five potential polyadenylation signals AATAAA at positions 4170, 4679, 4820, 4824, 5052, and 5678.

The *HSulf-1* gene spans ~211-kb genomic fragment on chromosome 8q13.3. Our analysis of the cDNA and gene agree with that reported by Morimoto-Tomita *et al.* (8) with one notable exception. Morimoto-Tomita *et al.* (8) reported the presence of a 280-bp noncoding exon in the 5′-UTR that they called exon 1

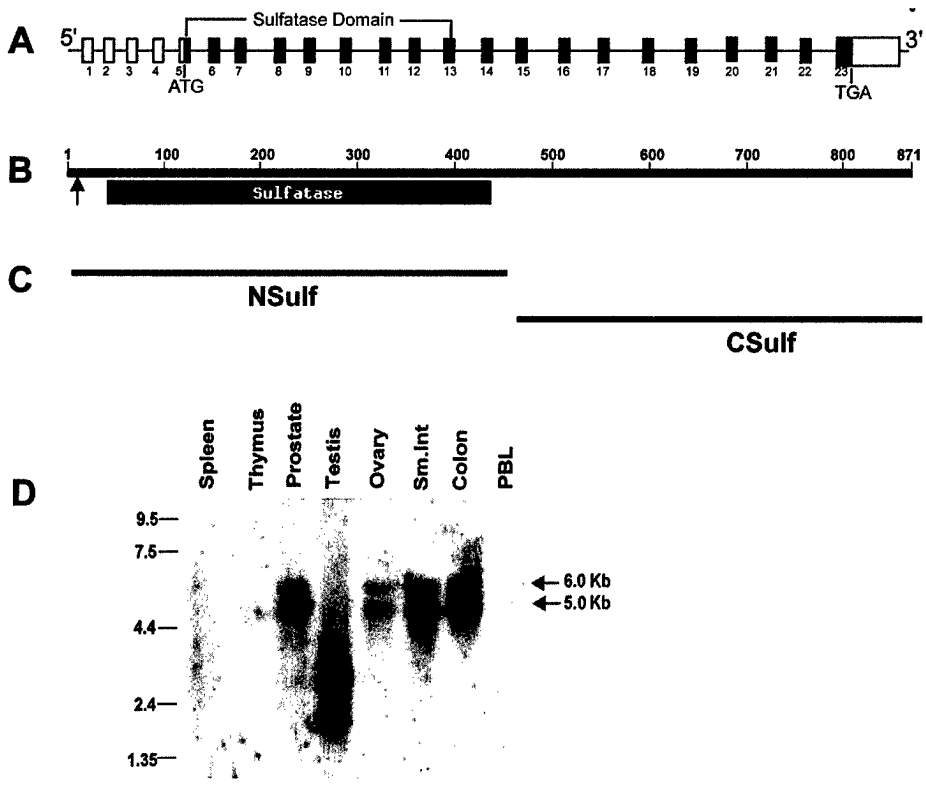

FIG. 1. **Genomic structure, domain structure, and expression profile of HSulf-1.** *A*, schematic representation of genomic structure of HSulf-1. The *numbered boxes* indicate exons; the *horizontal lines* indicate introns. The coding exons are indicated by *black boxes* and noncoding exons by *open boxes*. Not shown is the 280-bp exon reported by Morimoto-Tomito *et al.* (8) listed in Table III as exon 1A, as RT-PCR fails to demonstrate the transcription of this exon in mRNA from a variety of tissues. The sulfatase domain spans exons 5–13. *B*, HSulf-1 ORF is predicted to encode an 871-amino acid polypeptide with a 22-amino acid long signal peptide and 410-amino acid long sulfatase domain at the N terminus. *C*, portions of the polypeptide encoded by the truncation mutants N-Sulf and C-Sulf, which are utilized in subsequent experiments. *D*, multiple tissue Northern blot (Clontech, Palo Alto, CA) probed using radiolabeled full-length HSulf-1 ORF. The *arrows* point to the two different splice forms of HSulf-1 in prostate, ovary, small intestine, and colon. *PBL*, peripheral blood leukocytes. Testis expresses tissue-specific transcripts.

(8), and we will denote exon 1A. In addition to this sequence, we have identified two other noncoding exons, one 5′ to this exon (314 bases, which we call exon 1) and another 3′ to this sequence (165 bases, which we call exon 2). To determine which of these exons, 1, 1A, or 2, are present in transcribed message, primers in exons 1 and 5 were utilized to amplify a 950-bp 5′-UTR from normal ovarian epithelial cells, HMEC, and normal kidney. All of the cDNAs amplified lacked exon 1A. Instead, two different splice variants were amplified, a less abundant one lacking exon 1A but containing exons 1 and 2, and a more abundant one lacking both exon 1A and exon 2 (data not shown).

HSulf-1 Is Widely Expressed in Normal Tissue—Northern blot analysis using full-length HSulf-1 cDNA as a probe (Fig. 1*D*) revealed a 6.0-kb and a smaller 5.0-kb transcript. Expression was observed in all nonlymphoid tissues but was highest in small intestine, pancreas, and colon. Importantly, the blot shown in Fig. 1*D* contains message from total ovary. Further analysis (Fig. 2, *A* and *B*) demonstrated that HSulf-1 message was readily detected in purified human ovarian surface epithelial cells. Testis appears to express tissue-specific splice variants that have not been characterized further.

Decreased HSulf-1 Expression in Primary Ovarian Cancers—Because KIAA1077 was initially identified as a down-regulated transcript in SSH libraries of ovarian cancer, we next evaluated HSulf-1 expression ovarian cancer cell lines and primary tumor specimens. Although semi-quantitative PCR (Fig. 2, *A*, *C*, and *E*, *lane 1*) and Northern blotting (Fig. 2*B*) readily detected HSulf-1 mRNA in all normal ovarian surface epithelial samples examined, the message was undetectable in 5 of 7 ovarian cancer cell lines (Fig. 2, *A* and *B*). Moreover, semi-quantitative RT-PCR with overlapping primers spanning the entire HSulf-1 open reading frame (illustrated in Fig. 2*C* and summarized in Table II) demonstrated that HSulf-1 down-regulation is common in primary ovarian cancer specimens. In particular, HSulf-1 mRNA was undetectable in 40% of samples and extremely weak in another 37%. Among the histological subtypes of ovarian cancer, clear cell cancers have a particularly poor prognosis (26) and uniformly lack detectable HSulf-1 expression (Fig. 2*C* and Table II).

To begin to assess the mechanism by which HSulf-1 expression might be decreased in ovarian cancer, LOH analysis was performed. Genomic sequence analysis revealed microsatellite markers in the 5′-UTR, introns 1 and 2, and two within intron 3. The primers flanking these repeats are shown in Table I. Analysis in 30 primary ovarian tumor samples revealed that LOH of these markers ranged from 44 to 53% (Fig. 2*D*).

Decreased HSulf-1 Expression in Other Tumor Types—To assess the possibility that loss of HSulf-1 expression might be unique to ovarian cancer cells (Fig. 2, *A–C*), semi-quantitative RT-PCR was performed using cancer cell lines of breast, pancreas, kidney, and liver origin. For these studies, normal HMEC and normal kidney (Fig. 2*E*, *lanes 1* and *16*) served as positive controls. Results of this analysis revealed that the majority of cancer cell lines had either a complete loss or markedly diminished expression of HSulf-1 (Fig. 2*E*), raising the possibility that down-regulation of this transcript might be relatively widespread among epithelial malignancies. However, MCF10A cells derived from fibrocystic breast generally regarded as relatively normal (27) also had a complete loss of HSulf-1 expression, possibly implicating HSulf-1 loss as an early event in mammary carcinogenesis.

HSulf-1 Encodes an Active Sulfatase—To begin to analyze the function of HSulf-1, full-length cDNA was stably transfected into two lines lacking detectable message, SKOV3 and OV207, and multiple clones were isolated. Analysis by RT-PCR demonstrated varying levels of message within the clones (Fig. 3*A*). Both sets of lines were utilized in the analyses presented below.

To determine whether the stable transfectants exhibited sulfatase activity, cell lysates from clones displaying abundant HSulf-1 message were incubated with the fluorogenic substrate 4-MUS in the presence of estrone 3-*O*-sulfamate to specifically inhibit endogenous steroid sulfatase activity (Fig. 3, *B* and *C*). By using this nonspecific sulfatase substrate, an increase in activity comparable with that reported by Morimoto-Tomita *et*

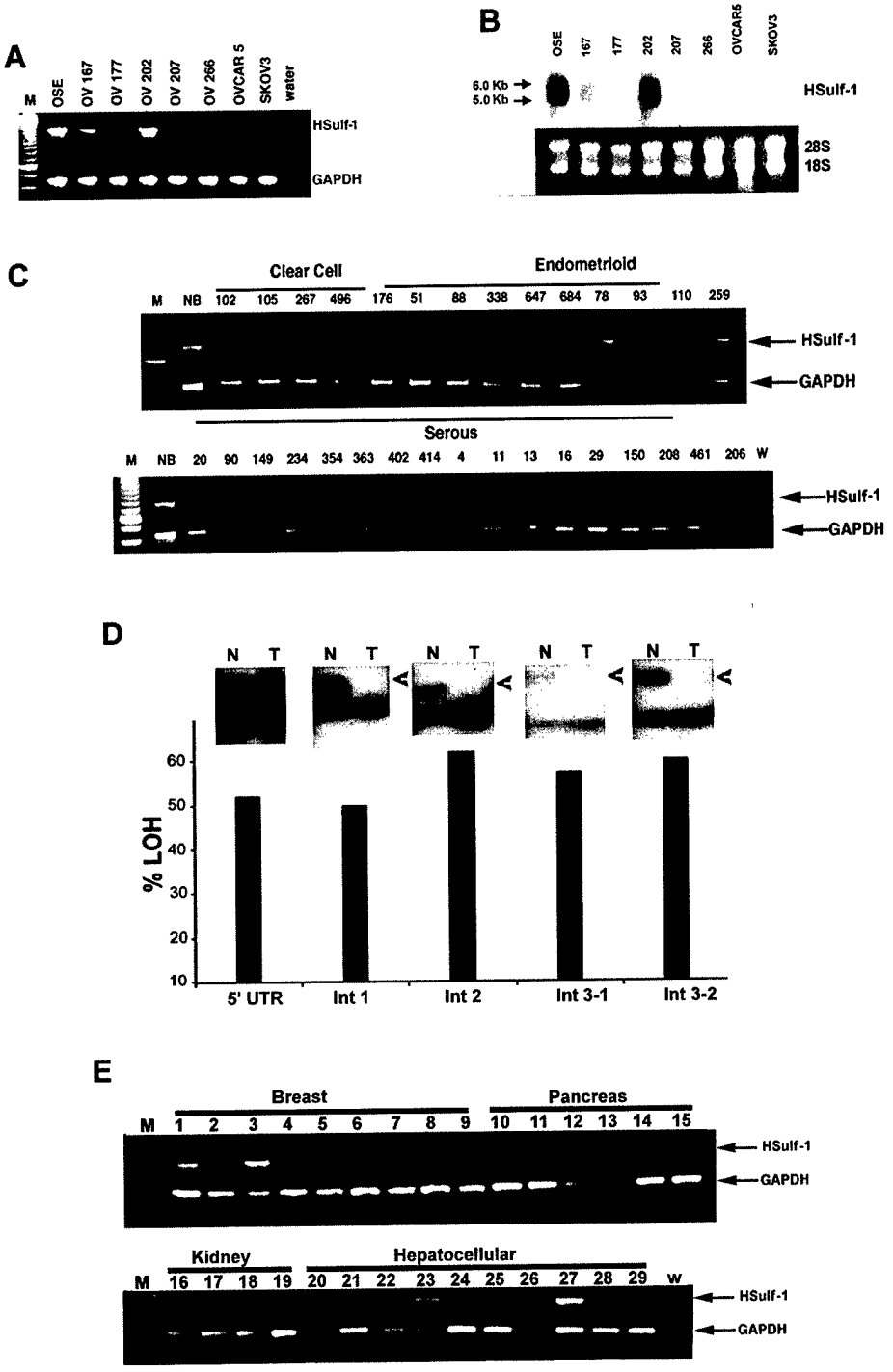

FIG. 2. **Expression of HSulf-1 mRNA is decreased in cancer cell lines and clinical cancer specimens.** *A*, RT-PCR in short term cultures of normal ovarian epithelial cells (*OSE*) and ovarian cancer cell lines. The *top band* is the product of amplification with HSulf-1 primers 1 and 2. The *bottom band* is the product of amplification with GAPDH primers F and R. *B*, *upper panel*, autoradiograph showing the Northern hybridization results with HSulf-1 ORF as probe in the same cell lines as in *A*. *Lower panel*, ethidium bromide-stained 18 S and 28 S RNA of the corresponding samples to show equal loading. *C*, agarose gel showing the products with HSulf-1 primers 1 and 2 by semi-quantitative RT-PCR in primary ovarian tumors resolved on a 1.6% agarose gel. Samples are numbered and grouped according to tumor histology. *M*, 100-bp ladder; *NB*, normal ovarian epithelial cell brushings. *D*, histogram showing the % LOH with microsatellite repeats in the introns of HSulf-1 in 33 matched normal/tumor tissue samples. Frequency of LOH with specific markers varied between 40 and 50%. For each marker, an autoradiograph of LOH analysis is illustrated using DNA from tumor OV 182 (*T*) and normal leukocytes (*N*) from the same patient. *Arrowhead* indicates loss of an allele in the corresponding tumor DNA. *E*, agarose gel showing the products with HSulf-1 primers 1 and 2 by semi-quantitative RT-PCR in breast lines (*lane 1*, HMEC; *lane 2*, BT474; *lane 3*, MCF-7; *lane 4*, MCF-10A; *lane 5*, MDA-MB-157; *lane 6*, MDA-MB-361; *lane 7*, MDA-MB-435; *lane 8*, UACC812; *lane 9*, UACC893), pancreas lines (*lane 10*, AsPc1; *lane 11*, BxPc3; *lane 12*, CAPAN-1; *lane 13*, CAPAN-2; *lane 14*, CFPAC-1; *lane 15*, Mia), kidney samples (*lane 16*, normal kidney; *lane 17*, HTB45; *lane 18*, HTB-49; *lane 19*, CRL-1633), and hepatocellular carcinoma lines (*lane 20*, Hep3B; *lane 21*, HepG2; *lane 22*, HUH7; *lane 23*, HSNU182; *lane 24*, SNU387; *lane 25*, SNU423; *lane 26*, SNU449; *lane 27*, SNU475; *lane 28*, SKHep1; and *lane 29*, PLC5). *Lane w*, water.

al. (8) was observed in HSulf-1-expressing clones compared with parental cells or clones transfected with empty vector. A comparable increase in sulfatase activity was also observed 48 h following transient transfection of full-length H-Sulf-1 cDNA into SKOV3 cells (data not shown).

HSulf-1 Is Localized to the Cell Surface—The avian ortholog of HSulf-1, QSulf1, was shown to localize to the cell surface (7). In contrast, Morimoto-Tomita *et al.* (8) reported that HSulf-1 is secreted to the medium after transfection into Chinese hamster ovary cells. To being to address this apparent inconsistency, cDNA encoding HSulf-1 fused to GFP was transiently transfected into SKOV3 cells. Blotting with anti-GFP antibody readily detected the fusion protein in whole cell lysates but not in medium that was concentrated 50-fold (Fig. 4*A*). This is similar to observations made previously with the HSulf-1 homologs QSulf-1 and RsulfFP1 (7, 28).

Confocal microscopy of cells expressing the HSulf-1/GFP fusion protein demonstrated that HSulf-1 localized to the plasma membrane (Fig. 4*B*). Further analysis demonstrated co-localization with growth factor receptors such as EGFR at the cell surface (Fig. 4*C*).

HSulf-1 Expression Is Associated with Decreased HSPG Sulfation—To assess the possibility that HSulf-1 affects HSPG sulfation, clones transfected with empty vector or HSulf-1 were stained with 10E4 antibody, which specifically recognizes sulfated glucosamine in HSPGs (29). Intense staining was observed in parental and vector transfected cells (Fig. 5*A*). In contrast, HSulf-1-expressing clones showed

reduced staining. Staining with anti-stub antibody 3G10 revealed that both HSulf-1-negative and HSulf-1-transfected cells express HSPGs equally (Fig. 5*B*).

To assess further the ability of HSulf-1 to modulate cell surface sulfation, OV202 cells, which endogenously express HSulf-1 (Fig. 2, *A* and *B*), were transiently transfected with HSulf-1 antisense cDNA. Cell surface staining for sulfated glucosamine in HSPGs was markedly increased (Fig. 5*C*). Collectively, these results provide preliminary evidence that HSulf-1 down-regulation increases HSPG sulfation and HSulf-1 re-expression decreases HSPG sulfation.

HSulf-1 Modulates Signaling by HB-EGF but Not EGF—To determine whether HSulf-1 modulates HB-GF signaling, we examined the action of HB-EGF in parental and HSulf-1-transfected ovarian cells. This growth factor was chosen because of its dependence on heparin binding for its action and because of its postulated role in ovarian carcinogenesis (30). Overexpression of HER2 and HER4, which mediate the effects of heparin-independent EGF and HB-EGF, respectively, is well documented in ovarian cancer cells (30, 31).

HB-EGF treatment of serum-starved parental and vector-transfected cells resulted in sustained phosphorylation of the EGFR on Tyr^{1068} (Fig. 6*A*, *upper panels*). Identical results were obtained with anti-Tyr^{992} antiserum (data not shown). Both Tyr^{1068} and Tyr^{992} have been implicated in EGFR-induced ERK pathway activation (32, 33). Consistent with the enhanced phosphorylation of these sites, ERK phosphorylation was demonstrated in these cells after HB-EGF treatment (Fig. 6*A*, *lower panels*). In contrast, HSulf-1-expressing clones demonstrated diminished EGFR phosphorylation and diminished ERK phosphorylation after HB-EGF treatment (Fig. 6*A*). These results suggest that HSulf-1 can modulate signaling by HB-EGF.

To determine whether this modulation was specific for HB-EGF, the same cells were treated with heparin-independent EGF. As indicated in Fig. 6*B*, there was no difference in either EGF-stimulated EGFR phosphorylation at Tyr^{1068} or ERK phosphorylation in HSulf-1-expressing clones compared with parental and vector-transfected controls.

HSulf-1 Also Modulates FGF-2 Signaling—Previous studies (4–6, 34–36) have shown that *N*-sulfation and 2-*O*-sulfation are critical for the interaction between HS-GAGs and FGF-2, whereas 6-*O*-sulfation is required for the interaction between HS-GAGs and FGFR1 in the formation of the FGF-2·HS-GAG·FGFR1 ternary complex. Conversely, it has been reported that cells containing GAG chains with reduced sulfation lose their proliferative response to FGF-2 (34, 35, 37). These observations, coupled with the demonstration of elevated FGF-2 and FGFR1 in ovarian cancer cells (38, 39), prompted us to examine the effect of HSulf-1 on FGF signaling.

As a read out for FGF signaling, we again measured mitogen-activated protein kinase pathway activation. Formation of the FGF-2·HS-GAG·FGFR1 ternary complex induces receptor dimerization, activation of the FGFR1 tyrosine kinase (36, 40), receptor autophosphorylation, and binding of the adaptor SNT/FRS, which then activates intracellular signaling pathways, including the ERK pathway (41).

When serum-starved vector-transfected cells were treated with FGF-2, sustained phosphorylation of ERK1 and ERK2 lasting >60 min in parental (not shown) and vector-transfected cells (Fig. 7*A*) was observed. In contrast, HSulf-1-expressing clones demonstrated lower basal levels of ERK phosphorylation and only transient elevation after FGF-2 treatment (Fig. 7*A*). Collectively, these results suggest that HSulf-1 not only down-regulates the basal activation of ERK pathway activation, but also inhibits a sustained activation of this pathway that may be required for cell survival and proliferation.

Several controls pointed to sulfation of HSPGs as a critical factor in this HB-GF signaling modulation. First, replacement of FGF-2 with heparinated FGF (heparin-stabilized FGF) abrogated the ability of HSulf-1 to modulate FGF-initiated signaling (Fig. 7*B*). In addition, transient transfection of SKOV3 cells with the sulfatase domain N-Sulf also dampened FGF

TABLE II
Expression analysis in primary ovarian tumors

HSulf-1 mRNA was examined by semiquantitative RT-PCR as illustrated in Fig. 2. Relative levels were scored as absent (0), barely detectable (1+), detectable but diminished compared with OSE (2+), or equal to ovarian surface epithelial cells (3+).

Samples	Tested	HSulf-1 = 0	HSulf-1 = 1+
Total	30	12 (40%)	11 (37%)
Clear cell	4	4 (100%)	0
Endo	9	6 (67%)	1 (11%)
Stage I	5	4 (80%)	1 (20%)
Stage III	4	3 (75%)	0
Serous	17	1 (6%)	16 (59%)
Stage I/II	5	1 (20%)	4 (80%)
Stage III	11	0	6 (55%)

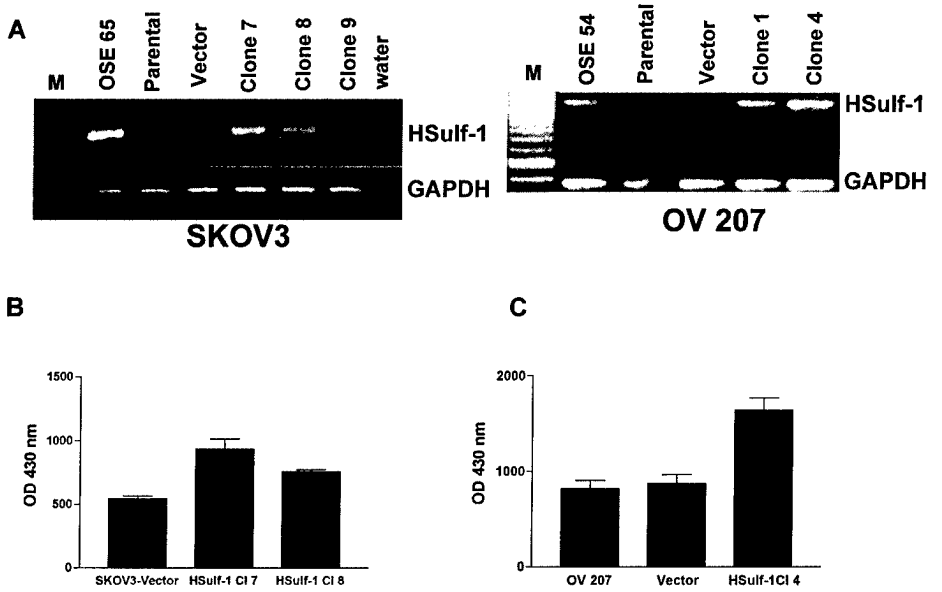

FIG. 3. **Increased sulfatase activity after Hsulf-1 re-expression.** *A*, RT-PCR of parental, vector-transfected, and HSulf-1-transfected clones obtained from SKOV3 (*left*) and OV207 (*right*) ovarian cancer cell lines. *B*, cell extracts from parental cells and stable SKOV3 clones were assayed for sulfatase activity using 10 μM 4-MUS in the presence of 10 μM estrone 3-*O*-sulfamate to inhibit endogenous steroid sulfatase activity. *C*, sulfatase activity in parental OV 207 cells and the indicated clones was measured as in *B*. No activity was detected in the absence of added substrate or lysate (data not shown). *M*, marker

signaling, whereas mutation of two conserved cysteines at the active site of this domain abrogated the modulation (Fig. 7*C*). Collectively, the results in Figs. 6 and 7 demonstrate the ability of HSulf-1 to modulate signaling by two different HB-GFs and the dependence of this modulation on an intact sulfatase domain.

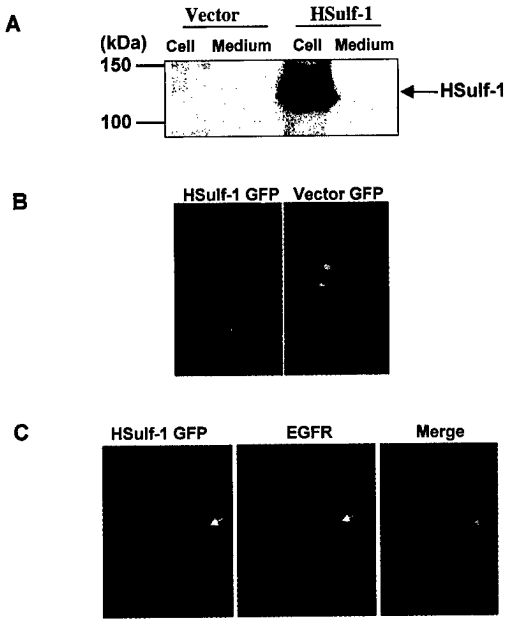

FIG. 4. **HSulf-1 is a cell surface-associated polypeptide.** *A*, 48 h after transient transfection with cDNA encoding an HSulf-1/GFP fusion protein, whole cell lysates and 50-fold concentrated conditioned medium were subjected to immunoblotting with anti-GFP antibodies. An intense band was detected at 135 kDa, the predicted size of the fusion protein, in the cell extracts but not the conditioned medium. *B*, confocal images of SKOV3 cells obtained 24 h after transient transfection of cDNA encoding an HSulf-1/GFP fusion protein (*left panel*) or GFP alone (*right panel*). *C*, co-localization of HSulf-1 and EGFR. SKOV3 cells transiently transfected with FLAG-tagged HSulf-1 were fixed and stained with rabbit anti-EGFR and TRITC-conjugated anti-rabbit IgG as well as FITC-conjugated anti-FLAG antibody. The *arrow* points to the co-localization of HSulf-1 and EGFR to the cell membrane in the merged panel.

HSulf-1 Modulates Proliferation and Apoptosis—Previous studies have demonstrated that stimulation of the Mek/ERK pathway leads to enhanced proliferation and inhibition of apoptosis (reviewed in Refs. 21 and 22). Based on the ability of HSulf-1 to modulate signaling through this pathway, we predicted that HSulf-1 re-expression in HSulf-1-deficient cells would lead to inhibition of proliferation and enhancement of apoptosis.

To test the first of these predictions, parental or HSulf-1-transfected clones were plated at 100,000 cells/dish and counted at various times. As predicted HSulf-1-expressing clones proliferated more slowly than parental or empty vector-transfected clones (Fig. 8*A*).

To examine the effects of HSulf-1 re-expression on apoptosis, stable transfectants were treated for 24 h with 5 μM cisplatin, an agent that is widely used to treat ovarian cancer (42), or diluent. Cells were then stained with DAPI under conditions where this agent preferentially enters apoptotic cells and examined for apoptotic morphological changes (nuclear fragmentation) by fluorescence microscopy (*schematic*, Fig. 8*B*). Results of this analysis indicated that cisplatin induced little apoptosis in parental or vector-transfected cells under these conditions. In contrast, cisplatin induced apoptosis in 25–40% of HSulf-1-transfected cells (Fig. 8*B*). HSulf-1 re-expression likewise sensitized OV207 clones to cisplatin (Fig. 8*C*). To rule out the possibility that these results were unique to cisplatin, the same cell lines were treated for 5 h with 1 μM staurosporine, a broad spectrum kinase inhibitor (43) that is widely used as a prototypic pro-apoptotic stimulus because it induces apoptosis in a wide variety of cells (44), or with UCN-01, a staurosporine analog currently in phase I clinical trials (45). Once again, HSulf-1-transfected clones were sensitized to the induction of apoptosis (Fig. 8*D*). Similar results were observed in the OV207 clones and in a second set of independently derived HSulf-1-expressing SKOV3 clones (data not shown). Further experiments revealed the typical biochemical hallmarks of apoptosis, including cytochrome *c* release from mitochondria and DNA

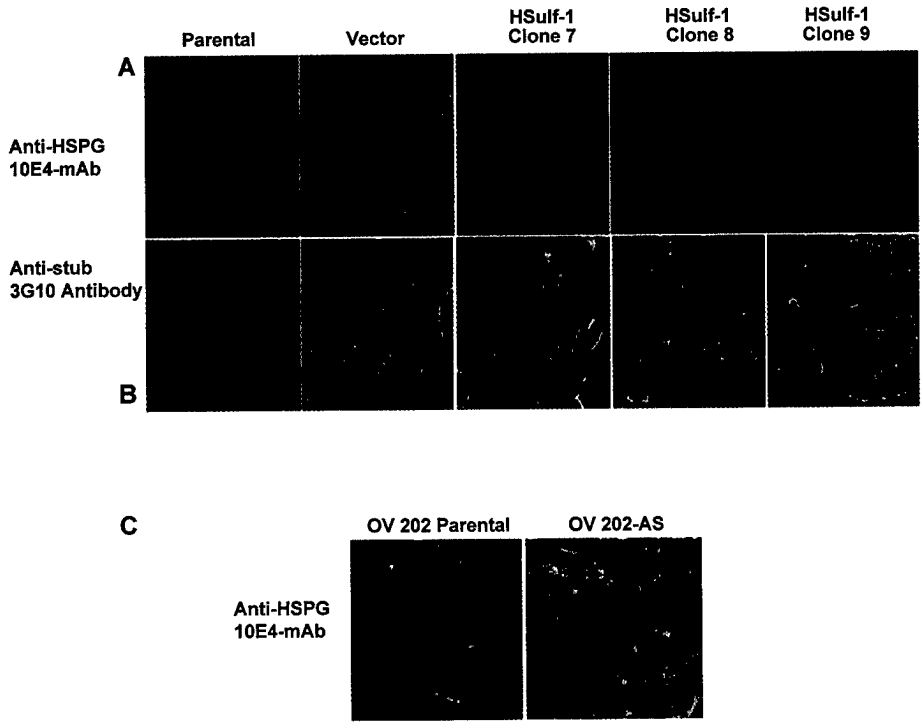

FIG. 5. **HSulf-1 expression is associated with decreased sulfation of cell surface HS-GAGs.** *A*, SKOV3 parental cells and the indicated stable, cloned transfectants were fixed and stained for sulfated HS-GAG using antibody 10E4, which recognizes native heparan sulfate with sulfated glucosamine residues (*A*) or antibody 3G10, which recognizes deglycosylated HS-GAG (*B*). *C*, OV202 cells, which express endogenous HSulf-1 (Fig. 2*A*), were transiently transfected with cDNA encoding full-length HSulf-1 in the antisense orientation (HSulf-1 AS) or empty vector and stained with antibody 10E4.

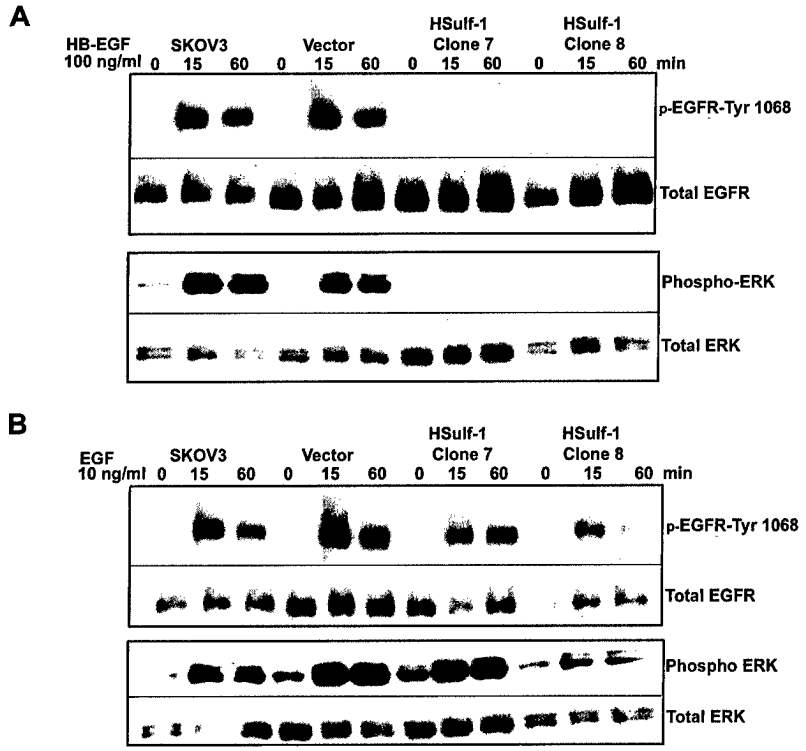

FIG. 6. **HSulf-1 modulates HB-EGF signaling but not EGF signaling.** *A*, effect of HB-EGF on EGFR phosphorylation and downstream signaling. After the indicated cell lines were cultured in serum-free medium for 12 h, 100 ng/ml HB-EGF was added for 15 and 60 min. Whole cell lysates were subjected to SDS-PAGE, transferred to nitrocellulose, and sequentially probed with antisera that recognize phospho-Tyr^{1068}-EGFR, total EGFR, phosphorylated ERK1/2, or total ERK1/2. *B*, effect of EGF on EGFR phosphorylation and downstream signaling. After cells were cultured in serum-free medium for 12 h, 10 ng/ml heparin-independent EGF was added. Whole cell lysates were prepared and probed as in *A*. In contrast to the diminished and unsustained EGFR phosphorylation observed in HSulf-1-expressing clones after treatment with HB-EGF, receptor phosphorylation and signaling were robust and sustained after EGF treatment.

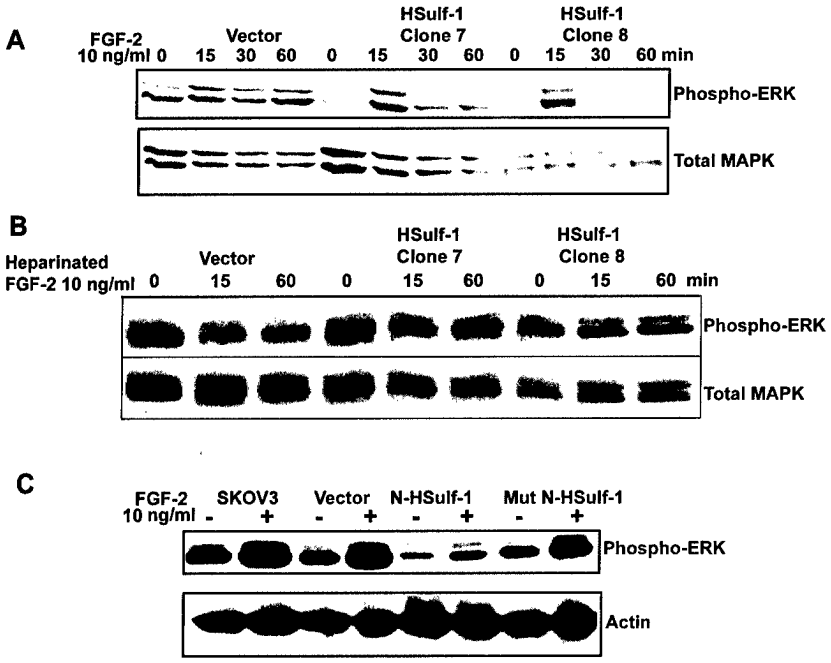

FIG. 7. **HSulf-1 modulates FGF-2 signaling but not heparinated FGF-2 signaling.** *A*, signaling by FGF-2. The indicated cells were cultured in serum-free medium for 8 h and then treated with 10 ng/ml FGF-2 for 15, 30, and 60 min. Whole cell lysates were probed with anti-phospho-ERK1/2 and anti-ERK1/2 as described in Fig. 6. *B*, signaling by heparinated FGF-2. The indicated cells were cultured in serum-free medium for 8 h and then treated with 10 ng/ml heparinated FGF-2 for 15 or 60 min. FGF-2 induced sustained phosphorylation of ERK1/2 in parental and vector-transfected cells but not HSulf-1 expressing clones. In contrast, heparinated FGF-2 induced sustained signaling in all four cell lines. *C*, an active sulfatase domain is required to modulate signaling. SKOV3 cells were transfected with cDNA encoding the N terminal domain of HSulf-1 (Fig. 1*C*), the C terminal domain, or an N terminal domain containing cysteine-alanine mutations of two conserved cysteines in the sulfatase domain (*Mut-N-Sulf*). After 12 h in serum-free medium, cells were incubated for 15 min with 10 ng/ml FGF-2. Phosphorylation of ERK1/2 was decreased in cells transfected with the N-Sulf construct but not the mutant construct.

fragmentation, when HSulf-1-transfected clones were drug-treated (data not shown). Two aspects of these results deserve particular emphasis. First, HSulf-1 by itself did not induce apoptosis but instead modulated the sensitivity of cells to other stimuli (Fig. 8, *B–D*). Second, higher expression of HSulf-1 correlated with somewhat higher induction of apoptosis (Fig. 8, *B–D*).

To confirm that this modulation of apoptosis reflected the sulfatase activity of HSulf-1, SKOV3 cells were transiently transfected with two truncation constructs and an active site mutant. Transfection with the C-terminal half of HSulf-1 (C-Sulf) had little effect on the ability of staurosporine and UNC-01 to induce apoptosis (Fig. 8*E*). In contrast, an N-terminal fragment containing the entire sulfatase domain (N-Sulf) enhanced the ability of staurosporine to induce apoptosis. Importantly, site-directed mutagenesis of the putative catalytic cysteines Cys^{87} and Cys^{88} in N-Sulf (Mut-N-Sulf) abolished the ability of HSulf-1 to modulate apoptosis (Fig. 8*E*), providing evidence that sulfatase activity is required for this modulation.

DISCUSSION

In the present experiments, we have examined the activity, localization, and function of HSulf-1, a recently cloned member of the HSPG sulfatase family. Earlier studies by Dhoot *et al.* (7) demonstrated that QSulf-1, the avian homolog of this enzyme, is a cell surface protein that modulates signaling by the HB-GF

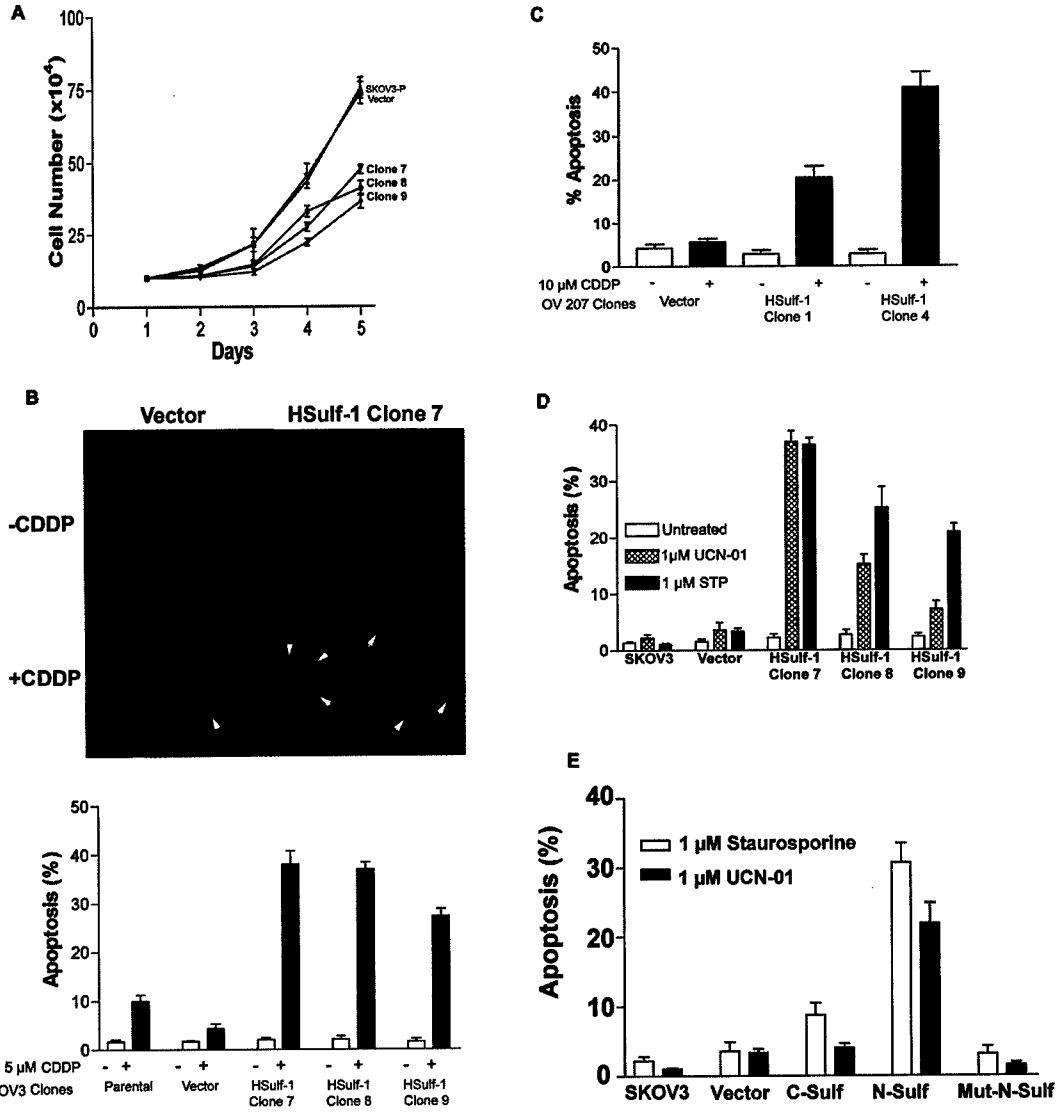

FIG. 8. **HSulf-1 modulates proliferation and apoptosis.** *A*, effect of HSulf-1 expression on proliferation. The indicated cell lines were plated at 100,000 cells/dish in triplicate and examined daily after trypan blue staining to determine the number of viable cells/plate. *B*, effect of HSulf-1 expression on induction of apoptosis by cisplatin (*CDDP*) in SKOV3 clones. The indicated SKOV3 lines were treated with 5 μM cisplatin for 24 h and then stained with DAPI. Representative micrographs are shown in the *schematic*. *Bars* indicate the percentage of total cells that exhibit nuclear condensation and fragmentation typical of apoptosis. *C*, effect of HSulf-1 expression on cisplatin-induced apoptosis in OV207 clones. The indicated clones were treated for 24 h with 10 μM cisplatin before apoptosis was assessed by DAPI staining. *D*, effect of HSulf-1 expression on induction of apoptosis by staurosporine and UCN-01. The indicated SKOV3 lines were treated for 5 h with 1 μM staurosporine or UCN-01 prior to DAPI staining and analysis as depicted in *B*. *E*, requirement for an active sulfatase domain to modulate apoptosis. 24 h after transient transfection of empty vector or cDNA encoding N-Sulf, C-Sulf, and mutated (C87A,C88A) N-Sulf, cells were treated with 1 μM staurosporine or UCN-01 for 5 h before staining with DAPI and analysis as depicted in *B*.

Wnt during quail muscle cell differentiation. Our studies extend this work by showing that HSulf-1 is a cell surface polypeptide that diminishes HSPG sulfation, inhibits signaling by heparin-dependent growth factors, diminishes proliferation, and facilitates apoptosis in response to exogenous stimuli. Further experiments have shown that HSulf-1 expression is diminished in a variety of cancer cell lines and in clinical cancer specimens. These observations provide new insight into the potential importance of HSPG sulfation and its regulation.

While these studies were in progress, Morimoto-Tomita *et al.* (8) reported cloning of the HSulf-1 cDNA and gene. Our analysis has extended this previous report by demonstrating the presence of two previously unrecognized upstream exons (Table III), both of which appear to be included in transcripts from a variety of human cell lines and cells.

Further studies by Morimoto-Tomita *et al.* (8) indicated that HSulf-1 exhibits sulfatase activity with a preference for glucosamine 6-sulfate substrates. Interestingly, transfection of Myc-tagged HSulf-1 into Chinese hamster ovary cells resulted in secretion of the protein into the culture medium rather than retention in or on the cells (8). In our experiments, HSulf-1 fused to GFP or tagged with the FLAG epitope was transfected into ovarian cancer cell lines that express undetectable amounts of endogenous HSulf-1 message. These experiments not only confirmed the induction of sulfatase activity (Fig. 3) but demonstrated desulfation of cell surface HSPGs upon HSulf-1 re-expression (Fig. 5). As was the case with QSulf-1 (7), however, our localization studies suggested that a substantial fraction of HSulf-1 remains associated with the cell surface. In particular, HSulf-1/EGFP was detected by immunoblotting in whole cell lysates but not 50-fold concentrated conditioned medium (Fig. 4). Moreover, both HSulf-1/EGFP and FLAG-tabbed HSulf-1 were localized to the cell surface by confocal microscopy (Fig. 4). Why these results differ from those of

TABLE III
Genomic structure of HSulf-1

Exon	Amino acids	Size	Intron size
1	5′-UTR	314	22,939
1A	5′-UTR	284	2917
2	5′-UTR	165	5994
3	5′-UTR	95	61,570
4	5′-UTR	73	304
5	5′-UTR, 1–57	232	11,821
6	58–137	240	10,147
7	138–188	152	2463
8	189–257	170	11,461
9	258–295	151	900
10	296–354	176	1362
11	355–397	129	277
12	398–416	57	1146
13	417–459	130	16,102
14	460–531	217	2690
15	532–617	256	3012
16	618–649	97	465
17	650–681	95	304
18	682–703	66	1267
19	704–761	176	8822
20	762–809	143	90
21	810–850	124	1949
22	851–862	34	17,656
23	863–893 3′-UTR	2408	

Morimoto-Tomita *et al.* (8) is at present unclear but might reflect the transfection of different cell lines or the use of different epitope tags.

Previous SSH analysis of two early and late stage tumors subtracted against normal ovarian epithelial brushings identified HSulf-1 as an mRNA that was diminished in several ovarian cancers compared with the cell of origin of these neoplasms (9). We have extended these studies by showing that HSulf-1 mRNA is markedly diminished or absent from 5 of 7 ovarian cancer cell lines and 23 of 30 epithelial ovarian cancers (Fig. 2). Further analysis has demonstrated that the *HSulf-1* locus is subject to allelic loss in 50–60% of ovarian cancers (Fig. 2*D*). As indicated in Table II, the lack of detectable HSulf-1 expression was particularly common in clear cell ovarian cancers. This variant accounts for ~10% of all epithelial ovarian cancers, but these tumors have a worse prognosis and are resistant to platinum-based chemotherapy (26, 46, 47). Interestingly, HSulf-1 expression was undetectable in the clear cell cancers even though all four of the tumors analyzed were early stage tumors. Equally important, analysis of a series of cancer cell lines demonstrated that HSulf-1 down-regulation is common in hepatocellular, renal, pancreatic, and breast carcinomas (Fig. 2*E*). This early and apparent widespread occurrence of HSulf-1 down-regulation raises the possibility that HSulf-1 down-regulation might be important in the carcinogenic process.

In order to examine the functional consequences of HSulf-1 down-regulation, we re-expressed HSulf-1 in two ovarian cancer cell lines lacking detectable message. Studies of Dhoot *et al.* (7) previously implicated QSulf-1 in the regulation of Wnt signaling and alluded to the possibility that QSulf-1 might also potentially regulate FGF signaling, which is controlled by 6-*O*-sulfation of *N*-acetylglucosamine in HSPGs (4). Based on the similarity of HSulf-1 to QSulf-1, we hypothesized that HSulf-1 down-regulation might modulate HB-GF signaling. Consistent with this possibility, we observed altered signaling by HB-EGF in cells after HSulf-1 re-expression (Fig. 6). In particular, we observed diminished HB-EGF-induced phosphorylation of at least two important sites on the EGFR, Tyr^{1068}, a binding site for Grb2 (32), and Tyr^{992}, a binding site for phospholipase C-γ (33). In previous studies (48), the interaction of HB-EGF with cell surface HSPGs was indirectly demonstrated by showing that sodium chlorate, which inhibits HS-GAG sulfation, and heparinase abrogate HB-EGF signaling. A subsequent report (49) indicated that ^{125}I-HB-EGF binding is diminished in Chinese hamster ovary cells deficient in HSPG. The present studies extend these earlier results by demonstrating that HSulf-1 re-expression, which diminishes cell surface HS-GAG sulfation (Fig. 5), interferes with HB-EGF signaling through the EGFR (Fig. 6). Consistent with these results, we observed diminished HB-EGF-induced activation of the ERK pathway (Fig. 6*A*). Importantly, these results were not seen with EGF (Fig. 6*B*), which lacks an HSPG binding domain and is thought to signal independent of the HS-GAGs.

The effect of HSulf-1 re-expression was not limited to HB-EGF. A variety of previous studies has demonstrated that FGF-2 binds to its receptor and to HSPGs, which act as co-receptors and promote formation of a ternary complex that is essential for cell proliferation and angiogenesis (50, 51). As indicated in the Introduction, previous reports have also demonstrated that sulfation of specific sites on the HS-GAGs is critical for this interaction. This interaction of FGF-2 with FGFR and HS-GAGs leads to receptor dimerization, activation, and autophosphorylation followed by activation of downstream signaling pathways, including the mitogen-activated protein kinase pathway (4, 37). Our experiments demonstrated that HSulf-1 also modulated FGF-2 signaling. In particular, FGF-2 induced sustained ERK phosphorylation in cells lacking detectable HSulf-1 expression but only transient ERK phosphorylation at 15 min in the HSulf-1 transfected clones (Fig. 7*A*). These observations are consistent with a recent report that chlorate treatment, which inhibits GAG sulfation, results in cells that exhibit a transient early (15 min) phosphorylation of ERK in response to FGF-2 but no sustained ERK phosphorylation (37). Once again the modulation of signaling by HSulf-1 was not observed when cells were treated with heparinated FGF-2 (Fig. 7*B*), which would be expected to signal independent of HS-GAGs. In summary, our results indicate that HSulf-1 transfection abrogates the sustained activation of ERK1 and ERK2 required for cell survival and proliferation.

Because sustained ERK phosphorylation has been implicated in proliferation (52) as well as resistance to apoptosis (22, 53, 54), we next examined the effect of HSulf-1 re-expression on these processes. Results of this analysis demonstrated that HSulf-1 re-expression diminished proliferation of SKOV3 and OV207 clones (Fig. 8*A* and data not shown). Moreover, HSulf-1 re-expression enhanced the sensitivity of these cells to a number of pro-apoptotic stimuli, including cisplatin, which is widely used to treat ovarian cancer (55), and staurosporine, a broadly active kinase inhibitor that is widely employed as a stimulus of the mitochondrial apoptotic pathway (44, 56). These results are consistent with previous studies (57, 58) demonstrating ERK phosphorylation and ability of the Mek1/2 inhibitor PD98059 to modulate cisplatin sensitivity in ovarian cancer cells. Further analysis demonstrated that an N-terminal fragment containing an intact sulfatase domain is responsible for this HSulf-1-induced modulation of apoptosis (Fig. 8*E*). Because HSulf-1 modulates sensitivity of cells to induction of apoptosis by cisplatin, which is considered the single most active agent currently available for the treatment of ovarian cancer, future studies to evaluate the relationship between HSulf-1 expression and clinical response in ovarian cancer appear to be warranted.

Although there is ample evidence that differences in the sulfation state of HS-GAGs introduced by altering sulfotransferase activity can modulate growth factor signaling *in vitro* (35, 59–62), there is little precedent for the idea that variations in sulfatase activity can alter survival signaling in human cancer. The functional results described above suggest that

HSulf-1 is a cell surface enzyme that desulfates critical sulfated moieties in HS-GAG, thereby inhibiting the action of heparin-dependent growth factors at their receptors and diminishing their ability to activate the ERK pathway. Because expression of HSulf-1 is undetectable or markedly attenuated in >75% of ovarian cancers relative to normal ovarian surface epithelium, these observations appear to outline a novel mechanism by which proliferative and anti-apoptotic signaling by heparin-dependent growth factors can be augmented during the process of carcinogenesis.

Acknowledgment—We thank Dr. Kim Kalli for providing the short term cultures of normal surface epithelial cells.

REFERENCES

1. Sasisekharan, R., Shriver, Z., Venkataraman, G., and Narayanasami, U. (2002) *Nat. Rev. Cancer* **2,** 521–528
2. Liu, D., Shriver, Z., Qi, Y., Venkataraman, G., and Sasisekharan, R. (2002) *Semin. Thromb. Hemostasis* **28,** 67–78
3. Rusnati, M., Coltrini, D., Caccia, P., Dell'Era, P., Zoppetti, G., Oreste, P., Valsasina, B., and Presta, M. (1994) *Biochem. Biophys. Res. Commun.* **203,** 450–458
4. Lundin, L., Larsson, H., Kreuger, J., Kanda, S., Lindahl, U., Salmivirta, M., and Claesson-Welsh, L. (2000) *J. Biol. Chem.* **275,** 24653–24660
5. Maccarana, M., Casu, B., and Lindahl, U. (1993) *J. Biol. Chem.* **268,** 23898–23905
6. Guimond, S., Maccarana, M., Olwin, B. B., Lindahl, U., and Rapraeger, A. C. (1993) *J. Biol. Chem.* **268,** 23906–23914
7. Dhoot, G. K., Gustafsson, M. K., Ai, X., Sun, W., Standiford, D. M., and Emerson, C. P., Jr. (2001) *Science* **293,** 1663–1666
8. Morimoto-Tomita, M., Uchimura, K., Werb, Z., Hemmerich, S., and Rosen, S. D. (2002) *J. Biol. Chem.* **277,** 49175–49185
9. Shridhar, V., Sen, A., Chien, J., Staub, J., Avula, R., Kovats, S., Lee, J., Lillie, J., and Smith, D. I. (2002) *Cancer Res.* **62,** 262–270
10. Hanahan, D., and Weinberg, R. A. (2000) *Cell* **100,** 57–70
11. Koury, M. J., and Bondurant, M. C. (1990) *Science* **248,** 378–381
12. Dudek, H., Datta, S. R., Franke, T. F., Birnbaum, M. J., Yao, R., Cooper, G. M., Segal, R. A., Kaplan, D. R., and Greenberg, M. E. (1997) *Science* **275,** 661–665
13. Gibson, S., Tu, S., Oyer, R., Anderson, S. M., and Johnson, G. L. (1999) *J. Biol. Chem.* **274,** 17612–17618
14. Liu, J. F., Crepin, M., Liu, J. M., Barritault, D., and Ledoux, D. (2002) *Biochem. Biophys. Res. Commun.* **293,** 1174–1182
15. Shin, E. Y., Ma, E. K., Kim, C. K., Kwak, S. J., and Kim, E. G. (2002) *J. Cancer Res. Clin. Oncol.* **128,** 596–602
16. Reynolds, C. M., Eguchi, S., Frank, G. D., and Motley, E. D. (2002) *Hypertension* **39,** 525–529
17. Di Blasio, A. M., Carniti, C., Vigano, P., and Vignali, M. (1995) *J. Steroid Biochem. Mol. Biol.* **53,** 375–379
18. Raab, G., and Klagsbrun, M. (1997) *Biochim. Biophys. Acta* **1333,** F179–F199
19. Valve, E., Martikainen, P., Seppanen, J., Oksjoki, S., Hinkka, S., Anttila, L., Grenman, S., Klemi, P., and Harkonen, P. (2000) *Int. J. Cancer* **88,** 718–725
20. Wang, J., Luo, F., Lu, J. J., Chen, P. K., Liu, P., and Zheng, W. (2002) *Int. J. Cancer* **97,** 163–167
21. Sebolt-Leopold, J. S. (2000) *Oncogene* **19,** 6594–6599
22. Dent, P., and Grant, S. (2001) *Clin. Cancer Res.* **7,** 775–783
23. Conover, C. A., Hartmann, L. C., Bradley, S., Stalboerger, P., Klee, G. G., Kalli, K. R., and Jenkins, R. B. (1998) *Exp. Cell Res.* **238,** 439–449
24. Nielsen, H., Engelbrecht, J., Brunak, S., and von Heijne, G. (1997) *Protein Eng.* **10,** 1–6
25. Stoffel, K. H. W. (1993) *Biol. Chem. Hoppe-Seyler* **374,** 166
26. Goff, B. A., Sainz de la Cuesta, R., Muntz, H. G., Fleischhacker, D., Ek, M., Rice, L. W., Nikrui, N., Tamimi, H. K., Cain, J. M., Greer, B. E., and Fuller, A. F., Jr. (1996) *Gynecol. Oncol.* **60,** 412–417
27. Soule, H. D., Maloney, T. M., Wolman, S. R., Peterson, W. D., Jr., Brenz, R., McGrath, C. M., Russo, J., Pauley, R. J., Jones, R. F., and Brooks, S. C. (1990) *Cancer Res.* **50,** 6075–6086
28. Ohto, T., Uchida, H., Yamazaki, H., Keino-Masu, K., Matsui, A., and Masu, M. (2002) *Genes Cells* **7,** 173–185
29. Clayton, A., Thomas, J., Thomas, G. J., Davies, M., and Steadman, R. (2001) *Kidney Int.* **59,** 2084–2094
30. Gilmour, L. M., Macleod, K. G., McCaig, A., Gullick, W. J., Smyth, J. F., and Langdon, S. P. (2001) *Cancer Res.* **61,** 2169–2176
31. Berchuck, A., Kamel, A., Whitaker, R., Kerns, B., Olt, G., Kinney, R., Soper, J. T., Dodge, R., Clarke-Pearson, D. L., Marks, P., *et al.* (1990) *Cancer Res.* **50,** 4087–4091
32. Rojas, M., Yao, S., and Lin, Y. Z. (1996) *J. Biol. Chem.* **271,** 27456–27461
33. Emlet, D. R., Moscatello, D. K., Ludlow, L. B., and Wong, A. J. (1997) *J. Biol. Chem.* **272,** 4079–4086
34. Ornitz, D. M., and Itoh, N. (2001) *Genome Biol.* **2,** 1–12
35. Ornitz, D. M. (2000) *Bioessays* **22,** 108–112
36. Selva, E. M., and Perrimon, N. (2001) *Adv. Cancer Res.* **83,** 67–80
37. Delehedde, M., Lyon, M., Gallagher, J. T., Rudland, P. S., and Fernig, D. G. (2002) *Biochem. J.* **366,** 235–244
38. Crickard, K., Gross, J. L., Crickard, U., Yoonessi, M., Lele, S., Herblin, W. F., and Eidsvoog, K. (1994) *Gynecol. Oncol.* **55,** 277–284
39. Di Blasio, A. M., Cremonesi, L., Vigano, P., Ferrari, M., Gospodarowicz, D., Vignali, M., and Jaffe, R. B. (1993) *Am. J. Obstet. Gynecol.* **169,** 1517–1523
40. Lepique, A. P., Forti, F. L., Moraes, M. S., and Armelin, H. A. (2000) *Endocr. Res.* **26,** 825–832
41. Rapraeger, A. C., Krufka, A., and Olwin, B. B. (1991) *Science* **252,** 1705–1708
42. Ozols, R. F., Rubin, S. C., and Thomas, G. M. (2000) *Principles and Practice of Gynecologic Oncology* (Hoskins, E., ed) 3rd Ed., Lippincott Williams & Wilkins, Baltimore
43. Gescher, A. (2000) *Crit. Rev. Oncol. Hematol.* **34,** 127–135
44. Bertrand, R., Solary, E., O'Connor, P., Kohn, K. W., and Pommier, Y. (1994) *Exp. Cell Res.* **211,** 314–321
45. Senderowicz, A. M. (2000) *Oncogene* **19,** 6600–6606
46. Sugiyama, T., Kamura, T., Kigawa, J., Terakawa, N., Kikuchi, Y., Kita, T., Suzuki, M., Sato, I., and Taguchi, K. (2000) *Cancer (Phila.)* **88,** 2584–2589
47. Behbakht, K., Randall, T. C., Benjamin, I., Morgan, M. A., King, S., and Rubin, S. C. (1998) *Gynecol. Oncol.* **70,** 255–258
48. Higashiyama, S., Abraham, J. A., and Klagsbrun, M. (1993) *J. Cell Biol.* **122,** 933–940
49. Aviezer, D., and Yayon, A. (1994) *Proc. Natl. Acad. Sci. U. S. A.* **91,** 12173–12177
50. Gallagher, J. T., and Turnbull, J. E. (1992) *Glycobiology* **2,** 523–528
51. Rusnati, M. P. M. (1996) *Int. J. Clin. & Lab. Res.* **26,** 15–23
52. Bhalla, U. S., Ram, P. T., and Iyengar, R. (2002) *Science* **297,** 1018–1023
53. Xia, Z., Dickens, M., Raingeaud, J., Davis, R. J., and Greenberg, M. E. (1995) *Science* **270,** 1326–1331
54. Bonni, A., Brunet, A., West, A. E., Datta, S. R., Takasu, M. A., and Greenberg, M. E. (1999) *Science* **286,** 1358–1362
55. Ozols, R. F. (2000) *Semin. Oncol.* **27,** Suppl. 7, 47–49
56. Budihardjo, I., Oliver, H., Lutter, M., Luo, X., and Wang, X. (1999) *Annu. Rev. Cell Dev. Biol.* **15,** 269–290
57. Hayakawa, J., Ohmichi, M., Kurachi, H., Ikegami, H., Kimura, A., Matsuoka, T., Jikihara, H., Mercola, D., and Murata, Y. (1999) *J. Biol. Chem.* **274,** 31648–31654
58. Persons, D. L., Yazlovitskaya, E. M., Cui, W., and Pelling, J. C. (1999) *Clin. Cancer Res.* **5,** 1007–1014
59. Yayon, A., Klagsbrun, M., Esko, J. D., Leder, P., and Ornitz, D. M. (1991) *Cell* **64,** 841–848
60. Ornitz, D. M., Yayon, A., Flanagan, J. G., Svahn, C. M., Levi, E., and Leder, P. (1992) *Mol. Cell. Biol.* **12,** 240–247
61. Miao, H. Q., Fritz, T. A., Esko, J. D., Zimmermann, J., Yayon, A., and Vlodavsky, I. (1995) *J. Cell. Biochem.* **57,** 173–184
62. Kobayashi, M., Habuchi, H., Yoneda, M., Habuchi, O., and Kimata, K. (1997) *J. Biol. Chem.* **272,** 13980–13985

MS#5

Oncogene (2003) 00, 1–8

www.nature.com/onc

A candidate tumor suppressor HtrA1 is downregulated in ovarian cancer

Jeremy Chien[1], Julie Staub[1], Shou-Ih Hu[2], Michele R Erickson-Johnson[1], Fergus J Couch[1], David I Smith[1], Robert M Crowl[2], Scott H Kaufmann[3] and Viji Shridhar*[,1]

[1]*Mayo Clinic Cancer Center and Department of Experimental Pathology, Mayo Clinic, Rochester, MN 55905, USA;* [2]*Arthritis Biology Unit, Novartis Pharmaceuticals, Summit, NJ 07901, USA;* [3]*Department of Oncology, Mayo Clinic, Rochester, MN 55905, USA*

E. Hanover/ 36/

We report here that HtrA1, a candidate tumor suppressor, is downregulated in ovarian cancer. Expression of HtrA1 is downregulated in five of seven ovarian cancer cell lines. In total, 59% of primary ovarian tumors have either a complete absence or markedly reduced levels of HtrA1 expression compared to the brushings of ovarian surface epithelium. Primary ovarian tumors show high frequencies of loss of an allele at microsatellite markers near *htrA1* locus on 10q26. Downregulation of HtrA1 in SKOV3 by antisense transfection promotes anchorage-independent growth, while exogenous expression of HtrA1 in OV202 induces cell death. HtrA1-induced cell death is not inhibited by the broad caspase inhibitor, zVAD(O-Me)fmk, but instead reflects serine protease activity associated with HtrA1. These observations raise the possibility of HtrA1 as a candidate tumor suppressor involved in promoting serine-protease-mediated cell death and that downregulation of HtrA1 in ovarian cancer may contribute to malignant phenotype.
Oncogene (2003) **0**, 000–000. doi:10.1038/sj.onc.1207271

Keywords: serine protease; HtrA; ovarian cancer; downregulation; loss of heterozygosity

Introduction

Ovarian cancer is one of the leading causes of gynecological-related deaths among women in the US. Of the 27 000 women diagnosed each year with this disorder, over half die of their disease (Greenlee *et al.*, 2000). These statistics highlight the need for improved understanding of the pathogenesis of this neoplasm.

Like cancers of other tissues, ovarian cancer is considered to result from an accumulation of a series of genetic alterations. Alterations in tumor-suppressor genes such as *p53* (Kohler *et al.*, 1993), *pRB* (Li *et al.*, 1991), and *NOEY2* (Yu *et al.*, 1999), and oncogenes such as *K-ras* (Enomoto *et al.*, 1991), *c-myc* (Katsaros *et al.*, 1995), and *HER-2/neu* (Ross *et al.*, 1999) have been shown to play an important role in ovarian carcinogenesis (Orsulic *et al.*, 2002). To search for additional alterations that might play a role in the biology of ovarian cancer, we recently generated suppression subtraction hybridization (SSH) cDNA libraries between normal ovarian epithelium and primary tumors. One of the differentially expressed genes identified from this screen (Shridhar *et al.*, 2002) was *htrA1*, a human homologue of bacterial *htrA/DegP* gene product.

HtrA1 belongs to the HtrA family of serine proteases that is well conserved from bacteria to humans. The bacterial HtrA gene product is one of the most well-characterized proteins of the HtrA family and its presence is necessary for bacterial thermotolerance (Clausen *et al.*, 2002). It has recently been shown that bacterial HtrA has dual roles, acting as a chaperone at normal temperature and as an active protease at high temperature (Spiess *et al.*, 1999; Krojer *et al.*, 2002).

Human HtrA1 was originally isolated from fibroblasts as a transformation-sensitive protein due to its downregulation by SV40 (Zumbrunn and Trueb, 1996). It contains an N-terminal insulin-like growth factor binding protein (IGFBP) domain, a Kazal-type trypsin inhibitor motif, and C-terminal trypsin-like protease and PDZ domains (Hu *et al.*, 1998). It is downregulated in malignant melanoma, and stable overexpression of HtrA1 inhibited proliferation in metastatic melanoma cell line (Baldi *et al.*, 2002).

RI ✓

To validate and extend our previous analysis indicating that HtrA1 is downregulated in all four ovarian tumor SSH libraries (Shridhar *et al.*, 2002), we examined the expression of HtrA1 in ovarian cancer cell lines and primary tumors by RT–PCR, Northern blot, Western blot, and Light-Cycler analyses. Furthermore, we investigated the functional significance of HtrA1 downregulation in an ovarian cancer cell line with endogenous HtrA1 expression, and the effect of HtrA1 re-expression in an ovarian cell line with low levels of HtrA1.

*Correspondence: V Shridhar, Division of Experimental Pathology, Mayo Foundation, 200 First Street SW, Rochester, MN 55905, USA; E-mail: shridv@exrch.mayo.edu
Received 2 September 2003; revised 6 October 2003; accepted 7 October 2003

Gml : Ver 6.0
Template: Ver 6.0

Journal: ONC ☐ Disk used Despatch Date: 25/10/2003
Article : NPG_ONC_6856 Pages: 1–8 OP: Solly Pouly

Results

HtrA1 is expressed in normal ovary and downregulated in ovarian cancer

Hybridization with the full-length coding sequence of HtrA1 to a multiple tissue Northern blot revealed that HtrA1 is widely expressed. Particularly noteworthy in the present context is the expression in ovary (Figure 1a). Further analysis revealed that HtrA1 is expressed in ovarian surface epithelial (OSE) cells (Figure 1b), the normal counterpart of ovarian cancer. Notably, compared to immortalized normal OSE cells, expression of HtrA1 is lost or markedly diminished in several ovarian cancer cell lines when analysed by RT–PCR and Western blot (Figure1b and 1c, respectively). Northern blot analysis of primary ovarian tumors (Figure 1d) indicates that HtrA1 is lost or reduced in both early- and late-stage tumors compared to normal ovarian epithelial cell brushings. Semiquantitative RT–PCR (Figure 1e) and Light-Cycler analyses (Figure 1f) confirmed the reduced levels of HtrA1 in several ovarian tumors of different histologies.

HtrA1 expression is aberrantly regulated in several types of cancer

RT–PCR analysis of HtrA1 expression in several types of cancer cell lines and tumors indicates that HtrA1 expression is aberrantly regulated. HtrA1 expression is downregulated in two of 13 primary brain tumors, three (BT474, MDA-MB-~~157~~, and UACC893) of eight breast cancer cell lines, two (HepG2 and Hep3B) of 10 liver cancer cell lines, and one (C33-A) of nine cervical cancer cell lines (Figure 2). Identities of other cell lines are listed in the figure legend.

361/

Loss of heterozygosity (LOH) at 10q26 is associated with HtrA1 downregulation

To investigate the mechanism of HtrA1 downregulation, LOH analysis was performed to determine if *htrA1* locus was a target for deletion. Utilizing six genetic markers around the *htrA1* locus, we analysed 39 ovarian tumors and matched normal DNA for LOH. The cytogenetic band locations, base position relative to *htrA1* locus, and the frequency of LOH are shown in Figure 3a. Two of the closest markers, the GT repeat marker (32 kb 5′ of exon 1) and the CT repeat marker (102 kb 3′ of exon 9), showed 32 and 42% LOH, respectively (Figure 3b). This is the first report of such high frequencies of LOH in this region in ovarian cancer. Representative autoradiographs indicative of LOH at each marker are shown in Figure 3c. No homozygous deletion was detected in the tumor samples tested. To determine if LOH corresponds with loss or reduced levels of expression, HtrA1 expression was analysed in 19 of 39 tumors for which

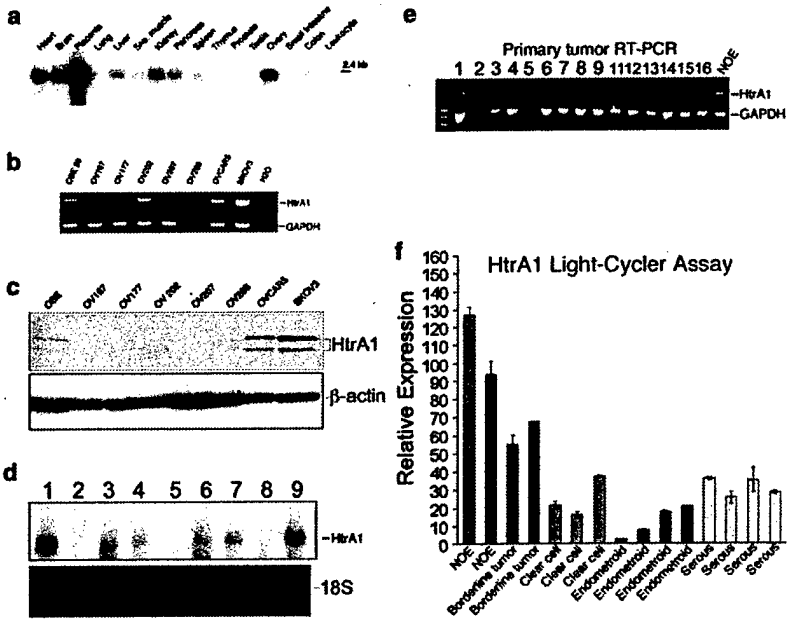

Figure 1 HtrA1 expression is downregulated in ovarian cancer. (**a**) Northern blot analysis of HtrA1 expression in normal tissues. The highest level of HtrA1 transcripts was detected in placenta followed by brain, heart, and ovary. (**b**) RT–PCR analysis of ovarian cancer cell lines indicates that HtrA1 is downregulated in four of seven cancer cell lines compared to short-term culture OSE50. (**c**) Western blot analysis of ovarian cancer cell lines also indicates a similar pattern of downregulation of HtrA1. (**d**) Diminished HtrA1 expression is observed in seven out of eight primary tumors (1–4, early stages; 5–9, late stages) by Northern blot. (**e, f**) Semiquantitative and quantitative RT–PCR of primary tumors. Absence or diminished expression of the HtrA1 transcript, compared to normal ovarian epithelial cells (NOE), is detected in primary tumors by semiquantitative RT–PCR (e) and by quantitative Light-Cycler (f). GAPDH is used as a loading control

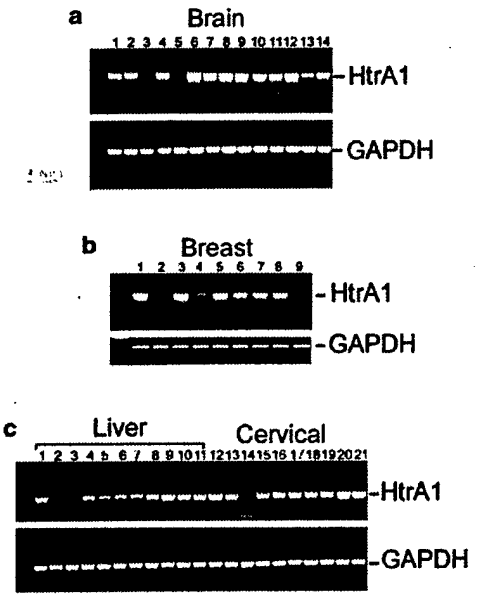

Figure 2 HtrA1 expression is aberrantly regulated in several types of cancer. (**a**) RT–PCR analysis of HtrA1 in primary brain tumors indicates downregulation of HtrA1 in two of 13 tumors. Lane 1: normal whole brain. (**b**) HtrA1 expression in downregulated in BT474 (lane 2), MDA-MB-~~453~~ (lane 4), and UACC893 (lane 9) breast cancer cell lines. 1, human mammary epithelial cells (HMEC control); 2, BT474; ~~3, MCF7~~; 4, MDA-MB-157; 5, MDA-MB-361; 6, MDA-MB-435; 7, MDA-MB-468; 8, T47D; 9, UACC812; and 10, UACC893. (**c**) HtrA1 expression is reduced in HepG2 (lane 2) and Hep3B (lane 3) liver cancer cell lines and C-33A (lane 14) cervical cancer cell line. 1, normal liver; 2, HepG2; 3, Hep3B; 4, Huh7; 5, PLC5; 6, SKHep1; 7, SNU182; 8, SNU387; 9, SNU475; 10, SNU423; 11, SNU449; 12, human keratinocyte; 13, C4a; 14,C-33A; 15, Caski; 16, HeLa; 17, HT3; 18, ME180; 19, Ms751; 20, SiHa; and 21, SW756

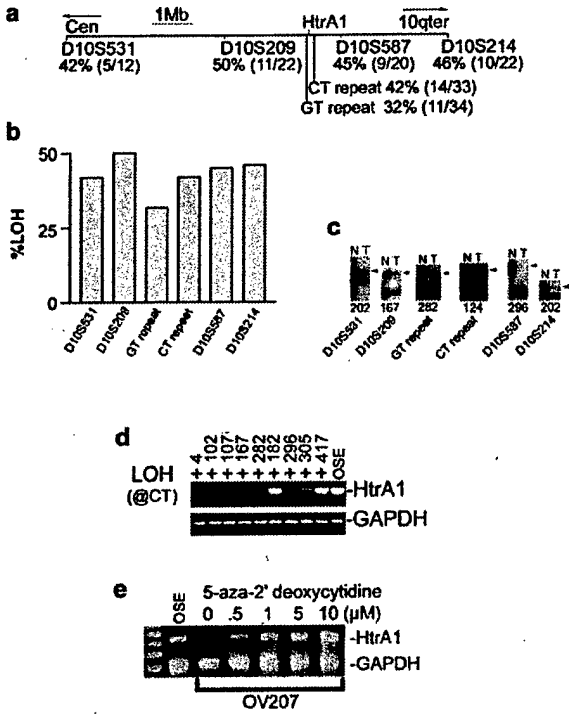

Figure 3 Mechanism of inactivation. (**a**) Markers used in the LOH studies, corresponding cytogenetic band location, and base position relative to htrA1 locus. (**b**) The frequencies of LOH calculated from informative samples at specific markers. (**c**) The representative LOH autoradiographs for each maker with LOH indicated by arrowheads. (**d**) LOH at CT repeat corresponds with reduced expression of HtrA1. (**e**) OV207 was treated with various concentrations of 5-aza-2′ deoxycytidine for 3 days, and HtrA1 expression was analysed by RT–PCR. A dose-dependent increase in HtrA1 expression was observed following this treatment

RNA was available. Of nine tumor samples that displayed LOH at CT repeat marker, seven tumors showed loss or reduced HtrA1 expression (Figure 3d). Tumors used in LOH analysis and the LOH score are listed in Table 1. To determine if additional mechanism, such as epigenetic silencing, could also be responsible for loss of HtrA1 expression, the ovarian cancer cell line OV207 was treated with the methyltransferase inhibitor 5-aza-2′ deoxycytidine. This treatment led to a dose-dependent increase in transcription of HtrA1 (Figure 3e), implicating methylation as another mechanism by which HtrA1 could be downregulated. However, additional experiments are needed to characterize specific sites of methylation regulating HtrA1 expression in ovarian cancer.

Mutational analysis by denaturing high-performance liquid chromatography (DHPCL)

To determine if mutations might also contribute to HtrA1 downregulation, a total of 96 tumor DNAs were analysed for mutations by the DHPLC (Schwartz *et al.*, 1999) using intronic primers (Table 2) flanking the nine exons present in *htrA1*. While single-nucleotide polymorphisms were detected in the intronic regions, no tumor-specific mutations were detected in any of the samples.

Downregulation of HtrA1 promotes anchorage-independent growth

A previous report indicated loss of HtrA1 expression in invasive melanoma and a decrease in matrix invasion *in vitro* following the re-expression of HtrA1 in melanoma LM cell line (Baldi *et al.*, 2002), suggesting that loss of HtrA1 may contribute to invasive phenotype. Since invasive phenotype depends not only on matrix migration but also on anchorage-independent growth, the latter was analysed in SKOV3 to determine the functional significance of HtrA1 downregulation in ovarian cancer. Since SKOV3 expresses endogenous HtrA1 (Figure 1c), HtrA1 expression was downregulated by antisense transfection. Of 12 stable clones expressing HtrA1 antisense, four clones displayed efficient downregulation of HtrA1 (Figure 4a, indicated by asterisks); thus they were used in the analysis of soft-

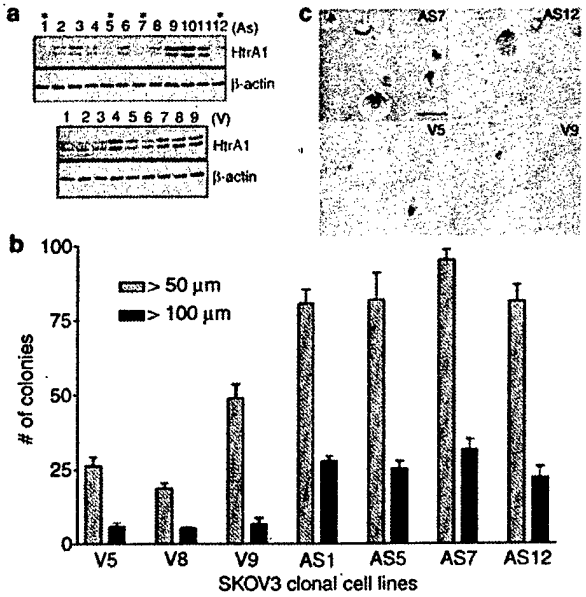

Figure 4 Downregulation of HtrA1 expression promotes the soft-agar growth of SKOV3. (**a**) HtrA1 expression is downregulated in four of 12 stable clones (upper panel). Clones used in soft-agar growth are indicated by asterisks. HtrA1 expression in nine stable clones transfected with vector control is shown for comparison (lower panel). β-Actin indicates loading control. (**b**) Downregulation of HtrA1 promotes anchorage-independent growth. A significantly higher number of colonies larger than 50 or 100 μm are observed in clones expressing antisense HtrA1. (**c**) A representative photomicrograph of soft-agar growth seen in antisense and vector-control clones

agar growth. As shown in Figure 4b and c, downregulation of HtrA1 resulted in a significant increase in the number of colonies grown on soft-agar compared to the vector-transfected controls. These results suggest that downregulation of HtrA1 may contribute to invasive phenotype.

Overexpression of HtrA1 induces cell death

Since HtrA1 also shares a high degree of sequence similarity with the proapoptotic HtrA2 (Suzuki *et al.*, 2001; Hegde *et al.*, 2002; Martins *et al.*, 2002; Verhagen *et al.*, 2002), particularly in the protease domain essential for apoptotic activity, the proapoptotic property of HtrA1 was tested in ovarian cancer cell line OV202. OV202 was selected in this analysis because it expresses very low levels of HtrA1 (Figure 1c). Exogenous expression of HtrA1 in OV202 induced cell rounding and death (Figure 5a, left panel) in a manner similar to that described in HEK293 cells following the transfection of HtrA2 (Suzuki *et al.*, 2001). Moreover, the cell rounding observed with HtrA1 expression in OV202 was not prevented by 100 μM zVAD(OMe)-fmk (fmk^*N*-(*N*α-benzyloxycarbonylvalinylalanyl) aspartic acid (*O*-methyl ester) fluoromethylketone) (Figure 5b), suggesting that this phenomenon may be caspase-independent. In contrast, OV202 cells transfected with the serine protease mutant S328A displayed a normal phenotype (Figure 5a, right panel). A significantly higher percentage of cell death was observed in cells transfected with the wild-type HtrA1 (Figure 5c and d). This increase in cell death was not observed with the serine protease mutant S328A (Figure 5c and d), suggesting that higher level of cell death was the result of the protease activity.

Discussion

In summary, this report describes the loss of HtrA1 expression in ovarian cancer and demonstrates the effects of HtrA1 downregulation and re-expression in ovarian cancer cell lines. In particular, we present evidence that expression of HtrA1 is reduced in several ovarian cancer cell lines and primary tumors. Moreover, the *htrA1* locus is subject to LOH and epigenetic inactivation. Previous analyses of glioblastoma, prostate cancer, malignant melanoma, and endometrial cancer with multiple markers on 10q have indicated evidence of two distinct loci for tumor-suppressor genes distal to 10q23 (Albarosa *et al.*, 1996). Although *PTEN* gene on 10q23.3 is probably the more proximal of these two loci, the distal locus is not yet well established. *DMBT1* (deleted in malignant brain tumors 1), mapping to 10q26.13, has been regarded as a potential tumor-suppressor gene representing the distal locus due to the presence of intragenic homozygous deletions and rare mutations (Mollenhauer *et al.*, 1997; Mueller *et al.*, 2002). However, the tumor suppressive role of the gene is still controversial. Two recent reports suggest that DMBT1 may not be a major target of inactivation in malignant melanoma and glioma (Deichmann *et al.*, 2002; Sasaki *et al.*, 2002). These reports underscore the importance of identifying another candidate tumor-suppressor gene in this frequently deleted region. Human *htrA1* gene maps to chromosome 10q26.13 in close proximity to DMBT1. The microsatellite markers used in the LOH analysis are within 10q25.3–10q26.2, encompassing both *htrA1* and *DMBT1*. These markers showed high frequency of deletion in ovarian tumors. Consistent with the notion of HtrA1 as a tumor suppressor, downregulation of HtrA1 in SKOV3 by antisense transfection promoted anchorage-independent growth. Additional support for HtrA1 as a putative tumor suppressor came from the study in malignant melanoma by Baldi *et al.* (2002). HtrA1 expression was significantly lower in autologous lymph node metastases (LM) compared to primary melanomas (Baldi *et al.*, 2002). Stable overexpression of HtrA1 in melanoma LM cell lines attenuated matrix invasion (Baldi *et al.*, 2002), and inhibited proliferation as well as cell growth *in vivo* in nu/nu mice. In addition, the fact that HtrA1 was originally identified as a SV40 transformation sensitive marker lends further support to the potential role of HtrA1 as a tumor suppressor. These observations raised the possibility that HtrA1 could potentially represent the long sought-after distal tumor suppressor in 10q26.

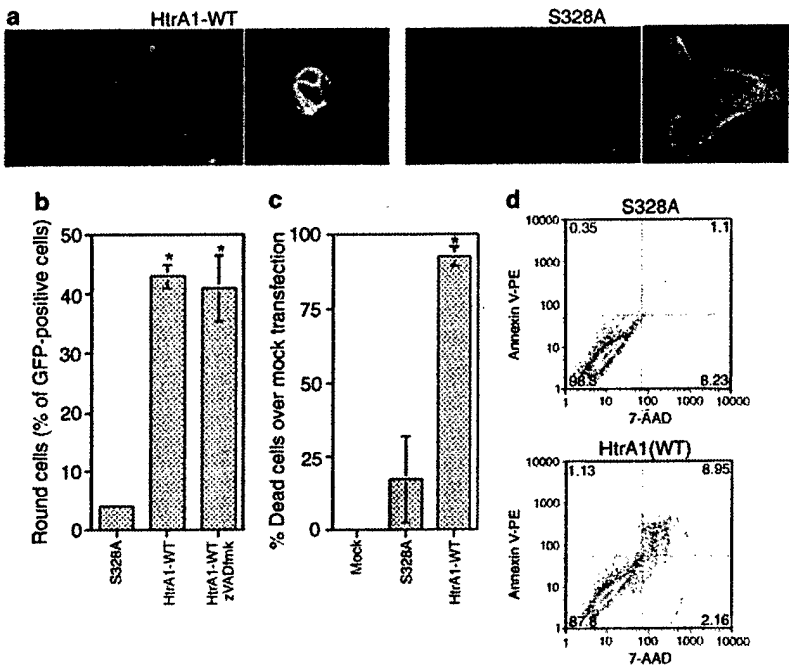

Figure 5 Exogenous expression of HtrA1 induces cell death. (**a**) OV202 cells were electroporated with 20 μg of plasmid encoding serine protease mutant HtrA1 (S328A) or wild-type HtrA1 (HtrA1-WT). After 24 h, GFP-positive cells were visualized by fluorescence microscopy. Cells transfected with HtrA1 displayed round morphology, whereas cells transfected with mutant remained flattened. (**b**) GFP-positive OV202 cells with round morphology were counted, and expressed as the percentage of total GFP-positive cells. (**c**) Comparison of % cell death (trypan blue positive) induced by S328A and wild-type HtrA1 normalized with cell death from mock transfection. The error bars represent the standard error of means (s.e.m.) calculated from triplicate samples. Asterisks indicate a statistically significant difference from the control as determined by one-way ANOVA ($P<0.05$). (**d**) When cell death was analysed with Annexin V-phycoerythrin (PE), a significantly higher percentage of cell death was observed in cells transfected with wild-type HtrA1 (WT) compared to protease mutant HtrA1 (S328A)

Loss of function of tumor suppressors requires inactivation of both alleles either by homozygous deletions, heterozygous deletions in combination with tumor-specific mutations, and/or epigenetic inactivation by hypermethylation. Our results indicated high frequency of LOH near the gene. However, neither homozygous deletions nor tumor-specific mutations within the coding exons were detected. Instead, our preliminary analysis indicated methylation as a second hit inactivating the function of HtrA1, as evidenced by the induction of transcription after 5-aza-2′-deoxycytidine treatment in the OV207 cell line. Future studies to delineate the specific CpG sites involved in this inactivation are ongoing.

In addition to its role in regulating cell growth, re-expression of HtrA1 induces cell death in ovarian cancer cells. HtrA1-induced cell death is not attenuated by the broad-spectrum caspase inhibitor zVAD(OMe)fmk (Garcia-Calvo *et al.*, 1998), but instead reflects serine protease activity. This is perhaps not unexpected given the fact that other proteases also induce cell death (Williams and Henkart, 1994; Suzuki *et al.*, 2001; Verhagen *et al.*, 2002). In particular, the human homologue HtrA2, which shares extensive homology with the C-terminal protease and postsynaptic density protein 95-Discs large-Zona occuldens 1 (PDZ) domains of HtrA1, also induces cell death independent of caspase activation (Suzuki *et al.*, 2001). In addition to induction of cell death via serine protease, HtrA2, when released from mitochondria during initial steps of apoptosis, also activates caspases by antagonizing inhibitors of apoptosis (IAPs) via its N-terminal tetrapeptide IAP-binding motif (Suzuki *et al.*, 2001; Hegde *et al.*, 2002; Martins, 2002; ~~Martins *et al.*, 2002~~; Verhagen *et al.*, 2002). In contrast, HtrA1 does not contain the N-terminal tetrapeptide IAP-binding motif, and therefore it is not expected to be involved in caspase activation. Nonetheless, both HtrA1 and HtrA2 can induce cell death via protease domain independent of caspases, suggesting a potential role of these proteases in caspase-independent cell death. Interestingly, HtrA1 was originally described as a secreted protease, yet it is detected in whole-cell lysates and induces cell death. Further analysis of this apparent paradox is required.

In addition to HtrA2, the identification and cloning of HtrA3 is recently described (Nie *et al.*, 2003). HtrA3 shares high degree of sequence and domain homologies with HtrA1, and therefore it may share functional similarity with HtrA1. Although both HtrA1 and HtrA3 are highly expressed in normal ovary (Nie *et al.*, 2003), semiquantitative RT–PCR analysis of ovarian cancer cell lines indicates that HtrA3 is lost in cell lines that

express HtrA1 (data not shown). The differential expression between HtrA1 and HtrA3 in ovarian cancer cells is intriguing, and necessitates further studies.

The N-terminus of HtrA1 also shares domain homology with the candidate tumor-suppressor Mac25. Mac25 (IGFBP-rP1) is differentially expressed in meningioma, prostate, and mammary cancers and is thought to regulate cell growth by affecting cell-cycle mechanisms (Swisshelm *et al.*, 1995; Baldi *et al.*, 2002). Addition of recombinant Mac25 to the culture medium suppressed the growth of cell lines of diverse origins including cervical and osteosarcomas (Kato, 2000). These data suggest the possibility that the N-terminal domain of HtrA1 may also regulate cell growth in similar fashion. It should be noted that the growth suppression by Mac25 domain might be affecting cell proliferation rather than cell death, since proteolytically inactive S328A mutant containing functional Mac25 domain has no effect in inducing cell death.

Here, we have shown that HtrA1 is consistently downregulated in ovarian cancer. Loss or lower levels of expression in ovarian cancer is due to deletion of an allele due to LOH, thus identifying a new region of deletion for ovarian cancer. Our further studies indicate that HtrA1 may modulate cell death and anchorage-independent growth of ovarian cancer cells. Collectively these results highlight the potential role of HtrA1 as a tumor suppressor. Further studies that identify molecular targets that interact with HtrA1 will enhance our understanding the role of HtrA1 in normal and malignant cells.

Materials and methods

Cell culture

OV167, OV177, OV202, OV207, and OV266 were low-passage ovarian cancer cell lines established at the Mayo Clinic (Conover *et al.*, 1998), while OVCAR-3, OVCAR-5, and SKOV-3 were purchased from American Type Culture Collection (Manassas, VA, USA). All other cells were grown according to the manufacturer's recommendations.

Tissue processing and tumors

All the tumors were snap-frozen tissues. Tumor contents of the tissues were assessed by hematoxylin and eosin (H&E)-stained sections and verified by a pathologist (Dr Gary Keeney) at the Mayo Clinic. Only tumors with 75–90% tumor content were used for RT–PCR analysis. For control, 20–30 normal ovarian epithelial cell brushings were pooled from patients without cancer and the epithelial nature of these brushings were verified by H&E staining.

Plasmids and antibodies

The plasmids encoding wild-type or mutant S328A HtrA1 were generated by PCR cloning into pcDNA3.1. vector as described previously (Hu *et al.*, 1998). To generate carboxyl terminus GFP fusion construct of HtrA1, PCR products flanking the entire ORF or C-terminal domain corresponding to codons 153–480 of HtrA1 were cloned into pcDNA3.1/CT-GFP TOPO vector. Proper construction of all the plasmids was confirmed by DNA sequencing. Antiserum specific for HtrA1 was raised as described previously (Hu *et al.*, 1998).

Northern blot analysis

In total, 15 μg of total RNA was resolved on 1.2%. formaldehyde agarose gels and blotted in 1 × SPC buffer onto Hybond N membranes (Amersham, Piscataway, NJ, USA). The probes were labeled using the random primer labeling system (Invitrogen, Carlsbad, CA, USA) and purified using spin columns (TE100) from Clontech (Palo Alto, CA, USA). Filters were hybridized at 68°C with radioactive probes in a microhybridization incubator (Robbins Scientific, Sunnyvale, CA, USA) for 1–3 h in Express Hybridization solution (Clontech, Palo Alto, CA, USA) and washed according to the manufacturer's guidelines. The probe corresponds to the open reading frame of HtrA1. It does not crosshybridize with HtrA2 or HtrA3.

Immunoblotting

Cell lysates were resolved by SDS–PAGE under reducing conditions, followed by transfer onto 0.45 μm nitrocellulose membrane. After the transfer, immunoblotting was carried out as previously described using affinity-purified polyclonal HtrA antibody (Hu *et al.*, 1998).

Semiquantitative RT–PCR

A total of 50–100 ng of reverse-transcribed cDNA was used in a multiplex reaction with the following primers: HtrA1 forward (5′-TAT CGC GGA CGT GGT GGA GAA GAT CG-3′) and HtrA1 reverse (5′-GTC CAG CTC ATG CCT CTG CCT-3′) to yield a 595 bp product and GAPDH forward (5′-ACC ACA GTC CAT GCC ATC AC-3′) and GAPDH reverse (5′-TCC ACC ACC CTG TTG CTT GTA-3′) to yield a 450 bp product. The PCR reactions contained 50 mM KCl, 10 mM Tris-HCl (pH 8.3), 1.5 mM $MgCl_2$, 400 μM of each HtrA1 primer and 50 μM of each GAPDH primer, and 0.5 U of *Taq polymerase* (Qiagen, Valencia, CA, USA) in a 12.5 μl reaction volume. The conditions for amplification were: 94°C for 3 min, then 30 cycles of 94°C for 30 s, 58°C for 30 s, and 72°C for 30 s in a Perkin Elmer-Cetus 9600 Gene-Amp PCR system. The products of the reaction were resolved on a 1.6% agarose gel. One amplicon was cut from the gel, purified with QIAquick Gel Extraction Kit (Qiagen, Valencia, CA, USA), and sequenced to verify the specificity of PCR reactions.

Light-cycler PCR analysis

Using HtrA1F1 (5′-TCC GCA ACT CAG ACA TGG AC-3′) and HtrA1R1 (5′-GGC CTC CCG AGT TTC CAT AG-3′) plus RPS9F (5′-TCG CAA AAC TTA TGT GAC CC-3′) and RPS9R (5′-TCC AGC ACC CCC AAT C-3′) primers, duplex PCR amplification was carried out with Light-Cycler (Roche, Indianapolis, IN, USA) in the presence of SYBR-Green dye according to the following conditions: 1 min at 95°C for initial denaturation, followed by 40 cycles at 95°C (10 s), 58°C (15 s), and 72°C (20 s), followed by the measurement of fluorescence at the end of each cycle. After the 40th cycle, melting curve analyses were performed with Light-Cycler software by denaturing the sample at 95°C, rapidly cooling down to 65°C for 15 s, and measuring the fluorescence as the sample temperature was gradually raised to 95°C in the steps of 0.1°C/s. Each run included a negative control.

LOH analysis of primary ovarian tumors

The markers used in this study are listed in Figure 2b, along with their chromosomal locations. The PCR reaction mix contained: 50 ng of genomic DNA, 50 mM KCl, 10 mM Tris-HCl (pH 8.3), 1.5 mM $MgCl_2$, 200 μM of each primer, 0.05 μl of [α-^{32}P]CTP (10 μCi/μl) and 0.5 U of *Taq polymerase* in a 10 μl reaction volume. The conditions for amplification were: 94°C for 2 min, then 30 cycles of 94°C for 30 s, 55–58°C for 30 s, and 72°C for 30 s in a Perkin Elmer-Cetus 9600 Gene-Amp PCR system in a 96-well plate. The PCR products were denatured and run on 6% polyacrylamide sequencing gels containing 8 M urea. The gels were dried, autoradiographed for 16–24 h and scored for LOH. Multiple exposures were used before scoring for LOH. Allelic imbalance indicative of LOH as scored when there was more than 50% loss of intensity of one allele in the tumor sample with respect to the matched allele from normal tissue.

Induction of HtrA1 expression by 5-aza-2′ deoxycytidine

The ovarian cancer cell line OV207 was treated with various concentration of 5-aza-2′ deoxycytidine (Sigma, St Louis, MO, USA) for 3 days, with addition of fresh 5-aza-2′ deoxycytidine every day, and HtrA1 expression was analysed by RT–PCR.

Mutational analysis by DHPLC

Samples used for mutation screening and sequencing were amplified in 20 μl reaction volumes containing 50 ng of genomic DNA, 25 pmoles each of sense and antisense primers, dNTPs (Perkin-Elmer, Foster City, CA, USA), 0.2 ml of *Taq polymerase* (AmpliTaq Gold, Perkin-Elmer), 1 × buffer provided by the manufacturer, and 1.5 mM of $MgCl_2$. PCR amplification was for 30 cycles using the following profile: 94°C for 30 s, the optimized annealing temperature for 30 s, and 72°C for 30 s. The enzyme was initially activated by denaturation at 95°C for 9 min, and final extension was performed at 72°C for 10 min. The annealing temperatures for various primer sets were 56°C for HtrA1 exons 2, 4, 6, 7, 8, and 9; 58°C for exon 3; 52°C for exon 5. Exon 1 was amplified using GC melt (Clontech, Palo alto, CA, USA) following the manufacturer's instructions. The primers used for DHPLC analysis are listed in Table 2.

Establishment of antisense HtrA1 stable transfectants

Exponentially growing SKOV3 cells in 100 mm dishes were washed with serum-free medium, and incubated with a mixture of 5 μg of plasmid, 30 μl of LipofectAmine, and 20 μl of Plus reagent (Invitrogen, Carlsbad, CA, USA). After 3 h incubation, complete medium with serum was added. Beginning 24 h after the start of transfection, G418 was added to a final concentration of 400 μg/ml to select the transfectants. For controls, cells were similarly transfected with empty pcDNA3.1 + vector and selected.

Soft-agar assay

Complete medium containing 1% low-melting point temperature agarose was poured into six-well plates (2 ml per well) and allowed to solidify at 4°C to form a bottom layer. SKOV cells (5000/well; vector or antisense transfected clones) were mixed in complete medium with 0.5% agarose and seeded as a top layer. The agarose was solidified at 4°C and then incubated at 37°C. On day 16, the colonies were stained with 1 ml of PBS containing 0.5 mg/ml *p*-iodonitrotetrazolium violet, which is converted into colored product by live cells only. Micrographs were taken at 10 × using a Spot II-RT digital camera (Nikon, Millburn, NJ, USA), and colonies larger than 50 and 100 μm in diameter were counted.

Electroporation

At 2 days prior to transfection, cells were incubated in antibiotic-free culture medium. On the day of transfection, two million cells in 0.4 ml Cytomix (van den Hoff *et al*., 1992) were mixed with 20 μg DNA, and electroporated in 0.4 cm cuvettes using BTX T820 square wave electroporator (BTX, San Diego, CA, USA). Typical settings for electroporation were two pulses of 5 ms duration at 330 V for OV202, resulting in 86% transfection efficiency. Immediately after electroporation, cells were allowed to recover for 10 min at room temperature before plating in antibiotic-free culture medium.

Assessment of cell death

At 24 h after the electroporation, free-floating cells in the medium were collected, stained with trypan blue, and counted in a hemacytometer. Approximately 20% of cells died from electroporation. The amount of cell death in mock electroporation served as a baseline for determining % cell death in S328A- or HtrA1-transfected groups.

Annexin V labeling and flow cytometry

Annexin V-PE (PharMingen, San Diego, CA, USA) labeling was performed according to the supplier's instruction. Briefly, cells transfected overnight with wild-type or protease mutant HtrA1 were released by trypsinization and sedimented at 200 *g* for 5 min. All further steps were performed at 4°C unless otherwise indicated. Samples were washed two times with cold PBS and resuspended in 1 × binding buffer at a concentration of 1 × 10^6 cells/ml. Then, 100 μl of solution was transferred to a new 5 ml culture tube, and 5 μl of Annexin V-PE and 7-AAD were added. Cells were incubated for 15 min at 25°C in the dark. In all, 400 μl of 1 × binding buffer was added into each tube before flow microfluorimetry on a Becton-Dickinson FACScan (San Jose, CA, USA). Annexin V-stained cells were analysed by FlowJo software (Ashland, OR, USA).

Abbreviations

DHPLC, denaturing high-performance liquid chromatography; IGFBP, insulin-like growth factor binding protein; PDZ, postsynaptic density protein 95-Discs large-Zona occuldens 1; LOH, loss of heterozygosity; OSE, ovarian surface epithelium; XIAP, X-linked inhibitor of apoptosis protein; H&E, hematoxylin and eosin; zVAD(OMe)-fmk, *N*-(*N*α-benzyloxycarbonylvalinylalanyl) aspartic acid (*O*-methyl ester) fluoromethylketone; PE, phycoerythrin; 7-AAD, 7-amino-actinomycin.

Acknowledgements

We thank Kim R Kalli for providing us with short-term culture of ovarian surface epithelial cells. This work is supported in part by DOD Grnt DAMD17-99-1-9504 to VS, DIS, and SHK and a John W Anderson Foundation grant to VS and the Mayo Foundation.

and Minnesota Ovarian Cancer Alliance grant

References

Albarosa R, Colombo BM, Roz L, Magnani I, Pollo B, Cirenei N, Giani C, Conti AM, DiDonato S and Finocchiaro G. (1996). *Am. J. Hum. Genet.*, **58**, 1260–1267.

Chien J, Wong E, Nikes E, Noble MJ, Pantazis CG and Shah GV. (1999). *Oncogene*, **22**, 3376–3382.

Clausen T, Southan C and Ehrmann M. (2002). *Mol. Cell*, **10**, 443–455.

Conover CA, Hartmann LC, Bradley S, Stalboerger P, Klee GG, Kalli KR and Jenkins RB. (1998). *Exp. Cell Res.*, **238**, 439–449.

Deichmann M, Mollenhauer J, Helmke B, Thome M, Hartschuh W, Poustka A and Naher H. (2002). *Oncology*, **63**, 166–172.

Enomoto T, Weghorst CM, Inoue M, Tanizawa O and Rice JM. (1991). *Am. J. Pathol.*, **139**, 777–785.

Garcia-Calvo M, Peterson EP, Leiting B, Ruel R, Nicholson DW and Thornberry NA. (1998). *J. Biol. Chem.*, **273**, 32608–32613.

Greenlee RT, Murray T, Bolden S and Wingo PA. (2000). *CA Cancer J. Clin.*, **50**, 7–33.

Hegde R, Srinivasula SM, Zhang Z, Wassell R, Mukattash R, Cilenti L, DuBois G, Lazebnik Y, Zervos AS, Fernandes-Alnemri T and Alnemri ES. (2002). *J. Biol. Chem*, **277**, 432–438.

Hu SI, Carozza M, Klein M, Nantermet P, Luk D and Crowl RM. (1998). *J. Biol. Chem.*, **273**, 34406–34412.

Kato MV. (2000). *Mol. Med.*, **6**, 126–135.

Katsaros D, Theillet C, Zola P, Louason G, Sanfilippo B, Isaia E, Arisio R, Giardina G and Sismondi P. (1995). *Anticancer Res.*, **15**, 1501–1510.

Kohler MF, Marks JR, Wiseman RW, Jacobs IJ, Davidoff AM, Clarke-Pearson DL, Soper JT, Bast Jr RC and Berchuck A. (1993). *J. Natl. Cancer Inst.*, **85**, 1513–1519.

Krojer T, Garrido-Franco M, Huber R, Ehrmann M and Clausen T. (2002). *Nature*, **416**, 455–459.

Li SB, Schwartz PE, Lee WH and Yang-Feng TL. (1991). *J. Natl. Cancer Inst.*, **83**, 637–640.

Martins LM, Iaccarino I, Tenev T, Gschmeissner S, Totty NF, Lemoine NR, Savopoulos J, Gray CW, Creasy CL, Dingwall C and Downward J. (2002). *J. Biol. Chem.*, **277**, 439–444.

Mollenhauer J, Wiemann S, Scheurlen W, Korn B, Hayashi Y, Wilgenbus KK, von Deimling A and Poustka A. (1997). *Nat. Genet.*, **17**, 32–39.

Mueller W, Mollenhauer J, Stockhammer F, Poustka A and von Deimling A. (2002). *Oncogene*, **21**, 5956–5959.

Nie GY, Hampton A, Li Y, Findlay JK and Salamonsen LA. (2003). *Biochem. J.*, **371** (Part 1), 39–48.

Orsulic S, Li Y, Soslow RA, Vitale-Cross LA, Gutkind JS and Varmus HE. (2002). *Cancer Cell*, **1**, 53–62.

Pallen MJ and Wren BW. (1997). *Mol. Microbiol.*, **26**, 209–221.

Ross JS, Yang F, Kallakury BV, Sheehan CE, Ambros RA and Muraca PJ. (1999). *Am. J. Clin. Pathol.*, **111**, 311–316.

Sasaki H, Betensky RA, Cairncross JG and Louis DN. (2002). *Cancer Res.*, **62**, 1790–1796.

Schwartz DI, Lindor NM, Walsh-Vockley C, Roche PC, Mai M, Smith DI, Liu W and Couch FJ. (1999). *Breast Cancer Res. Treat.*, **58**, 25–29.

Shridhar V, Sen A, Chien J, Staub J, Avula R, Kovats S, Lee J, Lillie J and Smith DI. (2002). *Cancer Res.*, **62**, 262–270.

Spiess C, Beil A and Ehrmann M. (1999). *Cell*, **97**, 339–347.

Suzuki Y, Imai Y, Nakayama H, Takahashi K, Takio K and Takahashi R. (2001). *Mol. Cell*, **8**, 613–621.

Swisshelm K, Ryan K, Tsuchiya K and Sager R. (1995). *Proc. Natl. Acad. Sci. USA*, **92**, 4472–4476.

van den Hoff MJ, Moorman AF and Lamers WH. (1992). *Nucleic Acids Res.*, **20**, 2902.

Verhagen AM, Silke J, Ekert PG, Pakusch M, Kaufmann H, Connolly LM, Day CL, Tikoo A, Burke R, Wrobel C, Moritz RL, Simpson RJ and Vaux DL. (2002). *J. Biol. Chem.*, **277**, 445–454.

Williams MS and Henkart PA. (1994). *J. Immunol.*, **153**, 4247–4255.

Yu Y, Xu F, Peng H, Fang X, Zhao S, Li Y, Cuevas B, Kuo WL, Gray JW, Siciliano M, Mills GB and Bast Jr RC. (1999). *Proc. Natl. Acad. Sci. USA*, **96**, 214–219.

Zumbrunn J and Trueb B. (1996). *FEBS Lett.*, **398**, 187–192.

Baldi A, De Luca A, Morini M, Battista T, Felsani A, Baldi F, Catricala C, Amantea A, Noonan DM, Albini A, Natali PG, Lombardi D, Paggi MG. (2002). Oncogene, 21, 6684-8.

MS #6

Oncogene (2001) 20, 980–988

www.nature.com/onc

Cloning and characterization of a senescence inducing and class II tumor suppressor gene in ovarian carcinoma at chromosome region 6q27

Francesco Acquati[1,8], Cristina Morelli[2,8], Raffaella Cinquetti[1], Marco Giorgio Bianchi[1], Davide Porrini[1], Liliana Varesco[3], Viviana Gismondi[3], Romina Rocchetti[4], Simona Talevi[4], Laura Possati[4], Chiara Magnanini[2], Maria G Tibiletti[5], Barbara Bernasconi[5], Maria G Daidone[6], Viji Shridhar[7], David I Smith[7], Massimo Negrini[2], Giuseppe Barbanti-Brodano[2] and Roberto Taramelli*[,1]

[1]Dipartimento di Biologia Strutturale e Funzionale, Universita' dell'Insubria, Varese, Italy; [2]Dipartimento di Medicina Sperimentale e Diagnostica, Sezione di Microbiologia, Università di Ferrara, I-44100 Ferrara, Italy; [3]Istituto Nazionale per la Ricerca sul Cancro Genova, Italy; [4]Istituto di Scienze Biomediche, Università di Ancona, I-60131 Ancona, Italy; [5]Laboratorio di Anatomia Patologica, Ospedale di Circolo, Varese, Italy; [6]Dipartimento Oncologia Sperimentale, Istituto Nazionale Tumori, Milano, Italy; [7]Division of Experimental Pathology, Department of Laboratory Medicine and Pathology, Mayo Clinic, Rochester, MN 55905, USA

Cytogenetic, molecular and functional analysis has shown that chromosome region 6q27 harbors a senescence inducing gene and a tumor suppressor gene involved in several solid and hematologic malignancies. We have cloned at 6q27 and characterized the RNASE6PL gene which belongs to a family of cytoplasmic RNases highly conserved from plants, to man. Analysis of 55 primary ovarian tumors and several ovarian tumor cell lines indicated that the RNASE6PL gene is not mutated in tumor tissues, but its expression is significantly reduced in 30% of primary ovarian tumors and in 75% of ovarian tumor cell lines. The promoter region of the gene was unaffected in tumors cell lines. Transfection of RNASE6PL cDNA into HEY4 and SG10G ovarian tumor cell lines suppressed tumorigenicity in nude mice. When tumors were induced by RNASE6PL-transfected cells, they completely lacked expression of RNASE6PL cDNA. Tumorigenicity was suppressed also in RNASE6PL-transfected pRPcT1/H6cl2T cells, derived from a human/mouse monochromosomic hybrid carrying a human chromosome 6 deleted at 6q27. Moreover, 63.6% of HEY4 clones and 42.8% of the clones of XP12ROSV, a Xeroderma pigmentosum SV40-immortalized cell line, transfected with RNASE6PL cDNA, developed a marked senescence process during *in vitro* growth. We therefore propose that RNASE6PL may be a candidate for the 6q27 senescence inducing and class II tumor suppressor gene in ovarian cancer. *Oncogene* (2001) **20,** 980–988.

Keywords: ovarian carcinoma; senescence; chromosome 6q27; Class II tumor suppressor gene; ribonuclease

*Correspondence: R Taramelli
[8]Francesco Acquati and Cristina Morelli contributed equally to this work.
Received 24 October 2000; revised 12 December 2000; accepted 14 December 2000

Introduction

Abnormalities of the long arm of chromosome 6 are associated with several solid neoplasms including carcinomas of the ovary (Saito *et al.*, 1992; Foulkes *et al.*, 1993; Cooke *et al.*, 1996; Orphanos *et al.*, 1995; Tibiletti *et al.*, 1996), breast (Develee *et al.*, 1991; Theile *et al.*, 1996; Chappel *et al.*, 1997), uterus (Tibiletti *et al.*, 1997), stomach (Queimado *et al.*, 1995), liver (DeSouza *et al.*, 1995), colon and rectum (Honchel *et al.*, 1996), kidney (Morita *et al.*, 1991), parathyroid gland (Tahara *et al.*, 1996), melanoma (Millikin *et al.*, 1991) and hematological malignancies such as non-Hodgkin B-cell lymphoma (Gaidano *et al.*, 1992) and acute lymphoblastic leukemia (Hayashi *et al.*, 1990). Among the solid tumors, ovarian cancers have been the focus of intense studies, because very little is known about the genetic pathways underlying ovarian carcinogenesis. Moreover, ovarian tumors are still associated with a rather high mortality rate, mostly due to delay in diagnosis which usually is performed at the late stages of the disease. The elucidation of the genetic events leading to inactivation of tumor suppressor genes or activation of oncogenes in ovarian tumors is therefore greatly needed.

By employing the loss of heterozygosity (LOH) assay with markers localized along the entire long arm of chromosome 6, several consensus regions of loss have been delineated. From centromere to telomere the order of these regions is 6q21–23.3 (Orphanos *et al.*, 1995; Shridhar *et al.*, 1999), 6q25.1–25.2 (Colitti *et al.*, 1998) and 6q26–27 (Saito *et al.*, 1992; Foulkes *et al.*, 1993; Cooke *et al.*, 1996; Orphanos *et al.*, 1995; Tibiletti *et al.*, 1996). The latter region has been deeply investigated and fine mapping has disclosed a genomic interval flanked by markers D6S193 and D6S149 as the shortest region lost in ovarian tumors (Cooke *et al.*, 1996; Saito *et al.*, 1996). Deletions at 6q27 were detected in 18 out of 20 benign ovarian tumors

(Tibiletti *et al.*, 1998), indicating that alterations in one or more genes mapping in this region are one of the earliest events in ovarian carcinogenesis.

Furthermore, the survey of more than 12 studies, reporting allele losses in ovarian carcinomas, allowed the identification of an even shorter region, defined by markers D6S193 and D6S297 which is included in the greater D6S193–D6S149 interval (Cooke *et al.*, 1996). The analysis of the critical D6S193–D6S149 interval resulted in the construction of a long range physical map and a YAC contig of the region (Tibiletti *et al.*, 1998; Hauptschein *et al.*, 1998). Physical measurements indicate that the distance between D6S193 and D6S149 is approximately 900 Kb, whereas the smaller D6S193–D6S297 interval spans about 100 Kb (Tibiletti *et al.*, 1998; Hauptschein *et al.*, 1998). Within the latter genomic region we have recently mapped, cloned and characterized a cDNA (RNASE6PL) (Trubia *et al.*, 1997; Acquati *et al.*, 2000) coding for a protein with a great similarity to a class of highly conserved cytoplasmic RNases present in plants (Anderson *et al.*, 1986; Clark *et al.*, 1990), animal viruses (Schneider *et al.*, 1993), bacteria (Meador and Kennell, 1990), fungi (McClure *et al.*, 1989), drosophila (Hime *et al.*, 1995) and mouse (Trubia *et al.*, 1997). Interestingly, although these enzymes from different organisms fulfill different biological functions, a common feature of their activity is the control of cell growth (McClure *et al.*, 1990). This effect is particularly challenging due to the chromosomal location of the human RNASE6PL gene at 6q27. Indeed, RNASE6PL may be a candidate tumor suppressor gene whose loss could contribute to the development or progression of ovarian cancers. We have assessed such potential role for RNASE6PL and we present here molecular and functional data supporting an involvement of this gene in senescence and in ovarian tumorigenesis.

Results

Genomic organization of the RNASE6PL gene

The structure of the RNASE6PL gene was determined by YAC subcloning (Tibiletti *et al.*, 1998, Hauptschein *et al.*, 1998) and cosmid assembling. This gene, which is present in a single copy in the genome, spans approximately 27 Kb of genomic DNA and is split into nine exons and eight introns (the accession number for the genomic sequence of the gene is AL159163).

Mutation analysis of the RNASE6PL gene in primary ovarian cancers

Fifty-five microdissected primary ovarian tumors, classified from stage II to stage IV, were selected for this analysis. These tumors were already known to contain 6q26-qter deletions in at least one of the chromosome 6 homologues (Tibiletti *et al.*, 1996; Tibiletti and Taramelli, unpublished results). According to the Knudson hypothesis, the remaining RNASE6PL allele or alleles (most of the tumors were aneuploid for chromosome 6) are expected to be altered by inactivating mutations or small deletions. Using exon 1, 2, 7, 8 and 9 primer pairs, several abnormal SSCP bands were observed. Sequence analysis revealed the presence of a missense common variant in exon 9 (a C to T at nucleotide position 708 with respect to the ATG replacing Arg with Trip). In addition, three silent base substitutions in exon 1, 8 and 9 and two common single-base changes in intron 1 and 6 were detected. It was possible to confirm the germline origin only of exon 9 and intron 1 modifications. Most likely these sequence variants are common polymorphisms because, at least in some cases, the same alterations were found to be present in the corresponding germ line. Also, the 5′ and 3′ regions of the gene, investigated by sequence analysis for the extension of 2 Kb, were found to be intact. On the whole, this analysis indicates that the RNASE6PL gene is not affected by mutations in primary ovarian cancers. Furthermore, the HEY4 and OVCAR3 ovarian cancer cell lines were also investigated, but as in the primary tumors no mutations were found.

Expression of RNASE6PL in normal tissues, primary ovarian tumors and ovarian tumor cell lines

Since the RNASE6PL gene does not seem to be mutated in primary ovarian tumors and tumor cell lines, we proceeded to study its expression in normal and neoplastic tissues. The 1.4 Kb message of the RNASE6PL gene is rather ubiquitous being present, although at variable levels, in all tissues that were examined (Figure 1a). When fourteen ovarian cell lines were studied and compared with normal ovarian tissue, several changes in RNASE6PL expression were detected. Figure 1b shows a representative example of eight cell lines where a reduced signal of RNASE6PL mRNA was detected in five samples (HEY4, OV1225, OV166, SW626, OVRS1000), while in one cell line (SG10G) the expression of the gene was totally abolished and in two cell lines (SKOV3 and OVCR3) was greatly enhanced. A series of 55 primary ovarian tumors were also analysed and decreased expression of RNASE6PL mRNA, below 25% of the normal ovarian tissue, was detected in 15 (30%) of them. As shown in Figure 1c, some samples displayed easily detectable levels of RNASE6PL mRNA, whereas in other samples the signal was barely detectable.

Transfection of tumor and immortal cell lines, induction of senescence and suppression of tumorigenicity

In order to verify whether the RNASE6PL gene suppresses *in vitro* the transformed and immortal phenotype, we transfected the ovarian cancer cell lines HEY4 and SG10G as well as the SV40-immortalized cell line XP12ROSV with the pcDNA/Neo-RNS6 vector, containing the full-length human RNASE6PL cDNA under the control of the cytomegalovirus immediate-early promoter. Suppression of tumorigeni-

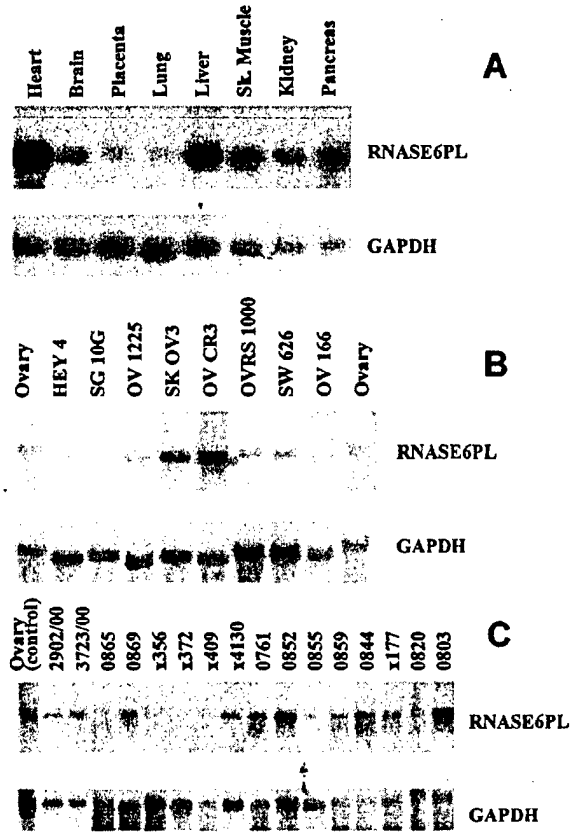

Figure 1 Expression pattern of RNASE6PL in normal and cancer cells. ^{32}P-labeled RNASE6PL and GAPDH cDNA probes were used for Northern blot hybridizations of a commercial poly (A)$^+$RNA filter representing several human tissues (**a**), a filter containing 25 μg per lane of total RNA from eight ovarian cancer-derived cell lines and a normal ovarian tissue (**b**), and a filter containing 20 μg per lane of total RNA from sixteen primary ovarian carcinomas and a normal ovarian tissue (**c**). Radioactive band intensity from each lane was measured by means of a PhosphorImage device and the RNASE6PL expression levels were calculated for each sample following normalization with the signals obtained with the GAPDH control probe

city was assessed in nude mice by inoculation of transfected HEY4 and SG10G cells as well as by inoculation of pRPc cells cotransfected with the plasmids pMT89, containing the RNASE6PL cDNA, and pGK (see Materials and methods). These cell lines were selected for transfection for the following reasons: the HEY4 cells show an expression of RNASE6PL reduced to 10% of normal ovarian tissue (Figure 1b), while the SG10G and XP12ROSV cells completely lack expression of the RNASE6PL gene. The SG10G cell line was found to miss completely chromosome 6 as evidenced by conventional cytogenetic and FISH analyses (data not shown). The pRPc cells are mouse cells derived from a tumor induced in nude mice by the human/mouse monochromosomic hybrid pRPcT1/H6 and harbor a human chromosome 6 deleted at 6q27 (Gualandri *et al.*, 1994).

Table 1 shows a summary of the results of transfection of the RNASE6PL cDNA into pRPc, HEY4, SG10G and XP12ROSV cells. Some characteristics of the results were common among the transfected cell lines. In fact, the number of living clones that could be propagated in culture, compared to the number of clones picked up after selection, was constantly lower in cells transfected with the RNASE6PL cDNA inserted in sense orientation (S) than in cells transfected with the RNASE6PL cDNA inserted in antisense orientation (AS) or with the vector alone, suggesting that the RNASE6PL cDNA exerts an inhibitory effect on cell growth and cloning efficiency. Moreover, all the clones transfected with the RNASE6PL cDNA-AS or with the vector alone were tumorigenic, whereas the pRPc and HEY4 cell clones transfected with the RNASE6PL cDNA-S were totally or partially suppressed in tumorigenicity (Tables 2 and 3). A greater tumorigenic activity was displayed by the clones of SG10G transfected with the RNASE6PL cDNA-S (Table 4). However, the tumors induced both by HEY4 and SG10G cell clones transfected with the RNASE6PL cDNA showed complete lack of expression of the inserted cDNA, indicating that the exogenous RNASE6PL cDNA was no longer functional in the neoplastic tissue (Tables 3 and 4, Figure 2). Finally, while pRPc and SG10G cells showed a normal phenotype *in vitro*, 63.6% of HEY cell clones and 42.8% of XP12ROSV clones displayed a senescent phenotype.

The analytical examination of the results of the single transfected cell lines indicates that pRPc normal cells and pRPc cells transfected with the empty vector were fully tumorigenic, whereas pRPc cells transfected with the RNASE6PL cDNA-S produced tumors in three out of eight inoculated animals (Table 2). Of these three tumors, two completely regressed 30 days after inoculation and the third failed to grow in culture, indicating a limited viability of the tumor cells.

Transfection of HEY cells with the RNASE6PL cDNA-S yielded two classes of clones, since, out of eleven clones expressing the inserted cDNA, seven (63.6%) showed a senescent phenotype *in vitro*, while four (36.4%) had a normal phenotype. The senescent phenotype gradually appeared and progressed during *in vitro* propagation of cell clones expressing RNASE6PL. Senescence was characterized by large and flattened cells, development of cytoplasmic vacuoles and nuclear shrinkage (Figure 3 a–c). The process of senescence was documented by a positive beta-galactosidase reaction (Figure 3 d–g) and by a decreased incorporation of [^{3}H]-thymidine in senescent cells: at 72 h the mean value of thymidine incorporation for three senescent clones was 245.6 ± 89.8 c.p.m. as compared to 900.5 ± 267.0 c.p.m. for three clones showing a normal *in vitro* growth phenotype ($P < 0.05$). When tumorigenicity was tested, four out of eight inoculated cell clones, expressing RNASE6PL cDNA, were suppressed in tumorigenicity. Of the nine tumors induced by the four tumorigenic clones, two completely

Table 1 Summary of the results of transfection of the RNASE6PL cDNA into pRPc, HEY4, SG10G and XP12ROSV cells

Cell line	*DNA*[a]	*Clone* (s)	*Pick* (ed)	*Living*[b]	*DNA*[c]	*RNA*[d]	In vitro *phenotype*	*Tumorigenicity*[e]
pRPc	RNASE6PL-S	29	29	25 (86.2%)	3 (12.0%)	2 (66.7%)	Normal 100%	2 PS
pRPc	PGK	>100	6	6 (100%)	NA	NA	Normal 100%	1 T
HEY4	RNASE6PL-S	78	78	47 (60.2%)	22 (46.8%)	11 (50.0%)	Normal 36.4% Senescent 63.6%	4 S; 3 PS; 1 T
HEY4	RNASE6PL-AS	>100	24	24 (100%)	8 (33.3%)	ND	Normal 100%	3 T
HEY4	pcDNA3	>100	4	4 (100%)	NA	NA	Normal 100%	3 T
SG10G	RNASE6PL-S	>100	68	49 (72.1%)	13 (26.5%)	6 (46.1%)	Normal 100%	1 PS; 4 T
SG10G	RNASE6PL-AS	>100	24	22 (91.7%)	7 (31.8%)	ND	Normal 100%	2T
SG10G	pcDNA3	>100	4	4 (100%)	NA	NA	Normal 100%	IT
XP12ROSV	RNASE6PL-S	>100	97	10 (10.3%)	8 (80.0%)	7 (87.5%)	Normal 57.2% Senescent 42.8%	ND
XP12ROSV	RNASE6PL-AS	85	10	6 (60.0%)	5 (83.3%)	ND	Normal 100%	ND
XP12ROSV	pcDNA3	>100	6	4 (66.7%)	NA	NA	Normal 100%	ND

[a]S and AS refer to the RNASE6PL cDNA inserted into the expression vectors in sense or antisense orientation; [b]Percentage of living clones over picked clones; [c]Percentage of RNASE6PL DNA positive clones over living clones; [d]Percentage of RNASE6PL expressing clones over DNA positive clones; [e]Number of inoculated cell clones which were tumorigenic or suppressed in tumorigenicity (T = tumorigenic; S = suppressed; PS = partially suppressed). ND, not done. NA, not applicable

Table 2 *In vitro* phenotype and tumorigenicity of pRPc cells after transfection of the RNASE6PL cDNA

Clone	*DNA*[a]	*RNA*[a]	*Phenotype*	*Tumorigenicity*[b]
pRPc-S9	+	+	Normal	1/4 (19)[c]
pRPc-S11	+	+	Normal	2/4 (26)[d]
pRPc-S7	+	–	Normal	ND
pRPc-pGKA3	NA	NA	Normal	4/4 (24.5)
pRPc	NA	NA	Normal	4/4 (18.5)

[a]DNA and RNA refer to RNASE6PL cDNA and RNA. [b]In parenthesis the mean value of the latency period for the appearance of tumors. [c]This tumor completely regressed 30 days after development. [d]One tumor regressed 30 days after development, the other failed to grow in culture. ND, not done. NA, not applicable

regressed (Table 3). Of the seven remaining tumors, three, derived from clones SA3, SB2 and SD14 (Table 3), were tested by RT–PCR and found to completely lack insert expression (Figure 2a), thereby confirming the tumor suppressing activity of the RNASE6PL cDNA. Three clones transfected by RNASE6PL-AS, three clones transfected with the pcDNA3 vector alone and one clone transfected by RNASE6PL-S, but not expressing the inserted cDNA, were tumorigenic (Table 3). Two clones, SB1 and SC10, showing a normal phenotype *in vitro*, were suppressed in tumorigenicity (Table 3), suggesting that senescence and suppression of tumorigenicity were induced through two different pathways by the RNASE6PL cDNA. Alternatively, the two phenotypes may depend on a quantitative difference in the expression of the RNASE6PL cDNA. Indeed, dot blot analysis of clones with the senescent and the normal phenotype showed that the senescent clones constantly exhibited a greater expression (twice to three times) of the inserted cDNA, as compared to clones with a normal phenotype which are suppressed in tumorigenicity (data not shown). This suggests that senescence is induced only when the RNase cDNA is expressed in HEY4 cells over a certain threshold, while suppression of tumorigenicity requires only a minimal expression of the insert.

Table 3 *In vitro* phenotype and tumorigenicity of HEY4 cells after transfection of the RNASE6PL cDNA

Clone	*DNA*[a]	*RNA*[a]	*Phenotype*	*Tumorigenicity*[b]
SA3[c]	+	+	Senescent	2/3 (56)
SA8[d]	+	–	Normal	3/3 (20)
SB1	+	+	Normal	0/3
SB2	+	+	Normal	1/3 (48)
SB10	+	+	Senescent	ND
SB11	+	+	Senescent	ND
SC7	+	+	Senescent	0/2
SC8	+	+	Senescent	ND
SC10	+	+	Normal	0/3
SD4	+	+	Senescent	2/3 (27)[e]
SD14	+	+	Normal	4/4 (24)
SD17	+	+	Senescent	0/3
AS cl.2	+	ND	Normal	4/4 (45)
AS cl.8	+	ND	Normal	4/4 (21)
AS cl.12	+	ND	Normal	3/3 (19)
pcDNA3A1	+	NA	Normal	4/4 (26)
pcDNA3B1	+	NA	Normal	4/4 (22)
pcDNA3C1	+	NA	Normal	4/4 (17)
HEY4	NA	NA	Normal	4/4 (21)

[a]DNA and RNA refer to RNASE6PL cDNA and RNA. [b]In parenthesis the mean value of the latency period for the appearance of tumors. [c]S and AS refer to the RNASE6PL cDNA inserted into the vector pcDNA3 in sense or antisense orientation. [d]Clone SA8, which does not express RNASE6PL cDNA, was used as a control in tumorigenicity assays. [e]The two tumors completely regressed 30 and 41 days after development. The two tumors induced by clone SA3, the tumor induced by clone SB2 and two tumors induced by clone SD14 were assayed by RT–PCR for the expression of RNASE6PL cDNA with negative results (see Figure 2A). ND, not done. NA, not applicable

Transfection of SG10G cells with RNASE6PL yielded six clones expressing the inserted cDNA (Table 4). The *in vitro* phenotype of these clones was normal and no signs of senescence were detected. Five of the six expressing clones, tested for tumorigenicity, were tumorigenic. However, when tumors, representative of each tumorigenic clone, were analysed by Northern blot hybridization, they were all found to be negative for the expression of the 1.4 Kb RNASE6PL transcript (Figure 2b). Two SG10G clones transfected with the

Table 4 *In vitro* phenotype and tumorigenicity of SG10G cells after transfection of the RNASE6PL cDNA

Clone	*DNA*[a]	*RNA*[a]	*Phenotype*	*Tumorigenicity*[b]
SA8	+	+	Normal	4/4 (18)
SB13	+	+	Normal	3/3 (18)
SB30	+	+	Normal	ND
SB31[c]	+	–	Normal	2/2 (5)
SD43	+	+	Normal	1/3 (33)
SD46	+	+	Normal	3/3 (22)
SE49	+	+	Normal	2/2 910)
SE53[c]	–	ND	Normal	2/2 (5)
ASA3	+	ND	Normal	4/4 (12)
ASA10	+	ND	Normal	4/4 (10)
pcDNA3D3	NA	NA	Normal	4/4 (10)
SG10G	NA	NA	Normal	4/4 (19)

[a]DNA and RNA refer to RNASE6PL cDNA and RNA. [b]In parenthesis the mean value of the latency period for the appearance of tumors. [c]Clone SB31, which does not express RNASE6PL, and clone S53, which does not contain the insert, were innoculated as controls in tumorigenicity assays. Two tumors induced by clone SA8, the three tumors induced by clones SB13 and SD46, the tumor induced by clone SD43 and one tumor induced by clone SE49 were assayed by Northern blot analysis for the expression of RNASE6PL with negative results (see Figure 2b). ND, not done. NA, not applicable

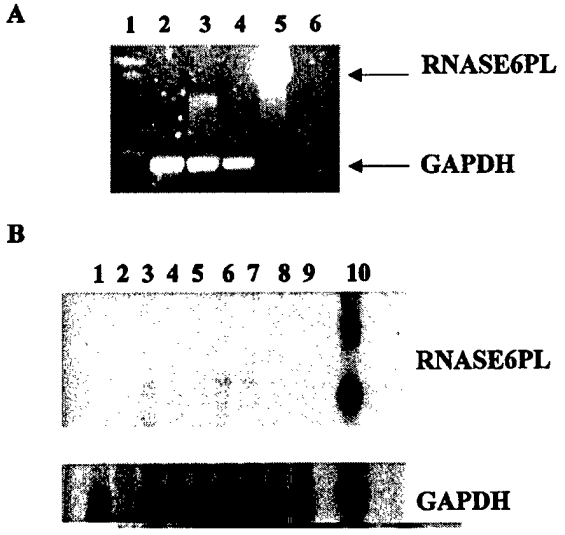

Figure 2 Lack of human RNASE6PL expression in mouse tumors. Total RNA was purified from several tumor samples obtained following s.c. injection in nude mice of HEY4 (**a**) and SG10G (**b**) clones which were previously selected in culture following transfection of an expression vector containing human RNASE6PL cDNA. Total RNA from HEY4-derived tumors (**a**) was analysed for RNASE6PL expression by RT–PCR, rather than Northern analysis due to the presence of endogenous RNASE6PL transcripts in this cell line. Lane 1: 1 kb DNA ladder standard; lanes 2–4: tumor samples representative of HEY4 clones SD14, SA3 and SB2, respectively (see Table 4); lane 5: RNASE6PL expression vector used for transfection of cell lines; lane 6: negative control. The RNA samples from SG10G-derived tumors (**b**) were analysed by Northern blot hybidization with ^{32}P-labelled RNASE6PL and GAPDH cDNA probes. The tumor analysed were derived from the following clones: lane 1: SA8; lanes 2–4: SB13; lanes 5–7: SD46; lane 8: SD43; lane 9: SE49; lane 10: placenta total RNA

RNASE6PL-AS cDNA, one clone transfected with the vector alone and two clones transfected with RNASE6PL-S, but not expressing the transfected cDNA, were fully tumorigenic.

CpG island methylation analysis of the RNASE6PL gene in ovarian cell lines and primary carcinomas

Hypermethylation of normally unmethylated CpG islands in the promoters and 5′ flanking regions of genes, down-regulated in cancers, is associated with loss or reduction of (Jones and Laird, 1999; Baylin and Herman, 2000). In order to carry out methylation studies, we determined the cap site, the proximal promoter region and more than 1 Kb of 5′-flanking sequences of the RNASE6PL gene. The region analysed spans the area of greatest CpG density immediately close to the transcription start site of RNASE6PL. Normal ovarian tissue, tumor cell lines and primary cancers were analysed by a methylation-specific PCR assay (Herman *et al.*, 1996) which revealed that RNASE6PL is present both in the methylated and unmethylated form in the same sample. No differences were detected between normal and tumor samples. Moreover, the HEY4, SW626 and OV166 cell lines were treated with the demethylating agent 5-aza-cytidine to see whether RNASE6PL expression could be increased but no changes were observed. These data suggest that molecular mechanisms other than promoter methylation may control RNASE6PL expression in primary tumors and tumor cell lines.

Discussion

In this study we have investigated the possible role of RNASE6PL as a tumor suppressor gene in ovarian cancer. The gene was cloned at 6q27 (Trubia *et al.*, 1997; Acquati *et al.*, 2000), a chromosome region often deleted in ovarian tumors and in different human neoplasms, such as melanoma, breast cancer, non-Hodgkin B-cell lymphoma and several others (Saito *et al.*, 1993; Foulkes *et al.*, 1993; Cooke *et al.*, 1996; Orphanos *et al.*, 1995; Tibiletti *et al.*, 1996; Develee *et al.*, 1991; Theile *et al.*, 1996; Chappel *et al.*, 1997; Queimado *et al.*, 1995; DeSouza *et al.*, 1995; Honchel *et al.*, 1996; Morita *et al.*, 1991; Tahara *et al.*, 1996; Millikin *et al.*, 1991; Gaidano *et al.*, 1992; Hayashi *et al.*, 1990). RNASE6PL belongs to a group of RNases which are very conserved among species (Trubia *et al.*, 1997; Anderson *et al.*, 1986; Clark *et al.*, 1990; Schneider *et al.*, 1993; Meadoe and Kennell, 1990; McClure *et al.*, 1989; Hime *et al.*, 1995). These enzymes display different functions. However, one of their main effects is regulation of cell growth (McClure *et al.*, 1990). In particular, a plant RNase, highly homologous to RNASE6PL, is responsible for the expression of gametophytic self-incompatibility in Nicotiana alata (McClure *et al.*, 1990). This enzyme exerts its action by inhibiting the growth of pollen tubes through degradation of pollen rRNA (McClure *et al.*, 1990) with consequent inhibition of protein synthesis. It may be

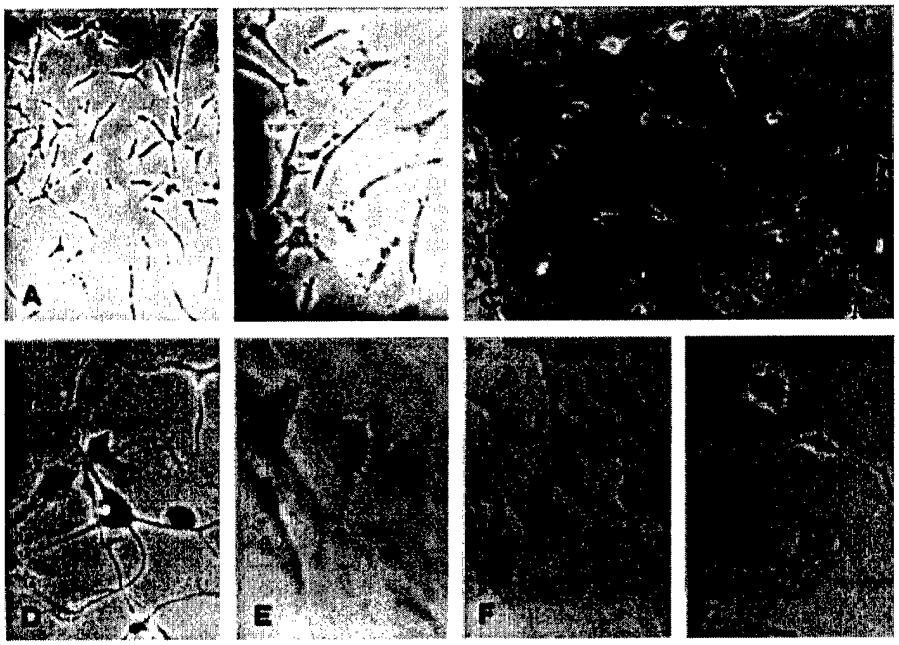

Figure 3 (**a** and **b**) Normal HEY4 cells. Magnification: **a**, 25×; **b**, 50×. **c**: HEY4 cell clone transfected with RNASE6PL cDNA and showing a senescent phenotype characeterized by flattened and enlarged cells with cytoplasmic vacuoles. Magnification: 50×. Note that **b** and **c** have the same magnification. **d**–**g**: Four cell clones transfected with the RNASE6PL cDNA show a positive reaction for beta-galactosidase. Magnification: 50×

conceivable that a similar mechanism could also be operative in the mammalian system, although at present we have no experimental evidence for this effect. On the other hand, it is worth noting that RNases like onconase (Ardelt *et al.*, 1991) and BS-RNase (D'Alessio, 1993) are potent inhibitors of cell proliferation and the inhibitory effect is much more evident on actively growing cells, such as immortalized or neoplastic cells (Schein 1997), lending support to the potential role of these enzymes as tumor suppressors. Indeed, onconase is currently being evaluated for the treatment of mesothelioma in phase III clinical trials (Smith *et al.*, 1999).

A mutation analysis on 55 ovarian tumors from stage II to stage IV indicated the absence of mutations in the RNASE6PL coding region as well as in the 5′ and 3′ regulatory regions. Only a few polymorphisms were detected. However, analysis of the same ovarian tumors by Northern blot hybridization showed absence or reduction of RNASE6PL expression in 30% of the samples as compared to normal ovarian tissue. Similarly, expression of the gene was reduced in 75% of ovarian tumor cell lines. In order to shed light on the possible mechanisms responsible for such down-regulation we have investigated whether the promoter of the RNASE6PL gene was methylated. Promoter methylation does not seem to account for the reduced RNASE6PL expression as most of the tumors, cell lines and normal ovary display both methylated and unmethylated alleles, without clear differences between normal and tumor tissues. Most likely other mechanisms are acting in the downregulation of this gene such as local chromatin alterations or mutations in a gene(s) acting upstream of RNASE6PL.

Furthermore, RNASE6PL-transfected ovarian tumor cell lines, inoculated into nude mice, were suppressed in tumorigenicity. All the induced tumors that were analysed resulted completely negative for the expression of the RNASE6PL RNA, confirming the role of this gene in controlling tumor growth.

Due to its behavior in tumors, RNASE6PL may be defined as a class II tumor suppressor gene. Indeed, tumor suppressor genes are distinguished into class I and class II. Class I tumor suppressor genes lose function by deletion, rearrangement or mutation (Haber and Harlow, 1997); class II tumor suppressor genes are structurally intact in their sequence, but are underexpressed or unexpressed, due to downregulation or silencing in transcription or translation (Jones and Laird, 1999; Baylin and Herman, 2000). Loss of expression may in turn depend on alterations affecting an upstream regulatory gene or on epigenetic mechanisms altering the function of the class II gene promoter. It is notable that all the genes which have convincingly been associated with tumor suppressing activity in human ovarian neoplasms belong to class II. Indeed no inactivating mutations in primary tumors and cell lines were reported for GPC3 (Lin *et al.*, 1999), NOEY2 (Yu *et al.*, 1999), OVCA1 (Bruening *et al.*, 1999), SPARC (Mok *et al.*, 1996) DOC-2 (Mok *et al.*, 1998), and ZAC/LOT1 genes (Abdollahi *et al.*, 1997; Bilanges *et al.*, 1999). The GPC3 gene promoter was found to be methylated in several ovarian cancer cell lines (Lin *et al.*, 1999), whereas the normal allele of the imprinted

NOEY2 gene is always deleted in tumors showing LOH (Yu *et al.*, 1999). Thus, with the inclusion of the RNASE6PL gene, these results seem to indicate that epigenetic mechanisms may play an important role in ovarian tumorigenesis, by inactivation or downregulation of tumor suppressor genes.

During the course of these experiments, when RNASE6PL cDNA was transfected into HEY4 and XP12ROSV cells, clear signs of senescence appeared in cell culture. The senescent phenotype was confirmed by a positive reaction for beta-galactosidase, an enzyme whose expression is specifically associated to the process of senescence (Dimri *et al.*, 1995). Induction of replicative senescence by RNASE6PL is particularly interesting in view of the fact that RNase activity increases in plants during senescence and in human serum in the course of ageing (Schein, 1997; Francesconi *et al.*, 1984). It is not clear at present why only a proportion of cell clones, both in HEY4 and in XP12ROSV cell cultures, displayed the senescence phenotype. With the single exception of angiogenin, most known RNases (e.g. fungal RNase, BS-RNase, onconase, EDN and the lectin RNases RCE and RJE) are highly selective towards specific cell types (D'Alessio, 1993; Schein, 1997), suggesting that the other cells are somehow protected from the inhibitory effect of RNases on cell growth. Therefore, it is possible that cell clones, not showing senescence after transfection of RNASE6PL, derive from single cells developing protective mutations towards the activity of this RNase. Alternatively, the RNASE6PL cDNA may be inactivated by mutation in transfected cell clones displaying a normal phenotype. Induction of senescence by RNASE6PL makes this gene a good candidate for the senescence-inducing gene (SEN6) mapped at 6q27 (Banga *et al.*, 1997), within the minimal region of LOH detected in ovarian cancer (Saito *et al.*, 1992; Foulkes *et al.*, 1993, Cooke *et al.*, 1996; Orphanos *et al.*, 1995; Tibiletti *et al.*, 1996, 1998) or induction of senescence may simply be a phenotypic aspect of the tumor suppressor function displayed by RNASE6PL. The relation of RNASE6PL to SEN6 could be relevant to establish whether an immortalization step is an early event in the process of ovarian tumorigenesis. Indeed, the region where the RNASE6PL gene resides is consistently deleted not only in benign ovarian tumors (Tibiletti *et al.*, 1998) but also in other benign conditions such as parathyroid adenomas (Tahara *et al.*, 1996) and breast benign tumors including fibroadenomas (Tibiletti *et al.*, 2000). In conclusion, RNASE6PL may represent the candidate gene at 6q27 fulfilling both functions of inducing senescence and of tumor suppressor gene in ovarian cancer.

Materials and methods

Primary tumors, cell lines and culture conditions

Fifty-five microdissected primary ovarian tumors, from stage II to stage IV, were selected for mutational and expression analysis in this study. The HEY4 cell line (Buick *et al.*, 1985), the SG10G cell line (Garzetti *et al.*, 1992), the Xeroderma Pigmentosum fibroblast cell line XP12ROSV, immortalized by SV40 (Simon *et al.*, 1981) and the ovarian cancer cell lines OV1225, SKOV3, OVCR3, OVRS1000, SW626 and OV166 were cultured in DMEM/F12 medium (GIBCO-BRL) supplemented with 10% fetal calf serum. pRPcT1/H6c12T (pRPc) cells, derived from a tumor induced by the human/mouse monochromosomic hybrid pRPcT1/H6, carrying a human chromosome 6 tagged with the *neo* gene (Gualandri *et al.*, 1994), were cultured in the same medium in the presence of 300 μg/ml of G418 (Boehringer, Mannheim).

Construction of plasmids and transfection of cells

pRPc cells were cotransfected with the RNASE6PL cDNA inserted in the plasmid pMT89 together with the pGK plasmid carrying the resistance to hygromicin. The HEY4 and SG10G cells, which do not express the RNASE6PL gene (see Results section), were transfected with the RNASE6PL cDNA inserted in the plasmid pcDNA3 (Invitrogen) which contains the *neo* gene and induces resistance to G418. In both constructs, the RNase cDNA was directed by the cytomegalovirus immediate early promoter. For transfection experiments, the plasmid containing the RNASE6PL cDNA (6 μg per 10^6 cells) was transfected into pRPc, HEY4, SG10G, and XP12ROSV cells with the Superfect reagent (Quiagen), following the manufacturer's instructions. The clones, appearing after approximately two weeks of selection, were harvested by trypsinization with glass cylinders and propagated as mass cultures.

Beta-galactosidase test staining

The test was performed directly in the culture flasks according to Dimri *et al.* (1995).

Thymidine incorporation test

Two $\times 10^4$ cells were cultured on glass dishes in 24-well plates in the presence of [^{3}H]thymidine (1 μCi/ml). After 72 h, cells were extensively washed in PBS, dishes were recovered from the wells, resuspended in 1 ml of INSTA-GEL II PLUS (Packard) and the radioactivity was measured in a Packard TRI-CARB 4530 beta counter.

Tumorigenicity assays

To test for tumorigenicity in nude mice, cells were trypsinized, harvested and washed twice. Five $\times 10^4$ pRPc cells, 1×10^5 HEY4 cells and 2×10^6 SG10G cells were suspended in 0.1 ml of serum-free medium and inoculated s.c. into 3-week-old nude BALB/c mice. Animals were examined for tumor formation for up to 6 months. After that time, if tumors had not appeared, the cells were considered suppressed in tumorigenicity.

PCR and RT-PCR

Cells from each clone were harvested from 18 mm wells and suspended in 0.5 ml of culture medium. Twenty per cent of the suspension was directly used for PCR to confirm the presence of the transfected cDNA, while the remaining 80% was used for RNA extraction followed by RT-PCR. For PCR reaction, the cell pellet was treated at 55°C for 1 h in 10 mM Tris pH 8.3, 1.25 mM $MgCl_2$, 0.01% gelatine, 0.45% Tween 20, 0.45% NP-40, 10 μg/ml proteinase K. After

inactivation of proteinase K for 10 min at 95°C, the reaction mixture was briefely centrifuged and 1 μl of the cell lysate was used for PCR analysis with T7 and Sp6 primers, designed on the arms of the expression vector. The conditions of the reaction were: 94°C for 30 s, 55°C for 30 s, 72°C for 60 s, 30 cycles. For RT–PCR analysis, total RNA was extracted with the RNAwiz reagent (Ambion) following the manufacturer's instructions and reverse transcription was carried out using the cDNA Synthesis System (Gibco–BRL). GAPDH amplification was performed to control cDNA synthesis. To discriminate from the endogenous RNASE6PL transcript, the expression of the transfected cDNA was tested using the T7 primer from the vector and a specific primer for the RNASE6PL cDNA (5′-TTGGGCATCAATGCTTGG-3′). cDNA amplification was then carried out as described for the PCR reaction.

RNASE6PL methylation status analysis by methylation specific PCR (MSP)

MSP was carried out as described by Herman *et al.* (1996). Two μg of sodium bisulfite-treated genomic DNA from the samples of interest was purified and used for MSP analysis using the following primers: 44bis-MetA: 5′ TTTGCGT-GGCGAAGGAACGTAGTCGTT-3′ and 44new-MetB: 5′-TACAACAACGACCACCGAATACGCCCG-3′ (to amplify methylated DNA); 44bis-UnmetA: 5′-GGTGTTTGTG-TGGTGAAGGAATGTAGTTGTT-3′, and 44new-UnmetB: 5′-TCCACTACAACAACAACCACCAAATACACCC-3′ (to amplify unmethylated DNA) PCR conditions were as follows: 94°C 2 min, then 40 cycles at 92°C 30 s, 61°C 30 s, 72°C 60 s with primers 44bis-MetA and 44new-MetB; :94°C 2 min, then 40 cycles at 92°C 30 s, 59°C 30 s, 72°C 60 s with primers 44bis-UnmetA and 44new-UnmetB. As a control for the specificity of the primers, the same PCR reactions were carried out using DNA which had not been treated with sodium bisulfite.

PCR-single-strand conformation polymorphism (SSCP)

DNA was prepared from 55 tumors and from the ovarian carcinoma cell line HEY4, using standard phenol-chloro-phorm extraction. Primer pairs were designed in intronic regions flanking each exon and in the 5′ and 3′ untranslated regions of the RNASE6PL gene. Every single exon of the RNASE6PL gene was PCR amplified (primer sequences and PCR conditions are available on request). SSCP analysis was performed on tumor DNAs as previously described (Varesco *et al.*, 1993).

Acknowledgments
R Taramelli was supported by grants from Associazione Italiana per la Ricerca sul Cancro (AIRC) and MURST Cofin 1998. L Possati and G Barbanti-Brodano were supported by grants from AIRC and MURST ex 60% and Cofin 1998.

References

Abdollahi A, Godwin A, Miller P, Getts L, Schultz D, Taguchi T, Testa J and Hamilton T. (1997). *Cancer Res.*, **57**, 2029–2034.
Acquati F, Nucci C, Bianchi M and Taramelli R. (2000). *Meth. Mol. Biol.*, (in press).
Anderson M, Cornish E, Mau S, Williams E, Hoggart R, Atkinson A, Bonig I, Grego B, Simpson R, Roche P, Penschow J and Clarke A. (1986). *Nature*, **321**, 38–41.
Ardelt W, Mikulsky S and Shogen K. (1991). *J. Biol. Chem.*, **266**, 245–251.
Banga S, Kim S, Hubbard K, Dasgupta T, Jha K, Patsalis P, Hauptschein R, Gamberi B, Dalla Favera R, Kraemer P and Ozer H. (1997). *Oncogene*, **14**, 313–321.
Baylin S and Herman J. (2000). *Trends Genet.*, **16**, 168–174.
Bilanges B, Varrault A, Basyuk E, Rodriguez C, Mazumdar A, Pantaloni C, Bockaert J, Theillet C, Spengler D and Journot L. (1999). *Oncogene*, **18**, 3979–3983.
Bruening W, Prowse A, Schultz D, Holgado Madruga M, Wong A and Gowin A. (1999). *Cancer Res.*, **59**, 4973–4983.
Buick RN, Pullano R and Trent JM. (1985). *Cancer Res.*, **45**, 3668–3676.
Chappell S, Walsh T, Walker R and Show J. (1997). *Br. J. Cancer*, **75**, 1324–1329.
Clark K, Okuley J, Collins P and Sims T. (1990). *Plant Cell*, **2**, 815–826.
Colitti C, Rodabaugh K, Welch W, Berkowitz R and Mok S. (1998). *Oncogene*, **16**, 555–559.
Cooke I, Cox S, Shelling A, LeMeuth V, Charnock M and Ganesan T. (1996). *Genes Chromosomes Cancer*, **15**, 13–20.
D'Alessio G. (1993). *Trends Cell. Biol.*, **3**, 106–109.
De Souza A, Hankins G, Washington M, Fine R, Orton T and Jirtle R. (1995). *Oncogene*, **10**, 1725–1729.
Develee P, van Vliet M, van Sloun Kuipers N, Hermans J, Pearson P and Cornelisse C. (1991). *Oncogene*, **6**, 1705–1711.
Dimri GP, Lee X, Basile G, Acosta M, Scott G, Roskelley C, Medrano EE, Linskens M, Rubelj I and Pereira-Smith O. (1995). *Proc. Natl. Acad. Sci. USA*, **92**, 9363–9367.
Foulkes W, Ragoussis J, Stamp G, Allan G and Trowsdale J. (1993). *Br. J. Cancer*, **67**, 551–559.
Francesconi M, Meryn S, Rogan AM, Szalay S, Graninger W and Schmidbauer CP. (1984). *Cancer*, **53**, 1927–1930.
Gaidano G, Hauptschein R, Parsa N, Offit K, Rao P, Lenoir G, Knowles D, Chaganti R and Dalla Favera R. (1992). *Blood*, **80**, 1781–1787.
Garzetti GG, Possati L, Ciavattini A, Recanatini E, Cignitti M, Valensise H and Romanini C. (1992). *Eur. J. Gynaecol. Oncol.*, **13**, 514–521.
Gualandi F, Morelli C, Pavan JV, Rimessi P, Sensi A, Bonfatti A, Gruppioni R, Possati L, Stanbridge EJ and Barbanti-Brodano G. (1994). *Genes Chrom. Cancer*, **10**, 77–84.
Haber D and Harlow E. (1997). *Nature Genet.*, **16**, 320–322.
Hauptschein R, Gamberi B, Pulivarthi R, Frigri F, Scotto L, Venkatraj, Gaidano G, Rutner T, Edwards Y, Chaganti R and Dalla-Favera R. (1998). *Genomics*, **50**, 170–186.
Hayashi Y, Raimondi S, Look T, Behm F, Kitchington G, Pui C, Rivera G and Williams D. (1990). *Blood*, **76**, 1626–1630.
Herman J, Graff J, Myohannen S, Nelkin B and Baylin S. (1996). *Proc. Natl. Acad. Sci. USA*, **93**, 9821–9826.
Hime G, Prior L and Saint R. (1995). *Gene*, **158**, 203–207.
Honchel R, McDonnell S, Schaid D and Thibodeau S. (1996). *Cancer Res.*, **56**, 145–149.
Jones P and Laird P. (1999). *Nature Genet.*, **21**, 163–167.

Lin H, Huber R, Schlessinger D and Morin P. (1999). *Cancer Res.*, **59**, 807–810.
McClure B, Haring V, Ebert P, Anderson M, Simpson R, Sakiyama F and Clarke A. (1989). *Nature*, **342**, 955–957.
McClure B, Gray J, Anderson M and Clarke A. (1990). *Nature*, **347**, 757–760.
Meador J and Kennell D. (1990). *Gene*, **95**, 1–7.
Millikin D, Meese E, Vogelstein B, Witkowski C and Trent J. (1991). *Cancer Res.*, **51**, 5449–5453.
Mok S, Chan W, Wong K, Muto M and Berkowitz R. (1996). *Oncogene*, **12**, 1895–1901.
Mok S, Chan W, Wong K, Cheung K, Lau C, Ng S, Baldini A, Colitti C, Rock C and Berkowitz R. (1998). *Oncogene*, **16**, 2381–2387.
Morita R, Saito S, Ishikawa J, Ogawa O, Yoshida O, Yamakawa K and Nakamura Y. (1991). *Cancer Res.*, **51**, 5817–5820.
Orphanos V, McGown G, Hey Y, Thorncroft M, Santibanez-Koref M, Russell S, Hickey I, Atkinson R and Boyle J. (1995). *Br. J. Cancer*, **71**, 666–669.
Queimado L, Seruca R, Costa-Pereira and Castedo S. (1995). *Genes Chromosomes Cancer*, **14**, 28–34.
Queimado L, Reis A, Fonseca I, Marins C, Lovett M, Soares J and Parreira L. (1998). *Oncogene*, **16**, 83–88.
Saito S, Saito H, Sagae S, Kudo R, Saito J, Noda K and Nakamura Y. (1992). *Cancer Res.*, **52**, 5815–5817.
Saito S, Sirahama S, Matsushima M, Suzuki M, Sagae S, Kudo R, Saito J, Noda K and Nakamura Y. (1996). *Cancer Res.*, **56**, 5586–5589.
Schein C. (1997). *Nature Biotech.*, **15**, 529–536.
Schneider R, Unger G, Stark R, Scheider-Scherzer E and Thiel H. (1993). *Science*, **261**, 1169–1171.
Shridhar V, Staub J, Huntley B, Cliby W, Jenkins R, Pass H, Hartmann L and Smith D. (1999). *Oncogene*, **18**, 3913–3918.
Simon L, Hazard RM, Maher VM and McCormick JJ. (1981). *Carcinogenesis*, **2**, 567–570.
Smith MR, Newton DL, Mikulski SM and Rybak SM. (1999). *Exp. Cell. Res.*, **247**, 220–232.
Tahara H, Smith A, Gas R, Cryns V and Arnold A. (1996). *Cancer Res.*, **56**, 599–605.
Theile M, Seitz S, Arnold W, Jandrig B, Frege R, Schlag P, Haensch W, Barret J and Scherneck S. (1996). *Oncogene*, **13**, 677–685.
Tibiletti MG, Bernasconi B, Furlan D, Riva C, Trubia M, Buraggi G, Franchi M, Bolis P, Mariani A, Frigerio L, Capella C and Taramelli R. (1996). *Cancer Res.*, **56**, 4493–4498.
Tibiletti M, Bernasconi B, Taborelli M, Furlan D, Fabbri A, Taramelli R, Trubia M and Capella C. (1997). *Br. J. Cancer*, **75**, 1831–1835.
Tibiletti MG, Trubia M, Ponti E, Sessa L, Acquati F, Furlan D, Bernasconi B, Fichera M, Mihalich A, Ziegler A, Volz A, Facco C, Riva C, Cremonesi L, Ferrari M and Taramelli R. (1998). *Oncogene*, **16**, 1639–1642.
Tibiletti MG, Sessa F, Bernasconi B, Cerutti R, Broggi B, Furlan D, Acquati F, Russo A, Capella C and Taramelli R. (2000). *Clin. Cancer Res.*, **6**, 1422–1431.
Trubia M, Sessa L and Taramelli R. (1997). *Genomics*, **42**, 342–344.
Yu Y, Xu F, Peng H, Fang X, Zhao S, Li Y, Cuevas B, Kou W, Gray J, Siciliano M, Mills G and Bast R. (1999). *Proc. Natl. Acad. Sci. USA*, **96**, 214–219.

MS#7

DOI 10.1002/cyto.10042

Cytometry 47:60-62 (2002)

Transcriptional Profiling Develops Molecular Signatures For Ovarian Tumors

David I. Smith

Mayo Clinic Cancer Center, Rochester, Minnesota

Of the cancers unique to women, ovarian cancer has the highest mortality rate. Over 26,000 women are diagnosed with this disease in the U.S. annually, and 60% of those diagnosed will die of the disease. One of the greatest problems with this disease is the lack of strong early warning signs or symptoms resulting in advanced stage at presentation in most women, followed by the outgrowth of chemotherapy-resistant disease in the majority of patients. The 5-year survival for patients with early stage disease ranges from 50-90%, but it is less than 25% for advanced-stage disease. In collaboration with researchers at Millennium Predictive Medicine (Cambridge, MA), the Ovarian Cancer Program of the Mayo Clinic Cancer Center analyzed gene expression in over 50 primary ovarian tumors, as compared with normal ovarian epithelial cells. The technologies utilized included microarray analysis with nitrocellulose filters containing 25,000 arrayed human cDNAs, as well as the construction of subtraction suppression hybridization cDNA libraries and their subsequent sequencing. Our specific focus has been on genes that are underexpressed during the development of ovarian cancer, although this analysis has revealed a large number of consistently up- and down-regulated genes. There were more down-regulated genes in ovarian tumors than up-regulated genes. In addition, the number of genes that had altered expression levels was quite large. For example, we found 409 genes down-regulated at least 5-fold, and 72 genes up-regulated at least 5-fold in 33% of the tumors analyzed. We also observed that most of the expression alterations observed in later stage (Stages III/IV) tumors were also observed in early-stage tumors (Stages I/II). This was corroborated using comparative genomic hybridization analysis on the same tumors that were expression profiled. This analysis revealed that the late-stage tumors had more gene amplification than early-stage tumors, but most regions of change (either increases or decreases) were in common between different stage tumors. We also have verified the altered expression levels of several of these genes using several complementary strategies. Finally, we are taking top candidate genes that are consistently under-expressed in ovarian tumors and attempting to determine their functional role in the development of ovarian cancer. Cytometry 47:60-62, 2002.

OBJECTIVES

Our goal was to analyze gene expression in ovarian tumors to identify genes that are consistently aberrantly regulated during the development of ovarian cancer. We partnered with researchers at Millennium Predictive Medicine (MPMx) to gain access to their high-throughput technologies for constructing and analyzing cDNA microarrays as well as for generating and characterizing subtraction suppression hybridization cDNA libraries. We wanted to compare the expression profiles of low-stage tumors with those of high-stage tumors to determine if genes that were differentially expressed between low- and high-stage tumors gave any insights into the dramatic differences in survival between patients with low-stage versus high-stage disease.

WHAT WE DID

Researchers at MPMx prepared 25K cDNA arrays which contained approximately 18,000 independent genes. High-quality RNA was prepared from over 50 primary ovarian tumors (representing different histologies and stages), radiolabeled and hybridized to the 25K arrays. Gene expression in the tumors was compared with that of noncultured normal ovarian epithelium. To complement the microarray analysis and potentially to identify additional genes, we also performed both differential display analysis (This work only identified 100 differentially expressed genes.) and constructed a number of SSH cDNA libraries that were sequenced and characterized by MPMx.

Ovarian-dedicated arrays containing any aberrantly regulated genes (identified from the microarrays, differential display, or SSH libraries) were then produced, and these are being used currently to analyze a much greater number of primary ovarian tumors. This analysis should

This work was supported by a Program Project Grant obtained from the Department of Defense (D.I. Smith, principal investigator), the Women's Cancer Program, and the Ovarian Cancer Program of the Mayo Clinic Cancer Center.

Correspondence to: David I. Smith, Cancer Genetics Program, Mayo Clinic Cancer Center, Rochester, MN 55905

E-mail:smith.david@mayo.edu

certainly yield a number of consistently over-expressed genes, several of which may make excellent genes for the early detection of ovarian cancer. This analysis also may yield a number of important genes that can differentiate among tumors with different histologies as well as among those with a distinct clinical outcome.

We then used a number of complementary techniques to verify that some of the genes identified were indeed aberrantly expressed in the primary tumors. These included Northern blot and reverse transcriptase polymerase chain reaction (RT-PCR) analyses in a panel of ovarian cancer cell lines followed by RT-PCR analysis with the primary tumors. We found that only 70% of the genes which appeared to be aberrantly expressed as determined by microarray analysis were indeed aberrantly expressed.

One of the greatest problems with this technology for global expression profiling is determining which genes of the hundreds or thousands of aberrantly regulated genes are worthy of study. We have employed functional analysis of several top candidates to demonstrate that aberrant regulation of these genes might have a functional consequence that would promote ovarian tumor development. Genes were reintroduced into ovarian cancer cell lines that were not expressing those genes, and the cell lines were analyzed for changes in growth characteristics, growth in soft agar, and sensitivity to chemotherapeutic agents (as chemoresistance is an important clinical part of the lethality of ovarian cancer).

WHAT WE OBSERVED

The 25K cDNA arrays were used to analyze over 50 primary ovarian tumors. Each tumor was hybridized to duplicate membranes, and the overall reproducibility on these filters was found to be quite high. Gene expression levels in the tumors were compared with noncultured ovarian epithelial cells (from brushings obtained from women without ovarian cancer that were having oophorectomies). We divided gene expression changes into > 2-fold, 5-fold, 10-fold, and 20-fold for both down- and up-regulated genes. Next we determined the proportion of the 50 tumors in which 2-fold, 5-fold, etc., changes in expression occurred. We found that there were many more down-regulated genes than up-regulated genes in ovarian tumors. For example, we found 24 genes that were down-regulated at least 5-fold in all the tumors profiled but only a single gene up-regulated 5-fold in all the samples.

How much of a change in expression is significant and in what proportion of the tumors must that change occur to be worthy of study? This is an important question as there were 5718 genes that were 2-fold down-regulated in at least 20% of the tumors and 4303 up-regulated genes, which is far too many genes to analyze. However, if we opt for the most stringent of criteria (for example, at least a 10-fold change in all of our samples), we find only 9 down-regulated genes and no up-regulated genes. We arbitrarily decided to examine genes that were at least 5-fold down-regulated in > 50% of the tumors analyzed (This is a list of 179 genes.).

The profound difference in survival between patients with early-stage disease as compared with those with late-stage disease suggests that there may be profound differences in gene expression between early- and late-stage disease and that some of these genes may be important in determining these differences. However, when we compared the expression profiles between early- and late-stage disease, we found that most of the genes that are aberrantly expressed in late-stage tumors are also aberrantly expressed in the early-stage tumors. There were indeed differences, and we detected several genes that were only aberrantly expressed in the late-stage tumors as well as several that were only aberrantly expressed in the early-stage tumors. We then used comparative genomic hybridization to analyze the same tumors that were transcriptionally profiled. This analysis revealed that the majority of the chromosomal regions that had either consistent losses or gains in ovarian tumors was common to both early- and late-stage tumors. The one important distinction that we did observe is that gene amplification was very infrequent in early-stage tumors but much more common in late-stage tumors.

Our strategy for verifying that these genes were indeed aberrantly regulated was to first analyze gene expression in a panel of ovarian cancer cell lines. We then tested gene expression in primary ovarian tumors using semi-quantitative RT-PCR analysis. To confirm that the aberrant expression detected was due to changes in the ovarian tumors themselves and not due to changes in contaminating stromal cells or infiltrating lymphocytes, we performed RNA in situ hybridization analysis of a number of our top candidate genes. These analyses revealed that only 70% of the genes determined to be aberrantly regulated from microarray analysis were indeed aberrantly regulated.

Finally we performed functional analysis with several of the consistently under-expressed genes. One gene, which was previously identified using differential display analysis, codes for a protein with a DNAJ domain. This gene, designated MCJ (for methylation-controlled J Protein), was consistently not expressed in ovarian tumors. We determined that this gene's expression is inactivated by loss of one allele (detected by loss of heterozygosity) and methylation of the remaining allele. This gene was introduced again into two ovarian cancer cell lines that did not express the gene, and we found that expression of this gene was associated with enhanced sensitivity to paclitaxel, topotecan, and cisplatin, suggesting that loss of MCJ expression may play a role in the de novo chemoresistance in ovarian carcinoma.

CONCLUSIONS AND FUTURE DIRECTIONS

We have used transcriptional profiling to analyze gene expression in primary ovarian tumors. This analysis has revealed that there are more genes that are down-regulated than up-regulated during the development of ovarian cancer. Surprisingly, most of the aberrantly regulated

genes in late-stage tumors also are aberrantly regulated in early-stage tumors. Indeed, the most profound difference that we observed between early- and late-stage tumors was that gene amplification was common only in late-stage tumors. Currently, a much larger number of primary ovarian tumors (representing all the distinct histologies of ovarian cancer) are being analyzed using arrays containing genes that appeared to be aberrantly regulated on the primary arrays or were identified from differential display or SSH cDNA libraries. This analysis should give us a large list of genes that we will need to examine before choosing a manageable number of genes to be characterized in much greater detail.

Our goal is to determine the number of genetic alterations that underlie the development of ovarian cancer. We also would like to identify the earliest genetic alterations that occur, as this will give much greater insight into the process whereby ovarian cancer develops. This work will generate markers that can be used to distinguish tumors of distinct histologies as well as clinical outcome. Our goal is to use this information to understand better the biology of this disease.

ACKNOWLEDGEMENTS

The author acknowledges all the members of the Ovarian Cancer Program of the Mayo Clinic Cancer Center. Special acknowledgement must go to Dr. Lynn Hartmann, the co-leader who started the Ovarian Program 10 years ago. Dr. Viji Shridhar performed much of the work described above in collaboration with the researchers at Millennium including Dr. Jim Lillie and John Lee.

MS#8

ARTICLE

A role for common fragile site induction in amplification of human oncogenes

Asaf Hellman,[1] Eitan Zlotorynski,[1] Stephen W. Scherer,[2] Joseph Cheung,[2] John B. Vincent,[2] David I. Smith,[3] Luba Trakhtenbrot,[4] and Batsheva Kerem[1,5]

[1]Department of Genetics, The Life Sciences Institute, The Hebrew University, Jerusalem 91904, Israel
[2]Department of Genetics, The Hospital for Sick Children, Toronto, Ontario, Canada M5G 1X8
[3]Department of Laboratory Medicine and Pathology, Mayo Foundation, Rochester, Minnesota 55905
[4]Department of Pediatric Hemato-Oncology and Institute of Hematology, The Chaim Sheba Medical Center, Tel Hashomer 52621, Israel
[5]Correspondence: kerem@mail.ls.huji.ac.il

Summary

Oncogene amplification is an important process in human tumorigenesis, but its underlying mechanism is currently unknown. Cytogenetic analysis indicates that amplification of drug-selected genes in rodent cells is driven by recurrent breaks within chromosomal common fragile sites (CFSs), via the breakage-fusion-bridge (BFB) mechanism. Here we show that BFB cycles drive the intrachromosomal amplification of the *MET* oncogene in a human gastric carcinoma. Our molecular evidence includes a "ladder-like" structure and inverted repeat organization of the *MET* amplicons. Furthermore, we show that the breakpoints, setting the centromeric amplicon boundaries, are within the CFS FRA7G region. Upon replication stress, this region showed perturbed chromatin organization, predisposing it to breakage. Thus, in vivo induction of CFSs can play an important role in human oncogenesis.

Introduction

A complex pattern of chromosomal aberrations is a common phenomenon in many cancers (Mitelman et al., 1997), but the mechanisms that initiate, direct, and enable this instability are still poorly understood. One form of cancer instability is intrachromosomal amplification of large genomic regions containing oncogenes. Amplification and subsequent overexpression of human oncogenes has been demonstrated for a variety of different neoplasias, and is thought to play an important role in the progression of tumor cells toward an increased malignancy (Brison, 1993).

Early events of gene amplification in cancer are usually unavailable for studying. Thus, model systems in cultured rodent cells were developed, in which amplification of genes conferring drug resistance is induced and selected for. Analysis of the structure and organization of such induced amplicons suggested that the mechanism underlying the early amplification events is breakage-fusion-bridge (BFB) cycles (Toledo et al., 1992). According to this model (McClintock, 1951) (Figure 1), an initial break (or telomere dysfunction) of a chromatid bearing the selected gene might lead to fusion of the uncapped sister chromatids after replication. The resulted dicentric chromosome forms an anaphase bridge between the centromeres, which will break while moving to opposite poles of the mitotic spindle. If this break occurs centromeric to the selected gene, a duplication of the region between the breaks is gained. Several recurrent cycles of chromosomal fusion and breakage under the appropriate selection lead to intrachromosomal amplification. Importantly, the recurrent breaks defining the boundaries of the induced amplicons were found to coincide with the cytogenetic location of specific hamster chromosomal loci (Kuo et al., 1994; Coquelle et al., 1997), defining as common fragile sites (CFSs) (Glover et al., 1984).

CFSs are specific regions in mammalian chromosomes that are prone to breakage and rearrangements. They appear as constrictions, gaps, or breaks in metaphase chromosomes of cells exposed to inhibitors of DNA replication, among which are known mutagens and carcinogens (Yunis et al., 1987), as well as inducers and enhancers of amplification events (Stark et al.,

SIGNIFICANCE

Here we provide molecular evidence that the chromosomal breakpoints that drive oncogene amplification occur nonrandomly. Our results show that the breaks setting the boundaries of amplified genomic regions might occur at specific chromosomal loci defined as fragile sites. There are ~100 fragile sites in the human genome estimated to encompass >100 Mb of DNA. The fragility of these sites is induced under conditions which interfere with DNA replication. We suggest that during in vivo tumorigenesis, cells can undergo genetic changes and/or be exposed to environmental factors that interfere with DNA replication and induce fragile site expression. Since many of the drugs used in cancer therapy are potential inducers of both fragile sites and gene amplification, they can lead to chromosomal rearrangements and further contribute to cancer development. Better understanding the effect of these drugs on the mechanisms that initiate, direct, and enable chromosomal instability is of major clinical importance and might lead to the development of better therapeutic approaches.

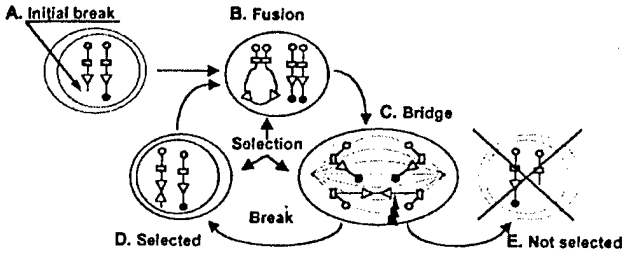

Figure 1. A scheme illustrating gene amplification via breakage-fusion-bridge cycles

Amplicons, yellow triangles; telomeres, orange (p-arm) or black (q-arm) circles; centromeres, orange rectangles. **A:** Interphase—an initial break gives rise to an uncapped chromatid carrying the selected gene. **B:** Metaphase—fusion of the 2 uncapped sister chromatids results in a dicentric chromosome. **C:** Anaphase—the dicentric chromosome forms a bridge between the opposite poles. A break of this chromosome leaves one daughter cell (D) with 3 copies of the selected gene, and only one copy in the other cell (E). Under a selection, recurrent cycles of BFB will occur, resulting in further accumulation of amplicon copies.

1989; Windle et al., 1991). They are classified as either rare or common, depending on their frequency within the population and their mode of induction. CFSs are considered to be part of the normal chromosome structure and thought to be present in all individuals (Sutherland and Richards, 1995). In tissue cultures, induced CFSs are preferential targets for chromosomal rearrangements, sister chromatid exchange, and integration of foreign DNA (Smith et al., 1998). So far, molecular analysis of CFSs has only been performed in human and mouse. This includes the partial identification of 4 sites (FRA3B, FRA7H, FRA7G, and FRA16D) out of ~90 that have been cytogenetically defined in the human genome (Boldog et al., 1997; Mishmar et al., 1998; Huang et al., 1998a; Paige et al., 2000; Shiraishi et al., 2001). These studies reveal that the fragile regions (the regions which exhibit fragility under the induction conditions) might encompass hundreds of kilobases (kb) of DNA. The molecular basis underlying their fragility is largely unknown; however, several studies show that intrinsic features of the fragile sequences might lead to perturbed fork progression. This can result in delayed replication along the fragile regions (Le Beau et al., 1998; Wang et al., 1999; Hellman et al., 2000), which is thought to interfere with the normal chromatin organization of the fragile region in metaphase, leading to fragility (Laird et al., 1987).

The ex vivo induction of CFSs was suggested to trigger and drive the amplification of drug-selected genes in rodent cells (Coquelle et al., 1997). However, the role of CFSs in the in vivo amplification of human oncogenes remains unclear. Here we investigate the possibility that recurrent chromosomal breaks in common fragile regions can drive BFB cycles, leading to amplification of human oncogenes. Under this model (Figure 1), the following would be predicted: (1) equal-spaced organization of intrachromosomal amplicons, visualized by fluorescence in situ hybridization (FISH) as a "ladder-like structure;" (2) clustering of the recurrent breaks within a CFS region; (3) inverted repeat organization of all the amplified copies along the same chromosomal arm; and (4) absence of sequences telomeric to the endogenous amplified region in the chromosome carrying the amplified copies. In this study, we reconstructed the molecular events that led to the amplification of the *MET* oncogene in a human gastric carcinoma and found that they fit with the BFB-CFS model. Our results suggest that recurrent breakage at CFS can lead to in vivo amplification of human oncogenes and other chromosomal rearrangements, thus shedding a new light on the role of CFSs in cancer.

Results

Equal-spaced organization of an amplified oncogene in a human cancer

If BFB cycles and recurrent breaks underlie oncogene amplifications, an equal-spaced organization of the amplified copies would be expected to be preserved in some amplification events, in which the initial organization was stabilized and preserved. We thus searched the literature for amplification of human oncogenes that resemble a ladder-like structure. Such a possible structure was noticed in the GTL-16 cell line, originating from a human gastric carcinoma (Motoyama et al., 1986). In this hypotetraploid cell line, 2 copies of a marker chromosome containing ~10 copies of the *MET* oncogene appear in all cells (Ponzetto et al., 1991), accompanied by overexpression and high activity of the MET tyrosine-kinase (Giordano et al., 1989). To study the amplicon organization in these cells, we applied FISH using clones from the vicinity of *MET*, and evaluated the results using confocal microscopy and computational image analysis (Hellman et al., 2000). As shown in Figure 2A, a clear ladder-like structure with 4 distinct intervals was visualized on the chromosomes carrying the amplification. This equal-spaced organization suggests that all the amplicons were bordered by breakpoints at the same chromosomal region. Thus, GTL-16 cells provide a suitable system to investigate the involvement of a BFB mechanism and the role of fragile site expression in cancer amplification.

Induction of perturbed chromatin organization along the CFS FRA7G region

Previous analysis in GTL-16 cells defined the centromeric boundary of the amplicons within an interval of several Mb at 7q31.1-7q31.2 (Ponzetto et al., 1991). The only CFS in this interval is FRA7G, cytogenetically mapped to 7q31.2 (Yunis et al., 1987). Although Huang et al. characterized ~300 kb spanning the fragile region (Huang et al., 1998a; 1998b), the entire FRA7G region and its location relative to *MET* have not yet been defined (Tatarelli et al., 2000).

To further define and characterize the entire FRA7G region, we constructed a physical map covering ~10 Mb of 7q31 by isolating BAC clones that bridged contiguous sequenced regions from the public and the Celera databases (Figure 3E). We further determined the location of clones relative to FRA7G gaps and constrictions by using FISH on metaphase chromosomes induced to exhibit CFSs. A clone was considered as spanning the fragile region if on different chromosomes from the same preparation its hybridization signals appeared centromeric or telomeric to the FRA7G gaps, or crossed the gaps ("both sides") (Mishmar et al., 1998). Since there are several CFSs along 7q, we used computational image analysis to identify FRA7G (Experimental Procedures). We were able to define 2 distinct zones within the region of FRA7G. One zone encompassed ~700 kb (dark blue in Figures 3B and 3F) and comprised clones (c169h6, AC002066, and V203C) that appear to span the FRA7G gaps (Figure 2B, Table 1). The more telomeric 19d10 clone (*RAY1/*

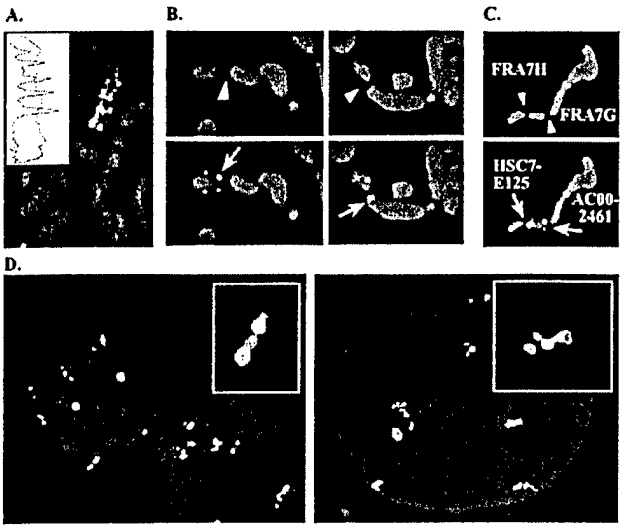

Figure 2. Organization of the *MET* amplicons relative to FRA7G region

A: The organization of the *MET* amplicons along a GTL-16 metaphase chromosome, analyzed by FISH using clone V193A as a probe. Insert: Computational representation of the FISH signals (red) and the DAPI staining (blue) along the amplified marker chromosome. **B:** FISH analysis of the FRA7G region. Upper panels: metaphase chromosomes expressing FRA7G (white triangles), stained with propidium iodide (PI). FRA7G are seen as unstained gaps. Bottom: the same chromosomes probed with a *MET* clone (cosmid c169h6, green arrow) and a reference clone from 7q32 to mark chromosome 7. The *MET* signals appear telomeric (left) or centromeric (right) to FRA7G gaps. **C:** Upper panel: A metaphase chromosome stained with PI, expressing both FRA7H and FRA7G. Bottom: The same chromosome probed with YAC HSC7E125 (FRA7H) and BAC AC002461 (FRA7G). Note the opposite orientation of both clones relative to the physical map. **D:** The order of clones along the FRA7G region, analyzed by FISH on interphase nuclei from the GM00847 cells (each has 4–6 chromosomes 7). Left: AC003080 (green); AC025297 (red); AC002461 (green); AC002465 (red). Right: HSC7E160 (7q31.1) (red); AC073137 (green); AC002461 (green); AC002465 (red). Inserts: a magnification of one chromosome from each nucleus. Note that the order found in these FISH experiments is the expected order, based on the sequenced contigs (Figure 3).

ST7 locus) showed hybridization signals only telomeric to the FRA7G gaps, indicating that the telomeric border of this zone must be between the *MET* and the *RAY1/ST7* loci (Figure 3 and Table 1).

The other zone encompassed 3–4 Mb (light blue in Figures 3B and 3F) and was comprised of clones showing an unusual hybridization pattern, since they hybridize mostly to the telomeric side of the FRA7G gaps, even though they are located more centromeric on the physical map (clones AC034112 to AC002463, Figure 2C and 3F and Table 1). The centromeric border of this zone was found between AC002463 and AC003080. To exclude the possibility that the opposite orientation of these clones resulted from an inversion or translocation of the region between AC002463 and AC034112 in the GM00847 cells, we performed a dual-color FISH analysis on interphase nuclei from cells grown under normal growth conditions. The signal order of 2 sets of clones was analyzed in at least 50 interphase chromosomes lying in a linear position (Figure 2D). This analysis showed that the order of clones along the entire region was as expected from the physical map, excluding the possibility of a chromosomal rearrangement in the GM00847 cells. To confirm the mapping of the opposite orientation region and to further exclude the possibility of a chromosomal rearrangement, we performed FISH on metaphase chromosomes expressing FRA7G in another human cell line, PANC-1. A similar telomeric orientation of clone AC002089 was identified in these cells (data not shown). These results suggest that the opposite-orientation pattern reflects an unusual chromatin organization of the fragile region in metaphase chromosomes exhibiting fragility. Thus, the analysis of the entire FRA7G region showed that fragile site induction can lead to an unusual chromatin organization (gaps, breaks, and spanning or opposite-orientation organization) along ~5 Mb of DNA.

Perturbed DNA replication along FRA7G

Perturbed DNA replication was previously found along CFS sequences (Le Beau et al., 1998; Wang et al., 1999; Hellman et al., 2000). To further define the region encompassed by FRA7G, we analyzed the replication pattern along that region, using FISH on S-phase nuclei. In this method, a high percentage of unreplicated alleles (single hybridization dot, S signal) indicates that the region is replicated relatively late in the S-phase, while a high percentage of replicated alleles (double dot, D signals), indicates a relatively early replication time. For most sequences, the 2 alleles replicate in a synchronous manner and have a low percentage (10%–20%) of SD signals (Selig et al., 1992).

First we analyzed the replication pattern of the nonfragile region telomeric to FRA7G (Figure 3). This analysis has revealed 2 distinct replication time zones: the region adjacent to FRA7G (cosmid clones c172d6 and c19d10, orange in Figures 3C and 3G) showed a relatively early replication time and an allelic synchronous replication pattern (18% and 19% SD, Table 2) while the more telomeric part (CW44 and CNH24, dark green in Figures 3C and 3G) showed a late and synchronous pattern (12% and 10% SD). Thus, the region defined by the cytogenetic analysis as the telomeric nonfragile region indeed presented a normal replication pattern with early and late replication time zones, which likely correspond to the R-band 7q31.2 and the G-band 7q31.3, respectively (Figure 3A).

We then analyzed the replication pattern of clones that span the FRA7G gaps. All of these clones (149e12, 182b3, 63e3, 19d5, and V193A, pink in Figures 3C and 3G) showed early replication time, but with high levels of allelic asynchrony (29%–32% SD, Table 2). Such high levels of asynchrony have previously been found along the CFS FRA7H and might reflect perturbed DNA replication (Hellman et al., 2000). However, it might also reflect allele-specific replication time of regions harboring parentally imprinted genes (Kitsberg et al., 1993a). We excluded this possibility by analyzing the replication pattern of this region in an isodisomic cell line (CF33-3) carrying 2 maternal chromosomes 7 (Hellman et al., 2000). The FRA7G clone V193A showed asynchronous replication in both normal (CF33-2) and the isodisomic cells (30% and 27% SD, respectively), indicating that its asynchrony is not a result of allele-specific replication time. It is important to note that the identified asynchrony might also result from an abnormal separation of the sister chromatids as part of the unusual chromatin organization of the region.

We further investigated the replication pattern along the FRA7G region by analyzing the replication time differences between adjacent sequences. The cosmid clone c63e3 replicated before c182b3 (35 kb apart) in 62% of the nuclei, and the clone c169h6 replicated before c149e12 (150 kb apart) in 76% of the

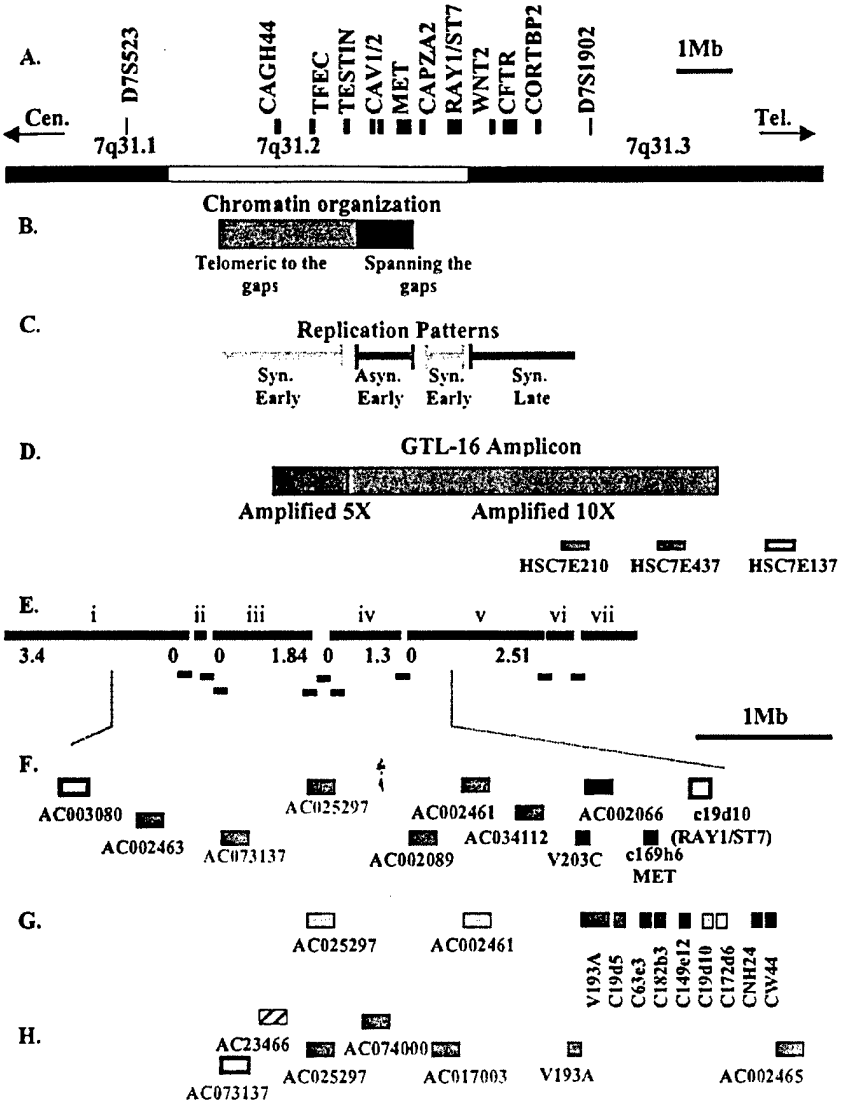

Figure 3. Maps of the FRA7G region

A: Reference genes and polymorphic markers at 7q31.1–7q31.3. **B:** A region spanning the cytogenetic gaps and constrictions (dark blue), and a region showing telomeric signals of clones that are located more centromeric on the physical map ("opposite oriented") (light blue). **C:** Regions showing normal (synchronous) and early replication pattern in orange, normal and late in dark green, and unusual (asynchronous) and early in pink. **D:** The boundaries of the GTL-16 amplicons, 5× region in red, 10× in green. Below are indicated the YAC clones used in the analysis of the telomeric boundary. **E:** The set of Celera DNA sequence scaffolds (upper line) connected by BAC clones (bottom lines). The numbers indicate the size of each sequence in Mb. The sequence names from left to right are: i-GA_x8Y8FG7; ii-GA_x8Y8FKQ; iii-GA_X2HTBKNJPOH; iv-GA_x2HTBL4GTR2; v-GA-x8WU11E; vi-GA_x2HTBKNGALA; vii-GA_x2HTBI2VJAN. The BAC clones or accession numbers from left to right are: AC073346; CIT-2172F3; AC032017; AC073901; CIT-2012G19; AC015621; NH032P06; NH516A21; AC005016. **F:** Clones used for the cytogenetic analysis of FRA7G gaps and constrictions. **G:** Clones used for the replication analysis. **H:** Clones used for the analysis of the amplicon boundaries and the copy number within the amplified region. The colors of the clones in **F–H** are the same as in **B–D**.

nuclei. The ability to clearly detect the replication time order of such adjacent clones suggested an unusual replication rate along FRA7G, as previously found along FRA7H (Hellman et al., 2000). Hence, the replication analysis supported the cytogenetic identification of the FRA7G region, and showed that this region has an intrinsic replication perturbation, in addition to its induced chromatin perturbation.

Breakpoints within FRA7G set the centromeric boundaries of the *MET* amplicons

If the amplification of *MET* in GTL-16 cells originated by a BFB-CFS mechanism, then the centromeric boundaries of the amplicons are expected to lie within the FRA7G region. In a previous study, the boundaries of the *MET* amplified region were estimated to lie at least 1 Mb centromeric and 2 Mb telomeric to *MET* (Ponzetto et al., 1991). To further define the boundaries, we applied dual-color FISH on GTL-16 nuclei using clones from 7q31. In this analysis, amplified sequences were detected as 2 groups of multiple hybridization signals (representing the 2 amplified chromosomes), while nonamplified sequences were detected as 4 isolated signals (representing the 4 copies of chromosome 7 in these cells; examples in Figure 4A). Using this approach, we defined the telomeric boundary of the amplified region between YACs HSC7E437 and HSC7E137 (Figure 3D) and the centromeric boundary between BACs AC025297 and AC073137 (Figure 3H). Very weak signals were seen with AC023466, indicating that the breakpoint is probably within this clone. These results show that the centromeric boundary of the amplified region is within the chromatin perturbation region of FRA7G, as expected from the model.

Since FRA7G encompasses a large genomic region, and assuming that the 10 amplified copies were generated by BFB cycles, more than one breakpoint was expected within the fragile region. In order to identify additional breakpoints, we ana-

Table 1. FISH analysis of hybridization signals on metaphase chromosomes exhibiting FRA7G

Clones	Number of signals		
	Centromeric	Both sides	Telomeric
c19d10 (*RAY1/ST7*)	0	0	21
c169h6 (*MET*)	2	1	17
AC002066/V203C	12	1	21
AC034112/AC002461	0	0	40
AC002089	1	2	43
AC025297	2	1	33
AC073137	1	0	54
AC002463	1	1	40
AC003080	18	0	3

The clones are ordered in accordance with the physical map, telomeric (top of the table) to centromeric (bottom). The results of clones covering the same genomic region were combined.

Table 2. Replication pattern (% SD, SS, and DD) of S-phase nuclei

Clones	SD	SS	DD
Synchronous and late			
CW44	12	73	15
CNH24	10	77	13
Synchronous and early			
C172d6	18	37	45
C19d10	19	45	36
Asynchronous and early			
C149e12	31	34	35
C182b3	29	31	40
C63e3	32	27	41
C19d5	30	33	37
V193A	29	28	43
Synchronous and early			
AC002461	18	25	57
AC025297	16	28	56

The clones are ordered according to the physical map, telomeric (top of the table) to centromeric (bottom).

lyzed the level of amplification along the amplified region by counting FISH signals in interphase nuclei (only nuclei in which the analyzed region was replicated were considered, Experimental Procedures). The analysis has revealed 2 distinct levels of amplification. Most (8/10 Mb) of the amplified region, covered by clones HSC7E437, AC002465, and V193A, showed 20 ± 5 signals per group (green in Figures 3D and 3H, and Figure 4B). This indicated that each marker chromosome carried 10 copies of the amplified region, in agreement with previous studies (Ponzetto et al., 1991). However, the centromeric 2 Mb of the amplified region, encompassed by BAC clones AC017003, AC074000, and AC025297 (red in Figures 3D and 3H), showed only 10 ± 3 signals/group, indicating only 5 copies/chromosome (Figure 4B). Hence, 2 breakpoints were identified in the centromeric boundary of the *MET* amplification: one between the high- and the low-amplified regions (between V193A and AC017003), and the other between the low- and the nonamplified regions (between AC025297 and AC073137). These 2 breakpoints lie within the FRA7G region, as predicted by the BFB-CFS mechanism. The final amplification break (accounting for >8 *MET* copies, Figure 5A, stage iv) is expected to appear in only one copy (Figure 5A, stage v). This final breakpoint could not be identified since a change in only one FISH signal is below the resolution of the analysis.

The GTL-16 amplicons are organized as inverted repeats

Another important prediction of the BFB model is an inverted repeat organization of the amplicons (Figure 1). The first indication for such an organization in GTL-16 cells was the 5-step ladder as demonstrated by hybridization with clone V193A, which is 2 Mb from the edge of the amplicon (Figure 2A). This type of pattern would be expected using a FISH probe from the edge of the amplicon, assuming an inverted repeat organization. An alternating pattern between close signals (below the resolution of FISH at metaphase) and distant signals should be observed, and this could result in a 5-step ladder, with each rung corresponding to 2 copies of the *MET* amplicon (Figure 5A). As can be seen in Figure 2A, this was indeed the identified pattern.

Since FISH resolution is much higher in interphase (>100 kb), we further examined the amplicon organization in interphase chromosomes. In the case of an inverted repeat organization, signals of a clone from the edge of the amplicon are expected to appear adjacent to each other, while signals of a clone from the center are expected to flank them (Figure 5A). In contrast, in the case of a direct repeat (head to tail) organization, the signals from the edge and those from the center are expected to alternate, and in a case of a random organization, no pattern is expected. The analysis of paired probes, one from the center and the other from the centromeric edge of the GTL-16 amplicon, showed a pattern (Figure 5B) consistent with an inverted repeat organization, as predicted by the BFB model.

The structure of the amplified chromosome

In many amplification events in cancer cells, the initial amplicon organization is hampered by secondary rearrangements which occur during the cancer development. However, in GTL-16 cells, the amplicon organization indicates that such secondary rearrangements did not occur in these cells. By using spectral karyotyping (SKY) and FISH analyses we found that the chromosome arm harboring the *MET* amplicons is fused to the centromere and the short arm of chromosome 12 (Figures 4C and 4D). Such a fusion could have prevented secondary BFB cycles, due to the recapping of the broken chromosome end (Toledo et al., 1992). Importantly, FISH analysis of clones from the telomeric part of 7q (clones HSC7E137 from 7q31.3 and c53g3 from the *MEST* locus in 7q32) showed that sequences telomeric to the endogenous amplified region are absent in the marker chromosome, as predicted by the BFB model. In addition, the karyotype analysis of GTL-16 showed that most chromosomes have 4 copies, while chromosome 7 has 2 normal and 2 deleted copies, and chromosome 12 and the 7-12 fused marker chromosome each appear in only 2 copies (Rege-Cambrin et al., 1992). This organization further supports our hypothesis that the amplified chromosome was stabilized by fusion with the short arm of chromosome 12 following the amplification. However, the fusion between the amplicons and chromosome 12 sequences could have also resulted from a recombination event prior to the BFB cycles.

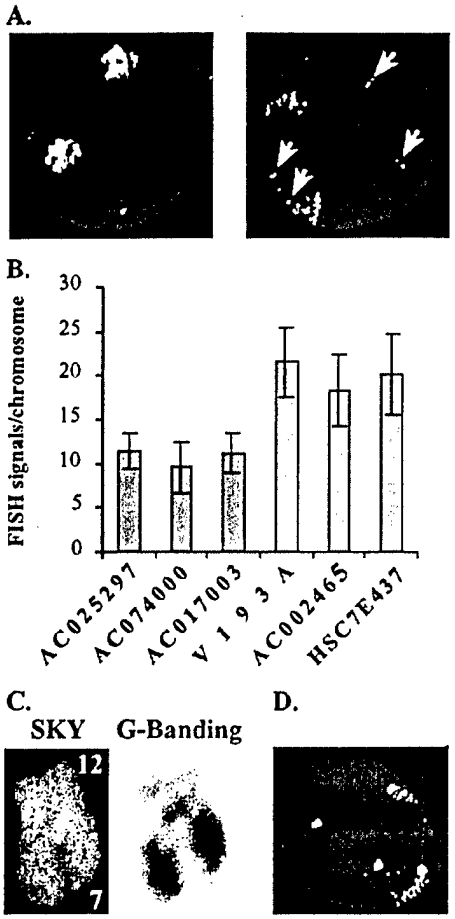

Figure 4. The organization of the amplified chromosome in the GTL-16 cells

A: FISH analysis of the amplicon boundaries. Left: an interphase nucleus hybridized with the *MET* clone c169h6 (green) and with clone V193A (red). The signals of both probes colocalize and appear yellow. Right: an interphase nucleus hybridized with V193A (red) and HSC7E137 (green). HSC7E137 signals appear only on the 4 nonamplified copies of chromosome 7 (arrowheads), indicating that this clone is not included in the amplicon. **B:** The level of amplification of clones encompasses the amplified region, determined by counting FISH signals in interphase nuclei. Only nuclei in which the analyzed region was replicated were considered. **C:** Left: SKY analysis of the amplified chromosome. Chromosome 12 sequences in green, chromosome 7 in orange. Right: G-banding of the same chromosome. **D:** An interphase nucleus from GTL-16 cells hybridized with a chromosome 12 centromeric probe (green) and V193A (red).

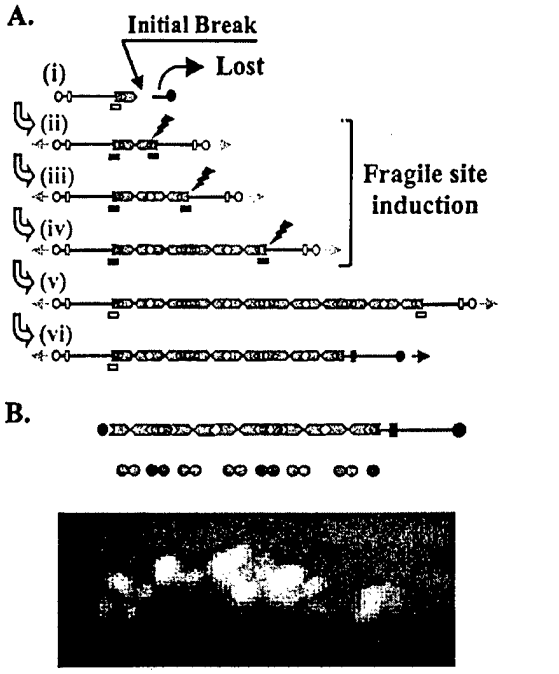

Figure 5. Reconstruction of the events which led to the *MET* amplification in GTL-16 cells

A: The sequence of events, leading to amplification of *MET* in the GTL-16 cells. The 5× region is shown in red, the 10× region in green, induced FRA7G as black rectangles, uninduced as empty rectangles. Only intact (nonrearranged) fragile regions are marked. Other elements have the same color code as in Figure 1. **B:** Upper: The expected hybridization pattern along one chromatid of the amplified chromosome. Bottom: A replicated amplified chromosome of a GTL-16 interphase, hybridized with clone AC025297, from the 5× amplified region (red) and AC002465 from the 10× amplified region (green).

Discussion

Here we demonstrate the role of a BFB-CFS mechanism in the amplification of a human oncogene in vivo. Our study provides evidence for all the predictions of this model: (1) An equal-spaced organization of the amplified units, visualized as a ladder-like structure. (2) Clustering of the recurrent breaks within CFS regions (rather then distribution of the breaks along the distance between the oncogene locus and the centromere). Our study provides molecular evidence that breakage leading to oncogene amplification preferentially occurs within CFS regions. Since human CFSs encompass large genomic regions, different breakpoints within the fragile region are expected to occur during subsequent BFB cycles. The regions between the breakpoints are expected to be included only in a subset of the amplicons (Figure 5). Here we identified 2 breakpoints (2 Mb apart) that set the centromeric boundaries of the *MET* amplicons. Both breakpoints lie in a region adjacent to the FRA7G spanning region, which showed unusual chromatin organization upon fragile site induction. Such an unusual organization (the "opposite orientated" phenomenon) was found around the spanning region of another CFS, FRA7H (Mishmar et al., 1998) (Figure 1C). Thus, we suggest that CFSs might consist of "core sequences" and "affected sequences." The core sequences (the spanning regions) have an unusual replication pattern (Le Beau et al., 1998; Wang et al., 1999; Hellman et al., 2000) (Table 2), which predispose them to additional replication delay under conditions that induce fragility. The replication delay might perturb the condensation of the chromatin, resulting in large regions showing perturbed chromatin organization at metaphase (Figure 1C). The unusual organization of the chromatin loops around the gaps might account for the "opposite-orientation" phenomenon. (3) Symmetric and alternate organization of the amplified copies, which fits with an inverted repeat organization of the amplified region. As can be seen in Figure 5B, such an organization was found for the 10× and 5× amplified regions in GTL-16 cells. (4) Absence of sequences telomeric to the endogenous

amplified region, in chromosomes carrying the amplified copies. In the GTL16 cells, no sequences telomeric to HSC7E137 were identified in the marker chromosome. Hence, for the amplification of *MET* in the GTL-16 cells, all the predictions of the BFB-CFS model have been verified at the molecular level. It therefore appears that intrachromosomal amplification of human oncogenes may arise by the same mechanism as suggested for the amplification of drug resistant genes in rodent cells.

We suggest the following sequence of events (diagrammed in Figure 5) for in vivo oncogene amplification in tumor cells: (1) An initial break sets the telomeric boundary of the amplified unit and leads to deletion of the region telomeric to the break (Figure 5A). The break might occur spontaneously, or as part of general chromosomal instability that characterizes early stages of many cancer types (Lengauer et al., 1998), such as nonreciprocal translocations caused by telomere dysfunction (Artandi et al., 2000). However, the initial break might also occur at CFSs due to exposure to induction conditions. In GTL-16 cells, this break occurred at 7q31.3, between YACs HSC7E437 and HSC7E137. (2) The initial break generates uncapped chromosomal ends, which can lead to end-fusion of the sister chromatids, resulting in a dicentric chromosome (Figure 5A). (3) At the same stage, the cells can undergo additional genetic changes and/or be exposed to environmental factors (e.g., hypoxia, deregulation of the nucleotides pools, and treatment with cytotoxic drugs) that interfere with DNA replication and induce fragile site expression (Yunis et al., 1987). All these conditions are also enhancers of gene amplification (Stark et al., 1989; Coquelle et al., 1998; Poupon et al., 1996). Importantly, FRA7G was shown to be induced by several agents, such as methotrexate or actinomycin D (Yunis et al., 1987), which are inducers of gene amplification. The unusual chromatin organization of induced fragile regions predisposes them to chromosomal breaks during anaphase, when the dicentric chromosome is segregating to opposite poles (Figure 5). In GTL-16 cells, this evidently led to a break within FRA7G, between the 10× and the 5× amplified regions. (4) Additional fusion-bridge-breakage cycles occur, giving rise to the amplification of the region between the breaks. In GTL-16 cells, 3 such BFB cycles presumably occurred, resulting in 16 extra copies of the *MET* amplicon. (5) Eventually, the selection pressure disappears once the oncogene has attained sufficient amplification. Since *MET* protein is known as a scatter factor, which triggers cell proliferation, cell survival, cell motility, invasion of extracellular matrix, and induced angiogenesis (Prat et al., 1998), we postulate that in the GTL-16 cells, the disappearance of the selection pressure (which also induces fragility) might have occurred as a result of the development of motility and/or angiogenesis ability in cells carrying extra copies of MET, leading to reoxygenation of the tumor cells. (6) Secondary BFB cycles can occur, hampering the initial organization of the amplicons, unless the uncapped chromosomal ends stabilize within a short time following amplification. In the GTL-16 cells, the amplified chromosome fused with chromosome 12, and the breakage of this dicentric 7-12 chromosome was stabilized, giving rise to the marker chromosome (Figures 4C and 4D and Figure 5A, stage vi), probably shortly following the amplification.

Recent studies suggest that BFB cycles represent a general mechanism leading to cancer instability. Gisselson et al. investigated cancer cells with high intratumor heterogeneity, and found evidence for frequent BFB events, including anaphase bridges, telomeric associations, and dicentric ring chromosomes, in both tissues and cell lines from a variety of solid tissues cancers (2000a). Artandi et al. showed that BFB cycles promote nonreciprocal translocations and epithelial cancers in mice (2000). Shuster et al. reported a pattern of rearrangements in oral squamous cell carcinoma cell lines that fit to the BFB mechanism of amplification in human chromosome 11q13, a region that harbors several oncogenes (2000). Our search of the literature identified additional examples of symmetric amplicon organization, which might indicate ladder-like organizations in amplifications of several human oncogenes, including *KRAS2* (Figure 7 in Gisselsson et al., 2000b), *MLL* (Figure 3C in Kakazu et al., 1999) and *C-MYC* (Figure 4 in Falzetti et al., 2000). Hence, the lack of visual ladder-like structures in most human tumors containing intrachromosomal amplifications probably reflects their late stage in the cancer progression, during which secondary rearrangements can hamper the recognition of the initial amplicon organization.

These findings show that the expected results of BFB-CFS amplification could be found in a variety of human tumors, suggesting that fragile sites may play an important role in cancer. Yunis and Soreng (1984) put forward the hypothesis that CFSs play a role in cancer instability, based on the correlation between chromosomal bands in which CFSs are mapped and bands harboring cancer breakpoints and/or oncogenes. Subsequently, deletions of regions containing tumor suppressor gene(s) were found at the human CFSs FRA3B, FRA7G, and FRA16D regions, indicating instability in cancer cells (reviewed in Smith et al., 1998; Mangelsdorf et al., 2000). However, these studies left open the question of whether this instability is the outcome of an intrinsic instability conferred by the fragile sites or due to the selection of altered cancer genes located in these regions (Smith et al., 1998). Our study suggests that these cancer breakpoints are indeed the outcome of an intrinsic instability conferred by the fragile site sequences, since in the case of intrachromosomal amplification of large genomic regions, the breaks are distant from the targeted genes and thus are not affected by selection. Thus, it is important to investigate the molecular organization of additional intrachromosomal oncogene amplifications (such as *C-MYC*, *cyclin D1*, *MLL*) and the role of the fragile sites in their vicinity (FRA8C or D, FRA11F or A, and FRA11G, respectively).

In many cancers, chromosomal instability precedes and promotes the dysfunction of specific cancer genes (Lengauer et al., 1998), leading to the generation and/or to the progression of malignancy (Rennstam et al., 2001). Our results suggest that under conditions which induce the expression of CFSs, these regions can direct chromosomal rearrangements that play a significant role in cancer development. Since many of the drugs used in cancer therapy are potential inducers of both fragile sites and amplification, they can lead to chromosomal rearrangements and further contribute to cancer development. Thus, a better understanding of the causal relationship between cancer therapeutic agents and their specific targets (specific fragile sites and oncogenes) will provide the required information for developing better therapeutic approaches.

Experimental procedures

Cells and growth conditions

The cell lines used in this study: GTL-16, a gastric carcinoma cell line with amplification of the *MET* oncogene (Motoyama et al., 1986); Manca, a lym-

phoma cell line; CF33-2, a normal lymphocyte cell line; and CF33-3, a chromosome 7 isodisomic lymphocyte cell line (Hellman et al., 2000). GM00847 (National Institute of General Medical Sciences, Camden, NJ), a simian virus 40 (SV40)-transformed human fibroblast cell line. PANC-1 (American Type Culture Collection, Rockville, MD), a tumor-cell line established from a carcinoma of the pancreas. All cell lines except GM00847 were grown in RPMI medium containing 10% fetal calf serum. GM00847 was grown in MEM-EAGLE medium supplemented with 10% fetal calf serum.

Contigs, sequences, and DNA probes

A DNA sequence-based map of chromosome 7q31.1 to 7q31.3 was constructed by comparing and combining information acquired from the Celera scaffold assemblies and from high-throughput (HTGS) and finished sequence from the public GenBank database. Physical gaps were bridged by BAC clones that have either been sequenced or whose end-sequence (TIGR BAC End Sequence Database) was known or generated. BLAST2 analysis was used to align all sequences. The assembled map with no physical (clone) gaps represents a consistent presentation of order of DNA markers, in comparison to our other studies which used the additional technologies of radiation and somatic cell hybrid mapping, and FISH (see http://www.genet.sickkids.on.ca/chromosome7/ for any additional information on clones required).

Fluorescent in situ hybridization (FISH) on interphase nuclei

FISH experiments on interphase nuclei (for mapping of FRA7G region, replication time analysis, and mapping of the amplicon boundaries and copy number) were performed as previously described (Hellman et al., 2000). To avoid misinterpretation of the amplification signals, only nuclei in which the 4 nonamplified copies of chromosome 7 were replicated (showed D signals) were considered in the analysis. Signals of 50 replicated amplified chromosomes were counted for each probe.

Cytogenetic analysis of the FRA7G region

GM00847 cells were grown on coverslips, and fragile sites were induced by growing the cells in M-199 medium in the presence of 0.4 μM aphidicolin and 0.5% ethanol for 24 hr prior to chromosome fixation. FISH mapping of the region encompassed by FRA7G was performed as previously described (Mishmar et al., 1998). Since there are several aphidicolin induced fragile sites on 7q, their positions had to be carefully determined. Using the Image-Pro Plus program (Media Cybernetics, Silver Spring, MD), the distance of the fragile sites from the tip of the long arm of chromosome 7 was measured, relative to the total length of the chromosome. According to the Genome DataBase mapping of the fragile sites, this value should be ~15% for FRA7H, ~30% for FRA7G, and ~37% for FRA7F. Analysis based on 150 FRA7G measurements indicated that it is located at 29% ± 2.5%. Observed cytogenetic gaps within 2 SD were considered to be FRA7G.

Spectral karyotyping analysis

Chromosome labeling was performed with the SKY fluorescent labeling kit (Applied Spectral Imaging, Migdal HaEmek, Israel) according to the manufacturer's protocol. Chromosomes were counterstained with DAPI. Image acquisition was performed by use of a SD200 Spectracube (Applied Spectral Imaging, Inc.) mounted on an Olympus BH-2 microscope using a custom designed optical filter (SKY-1, Chroma Technology, Brattleboro, VT, USA). Automatic identification of chromosomes was based on the measurement of the spectrum for each chromosome.

Acknowledgments

The authors wish to thank Dr. Silvia Giordano, Italy, for providing the GTL-16 cells.

Received: November 2, 2001
Revised: December 19, 2001

References

Artandi, S.E., Chang, S., Lee, S.L., Alson, S., Gottlieb, G.J., Chin, L., and DePinho, R.A. (2000). Telomere dysfunction promotes non-reciprocal translocations and epithelial cancers in mice. Nature *406*, 641–645.

Boldog, F., Gemmill, R.M., West, J., Robinson, M., Robinson, L., Li, E., Roche, J., Todd, S., Waggoner, B., Lundstrom, R., et al. (1997). Chromosome 3p14 homozygous deletions and sequence analysis of FRA3B. Hum. Mol. Genet. *6*, 193–203.

Brison, O. (1993). Gene amplification and tumor progression. Biochim. Biophys. Acta *1155*, 25–41.

Coquelle, A., Pipiras, E., Toledo, F., Buttin, G., and Debatisse, M. (1997). Expression of fragile sites triggers intrachromosomal mammalian gene amplification and sets boundaries to early amplicons. Cell *89*, 215–225.

Coquelle, A., Toledo, F., Stern, S., Bieth, A., and Debatisse, M. (1998). A new role for hypoxia in tumor progression: induction of fragile site triggering genomic rearrangements and formation of complex DMs and HSRs. Mol. Cell *2*, 259–265.

Falzetti, D., Vermeesch, J.R., Matteucci, C., Ciolli, S., Martelli, M.F., Marynen, P., and Mecucci, C. (2000). Microdissection and FISH investigations in acute myeloid leukemia: a step forward to full identification of complex karyotypic changes. Cancer Genet. Cytogenet. *118*, 28–34.

Giordano, S., Ponzetto, C., Di Renzo, M.F., Cooper, C.S., and Comoglio, P.M. (1989). Tyrosine kinase receptor indistinguishable from the c-met protein. Nature *339*, 155–156.

Gisselsson, D., Pettersson, L., Hoglund, M., Heidenblad, M., Gorunova, L., Wiegant, J., Mertens, F., Dal Cin, P., Mitelman, F., and Mandahl, N. (2000a). Chromosomal breakage-fusion-bridge events cause genetic intratumor heterogeneity. Proc. Natl. Acad. Sci. USA *97*, 5357–5362.

Gisselsson, D., Mandahl, N., Palsson, E., Gorunova, L., and Hoglund, M. (2000b). Locus-specific multifluor FISH analysis allows physical characterization of complex chromosome abnormalities in neoplasia. Genes Chromosomes Cancer *28*, 347–352.

Glover, T.W., Berger, C., Coyle, J., and Echo, B. (1984). DNA polymerase alpha inhibition by aphidicolin induces gaps and breaks at common fragile sites in human chromosomes. Hum. Genet. *67*, 136–142.

Hellman, A., Rahat, A., Scherer, S.W., Darvasi, A., Tsui, L.C., and Kerem, B. (2000). Replication delay along FRA7H, a common fragile site on human chromosome 7, leads to chromosomal instability. Mol. Cell. Biol. *20*, 4420–4427.

Huang, H., Qian, J., Proffit, J., Wilber, K., Jenkins, R., and Smith, D.I. (1998a). FRA7G extends over a broad region: coincidence of human endogenous retroviral sequences (HERV-H) and small polydispersed circular DNAs (spcDNA) and fragile sites. Oncogene *16*, 2311–2319.

Huang, H., Qian, C., Jenkins, R.B., and Smith, D.I. (1998b). Fish mapping of YAC clones at human chromosomal band 7q31.2: identification of YACS spanning FRA7G within the common region of LOH in breast and prostate cancer. Genes Chromosomes Cancer *21*, 152–159.

Kakazu, N., Taniwaki, M., Horiike, S., Nishida, K., Tatekawa, T., Nagai, M., Takahashi, T., Akaogi, T., Inazawa, J., Ohki, M., and Abe, T. (1999). Combined spectral karyotyping and DAPI banding analysis of chromosome abnormalities in myelodysplastic syndrome. Genes Chromosomes Cancer *26*, 336–345.

Kitsberg, D., Selig, S., Brandeis, M., Simon, I., Keshet, I., Driscoll, D.J., Nicholls, R.D., and Cedar, H. (1993a). Allele-specific replication timing of imprinted gene regions. Nature *364*, 459–463.

Kuo, M.T., Vyas, R.C., Jiang, L.X., and Hittelman, W.N. (1994). Chromosome breakage at a major fragile site associated with P-glycoprotein gene amplification in multidrug-resistant CHO cells. Mol. Cell. Biol. *14*, 5202–5211.

Laird, C.E., Jaffe, G., Karpen, M., Lamb, M., and Nelson, R. (1987). Fragile sites in human chromosomes as regions of late-replicating DNA. Trends Genet. *3*, 274.

Le Beau, M.M., Rassool, F.V., Neilly, M.E., Espinosa, R., III, Glover, T.W., Smith, D.I., and McKeithan, T.W. (1998). Replication of a common fragile site, FRA3B, occurs late in S phase and is delayed further upon induction: implications for the mechanism of fragile site induction. Hum. Mol. Genet. *7*, 755–761.

Lengauer, C., Kinzler, K.W., and Vogelstein, B. (1998). Genetic instabilities in human cancers. Nature *396*, 643–649.

Mangelsdorf, M., Ried, K., Woollatt, E., Dayan, S., Eyre, H., Finnis, M., Hobson, L., Nancarrow, J., Venter, D., Baker, E., and Richards, R.I. (2000). Chromosomal fragile site FRA16D and DNA instability in cancer. Cancer Res. *60*, 1683–1689.

McClintock, B. (1951). Chromosome organization and genic expression. Cold Spring Harb. Symp. Quant. Biol. *16*, 13–47.

Mishmar, D., Rahat, A., Scherer, S.W., Nyakatura, G., Hinzmann, B., Kohwi, Y., Mandel-Gutfroind, Y., Lee, J.R., Drescher, B., Sas, D.E., et al. (1998). Molecular characterization of a common fragile site (FRA7H) on human chromosome 7 by the cloning of an SV40 integration site. Proc. Natl. Acad. Sci USA *95*, 8141–8146.

Mitelman, F., Mertens, F., and Johansson, B. (1997). A breakpoint map of recurrent chromosomal rearrangements in human neoplasia. Nat. Genet. *15*, 417–474.

Motoyama, T., Hojo, H., and Watanabe, H. (1986). Comparison of seven cell lines derived from human gastric carcinomas. Acta Pathol. Jpn. *36*, 65–83.

Paige, A.J., Taylor, K.J., Stewart, A., Sgouros, J.G., Gabra, H., Sellar, G.C., Smyth, J.F., Porteous, D.J., and Watson, J.E. (2000). A 700-kb physical map of a region of 16q23.2 homozygously deleted in multiple cancers and spanning the common fragile site FRA16D. Cancer Res. *60*, 1690–1697.

Ponzetto, C., Giordano, S., Peverali, F., Della Valle, G., Abate, M.L., Vaula, G., and Comoglio, P.M. (1991). c-met is amplified but not mutated in a cell line with an activated met tyrosine kinase. Oncogene *6*, 553–559.

Poupon, M.F., Smith, K.A., Chernova, O.B., Gilbert, C., and Stark, G.R. (1996). Inefficient growth arrest in response to dNTP starvation stimulates gene amplification through bridge-breakage-fusion cycles. Mol. Biol. Cell *7*, 345–354.

Prat, M., Crepaldi, T., Pennacchietti, S., Bussolino, F., and Comoglio, P.M. (1998). Agonistic monoclonal antibodies against the Met receptor dissect the biological responses to HGF. J. Cell Sci. *111*, 237–247.

Rege-Cambrin, G., Scaravaglio, P., Carozzi, F., Giordano, S., Ponzetto, C., Comoglio, P.M., and Saglio, G. (1992). Karyotypic analysis of gastric carcinoma cell lines carrying an amplified c-met oncogene. Cancer Genet. Cytogenet. *64*, 170–173.

Rennstam, K., Baldetorp, B., Kytola, S., Tanner, M., and Isola, J. (2001). Chromosomal rearrangements and oncogene amplification precede aneuploidization in the genetic evolution of breast cancer. Cancer Res. *61*, 1214–1219.

Selig, S., Okumura, K., Ward, D.C., and Cedar, H. (1992). Delineation of DNA replication time zones by fluorescence in situ hybridization. EMBO J. *11*, 1217–1225.

Shiraishi, T., Druck, T., Mimori, K., Flomenberg, J., Berk, L., Alder, H., Miller, W., Huebner, K., and Croce, C.M. (2001). Sequence conservation at human and mouse orthologous common fragile regions, FRA3B/FHIT and Fra14A2/Fhit. Proc. Natl. Acad. Sci. USA *98*, 5722–5727.

Shuster, M.I., Han, L., Le Beau, M.M., Davis, E., Sawicki, M., Lese, C.M., Park, N.H., Colicelli, J., and Gollin, S.M. (2000). A consistent pattern of RIN1 rearrangements in oral squamous cell carcinoma cell lines supports a breakage-fusion-bridge cycle model for 11q13 amplification. Genes Chromosomes Cancer *28*, 153–163.

Smith, D.I., Huang, H., and Wang, L. (1998). Common fragile sites and cancer. Int. J. Oncol. *12*, 187–196.

Stark, G.R., Debatisse, M., Giulotto, E., and Wahl, G.M. (1989). Recent progress in understanding mechanisms of mammalian DNA amplification. Cell *57*, 901–908.

Sutherland, G.R., and Richards, R.I. (1995). The molecular basis of fragile sites in human chromosomes. Curr. Opin. Genet. Dev. *5*, 323–327.

Tatarelli, C., Linnenbach, A., Mimori, K., and Croce, C.M. (2000). Characterization of the human TESTIN gene localized in the FRA7G region at 7q31.2. Genomics *68*, 1–12.

Toledo, F., Le Roscouet, D., Buttin, G., and Debatisse, M. (1992). Co-amplified markers alternate in megabase long chromosomal inverted repeats and cluster independently in interphase nuclei at early steps of mammalian gene amplification. EMBO J. *11*, 2665–2673.

Wang, L., Darling, J., Zhang, J.S., Huang, H., Liu, W., and Smith, D.I. (1999). Allele-specific late replication and fragility of the most active common fragile site, FRA3B. Hum. Mol. Genet. *8*, 431–437.

Windle, B., Draper, B.W., Yin, Y.X., O'Gorman, S., and Wahl, G.M. (1991). A central role for chromosome breakage in gene amplification, deletion formation, and amplicon integration. Genes Dev. *5*, 160–174.

Yunis, J.J., and Soreng, A. (1984). Constitutive Fragile Sites and Cancer. Science *226*, 1199–1204.

Yunis, J.J., Soreng, A.L., and Bowe, A.E. (1987). Fragile sites are targets of diverse mutagens and carcinogens. Oncogene *1*, 59–69.

MS#9

GENES, CHROMOSOMES & CANCER 34:406–415 (2002)

Transcriptional Profiling Reveals That Several Common Fragile-Site Genes Are Downregulated in Ovarian Cancer

Stacy R. Denison,[1] Nicole A. Becker,[1] Matthew J. Ferber,[2] Leslie A. Phillips,[1] Kimberly R. Kalli,[3] John Lee,[4] Jim Lillie,[4] David I. Smith,[1]* and Viji Shridhar[1]

[1]Division of Experimental Pathology, Department of Laboratory Medicine and Pathology, Mayo Foundation, Rochester, Minnesota
[2]Biochemistry and Molecular Biology, Mayo Foundation, Rochester, Minnesota
[3]Endocrine Research Unit, Mayo Foundation, Rochester, Minnesota
[4]Millenium Pharmaceuticals, Inc., Cambridge, Massachusetts

Previous transcriptional profiling analysis of 14 primary ovarian tumors identified approximately 12,000 genes as decreased in expression by at least twofold in one or more of the tumors sampled. Among those genes were several known to be mapped to common fragile sites (CFSs), some of which had previously been shown to exhibit a loss of expression in ovarian carcinoma. Therefore, we selected a subset of genes to determine whether they localized within CFSs. Of the 262 genes that were downregulated at least twofold in 13 of 14 tumors, 10 genes were selected based on the following criteria: localization to a CFS band; documented aberrations in at least one malignancy; and feasibility of scoring breakage at the specific CFS. Fluorescence in situ hybridization analysis was performed using bacterial artificial chromosome clones encompassing portions of the genes to determine the position of the genes relative to their corresponding CFSs. Nine genes were determined to localize within seven previously uncloned CFSs. Semiquantitative reverse-transcription/polymerase chain reaction analysis of the cell lines and primary ovarian tumors validated the downregulation of seven of the 10 genes. We identified portions of seven uncloned CFSs and provide data to suggest that several of the genes mapping within CFSs may be inactivated in ovarian cancer.

INTRODUCTION

Present in virtually all individuals, the common fragile sites (CFSs) are chromosomal loci at which gaps/breaks and rearrangements are visualized when cells are challenged under appropriate tissue culture conditions. Hypotheses have suggested that CFSs are causally related to cancer. Initially, the evidence supporting a relationship between CFSs and cancer was the observation that many CFSs localized within cytogenetic bands were frequently altered or rearranged during cancer development (Yunis, 1983; Hecht and Glover, 1984; Hecht and Sutherland, 1984; Yunis and Soreng, 1984). Since that initial observation, regions of chromosomal fragility have also been shown to be associated with gene amplification as well as sites of preferential viral integration (Wilke et al., 1996; Coquelle et al., 1997; Mishmar et al., 1998; Thorland et al., 2000). However, these data did not conclusively demonstrate a link between CFSs and cancer development. Therefore, in an attempt to determine the role that the CFSs play in cancer development, a substantial effort has been made to clone and characterize the CFSs, to characterize the genes that localize within these fragile regions, and to determine the role that these genes may play in tumorigenesis and cancer progression.

To date, five of the 87 currently recognized CFSs have been cloned and characterized [FRA3B (3p14.2), FRA7G (7q31.2), FRA7H (7q32.3), FRA16D (16q23.2), and FRAXB (Xp22.3)] (Wilke et al., 1996; Huang et al., 1998; Mishmar et al., 1998; Krummel et al., 2000; Mangelsdorf et al., 2000; Paige et al., 2000; Arlt et al., 2002). Many of these CFSs have been associated with a cancer-specific chromosomal rearrangement, a region of high loss of heterozygosity (LOH) in one or more tumor types, and/or a site of viral integration (Wilke et al., 1996; Huang et al., 1998; Mishmar et al., 1998; Smith et al., 1998; Krummel et al., 2000;

Supported by: National Cancer Institute; Grant number: CA48031; Department of Defense; Grant number: DAMD-99-1-9504; Mayo Clinic Cancer Center Ovarian Cancer Working Group.

*Correspondence to: Dr. David I. Smith, Director of the Cancer Genetics Program, Mayo Clinic Cancer Center, Division of Experimental Pathology, Mayo Foundation, 200 First Street SW, Rochester, MN 55905.

Received 16 November 2001; Accepted 28 January 2002
DOI 10.1002/gcc.10084
Published online 21 March 2002 in
Wiley InterScience (www.interscience.wiley.com).

Mangelsdorf et al., 2000; Paige et al., 2001). In addition, chromosomal deletions involving all five of these fragile sites have been observed in several different cancer types (Inoue et al., 1997; Huang et al., 1998; Smith et al., 1998; Mimori et al., 1999; Mangelsdorf et al., 2000; Paige et al., 2001; Arlt et al., 2002). These observations initiated the search for genes located within these breakage regions that were potential targets for alterations. A total of eight genes, the fragile histidine triad gene (*FHIT*, FRA3B), caveolin-1 and -2 (*CAV1* and *CAV2*, FRA7G), *TESTIN* (FRA7G), the WW domain containing the oxidoreductase gene (*WWOX*, FRA16D), and *GSI*, *TLR5A*, and the steroid sulfatase genes (*STS*, FRAXB), have been identified within these fragile regions (Ohta et al., 1996; Engelman et al., 1998; Bednarek et al., 2001; Tatarelli et al., 2000; Arlt et al., 2002). Several of these genes have been shown to have a loss of expression (LOE) in a variety of different tumor types including lung, breast, and ovarian cancer (Lee et al., 1998; Smith et al., 1998; Tatarelli et al., 2000). Two of these genes, *FHIT* and *WWOX*, have been shown to act functionally as tumor suppressors (Ohta et al., 1996; Siprashvili et al., 1997; Bednarek et al., 2001).

Transcriptional profiling is a powerful technique for the identification of a large number of genes that are aberrantly regulated during cancer development. Utilizing transcriptional profiling technology, 14 primary ovarian tumors (seven early and seven late stage) were analyzed previously to identify genes that were downregulated in ovarian cancer (Shridhar et al., 2001). Analysis of the 14 tumors identified approximately 12,000 genes, including several known CFS genes, as downregulated by $\geq$ twofold in at least one of the 14 tumors sampled. Prior analyses of *FHIT*, *WWOX*, and *CAV1* had also indicated the downregulation of these genes during ovarian cancer development (Mandai et al., 1998; Manning et al., 1999; Bagnoli et al., 2000; Ozaki et al., 2001; Paige et al., 2001). Therefore, we selected a subset of 10 genes to determine whether genes located within CFSs were inactivated in ovarian cancer. Using selective criteria, which limited analysis to genes found in CFSs that had been implicated previously as playing a role in cancer, 10 genes were selected from the 262 genes downregulated in at least 13 of the 14 tumors analyzed (Shridhar et al., 2001). Fluorescence in situ hybridization (FISH) analysis of bacterial artificial chromosome (BAC) clones identified as spanning portions of these 10 genes indicated that nine of the 10 were contained within CFSs. As a result, portions of seven previously uncloned CFSs were identified and the genes within them localized relative to their specific CFS. LOE analysis of the nine CFS genes confirmed that six were downregulated in primary ovarian tumors. Therefore, not only have portions of seven uncloned CFSs been identified, but also our data suggest that many of the genes within CFSs may be inactivated during ovarian tumorigenesis and/or cancer development.

MATERIALS AND METHODS

Transcriptional Profiling

For a detailed description of the tumor processing and selection, the RNA isolation and labeling, the cDNA microarray, and the image analysis and data recovery, see Shridhar et al. (2001).

Clone Selection

For each of the 10 genes, gene-specific primers were designed using Oligo 6.4 software (Molecular Biology Insights, Cascade, CO) and utilized for polymerase chain reaction (PCR) screening of the CITB Human BAC DNA Library (Release IV; Research Genetics, Huntsville, AL) (Table 1). Clones were then obtained from Research Genetics and grown according to the manufacturer's specifications. The protocol for the isolation of the BAC clones is available upon request.

Localization of Clones

Metaphase chromosomes were obtained from blood cultures established from 1 ml of whole blood and 9 ml of Chang Media PB (Irvine Scientific, Santa Ana, CA). Cultures were incubated at 37°C in 5% CO_2 for 72 hr and inoculated with 0.2 ml of a 0.2 μM (0.4 μM final concentration) aphidicolin (APC) solution approximately 24 hr before harvest. For those CFSs that were low expressing, 500 μl of 50 mM (2.5 mM final concentration) caffeine was added to the culture medium 4 hr prior to harvest, to increase the observed breakage at those particular loci. Cell harvest and metaphase preparations were performed using routine cytogenetic techniques.

For each BAC clone, 1 μg of purified DNA was labeled with biotin-16-dUTP (Boehringer/Roche, Indianapolis, IN) by nick translation, precipitated, and hybridized to the APC-treated metaphase cells according to the protocol of Verma and Babu (1995). Probe detection was accomplished using minor modifications of the manufacturer's protocol (Ventana Medical Systems, Tucson, AZ), and the chromosomes were subsequently counterstained

TABLE 1. Downregulated Genes Selected for Further Analysis Using FISH and/or Semiquantitative RT-PCR*

Gene	Image clone	Accession no.	Band	CFS	BAC primers	Clone	RT primers
NOEY2	345680	W72033	1p31	FRA1C	5′-AGGACCGCCTTCCAATTTTT-3′ 5′-TTTCTTTTTCCCAGGCCAGA-3′	15D15	5′-GCTTTGGCTCCAAGGAAC-3′ 5′-GGGCTCACATGATTATGCAC-3′
RGS4	429349	AA007419	1q21	FRA1F	5′-CCCGATGTTTGGAATGAAAT-3′ 5′-AATGGCTCTGGGCTATATGC-3′	112M12	5′-TGAGGAGTGCAAAAGATATG-3′ 5′-GAGAATTAGGCACACTGAGG-3′
FHIT	—	XM043137	3p14.2	FRA3B	—	—	5′-GGCCAACATCTCATCAAG-3′ 5′-TTTCCTCCTCTGATCTCC-3′
PDGFRA	52096	H23235	4q12	FRA4B	5′-ATGCTAAATGTGTAATAATGTA-3′ 5′-TTACTTTGTTCTCTATGCTC-3′	574J21	5′-CAAATGAAAATGAAAAGGTTG-3′ 5′-TAATCTCCACTGTCTTTCACC-3′
FST	434768	AA701860	5p14; 5q11	FRA5E; Hecht et al., 1988	5′-TTTCAAGGTTGGGAGAGG-3′ 5′-GCTTTACTTCCAGTAGCACACC-3′	326J12	5′-TACAGGACCGAACTGAGC-3′ 5′-GCTTTGATACACTTTCCC-3′
IGF2R	67055	T70421	6q26	FRA6E	5′-GTCGGGCCAGAACAAG-3′ 5′-AGGGCAACGATCACCATTCA-3′	421P10	5′-ATTGTCCAGTGCGGGCCATC-3′ 5′-CCCAGGGTTTTCCCACACAG-3′
PLG	875979	T73187	6q26	FRA6E	—[a]	81D8	5′-AAGGAGAGCCTCTGGATGAC-3′ 5′-AGGTCTGTGGGGAGAAGTGG-3′
SLC22A3	127120	R08121	6q26	FRA6E	—[a]	81D8	5′-CAGAGACAGTGGATGATG-3′ 5′-GCTTCTTTGTTAAACTGG-3′
CAV1	—	XM057981	7q31.2	FRA7G	—	—	5′-ATGTGATTGCAGAACCAG-3′ 5′-CAACTTGGAACTTGAAATTG-3′
CAV2	—	NM001233	7q31.2	FRA7G	—	—	5′-TTGTTTGTCTGTTTTTACTCTG-3′ 5′-ATGAAGTTTACCTTGTGGG-3′
TESTIN	—	?	7q31.2	FRA7G	—	—	5′-TTTCACCATGTTAGCCAG-3′ 5′-ATTTGATATATCCATGGACAG-3′
PSAP	291255	N72215	10q21-22	FRA10C; FRA10D	5′-ATCTGCCTGAATGTAACCTG-3′ 5′-AACTTCATGTCCTGCTGG-3′	31K4	5′-TATGCTGAAGGACAATGC-3′ 5′-ATCAGACTTTGCTGGGAC-3′
TSG101	123087	R02529	11p15	FRA11C; FRA11D; FRA11E	5′-TCTCTGATACCAGCTGGAG-3′ 5′-AGTCCCAACATTCAGCAC-3′	296P21	5′-TCTCTGATACCAGCTGGAG-3′ 5′-AGTCCCAACATTCAGCAC-3′
TPM1	341328	W58092	15q22.1	FRA15A	5′-AACACAGTGTGCTTAGTCAG-3′ 5′-TGGACAGAGTTCTACATTGTAC-3′	368M11	5′-AAGATGAGCTGGTGTCAC-3′ 5′-GTCATATCGTTGAGAGCG-3′
WWOX	—	NM016373	16q23.2	FRA16D	—	—	5′-GGGGAGACAAATCTCAGAAC-3′ 5′-TACAATGTGAAAGCAAGAGAA-3′

*The possible band location(s) as identified by UniGene (band), potential CFS, gene-specific BAC clone (clone), and the gene-specific primers for BAC slection and RT analysis are provided for each of the genes analyzed.

[a]BAC primers not designed as BACs were identified by the Sanger Centre.

TABLE 2. FISH Localization of Downregulated Genes Relative to their Respective Common Fragile Site

Gene	Band	FS	Breakage[a]			LOE cell lines (tumors)	Position relative to FS
			Centromeric	Crossing	Telomeric		
NOEY2	1p31	FRA1C	12	0	13	100% (100%)	Within
RGS4	1q21	FRA1F	20	0	0	85.7% (100%)	Off; centromeric
PDGFRA	4q12	FRA4B	0	1	19	100% (100%)	Telomeric end
FST	5q11	Hecht et al., 1988	19	0	1	57.1% (0%)	Centromeric end
IGF2R	6q26	FRA6E	18	0	2	57.1% (100%)	Centromeric end
PLG	6q26	FRA6E	16	0	6	0% (0%)	Within
SLC22A3	6q26	FRA6E	—[b]	—[b]	—[b]	85.7% (100%)	Within
PSAP	10q22	FRA10D	13	0	8	37% (35.7%)	Within
TSG101	11p15.1	FRA11C	13	2	5	42.9% (100%)	Within
TPM1	15q22.1	FRA15A	11	2	7	85.7% (100%)	Within

[a]The number and position (centromeric/crossing/telomeric) of observed hybridization signals relative to each particular common fragile site.
[b]*PLG* and *SLC22A3* localize to the same BAC; therefore, the counts for *SLC22A3* are identical to that of *PLG* (Table 1).

with 4′-6-diamidino-2-phenylindole (DAPI; Vector Laboratories, Burlingame, CA). A Zeiss Axioplan 2 fluorescence microscope (Zeiss, Thornwod, NY) and the IPLab Spectrum P software (Scanalytics Inc., Fairfax, VA) were used for photomicroscopy. The cytogenetic location of each individual clone was established by DAPI banding (Table 2). The position of the clone relative to the fragile site was determined from the analysis of a minimum of 20 APC-treated metaphase cells with breakage at that particular fragile site. A BAC was considered to be crossing the fragile site if the hybridization signal was observed on both sides of the breakage, or was observed proximal to the fragile site (centromeric) in one metaphase cell and distal (telomeric) to the fragile site in a different metaphase cell.

Semiquantitative Reverse Transcription/Polymerase Chain Reaction (RT-PCR)

Normal ovarian surface epithelial (OSE) cells were collected following oophorectomy for reasons unrelated to gynecological malignancy, and were used as either uncultured brushings or grown as short-term cultures as described by Kruk et al. (1990). Only OSE cultures between passages two and five with epithelial morphology and uniform cytokeratin staining were utilized. Total RNA was extracted from normal ovarian epithelial brushings, short-term cultured normal OSE, seven ovarian tumor-derived cell lines [Mayo cell lines: OV167, OV177, OV202, OV207, OV266 (Conover et al., 1998), SKOV3, and OVCAR5], and 14 primary ovarian tumors (stages 1–4) using Trizol reagent (GibcoBRL, Rockville, MD) according to the manufacturer's specifications. Approximately 5 μg of total RNA from each sample was treated with RNase-free DNase for 30 min at 37°C, and the DNase was inactivated by incubation of the reaction for 10 min at 90°C. The DNase-treated RNA was reverse-transcribed according to the manufacturer's protocol (GibcoBRL).

Unique primers (Table 2) were designed for all 10 genes by use of the Oligo 6.4 software (Molecular Biology Insights) and used in a multiplex reaction with *GAPDH* (5′-ACCACAGTCCATGCCATCAC-3′, 5′-TCCACCACCCTGTTGCTTGTA-3′; 450-bp product), β-tubulin (5′-GCATCAACGTGTACTACAA-3′, 5′-TACGAGCTGGTGGACTGAGA-3′; 454-bp product), or β2-microglobulin primers (5′-AGCTGTGCTCGCGCTACTCTCTC-3′, 5′-GTGTCGGATTGATGAAACCCAGACAC-3′; 140-bp product) as an internal control. The PCR reaction consisted of reverse-transcribed cDNA, 50 mM KCl, 10 mM Tris–HCl (pH 8.3), 1.5 mM $MgCl_2$, 400 μM concentration of forward and reverse primers for the specific genes, 50 μM concentration of the control primer, and 0.1 U *Taq* polymerase (Promega, Madison, WI). Amplification conditions were 95°C for 3 min, 28 cycles of 95°C for 30 sec, 55–67°C for 30 sec, and 72°C for 30 sec, and a final extension at 72°C for 10 min.

RESULTS

Based on the data provided by Shridhar et al. (2001), 10 genes were selected from a total of 262 genes that were downregulated by at least twofold in at least 13 of the 14 primary ovarian tumors analyzed. Genes were selected if the cytogenetic location, determined by the UniGene database, was within a band known to contain a CFS. Additional criteria included the localization of the gene to a known region of LOH in one or more tumor types or a documented loss of gene expression in at

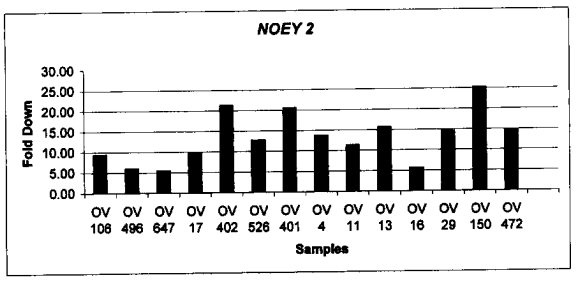

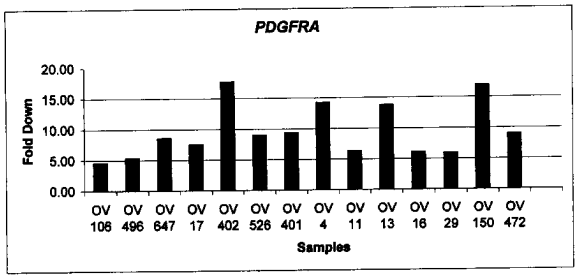

Figure 1. Representative examples of expression profiles obtained from transcriptional profiling of 14 primary ovarian tumors. The decreased expression levels of the tumor compared to levels of normal ovarian surface epithelial brushings (fold down) are provided for each of the tumors sampled.

least one type of cancer. Finally, genes were selected based on the ease of scoring breakage at the CFS of interest. Ease of scoring was evaluated by whether the possible CFS had a relatively high frequency of breakage and could be easily discerned from neighboring CFSs. Using these criteria, we selected 10 genes for FISH and semiquantitative RT-PCR analysis: *RAS* homolog gene family, member 1 (*NOEY2*); regulator of G-protein signaling 4 (*RGS4*); platelet-derived growth factor receptor, alpha polypeptide (*PDGFRA*); follistatin (*FST*); mannose 6 phosphate/insulin-like growth factor receptor II (*IGF2R*); plasminogen (*PLG*); solute carrier family 22, member 3 (*SLC22A3*); prosaposin (*PSAP*); tumor susceptibility gene 101 (*TSG101*); and tropomyosin 1, alpha (*TPM1*) (Table 1).

Figure 1 shows the expression levels of two of the 10 genes, *NOEY2* and *PDGFRA*, analyzed in the ovarian tumors, compared to normal OSE. Table 1 lists the Image clone and GenBank accession numbers, cytogenetic localization, and the CFS(s) located within that region for each of the 10 genes.

FISH analysis of the 10 genes required the identification of BAC clones that contained a portion of the gene to be analyzed. For eight of the 10 genes (*NOEY2, RGS4, PDGFRA, FST, IGF2R, PSAP, TPM1*, and *TSG101*), a gene-specific BAC clone was identified by screening of the CITB Human BAC DNA Library (Release IV; Research Genetics) with gene-specific primers (Table 1). By use of the Sanger Centre database (www.sanger.ac.uk.; Cambridge, UK), a single BAC clone was identified as encompassing portions of both the *SLC22A3* and *PLG* genes (Table 1). Confirmation for the presence of portions of *SLC22A3* and *PLG* in BAC 81D8 was established by PCR (data not shown). Therefore, a total of nine BACs were identified and hybridized to APC-induced metaphase chromosomes to determine the position of the genes relative to their respective CFSs (Table 1, Fig. 2).

For any CFS for which there were CFSs located in neighboring bands, inverse-DAPI banding was used to ensure that the breakage was occurring in the CFS of interest. FISH analysis of the nine BACs determined that nine of the 10 genes were localized within CFS regions (Table 2). A gene was determined to localize within a CFS region if the BAC, containing portions of that gene, hybridized proximal to the site of APC-induced decondensation/breakage in some metaphase cells and distal in others. *RGS4* was the only gene that did not localize to a CFS; *RGS4* maps centromeric to FRA1F (1q21). BACs containing a portion of each of the remaining nine genes mapped to the following CFSs: FRA1C (*NOEY2*), FRA4B (*PDGFRA*), 5q11 [a CFS described by Hecht et al. (1988) that was never given an FRA designation; *FST*], FRA6E (*IGF2R, PLG*, and *SLC22A3*), FRA10D (*PSAP*), FRA11C (*TSG101*), and FRA15A (*TPM1*) (Table 2). Table 2 lists the observed counts (centromeric/crossing/telomeric) for each gene/BAC. Based on the proportion of hybridization signals observed as centromeric, crossing, or telomeric to the region of breakage, the position of the gene relative to its respective fragile site could be determined (Table 2). Three of the genes (*FST, IGF2R*, and *PDGFRA*) localized to the ends of their respective CFSs, centromeric for *FST* and *IGF2R* and telomeric for *PDGFRA*, with counts of 19/0/1, 18/0/2, and 0/1/19, respectively. The six remaining CFS genes localized within the centers of their respective fragile sites as they hybridized with approximately equal frequency proximal and distal to the region of decondensation/breakage within each of the respective sites (Table 2).

To confirm whether the 10 genes were downregulated in ovarian cancer, we analyzed all of the genes by semiquantitative RT-PCR on cDNAs generated from tumor-derived cell lines and primary tumors and tested for decreased expression

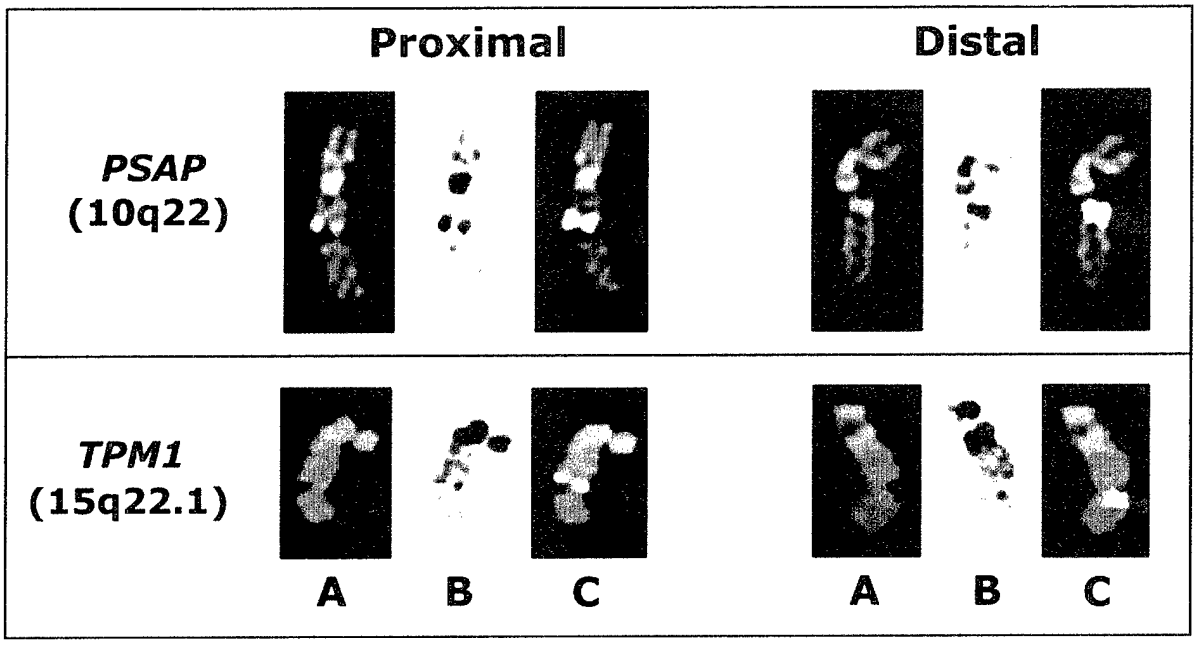

Figure 2. Depiction of FISH clones obtained for *PSAP* and *TPM1* and determined to be crossing FRA10D and FRA15A, respectively. For each APC-induced break analyzed, the presence of breakage at 10q22 (FRA10D) and 15q22.1 (FRA15A) was initially scored from a DAPI-counterstained image (**A**). Breakage was confirmed as mapping to the region of interest by inverted DAPI bands (**B**). Both centromeric and telomeric hybridization signals for the FITC-labeled BAC clone are provided (**C**).

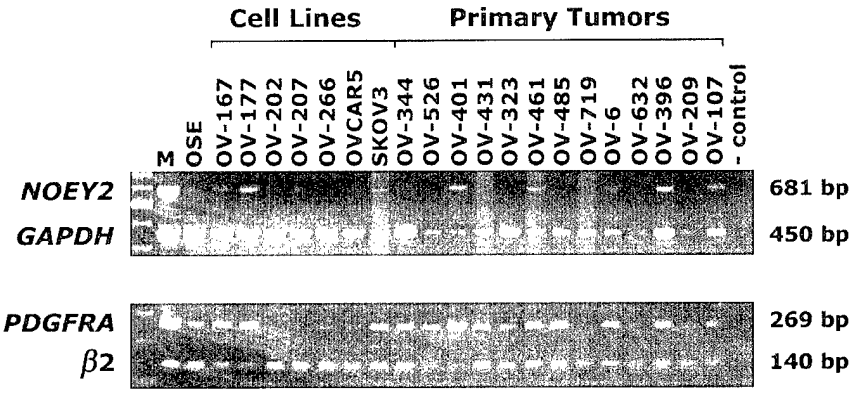

Figure 3. Semiquantitative RT-PCR analysis for two of the 10 genes (*NOEY2* and *PDGFRA*) selected for analysis in this study. The expression levels for both genes were analyzed in short-term cultured normal ovarian surface epithelium (OSE), seven tumor-derived ovarian cell lines (OV166, OV177, OV202, OV207, OV266, OVCAR5, and SKOV3), and 13 primary ovarian tumors. *GAPDH* and β2 primers were used as internal controls. A negative H_2O control (−) and a marker ladder (M) are also provided.

levels. Initially, all 10 genes were tested on cDNA obtained from normal OSE brushings, to ensure that each gene was expressed in normal OSE. Analysis of the 10 genes confirmed the expression of each in normal OSE (data not shown). Expression levels for all the genes were then analyzed in 14 primary ovarian tumors (stages 1–4) and seven tumor-derived cell lines and compared to the expression level in the short-term culture of OSE (Fig. 3, Table 2). Unique primers for each of the 10 genes were initially used in a multiplex reaction with an internal control primer. To ensure that there was no preferential amplification of the control primer in the multiplex reaction, unique primers for several of the 10 genes were analyzed on the same primary tumor panel and yielded similar results (data not shown). Representative examples of the PCR analysis and the observed expression patterns are provided in Figure 3 and Table 3, respectively.

Expression analysis of the tumor-derived cell line and primary tumor panels determined that eight of the 10 genes showed LOE (i.e., decreased or complete absence of expression) in at least one or more of the samples. However, *IGF2R* and *PLG* did not exhibit LOE in any of the cell lines or primary tumors analyzed. Of the eight genes with LOE, five (*NOEY2*, *RGS4*, *PDGFRA*, *SLC22A3*, and *TSG101*) showed decreased expression, and in some cases complete absence of expression, in the

TABLE 3. Loss of Expression Analysis in Tumor-Derived Cell Lines and Primary Tumors

Cell lines/tumors	*NOEY2*	*RGS4*	*PDGFRA*	*FST*	*IGF2R*	*PLG*	*SLC22A3*	*PSAP*	*TPM1*	*TSG101*
OSE	●[a]	●	●	●	●	●	●	●	●	●
OV167	◍[b]	○[c]	◍	●	●	●	◍	◍	●	●
OV177	◍	○	◍	●	●	●	◍	●	●	◍
OV202	◍	○	●	○	●	●	◍	◍	●	◍
OV207	◍	◍	◍	○	●	●	◍	●	●	◍
OV266	◍	◍	◍	○	●	●	◍	●	○	◍
OVCAR5	○	●	◍	○	●	●	●	◍	○	◍
SKOV3	○	○	◍	●	●	●	◍	●	○	◍
% downregulated	100.0	85.7	85.7	57.1	0.0	0.0	85.7	42.9	42.9	85.7
344	◍	◍	◍	●	●	●	◍	●	○	◍
526	○	◍	◍	●	●	●	◍	●	○	○
401	○	◍	◍	●	●	●	◍	●	○	◍
431	◍	◍	●	●	●	●	◍	●	○	◍
323	○	◍	◍	●	●	●	N/A	●	○	◍
461	○	◍	◍	●	●	●	○	●	○	○
485	◍	◍	◍	●	●	●	○	N/A	◍	◍
426	○	◍	◍	●	●	●	◍	●	○	○
719	○	○	◍	●	●	●	○	◍	○	◍
6	◍	◍	◍	●	●	●	○	◍	○	◍
632	○	◍	◍	●	●	●	○	N/A	○	◍
396	◍	◍	◍	●	●	●	◍	◍	○	◍
209	○	◍	◍	●	●	●	◍	●	○	◍
107	◍	◍	◍	●	●	●	○	◍	○	◍
% downregulated	100.0	100.0	92.9	0.0	0.0	0.0	100.0	33.3	100.0	100.0

[a]Normal expression.
[b]Reduced expression.
[c]Complete absence of expression.

majority (≥85.7%) of the cell lines and primary tumors analyzed (Fig. 3).

RT-PCR analysis of the cell lines determined that the remaining three genes showed LOE in at least one of the cell lines. The numbers of cell lines exhibiting LOE were three (42.9%) for *PSAP* and *TPM1* and four (57.1%) for *FST* (Fig. 3, Table 3). Semiquantitative RT-PCR analysis of the primary ovarian tumors determined that only *PSAP* and *TPM1* showed LOE in one or more of the tumors sampled; *FST* did not exhibit any LOE in any of the 14 tumors. The number of tumors that had LOE were three (33.3%) for *PSAP* and 14 (100%) for *TPM1* (Table 3).

To determine whether the five previously identified CFS genes (*FHIT, CAV1, CAV2, TESTIN,* and *WWOX*) also showed LOE in our panel of cell lines and primary tumors, we designed unique primers for each gene and used them in semiquantitative RT-PCR analysis. *FHIT, CAV1, CAV2,* and *WWOX* each showed LOE in at least one of the cell lines tested, whereas *TESTIN* showed normal expression levels compared to that of short-term culture OSE (Fig. 4). When analyzed on the primary tumor panel, all five genes exhibited downregulation (Fig. 4). The percentage of tumors exhibiting LOE ranged from 21.4% (*TESTIN*) to 78.6% (*FHIT*) (Fig. 4).

DISCUSSION

There are considerable data suggestive of a causal relationship between CFSs and cancer; however, the evidence is limited to data obtained from only five CFSs (FRA3B, FRA7G, FRA7H, FRA16D, and FRAXB). The cloning and characterization of these five CFSs and the genes localizing within them, however, have generated significant interest in the potential role of CFSs in tumorigenesis and/or cancer progression. One such observation is that several of the genes localizing within the cloned CFSs (*FHIT, CAV1, TESTIN,* and *WWOX*) exhibit LOE in a variety of different tumor types (Lee et al., 1998; Smith et al., 1998; Tatarelli et al., 2000; Paige et al., 2001). Based on this observation, we selected 10 genes, determined by transcription profiling to be downregulated in primary ovarian tumors and localizing to chromosomal bands containing a CFS, to determine whether genes located within CFSs were inactivated during the development of ovarian cancer.

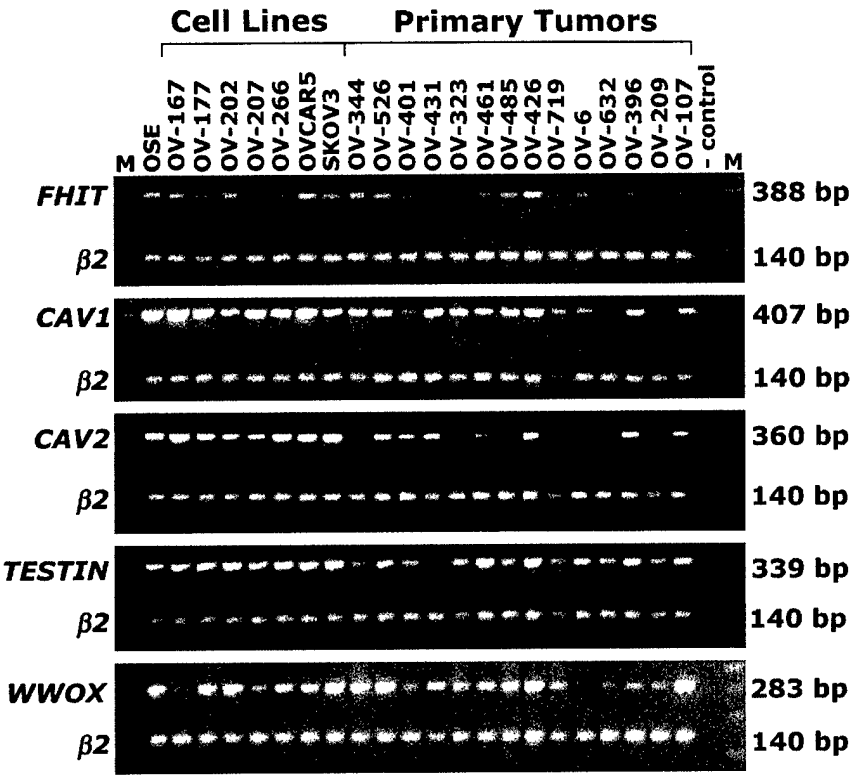

Figure 4. Semiquantitative RT-PCR analysis for the five known CFS genes (*FHIT, CAV1, CAV2, TESTIN,* and *WWOX*). The expression levels for these genes were analyzed in short-term culture normal ovarian surface epithelium (OSE), seven tumor-derived ovarian cell lines (OV166, OV177, OV202, OV207, OV266, OVCAR5, and SKOV3), and 14 primary ovarian tumors. β2 microglobulin primers were used as an internal control for each primer set. A negative H_2O control (−) and a marker ladder (M) are also provided.

FISH analysis of the 10 genes established that nine (90%) localized within seven different CFSs (Table 2); three of the genes (*IGF2R, SLC22A3,* and *PLG*) were all derived from the same chromosomal band (6q26) and were determined to map within the CFS FRA6E. As a result, BACs have been identified that cross a portion of the previously uncloned CFSs mapping to 1p31 (FRA1C), 4q12 (FRA4B), 5q11 (Hecht et al., 1988), 6q26 (FRA6E), 10q22 (FRA10D), 11p15.1 (FRA11C), and 15q22 (FRA15A). Only *RGS4* mapped outside a CFS region. The complete cloning and characterization of these CFSs, however, will require the definition of both the centromeric and telomeric ends for each of these CFSs; this work is ongoing in our laboratory.

Transcriptional profiling, though considered to be a powerful technique for identifying aberrantly regulated genes, can result in the identification of numerous false positives (Mills et al., 2001). To validate the expression profiles provided by the microarray analysis, we confirmed the expression levels for all 10 genes by semiquantitative RT-PCR analysis of a panel of seven ovarian cancer cell lines and 14 primary tumors. RT-PCR analysis of the cell line/tumor panels indicated that seven of the 10 genes (70%) were downregulated in one or more of the cell lines and primary tumors analyzed (Fig. 3, Table 3). There was no direct correlation between genes that were downregulated and those that were localized within CFSs. Three of the genes that mapped within a CFS (*FST, IGF2R,* and *PLG*) did not show LOE, and *RGS4,* the gene located outside FRA1F, did exhibit LOE in both the cell line and primary tumor panels (Table 3). Six of the nine (66.7%) CFS genes, however, exhibited LOE in the primary tumors analyzed, therefore suggesting that several CFS genes are inactivated in ovarian cancer.

LOE analysis of the five known CFS genes (*FHIT, CAV1, CAV2, WWOX,* and *TESTIN*) has indicated that *FHIT, CAV1,* and *WWOX* are downregulated in ovarian tumors (Mandai et al., 1998; Manning et al., 1999; Bagnoli et al., 2000; Paige et al., 2001). Expression analysis on primary ovarian tumors was not previously performed for either *CAV2* or *TESTIN.* We therefore analyzed the expression levels for *FHIT, CAV1, CAV2, WWOX,* and *TESTIN* on the ovarian cell line and primary tumor panels (Fig. 4). All five genes were identified as being downregulated in at least one of the primary ovarian tumors analyzed. The percentage of tumors exhibiting LOE ranged from 21.4% (*TESTIN*) to 78.6% (*FHIT*). Therefore, the majority of the 15

CFS genes (13/15) are downregulated in primary ovarian tumors, indicating that CFS genes may play a role in the development and/or progression of ovarian cancer. Additionally, these data provide further evidence supporting the hypothesis that CFSs and the genes contained within them are causally related to cancer.

The data provided in this study also suggest that genes mapping within the same CFS may exhibit different expression patterns depending on the tumor type. Previous expression analyses of *CAV1* and *CAV2* in lung carcinoma identified an inverse correlation in expression patterns (Racine et al., 1999). *CAV1* was determined to be downregulated in all of the lung cancer cell lines analyzed, but *CAV2* had expression levels similar to those of normal bronchial epithelial cells (Racine et al., 1999); *TESTIN* expression levels have not been examined in lung carcinoma. In this study, all three genes (*CAV1*, *CAV2*, and *TESTIN*) exhibited LOE in the primary ovarian tumors, 28.6, 57.1, and 21.4%, respectively (Fig. 4). These data indicate that the expression levels for CFS genes may be dependent on the tumor type. This is further supported by the observation that the three FRA6E genes *IGF2R*, *SLC22A3*, and *PLG* also exhibited alternative expression patterns. Although *SLC22A3* was validated as exhibiting LOE in ovarian tumors, the expression levels for *IGF2R* and *PLG* were normal compared to that of normal OSE. The expression levels for *IGF2R*, *PLG*, and *SLC22A3* have not been compared in any other tumor types. Nevertheless, if the instability within the CFSs were solely responsible for gene inactivation, LOE would be expected for all the genes within the region. Therefore, these data would suggest that, although the genes are located within the same CFS region, there might be a selection pressure for the loss of specific genes, but not of others.

Additionally, the data provided in this study indicate that a number of currently recognized tumor-suppressor genes not only map within CFS regions but also may play a role in the development and/or progression of ovarian cancer. Three of the nine genes identified in this study as localizing within CFSs (*NOEY2*, *IGF2R*, and *TSG101*) have already been determined to be putative tumor-suppressor genes (De Souza et al., 1995; Li et al., 1997; Sun et al., 1997; Oates et al., 1998; Yu et al., 1999; Kong et al., 2000; Luo et al., 2001). LOE has been documented for *NOEY2* in breast and ovarian carcinomas (Yu et al., 1999) and *IGF2R* in breast, hepatocellular, and lung carcinomas (De Souza et al., 1995; Oates et al., 1998; Kong et al., 2000). In the case of *TSG101*, aberrant transcripts have been identified in both breast and prostate cancer (Li et al., 1997; Sun et al., 1997). The identification of these genes as downregulated in primary ovarian tumors by transcriptional profiling suggests that some of these genes may be functioning as tumor suppressors, as has already been demonstrated for *FHIT* (Ohta et al., 1996; Siprashvili et al., 1997). Localization of *NOEY2*, *IGF2R*, and *TSG101* to CFSs, in addition to the previously localized candidate tumor-suppressor genes *FHIT*, *CAV1*, *WWOX*, and *TESTIN* (Ohta et al., 1996; Siprashvili et al., 1997; Tatarelli et al., 2000; Liu et al., 2001; Paige et al., 2001), also suggests that CFSs may preferentially harbor tumor-suppressor genes.

ACKNOWLEDGMENTS

We thank Gwen Callahan for providing the tissue samples. This work was supported, in part, by National Cancer Institute Grant CA48031 and Department of Defense Grant DAMD-99-1-9504 (both to D.I.S.).

REFERENCES

Arlt MF, Miller DE, Beer DG, Glover TW. 2002. Molecular characterization of FRAXB and comparative common fragile site instability in cancer cells. Genes Chromosomes Cancer 33:82–92.

Bagnoli M, Tomassetti A, Figini M, Flati S, Dolo V, Canevari S, Miotti S. 2000. Downmodulation of caveolin-1 expression in human ovarian carcinoma is directly related to alpha-folate receptor overexpression. Oncogene 19:4754–4763.

Bednarek AK, Laflin KJ, Daniel RL, Liao Q, Hawkins KA, Aldaz CM. 2000. WWOX, a novel WW domain-containing protein mapping to human chromosome 16q23.3–24.1, a region frequently affected in breast cancer. Cancer Res 60:2140–2145.

Conover CA, Hartmann LC, Bradley S, Stalboerger P, Klee GG, Kalli KR, Jenkins RB. 1998. Biological characterization of human epithelial ovarian carcinoma cells in primary culture: the insulin-like growth factor system. Exp Cell Res 238:439–449.

Coquelle A, Pipiras E, Toledo F, Buttin G, Debatisse M. 1997. Expression of fragile sites triggers intrachromosomal mammalian gene amplification and sets boundaries to early amplicons. Cell 89:215–255.

De Souza AT, Hankins GR, Washington MK, Orton TC, Jirtle RL. 1995. M6P/IGF2R gene is mutated in human hepatocellular carcinomas with loss of heterozygosity. Nat Genet 11:447–479.

Engelman JA, Zhang XL, Lisanti MP. 1998. Genes encoding human caveolin-1 and -2 are co-localized to the D7S522 locus (7q31.1), a known fragile site (FRA7G) that is frequently deleted in human cancers. FEBS Letters 436:403–410.

Hecht F, Glover TW. 1984. Cancer chromosome breakpoints and common fragile sites induced by aphidicolin. Cancer Genet Cytogenet 13:185–188.

Hecht F, Sutherland GR. 1984. Fragile sites and cancer breakpoints. Cancer Genet Cytogenet 12:179–181.

Hecht F, Tajara EH, Lockwood D, Sandberg AA, Hecht BK. 1988. New common fragile sites. Cancer Genet Cytogenet 33:1–9.

Huang H, Qian C, Jenkins RB, Smith DI. 1998. FISH mapping of YAC clones at human chromosomal band 7q31.2: identification of YACs spanning FRA7G within the common region of LOH in breast and prostate cancer. Genes Chromosomes Cancer 21:152–159.

Inoue H, Ishii H, Alder H, Snyder E, Druck T, Huebner K, Croce CM. 1997. Sequence of the FRA3B common fragile region: implications for the mechanism of FHIT deletion. Proc Natl Acad Sci USA 94:14584–14589.

Kong FM, Anscher MS, Washington MK, Killian JK, Jirtle RL. 2000.

M6P/IGF2R is mutated in squamous cell carcinoma of the lung. Oncogene 19:1572–1578.
Kruk PA, Maines-Bandiera SL, Auersperg N. 1990. A simplified method to culture human ovarian surface epithelium. Lab Invest 63:132–136.
Krummel KA, Roberts LR, Kawakami M, Glover TW, Smith DI. 2000. The characterization of the common fragile site FRA16D and its involvement in multiple myeloma translocations. Genomics 69:37–46.
Lee SW, Reimer CL, Oh P, Campbell DB, Schnitzer JE. 1998. Tumor cell growth inhibition by caveolin re-expression in human breast cancer cells. Oncogene 16:1391–1397.
Li L, Li X, Francke U, Cohen SN. 1997. The TSG101 tumor susceptibility gene is located in chromosome 11 band p15 and is mutated in human breast cancer. Cell 88:143–154.
Liu J, Lee P, Galbiati F, Kitsis RN, Lisanti MP. 2001. Caveolin-1 expression sensitizes fibroblastic and epithelial cells to apoptotic stimulation. Am J Physiol Cell Physiol 280:C823–C835.
Luo RZ, Peng H, Xu F, Bao J, Pang Y, Pershad R, Issa JP, Liao WS, Bast RC Jr, Yu Y. 2001. Genomic structure and promoter characterization of an imprinted tumor suppressor gene ARHI. Biochim Biophys Acta 1519:216–222.
Mandai M, Konishi I, Kuroda H, Nanbu K, Matsushita K, Yura Y, Hamid AA, Mori T. 1998. Expression of abnormal transcripts of the FHIT (fragile histidine triad) gene in ovarian carcinoma. Eur J Cancer 34:745–749.
Mangelsdorf M, Ried K, Woollatt E, Dayan S, Eyre H, Finnis M, Hobson L, Nancarrow J, Venter D, Baker E, Richards RI. 2000. Chromosomal fragile site FRA16D and DNA instability in cancer. Cancer Res 60:1683–1689.
Manning AP, Mes-Masson AM, Seymour RJ, Tetrault M, Provencher DM, Tonin PN. 1999. Expression of FHIT in primary cultures of human epithelial ovarian tumors and malignant ovarian ascites. Mol Carcinog 24:218–225.
Mills JC, Roth KA, Cagan RL, Gordon JI. 2001. DNA microarrays and beyond: completing the journey from tissue to cell. Nat Cell Biol 3:E175–E178.
Mimori K, Druck T, Inoue H, Alder H, Berk L, Mori M, Huebner K, Croce CM. 1999. Cancer-specific chromosome alterations in the constitutive fragile region FRA3B. Proc Natl Acad Sci USA 96:7456–7461.
Mishmar D, Rahat A, Scherer SW, Nyakatura G, Hinzmann B, Kohwi Y, Mander-Gutfroind Y, Lee JR, Drescher B, Sas DE, Margalit H, Platzer M, Weiss A, Tsui LC, Rosenthal A, Kerem B. 1998. Molecular characterization of common fragile site (FRA7H) on human chromosome 7 by the cloning of a simian virus 40 integration site. Proc Natl Acad Sci USA 95:8141–8146.
Oates AJ, Schumaker LM, Jenkins SB, Pearce AA, DaCosta SA, Arun B, Ellis MJ. 1998. The mannose 6-phosphate/insulin-like growth factor 2 receptor (M6P/IGF2R), a putative breast tumor suppressor gene. Breast Cancer Res Treat 47:269–281.
Ohta M, Inoue H, Cotticelli MG, Kastury K, Baffa R, Palazzo J, Siprashvili Z, Mori M, McCue P, Druck T, Croce CM, Huebner K. 1996. The *FHIT* gene, spanning the chromosome 3p14.2 fragile site and renal carcinoma-associated t(3;8) breakpoint, is abnormal in digestive tract cancers. Cell 84:587–597.
Paige AJ, Taylor KJ, Stewart A, Sgouros JG, Gabra H, Sellar GC, Smyth JF, Porteous DJ, Watson JE. 2000. A 700-kb map of a region of 16q23.2 homozygously deleted in multiple cancers and spanning the common fragile site FRA16D. Cancer Res 60:1690–1697.
Paige AJW, Taylor KJ, Taylor C, Hillier SG, Farrington S, Scott D, Porteous DJ, Smyth JK, Gabra H, Watson JEV. 2001. WWOX: a candidate tumor suppressor gene involved in multiple tumor types. Proc Natl Acad Sci USA 98:11414–11422.
Racine C, Belanger M, Hirabayashi H, Boucher M, Chakir J, Couet J. 1999. Reduction of caveolin 1 gene expression in lung carcinoma cell lines. Biochem Biophys Res Commun 255:580–586.
Shridhar V, Lee J, Pandita A, Iturria S, Avula R, Staub J, Morrissey M, Calhoun E, Sen A, Kalli K, Keeney G, Roche P, Cliby W, Lu K, Schmandt R, Mills GB, Bast RC Jr, James CD, Couch FJ, Hartmann LC, Lillie J, Smith DI. 2001. Genetic analysis of early- versus late-stage ovarian tumors. Cancer Res 61:5895–5904.
Siprashvili Z, Sozzi G, Barnes LD, McCue P, Robinson AK, Eryomin V, Sard L, Tagliabue E, Greco A, Fusetti L, Schwartz G, Pierotti MA, Croce CM, Huebner K. 1997. Replacement of Fhit in cancer cells suppresses tumorigenicity. Proc Natl Acad Sci USA 94:13771–13776.
Smith DI, Huang H, Wang L. 1998. Common fragile sites and cancer [review]. Int J Oncol 12:187–196.
Sun Z, Pan J, Bubley G, Balk SP. 1997. Frequent abnormalitites of TSG101 transcripts in human prostate cancer. Oncogene 15:3121–3125.
Tatarelli C, Linnenbach A, Mimori K, Croce CM. 2000. Characterization of the human testin gene localized in the FRA7G region at 7q31.2. Genomics 68:1–12.
Thorland EC, Myers SL, Persing DH, Sarkar G, McGovern RM, Gostout BS, Smith DI. 2000. Human papillomavirus type 16 integrations in cervical tumors frequently occur in common fragile sites. Cancer Res 60:5916–5921.
Verma RS, Babu A. 1995. Human chromosomes: principles and techniques, Second Ed. New York: McGraw-Hill. 419 p.
Wilke CM, Hall BK, Hoge A, Paradee W, Smith DI, Glover TW. 1996. FRA3B extends over a broad region and contains a spontaneous HPV16 integration site: direct evidence for the coincidence of viral integration sites and fragile sites. Hum Mol Genet 5:187–195.
Yu Y, Xu F, Peng H, Fang X, Zhao S, Li Y, Cuevas B, Kuo WL, Gray JW, Siciliano M, Mills GB, Bast RC Jr. 1999. NOEY2 (ARHI), an imprinted putative tumor suppressor gene in ovarian and breast carcinomas. Proc Natl Acad Sci USA 96:214–219.
Yunis JJ. 1983. The chromosomal basis of neoplasia. Science 221: 227–236.
Yunis JJ, Soreng AL. 1984. Constitutive fragile sites and cancer. Science 226:1199–1204.

MS #10

Oncogene (2002) 21, 7266–7276

www.nature.com/onc

Cloning and characterization of the common fragile site *FRA6F* harboring a replicative senescence gene and frequently deleted in human tumors

Cristina Morelli[1], Efthimia Karayianni[1], Chiara Magnanini[1], Andrew J Mungall[2], Erik Thorland[3], Massimo Negrini[1], David I Smith[3] and Giuseppe Barbanti-Brodano*,[1]

[1]*Department of Experimental and Diagnostic Medicine, Section of Microbiology and Center for Biotechnology, University of Ferrara, I-44100 Ferrara, Italy;* [2]*The Sanger Centre, Wellcome Trust Genome Campus, Hinxton, Cambridgeshire, CB10 1SA, UK;* [3]*Division of Experimental Medicine, Department of Laboratory Medicine and Pathology, Mayo Clinic Foundation, Rochester, Minnesota MN 55905, USA*

The common fragile site *FRA6F*, located at 6q21, is an extended region of about 1200 kb, with two hot spots of breakage each spanning about 200 kb. Transcription mapping of the *FRA6F* region identified 19 known genes, 10 within the *FRA6F* interval and nine in a proximal or distal position. The nucleotide sequence of *FRA6F* is rich in repetitive elements (LINE1 and LINE2, Alu, MIR, MER and endogenous retroviral sequences) as well as in matrix attachment regions (MARs), and shows several DNA segments with increased helix flexibility. We found that tight clusters of stem-loop structures were localized exclusively in the two regions with greater frequency of breakage. Chromosomal instability at *FRA6F* probably depends on a complex interaction of different factors, involving regions of greater DNA flexibility and MARs. We propose an additional mechanism of fragility at *FRA6F*, based on stem-loop structures which may cause delay or arrest in DNA replication. A senescence gene likely maps within *FRA6F*, as suggested by detection of deletion and translocation breakpoints involving this fragile site in immortal human-mouse cell hybrids and in SV40-immortalized human fibroblasts containing a human chromosome 6 deleted at q21. Deletion breakpoints within *FRA6F* are common in several types of human leukemias and solid tumors, suggesting the presence of a tumor suppressor gene in the region. Moreover, a gene associated to hereditary schizophrenia maps within *FRA6F*. Therefore, *FRA6F* may represent a landmark for the identification and cloning of genes involved in senescence, leukemia, cancer and schizophrenia.
Oncogene (2002) **21**, 7266–7276. doi:10.1038/sj.onc.1205573

Keywords: *FRA6F*; fragile sites; chromosome 6q21; senescence; human tumors; schizophrenia

*Correspondence: G Barbanti-Brodano, Department of Experimental and Diagnostic Medicine, Section of Microbiology, University of Ferrara, Via Luigi Borsari 46, I-44100 Ferrara, Italy;
E-mail: brb@unife.it
Received 13 December 2001; revised 29 March 2002; accepted 15 April 2002

Introduction

Gaps, breaks and other chromosome aberrations are induced in cells cultured under specific conditions, generally in the presence of drugs inhibiting or delaying DNA replication. Regions that show a statistically significant increase in the frequency of such abnormalities, above that occurring by chance throughout the human genome, are defined as fragile sites (Sutherland *et al.*, 1998). In recent years, fragile sites have raised considerable interest, because they appear to participate in chromosomal rearrangements involved in cancer, leukemia, mental retardation and aging (Le Beau and Rowley, 1984; Yunis and Soreng, 1984; Smith *et al.*, 1998; Sutherland *et al.*, 1998).

Fragile sites are classified into two categories, rare and common or constitutive, depending on the frequency observed in the population and on the culture conditions inducing their expression (Smith *et al.*, 1998; Sutherland *et al.*, 1998). The 89 common fragile sites are expressed constitutively in all individuals, although the level of expression can vary from 1 to 70% of metaphases for different fragile sites. Variations in expression may also be observed in different individuals for the same fragile site. Most common fragile sites (84 out of 89) are induced by aphidicolin, a drug which inhibits DNA polymerases α and δ, but other common fragile sites are induced by 5-azacytidine or bromo-deoxyuridine (Glover *et al.*, 1984; Smith *et al.*, 1998; Sutherland *et al.*, 1998).

The structure and molecular features of common fragile sites are not well characterized. However, those which have been better defined or cloned, such as *FRA3B* at 3p14.2, *FRA7G* at 7q31.2, *FRA7H* at 7q32.3, *FRA16D* at 16q23.2 and *FRAXB* at Xp22.1, share some characteristics. Constitutive fragile sites are generally rich in repetitive sequences (LINE, Alu, MER). They may also contain small polydispersed circular DNA sequences, endogenous retroviral sequences and integration sites for plasmids or for DNA tumor viruses such as HPV16 and SV40 (Rassool *et al.*, 1996; Wilke *et al.*, 1996; Boldog *et al.*, 1997; Inoue *et al.*, 1997; Huang *et al.*, 1998b; Huebner *et al.*, 1998; Mishmar *et al.*, 1998; Mimori *et al.*, 1999). Studies carried out on fragile sites

FRA3B (Mimori *et al.*, 1999) and *FRA7H* (Mishmar *et al.*, 1998) have shown coincidental regions of greater DNA flexibility and lower DNA stability within the fragile sites compared to genomic regions not harboring sites of fragility. Areas of high flexibility and low stability colocalized with clusters of DNA sequences with non-B and triple-helix conformation (Mishmar *et al.*, 1998) which are known to inhibit DNA replication and enhance homologous recombination. Finally, all the common fragile sites are regions of late DNA replication, and this delay in replication is enhanced by aphidicolin (Le Beau *et al.*, 1998; Wang *et al.*, 1999; Hellman *et al.*, 2000). It has been suggested that late-replicated DNA regions would affect locally the chromatin structure, leading to the unstable and recombinogenic properties of fragile sites (Smith *et al.*, 1998; Sutherland *et al.*, 1998; Wang *et al.*, 1999). Indeed, since DNA replication must be completed before the initiation of mitosis, delayed replication may cause the incomplete packaging and collapse of the chromosome structure during metaphase, resulting in expression of fragile sites (Simonic and Gericke, 1996). In spite of this knowledge on the characteristics of common fragile sites, a molecular basis and a clear explanation for the mechanisms of their fragility are still lacking. Hence, the need to clone further fragile sites in order to clarify what DNA sequence elements and molecular organization give rise to such regions in the human genome.

Common fragile sites seem to play a functional role and to be involved in cancer. In fact, cancer associated deletions and translocations often affect chromosome regions containing fragile sites. Recently, it was shown that expression of fragile sites triggers intrachromosomal gene amplification (Coquelle *et al.*, 1997). Through these chromosomal aberrations, fragile sites may play a role both in loss of tumor suppressor genes and in amplification of oncogenes. These hypotheses have recently gained more credit by the observation that *FRA3B*, the most frequently expressed human common fragile site, maps within the sequence of the tumor suppressor gene *FHIT* at 3p14.2. The *FHIT* gene has abnormal transcripts in colorectal, lung and breast carcinomas as well as in other human tumors, resulting primarily from deletions generated by recombination between or within LINE sequences in the region of *FRA3B* (Huebner *et al.*, 1998). The common fragile site *FRA7G* maps at 7q31.2, in a region of frequent loss of heterozygositey (LOH) in breast and prostate cancer (Huang *et al.*, 1998a). A detailed LOH analysis in ovarian cancer showed the highest frequency of deletion breakpoints within the sequences of *FRA7G* (Huang *et al.*, 1999). Recently, homozygous deletions have been detected at 16q23.2, within the common fragile site *FRA16D*, in tumor cell lines derived from colonic, gastric, ovarian and small cell lung carcinoma (Mangelsdorf *et al.*, 2000; Paige *et al.*, 2000; Ried *et al.*, 2000; Krummel *et al.*, 2000). *FRA16D* associated deletions affect the transcripts of the *FOR* gene, also named WWOX (Bednarek *et al.*, 2000, 2001), spanning *FRA16D* and belonging to the family of oxidoreductases (Ried *et al.*, 2000).

The process of immortalization of human diploid fibroblasts by simian virus 40 (SV40) involves nonrandom chromosomal aberrations induced by SV40 T antigen (Ray *et al.*, 1990). Most of the chromosomal alterations are gaps and breaks identical to those induced by aphidicolin and may therefore involve fragile sites. The highest frequency of chromosomal aberrations in human diploid fibroblasts immortalized by SV40 is detected in the long arm of chromosome 6 (Hubbard-Smith *et al.*, 1992; Ray and Kraemer, 1992; Sandhu *et al.*, 1994) which harbors five common fragile sites. We have mapped a gene inducing replicative senescence in a 4 Mb region at 6q21, where we have constructed a complete YAC contig and a partial BAC/PAC contig (Morelli *et al.*, 1997a,b). This region is the most common breakpoint in a panel of translocation, deletion and radiation monochromosome human/mouse cell hybrids containing human chromosome 6 (Pappas *et al.*, 1995; C Morelli and G Barbanti-Brodano, unpublished). In preliminary fluorescence *in situ* hybridization (FISH) experiments with YACs of the 4 Mb contig, we detected breaks at 6q21 in metaphases of aphidicolin-treated human lymphocytes, suggesting that the common fragile site *FRA6F*, cytogenetically mapped at 6q21 (Smith *et al.*, 1998), lies within the region harboring the senescence gene. We therefore decided to finely map and clone *FRA6F* as a possible landmark of the gene at 6q21 inducing replicative senescence.

Results

Localization of FRA6F

A senescence gene was mapped at chromosome region 6q21 by chromosome transfer experiments. Introduction of an intact human chromosome 6 into immortalized mouse cells by microcell fusion induced senescence in most recipient cells. The few clones that grew up and maintained the immortalized phenotype of the original cell line invariably showed a common region of deletion involving chromosome bands 6q21-q22 (Gualandi *et al.*, 1994). Subsequently, the region containing the senescence gene was restricted to 4 Mb by molecular analysis and localized between markers D6S1499 and D6S266 at chromosome region 6q21 (Morelli *et al.*, 1997a,b). During our studies on the senescence gene, we characterized several translocation, deletion and radiation monochromosomic human-mouse somatic cell hybrids containing a rearranged chromosome 6 or portions of the chromosome (Pappas *et al.*, 1995; Morelli *et al.*, 1997a; Karayianni *et al.*, 1999). The majority of the hybrids show breakpoints within the 4 Mb region containing the senescence gene. Since fragile sites are regions particularly prone to breaking and the 4 Mb region at 6q21 is frequently deleted in immortalized cells (Ray and Kraemer, 1992; Morelli *et al.*, 1997b), it is possible that *FRA6F*, cytogenetically mapped at 6q21, lies within the

senescence gene region. We therefore used three YAC clones, belonging to the contig covering the 4 Mb portion of the 6q21 region (Morelli *et al.*, 1997b), in FISH experiments on aphidicolin-treated human lymphocyte metaphases to assess whether *FRA6F* is located in the senescence gene region. We chose YAC clones 852d6, 933c4 and 856g2 because they are not chimeric and cover the whole 4 Mb region (Morelli *et al.*, 1997b). Since *FRA6F* is expressed at low frequency (1–2%) on human chromosome 6, the location of the signal relative to the position of the fragile site (proximal, crossing or distal) was scored on 15 metaphases expressing *FRA6F*, corresponding to a total of 800 metaphases, for each probe. YAC clones 852d6 and 933c4 show proximal, crossing and distal signals relative to the fragile site, whereas YAC clone 856g2 gives only distal and a single crossing signal (Table 1 and Figure 1). The ratio of the number of distal plus crossing over proximal plus crossing signals (D+C/P+C) is also reported in Table 1. This value indicates that YAC clones 852d6 and 933c4, despite giving proximal, crossing and distal signals, do not contain the whole fragile site, since the D+C/P+C ratio is 0.5 and 1.7 respectively instead of 1. From these data we argue that *FRA6F* may extend proximally in a region larger than the overlapping region of the 852d6 and 933c4 YAC clones.

Characterization of FRA6F

In order to address this question and to precisely define *FRA6F*, we assembled a contig of 14 PAC clones covering the whole region from marker CMFE7 to marker D6S1066 and extending centromerically beyond the overlapping region of YAC clones 852d6 and 933c4 (Figure 1). The continuity of the PAC contig was assessed by known STS content and by developing new STSs from PAC end sequences. The correct orientation of PAC clones in relation to centromere and telomere was defined in triple color FISH experiments using a proximal or distal probe as the anchor point. Each PAC clone was used as a probe in FISH experiments on aphidicolin-treated metaphases of human lymphocytes (Figure 2). At least 11 metaphases expressing *FRA6F* were scored for each probe as previously described for YAC clones. The number of proximal, crossing and distal signals was recorded. Based on the number of crossing signals given by each PAC (Table 1), two hot spots of breaking, measuring each about 200 kb, were detected, one proximal involving PACs RP3-442M11, RP3-415N13 and RP3-487J7, the other distal involving PACs RP1-139A3, RP1-96N13, RP1-97J1 and RP1-276A6 (Table 1; Figure 1). The value of D+C/P+C ratio was calculated (Table 1), although it is less significant as compared to the same value obtained with YAC clones. However, the small size of PAC probes allowed a more detailed analysis which detected two regions of breakage.

Table 1 Localization of *FRA6F* by FISH analysis

Position of signals relative to the aphidicolin-induced breakpoints at 6q21				
Clone[a]	*Proximal*	*Crossing*	*Distal*	*D+C/P+C*[b]
Y852d6	9	3	3	0.5
Y933c4	3	4	8	1.71
Y856g2	0	1	14	15
RP3-50514	8	2	1	0.3
RP1-153M21	15	0	7	0.47
RP3-442M11	6	3	2	0.55
RP3-415N13	4	6	2	0.8
RP3-487J7	9	3	7	0.83
RP1-66H14	10	1	8	0.82
RP1-182A16	7	0	10	1.42
RP1-139A3	9	2	8	0.91
RP1-96N13	8	4	8	1
RP1-97J1	9	3	10	1.08
RP1-276A6	8	2	9	1.1
RP1-142L7	6	2	9	1.37
RP3-403D1	6	2	12	1.75
RP1-166K4	1	2	10	4

[a]Clones used as probes in FISH experiments. Y before the number of the clone indicates a YAC clone, whereas PAC clones are indicated with the denominations given in the library of origin; [b]Ratio of distal+crossing (D+C) to proximal+crossing (P+C) signals relative to the breakpoints at 6q21

Transcription map of the FRA6F *region*

Ten known genes map within the fragile site region. In a proximal to distal position they are: dj*1112D6.1*, *REV3L* (Gibbs *et al.*, 1998; Morelli *et al.*, 1998), *DIF13*, *C6UAS* and *C6ORF4-6* (Morelli *et al.*, 2000), *FYN* (Karayianni *et al.*, 1999), *H3F3A*, *FKHRL1* (Hillion *et al.*, 1997), *dj142L7.3*, *LAMA4*, (Figure 1). Furthermore, nine other genes map close to *FRA6F*, in a proximal or distal position (Figure 1). Three CpG islands, indicating the presence of putative new genes and corresponding to markers D6S1499, D6S302 and D6S416, were detected within *FRA6F*.

Sequence analysis of FRA6F

To analyse the nucleotide sequence of *FRA6F*, PACs RP5-1112D6, RP3-442M11, RP3-415N12, RP3-487J7, RP1-66H14, RP1-139A3, RP1-97J1, RP1-276A6 and RP1-142L7 were sequenced. These PACs cover essentially all the region of *FRA6F* in the contig (Figure 1), since a total of 1100 kb were sequenced. In particular, the regions corresponding to the two hot spots of breakage were completely sequenced on PACs RP3-422M11, RP3-415N12, RP3-487J7, RP1-97J1 and RP1-276A6 (Figure 1). The nucleotide sequence of the contig was used to measure the length of *FRA6F*. By subtracting the overlapping regions of the clones, the length of the whole fragile site and of each of the two hot spots was found to be 1200 and 200 kb, respectively.

The DNA sequence spanning *FRA6F* was analysed for the type and quantity of DNA repeats (Figure 3), since DNA repeats have been proposed to have a role in common fragile site instability (Inoue *et al.*, 1997; Mimori *et al.*, 1999). Total repetitive elements represent 35.7% of the entire DNA sequence in *FRA6F*, an amount which is not significantly different

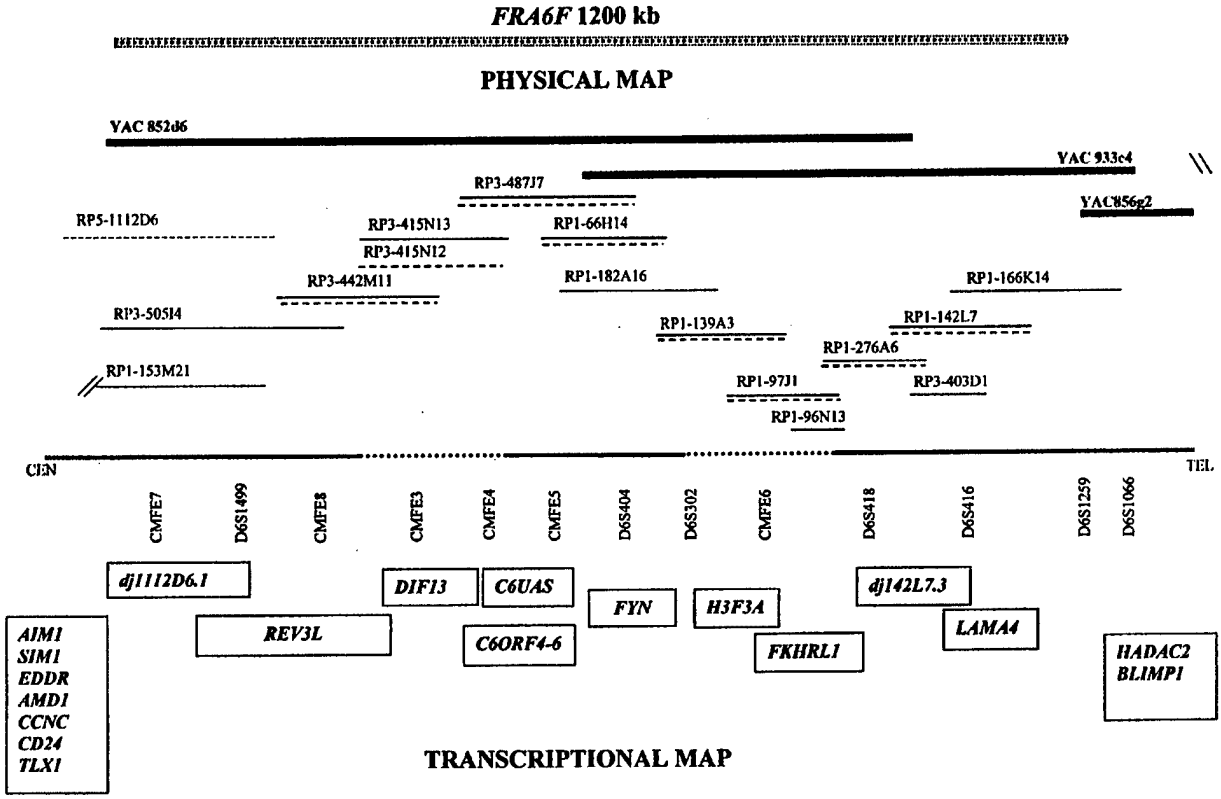

Figure 1 Physical and transcriptional map of the *FRA6F* region. The physical map and the whole region of breaking are reported in the top part of the figure with the markers distributed along the region. Dotted lines indicate the two hot-spots of breaking, revealed by FISH experiments with PAC probes. Thick bold lines represent the YAC clones used for initial *FRA6F* localization. PAC clones used in FISH experiments are shown in the figure with plain lines. PAC clones subjected to sequence analysis are indicated with dashed lines. PAC clones marked with both continuous and dashed lines have been used for FISH experiments and sequence analysis. The transcriptional map of *FRA6F* is shown in the lower part of the figure with genes distributed in the regions proximal to, within and distal to *FRA6F*

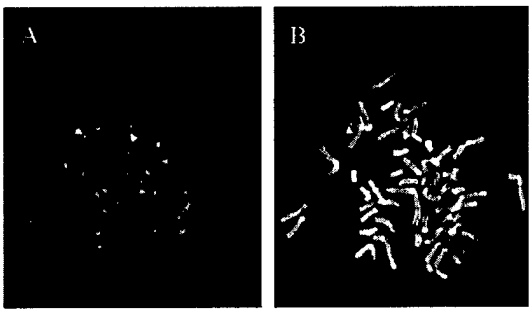

Figure 2 Chromosomal localization of *FRA6F* by FISH analysis. (**a**) In this experiment *FRA6F* was detected on metaphases of aphidicolin-treated normal human lymphocytes, using PAC RP1-97J1 (see Figure 1) as the probe. Only one of the two copies of chromosome 6 shows a break at *FRA6F* (right green dots). Due to the rare expression of *FRA6F*, this was the general pattern observed in most of the metaphases analysed. (**b**) The propidium iodide staining of the same metaphase is shown in black and white. In **a** and **b** arrows indicate the position of *FRA6F* at 6q21

from a standard region of the genome (37.4%) with a similar GC content (Genome 1 in Figure 3). Notable features of *FRA6F* were a high content of Alu sequences in the proximal hot spot and the regions outside the hot spots and a considerable amount of DNA transposons of the MER type in the proximal hot spot (Figure 3). Although LINE (LINE1+-LINE2) sequences were consistently represented in the two hot spots and in the other regions of *FRA6F*, they were less abundant than in the region of the genome (Genome 1) with the corresponding GC content (Figure 3). Twenty-two sequences with the typical characteristics of matrix attachment regions (MARs), which have been suggested to participate in chromosomal instability (Wang *et al*., 1997; Mishmar *et al*., 1998), were detected in *FRA6F* (Table 2). While the average density of MARs in the human genome is of one every 80–90 kb (Luderus *et al*., 1992), the density in *FRA6F*, corresponding to 22 MARs in 1200 kb, is of one every 54 kb. Moreover, in some portions of *FRA6F* MARs were clustered, such as in PAC RP5-1112D6 (five MARs in 67 kb) or in PAC RP1-66H14 (four MARs in 57 kb) (Table 2). No CCG repeats or long AT-rich sequences were detected in *FRA6F*.

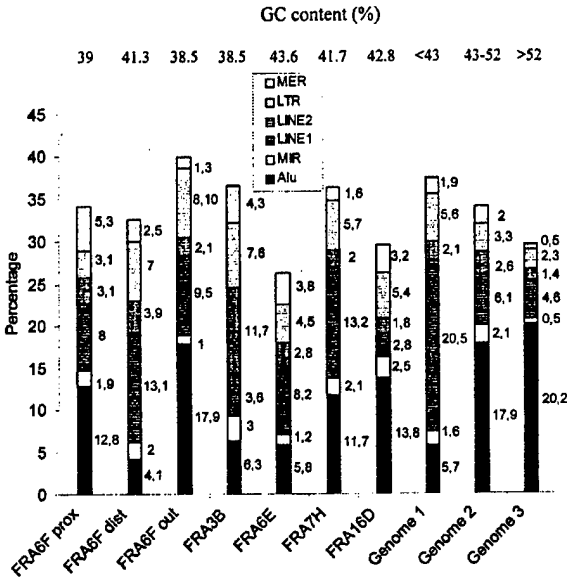

Figure 3 DNA repeat composition of *FRA6F* proximal (prox) and distal (dist) hot spots of breakage and of the regions outside (out) the hot spots. The DNA repeat composition of the other fragile sites *FRA3B, FRA6E, FRA7H, FRA16D* and of three regions of the whole genome with increasing GC content (Genomes 1, 2 and 3) are also shown for comparison. Values of percentage refer to the percentage of repetitive elements relative to the entire sequence of *FRA6F*. Values for *FRA3B, FRA6E, FRA7H* and *FRA16D* are from Ried *et al.* (2000), values for Genomes 1, 2 and 3 are from Smit (1996)

Table 2 Analysis for MAR sequences within *FRA6F*

Clones	*MAR*[a]	*Repeats*[b]	*ORI*[b,c]	*T/G*[b,d]	*A/T*[b,e]	*TOPOII*[b,f]
RP5-1112D6	14.6–14.9	Alu	27	0	78	5
RP5-1112D6	31.6–32.0	Harlequin	39	1	92	10
RP5-1112D6	41.8–42.6	Alu	53	0	108	7
RP5-1112D6	46.5–47.0	Alu	45	0	117	7
RP5-1112D6	81.1–82.0	MIR	86	0	154	9
RP3-442M11	30.3–31.1	Alu	47	1	112	26
RP3-415N12	36.6–36.8	Alu	43	1	120	10
RP3-487J7	50.1–50.6	Alu, MIR	56	0	91	7
RP3-487J7	91.3–92.1	L1, MIR	42	0	62	9
RP3-487J7	114.0–114.9	Alu, MLT	23	0	51	8
RP1-66H14	61.9–62.6	Alu	32	0	52	4
RP1-66H14	96.3–96.9	Alu, MIR	32	0	37	11
RP1-66H14	118.0–118.2	Alu	43	0	54	6
RP1-66H14	118.4–118.6	Alu	43	0	54	6
RP1-139A3	38.1–38.3	Alu	30	0	67	9
RP1-139A3	71.4–72.2	MIR	47	3	103	10
RP1-139A3	171.0–171.9	Alu	53	0	116	34
RP1-97J1	129.7–130.4	Alu	57	0	77	58
RP1-97J1	155.3–156.0	None	38	0	82	14
RP1-97J1	176.8–177.1	MIR	42	1	71	8
RP1-142L7	13.7–14.1	Alu	67	1	141	12
RP1-142L7	91.7–92.4	Alu, MIR	72	1	151	14

[a]Values represent the sequence intervals (kb) where the MAR elements were detected. [b]The analysis was performed within the MAR element as well as 2 kb upstream and downstream the MAR sequence. [c]Number of motifs (ATTA, ATTTA, ATTTTA) identifying the origins of replication. [d]Number of T- or G-rich sequences. [e]Number of A- or T-rich sequences. [f]Topoisomerase II binding and cleavage sites

In the *FRA6F* sequence we detected stem-loop structures with a stem of 20–50 bp and a loop of 20–200 bp, often aggregated in clusters of more than 80 stem-loops in 2 kb of DNA sequence (Table 3). Clusters with the highest density were found in the proximal and distal hot spots of *FRA6F* (PAC clones RP3-415N12, RP1-139A3 and RP1-97J1; Figure 1 and Table 3), whereas the regions outside the hot spots, (PAC clones RP5-1112D6, RP3-487J7, RP1-66H14 and RP1-142L7; Figure 1 and Table 3), a genomic region (9p23) selected at random and other fragile sites, with the exception of *FRA6E*, had a much lower density of stem-loop structures (Table 3). Interestingly, the genomic region 22q11, frequently involved in chronic myeloid leukemia translocations, with consequent truncation of the BCR gene, shows a high density of stem-loops, similarly to the unstable hot spot regions of *FRA6F* (Table 3). Contrary to *FRA6F* and *FRA6E*, in fragile sites *FRA3B, FRA7G, FRA7H* and *FRA16D* clusters of stem-loops were detected in connection to the presence of dinucleotide repeats (Table 3).

The analysis of DNA helix flexibility in the *FRA6F* sequence was carried out with the bend.it program. This program measures the flexibility parameter which is expressed as fluctuation in the twist angle. The analysis revealed six regions with potential high flexibility (predicted curvature parameter greater than 14) in the proximal hot spot and five regions in the distal hot spot of *FRA6F*. The analysed sequences of other fragile sites *FRA3B* (180 kb), *FRA6E* (330 kb) and *FRA16D* (270 kb) showed 14, 10 and 11 regions of greater flexibility, while the control genomic DNA showed no regions of high flexibility (Figure 4). Stem-loop clusters in *FRA6F* and *FRA6E* were located in regions of greater stability, close to high flexibility sites of the DNA helix (Figure 4).

Detection of deletion and translocation breakpoints involving FRA6F *in immortal cells, leukemia and cancer*

A gene inducing replicative senescence was mapped in a 4 Mb region at 6q21 containing *FRA6F* (Morelli *et al.*, 1997a,b). Therefore, to assess directly whether breaks occur at *FRA6F* and are involved in the process of immortalization, we carried out a deletion analysis by PCR (see Materials and methods) on a series of immortal cell lines bearing translocation and deletions involving region 6q21 (Figure 5). In all the eight cell lines examined (two translocations human-mouse fusion cell hybrids, one monochromosomic human-mouse hybrid containing a human chromosome 6, two SV40-immortalized intraspecific human fibroblast hybrids carrying an additional exogenous chromosome 6 and three human fibroblast cell lines immortalized by SV40; see Materials and methods) one breakpoint end was detected within *FRA6F*, either in the distal hot spot, in the region between the two hot spots or in the telomeric portion of the fragile site (Figures 5 and 6). These results indicate that *FRA6F* is a true region of instability in the human genome and that a senescence inducing gene likely maps within *FRA6F*. Moreover,

Table 3 Distribution of stem-loop structures in *FRA6F*, other fragile sites and control genomic DNA

	FRA6F				*Other fragile sites*					*Genomic DNA*			
		No. stem-loops				*No. stem-loops*					*No. stem-loops*		
PAC clones	*Size*[a]	*Total*[d]	*Max*[e]	*Average kb*[b]	*Fragile sites*	*Size*[a]	*Total*[d]	*Max*[e]	*Average kb*[b]	*Regions*[c]	*Size*[a]	*Total*[d]	*Max*[e]	*Average kb*[b]
RP5-1112D6	135	34	7	4.0	*FRA3Bex4*[f]	185	41	9[g]	4.4	9p23	152	20	3	7.6
RP3-415N12	177	153	80	1.1	*FRA3*in5[f]	110	38	11[g]	2.9	22q11	152	378	25	0.4
RP3-487J7	116	53	5	2.2	*FRA3B*ex5[f]	207	30	14[g]	6.9					
RP1-66H14	156	63	5	2.5	*FRA3B*ex6[f]	246	16	4	15.4					
RP1-139A3	208	246	164	0.8	*FRA6E*	331	546	184	0.6					
RP1-97J1	217	178	114	1.2	*FRA7G*	152	46	23[g]	3.5					
RP1-142L7	190	36	5	5.3	*FRA7H*	161	55	11	2.9					
					FRA16D	270	131	42[g]	2.1					

[a]Size (kb) of analysed sequence (see Materials and methods). [b]Average number of kb where a stem-loop is detected, obtained by dividing the size in kb of the region analysed by the total number of stem-loops found in the region. [c]Genomic regions analysed at random for the presence of stem-loop structures. [d]Total number of stem-loops per analysed sequence. [e]Highest number of stem-loops clustered within the 2 kb of maximum stem-loop density for each analysed sequence. [f]The sequences of *FRA3B* analysed for the presence of stem-loop structures correspond to the region of the fragile site encompassing *FHIT* exons 4, 5 and 6 as well as intron 5. [g]Stem-loops are clustered within a dinucleotide repeat region

Table 4 Deletions within *FRA6F* in human leukemias

Tumor type	*Minimal deletion*	*Markers*[a]	*Reference*[b]
Acute lymphoblsatic leukemia	6q15-q21	*M6P1-FYN*	Menasce *et al.*, 1994
Acute lymphoblastic leukemia	6q21	D6S447-*FYN*	Jackson *et al.*, 1998
Non-Hodgkin's lymphoma	6q21-q22.1	D6S246-D6S261	Starostik *et al.*, 2000
Breast carcinoma	6q21-q23	D6S268-D6S261	Sheng *et al.*, 1996
Breast carcinoma	6q21	D6S1040-D6S262	Utada *et al.*, 2000
Gastric carcinoma	6q16.3-q21	D6S283-D6S302	Queimado *et al.*, 1995
Ovarian carcinoma	6q21-q22.3	D6S301-D6S292	Shridhar *et al.*, 1999
Prostate carcinoma	6q14-q21	D6S404	Cooney *et al.*, 1996
Salivary gland carcinoma	6q21-q23.3	D6S262-D6S302	Queimado *et al.*, 1998
Melanoma	6q21-q23.3	D6S357	Talwalkar *et al.*, 1998
Melanoma	6q16.3-q21	D6S268-D6S292	Miele *et al.*, 2000
Mesothelioma	6q16.3-6q21	D6S301-D6S474	Bell *et al.*, 1997

[a]Markers are listed in centromeric to telomeric order. At least one breakpoint marker always lies within *FRA6F*. [b]The complete references are reported in the reference list

deletions involving breaks at *FRA6F* are detected in human leukemias and lymphomas, in breast, gastric, ovarian, prostate and salivary gland carcinoma, in melanoma and mesothelioma (Table 4).

Discussion

We have cloned and characterized the common fragile site *FRA6F* in a 1200 kb region at 6q21. It is notable that numerous genes map within *FRA6F*, in contrast to other fragile sites such as *FRA3B* and *FRA16D* that are associated each to only one gene, *FHIT* and *FOR* respectively (Huebner *et al.*, 1998; Ried *et al.*, 2000). The richness of genes in *FRA6F* may be relevant to the biological consequences of DNA instability at this fragile site.

Molecular mechanisms of FRA6F *instability*

Repetitive elements may constitute the molecular basis of common fragile site expression, as the expansion of repeat elements is the only known cause for the instability of rare fragile sites (Sutherland *et al.*, 1998). The DNA, affected at the fragile region by aphidicolin, carcinogens or other damaging agents, may break and be repaired during replication. If the break falls within or close to a LINE repeat, annealing of the homologous sequences of the repeat element may generate a stem-loop structure inducing deletion of a DNA segment, by nonhomologous or unequal homologous recombination, during the process of replication/repair in the damaged region (Mimori *et al.*, 1999). In agreement with this model, association of LINE1 elements and cancer deletion breakpoints was observed at the proximal end of *FRA3B* (Inoue *et al.*, 1997). However, no association was found between repetitive sequences and aphidicolin-induced or cancer deletion breakpoints located at the distal end of *FRA3B* (Wang *et al.*, 1997) or at *FRA16D* (Ried *et al.*, 2000). A considerable degree of variation in the type and quantity of repeat DNA sequences was observed in the three regions of *FRA6F*. In particular, LINE1 elements were significantly under-represented when compared with the normal human genome. Variation in repeat element composition and under-representation of LINE1 elements was observed also in *FRA16D* (Ried *et al.*, 2000). On the whole, these observations suggest that a specific repeat composition

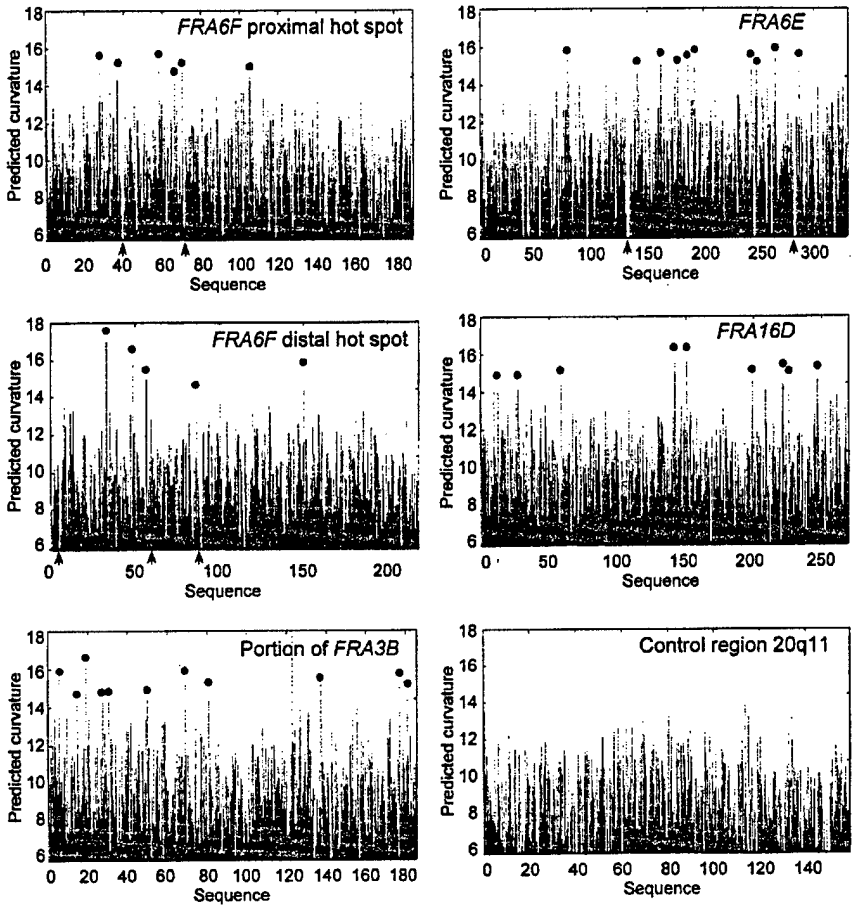

Figure 4 Analysis of DNA helix flexibility in the sequence of *FRA6F* proximal and distal regions of maximum breakage (proximal hot spot and distal hot spot) as well as in the other fragile sites *FRA3B*, *FRA6E*, *FRA16D* and in a non fragile control region (20q11) of the genome. The *FRA3B* sequence analysed for flexibility corresponds to the 180-kb region encompassing *FHIT* exon 4 (Boldog *et al*., 1997; Inoue *et al*., 1997; Mimori *et al*., 1999). The values of the curvature of the DNA helix are expressed in the *y* axis in degrees per helical turn. Values of the curvature above 14 (marked by dots) are considered indicative of high flexibility. The *x* axis reports the size (kb) of the region subjected to the flexibility analysis. The arrows indicate the positions where stem-loop clusters were detected

is unlikely to be related to the mechanism of DNA instability of fragile sites.

DNA helix flexibility correlated with DNA instability at *FRA3B* and *FRA16D* (Mimori *et al*., 1999; Ried *et al*., 2000). Regions of greater DNA helix flexibility influence protein-DNA interactions (Mishmar *et al*., 1998, 1999), and may therefore affect chromatin structure and condensation, generating DNA instability. The high flexibility peaks detected in *FRA6F* proximal and distal hot spots of breakage are therefore candidate regions for the DNA instability of this fragile site. Delay in DNA replication plays a crucial role in DNA instability at fragile sites. Cytogenetic analysis indicated that aphidicolin-induced breaks at *FRA3B* preferentially occurred on the chromosome 3 with a late replicating allele (Wang *et al*., 1999). *In situ* hybridization and FISH analysis showed that the *FRA7H* region has a replication delay during S phase in about 35% of the nuclei. The results of this study indicated that replication delay was due to perturbation of replication fork progression (Hellman *et al*., 2000). This effect could depend on two peculiar structures present in *FRA6F*: MARs and stem-loop clusters.

Due to the attachment of MARs to the nuclear matrix, progression of the replication fork through these DNA elements may be hindered and these regions may normally replicate late in S phase. They could replicate even later under aphidicolin treatment and fail to complete replication by the time chromatin is packaged into chromosomes. Further replication delay may derive from the greater density and aggregation of MARs in clusters at *FRA6F* as well as from generation at MARs of independent loop domains, due to unwinding of the DNA helix and continuous base unpairing (Kohwi-Shigematsu and Kohwi, 1990; Bode *et al*., 1992). MARs were detected in *FRA3B* (Wang *et al*., 1997) and *FRA7H*. In *FRA7H*,

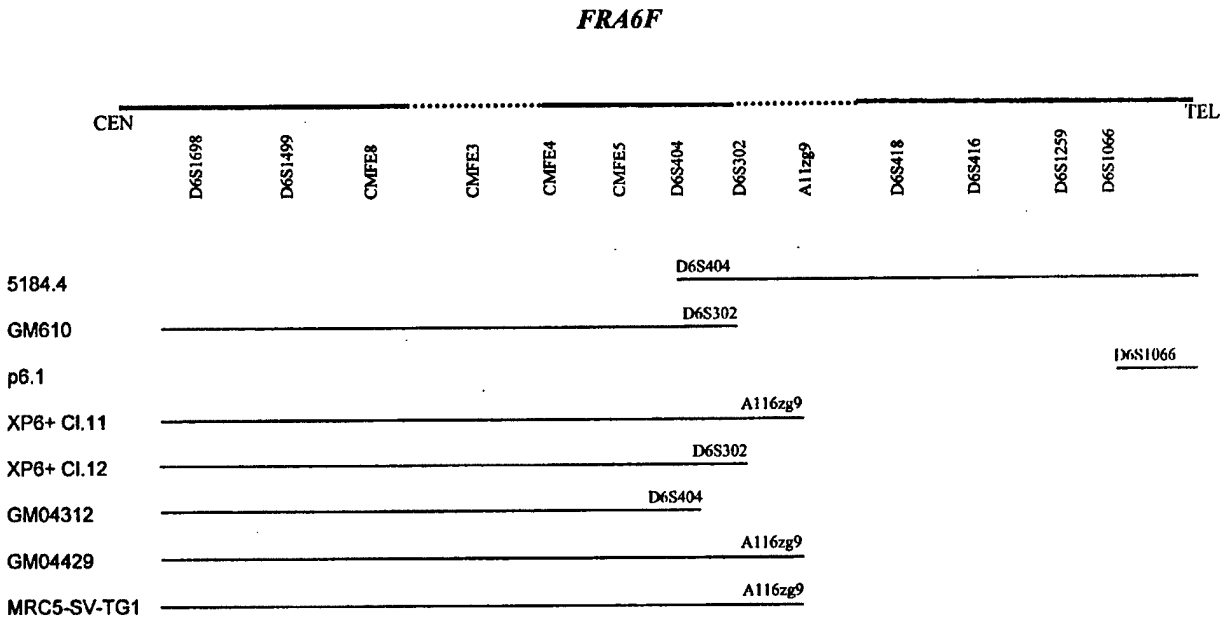

Figure 5 Breakpoint ends within *FRA6F* in cell lines (left column) showing translocations and deletions involving region 6q21 (see the sections on Materials and methods and Results for details). *FRA6F* is depicted with the two hot spots of breakage represented by dotted lines. Markers below *FRA6F* were used for the molecular analysis of cell lines by PCR. Solid lines corresponding to the cell line names indicate the conserved portion of chromosome 6. Markers at breakpoint ends indicate the chromosome 6 region of break in each cell line

six MARs colocalize in a cluster with a high flexibility region and an SV40 integration site (Mishmar *et al.*, 1998), strongly suggesting that they participate in chromosomal instability at this fragile site. We detected clusters of stem-loops in *FRA6F*. Similar multiple hairpin structures were detected close to the eight breakpoints at the distal region of breakage in *FRA3B*, and in *FRA16D* in coincidence with some of the breakpoint locations in AGS and HCT116 tumor cell lines (Ried *et al.*, 2000). The expanded trinucleotide repeats and the AT-rich minisatellite repeats, responsible for the DNA instability at the rare fragile sites *FRA10B* and *FRA16B*, are also capable of forming hairpin structures (Sutherland *et al.*, 1998). Stem-loop and hairpin structures are candidates to directly induce deletions by nonhomologous recombination, according to a mechanism akin to that proposed for LINE1 sequences. Moreover, they may generate localized sequence elements with the properties of DNA polymerase pause sites, representing areas of the genome where progression of the DNA polymerase is hindered or delayed. These sites would play an important role in inhibiting or delaying DNA replication. Since clusters of stem-loops were detected in *FRA6F* and *FRA6E* exclusively at regions of high stability, adjacent to flexibility zones of the DNA helix, clustered stem-loops may cooperate with high DNA flexibility in inducing DNA breaks. It will be interesting to search for clustered stem-loops in future cloned fragile sites to confirm if such structures really represent a common mechanism of fragility.

Involvement of FRA6F *in senescence, oncogenesis and schizophrenia*

Convincing data exist linking expression of common fragile sites to leukemia and cancer. Activation of common fragile sites by aphidicolin was detected in lymphocytes from colon, rectum, head and neck cancer patients and in their first-degree relatives, with a significant difference compared to lymphocytes of normal controls (Egeli *et al.*, 2000; Tunca *et al.*, 2000a,b). Moreover, several tumor suppressor genes have been cloned from regions containing fragile sites: *FHIT* from *FRA3B* (Huebner *et al.*, 1998), *TESTIN* from *FRA7G* (Tatarelli *et al.*, 2000) and *FOR* from *FRA16D* (Ried *et al.*, 2000). Our study shows that breaks at *FRA6F* are involved in cell immortalization and oncogenesis, suggesting the presence of a senescence gene and perhaps of a tumor suppressor gene within or close to this fragile site. Hereditary schizophrenia has also been associated with fragile sites. Lymphocytes from schizophrenia patients show activation of a rare fragile site at 2q11.2 and of a common fragile site at 9q12 with a significant difference compared to lymphocytes of normal controls (Chen *et al.*, 1998). A gene involved in hereditary schizophrenia was localized at 6q21. The greatest allele sharing in members of affected families was defined by marker D6S416 (Cao *et al.*, 1997) which maps within *FRA6F* (Morelli *et al.*, 1997a,b; Karayianni *et al.*, 1999; Morelli *et al.*, 2000 and this study). Therefore, *FRA6F* may be a landmark for the identification and cloning of genes involved in senescence, leukemia, cancer and schizophrenia.

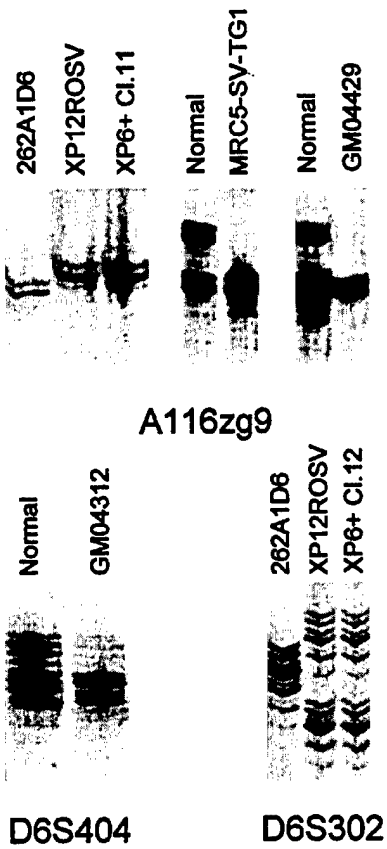

Figure 6 LOH analysis for markers A116zg9, D6S404 and D6S302, located within *FRA6F*, in immortal human cell lines (see Materials and methods). XP6+Cl.11 and XP6+Cl.12 are two clones of immortal cells derived from transfer of a normal human chromosome 6 from the donor cell line 262A1D6 to the recipient cell line XP12ROSV. The two clones are compared with the donor and recipient cell lines. MRC5-SV-TG1, GM04429 and GM04312 are human diploid fibroblasts immortalized by SV40. They are compared with the normal parental fibroblast strains. Note that polymorphic markers present in the donor cell line 262A1D6 are lost in clones XP6+Cl.11 and XP6+Cl.12. Likewise, markers present in normal parental fibroblasts are lost in the derived SV40-immortalized cell lines

Materials and methods

Fluorescent in situ *hybridization (FISH)*

Whole blood was cultured in the presence of PHA for 72 h, followed by colcemid treatment (20 min at 37°C) and standard procedures for harvesting and fixation. For interphase physical mapping of PAC clones, 2.5 mM of sodium borate was added to the hypotonic solution. For fragile site induction, cells were cultured in the presence of 0.4 μM aphidicolin for 24 h before harvesting. After spreading, slides were fixed for 1 h at room temperature in 3:1 methanol:acetic acid solution and then dehydrated in an ethanol series. Slides were used for hybridization after aging overnight at 42°C and a 10 min treatment in acetone. YAC and PAC DNA was used to prepare probes for FISH analysis. DNA was extracted from broth cultures by standard techniques. One μg of YAC DNA or 400 ng of PAC DNA were labeled by nick-translation with biotin-16-dUTP or 11-digoxigenin-dUTP. After precipitation in the presence of a 15-fold excess of human Cot1 DNA and a 30-fold excess of sonicated salmon sperm DNA, probes were resuspended in 10 μl of hybridization buffer (50% formamide, 10% dextran sulfate in 2×SSC). For hybridization, chromosomal DNA was denatured by placing the slides in 2×SSC, containing 70% formamide, at 75°C for 5 min. The preparations were then immediately dehydrated through a cold ethanol series. Probes were denatured at 75°C for 5 min and preannealed on slides for 30 min before hybridization. Hybridization was carried out at 37°C for 72 h for YAC probes and once overnight for PAC probes. After washing in stringent conditions (50% formamide in 2×SSC twice at 42°C, 1×SSC twice at 42°C), biotin-labeled probes were visualized with avidin-FITC or avidin-Texas Red, performing a cycle of signal amplification with biotinylated anti-avidin antibody. Digoxigenin-labeled probes were detected using a sheep anti-digoxigenin antibody, a rabbit-FITC anti-sheep antibody and goat-FITC anti-rabbit antibody (Southern Biotechnology Associates, Birmingham, AL, USA). Cell metaphases were counterstained with propidium iodide or DAPI and observed with a Zeiss Axioplan microscope equipped with a triple-pass filter (VYSIS) using the IPLAB Spectrum P software.

Assembly of YAC and PAC contigs and DNA sequence determination

Direct sequencing of PAC clone ends was performed on 1 μg of purified PAC DNA with T7 or Sp6 standard primers. PAC end amplification was carried out by PCR (33 cycles with 30″ at 94°C, 30″ at the appropriate annealing temperature and 30″ at 72°C) in a 10 μl reaction mixture, using 50 ng of YAC DNA or 25 ng of PAC DNA. Complete sequence of all PAC clones in the contig at 6q21 was carried out using established shotgun methods, available at the Sanger Center (http://www.sanger.ac.uk/HGP/overview.shtml).

Sequence analysis

Sequence analysis of *FRA6F*, other fragile sites and control genomic DNA was carried out on DNA sequences with the following GenBank accession numbers. *FRA3B*ex4: AF152363; *FRA3B*in5: U66722; *FRA3B*ex5: AF020503; *FRA3B*ex6: AF152365; *FRA6E*: AB016897; *FRA6F*: RP5-1112D6: AL080317; RP3-442M11: AL512325; RP3-415N12: AL136310; RP3-487J7: AL008730; RP1-66H14: Z97989; RP1-139A3: AL109916; RPI-97J1: AL158035; RP1-276A6: AL512299; RP1-142L7: Z99289; *FRA7G*: AC002066; *FRA7H*: AF017104; *FRA16D*: AF217490; region 9p23: AL135923; region 20q11: AL355392; region 22q11: U07000. The composition in DNA repeats was analysed using the RepeatMasker program (http://repeatmasker.genome.washington.edu) which compares DNA sequences to a library of repetitive elements and detects low complexity regions. For the analysis of DNA helix flexibility, the bendability/curvature propensity plot were calculated with the bend.it server (http://www2.icgeb.trieste.it/~dna/bend_it.html) using the DNase I based bendability parameters (Brukner *et al.*, 1995) and the consensus bendability scale (Gabrielian and Pongor, 1996). This server predicts DNA curvature from DNA sequences. The curvature is calculated as a vector sum of dinucleotide geometries (roll, tilt and twist angles) using the BEND algorithm of Godsell and Dickerson, and is expressed as degrees per helical turn (10.5 degrees/helical turn = 1 degree/base pair). The STEMLOOP program of the Genetics Computer Group (GCG) at the UK Human Gene

Mapping Project (http://www.hgmp.mrc.ac.uk) was used to determine the presence and distribution of stem-loop structures within the sequences analysed. MARs were identified using the MarFinder program (http://ncgr.org/MarFinder). This computational approach to find MARs is based on the simultaneous presence of several motifs occurring in the neighborhood of MAR sequences. The density of these motifs in a region of DNA indicates the presence of a MAR in that region.

Cell lines

The following cell lines, cultured in DMEM/F12 medium (GIBCO-BRL) supplemented with 10% fetal calf serum, were subjected to molecular analysis by PCR to detect breakpoints within *FRA6F*: 5184.4 and GM610, two human-mouse cell fusion hybrids where portions of chromosome 6 are translocated to the X chromosome and to other human and mouse chromosomes, with breaks at 6q21 (Pappas *et al.*, 1995); p6.1, a monochromosomic human-mouse somatic cell hybrid containing, as a sole human genetic complement, a human chromosome 6 deleted at q16.3-q21 (Morelli *et al.*, 1997b); XP6+C1.11 and XP6+C1.12, two clones derived from the SV40-immortalized human fibroblast cell line XP12ROSV after transfer of an exogenous normal human chromosome 6 by microcell fusion from the donor cell line 262A1D6; GMO4312, GMO4429 (NIGMS Human Genetic Mutant Cell Repository, Coriell Institute for Medical Research, Camden, NJ, USA) and MRC5-SV-TG1 (Huschtscha and Holliday, 1983), derived by immortalization of human diploid fibroblasts with SV40. The molecular analysis of cell lines was carried out by PCR with markers located within *FRA6F*. The markers used were D6S1698, D6S1499, CMFE8, CMFE3, CMFE4, CMFE5, D6S404, D6S302, A116zg9, D6S418, D6S416, D6S1259 and D6S1066. Only polymorphic markers were used to characterize the human cell lines. XP6+C1.11 and XP6+C1.12 cells were compared in a LOH analysis with the donor (262A1D6) and the recipient (XP12ROSV) cell lines, while GMO4312, GMO4429 and MRC5-SV-TG1 cells were compared with the normal parental fibroblast strains (Figure 6).

Acknowledgements
We thank all members of the chromosome 6 project group at the Sanger Centre, funded by the Wellcome Trust, for continuous support in sequence determination. We also thank Annalisa Peverati, Augusto Bevilacqua, Pietro Zucchini and Iva Pivanti for excellent technical assistance. C Morelli was supported by a fellowship from Fondazione Italiana per la Ricerca sul Cancro (FIRC). This work was supported by grants from Associazione Italiana per la Ricerca sul Cancro (AIRC) and from MURST ex 60%.

References

Bednarek AK, Laflin KJ, Daniel RL, Liao Qiaoyin, Hawkins KA and Aldaz CM. (2000). *Cancer Res.*, **60**, 2140–2145.
Bednarek AK, Keck-Waggoner CL, Daniel RL, Laflin KJ, Bergsagel PL, Kiguchi K, Brenner AJ and Aldaz CM. (2001). *Cancer Res.*, **61**, 8068–8073.
Bell DW, Jhanwar SC and Testa JR. (1997). *Cancer Res.*, **57**, 4057–4062.
Bode J, Kohwi Y, Dickinson L, Joh T, Klehr D, Mielke C and Kohwi-Shigematsu T. (1992). *Science*, **255**, 195–197.
Boldog F, Gemmill RM, West J, Robinson M, Robinson L, Li E, Roche J, Todd S, Waggoner B and Lundstrom R. (1997). *Hum. Mol. Genet.*, **6**, 193–203.
Brukner I, Sanchez R, Suck D and Pongor S. (1995). *EMBO J.*, **14**, 1812–1818.
Cao Q, Martinez M, Zhang J, Sanders AR, Badner JA, Cravchik A, Markey CJ, Beshah E, Guroff JJ and Maxwell ME. (1997). *Genomics*, **43**, 1–8.
Chen C-H, Shih H-H, Wang-Wuu S, Jen Tai J and Wuu K-D. (1998). *Hum. Genet.*, **103**, 702–706.
Cooney KA, Wetzel JC, Consolino CM and Wojno KJ. (1996). *Cancer Res.*, **56**, 4150–4153.
Coquelle A, Pipiras E, Toledo F, Buttin G and Debatisse M. (1997). *Cell*, **89**, 215–225.
Egeli U, Ozkan L, Tunca B, Kahraman S, Cecener G, Ergul E and Engin K. (2000). *Head Neck J.*, **22**, 591–598.
Gabrielian A and Pongor S. (1996). *FEBS Lett.*, **393**, 65–68.
Gibbs PEM, McGregor WG, Maher VM, Nisson P and Lawrence CW. (1998). *Proc. Natl. Acad. Sci. USA*, **95**, 6876–6880.
Glover TW, Berger C, Coyle J and Echo B. (1984). *Hum. Genet.*, **67**, 136–142.
Gualandi F, Morelli C, Pavan JV, Rimessi P, Sensi A, Bonfatti A, Gruppioni R, Possati L, Stanbridge EJ and Barbanti-Brodano G. (1994). *Genes Chrom. Cancer*, **10**, 77–84.
Hellman A, Rahat A, Scherer SW, Darvasi A, Tsui L-C and Kerem B. (2000). *Mol. Cell. Biol.*, **20**, 4420–4427.
Hillion J, Le Coniat M, Jonveaux P, Berger R and Bernard OA. (1997). *Blood*, **90**, 3714–3719.
Huang H, Qian C, Jenkins RB and Smith DI. (1998a). *Genes Chrom. Cancer*, **21**, 152–159.
Huang H, Qian J, Proffit J, Wilber K, Jenkins R and Smith DI. (1998b). *Oncogene*, **16**, 2311–2319.
Huang H, Reed CP, Mordi A, Lomberk G, Wang L, Shridhar V, Hartmann L, Jenkins R and Smith DI. (1999). *Genes Chrom. Cancer*, **24**, 48–55.
Hubbard-Smith K, Patsalis K, Pardinas JR, Jha KK, Henderson AS and Ozer HL. (1992). *Mol. Cell. Biol.*, **12**, 2273–2281.
Huebner K, Garrison PN, Barnes LD and Croce CM. (1998). *Annu. Rev. Genet.*, **32**, 7–31.
Huschtscha LI and Holliday R. (1983). *J. Cell Sci.*, **63**, 77–99.
Inoue H, Ishii H, Alder H, Snyder E, Druck T, Huebner K and Croce CM. (1997). *Proc. Natl. Acad. Sci. USA*, **94**, 14584–14589.
Jackson A, Panayiotidis P and Foroni L. (1998). *Genomics*, **50**, 34–43.
Karayianni E, Magnanini C, Orphanos V, Negrini M, Maniatis GM, Spathas DH, Barbanti-Brodano G and Morelli C. (1999). *Cytogenet. Cell Genet.*, **86**, 263–266.
Kohwi-Shigematsu T and Kohwi Y. (1990). *Biochemistry*, **29**, 9551–9560.
Krummel KA, Roberts LR, Kawakami M, Glover TW and Smith DI. (2000). *Genomics*, **69**, 37–46.
Le Beau MM, Rassool FV, Neilly ME, Espinosa III R, Glover TW, Smith DI and McKeithan TW. (1998). *Hum. Mol. Genet.*, **7**, 755–761.
Le Beau MM and Rowley JD. (1984). *Nature*, **308**, 607–608.

Luderus MEE, De Graaf A, Mattia E, Den Blaauwen JL, Grande MA, De Jong L and Van Driel R. (1992). *Cell*, **70**, 949–959.

Mangelsdorf M, Ried K, Woolatt E, Dayan S, Eyre H, Finnis M, Hobson L, Nancarrow J, Ventner D and Baker E. (2000). *Cancer Res.*, **60**, 1683–1689.

Menasce LP, Orphanos V, Santibanez-Koref M, Boyle JM and Harrison CJ. (1994). *Genes Chrom. Cancer*, **10**, 286–288.

Miele ME, Jewett MD, Goldberg SF, Hyatt DL, Morelli C, Gualandi F, Rimessi P, Hicks DJ, Weissman BE, Barbanti-Brodano G and Welch DR. (2000). *Int. J. Cancer*, **86**, 524–528.

Mimori K, Druck T, Inoue H, Alder H, Berk L, Mori M, Huebner K and Croce CM. (1999). *Proc. Natl. Acad. Sci. USA*, **96**, 7456–7461.

Mishmar D, Mandel-Gutfroind Y, Margalit H, Rahat A and Kerem B. (1999). *Am. J. Hum. Genet.*, **64**, 908–910.

Mishmar D, Rahat A, Scherer SW, Nyakatura G, Hinzmann B, Kohwi Y, Mandel-Gutfroind Y, Lee JR, Drescher B and Sas DE. (1998). *Proc. Natl. Acad. Sci. USA*, **95**, 8141–8146.

Morelli C, Cardona F, Boyle JM, Negrini M and Barbanti-Brodano G. (1997a). *Cytogenet. Cell Genet.*, **79**, 97–100.

Morelli C, Magnanini C, Mungall AJ, Negrini M and Barbanti-Brodano G. (2000). *Gene*, **252**, 217–225.

Morelli C, Mungall AJ, Negrini M, Barbanti-Brodano G and Croce CM. (1998). *Cytogenet. Cell Genet.*, **83**, 18–20.

Morelli C, Sherratt T, Trabanelli C, Rimessi P, Gualandi F, Greaves MJ, Negrini M, Boyle JM and Barbanti-Brodano G. (1997b). *Cancer Res.*, **57**, 4153–4157.

Paige AJW, Taylor KJ, Stewart A, Sgouros JG, Gabra H, Sellar GC, Smyth JF, Porteous DJ and Watson JEV. (2000). *Cancer Res.*, **60**, 1690–1697.

Pappas GJ, Polymeropoulos MH, Boyle JM and Trent JM. (1995). *Genomics*, **25**, 124–129.

Queimado L, Reis A, Fonseca I, Martins C, Lovett M, Soares J and Parreira L. (1998). *Oncogene*, **16**, 83–88.

Queimado L, Seruca R, Costa-Pereira A and Castedo S. (1995). *Genes Chrom. Cancer*, **14**, 28–34.

Rassool FV, Le Beau MM, Shen ML, Neilly ME, Espinosa III R, Ong ST, Boldog F, Drabkin H, McCarroll R and McKeithan TW. (1996). *Genomics*, **35**, 109–117.

Ray FA and Kraemer PM. (1992). *Cancer Genet. Cytogenet.*, **59**, 39–44.

Ray FA, Peabody DS, Cooper JL, Scott-Cram L and Kraemer PM. (1990). *J. Cell. Biochem.*, **42**, 13–31.

Ried K, Finnis M, Hobson L, Mangelsdorf M, Dayan S, Nancarrow JK, Woollatt E, Kremmidiotis G, Gardner A and Venter D. (2000). *Hum. Mol. Genet.*, **9**, 1651–1663.

Sandhu AK, Hubbard-Smith K, Kaur GP, Jha KK, Ozer HL and Athwal RS. (1994). *Proc. Natl. Acad. Sci. USA*, **91**, 5498–5502.

Sheng ZM, Marchetti A, Buttitta F, Champeme MH, Campani D, Bistocchi M, Lidereau R and Callahan R. (1996). *Br. J. Cancer*, **73**, 144–147.

Shridhar V, Staub J, Huntley B, Cliby W, Jenkins R, Pass HI, Hartmann L and Smith DI. (1999). *Oncogene*, **18**, 3913–3918.

Simonic I and Gericke GS. (1996). *Hum. Genet.*, **97**, 524–531.

Smit A. (1996). *Curr. Opin. Genet. Dev.*, **6**, 743–748.

Smith DI, Huang H and Wang L. (1998). *Int. J. Oncol.*, **12**, 187–196.

Starostik P, Greiner A, Schultz A, Zettl A, Peters K, Rosenwald A, Kolve M and Muller-Hermelink HK. (2000). *Blood*, **95**, 1180–1187.

Sutherland GR, Baker E and Richards RI. (1998). *Trends Genet.*, **14**, 501–506.

Talwalkar VR, Scheiner M, Hedges LK, Butler MG and Schwartz HS. (1998). *Cancer Genet. Cytogenet.*, **104**, 111–114.

Tatarelli C, Linnenbach A, Mimori K and Croce CM. (2000). *Genomics*, **68**, 1–12.

Tunca B, Egeli U, Zorluoglu A, Yilmazlar T, Yerci O and Kizil A. (2000a). *Cancer Genet. Cytogenet.*, **119**, 139–145.

Tunca B, Egeli U, Zorluoglu A, Yilmazlar T, Yerci O and Kizil A. (2000b). *Cancer Lett.*, **152**, 201–209.

Utada Y, Haga S, Kajiwara T, Kasumi F, Sakamoto G, Nakamura Y and Emi M. (2000). *Jpn. J. Cancer Res.*, **91**, 293–300.

Wang I, Darling J, Zhang JS, Huang H, Liu W and Smith DI. (1999). *Hum. Mol. Genet.*, **8**, 431–437.

Wang L, Paradee W, Mullins C, Shridhar R, Rosati R, Wilke CM, Glover TW and Smith DI. (1997). *Genomics*, **41**, 485–488.

Wilke CM, Hall BK, Hoge A, Paradee W, Smith DI and Glover TW. (1996). *Hum. Mol. Genet.*, **5**, 187–195.

Yunis JJ and Soreng AL. (1984). *Science*, **226**, 1199–1204.

MS#11

Oncogene (2002) 21, 8713–8722

www.nature.com/onc

Evidence that instability within the FRA3B region extends four megabases

Nicole A Becker[1], Erik C Thorland[2], Stacy R Denison[1], Leslie A Phillips[1] and David I Smith*[,1]

[1]*Department of Experimental Pathology, Mayo Foundation, Rochester, Minnesota, MN 55905, USA;* [2]*Departments of Biochemistry and Molecular Biology, Mayo Foundation, Rochester, Minnesota, MN 55905, USA*

FRA3B is the most frequently expressed common fragile site localized within human chromosomal band 3p14.2, which is frequently deleted in many different cancers, including cervical cancer. Previous reports indicate aphidicolin-induced FRA3B instability occurs over ~500 kb which is spanned by the 1.5 Mb fragile histidine triad (FHIT) gene. Recently an HPV16 cervical tumor integration, 2 Mb centromeric to the published FRA3B region, has been identified. FISH-based analysis with a BAC spanning the integration has demonstrated this integration occurs within the FRA3B region of instability. These data suggest that the unstable FRA3B region is much larger than previously reported. FISH-based analysis of aphidicolin-induced metaphase chromosomes allowed for a complete characterization of instability associated with FRA3B. This analysis indicates that fragility extends for 4 Mb. Within this region are a total of five genes, including FHIT. FRA3B gene expression analysis on a panel of cervical tumor-derived cell lines revealed that three of the five genes within FRA3B were aberrantly regulated. A similar analysis of genes outside of FRA3B indicated that the surrounding genes were not aberrantly expressed. These data provide additional support that regions of instability associated with CFSs and the genes contained within them, may play an important role in cancer development.
Oncogene (2002) **21,** 8713–8722. doi:10.1038/sj.onc.1205950

Keywords: common fragile sites; FRA3B; human papillomavirus; cervical cancer; viral integration

Introduction

The development of cervical cancer is highly associated with HPV infection (Choo, 1998). HPV sequences have been identified within more than 95% of analysed cervical tumors, with high-risk subtypes HPV16 and HPV18 being the most prevalently recovered sub-types (Walboomers *et al.*, 1999).

In premalignant cervical lesions, the HPV genome is typically maintained in its episomal form. However, in the majority of invasive cervical carcinomas the HPV genomic DNA has been integrated into the host cell genome. Initial analysis involving cervical integration sites proposed that the integration events occurred randomly, but later cytogenetic analysis suggested a correlation between the sites of HPV integration and chromosomal bands containing common fragile sites (CFSs; Ref. Popescu *et al.*, 1990). We rescued the sites of HPV integration from a number of HPV16-positive cervical tumors and confirmed at the molecular level that HPV16 preferentially integrates into different CFS regions in ~50% of cervical tumors analysed (Thorland *et al.*, 2000, 2002; Denison *et al.*, submitted).

Fragile sites (FSs) are reproducible, non-random regions of chromosomal instability that are observed when cells are cultured under appropriate tissue culture conditions. FSs are divided into two classifications, rare fragile sites (RFSs) and common fragile sites (CFSs). RFSs are defined as sites that are observed in less than 5% of the population. CFSs appear to be present in all individuals with varying levels of expression. Molecular analysis of four CFSs (FRA6E, FRA7G, FRA7H, and FRA16D) has revealed that aphidicolin-induced decondensation/breakage within these CFSs occurs over broad genomic regions ranging from 200 kb to greater than 2 Mb (Huang *et al.*, 1998; Krummel *et al.*, 2000; Mishmar *et al.*, 1998; Tatarelli *et al.*, 2000). Additionally, CFSs have been demonstrated to be sites of elevated sister chromatid exchange (Glover and Stein, 1987), translocations and deletions in tumors (Boldog *et al.*, 1997; Fang *et al.*, 2001; Glover *et al.*, 1988; Glover and Stein, 1988), intrachromosomal gene amplification (Coquelle *et al.*, 1997), and *in vivo* tumor-associated viral integration (Mishmar *et al.*, 1998; Rassool *et al.*, 1991; Thorland *et al.*, 2000; Wilke *et al.*, 1996). These observations suggest that the inherently unstable regions within CFSs may be predisposed to chromosomal breakage and rearrangement during cancer development (Popescu *et al.*, 1990).

The most commonly expressed CFS in humans is FRA3B, cytogenetically located at 3p14.2 (Smeets *et al.*, 1986). The region 3p14.2 is deleted in a variety of histologically different cancers including renal cell carcinoma, and cancers of the lung, pancreas, and cervix (Connolly *et al.*, 2000; Herzog *et al.*, 2001; Rabbitts, 1994; Sandberg, 1990; Solomon *et al.*, 1991).

*Correspondence: DI Smith, Department of Experimental Pathology, Mayo Foundation, Hilton 800, 200 First Street S.W., Rochester, MN 55905, USA; E-mail: smith.david@mayo.edu
Received 10 April 2002; revised 31 July 2002; accepted 7 August 2002

Previous data mapped a HPV16 viral integration from a cervical tumor within FRA3B (Wilke *et al.*, 1996). Both ends of this integration were defined, revealing the integration is associated with a 96 kb deletion within intron 4 of the FHIT gene. Recently an additional HPV16 cervical integration has been mapped to the 3p14.1 region with FISH-based analysis indicating the position of the integration is contained within the region of FRA3B fragility (Thorland *et al.*, 2002). Previous analyses had defined FRA3B as a large region of genomic instability covering ~500 kb (Paradee *et al.*, 1996; Rassool *et al.*, 1996; Wilke *et al.*, 1996; Zimonjic *et al.*, 1997). Unfortunately, the original data describing the instability at FRA3B did not fully define the boundaries of the fragility, with the telomeric boundary being defined by a cosmid that hybridizes centromeric to breakage at FRA3B in 10% of the metaphases. Similarly, the centromeric boundary is defined by a cosmid that hybridizes telomeric to breakage at FRA3B in 8% of the metaphases (Zimonjic *et al.*, 1997). The new HPV16 integration is located 2 Mb centromeric to the previously defined FRA3B region of instability therefore this led us to re-investigate the entire FRA3B region to completely characterize the 'center' as well as the 'ends' of the fragility. FISH and sequence-based analysis reveals fragility at FRA3B extends over a 4 Mb region containing five genes. In addition to FHIT, FRA3B contains protein tyrosine phosphatase receptor, gamma (PTPRG), HT021, calcium dependent activators for protein secretion (CADPS), spinocerebellar ataxia 7 (SCA7, Table 1). Gene expression analysis using cervical tumor-derived cell lines reveal that the majority of the genes in FRA3B are down-regulated whereas the surrounding genes do not demonstrate aberrant gene expression. Our data indicate that the region of genomic instability associated with FRA3B, is much larger than previously believed. This large region of defined genomic instability offers a possible explanation for the frequent deletions and alterations 3p14.2 in a variety of human cancers.

Results

Cervical tumor HPV16 integration at 3p14.2

RS–PCR, was previously employed to identify HPV16 genomic integrations into cervical tumor DNA (Thorland *et al.*, 2000, 2002). Initial sequence data revealed an HPV16 integration into a specific, non-repetitive region of the human genome localizing to 3p14.2.

We sought to confirm and further characterize this new HPV16 integration relative to the published FRA3B region. PCR was performed to validate the HPV16 integration site. A specific PCR primer in the cellular integration flanking sequence was designed. PCR amplification on cervical tumor DNA was performed using the cellular primer and HPV16 RS–PCR primers (Figure 1a). PCR products of the expected sizes were obtained for all three of the HPV16/cellular primer combinations (Figure 1b). These HPV16/cellular primer combinations did not amplify from normal human genomic DNA (data not shown). These data validate the viral integration and eliminate the possibility of a RS–PCR artifact. RS–PCR hybrid products were BLASTN searched in the NCBI non-redundant complete sequences (nr) and high throughput genomic sequences (htgs) databases to determine what similarities existed to the HPV16 and human genomes (Figure 1a). The BLASTN searches of the HPV16/human sequence hybrid reveals that the HPV16 portion of the PCR-rescued DNA fragment mapped to the HPV16 regulatory protein E2, whereas the human genomic portion mapped to unordered BAC clone RP11 129_K_20 localized to chromosome 3. Analysis of the integration site sequence reveals a 15 bp orphan sequence that can not be aligned with either the HPV16 or the human genomic sequence and creates a 12 bp direct repeat (Figure 1a). These results confirm the initial RS–PCR results and validate the site of viral integration within cervical tumor, CC61. FISH analysis on aphidicolin-treated metaphase chromosomes further positioned clone 129_K_20 cytogenetically to 3p14.2. As the ends of FRA3B had only been loosely defined, BAC 129_K_20 was used as a FISH-based probe to determine whether it was within the FRA3B region of instability.

FISH-based analysis of 50 aphidicolin-induced metaphase breaks at 3p14.2 revealed that clone 129_K_20 was contained within FRA3B. This BAC hybridized proximal to the region of aphidicolin-induced breakpoints in 42 out of 50 metaphases and distal in eight out of 50 metaphases (Figure 2; Table 2). Since FRA3B is cytogenetically localized to 3p14.2, we sought to further localize clone 129_K_20 relative to the published FRA3B site. Using the NCBI, the Santa Cruz Genome Center, and the San Antonio Genome Center public databases, we assembled a BAC contig around the published FRA3B fragile site (Paradee *et al.*, 1996; Rassool *et al.*, 1996). Unassembled BACs were aligned with the use of Sequencher 4.1.2 (Figure 3a). This revealed the cervical tumor CC61 integration to be ~2 Mb centromeric (proximal) to the previously defined HPV16 integration (Figure 3b). Only one end of this novel HPV16 integration has been localized at this time. This end localizes between two known genes, CADPS and SCA7. Therefore, unlike the previously identified HPV16 integration into FRA3B, in which a 96 kb intronic deletion between FHIT exons 4 and 5 was identified, it is not known whether this novel integration is also associated with a deletion or a more complex rearrangement.

Mapping the complete region of instability within FRA3B

Previous published reports estimated the size of FRA3B to be ~500 kb and completely contained within the FHIT locus (Paradee *et al.*, 1996; Rassool *et al.*, 1996). These previous data did not define the boundaries of fragility, but instead focused on the 'active' region which contains the previous HPV16 integration, a hereditary

Table 1 Genes contained within and surrounding common fragile site FRA3B (3p14.2)

Gene	*UniGene*	*Gene definition*	*Genomic size*[a]	*Approx. position*[b]	*RT oligonucleotide primers*[c]	*Produce size*[d]
ARHGEF3	Hs.6066	Rho guanine nucleotide exchange factor 4	120 kb	1.1 Mb	GTTCCTAAATCCCACCACC TGCTTCTCCAAACCGTTC	269
APPL	Hs.27413	Adaptor protein containing pH domain	45 kb	750 kb	ATGTGATTCTGTTGGACTG CCAAGGGGGAATATCTAC	317
ARF4	Hs.75290	ADP-ribosylation factor 4	20 kb	650 kb	TGCTACTTTTTGCAAACAAAC CCAAACCAGTCCCAGATAC	291
TU3A	Hs.8022		16 kb	500 kb	CCAGCTCATCAAGAAGAAG GTACAGAAGGGCTGAAGG	271
FHIT	Hs.77252	Fragile histidine triad gene	1.4 Mb	within FRA3B	GGCCAACATCTCATCAAG TTTCCTCCTCTGATCTCC	388
PTPRG	Hs.89627	Protein tyrosine phosphatase, receptor type, G	680 kb	within FRA3B	CAACTGGAGAATGAAAATG CTAGAGTCTGGCAAAAAAG	322
HT021	Hs.47166		15 kb	within FRA3B	AAAGATGACTTCCTTGTTTG GCTCTTCCTAAAAGAAACTG	321
CADPS	Hs.151301	Calcium dependent activator protein for secretion	70 kb	within FRA3B	TACAAGCAATATGGAGCAC GGTTCATTTTTTGGTTTTAG	335
SCA7	Hs.108447	Spinocerebellar ataxia 7	130 kb	within FRA3B	GTCTGTTTTCCCAACCTC GAAAGGTCTACAGTAACG	300
BAIAP1	Hs.169441	Brain-specific angiogenesis inhibitor-assoc. protein	200 kb	500 kb	AATTTTAGAGATCAATGGTGAG CACGTAAGCAAGCAAAAG	319
UBE1C	Hs.154320	Ubiquitin-activating enzyme E1C	40 kb	750 kb	ATTCCCTTGAATAATTACTTG GTTACCGACTGTAAGTAAAGTG	248
MITF	Hs.166017	Microphthalmai-associated transcription factor	286 kb	1 Mb	GCATCATGCAGACCTAAC GTCTCTTCCATGCTCATAC	255
β-tubulin	Hs.336780	Tubulin, beta polypeptide		Control gene	GCATCAACGTGTACTACAA TACGAGCTGGTGGACTGAGA	454
GAPDH	Hs.169476	glyceraldehyde-3-phosphate dehydrogenase		Control gene	ACCACAGTCCATGCCATCAC TCCACCACCCTGTTGCTTGTA	450
β2	Hs.75415	Beta-2-microglobulin		Control gene	AGCTGTGCTCGCGCTACTCTCTC GTGTCGGATTGATGAAACCCAGACAC	140

[a]Estimated genomic size as determined by sequence alignment and Santa Cruz genomic database. [b]Approximate gene distance relative to the proximal or distal ends of FRA3B as determined by sequence alignment and Santa Cruz genomic database. [c]Semi-quantitative RT–PCR oligonucleotide primers upper (forward) and lower (reverse) are shown 5′ to 3′. [d]Semi-quantitative RT–PCR product size (bp)

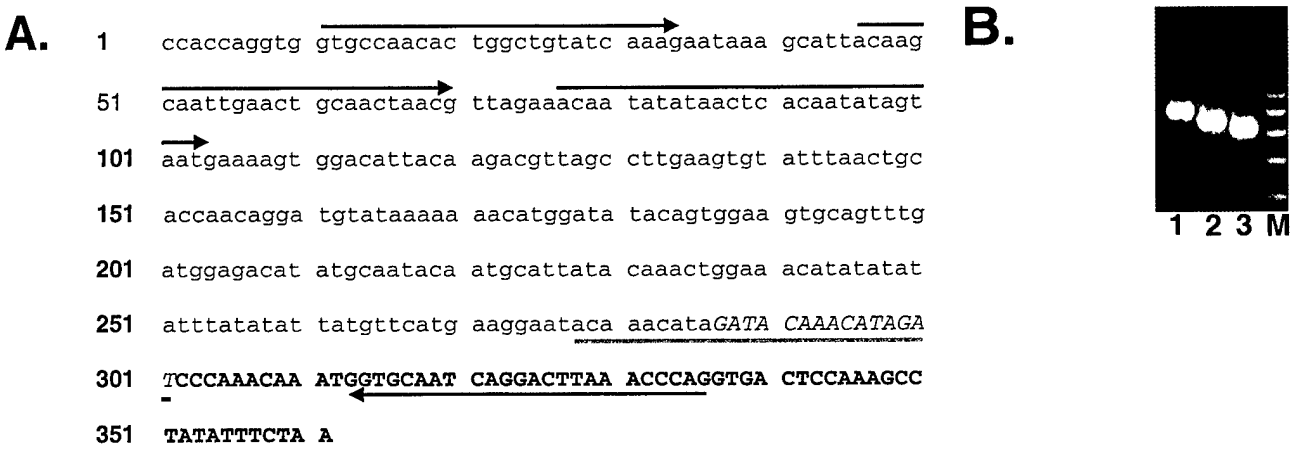

Figure 1 RS–PCR sequence results and integration confirmation for tumor CC61. (**a**) Lowercase letters indicate HPV16 sequence. Uppercase bold letters indicated human genomic sequence corresponding to BAC clone RP11 129_K_20 flanking the site of HPV16 integration. Uppercase italicized letters indicate bases that match neither HPV16 nor 129_K_20 sequences. The gray underlined letters indicate a 12 bp direct repeat at the site of viral integration. (**b**) Integration verification of the HPV16 integration in CC61. PCR was performed with three different oligonucleotides derived from HPV16 sequence (Thorland *et al*., 2000) (Lane 1: HPV16-2929-24D; Lane 2: HPV16-2964-25D; Lane 3: HPV16-2995-28D) and an oligonucleotide derived from the sequence flanking the site of HPV16 integration (5′-CTGGGTTTAAGTCCTGATTGCACC) corresponding to BAC 129_K_20. These primer combinations produce products of 326, 291, and 260 bp, respectively. Forward HPV16 specific (black arrows above sequence) and reverse 3p14.2 specific (black arrow below sequence) primers are indicated. Fifty bp ladder (M) is shown (right)

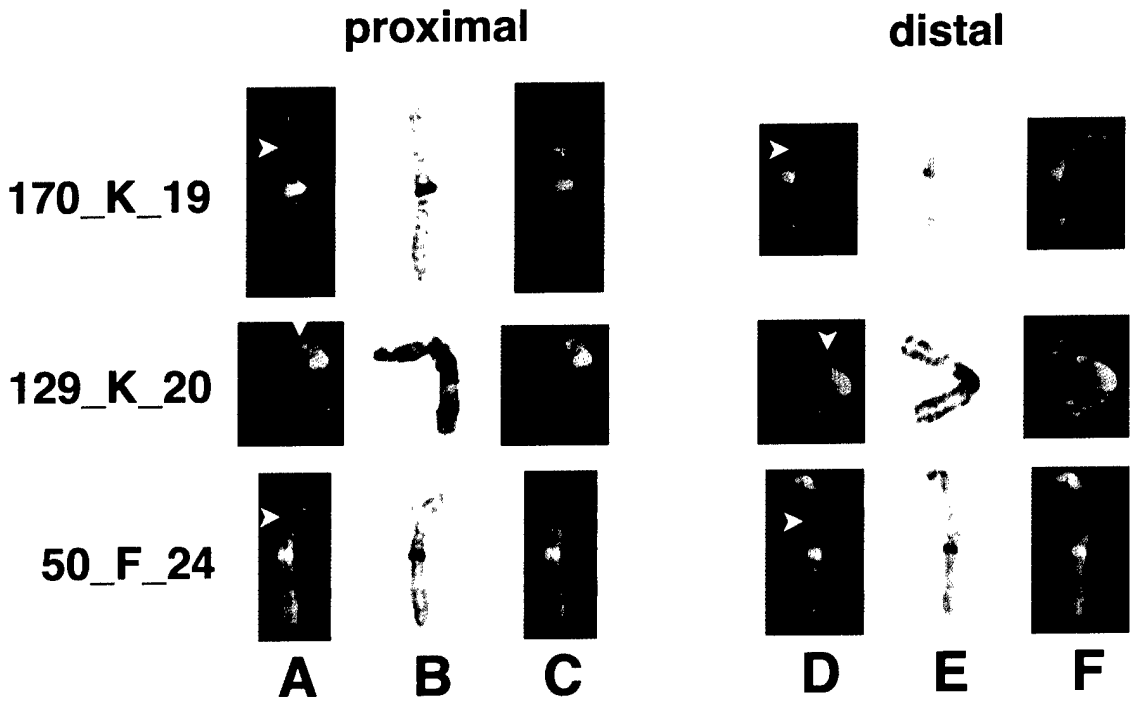

Figure 2 FISH-based analysis depicting aphidicolin-induced breakage at proximal and distal end of FRA3B (3p14.2). Breakage at 3p14.2 (white arrows) was initially identified using a DAPI image (**a**,**d**). Inverted DAPI banding confirmed breakage at 3p14.2 (**b**,**e**). Hybridization signal (green) of biotin-labeled specific BACs on the same aphidicolin-induced metaphase (**c**,**f**). Proximal (**a**–**c**) and distal (**d**,**e**) are shown for three BACs spanning the region of fragility. A summary of FISH results are shown in Table 2. BAC 170_K_19 (distal), 129_K_20 (HPV16 integration), 50_F_24 (proximal) are listed (left of panel)

Table 2 FISH analysis for BAC clones spanning the fragile site 3p14.2 (FRA3B)

		Location of fluorescent signal relative to chromosomal location 3p14.2		
Clones[a]	*# Breaks*[b]	*Proximal* (%)	*Crossing* (%)	*Distal* (%)
719_N_22	51	0 (0)	0 (0)	51 (100)
70_P_20	50	0 (0)	2 (4)	48 (96)
170_K_19	50	3 (6)	0 (0)	47 (94)
29_O_20	21	2 (9.5)	2 (9.5)	17 (81)
1_A_6	50	32 (64)	7 (14)	11 (22)
137_N_22	20	15 (75)	3 (15)	2 (10)
154_D_3	20	13 (65)	2 (10)	5 (25)
204_J_18	21	17 (80.9)	0 (0)	4 (19.1)
129_K_20	50	42 (80)	0 (0)	8 (20)
284_K_18	53	47 (88.7)	4 (7.5)	2 (3.7)
585_O_21	50	45 (90)	0 (0)	5 (10)
50_F_24	20	18 (90)	0 (0)	2 (10)
152_N_21	50	50 (100)	0 (0)	0 (0)

[a]Research Genetics RP-11 BAC clones hybridized to APC treated metaphase spreads. [b]Number of APC induced metaphase breaks analysed for breakage at 3p14.2. The breaks were scored as either proximal (centromeric), crossing the break, or distal (telomeric)

renal cell carcinoma translocation breakpoint (hRCC t(3:8) translocation), and aphidicolin induced breakpoint clusters (Wang *et al*., 1997; Zimonjic *et al*., 1997). Since clone 129_K_20, which is 2 Mb proximal to the previous HPV16 integration, still localizes within the region of aphidicolin-induced instability, this suggests that instability at FRA3B is significantly larger than previously published results indicate. To define the entire region of instability, we chose BACs across the region for FISH analysis on aphidicolin-induced metaphase chromosomes (Figure 3a). Using a single individuals blood culture, 50 metaphase breaks at FRA3B (3p14.2) were used to define the boundaries of fragility. A minimum of 20 breaks was counted when both proximal and distal breaks were observed for an individual BAC (Table 2). Our data indicates that RP11 152_N_21 and RP11 719_N_22 reside outside of FRA3B at its proximal and distal ends, respectively. Contig assembly across the region reveals that FRA3B fragility extends for approximately 4 Mb with the distal end contained within 3p14.2 and the proximal end extending into 3p14.1 (Figure 3a). One sequence gap is present that could not be closed by available sequence from the public databases (Figure 3a, double vertical black lines). This gap is located between FHIT exons 3 and 4.

Individual BAC clones hybridizing with approximately equal frequency proximally and distally to decondensation/breakage are observed within the FHIT locus between RP11 clones 137_N_22 and 29_O_20 (Figure 3a, Table 2). This localized region is considered the 'active' region, containing the previously published HPV16 integration site, the hRCC t(3:8) translocation, and the aphidicolin breakpoint clusters (Boldog *et al*., 1993; Cohen *et al*., 1979; Wang *et al*., 1997; Wilke *et al*., 1996; Zimonjic *et al*., 1997) (Figure 3b). Our assembled BAC contig for FRA3B contains five known genes: SCA7, CADPS, HT021, PTPRG, and FHIT. The first four genes are completely

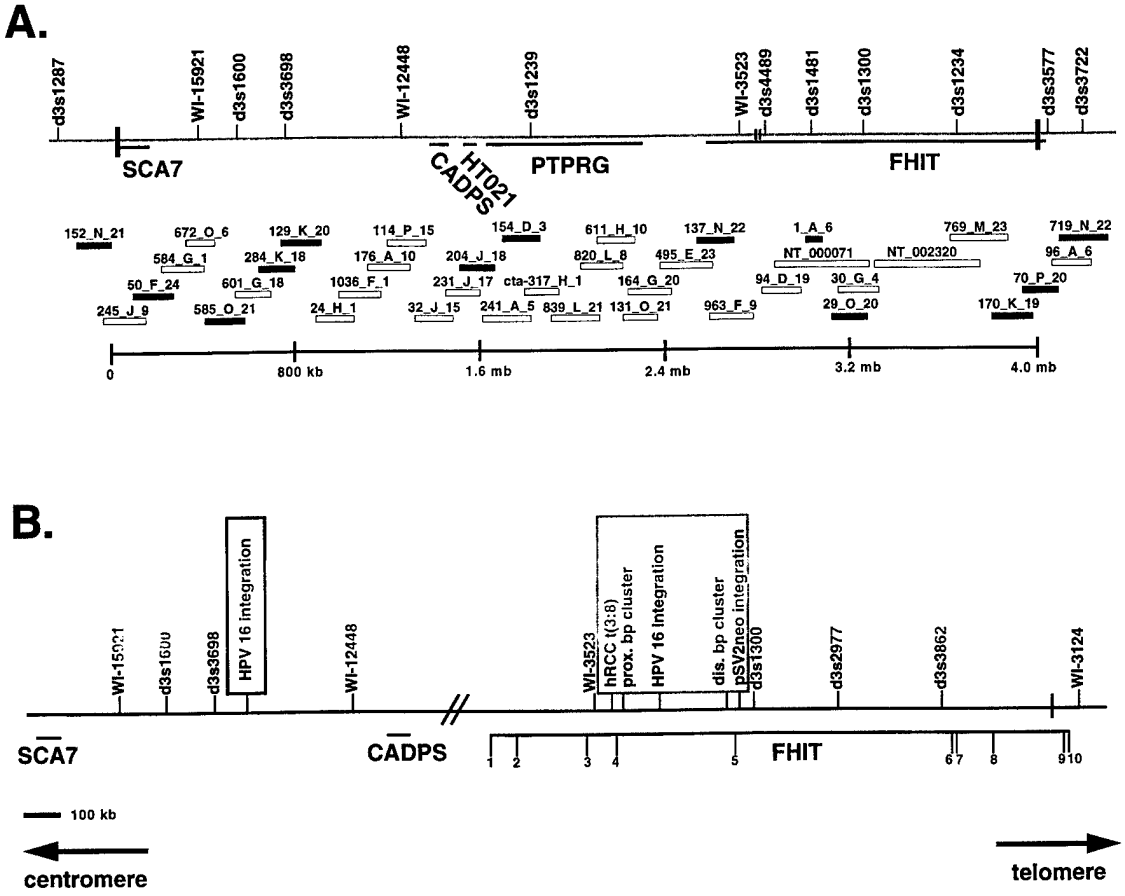

Figure 3 FRA3B BAC contig. (**a**) FRA3B BAC contig defining the proximal (centromeric) and distal (telomeric) ends. Markers across the region are indicated above the light gray line. The black vertical lines represent the proximal and distal ends for FRA3B. The double black vertical lines indicate sequence gaps of unknown size. The FRA3B genes and their relative genomic size (horizontal black lines) are indicated below the solid gray line. The NT numbers refer to complete NCBI sequences, 1_A_6 is a P1 cosmid clone (Paradee *et al.*, 1996), and cta-317_H_1 is a BAC clone sequenced by Washington University. All other clones are Research Genetics RP-11 BACs. BACs analysed by FISH (gray boxes) and BACs spanning the fragile site (white boxes) are indicated. The estimated genomic bp size of the region is indicated. (**b**) FRA3B 'active' site and new HPV16 integration. FRA3B 'active region' (gray box) depicts sites of integration, aphidicolin break points, a hRCC t(3:8) translocation previously mapped to the region (Paradee *et al.*, 1996; Wilke *et al.*, 1996). New HPV16 integration (black box) from tumor CC61 is indicated. FRA3B genes and their genomic size (horizontal black lines) are indicated with FHIT exons marked. Markers across the region are indicated above the black line. The black vertical line (telomeric end) represents the FRA3B proximal end. Double black vertical lines indicate sequence break FRA3B genes CADPS and FHIT. Directions of centromere and telomere are shown (bottom). A 100 kb reference size is also provided

contained within the fragile site with SCA7 being on the very proximal end of FRA3B. Sequence analysis indicates that the 3′ end of SCA7 is approximately 10 kb from BAC 152_N_21, which is outside the region of FRA3B fragility (Figure 3a). Only FHIT has a portion of the gene outside of the fragile site, with exons 9 and 10 localizing distal to the region of fragility (Figure 3).

Expression analysis of genes in and surrounding FRA3B

We assessed the expression of all genes within and surrounding the FRA3B region of instability in nine tumor-derived cervical cell lines. Previous work has demonstrated aberrant transcripts and loss of FHIT expression in cervical cell lines (Connolly *et al.*, 2000; Greenspan *et al.*, 1997; Hendricks *et al.*, 1997). In addition, FHIT and PTPRG, two genes contained within FRA3B, have been proposed to be tumor suppressor genes (Cool and Fischer, 1993; Druck *et al.*, 1998).

For this analysis, we performed semi-quantitative RT–PCR on tumor-derived cervical cell lines using cultured keratinocytes as our normal control. Oligonucleotide DNA primers were designed to specifically amplify each of the five FRA3B genes (Table 1). These primers were optimized and multiplex RT–PCR was performed with either GAPDH primers or β-tubulin primers as controls. CADPS was not expressed in normal keratinocytes and was not further analysed for expression in the cervical cell lines. Of the remaining four genes, three (FHIT, PTPRG, and HT021) demonstrated aberrant gene expression (Figure 4). SCA7 was expressed in all cell lines analysed with intensities similar to normal keratinocytes. FHIT, however, had a complete loss of detectable expression in 66% (six out of nine) of the cell lines with apparent down regulation in the remaining three cell lines (Figure 4).

HT021 and PTPRG had complete LOE in 44.4% (four out of nine) and 22.2% (two out of nine), respectively. PTPRG was up regulated in two of the cell lines (Figure 4, lanes 7 and 9) and down regulated in an additional two cell lines (Figure 4, lanes 4 and 5). By comparison, HT021 had down regulation in one cell line (Figure 4, lane 4) and normal expression in the remaining four cell lines (Figure 4, lanes 6, 9, 10, and 11). These data reveal that three out of five genes in FRA3B have either complete loss of expression or aberrant gene expression in the analysed cervical cell lines.

To determine if only genes contained within FRA3B demonstrated aberrant gene expression, we also analysed genes outside the region of fragility (Figure 4, Table 1). Genes outside of FRA3B were chosen at random for analysis. The genes chosen localized between 500 kb and 1 Mb proximal or distal to the BACs, which defined the proximal and distal ends of the FRA3B region of instability (Table 1). Four distal (telomeric) genes were analysed, ARHGEF3, APPL, ARF4, and TU3A (Table 1). TU3A was not expressed in normal keratinocytes and was not further analysed for expression in the cervical cell lines. The remaining three genes (ARHGEF3, APPL, ARF4) all demonstrated expression levels similar to the normal control (Figure 4). Only APPL indicated lower expression levels, but no complete loss in any of the cell lines analysed (Figure 4). Three proximal (centromeric) genes were analysed, BAIAP1, UBE1C, and MITF (Table 1). Two of the three (UBE1C and BAIAP1) proximal genes did not demonstrate aberrant gene expression (Figure 4). MITF was up-regulated in two of the examined cervical cell lines (Figure 4, lanes 3 and 6), but did not demonstrate loss of expression in any of the remaining cell lines (Figure 4).

Discussion

The integration of high-risk HPV subtypes is temporally associated with the development and/or progression of cervical cancer (Choo, 1998). It remains to be determined, however, if these integration events are pivotal in the development of cervical cancer. The genomic positions of HPV integrations have been of great interest to determine the significance of the integration site in cervical cancer development. Initial cytogenetic studies localized a high percentage of HPV genomic integrations to bands containing CFSs (Popescu *et al*., 1990). We previously demonstrated at the molecular level that HPV16 integration events preferentially occur (~ 50% of integrations analysed) within CFSs (Thorland *et al*., 2000, 2002). Preferential viral integration suggests that a unique feature exists within these unstable regions, but it is not known if this feature is solely the fragility within CFSs or the targeting of specific genes. Interestingly, many of the characterized integration events occurred within or immediately adjacent to genes proposed to play a role in cancer development. This not only supports the

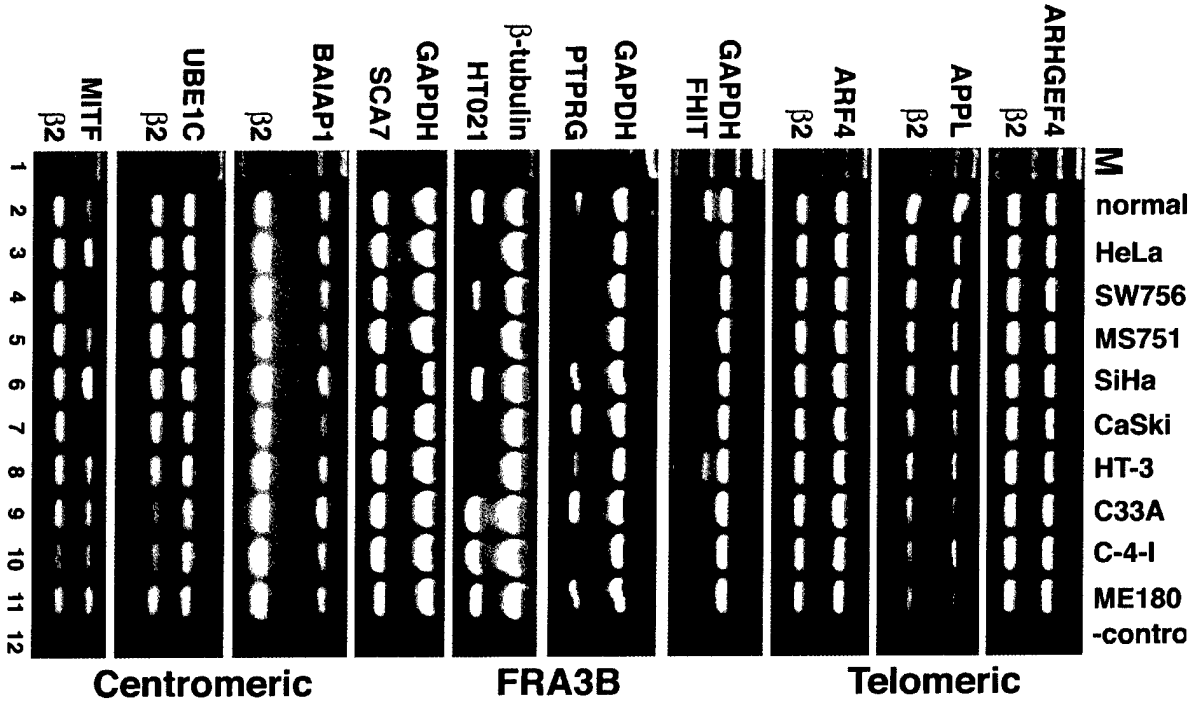

Figure 4 Semi-quantitative RT–PCR for genes in and surrounding FRA3B. Genes analysed along with internal control are indicated (left of panel). The normal control (cultured keratinocytes), tumor-derived cell lines, and negative control (H_2O) are shown (top of panel). Relative gene position is indicated (right of panel). Expected gene product size is described in Table 1. One hundred bp ladder (M, lane 1)

hypothesis that the integration events may be targeting regions of instability, such as the CFSs, but also indicates that genes at the site of integration may be important in the development of cervical cancer.

In this report, we further characterized a previously defined (Thorland *et al.*, 2002) single HPV16 integration event that occurred within FRA3B at 3p14.2. FISH analysis revealed that a BAC clone which spanned this integration mapped within the proximal end of FRA3B even though the integration occurred more than 2 Mb centromeric to the HPV16 integration originally described by Wilke *et al.*, 1996 (Figure 3a). The new HPV16 integration did not occur within any known gene or EST, but instead localizes between the two known genes SCA7 and CADPS (Figure 3). The other end of this HPV16 integration has not been identified, so it is not known if this integration is associated with a deletion at 3p14.2 or a more complex translocation. In addition, sequence analysis at the HPV16 integration site identified a short 15 bp sequence that is not associated with either HPV16 or human sequences at 3p14.2 (Figure 1a). This unknown sequence creates a 12 bp direct repeat that is located at the junction between the HPV and human sequences (Figure 1a). Orphan sequences such as this have been observed at the junctions of other HPV integrations (Gallego *et al.*, 1997). These sequences may be derived from cellular sequences involved in the integration process or may be due to illegitimate repair after the integration event. However, this novel sequence was not observed in any of the other HPV16 integrations described by Thorland *et al.* (2000, 2002).

The identification of this new HPV16 integration led to the complete characterization of the region of instability surrounding FRA3B. In the previous analysis of FRA3B, a 500 kb cosmid contig around the HPV16 integration described by Wilke *et al.*, 1996 was constructed with cosmids derived from the original YAC (850A6) that was found to span the hRCC (Paradee *et al.*, 1996; Rassool *et al.*, 1996). These cosmid clones were used as FISH-based probes to characterize the FRA3B region and this defined the 'center' of FRA3B instability as localizing between FHIT exons 4 and 5. However, these data did not define the 'ends' or boundaries of fragility in FRA3B. Based upon the HPV16 integration which is 2 Mb centromeric of the 'center' of FRA3B, but which still occurs within the region of instability, we sought to completely characterize the region of instability at FRA3B. To define the boundaries of fragility we assessed 50 metaphase breaks for each BAC clone at 3p14.1-3p14.2, offering a more comprehensive definition of the ends of FRA3B (Table 2).

In addition to defining the boundaries of fragility, we also wanted to determine the FRA3B 'active' site and compare this with results with previous reports (Paradee *et al.*, 1996; Rassool *et al.*, 1996). The 'active' site for a CFS can be defined as the region of instability where breakage, determined by FISH-based analysis, occurs with a relatively equal frequency both proximal and distal to the large insert clone tested. Our data indicate the FRA3B 'active' site remains between exons 4 and 5 of the FHIT locus, which agrees with previous reports (Paradee *et al.*, 1996; Rassool *et al.*, 1996). However, the 'active' site is not in the physical center of the fragile site. The proximal end for FRA3B extends ~3 Mb beyond the center of instability, whereas the distal end only extends ~700 kb (Figure 3). Interestingly, the most proximal gene, SCA7, contains an unstable (CAG) trinucleotide repeat in the coding sequence. In RFSs a link has been made between unstable repeats, either trinucleotide (CCG) repeats or mini-satellite (AT) expansions, and the mechanism of RFS fragility (Usdin and Woodford, 1995; Verkerk *et al.*, 1991). Although the trinucleotide expansion in SCA7 patients is different (CAG *vs* CCG), both of these expansions result in unusual structures *in vitro* that could inhibit replication machinery (Kang *et al.*, 1995; Parniewski *et al.*, 1999; Usdin and Woodford, 1995). Since the mechanism for RFS fragility is not completely understood, but known to be linked to unstable expansions associated with a disease-state, it is possible that the variable, unstable SCA7 CAG repeat found even in normal individuals is sufficient to affect fragility without having the full disease state expansion. The presence of SCA7 in FRA3B is the first unstable trinucleotide repeat that has been shown to be contained within a CFS and may offer a potential link between CFSs and RFSs in terms of their mechanism of fragility.

To determine if any of the five known genes within FRA3B are targeted for gene inactivation in cervical cancer, we assessed gene expression in nine tumor-derived cervical cell lines. Expression analysis revealed that the very large PTPRG and FHIT genes were down-regulated or showed LOE in cervical tumor cell lines. This indicates that there may be a targeting of the 'large' genes in FRA3B, but HT021 (an average-sized gene covering ~60 kb) also had marked inactivation. The most proximal gene, SCA7, did not reveal any down regulation (Figure 4). Since this gene is on the very end proximal of FRA3B, the instability associated with this site may not have an effect on gene regulation. In order to confirm that the genes within FRA3B may be specifically targeted for gene inactivation in cervical tumor-derived cell lines, we also assessed the expression of genes outside the region of FRA3B instability (Figure 4). The surrounding genes did not indicate loss of expression or down-regulation (Figure 4). These data support our FISH-based observations of a 4 Mb region of FRA3B instability and demonstrates that the genes within the region of fragility are being targeted for gene inactivation. Several previous studies, using different tumor types, have determined that the aberrant and alternative transcripts associated with FHIT expression are a complex combination of methylation changes and genomic deletions (Gonzalez *et al.*, 1998; Huebner *et al.*, 1998; Tanaka *et al.*, 1998; Vertino *et al.*, 1993; Zochbauer-Muller *et al.*, 2001). In addition, a recent publication studied alterations in the FHIT/FRA3B

region by generating somatic cell hybrid that separated chromosome 3 homologs from each. The data reveal multiple different chromosome 3 homologs isolated from each individual cell line (Corbin *et al.*, 2002). The net effect is that the instability within this region generates a great deal of heterogeneity and complexity.

The data generated in this paper is in complete agreement with previously published reports characterizing FRA3B (Kastury *et al.*, 1996; Paradee *et al.*, 1996). The key distinction is that we have now more comprehensively analysed clones from this region to define the ends of decondensation/breakage in the FRA3B region. It is interesting that the 'active' center of this region is not in the physical center of this fragile site. The proximal end for FRA3B extends for ~3 Mb beyond the center of instability, whereas the distal end extends ~700 kb. FISH and sequence analysis reveals the region of instability for FRA3B fully extends over a 4 Mb region containing five genes. Our data indicates that the regions of genomic instability associated with CFSs, specifically FRA3B, are much larger than previously believed. This large region of defined genomic instability offers an explanation for why 3p14.2 has been shown to be involved in a variety of cancers including cervical cancer. The data generated defining the FRA3B ends will allow for further analysis of this region of instability.

Materials and methods

Cervical tumor samples, RS–PCR, and HPV16 integration identification

Cervical tumors, grade 2–4 squamous cell carcinomas, were obtained from 26 patients. DNA was extracted and HPV typing was preformed as described in Gostout *et al.* (1998). RS–PCR (Sarkar *et al.*, 1993) was performed on samples using oligonucleotide primers and conditions previously described (Thorland *et al.*, 2000, 2002).

BAC clone selection and FRA3B contig assembly

Sequenced RS–PCR products were BLASTN searched in both the National Center for Biotechnology Information (http://www.ncbi.nlm.nih.gov) non-redundant complete sequences (nr) and high throughput genomic sequences (htgs) databases to determine what similarities existed to the HPV16 and human genomes. BACs containing the human genomic sequence were obtained from Research Genetics and extracted BAC DNA was used as a probe for FISH-based cytogenetic localization. A BAC contig surrounding the published FRA3B region was assembled using the NCBI, the Santa Cruz Genome Center (http://genome.ucsc.edu), and the San Antonio Genome Center (http://apollo.uthscsa.edu) public databases. Unassembled BACs were aligned using Sequencher 4.1.2 (Gene Codes Corp., Ann Arbor, MI, USA).

Cytogenetic localization of clones

Metaphase preparations were obtained from blood cultures established from 1 ml of peripheral whole blood and 9 ml of Chang Media PB (Irvine Scientific, Santa Ana, CA, USA). Cultures were incubated at 37°C in 5% CO_2 for 72 h. Twenty-four hours prior to harvest, the cultures were induced with 0.4 μM aphidicolin (Sigma-Aldrich, St. Louis, MO, USA) solution. Cell harvest and metaphase preparations followed routine cytogenetic techniques.

For each BAC clone, standard nick translation was used to incorporate biotin-16-dUTP (Boehringer/Roche, Indianapolis, IN, USA) into 1 μg of purified BAC DNA followed by precipitation and hybridization to aphidicolin-treated metaphase chromosomes according to the protocol described by Verma and Babu (1989). Probe detection and amplification followed the manufacturer's protocols (Ventana Medical Systems, Tucson, AZ, USA) with minor modifications. Chromosomes were counterstained with DAPI. Photomicroscopy was performed using a Zeiss Axioplan 2 fluorescence microscope and Powergene MacProbe software (Applied Imaging, Santa Clara, CA, USA). The position of each individual BAC clone relative to FRA3B was determined by the analysis of aphidicolin-treated metaphases with breakage at 3p14.2. A minimum of 50 breaks at 3p14.2 was used to define the proximal and distal ends. Breakage at 3p14.2 was identified by band location as established by DAPI banding. A clone was determined to be within the fragile site region if hybridization signal was observed on both sides of decondensation/breakage or if signal was observed as occurring proximal (centromeric) in one metaphase and distal (telomeric) in a separate metaphase.

Cell culture and RNA isolation

Primary keratinocytes were cultured as previously described and used as a normal control (Poumay and Pittelkow, 1995). Nine cervical tumor-derived cell lines (HeLa, SW756, MS751, SiHa, CaSki, HT-3, C-33-A, C-4-I, and ME-180) were obtained from the American Type Culture Collection. The cells were maintained at 37°C in 5% CO_2 in their recommended media. Total RNA was extracted from normal cultured keratinocytes and tumor-derived cervical cell lines using TRIZOL reagent (GibcoBRL, Rockville, MD, USA) following the manufacturer's instructions.

Semi-quantitative RT–PCR

For each reverse transcription (RT) reaction, DNA was eliminated by treating 5 μg of total RNA with RNase-free DNase I for 15 min at 25°C followed by DNase I inactivation by addition of 2 mM $MgCl_2$ and incubation at 65°C for 10 min. DNase-treated RNA RT was performed using MMLV-RT (GibcoBRL, Rockville, MD, USA).

Gene specific DNA oligonucleotide primers were designed for the genes contained within and surrounding FRA3B using Oligo 6.4 software (Molecular Biology Insights, Cascade, CO, USA) and multiplexed for semi-quantitative RT–PCR with either β-tubulin, GAPDH, or β2 control primers (Table 1). Oligonucleotide primers were obtained from Integrated DNA Technologies (Coralville, IA, USA). The semi-quantitative RT–PCR reactions (12.5 μl total volume) contained 50 ng of reverse-transcribed cDNAs, 50 mM KCl, 10 mM Tris-HCl (pH 8.3), 0.2 mM dNTPs, 1.5 mM $MgCl_2$, 5 pmol of each gene specific primer, 0.5 pmol of the control primer and 0.1 U of Taq polymerase (Promega, Madison, WI, USA). The conditions for amplification were: 98°C for 3 min, then two cycles of 98°C for 30 s, 55–59°C for 30 s, and 72°C for 30 s, followed by 28 cycles of 94°C for 30 s, 55–59°C for 30 s, and 72°C for 30 s with a final extension of 72°C for 10 min. Samples were analysed by ethidium bromide agarose gel electrophoresis.

Abbreviations

BAC, bacterial artificial chromosome; CFS, common fragile site; FISH, fluorescence *in situ* hybridization; FS, fragile site; HPV, human papillomavirus; Mb, megabase pairs

Acknowledgments

Supported by NIH Grant CA 48031 and Department of Defense Grant DAMD 17-99-1-9504 to DI Smith.

References

Boldog FL, Gemmill RM, West J, Robinson M, Robinson L, Li E, Roche J, Todd S, Waggoner B, Lundstrom R, Jacobson J, Mullokandov MR, Klinger H and Drabkin HA. (1997). *Hum. Mol. Genet.*, **6,** 193–203.

Boldog FL, Gemmill RM, Wilke CM, Glover TW, Nilsson AS, Chandrasekharappa SC, Brown RS, Li FP and Drabkin HA. (1993). *Proc. Natl. Acad. Sci. USA,* **90,** 8509–8513.

Choo KR. (1998). *The genetic basis of human cancer.* Vogelstein B and Kinzler KW (ed). New York: McGraw-Hill, Inc., pp. 631–637.

Cohen AJ, Li FP, Berg S, Marchetto DJ, Tsai S, Jacobs SC and Brown RS. (1979). *N. Engl. J. Med.*, **301,** 592–595.

Connolly DC, Greenspan DL, Wu R, Ren X, Dunn RL, Shah KV, Jones RW, Bosch FX, Munoz N and Cho KR. (2000). *Clin. Cancer Res.*, **6,** 3505–3510.

Cool DE and Fischer EH. (1993). *Semin. Cell Biol.*, **4,** 443–453.

Coquelle A, Pipiras E, Toledo F, Buttin G and Debatisse M. (1997). *Cell,* **89,** 215–225.

Corbin S, Neilly ME, Espinosa III R, Davis EM, McKeithan TW and LeBeau MM. (2002). *Cancer Res.*, **62,** 3477–3484.

Druck T, Berk L and Huebner K. (1998). *Oncol. Res.*, **10,** 341–345.

Fang JM, Arlt MF, Burgess AC, Dagenais SL, Beer DG and Glover TW. (2001). *Genes Chromosomes Cancer,* **30,** 292–298.

Gallego MI, Schoenmakers EFPM, Van de Ven WJM and Lazo PA. (1997). *Mol. Carcinog.*, **19,** 114–121.

Glover TW, Coyle-Morris JF, Li FP, Brown RS, Berger CS, Gemmill RM and Hecht F. (1988). *Cancer Genet. Cytogenet.*, **31,** 69–73.

Glover TW and Stein CK. (1987). *Am. J. Hum. Genet.*, **41,** 882–890.

Glover TW and Stein CK. (1988). *Hum. Genet.*, **43,** 265–273.

Gonzalez MV, Pello MF, Ablanedo P, Suarez C, Alvarez V and Coto E. (1998). *J. Clin. Pathol.*, **51,** 520–524.

Gostout BS, Podratz KC, McGovern RM and Persing DH. (1998). *Am. J. Obstet. Gynecol.*, **179,** 56–61.

Greenspan DL, Connolly DC, Wu R, Lei RY, Vogelstein JT, Kim YT, Mok JE, Munoz N, Bosch FX, Shah KV and Cho KR. (1997). *Cancer Res.*, **57,** 4692–4698.

Hendricks DT, Taylor R, Reed M and Birrer MJ. (1997). *Cancer Res.*, **57,** 2112–2115.

Herzog C, Crist K, Sabourin C, Kelloff G, Boone C, Stoner G and You M. (2001). *Mol. Carcinog.*, **30,** 159–168.

Huang H, Qian JH, Proffit J, Wilber K, Jenkins RB and Smith DI. (1998). *Oncogene,* **16,** 2311–2319.

Huebner K, Garrison PN, Barnes LD and Croce CM. (1998). *Ann. Rev. Genet.*, **32,** 7–31.

Kang S, Oshshima K, Shimizu M, Amirhaeri S and Wells RD. (1995). *J. Biol. Chem.*, **270,** 27014–27021.

Kastury K, Ohta M, Lasota J, Moir D, Dorman T, LaForgia S, Druck T and Huebner K. (1996). *Genomics,* **32,** 225–235.

Krummel KA, Roberts LR, Kawakami M, Glover TW and Smith DI. (2000). *Genomics,* **69,** 37–46.

Mishmar D, Rahat A, Scherer SW, Nyakatura G, Nihzmann B, Kohwi Y, Mandel-Gutfroind Y, Lee JR, Drescher B, Sas DE, Margalit H, Platzer M, Weiss A, Tsui LC, Rosenthal A and Kerem B. (1998). *Proc. Natl. Acad. Sci. USA,* **95,** 8141–8146.

Paradee W, Wilke CM, Wang L, Shridhar R, Mullins CM, Hoge AW, Glover TW and Smith DI. (1996). *Genomics,* **35,** 87–93.

Parniewski P, Bacolla A, Jaworski A and Wells RD. (1999). *Nucleic Acids Res.*, **27,** 616–623.

Popescu NC, Zimonjic DB and DiPaolo JA. (1990). *Hum. Genet.*, **84,** 383–386.

Poumay Y and Pittelkow MR. (1995). *J. Invest. Dermatol.*, **104,** 271–276.

Rabbitts TH. (1994). *Nature,* **372,** 143–149.

Rassool FV, Le Beau MM, Shen ML, Neilly ME, Espinosa III R, Ong ST, Boldog FL, Drabkin H, McCarroll R and McKeithan TW. (1996). *Genomics,* **35,** 109–117.

Rassool FV, McKeithan TW, Neilly ME, van Melle E, Espinosa R and Le Beau MM. (1991). *Proc. Natl. Acad. Sci. USA,* **88,** 6657–6661.

Sandberg AA. (1990). *The chromosome in human cancer and leukemia.* 2nd edn. New York: Elsevier Science Publishing Co., Inc, 1315 pp.

Sarkar G, Turner RT and Bolander ME. (1993). *PCR Methods Appl.*, **2,** 318–322.

Smeets DF, Scheres JM and Hustinx TW. (1986). *Hum. Genet.*, **72,** 215–220.

Solomon E, Borrow J and Goddard AD. (1991). *Science,* **254,** 1153–1160.

Tanaka H, Shimada Y, Harada H, Shinoda M, Hatooka S, Imamura M and Ishizaki K. (1998). *Cancer Res.*, **58,** 3429–3434.

Tatarelli C, Linnenbach A, Mimori K and Croce CM. (2000). *Genomics,* **68,** 1–12.

Thorland EC, Myers SL, Persing D, Sarkar G, McGovern RM, Gostout BS and Smith DI. (2000). *Cancer Res.*, **60,** 5916–5921.

Usdin K and Woodford KJ. (1995). *Nucleic Acids Res.*, **23,** 4202–4209.

Verkerk A, Pieretti M, Sutcliffe JS, Fu YH, Kuhl D, Pizzuti A, Reiner O, Richards S, Victoria MF, Zhang F, Eussen BE, van Ommen G-JB, Blonden L, Riggins GJ, Chastain JL, Kunst GH, Caskey CT, Nelson D, Oostra BA and Warren ST. (1991). *Cell,* **65,** 905–914.

Verma RS and Babu A. (1989). *Human Chromosomes: Manual of Basic Techniques.* Verma RS and Babu A (ed). New York: Pergamon Press, Inc., 240 pp.

Vertino PM, Spillare EA, Harris CC and Baylin SB. (1993). *Cancer Res.*, **53,** 1684–1689.

Walboomers JMM, Jacobs MV, Manos MM, Bosch FX, Kummer A, Shah KV, Sniders PJF, Peto J, Meuer CJLM and Munoz N. (1999). *J. Path.*, **189,** 12–19.

Wang L, Paradee W, Mullins C, Shridhar R, Rosati R, Wilke CM, Glover TW and Smith DI. (1997). *Genomics,* **41,** 485–488.

Wilke CM, Hall BK, Hoge AW, Pardee W, Smith DI and Glover TW. (1996). *Hum. Mol. Genet.*, **5,** 187–195.

Zimonjic DB, Druck T, Ohta M, Kastury K, Croce CM, Popescu NC and Huebner K. (1997). *Cancer Res.*, **57**, 1166–1170.

Zochbauer-Muller S, Fong KM, Maitra A, Lam S, Geradts J, Ashfaq R, Virmani AK, Milchgrub S, Gazdar AF and Minna JD. (2001). *Cancer Res.*, **61**, 3581–3585.

MS#12

Oncogene (2003) 22, 590–601

www.nature.com/onc

Characterization of the common fragile site *FRA9E* and its potential role in ovarian cancer

Gwen Callahan[1,2], Stacy R Denison[2], Leslie A Phillips[2], Viji Shridhar[2] and David I Smith*[,2]

[1]*Tumor Biology Program, Mayo Graduate School, Mayo Foundation, 200 First Street SW, Rochester, MN 55905, USA;* [2]*Division of Experimental Pathology, Department of Laboratory Medicine and Pathology, Mayo Foundation, 200 First Street SW, Rochester, MN 55905, USA*

Common fragile sites (CFSs) are regions of profound genomic instability that have been hypothesized to play a role in cancer. The major aim of this study was to locate a fragile region associated with ovarian cancer. Differential display (DD)-PCR analysis comparing normal ovarian epithelial cultures and ovarian cancer cell lines identified pregnancy-associated plasma protein-A (*PAPPA*) because of its frequent loss of expression (LOE) in ovarian cancer cell lines. *PAPPA* is localized to human chromosome 9q32–33.1, a region associated with significant loss of heterozygosity (LOH) in ovarian tumors (>50%) and in close proximity to the *FRA9E* CFS. FISH analysis determined that *PAPPA* was contained within the distal end of *FRA9E*. Characterization of *FRA9E* determined that aphidicolin-induced instability extended over 9 Mb, identifying *FRA9E* as the largest CFS characterized to date. Comprehensive LOH analysis revealed several distinct peaks of LOH within *FRA9E*. Semiquantitative RT–PCR analysis of 16 genes contained within *FRA9E* indicated that genes showing LOE in ovarian tumors coincided with regions of high LOH. *PAPPA* displayed the most significant loss (72%). This study provides evidence to suggest that instability within *FRA9E* may play an important role in the development of ovarian cancer and lends further support for the hypothesis that CFSs may be causally related to cancer.
Oncogene (2003) **22,** 590–601. doi:10.1038/sj.onc.1206171

Keywords: common fragile sites; *FRA9E*; chromosomal deletions; ovarian cancer; *PAPPA*

Introduction

A chromosomal fragile site is a locus that experiences nonrandom gaps or breakage when cells are cultured under appropriate conditions. Fragile sites have been categorized into two classes, rare and common, based on their relative frequency of occurrence and further subcategorized according to the specific chemicals that induce their expression. Rare fragile sites (RFSs) are observed in less than 5% of the population and inherited in a Mendelian codominant fashion. In contrast, the common fragile sites (CFSs) are present in virtually all individuals. The vast majority of the CFSs (84 of 89) are induced by aphidicolin (APC), a DNA polymerase α/δ inhibitor.

Most of the molecular information about fragile sites was obtained from the cloning and characterization of several RFSs. Each of these has been associated with the expansion of unstable repeat sequences (Oberle *et al.*, 1991; Verkerk *et al.*, 1991; Knight *et al.*, 1993; Jones *et al.*, 1994; Nancarrow *et al.*, 1994; Ritchie *et al.*, 1994; Yu *et al.*, 1997; Hewett *et al.*, 1998). For three of the 29 known RFSs, an association between expanded repeat sequences, chromosomal fragility, and a disease phenotype has been established. Trinucleotide repeat expansions at *FRAXA* (Xq27.3) and *FRAXE* (Xq28) are associated with heritable mental retardation, and similar expansions at *FRA11B* (11q23.3) have been implicated in a predisposition to the chromosomal deletion disorder, Jacobsen syndrome (Jones *et al.*, 1995; Sutherland *et al.*, 1998).

Unlike the RFSs, the biological consequence of instability within the CFSs is unclear, as is the underlying cause of their instability. Yunis and Soreng (1984) first proposed that CFSs play a causal role in the oncogenic process. This hypothesis originated from the observation that structural anomalies documented in various cancers cytogenetically coincided with the positions of CFSs. In addition, each of the five cloned and characterized CFSs, *FRA3B* (3p14.2), *FRA7G* (7q31.2), *FRA7H* (7q32.3), *FRA16D* (16q23.2), and *FRAXB* (Xp22.3), has been associated with either cancer-specific chromosomal rearrangements, a region of high loss of heterozygosity (LOH) in many cancer types, sites of viral integration, and or gene(s) showing a loss of expression (LOE) in one or more tumor types (Wilke *et al.*, 1996; Huang *et al.*, 1998a, b; Mishmar *et al.*, 1998; Smith *et al.*, 1998; Bednarek *et al.*, 2000; Krummel *et al.*, 2000; Mangelsdorf *et al.*, 2000; Paige *et al.*, 2000; Arlt *et al.*, 2002). However, there remains no concrete evidence of a causal relation between the genomic instability within the CFSs and the development and/or progression of cancer.

Today, ovarian cancer comprises approximately 4% of new cancer cases and 5% of cancer deaths in females, making it the most common cause of death from

*Correspondence: DI Smith, E-mail: smith.david@mayo.edu
Received 9 September 2002; revised 15 October 2002; accepted 22 October 2002

gynecological malignancy (Gabra and Smyth, 1997; Landis *et al*., 1998). In the United States, during 2002, the estimated numbers of new ovarian cancer cases and deaths are projected to be 23,300 and 13,900, respectively (Jemal *et al*., 2002). In order to identify genes important in the development of ovarian cancer, we performed differential display-PCR (DD-PCR) analysis of short-term cultured normal ovarian surface epithelial (OSE) cells versus five low-passage ovarian cancer cell lines established at the Mayo Clinic, as well as the NIH ovarian cancer cell line, OVCAR5 (Hamilton *et al*., 1984; Conover *et al*., 1998). One of the consistently downregulated genes encodes pregnancy-associated plasma protein-A (PAPP-A), one of four proteins originally isolated in 1974 from normal human pregnancy serum and more recently described as the IGF-dependent protease that cleaves insulin-like growth factor binding protein-4 (IGFBP-4) (Lin *et al*., 1974; Lawrence *et al*., 1999). *PAPPA* has been localized to human chromosome 9q32–33, a region associated with a high frequency of LOH in ovarian tumors, which also contains the CFS, *FRA9E* (Glover *et al*., 1984; Silahtaroglu *et al*., 1993; Schultz *et al*., 1995). In addition, recurrent under-representation of the chromosome arm 9q has been documented by comparative genomic hybridization (CGH) analysis (Sonoda *et al*., 1997). We determined that *PAPPA* was situated within the distal portion of *FRA9E*; therefore, we fully characterized the *FRA9E* CFS and investigated this highly unstable chromosomal region for LOH in ovarian tumors and for LOE of genes mapped within this CFS, including *PAPPA*.

Results

Cloning and characterization of FRA9E

DD-PCR was performed on short-term cultures of normal OSE versus five low-passage, ovarian cancer-derived cell lines generated at the Mayo Clinic and the accessible NIH cell line, OVCAR5 (Hamilton *et al*., 1984; Conover *et al*., 1998). Partial sequence from *PAPPA* was recovered from this technique because of its presence in OSE, but absence from some of the cancer cell lines. A previous report had mapped *PAPPA* to 9q33.1, possibly close to *FRA9E* (9q32) (Silahtaroglu *et al*., 1993). Consequently, we selected two overlapping BACs, which together contained the entirety of the *PAPPA* genomic sequence, and performed fluorescence *in situ* hybridization (FISH) on APC-induced chromosomes. Analysis of a BAC clone harboring *PAPPA* exons 11–22, RPCI-11.1-45A16, on 20 APC-induced metaphases determined that all 20 signals hybridized distal to the observed breakage at 9q32, positioning this BAC clone distal to the *FRA9E* CFS. However, FISH analysis of BAC clone RPCI-11.1-58C3, verified to contain *PAPPA* exons 1–10, indicated that seven of the 20 signals hybridized proximal and 13 signals hybridized distal to breakage at 9q32 (Figure 1, Table 1). Therefore, the 5′ end of *PAPPA* was found to lie within the distal portion of *FRA9E*. As these two clones are overlapping and clone 45A16 hybridized completely distal to the site of breakage, the telomeric end of *FRA9E* resides within clone 58C3. BAC clones positioned 1 Mb (RPCI-11.1-445L6) and 2 Mb (RPCI-11-46P18) centromeric to 58C3 hybridized both proximal and distal to the aphidicolin-induced breakage/decondensation at approximately equal frequencies among the scored metaphases (Figures 1 and 2, and Table 1). Therefore, we continued this analysis with additional BAC clones further centromeric to 46P18. BAC clones RPCI-11.2-444K11, 430K21, and 406O23 all produced signals that were observed equally proximal and distal to the site of breakage at 9q32, even though clone 406O23 was at least 6 Mb centromeric to 58C3 (Figures 1 and 2, and Table 1). Definition of the centromeric boundary of *FRA9E* was determined by analysis of clone RPCI-11.2-308N19. The hybridization signal for this clone was observed distal to *FRA9E* breakage only twice in 20 metaphases with the remaining 18 signals observed as proximal (Table 1). These data indicate that the centromeric edge of *FRA9E* is in close proximity to 308N19. A total of 11 BAC clones located in between the proximal and distal boundaries of *FRA9E* were examined to ascertain the distribution of breakage frequency across the region (Figure 2, Table 1). Interestingly, the majority of these clones hybridized proximal in approximately half of the metaphases and distal to the site of breakage in the other half of the metaphases. As a result of this unusual pattern of breakage, *FRA9E* appears to have a broad plateau of fragility rather than the typical core peak.

As a result of the efforts of the Human Genome Project, we were able to construct a sequence-based contig of *FRA9E*. BACs assigned to the *FRA9E* region were obtained from the University of California at Santa Cruz (UCSC) Human Genome Project Working Draft (http://genome.ucsc.edu/, Santa Cruz, CA, USA). Fully and partially sequenced BACs were assembled using the Sequencher computer program (Version 3.1, Gene Codes Corp., Ann Arbor, MI, USA). The sequence alignment was contiguous across the established region of fragility with flanking ends, eliminating gaps present in the UCSC database near D9S1832 and D9S174/*ZFP37*. As a result, we are able to estimate that the distance between the most proximal and most distal BACs, which define *FRA9E*, extends approximately 9.8 Mb. In addition, *PAPPA* was found to encompass approximately 244 kb of genomic DNA, consisting of 22 exons.

Considering the exceptionally large size of *FRA9E*, determined by the initial analysis of lymphocytes obtained from a single individual, we chose to analyze metaphases from two additional individuals using BACs within the proposed *FRA9E* region. Metaphases from the first individual were hybridized with BAC clones 272G11, 45E19, and 81L14 (Figure 2). Although the proximal edge was similar in position, as determined by hybridization of clone 272G11, the distal end was found to be closer to clone 45E19 than clone 81L14. Clone 81L14 hybridized distal in all 20 metaphases analyzed in this individual, whereas clone 45E19, more centromeric

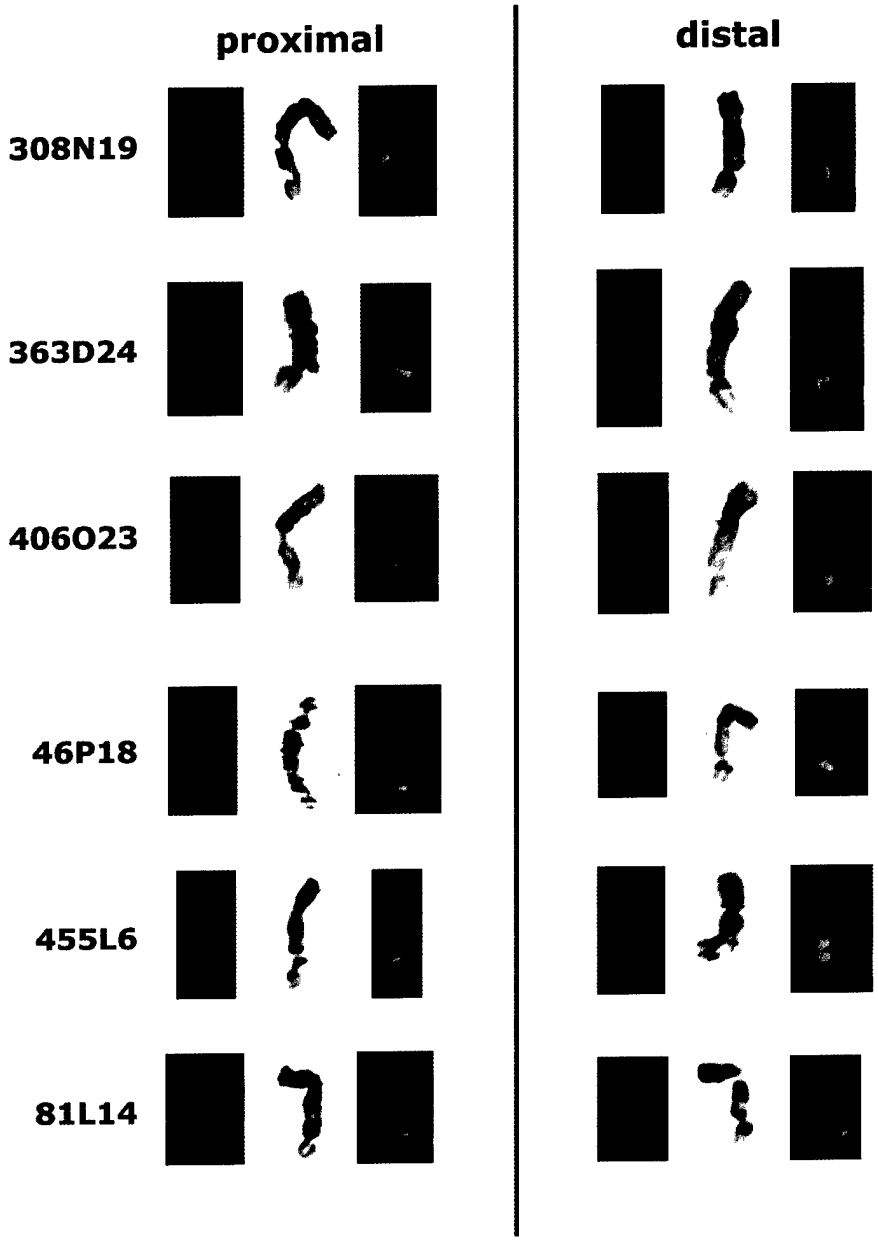

Figure 1 Representative examples of FISH across the region of *FRA9E* breakage. Seven BACs across the *FRA9E* region are shown. Chromosomes were obtained from separate APC-treated metaphases. Presence of breakage at 9q32 was initially identified from a DAPI image. The inverted DAPI image was used for confirmation of breakage at the 9q32 locus. Hybridization signals of the biotin-labeled BACs, detected by FITC–avidin (green), are shown as occurring both proximal and distal to the breakage at *FRA9E*. A summary of FISH results are shown in Table 1

than 81L14, hybridized twice proximal to the observed breakage with the remaining 18 metaphases showing distal hybridization. In the second individual, clone 81L14 displayed hybridization proximal (2 times) and distal (9 times) to breakage, comparable to initial findings. These results indicate that, in one of three individuals, the distal edge of fragility is positioned slightly more centromeric. However, these observations still confirm a similar size of *FRA9E* within three separate individuals, indicating that the unusual dimensions of this fragile site are not unique to a single individual.

LOH analysis of primary ovarian tumors

Previous studies have indicated a high frequency of LOH in ovarian cancer at 9q32 based on the analysis of only a few markers from the region (Schultz *et al*., 1995). Owing to the large region of aphidicolin-induced instability determined by our FISH analysis, we sought

to achieve a more comprehensive LOH analysis of the region in ovarian cancer. Therefore, 16 microsatellite markers across *FRA9E* were selected for LOH analysis on 21 primary ovarian tumors (serous, stages I–III). Of these markers, 14 localized within the fragile region, while the other two markers, D9S1866 and D9S154, were positioned beyond the centromeric and telomeric boundaries of fragility, respectively (Figure 2). Representative examples of LOH analysis are shown in Figure 3. Figure 4 shows the results obtained, with the percentage of LOH ranging from 14.3 to 69%. Of the 21 samples examined, 17 tumors (81%) displayed LOH at a minimum of one marker, and the number of markers exhibiting LOH for any one tumor ranged from one to 14 markers. The marker near *PAPPA*, D9S177, had the highest frequency of LOH at 69%. In addition, prominent peaks of LOH were observed with D9S1832 (52.6%), D9S105 (57%), and D9S1824 (55%). Within *FRA9E*, a distinct depression in LOH frequency was located in the center of the fragile region at markers D9S1856 (15%) and D9S930 (18.8%).

Table 1 FISH analysis for BAC clones spanning *FRA9E*

Clone[a]	*# of breaks*[b]	*Proximal (%)*	*Crossing (%)*	*Distal (%)*
308N19	21	18 (86)	1 (5)	2 (9)
363D24	16	13 (81)	0 (0)	3 (19)
272G11	20	17 (85)	0 (0)	3 (15)
143P10	20	14 (70)	1 (5)	5 (25)
406O23	20	12 (60)	2 (10)	6 (30)
430K21	21	9 (43)	3 (14)	9 (43)
444K11	10	5 (50)	0 (0)	5 (50)
46P18	20	10 (50)	0 (0)	10 (50)
46E19	15	8 (53)	1 (7)	6 (40)
445L6	20	9 (45)	1 (5)	10 (50)
81L14	20	7 (35)	0 (0)	13 (65)
49C22	20	7 (35)	0 (0)	13 (65)
58C3	20	7 (35)	0 (0)	13 (65)
45A16	20	0 (0)	0 (0)	20 (100)

[a]Research Genetics RPCI-11 BAC clones hybridized to APC-treated metaphases. [b]Number of APC-induced metaphase breaks observed for breakage at 9q32. The breakage was scored as proximal (centromeric), crossing, or distal (telomeric)

Gene expression analysis across FRA9E

The 9.8 Mb *FRA9E* region was found to contain a total of 36 known genes, including *PAPPA* at the telomeric end. Since the expression of genes that reside within CFSs have previously been shown to be reduced or

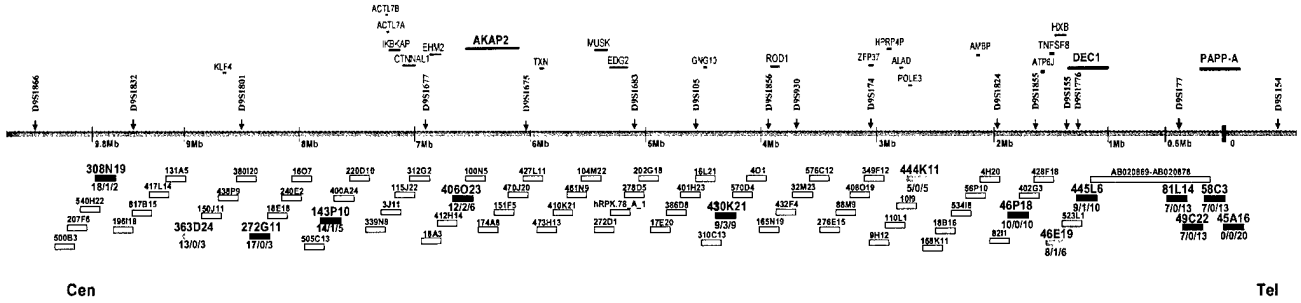

Figure 2 Approximately 9.8 Mb sequence-based contig for the *FRA9E* region. A *FRA9E* contig defining the proximal (centromeric) and distal (telomeric) ends is depicted. BACs analysed by FISH in 20 APC-induced metaphases (black boxes; ▬) and BACs scored in less than 20 APC-induced metaphases (gray boxes; ▭) are represented with the final counts indicated below each box as proximal/crossing/distal. BACs spanning the fragile site (white boxes; ▭) are also shown. AB020869-AB020878 (represented by long white box) is a series of Genbank accession numbers for human genomic sequence. All clones are Research Genetics RPCI-11 BACs. The estimated genomic size of the region is indicated starting at the distal end (*PAPPA*), based upon the order the fragile site was initially characterized. The relative positions of genes and microsatellite markers analyzed in this study are provided above the gray line

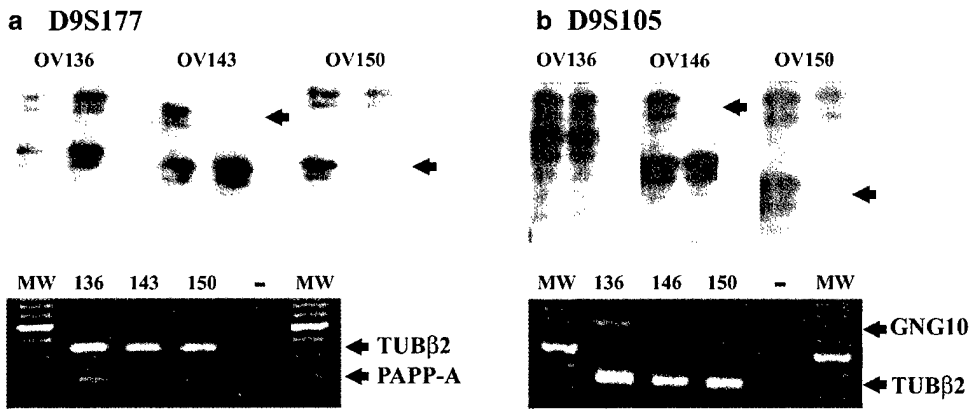

Figure 3 Representative examples of LOH and corresponding LOE. For both D9S177 (**a**) and D9S105 (**b**), one example of intact alleles without downregulation of nearby gene expression is shown, along with two examples of LOH showing concurrent LOE. Scored LOH is indicated with arrows

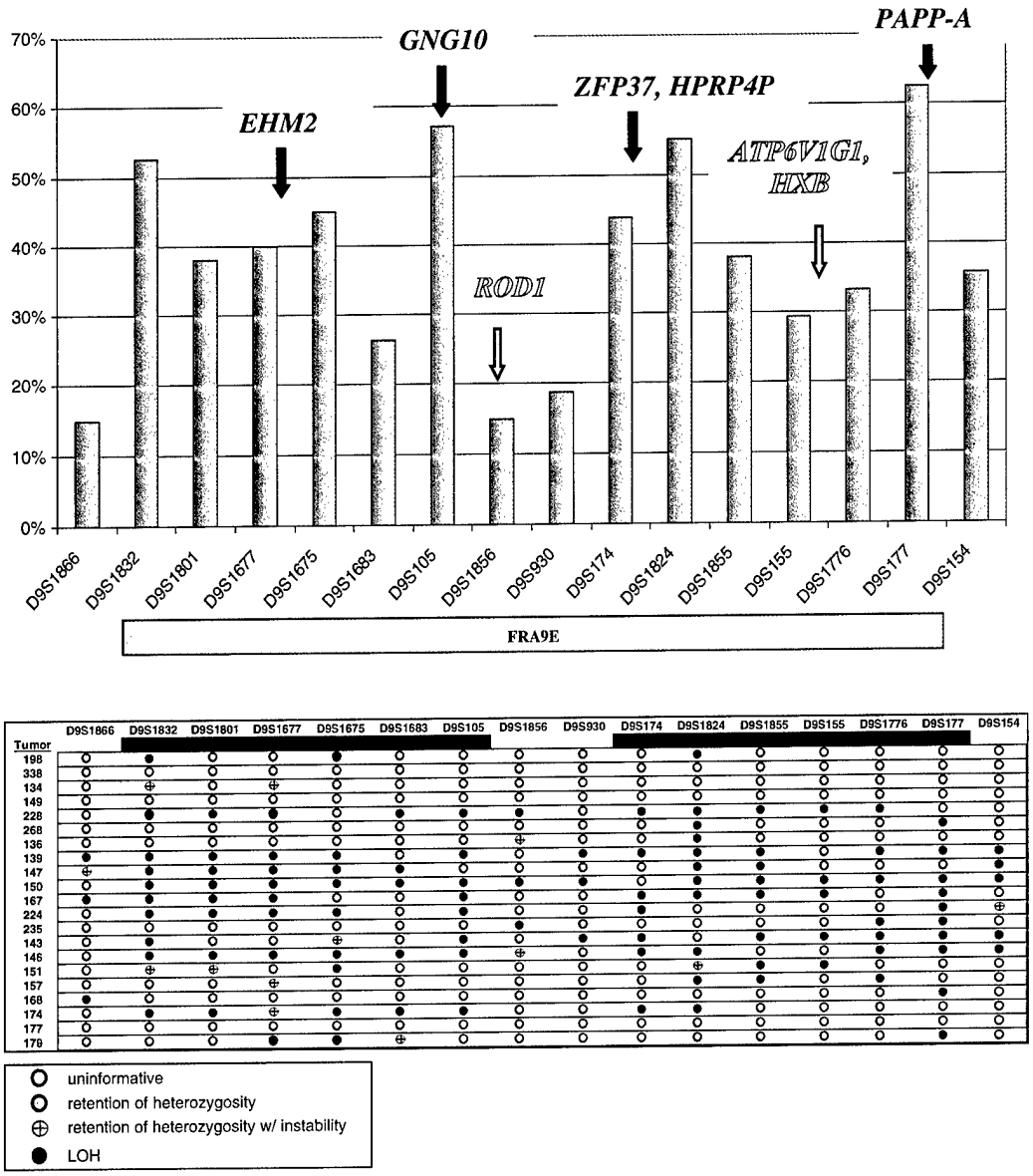

Figure 4 LOH analysis across the *FRA9E* region. The upper panel shows a bar graph representation of the frequency of LOH observed at the 16 microsatellite markers localizing within or near the *FRA9E* region. The gray bar at the bottom of the graph depicts the *FRA9E* region. The relative positions of genes to microsatellite markers are indicated with solid (LOE) or open arrows (no LOE). The lower panel shows the pattern of LOH for each individual tumor sample. Open circles (○) indicate an uninformative result; gray circles (**O**) indicate retention of heterozygosity; gray circles with a cross (⊕) indicate retention of heterozygosity with microsatellite instability; and solid black circles (●) indicate LOH. The solid bars display the two apparent regions of high LOH within the sample set

absent in tumor samples (Denison *et al.*, 2002), we sought to investigate the expression pattern of genes across the *FRA9E* region. Unique primers were designed for the majority of the genes within *FRA9E* to analyze a panel consisting of short-term cultured, normal ovarian surface epithelium (OSE), ovarian cancer cell lines, and primary serous tumors (Table 2). Each gene was initially checked for expression in normal ovarian epithelial brushings (data not shown). Of the 22 genes, six were not expressed in the normal ovary, including *DEC1*, *AMBP*, *TNFSF8*, *MUSK*, *ACTL7A*, and *ACTL7B*, and therefore were not examined on the complete panel of samples. Semiquantitative RT–PCR was performed for the remaining set of genes on the entire panel of tumor-derived cell lines and primary tumors (stages I–IV) (Figure 5). The optimal control primers that were included with the PCR reaction for each individual gene were based on the required PCR conditions for the combined primers and the relative size of the two, specific and control, products. Control primers were designed from the sequences of the glyceraldehyde-3-phosphate dehydrogenase (*GAPDH*), beta-actin (*ACTB*), beta-2-tubulin (*TUBB2*), and beta-2-microglobulin (*B2M*) genes (Table 2).

PAPPA had the most significant reduction of gene expression in both the cell lines and primary tumors as

Table 2 Genes mapping within the *FRA9E* CFS region

Gene	*Unigene*	*Gene definition*	*Genomic size (kb)*[a]	*Primers*[b]	*Product size (bp)*
KLF4	Hs.356370	Kruppel-like factor 4	3.9	CAGAGGAGCCCAAGCCAAAGAG CACAGCCGTCCCAGTCACAGT	174
ACTL7B	Hs.119287	Actin-like 7B	1.3	GCCACGCATTCACGGACGAC AGCATCTCAGAGCAACGGAAGC	184
ACTL7A	Hs.123530	Actin-like 7A	1.4	CAATGCACATCGCCTACCAGTC CCCGTGTTCCTCGTACTCAA	695
IKBKAP	Hs.31323	Inhibitor of κ light polypeptide gene enhancer in B-cells, kinase complex-associated protein	65.5	GCCCAGCTTAACTTTACCAA CATCTCACTGCCACTCACGACA	430
CTNNAL	Hs.58488	Catenin, alpha-like 1	70.9	AGACGCTACTCCCGCTGGTTT TGGGCTGATTCGCAGTTAGGAT	650
EHM2	Hs.267997	EHM2 gene	67.2	GCCTGGACGAGTCATTTC TAGGGCAACAACCATCTCAT	598
AKAP2	Hs.42322	A kinase (PRKA) anchor protein 2	392.2	TAAACGTGGGCCCTTATCTAAA GCTTCCTCTACAGTCGCTTCA	564
TXN		Thioredoxin	12.5	AGTCAAATGCACGCCAACA GCAGATGGCAACTGGTTATGTC	207
MUSK	Hs.156465	Muscle, skeletal, receptor tyrosine kinase	132.1	GGTCATTTACTACGTGCGAGAT CTCACACATGCGTTCCAG	154
EDG2	Hs.75794	Endothelial differentiation, lysophosphatidic acid G-protein-coupled receptor, 2	163.8	TGGTCATGGTGGCAATCTATGT TCATTTCTTTGTCGCGGTAGG	750
GNG10	Hs.79126	Guanine nucleotide binding protein 10	8.6	CCTGTGGCCTGGTCCTAT CAAAGGCACATCGTCGAAGTAA	780
ROD1	Hs.145078	Regulator of differentiation	74.1	AGACTTCACTCGCTTAGACCTT GCCCATGTGGTGTGATAAGAT	310
ZFP37	Hs.150406	Zinc-finger protein 37 homolog (mouse)	14.8	TATACATCAGCGATCCC AGAAGCCAACACAGACATTAAG	602
HPRP4P	Hs.374973	Pre-mRNA processing factor 4 homolog (yeast)	16.5	AAACTAAAGCACCCGACGACTT GGCCTCTTCCAAGCGTTTCA	550
ALAD	Hs.1227	Aminolevulinate, delta-, dehydratase	5.4	CGGCTACTTCCACCCACTACTT AAGATCAAGACACAGCGTAGGC	210
POLE3	Hs.108112	Polymerase (DNA directed), epsilon 3 (p17 subunit)	3.1	CGCTCCCGGACGGTGTCAACA TTTCTGCTCCCGCCTATATGCT	225
AMBP	Hs.76177	Alpha-1-microglobulin/bikunin precursor	18.1	CCCAAGAAGAGGAAGGATCAGG GCAGACCGGCCAGTTGTC	450
ATP6V1G1	Hs.90336	ATPase, H+ transporting, lysosomal 13 kDa, V1 subunit G isoform 1	10	GAAATTGAACAGTACCGCCTGC GGATTTCTGGCCGAATGTCAC	205
TNFSF8	Hs.1313	Tumor necrosis factor (ligand) superfamily, member 8	27.6	TGGACAGAAAGGGCATAATGA TGGCCAGAGACAAGAACTTAGA	240
HXB	Hs.289114	Tenascin C (hexabrachion)	97.6	AGGTCTCTCGCCCATCGGAAAG TCTGGCAGGGTGGCGTTCA	250
DEC1	Hs.158035	Deleted in esophageal cancer 1	291	AATCCGTTTAGAATCATCTATT AGCACTTCTAGGACGTGGT	250
PAPPA[c]	Hs.75874	Pregnancy-associated plasma protein A	243	ACAACACAGAGGTCATTGCCAG TGCACTCGGGGTCACAGTTCTCATC	290
PAPPA[d]				TGGCTAAGGAAGGACAAGAAGTTGT CACAGATGTTTGTATGGGTGTGTAT	380
ACTB	Hs.288061	Actin, beta		GCTCCGGCATGTGCAAGG ATGAGGTAGTCAGTCAGGTC	550
B2M	Hs.75415	Beta-2-microglobulin		AGCTGTGCTCGCGCTACTCTCTC GTGTCGGATTGATGAAACCCAGACAC	140
GAPDH	Hs.169476	Glyceraldehyde-3-phosphate dehydrogenase		ACCACAGTCCATGCCATCAC TCCACCACCCTGTTGCTTGTA	450
TUBB2	Hs.251653	Tubulin, beta, 2		ACCACAGTCCATGCCATCAC TCCACCACCCTGTTGCTTGTA	454

[a]Estimated genomic size (kb) as determined by UCSC database. [b]Upper (forward) and lower (reverse) primers are shown 5′ to 3′. [c]Semiquantitative RT–PCR oligonucleotide primers. [d]Real-time PCR oligonucleotide primers

72% showed partial or complete LOE (Figure 5). *PAPPA* expression was found to be consistently high in multiple normal ovarian samples, including three different short-term cultured OSE and two samples of ovarian epithelial brushings (data not shown). Five genes located near the middle of the fragile site were found to be downregulated compared to expression levels in OSE. The endothelial differentiation gene 2 (*EDG2*), part of the lysophosphatidic acid receptor family, exhibited LOE in one of the seven cancer cell lines (14%) and nine of the 18 primary tumor samples (50%). The guanine-nucleotide binding protein, gamma

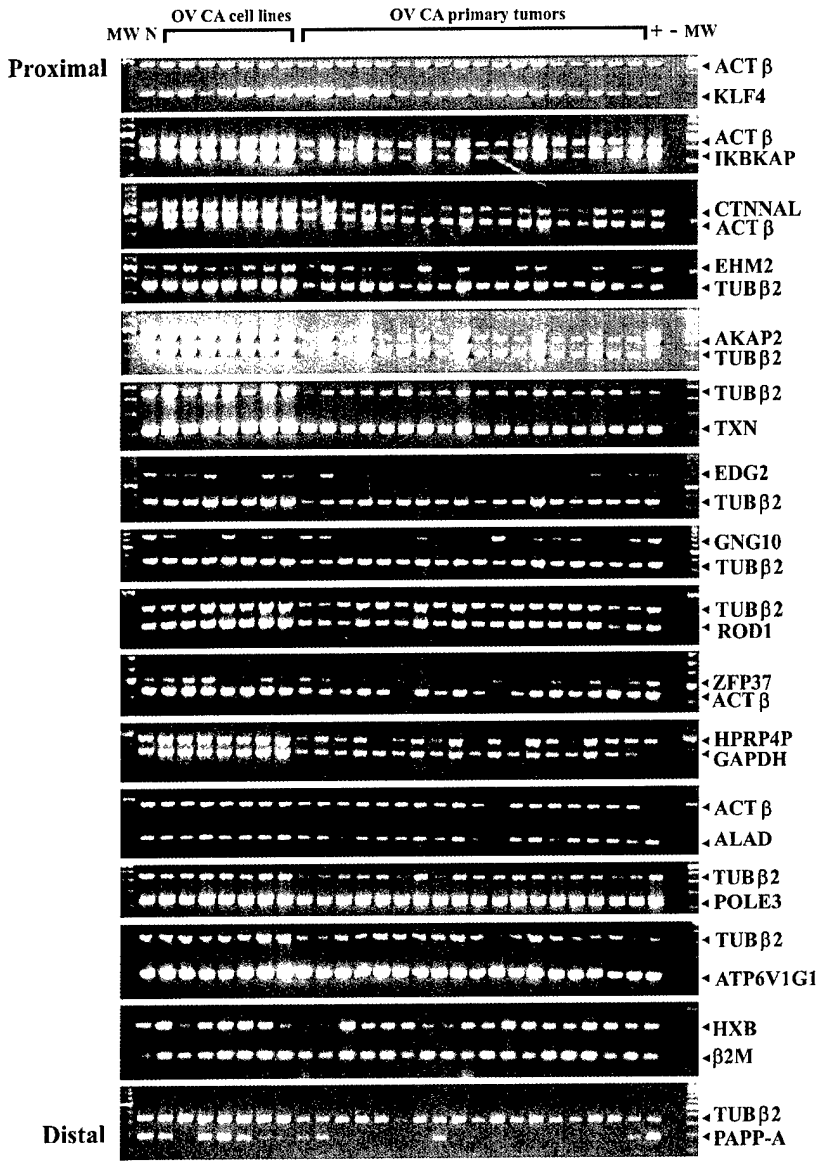

Figure 5 Semiquantitative RT–PCR analysis of 16 genes mapping to the *FRA9E* region. Each gene was tested for expression levels in OSE (N), seven tumor-derived cell lines, and 18 primary ovarian tumors. The internal control (*ACTB*, *GAPDH*, *B2M*, or *TUBB2*) used with each specific primer set is indicated. Positive (+) and negative (−) water controls are shown, along with molecular weight ladder (MW)

10 gene (*GNG10*) demonstrated a considerable decrease of expression in 57% of cancer cell lines (4/7) and 39% of primary tumors (7/18). Diminished expression of the gene encoding for the zinc-finger protein 37, *ZFP37*, was detected in three of the cancer cell lines (43%) and nine of the primary tumor samples (50%). *EHM2* that encodes for a protein involved in cytoskeletal structure, and *HPRP4P*, a U4/U6-associated splicing factor gene, did not show reduction of expression in the cancer cell lines; however, these did display reduced expression in 33% (6/18) and 17% (3/18) of the primary tumors, respectively (Figure 5). The remaining 10 genes displayed no LOE in either cancer cell lines or primary tumors: *KLF4*, *IKBKAP*, *CTNNAL*, *AKAP2*, *TXN*, *ROD1*, *ALAD*, *POLE3*, *ATP6J*, and *HXB* (Figure 5).

Interestingly, superimposition of the LOH pattern across the *FRA9E* region revealed a correlation between the expression of genes and the observed frequency of LOH (Figure 4). For example, *ROD1*, the only known gene analyzed, which lies within the central LOH depression, had normal levels of expression in both the cell lines and primary tumors. In addition, the gene with the highest LOE, *PAPPA*, coincided with the highest peak of LOH, at the distal edge of *FRA9E*. Figure 3 displays representative examples of LOE associated with LOH. This figure includes examples of allelic loss consistent with loss of expression for *PAPPA* and *GNG10*, both of which are genes near the two highest peaks of LOH. Although not all samples with observed LOE had associated LOH, any sample with LOH was

found to have decreased expression. Markers D9S1832 and D9S1824, both with a high frequency of LOH, did not have any known genes nearby that were normally expressed in the ovarian epithelium to correlate LOE with the observed LOH from these regions.

Since *PAPPA* had the most significant LOE within the *FRA9E* region, real-time PCR was performed to quantitatively confirm the results observed with semi-quantitative RT–PCR (Figure 6). Real-time PCR analysis was also performed with the *ACTB* gene to control for differences in the amount of RNA in each sample and for the reverse transcription efficiency. Once normalized, tumor samples were compared with OSE to determine the percentage reduction in expression. All of the ovarian cell lines were downregulated, with averages ranging from only 0.1% (OVCAR3) to 14.1% (OV202) of normal OSE expression levels (Figure 6a). In addition, the expression levels of the primary ovarian tumor samples were significantly lower than normal with averages from 0.7% (sample 14) to 15.9% (sample 3) of OSE expression (Figure 6b). Therefore, the quantitative expression data for *PAPPA* was consistent with the results obtained with semiquantitative RT–PCR.

Discussion

In this study, we sought to identify genes that are consistently downregulated during the development of ovarian cancer. DD-PCR was utilized to compare the expression of genes in short-term cultures of normal OSE to ovarian cancer cell lines. This analysis revealed numerous genes that are normally expressed in the ovarian epithelium, but displayed LOE in ovarian cancer. One of these genes encodes for PAPP-A, one of the four proteins originally isolated in 1974 from normal human pregnancy serum (Lin *et al*., 1974). Even though the biological function of PAPP-A was unclear at that time, particular interest in PAPP-A had been generated because of its clinical utility as an index of placental function and a first-trimester screen for Down's syndrome (Stabile *et al*., 1988; Wald *et al*., 1996). Recently, PAPP-A was identified as the IGF-dependent protease that cleaves the 26 kDa insulin-like growth factor binding protein-4 (IGFBP-4) into two proteolytic products (Lawrence *et al*., 1999). This protease activity has been detected in medium conditioned by normal human osteoblasts, but not by transformed osteoblastic cells (Durham *et al*., 1995). In agreement with these findings, Northern blot analysis has displayed *PAPPA* expression in normal osteoblasts with a corresponding lack of expression in several osteosarcoma cell lines (Lawrence *et al*., 1999). Interestingly, human fibroblasts treated with the phorbol ester tumor promoter, beta-phorbol 12,13-didecanoate, or transformed with SV40 large T antigen exhibit diminished IGFBP-4 protease activity, by induction of the PAPP-A inhibitor, proMBP (Chen *et al*., 2002).

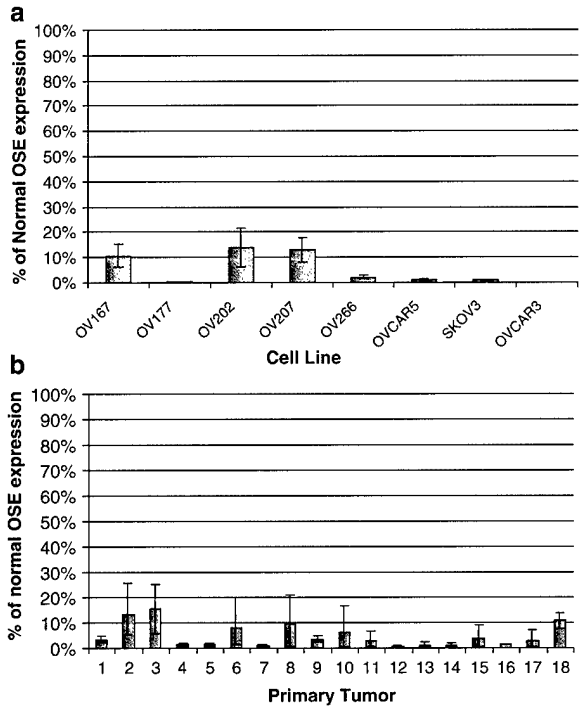

Figure 6 Real-time PCR analysis of *PAPPA* expression. Bar graph representations of average *PAPPA* expression for each ovarian cancer cell line (**a**) and 18 primary ovarian tumors (**b**). Both graphs are represented as the percentage of normal OSE expression after normalization with *ACTB* expression level for each sample

PAPPA has previously been localized to human chromosome 9q32–33, a region associated with a high frequency of LOH in ovarian tumors (Silahtaroglu *et al*., 1993; Schultz *et al*., 1995). In addition, the 9q32 band contains the *FRA9E* CFS; hence, we were interested in the genomic position of *PAPPA* relative to this region of instability. FISH was performed on two overlapping BAC clones, each of which contained a portion of the 244 kb *PAPPA* gene, to determine their association with the *FRA9E* region. The more telomeric BAC clone, 45A16, hybridized distal to *FRA9E* breakage in each of the 20 scored metaphases, placing this clone distal to the *FRA9E* region. In contrast, the hybridization of the BAC clone immediately centromeric to 45A16, RPCI-11.1-58C3, produced a distal signal to the aphidicolin-induced decondensation/breakage at *FRA9E* in only 13 of 20 metaphases with proximal signal in the remaining seven metaphases. Thus, BAC clone 58C3 spans some of the telomeric portion of this CFS, incorporating *PAPPA* within the *FRA9E* region.

The placement of *PAPPA* within the telomeric portion of *FRA9E* led to the complete characterization of this unstable genomic region. The centromeric boundary of *FRA9E* was defined with BAC clone RPCI-11.2-308N19, as this clone hybridized proximal to *FRA9E* breakage in 18 of 20 examined metaphases. A total of 11 BAC clones from the region were examined between RPCI-11.1-45A16 and RPCI-11.2-308N19 with the majority of these BAC clones hybridizing at approximately equal frequencies proximal and distal to the aphidicolin-induced breakage at *FRA9E* (Table 1). Sequence-based assembly of the region determined that

9.8 Mb of genomic sequence is present between 308N19, near the centromeric boundary of *FRA9E*, and 45A16, at the telomeric end of this region (Figure 2). This broad region of instability was confirmed with aphidicolin-induced metaphases obtained from three separate individuals. As a result, this study defines *FRA9E* as the largest described CFS to date.

CFSs, in contrast to the RFSs, have been observed to span broad genomic regions. *FRA3B* (3p14.2), the most active of the CFSs, was originally thought to span a 500 kb region (Paradee *et al*., 1996; Rassool *et al*., 1996; Wilke *et al*., 1996). However, these original characterizations of *FRA3B* solely defined the active center of instability without full delineation of the boundaries. Recently, the complete region of instability within the *FRA3B* CFS has been documented to extend as much as 4 Mb (Becker *et al*., 2002). Molecular analysis of other CFSs (*FRA7G*, *FRA7H*, *FRA16D*, and *FRAXB*) has revealed that instability within these CFSs occurs over genomic regions ranging from 200 kb to 2 Mb in size (Huang *et al*., 1998b; Mishmar *et al*., 1998; Krummel *et al*., 2000; Arlt *et al*., 2002). As *FRA9E* is a less active CFS relative to *FRA3B*, *FRA16D*, and *FRAXB* (Glover *et al*., 1984), our observation that instability within *FRA9E* comprises more than 9 Mb suggests that there may not be a relation between the frequency of observed aphidicolin-induced decondensation/breakage that occurs within any one CFS *in vitro* and the size of that unstable region.

The *FRA9E* CFS was examined to determine the frequency of LOH across this region in a panel of primary ovarian tumors. This detailed analysis revealed that there was frequent LOH across this CFS, with the marker near *PAPPA*, D9S177, showing the highest frequency of loss (69%; Figure 4). In addition, two distinct regions of high LOH were apparent within *FRA9E*, emphasized by a central region of two microsatellite markers (D9S930 and D9S1856) with negligible LOH (Figure 4). Therefore, in the midst of this high occurrence of allelic loss in ovarian cancer, there remains a relatively low frequency of LOH in the middle of *FRA9E*.

There are a total of 36 known genes contained within the *FRA9E* region. We examined the expression of 22 of these genes in brushings from normal ovarian surface epithelial cells, and found that six genes were not normally expressed in the ovarian epithelium. The comparative expression profiles of the remaining 16 genes were varied, as some genes did not demonstrate altered expression in the ovarian cancer cell lines or primary tumors (Figure 5). Six genes, including *PAPPA*, had frequent LOE in the panel of cell lines and primary tumors. Interestingly, the genes that displayed the greatest LOE were derived from regions of high LOH, whereas one of the genes that did not show a decrease in expression localized to a region with less LOH. Not all genes within regions of high LOH displayed LOE, which emphasizes the complexity of this large region of genomic instability.

Traditionally, CFSs are characterized by the frequency that large-insert clones within those regions hybridize proximal, distal or crossing to aphidicolin-induced decondensation/breakage in 20 separate metaphases with clear, discernible breakage at that CFS. Clones that always hybridize centromeric to the region of breakage are considered proximal to that CFS, whereas clones with solely telomeric hybridization are considered distal to that CFS. Hybridization of clones both proximal and distal to CFS breakage at approximately equal frequencies typically defines the active 'center' of that CFS region. Previously characterized CFSs, which include *FRA3B*, *FRA16D*, *FRA7G*, *FRA7H*, and *FRAXB*, have all been found to have compact, definitive 'center' regions flanked by trailing regions with a propensity toward proximal or distal hybridization relative to the breakage. In contrast, our analysis of *FRA9E* shows a more extensive region of instability than observed with any other CFS, with an extremely broad active center or 'plateau' extending over 5 Mb of genomic sequence. The LOH and LOE data for *FRA9E* suggest that contained within this large region of instability may be two subregions of instability with a more stable middle region. These observations raise the possibility of two or more CFSs present within this genomic region. With resolution limitations of the FISH-based assay used to clone the CFSs, more than one CFS within the same chromosomal band would be cytogenetically indistinguishable from one another. If two or more CFSs were present within the region, the typical 'centers' of active fragility would effectively merge, creating a 'plateau' across the majority of the CFS. Since FISH is currently the only technique used to characterize a CFS, we are unable to directly test the possibility of the existence of more than one CFS within 9q32.

This study represents the first characterization of the *FRA9E* region and the first observation of altered expression of the *PAPPA* gene in ovarian tumors. Of the genes analyzed within the *FRA9E* region, *PAPPA* had the most significant loss of gene expression in ovarian cell lines and primary tumors, with downregulation in 100% of the samples analyzed by quantitative real-time PCR (Figure 6). Loss of *PAPPA*, as an IGFBP-4 protease or perhaps as another yet unknown function, may provide an environment for preferential tumor growth. Intriguingly, many genes within CFSs have been associated with decreased expression in various tumor types (Lee *et al*., 1998; Smith *et al*., 1998; Tatarelli *et al*., 2000; Paige *et al*., 2001; Arlt *et al*., 2002; Denison *et al*., 2002). Whether these genes lose expression as a result of their location within inherently unstable regions of the genome or because of a selective growth advantage within cancer cells remains to be determined. The role of *PAPPA* in cancer development, along with several other genes from the *FRA9E* region, requires further investigation.

Materials and methods

Primary ovarian tissue and ovarian cell lines

Samples of primary serous ovarian tumors were obtained from surgical specimens taken at the Mayo Clinic. Material was

promptly snap-frozen and stored at −70°C until the time of processing. For LOH analysis, three stage-I, one stage-II, and 17 stage-III high-grade ovarian tumors were analysed. For semiquantitative RT–PCR, six stage-I, six stage-II, four stage-III, and two stage-IV high-grade ovarian tumors were examined. All specimens were collected under approval of the Institutional Review Board.

Normal OSE cells were obtained following oophorectomy for reasons unrelated to gynecological malignancy, then used as uncultured brushings or cultured as described (Kruk *et al.*, 1990). Only short-term OSE cultures with epithelial morphology and uniform cytokeratin staining were utilized. OV167, OV177, OV202, OV207, and OV266 cultures were low-passage cancer cell lines established at the Mayo Clinic (Conover *et al.*, 1998). OVCAR-5 was an established NIH cell line (Hamilton *et al.*, 1984), and SKOV-3 was obtained through American Type Culture Collection (Manassas, VA, USA). All cells were maintained according to the providers' recommendations.

Selection of clones

BAC clones were selected based on their localization to the 9q32 region by The Sanger Center (Cambridge, UK), the University of California at Santa Cruz (UCSC) Human Genome Project Working Draft (Santa Cruz, CA, USA), or by a PCR-based screen of the Research Genetics CITB Human BAC DNA Library (Release IV) (Huntsville, AL, USA), using primers designed to amplify STS markers in the region. BAC DNA was isolated according to the protocol of Kirschner and Stratakis (1999).

FISH

Lymphocyte cultures were established from 1 ml of peripheral whole blood and 9 ml of Chang Media PB (Irvine Scientific, Santa Ana, CA, USA). Cell cultures were incubated for a total of 72 h at 37°C in 5% CO_2. At 24 h prior to harvest, APC solution was added to a final concentration of 0.4 μM. Cell harvest and metaphase preparations followed standard cytogenetic techniques.

For localization, 1 μg of BAC DNA was labeled with biotin-16-dUTP (Roche Applied Science, Indianapolis, IN, USA) by nick translation, then precipitated and hybridized to APC-treated metaphase spreads according to the protocol described by Verma and Babu (1989). The biotin-labeled probe was detected following minor modifications of the manufacturer's protocols (Ventana Medical Systems, Tucson, AZ, USA). The chromosomes were counterstained with DAPI. Hybridization signals were observed with a Zeiss Axioplan2 fluorescence microscope, and the images were digitized using the IPLab SpectrumP software (Scanalytics Inc., Fairfax, VA, USA). The position of each clone relative to *FRA9E* was determined by analysis of 20 APC-treated metaphases with breakage at 9q32. Assignment of a BAC clone within the *FRA9E* fragile site was determined by hybridization signal observed on both sides of breakage or by signal observed on the proximal (centromeric) side of breakage in one metaphase and on the distal (telomeric) side of breakage in a separate metaphase.

LOH analysis

The percent LOH was determined by analysis of 16 microsatellite markers with a minimum of 60% heterozygosity within the human population. Primers specific for each marker were tested in matched normal blood and ovarian tumor DNA obtained from 21 patients (serous, stages I–III). DNA was obtained using standard phenol–chloroform methods. The forward primer for each marker was end-radiolabeled with γP^{32} ATP (10 μCi/μl) using T4 polynucleotide kinase (Invitrogen, Carlsbad, CA, USA) according to the manufacturer's protocol. PCR was completed in a 12.5 μl reaction volume, containing 50 ng of genomic DNA, 10 mM Tris-HCl, 50 mM KCl, 1.5 mM $MgCl_2$, 0.3 μM each primer, 200 μM dNTPs, and 0.5 units of Taq DNA polymerase (Promega, Madison, WI, USA) or AmpliTaq Gold polymerase (Applied Biosystems, Foster City, CA, USA). After 3 (for Promega Taq) or 10 (for AmpliTaq) min of initial denaturation at 95°C, amplification was performed for 30 cycles (95°C for 30 s, 50–62°C for 30 s, and 72°C for 30 s) with a final extension cycle at 72°C for 10 min. Products were denatured and electrophoresed on 6% polyacrylamide-sequencing gels containing 8 M urea. Gels were dried and autoradiographed for 16–24 h. LOH was scored by allelic imbalance, displayed through more than 50% loss of intensity of one allele in the tumor sample, in comparison with the same allele from matched normal tissue.

Semiquantitative RT–PCR

Total RNA was extracted from normal ovarian epithelial brushings, short-term cultured normal OSE, seven ovarian tumor-derived cell lines, and 18 primary serous tumors (stages I–IV) using TRIzol reagent following the manufacturer's protocol (Invitrogen, Carlsbad, CA, USA). For each sample, 5 μg of total RNA was treated with RNase-free DNase for 30 min at 37°C to eliminate genomic DNA contamination, followed by heat inactivation of the DNase at 65°C. Reverse transcription of DNase-treated RNA was performed with M-MLV RT (Invitrogen, Carlsbad, CA, USA) following the manufacturer's protocol.

Unique primers were designed for a subset of genes within the *FRA9E* region (Table 2) using the Oligo 6.4 software (Molecular Insights, Cascade, CO, USA), and used in a multiplex reaction with *GAPDH*, *ACTB*, *TUBB2*, or *B2M* control primers (Table 2). RT–PCR was routinely performed in a 12.5 μl reaction volume, containing 10 mM Tris-HCl, 50 mM KCl, 1.5 mM $MgCl_2$, 0.4 μM each primer, 200 μM dNTPs, and 0.5 units of Taq DNA polymerase (Promega, Madison, WI, USA). After 3 min of initial denaturation at 95°C, amplification was performed for 30 cycles (95°C for 30 s, 55–60°C for 30 s, and 72°C for 30 s) with a final extension cycle at 72°C for 10 min. Levels of expression were determined by the ratios of band intensity of the target gene to the control gene within a single sample, followed by comparison relative to the normal (OSE) expression level ratio.

Real-time PCR

Unique primers were designed within the 3′ end of *PAPPA* using the Oligo 6.4 software (Molecular Insights, Cascade, CO, USA), and control primers were derived from the *ACTB* gene (Table 2). All PCR reactions were performed using a LightCycler instrument (Roche Applied Science, Indianapolis, IN, USA) in a total volume of 20 μl, containing 20 mM Tris pH 8.4, 50 mM KCl, 4 mM $MgCl_2$, 0.5 μM each primer, 200 μM dNTPs, 0.05% BSA, 0.3X SYBR® Green I (Molecular Probes, Eugene, OR, USA), and 0.5 units of Platinum Taq DNA polymerase (Invitrogen, Carlsbad, CA, USA). The amplification conditions comprised an initial denaturation at 95°C for 1 min and 32 cycles at 95°C for 0 s, 63°C for 16 s, and 72°C for 20 s. At the end of the extension step for every cycle, the fluorescence of each sample was measured to allow quantification of product. Following amplification, a melting curve was obtained by heating at 20°C/s to 95°C, cooling at 20°C/s to 63°C, then slowly heating at 0.1°C/s to 99°C with fluorescence data

collection at 0.1°C intervals. Experiments were performed in triplicate.

Quantitative analysis of the data was determined through the use of LightCycler analysis software. The SYBR Green fluorescence signal of each sample was plotted against the number of cycles. The background fluorescence is removed by establishing a noise band; then the resulting threshold is used to resolve the cycle numbers that correlate inversely with the log of the initial template concentration. The crossing points are the intersections between the best-fit lines, calculated from the log-linear portion of the amplification curve, and the noise band. A standard curve was created for both *PAPPA* and *ACTB* by performing PCR on 1:10, 1:100, and 1:1000 dilutions of the normal sample, OSE. Fold reduction was calculated from applying the crossing points of the samples to the standard curve. The fold reduction determined for *PAPPA* was normalized to that of *ACTB* to compensate for the amount of RNA in each sample and for the reverse transcription efficiency.

Acknowledgments

We thank Dr Kimberly Kalli and Kimberly Stephens for providing the short-term normal ovarian epithelial (OSE) cultures. This study was conducted as a component of GC's doctoral thesis requirements in the Mayo Graduate School. GC's training has been supported, in part, by an NIH training Grant (CA 75926) to the Tumor Biology Program of the Mayo Graduate School and by the Mayo Clinic Foundation. This work was supported by NCI Grant CA48031 and DOD Grant DAMD17-99-1-9504 (both to DIS).

References

Arlt MF, Miller DE, Beer DG and Glover TW. (2002). *Genes Chromosomes Cancer*, **33,** 82–92.

Becker NA, Thorland EC, Denison SR, Phillips LA and Smith DI. (2002). *Oncogene* (in Press).

Bednarek AK, Laflin KJ, Daniel RL, Liao Q, Hawkins KA and Aldaz CM. (2000). *Cancer Res.*, **60,** 2140–2145.

Chen BK, Overgaard MT, Bale LK, Resch ZT, Christiansen M, Oxvig C and Conover CA. (2002). *Endocrinology*, **143,** 1199–1205.

Conover CA, Hartmann LC, Bradley S, Stalboerger P, Klee GG, Kalli KR and Jenkins RB. (1998). *Exp. Cell Res.*, **238,** 439–449.

Denison SR, Becker NA, Ferber MJ, Phillips LA, Kalli KR, Lee J, Lillie J, Smith DI and Shridhar V. (2002). *Genes Chromosomes Cancer*, **34,** 406–415.

Durham SK, Riggs BL, Harris SA and Conover CA. (1995). *Endocrinology*, **136,** 1374–1380.

Gabra H and Smyth JF. (1997). *Biology of Female Cancers*. Langdon SP, Miller WR, Berchuck A (eds). CRC Press: Boca Raton, FL, pp. 93–113.

Glover TW, Berger C, Coyle J and Echo B. (1984). *Hum. Genet.*, **67,** 136–142.

Hamilton TC, Young RC and Ozols RF. (1984). *Semin. Oncol.*, **11,** 285–298.

Hewett DR, Handt O, Hobson L, Mangelsdorf M, Eyre HJ, Baker E, Sutherland GR, Schuffenhauer S, Mao JI and Richards RI. (1998). *Mol. Cell*, **1,** 773–781.

Huang H, Qian C, Jenkins RB and Smith DI. (1998a). *Genes Chromosomes Cancer*, **21,** 152–159.

Huang H, Qian J, Proffit J, Wilber K, Jenkins R and Smith DI. (1998b). *Oncogene*, **16,** 2311–2319.

Jemal A, Thomas A, Murray T and Thun M. (2002). *CA: Cancer J. Clin.*, **52,** 23–47.

Jones C, Penny L, Mattina T, Yu S, Baker E, Voullaire L, Langdon WY, Sutherland GR, Richards RI and Tunnacliffe A. (1995). *Nature*, **376,** 145–149.

Jones C, Slijepcevic P, Marsh S, Baker E, Langdon WY, Richards RI and Tunnacliffe A. (1994). *Hum. Mol. Genet.*, **3,** 2123–2130.

Kirschner LS and Stratakis CA. (1999). *Biotechniques*, **27,** 72–74.

Knight SJL, Flannery AV, Hirst MC, Campbell L, Christodoulou Z, Phelps SR, Pointon J, Middleton-Price HR, Barnicoat A, Pembrey ME. (1993). *Cell*, **74,** 127–134.

Kruk PA, Maines-Bandiera SL and Auersperg N. (1990). *Lab. Invest.*, **63,** 132–136.

Krummel KA, Roberts LR, Kawakami M, Glover TW and Smith DI. (2000). *Genomics*, **69,** 37–46.

Landis SH, Murray T, Bolden S and Wingo PA. (1998). *CA: Cancer J. Clin.*, **48,** 6–30.

Lawrence JB, Oxvig C, Overgaard MT, Sottrup-Jensen L, Gleich GJ, Hays LG, Yates 3rd JR and Conover CA. (1999). *Proc. Natl. Acad. Sci. USA*, **96,** 3149–3153.

Lee SW, Reimer CL, Oh P, Campbell DB and Schnitzer JE. (1998). *Oncogene*, **16,** 1391–1397.

Lin TM, Galbert SP, Kiefer D, Spellacy WN and Gall S. (1974). *Am. J. Obstet. Gynecol.*, **118,** 223–236.

Mangelsdorf M, Ried K, Woollatt E, Dayan S, Eyre H, Finnis M, Hobson L, Nancarrow J, Venter D, Baker E and Richards RI. (2000). *Cancer Res.*, **60,** 1683–1689.

Mishmar D, Rahat A, Scherer SW, Nyakatura G, Hinzmann B, Kohwi Y, Mandel-Gutfroind Y, Lee JR, Drescher B, Sas DE, Margalit H, Platzer M, Weiss A, Tsui LC, Rosenthal A and Kerem B. (1998). *Proc. Natl. Acad. Sci. USA*, **95,** 8141–8146.

Nancarrow JK, Kremer E, Holman K, Eyre H, Doggett NA, Le Paslier D, Callen DF, Sutherland GR and Richards RI. (1994). *Science*, **264,** 1938–1941.

Oberle I, Rousseau F, Heitz D, Kretz C, Devys D, Hanauer A, Boue J, Bertheas MF and Mandel JL. (1991). *Science*, **252,** 1097–1102.

Paige AJ, Taylor KJ, Stewart A, Sgouros JG, Gabra H, Sellar GC, Smyth JF, Porteous DJ and Watson JE. (2000). *Cancer Res.*, **60,** 1690–1697.

Paige AJ, Taylor KJ, Taylor C, Hillier SG, Farrington S, Scott D, Porteous DJ, Smyth JF, Gabra H and Watson JE. (2001). *Proc. Natl. Acad. Sci. USA*, **98,** 11417–11422.

Paradee W, Wilke CM, Wang L, Shridhar R, Mullins CM, Hoge A, Glover TW and Smith DI. (1996). *Genomics*, **35,** 87–93.

Rassool FV, Le Beau MM, Shen ML, Neilly ME, Espinosa 3rd R, Ong ST, Boldog F, Drabkin H, McCarroll R and McKeithan TW. (1996). *Genomics*, **35,** 109–117.

Ritchie RJ, Knight SJ, Hirst MC, Grewal PK, Bobrow M, Cross GS and Davies KE. (1994). *Hum. Mol. Genet.*, **3,** 2115–2121.

Schultz DC, Vanderveer L, Buetow KH, Boente MP, Ozols RF, Hamilton TC and Godwin AK. (1995). *Cancer Res.*, **55,** 2150–2157.

Silahtaroglu AN, Tumer Z, Kristensen T, Sottrup-Jensen L and Tommerup N. (1993). *Cytogenet. Cell Genet.*, **62,** 214–216.

Smith DI, Huang H and Wang L. (1998). *Int. J. Oncol.*, **12,** 187–196.

Sonoda G, Palazzo J, du Manoir S, Godwin AK, Feder M, Yakushiji M and Testa JR. (1997). *Genes Chromosomes Cancer*, **20,** 320–328.

Stabile I, Grudzinskas JG and Chard T. (1988). *Obstet. Gynecol. Surv.*, **43,** 73–82.

Sutherland GR, Baker E and Richards RI. (1998). *Trends. Genet.*, **14,** 501–506.

Tatarelli C, Linnenbach A, Mimori K and Croce CM. (2000). *Genomics*, **68,** 1–12.

Verkerk AJMH, Rieretti M, Sutcliffe JS, Fu Y, Kuhl DP, Pizzuti A, Reiner O, Richards S, Victoria MF, Zhang F, Eussen BE, van Ommen GB, Blonden LAJ, Riggins GJ, Chastain JL, Kunst CB, Galjaard H, Caskey CT, Nelson DL, Oostra MA and Warren ST. (1991). *Cell*, **65,** 905–914.

Verma RS and Babu A. (1989). *Human Chromosomes: Manual of Basic Techniques*. Verma RS, Babu A (eds). Pergamon Press Inc.: New York, p. 240.

Wald NJ, George L, Smith D, Densem JW and Petterson K. (1996). *Br. J. Obstet. Gynaecol.*, **103,** 407–412.

Wilke CM, Hall BK, Hoge A, Paradee W, Smith DI and Glover TW. (1996). *Hum. Mol. Genet.*, **5,** 187–195.

Yu S, Mangelsdorf M, Hewett D, Hobson L, Baker E, Eyre HJ, Lapsys N, Le Paslier D, Doggett NA, Sutherland GR and Richards RI. (1997). *Cell*, **88,** 367–374.

Yunis JJ and Soreng AL. (1984). *Science*, **226,** 1199–1204.

MS#13

GENES, CHROMOSOMES & CANCER 38:40–52 (2003)

Characterization of FRA6E and Its Potential Role in Autosomal Recessive Juvenile Parkinsonism and Ovarian Cancer

Stacy R. Denison,[1] Gwen Callahan,[2] Nicole A. Becker,[1] Leslie A. Phillips,[1] and David I. Smith[1]*

[1]Division of Experimental Pathology, Department of Laboratory Medicine and Pathology, Mayo Foundation, Rochester, Minnesota
[2]Tumor Biology Program, Mayo Foundation, Rochester, Minnesota

Characterization of FRA6E (6q26), the third most frequently observed common fragile site (CFS) in the human population, determined that aphidicolin-induced instability at FRA6E extends over a very large region (3.6 Mb). Sequence analysis identified eight genes (*IGF2R*, *SLC22A1*, *SLC22A2*, *SLC22A3*, *PLG*, *LPA*, *MAP3K4*, and *PARK2*) as mapping within the large FRA6E region. *PARK2*, the gene associated with autosomal recessive juvenile parkinsonism (ARJP), accounts for more than half of the CFS. Homozygous deletions and large heterozygous deletions have been observed in *PARK2* in ARJP patients. RT-PCR analysis of the eight genes localizing to FRA6E indicated that 50% of the genes, including *PARK2*, were down-regulated in one or more of the primary ovarian tumors analyzed. *PARK2* expression was down-regulated in 60.0% of the primary ovarian tumors analyzed. Additionally, we found tumor-specific alternative transcripts of *PARK2*. Loss of heterozygosity analysis of primary ovarian tumors by use of polymorphic markers in the 6q26 region demonstrated 72% LOH in the center of the *PARK2* gene, the highest of any of the markers tested. FRA6E shares many similarities with FRA3B (3p14.2) and FRA16D (16q23.2) in representing a large region of genomic instability and containing an extremely large gene that may play a role in the development of ovarian and many other cancers.

INTRODUCTION

Chromosomal fragile sites are specific loci that are susceptible to forming gaps, breaks, and rearrangements when cells are challenged under specific tissue culture conditions. Fragile sites are currently classified into two classes on the basis of their relative frequency of occurrence in the general population. Rare fragile sites (RFSs) have been defined as sites observed in less than 5% of the population and inherited as Mendelian co-dominant alleles. In contrast, the common fragile sites (CFSs) are purported to be present in all individuals.

Most of what is known about chromosomal fragile sites pertains primarily to the RFSs. A correlation between chromosomal fragility and an observable clinical phenotype has been demonstrated with certain RFSs. FRAXA (Xq27.3) and FRAXE (Xq28) are associated with heritable mental retardation, and FRA11B (11q23.3) has been implicated in the generation of a chromosomal deletion characteristic of Jacobsen syndrome (Oberle et al., 1991; Knight et al., 1993; Jones et al., 1995). The potential biological significance of the CFSs, however, remains somewhat unclear. There are data to suggest that the CFSs play a causal role in tumorigenesis and/or cancer progression. All seven of the CFSs that have been cloned and well characterized, FRA3B (3p14.2), FRA7G (7q31.2), FRA7H (7q32.3), FRA9E (9q32), FRA16D (16q23.2), FRA2G (Limongi et al., 2003) and FRAXB (Xp22.3) (Wilke et al., 1996; Huang et al., 1998a,b; Mishmar et al., 1998; Krummel et al., 2000; Mangelsdorf et al., 2000; Paige et al., 2000; Arlt et al., 2002; Callahan et al., 2003) have been associated with a cancer-specific chromosomal rearrangement, a putative tumor-suppressor gene, and/or a region of high loss of heterozygosity (LOH) (Wilke et al., 1996; Huang et al., 1998b; Mishmar et al., 1998; Smith et al., 1998; Bednarek et al., 2000; Krummel et al., 2000; Mangelsdorf et al., 2000; Paige et al., 2000; Arlt et al., 2002). There is also evidence demonstrating that CFSs participate in gene amplification, and that they are preferred sites for DNA integration in vitro and viral integration in vivo (Popescu et al., 1990; Rassool et al., 1991;

Supported by: National Cancer Institute; Grant number: CA48031; Department of Defense; Grant number: DAMD17-99-1-9504; Mayo Clinic Cancer Center Ovarian Cancer Working Group.

*Correspondence to: Dr. David I. Smith, Professor, Director of the Cancer Genetics Program, Mayo Clinic Cancer Center, Division of Experimental Pathology, Mayo Foundation, 200 First Street SW, Rochester, MN 55905. E-mail: smith.david@mayo.edu

Received 14 November 2002; Accepted 25 April 2003

DOI 10.1002/gcc.10236

Published online 16 June 2003 in Wiley InterScience (www.interscience.wiley.com).

Coquelle et al., 1997; Thorland et al., 2000; Becker et al., 2002; Hellman et al., 2002).

Although these sites represent a small fraction of the 89 currently recognized CFSs, there is one noticeable similarity among them. Several of them contain very large genes that play an important role in tumorigenesis and/or cancer development. The focus of this study was to clone and characterize the CFS FRA6E (6q26), the third most frequently observed CFS in the human population. Chromosomal band 6q26 has been associated with a high frequency of LOH in squamous cell lung, ovarian, hepatocellular, and breast cancers (De Souza et al., 1995; Oates et al., 1998; Shridhar et al., 1999; Kong et al., 2000). Additionally, the putative tumor-suppressor gene *IGF2R* has been localized to the 6q26–27 region (De Souza et al., 1995). We report on the characterization of this unstable CFS and find that instability in this region extends for 3.6 megabases. The FRA6E CFS contains *IGF2R* (at its centromeric end), six small genes, and the very large *PARK2* gene (which is mutated in patients with autosomal recessive juvenile parkinsonism [ARJP]) spans the telomeric half of this fragile site. The most unstable region within FRA6E coincides with polymorphic markers that demonstrate the greatest LOH in primary ovarian tumors and occurs within the *PARK2* gene. Instability within this CFS may play an important role in cancer development and in the frequent *PARK2* deletions observed in ARJP patients.

MATERIALS AND METHODS

Selection of Clones

Bacterial artificial chromosome (BAC)/P1 artificial chromosome (PAC) clones were selected based on their localization to 6q26 by The Sanger Centre (Cambridge, UK), the Washington School of Medicine Genome Sequencing Center FPC Database (St. Louis, MO), or by PCR screening of the Research Genetics CITB Human BAC DNA Library (Release IV; Huntsville, AL), by use of primers designed to amplify known STS/EST markers in the 6q26 region. The protocol for the growth and isolation of clones is available on request.

Cytogenetic Localization of Clones

Metaphase preparations were obtained from blood cultures established from 1 ml of peripheral whole blood and 9 ml of Chang Media PB (Irvine Scientific, Santa Ana, CA). Cultures were incubated at 37°C in 5% CO_2 for 72 hr. Twenty-four hours before harvest, the cultures were inoculated with 0.2 μM aphidicolin (APC). Cell harvest and metaphase preparations followed routine cytogenetic techniques.

For each clone, 1 μg of purified BAC or PAC DNA was labeled with biotin-16-dUTP (Boehringer/Roche, Indianapolis, IN) by nick translation, precipitated, and hybridized to the APC-treated metaphase chromosomes according to the protocol described by Verma and Babu (Pennington and Sheinis, 1989). Probe detection followed minor modifications of the manufacturer's protocols (Ventana Medical Systems, Tucson, AZ). After overnight hybridization at 37°C, the slides were washed twice in 2× SSC (pH 7.0), twice in 2× SSC/50% formamide, and twice in 2× SSC (pH 7.0), all at 42°C for 5 min. Slides were then washed two times in room-temperature 2× SSC/0.2% Tween 20 for 5 min. Before detection, slides were incubated in room-temperature BT buffer (100 mM $NaHCO_3$, 300 mM NaCl, 0.05% Tween 20). A total of 75 μl of 5% BSA/BT buffer was added to each slide, and the slide was incubated for 5 min at room temperature. Amplification of the probe signal was performed by adding 100 μl of a 0.33% avidin/BT buffer mixture to each slide, incubating the slide(s) for 30 min at 37°C, and washing them in three 6-min washes of BT buffer at 39°C. A 1.5% solution of biotinylated anti-avidin in 5% normal goat serum (5% NGS/BT buffer) was then added to each slide for probe detection. Slides were washed three times in BT buffer at 39°C, and the chromosomes were counterstained with DAPI. Photomicroscopy was performed by use of a Zeiss Axioplan 2 fluorescence microscope and IPLab Spectrum P software (Scanalytics, Fairfax, VA). The position of each individual clone relative to FRA6E was determined by the analysis of a minimum of 20 APC-treated metaphase cells with breakage at 6q26. Breakage at 6q26 was identified by band location as established by DAPI banding. A clone was identified as crossing the fragile site if a hybridization signal was observed on both sides of the breakage or if a signal was observed as occurring proximal (centromeric) in one metaphase cell and distal (telomeric) in a separate metaphase cell (Fig. 1).

LOH Analysis of Primary Ovarian Tumors

The percentage LOH throughout the FRA6E region was determined by analysis of eight microsatellite markers identified as being heterozygous in a minimum of 60% of the human population. DNA primers specific for each marker were either obtained from Research Genetics (Huntsville, AL; MapPairs *D6S305*, *D6S411*, *D6S1008*, *D6S1579*,

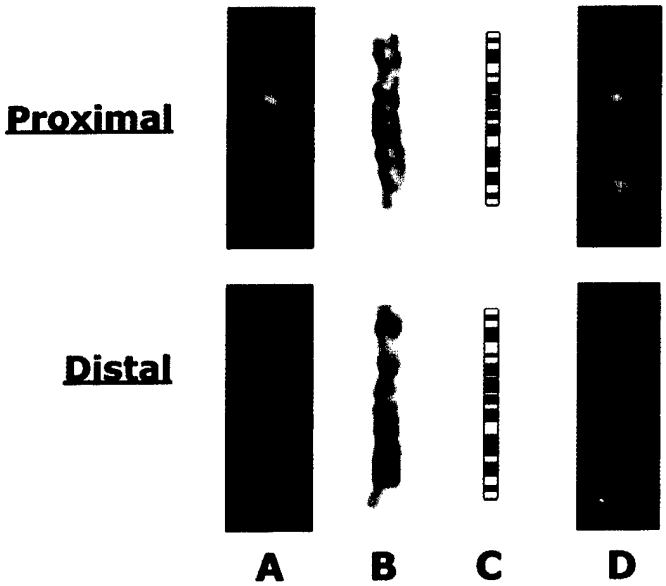

Figure 1. Depiction of clone RP1-81D8 determined to be crossing the region of FRA6E breakage. Chromosomes were obtained from separate APC-treated metaphase cells. For each break analyzed, the presence of breakage at 6q26 was initially scored from a DAPI-counterstained image. Breakage was confirmed as mapping to 6q26 by comparing the inverted DAPI image to a G-banded ideogrammatic representation of chromosome 6. Hybridization of the FITC-labeled clone (green) is shown as occurring both proximal and distal to the FRA6E region. Rhodamine-labeled RP1-119H20 (red) was in some instances hybridized simultaneously with clone RP1-81D8 and is shown as also hybridizing distal to FRA6E.

D6S1581) or synthesized by the Mayo Foundation Molecular Core Facility (Rochester, MN; *IGF2R*, *D6S1719*, and *D6S1599*). Primer sets specific for each marker were tested in both normal and tumor ovarian DNA (serous; stages 2–4) pairs obtained from 21 different patients. For each patient, tumor DNA was obtained from snap-frozen tissue, and paired noncancerous DNA was isolated from blood by standard phenol-chloroform methods. The forward primer for each microsatellite marker was end-radiolabeled with [γ^{32}P]ATP (10 μCi/μL) by use of the RTS T4 Kinase Labeling System (GibcoBRL, Rockville, MD). End-labeling was performed following the manufacturer's protocol. The PCR mix (12.5 μL reaction volume) contained: 50 ng of genomic DNA, 50 mM KCl, 10 mM Tris-HCl (pH 8.3), 1.5 mM $MgCl_2$, 200 μM concentration of the radiolabeled forward primer, 200 μM concentration of the unlabeled reverse primer, and 0.1 U *Taq* polymerase (Promega, Madison, WI). The conditions for amplification were: 94°C for three min, then 30 cycles of 94°C for 30 sec, 55–61°C for 30 sec, and 72°C for 30 sec, with a final extension of 72°C for 10 min. PCR products were denatured and electrophoresed on 6% denaturing polyacrylamide-sequencing gels containing 8 M urea. The gels were dried, autoradiographed for 16–24 hr, and subsequently scored for LOH. Allelic imbalance, indicative of LOH, was scored when there was more than 50% loss of intensity of one allele in the tumor sample with respect to the matched allele from normal tissue.

RT-PCR

RT-PCR products were obtained from total RNA extracted from normal ovarian epithelial brushings, short-term–cultured normal ovarian surface epithelium, seven ovarian tumor-derived cell lines (Mayo cell lines OV167, OV177, OV202, OV207, and OV266 [Conover et al., 1998], SKOV3, and OVCAR5), and 15 primary tumors (serous) ranging from stage 1 to stage 4 by use of Trizol reagent (GibcoBRL) following the manufacturer's instructions. For each reaction, DNA was eliminated by treating 5 μg of total RNA with RNase-free DNase for 30 min at 37°C, and the DNase was inactivated by incubating the reaction for 10 min at 90°C. Reverse transcription of DNase-treated RNA was performed following the manufacturer's protocol (GibcoBRL).

Unique primers were designed for genes localized to the FRA6E region (Table 1) by use of Oligo 6.4 software (Molecular Biology Insights, Cascade, CO) and used in a multiplex reaction with *GAPDH*, *ACTB*, or *TUBB2* internal control primers (Table 1). The PCR samples (20 μL total volume) contained 50–100 ng of reverse-transcribed cDNAs, 1× PCR buffer (as supplied with enzyme), 0.5 mM BSA, 200 μM dNTPs, 4 mM $MgCl_2$, 750 μM concentration of forward and reverse primers for the specific genes, and 0.1 U Platinum *Taq* polymerase (Invitrogen, Carlsbad, CA). The conditions for amplification were: 94°C for three min, then 28 cycles of 94°C

TABLE 1. STS and EST Markers Mapped to the FRA6E Region*

STS/EST marker	GenBank accession	LOH/RT-PCR/ BAC/AT	Primer sequence 5′ → 3′	Product size (bp)	Het
ACTB	NM_001101	RT-PCR	GCTCCGGCATGTGCAAGG	550	
			ATGAGGTAGTCAGTCAGGTC		
B2M	AH002619	RT-PCR	AGCTGTGCTCGCGCTACTCTCTC	140	
			GTGTCGGATTGATCAAACCCAGACAC		
D6S305	Z17103	LOH	CACCAGCGTTAGAGACTGC	218	0.84
			GCAAATGGAGCATGTCACT		
D6S411	Z23573	LOH	TGGTTGATTGACCCACTTAT	155	0.59
			TCACAGTGCCTGGTCC		
D6S1008	G08541	LOH/BAC	AAGAAAGACTAGAGAGACAGACAGC	246	
			ATCATTTGCCCATTTACCAA		
D6S1579	Z52681	LOH	TACTCACACATGCACAGGC	161	0.70
			CTTCCTACCCACATGCAG		
D6S1581	Z52717	LOH	AGGCTCATCCATGTTTCTG	219	0.72
			TGCATTCCCACATTTACTG		
D6S1599	Z52945	LOH	TGTTTTCCACAGGTTCCAG	133	0.69
			CTTCAGATGTAGGCTCCACG		
D6S1719	Z51973	LOH	GGAACTACTCCCATTCCAAC	178	0.75
			GAGATACAAGCAGGAGGTAGC		
GAPDH	M33197	RT-PCR	ACCACAGTCCATGCCATCAC	450	
			TCCACCACCCTGTTGCTTGTA		
IGF2R	Y00285	LOH	TTGCCGGCTGGTGAATTCAA	162	0.63
			GTATCATGAGAACCTGAAGAG		
IGF2R	NM_000876	RT-PCR	ATTGTCCAGTGCGGGCCATC	197	
			CCCAGGGTTTTCCCACACAG		
IGF2R	AF109281	BAC	GTCGGGCCAGAACAAG	156	
			AGGGCAACGATCACCATTCA		
MAP3K4	NM_005922	RT-PCR	AGGATGATTCTCTTGGCTGG	553	
			TCGGGCTTCTCCAAGTC		
LPA	X06290	RT-PCR	ACGTACTCCACCACTGTC	156	
			CGTATAACAATAAGGAGCTG		
PARK2	AB009973	RT-PCR	GTTGCTAAGCGACAGG	587	
			GCTACTGGTGTTTCCTTGTC		
PARK2	AB009973	AT	CCAGTGACCATGATAGTGTT	600	
			TGATGTTCCGACTATTTGTTG		
PARK2	AB009973	AT	TGACCCAGGGTCCATCTT	1067	
			TTTTCATGGACATAGTGAAG		
PLG	X05199	RT-PCR	AAGGAGAGCCTCTGGATGAC	353	
			AGGTCTGTGGGGAGAAGTGG		
SLC22A1	XM_004236	RT-PCR	ATGACATTCTGGAGCAGG	527	
			CAGGAGACACAGCTTACG		
SLC22A2	XM_004235	RT-PCR	CGTCCATCGTCACCGAG	1383	
			CAGGGGTAAGTTTGGTTGAG		
SLC22A3	XM_011436	RT-PCR	CAGAGACAGTGGATGATG	330	
			GCTTCTTTGTTAAACTGG		
TUBB2	BC007889	RT-PCR	GCATCAACGTGTACTACAA	454	
			TACGAGCTGGTGGACTGAGA		

*The GenBank accession number (when available), primer sequence, PCR product size, and percentage heterozygosity (Het) in the population (when applicable) are provided for each STS/EST marker. Also included is the experiment for which the primers were used. LOH primers were used to assess loss of heterozygosity throughout the FRA6E region. RT-PCR primers were used for expression analysis. BAC primers were used in BAC screens for potential BAC clones in the region, and AT primers were used for screening the ovarian panel for alternative transcripts.

for 30 sec, 55–67°C for 30 sec, and 72°C for 30 sec, with a final extension of 72°C for 10 min.

RESULTS

Cloning and Characterization of FRA6E

Fluorescence in situ hybridization (FISH) of large insert clones localized to the 6q26 band region identified seven clones that define FRA6E (Figs. 1 and 2). Analysis of BAC clone RPCI-1-249F5 on 20 APC-induced metaphase cells determined that all 20 signals hybridized proximal to the observed breakage at 6q26. FISH analysis of clone 424P10, identified by screening of the Research Genetics CITB BAC library by use of primers

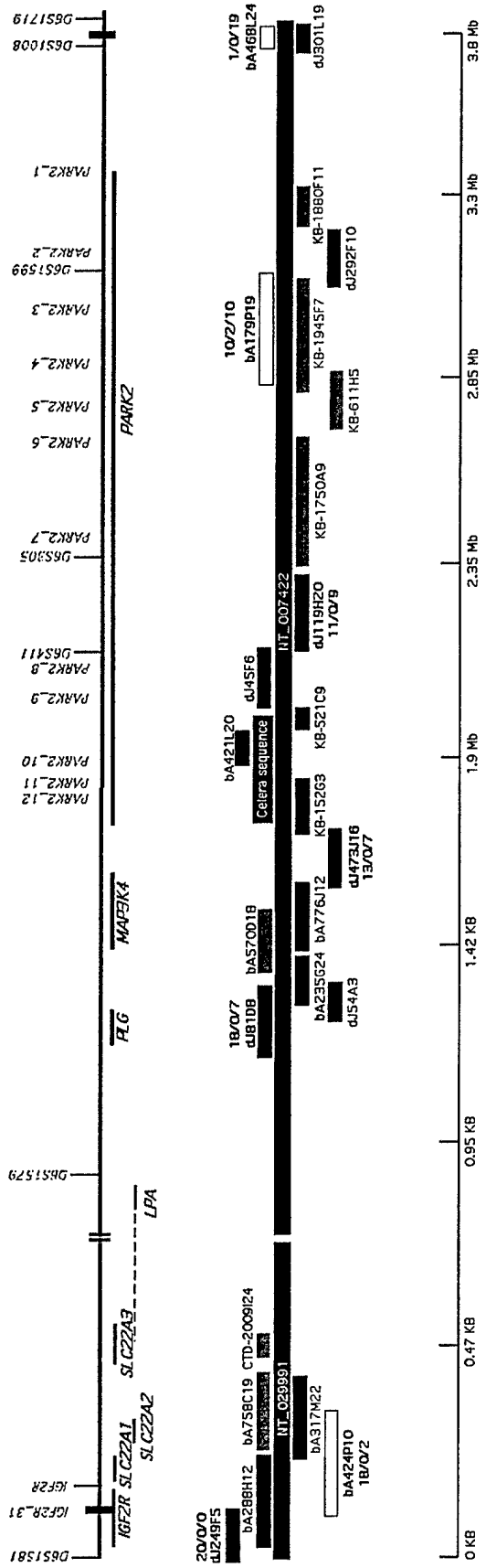

Figure 2. Approximately 3.6-Mb sequence-based contig for the FRA6E region. Clone representations are proportional to the size of inserted sequence. Black rectangles (■) represent clones for which the complete ordered sequence has been assembled. Clones that have been sequenced but remain unordered are represented by a gray rectangle (▤). Open rectangles represent unsequenced clones. A gap in the sequence is indicated by double vertical bars. The placement and relative size are provided for the eight genes that align to sequence in the region. The size of *LPA* remains undetermined and is therefore represented by a dashed line (– – –). FISH data for those clones for which 20 APC-treated metaphase cells were analyzed are provided above the particular clone (proximal/crossing/distal). Vertical blocks indicate the boundaries of FRA6E. The relative position of STS/EST markers used in this study relative to the fragile site is also provided.

designed for *IGF2R* exon 38, determined that 18 of the 20 signals hybridized proximal to the breakage at 6q26. The remaining two signals were observed as distal to the fragile site, indicating that the centromeric end of FRA6E lies between clones RPCI-1-245F9 and 424P10 (Fig. 2). Definition of the telomeric end of FRA6E was determined by FISH analysis of clone 468L24 (identified by screening of the BAC library by use of the MapPair for *D6S1008*). The hybridization signal was observed proximal to the region of breakage only once in the 20 metaphase cells analyzed. The remaining 19 hybridization signals were observed distal, indicating that the telomeric boundary of FRA6E is in close proximity to 468L24 (Fig. 2). Five additional clones encompassed within the boundaries of FRA6E were hybridized and analyzed to determine the "center" of the FRA6E fragile site. Hybridization signals for clones RPCI-1 119H20 and 179P19 were observed nearly 50% of the time proximal and 50% of the time distal to the region of breakage. Therefore, these clones were determined to define the "center" of FRA6E (Fig. 2). Although the region between these two clones does not fall in the geographic center, for the purposes of this study, this region will be referred to as the "center" of FRA6E.

Because of the large effort of the Human Genome project, we were able to obtain the sequence for BAC and PAC clones mapping throughout the FRA6E region. Through the use of the original seven clones as landmarks, a sequence-based contig of the FRA6E region was assembled with the Sequencher computer program (Version 3.1; Gene Codes, Ann Arbor, MI). The Sanger Centre (http://www.sanger.ac.uk; Cambridge, UK) has this region divided into two separate contigs (chr_6ctg5 and chr_6ctg9). Contig 111 (chr_6ctg111) consists of clones RPCI-1 111C20 through RP-11 178P20 and includes the *IGF2R* locus, and contig 5 (chr_6ctg5) begins with clone RP-3 366M24 and encompasses the *PARK2* locus. The sequence-based contig we have assembled combines these into a single contig. Based on this sequence alignment, we were able to assemble contiguously a majority of the FRA6E region (Fig. 2). We attempted to eliminate gaps in the contig by use of sequence data made available by Celera Genomics (www.celera.com; Rockville, MD) (Venter et al., 2001) and by end-sequencing of clones indicated by the FPC database to span the noncontiguous regions. However, the Celera sequence data and the remaining FPC-identified clones did not aid in the completion of sequence alignment within the region. As a result, there is a single gap remaining in the assembled contig located near marker *D6S1579*. On the basis of the aligned sequence, we estimate FRA6E to span approximately 3.6 Mb.

The available sequence localized to 6q26 also allowed for the positioning of genes relative to FRA6E. To date, eight genes have been localized within the FRA6E region: apolipoprotein-A (*LPA*), mannose-6-phosphate/insulin-like growth factor 2 receptor (*IGF2R*), mitogen-activated protein kinase kinase kinase 4 (*MAP3K4*), plasminogen (*PLG*), *PARK2*, and solute carrier 22, members 1, 2, and 3 (*SLC22A1*, *SLC22A2*, and *SLC22A3*, respectively). The position of these genes relative to FRA6E is indicated in Figure 2. FRA6E localizes between *IGF2R* and *PARK2*. Whereas the *PARK2* gene is contained completely within the fragile site, data suggest that only portions of *IGF2R* localize to the region. End-sequencing of clone 424P10 indicated that exons 32–48 of *IGF2R* definitively map within FRA6E. Because the proximal end of FRA6E is located in the region between clones RPCI-1-249F5 and 424P10, additional FISH analysis is required to delineate what portion of the *IGF2R* gene resides within this region. Of the six remaining genes, five (*MAP3K4*, *PLG*, *SLC22A1*, *SLC22A2*, and *SLC22A3*) are definitely encompassed within the fragile site. The portion of the *LPA* gene contained within FRA6E, however, remains unknown. The highly repetitive nature of *LPA* does not allow for complete alignment of its genomic sequence with that for FRA6E. Therefore, it remains unclear as to whether *LPA* is completely encompassed by FRA6E or whether it extends into the region proximal to the fragility at 6q26.

LOH Analysis of Primary Ovarian Tumors

Eight microsatellite markers were used to test 21 primary ovarian tumors (serous, stages 2–4) for LOH. Six of the selected markers localized within the FRA6E region; the remaining two markers, *D6S1581* and *D6S1719*, localized outside of FRA6E, centromeric and telomeric, respectively (Fig. 2). LOH analysis of these eight markers determined that 19 (90.4%) of the tumors sampled had LOH of at least one of the markers tested (Table 2). The number of markers at which a single tumor displayed LOH ranged from one to seven; no tumors had LOH at all of the microsatellite markers sampled (Table 2). The percentage LOH of the eight markers ranged from 25.0% to 64.7%. The lowest frequency of LOH was observed at *D6S1581* (25.0%) and *D6S1719* (33.3%).

TABLE 2. Observed Loss of Heterozygosity (LOH) in 21 Primary Ovarian Tumors (serous; stages 2–4) at Eight Microsatellite Markers Located Throughout the FRA6E Region

Marker	1	2	3	4	5	6	7	8	9	10	11	12	13	14	15	16	17	18	19	20	21	P[a]
D6S1581	UI[b]	○[c]	UI	UI	UI	UI	○	UI	—[d]	○	UI	MI[e]	○	UI	●[f]	MI	●	○	○	○	●	25.0
IGF2R	○	○	●	○	○	○	●	○	●	UI	○	○	UI	○	●	UI	○	●	○	UI	●	35.3
D61579	—	UI	●	—	○	●	UI	○	○	○	UI	●	●	○	UI	○	●	●	UI	●	○	50.0
D6S411	○	○	○	○	UI	UI	○	●	●	—	●	UI	UI	UI	●	UI	●	○	●	○	MI	42.9
D6S305	●	UI	●	●	○	○	○	UI	●	—	●	●	UI	●	●	○	●	○	○	●	●	64.7
D6S1599	UI	○	●	—	UI	○	UI	MI	○	UI	●	●	UI	—	MI	UI	●	●	●	●	●	61.5
D6S1008	○	○	●	—	●	○	○	MI	●	●	○	○	○	○	●	○	●	UI	UI	UI	—	40.0
D6S1719	UI	○	○	—	UI	○	○	○	●	○	●	○	UI	○	○	○	●[z]	—	●	—	●	33.3

[a]Percentage of tumors with LOH at that locus.
[b]The marker was uninformative.
[c]LOH was not observed.
[d]Marker amplified in normal DNA but would not amplify in tumor DNA.
[e]Microsatellite instability observed at that locus.
[f]LOH was observed at that marker.

The highest frequency of LOH was observed at *D6S305* (64.7%). This marker was localized within FRA6E by sequence alignment and was located telomeric to RPCI-1 179P19, in the middle of the *PARK2* gene (Fig. 2).

RT-PCR

RT-PCR was performed on short-term culture normal ovarian epithelium (OSE), ovarian cancer cell lines, as well as primary tumors by use of primers designed specifically for the eight genes in FRA6E (Table 1). Initially, each gene was analyzed for expression in normal ovarian epithelium by use of cDNA products derived from normal ovarian epithelial brushings (data not shown). All but three of the genes analyzed (*SLC22A1*, *SLC22A2*, and *LPA*) were expressed in the normal ovarian brushings. Because *SLC22A1*, *SLC22A2*, and *LPA* were not expressed in the brushings, RT-PCR was not performed for the ovarian cell lines or primary tumors. The expression levels for the five remaining genes were subsequently analyzed in both primary ovarian tumors (serous, stages 1–4) and tumor-derived cell lines and compared to the expression level in OSE (Fig. 3). Gene-specific primer sets for all of the genes tested were multiplexed with *B2M*, *GAPDH*, *ACTB*, or *TUBB2* control primers. The appropriate control genes were chosen for each gene tested so that the PCR products obtained were similar in size (Fig. 3). Expression analysis for the five genes indicated that all but *MAP3K4* showed decreased expression in at least one cell line and/or primary tumor when expression levels were compared to that of the OSE (Fig. 3).

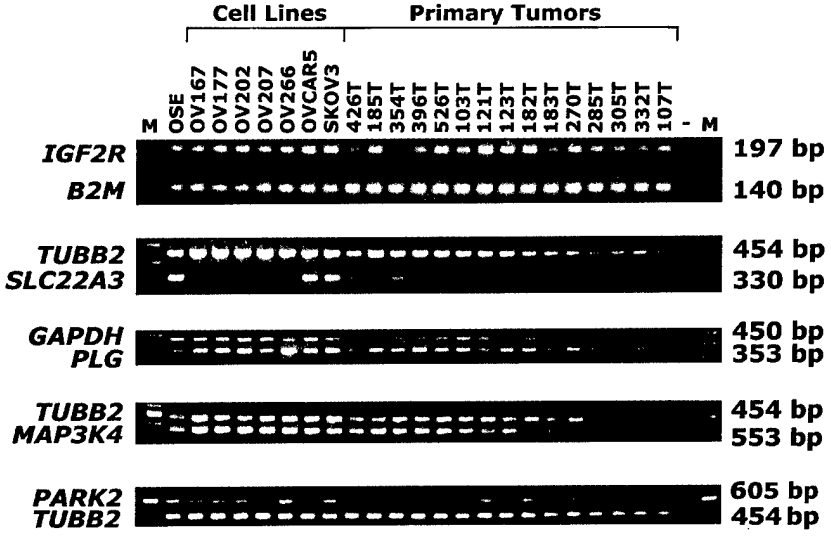

Figure 3. RT-PCR analysis of the genes mapping to the FRA6E region. Each gene was tested for the presence or absence of expression in short-term cultured normal ovarian surface epithelium (OSE), seven tumor-derived ovarian cell lines (OV167, OV177, OV202, OV207, OV266, OVCAR5, and SKOV3), and 15 primary ovarian tumors. The internal control (*GAPDH*, *B2M*, or *TUBB2*) used for each specific primer set is indicated. A negative control (−) is also provided. Marker ladder is indicated as M.

When expression levels for *MAP3K4* in OSE were compared to that of the cell lines and the primary tumors, none showed any decrease in expression. *IGF2R*, *PLG*, and *PARK2* were expressed in all of the cell lines and primary tumors tested, but did show a decrease of expression in some of the cell lines and primary tumors analyzed (Fig. 3). *IGF2R* and *PLG* were down-regulated only in the primary tumors, 6/15 (40.0%) and 1/15 (6.7%), respectively. *PARK2* exhibited decreased expression in 2/7 (28.5%) of the tumor-derived cell lines and 7/15 (46.7%) of the primary tumors analyzed. *SLC22A3* showed an absence of expression in both the cell lines and primary tumors examined. RT-PCR analysis of *SLC22A3* expression determined the lack of expression in 4/7 (57.1%) of the tumor-derived cell lines and in 9/15 (60.0%) of the primary ovarian tumors (Fig. 3).

Although *PARK2* was not the gene with the highest loss of expression (LOE) from this region, RT-PCR analysis of *PARK2*, by use of primers encompassing exons 2 to 6, revealed the presence of alternative transcripts in both the ovarian cell lines and primary ovarian tumors tested (Fig. 4). These alternative transcripts were never observed in OSE, or in any other normal tissues analyzed, including liver, kidney, prostate, and OR normal keratinocytes (Fig. 4). Various intragenic homozygous and heterozygous deletions/duplications and point mutations in *PARK2* have been identified in patients with ARJP, characterized by an early onset of parkinsonism (before the age of 40), and result in either protein truncation or an amino acid substitution (Kitada et al., 1998; Lucking et al., 1998; Abbas et al., 1999; de Silva et al., 2000; Hedrich et al., 2001; Terreni et al., 2001). In particular, variable deletions and duplications have been documented throughout *PARK2*, with the majority of them localizing between exons 3 and 8 (Fig. 4a) (Kitada et al., 1998; Lucking et al., 1998; Abbas et al., 1999; de Silva et al., 2000; Hedrich et al., 2001; Terreni et al., 2001). We designed two sets of RT primers (Table 1), one encompassing *PARK2* coding sequence from exons 1–6 and the other from exons 5–12, which together encompassed the complete coding sequence for *PARK2*, to analyze seven ovarian cell lines and 22 primary ovarian tumors, 15 of which had been analyzed by RT-PCR (Fig. 3), for alternative transcripts in *PARK2*. The seven additional tumors were analyzed by RT-PCR by use of primers specific to *GAPDH* (data not shown) to control for the amount of RNA in each sample (Fig. 3). Previous alternative-transcript analyses of *FHIT* and *WWOX* were performed by nested PCR analysis of cell lines and primary tumors (Druck et al., 1998; Bednarek et al., 2001). However, because we observed alternative transcripts by use of conventional single-round (28-cycle) PCR, we opted merely to increase the number of PCR cycles to 35 rather than perform nested PCR. RT-PCR analysis of the cell line/primary tumor panel identified several alternative transcripts in both the cell lines and primary tumors analyzed that were not observed in normal OSE (Fig. 4b). Sequence analysis of these transcripts determined that they were alternative *PARK2* transcripts. In some instances, however, a normal transcript was observed for *Parkin* by use of the alternative transcript primers when a normal transcript was not observed with the RT primers (Figs. 3 and 4). This inconsistency in observed transcripts may be the result of the position of the primers in the coding region of *Parkin*. If a primer was designed in an exon that was either partially or completely deleted in a portion of the *Parkin* transcripts for that particular tumor, no transcript or a lesser amount of transcript would be observed by use of that primer set. We detected no tumor-specific alternative transcripts for any of the other genes in the FRA6E region.

DISCUSSION

In this study, we cloned and characterized the CFS FRA6E (6q26), the third most frequently observed CFS in the human population. FISH analysis of large insert clones localized to the 6q26 band region allowed for the identification of seven clones that define the FRA6E region (Fig. 2). In addition, a sequence-based contig was constructed across the FRA6E region and allowed for an estimation of the size of the FRA6E region of instability. The fragility at FRA6E extends approximately 3.6 Mb, making it the third largest CFS characterized to date; the two largest CFSs are FRA3B at 3p14 (4 Mb), the most frequently observed CFS in the human population, and FRA9E at 9q32 (9.8 Mb), a less frequently observed CFS (Becker et al., 2002; Callahan et al., 2003). The other CFSs that have been cloned and characterized are much smaller in size compared to FRA9E, FRA3B, and FRA6E. FRA16D (16q23.2) has been estimated at 1.5 Mb and FRA7G, FRA7H, and FRAXB are estimated at only 161 to 500 kb in size (Wilke et al., 1996; Huang et al., 1998b; Mishmar et al., 1998; Krummel et al., 2000; Mangelsdorf et al., 2000; Paige et al., 2000; Arlt et al., 2002). The data on two of these CFSs (FRA7G and FRA7H), however, are incomplete. The ends of these sites remain only loosely defined, and thus these CFSs may represent larger

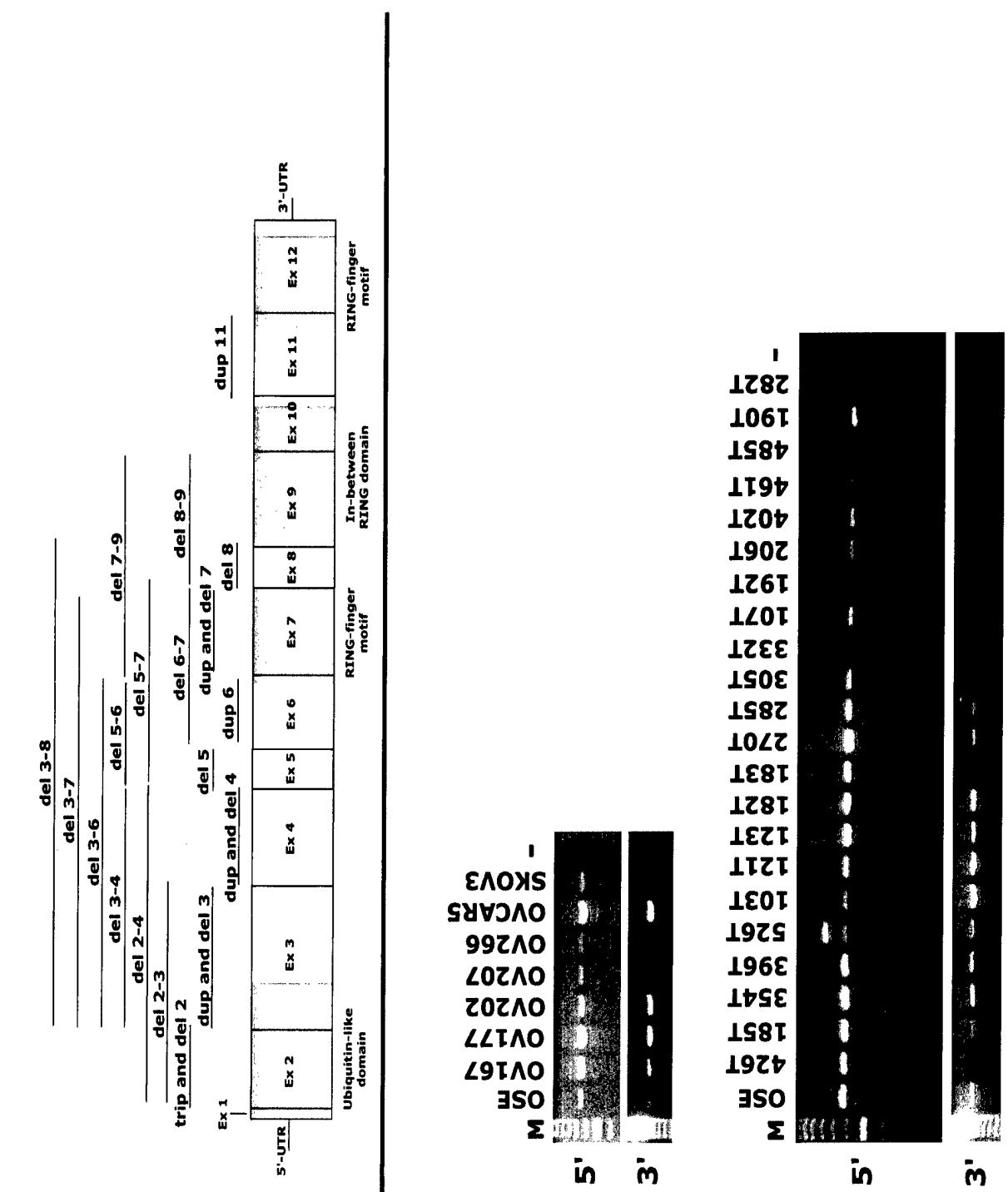
a
del 3-8
del 3-7
del 3-6
del 3-4
del 5-6
del 7-9
del 2-4
del 5-7
del 2-3
del 6-7
del 8-9
trip and del 2
dup and del 3
del 5
dup and del 7
dup 11
dup and del 4
dup 6
del 8
Ex 1
Ex 2
Ex 3
Ex 4
Ex 5
Ex 6
Ex 7
Ex 8
Ex 9
Ex 10
Ex 11
Ex 12
5'-UTR
3'-UTR
Ubiquitin-like domain
RING-finger motif
In-between RING domain
RING-finger motif
b
M
OSE
OV167
OV177
OV202
OV207
OV266
OVCAR5
SKOV3
-
5'
3'
M
OSE
426T
185T
354T
396T
526T
103T
121T
123T
182T
183T
270T
285T
305T
332T
107T
192T
206T
402T
461T
485T
190T
282T
-
5'
3'

Figure 4.

regions of fragility. However, if the size estimations for the currently cloned and characterized CFSs are correct, then the data suggest that there is no correlation between the size of a CFS region of instability and the observed frequency of its expression in vitro.

Eight genes were identified as being either partially or completely contained within FRA6E (Fig. 2). FRA6E is very similar in genomic structure to the previously cloned highly active CFSs FRA3B (Becker et al., 2002) and FRA16D (Bednarek et al., 2000), given that genomic instability extends over a large region, and contained within the center of this region of instability is an extremely large gene. *PARK2* is estimated at 1.5 MB in size (Kitada et al., 1998). Five of the eight genes that localize within FRA6E were expressed in normal ovarian epithelium, and these were analyzed for their expression in ovarian cancer cell lines and primary tumors. Only *MAP3K4* showed normal expression in ovarian cancer cell lines and primary tumors. The remaining four genes all exhibited decreased mRNA expression in either a tumor-derived cell line or a primary ovarian tumor. There was no obvious pattern of LOE across the cell lines and primary tumors, and no tumor or cell line exhibited a loss or decrease of expression for all of the genes in FRA6E. These data are consistent with expression data obtained for genes that were localized to other cloned CFSs (Le Beau et al., 1998; Lee et al., 1998; Smith et al., 1998; Arlt et al., 2002; Denison et al., 2002).

LOH is frequently observed within FRA3B and FRA16D in a variety of different tumor types, including ovarian cancer. We therefore examined microsatellite markers throughout FRA6E against a panel of primary ovarian tumors, with matched blood from each patient. Percentage LOH observed across the eight markers mapping to the FRA6E region ranged from 25.0% (*D6S1581*) to 64.7% (*D6S305*) (Table 2). LOH analysis of these eight markers identified a significantly high frequency of LOH at *D6S1599* (61.5%) and *D6S305* (64.7%) (Table 2). These markers localize to introns 2 and 6, respectively, of the *PARK2* gene (Fig. 2). These markers are also contained within the center of the FRA6E CFS, demonstrating at the molecular level that the center of FRA6E contains markers that show the highest LOH in ovarian tumors.

Previous studies have shown that many of the genes mapping to other cloned CFSs show LOE in various tumor types and/or tumor-derived cell lines (Le Beau et al., 1998; Lee et al., 1998; Smith et al., 1998; Tatarelli et al., 2000; Arlt et al., 2002; Denison et al., 2002). RT-PCR on normal ovarian epithelial brushings, OSE, ovarian cell lines, and primary tumors revealed that five of the eight genes were expressed in normal ovarian epithelium; thus, only these five were analyzed for their level of expression in ovarian cancer cell lines and primary tumors. Only *MAP3K4* showed normal expression when the expression levels in tumor-derived cell lines and primary ovarian tumors were compared to that of OSE (Fig. 3). Of the remaining four genes (*IGF2R*, *PLG*, *SLC22A3*, and *PARK2*), all exhibited decreased expression in either a tumor-derived cell line and/or a primary ovarian tumor. *SLC22A3* expression levels were determined to be down in 57.1% (4/7) cell lines and 60.0% (9/15) of the primary ovarian tumors analyzed. There was no obvious pattern for LOE across the cell lines and the primary tumors. No one cell line or primary tumor exhibited a loss or decrease of expression for all of the genes in the FRA6E region. These data are consistent with expression data collected for genes localized to other cloned CFSs.

The "center" of a common fragile site is generally defined as the region where clones hybridize with approximately equal frequency and distal to aphidicolin-induced breakage in this unstable region. We have now observed for FRA3B and FRA6E that the center regions of the CFSs do not coincide with the physical center of the fragile site. Instead, the "center" of these two fragile sites spans the middle of two extremely large genes, *FHIT* (in FRA3B) and *PARK2* (in FRA6E). We have also observed that markers within the "center" of the FRA6E CFS showed the greatest LOH in primary ovarian tumors, as has been observed for markers within the "center" of FRA3B and *FHIT*.

Constitutional mutations in the *PARK2* gene have been associated with the neurodegenerative disorder referred to as autosomal recessive juvenile Parkinson's disease, characterized by an early onset of parkinsonism (before the age of 40 years) (Kitada et al., 1998). Mutational screening of ARJP patients has revealed the presence of various intragenic

Figure 4. *PARK2* mutations and aberrant transcripts. **a:** Previously identified mutations in *PARK2* in ARJP patients. [Adapted from Lucking et al. (1998), de Silva et al. (2000), Hedrich et al. (2001), and Terreni et al. (2001).] **b:** Alternative transcript analysis of short-term-cultured normal ovarian surface epithelium (OSE), normal liver, normal kidney, normal prostate, normal keratinocytes, seven tumor-derived cell lines (OV167, OV177, OV202, OV207, OV266, OVCAR5, and SKOV3), and 22 primary ovarian tumors by use of primer sets specifically designed to encompass exons 1 to 6 (5′) and exons 5 to 12 (3′) of the *PARK2* coding sequence. A negative control (−) and marker ladder (M) are provided.

homozygous and heterozygous deletions/duplications and point mutations in *PARK2* in those patients (Kitada et al., 1998; Lucking et al., 1998; Abbas et al., 1999; de Silva et al., 2000; Hedrich et al., 2001; Terreni et al., 2001). Many of the heterozygous mutations were found to be quite large (Kitada et al., 1998; Lucking et al., 1998; Abbas et al., 1999; de Silva et al., 2000; Hedrich et al., 2001; Terreni et al., 2001). Although variable deletions and duplications have been documented throughout the major portion of *PARK2*, most of them localize between exons 3 and 8, which spans the center of FRA6E (Fig. 4a; Abbas et al., 1999).

Detailed analyses of the genomic alterations that occur in *FHIT* in human tumors have not been carried out because this gene spans more than 1 Mb of highly unstable genomic DNA within the center of FRA3B. One technique for characterizing such a large gene was to focus on the relatively small 1.1-kb final processed transcript and use RT-PCR to amplify and characterize *FHIT* transcripts. Through the use of nested PCR primers, a number of groups detected multiple aberrant *FHIT* transcripts that appeared to be tumor-specific (Mao et al., 1996; Yanagisawa et al., 1996; Simon et al., 1998). We carried out a similar analysis on *PARK2* with two sets of RT-PCR primers specifically designed to amplify the whole *PARK2* coding region, which also spans the "center" of FRA6E. We analyzed seven ovarian cell lines and 22 primary ovarian tumors for alternative transcripts in *PARK2*. Screening of the cell line/primary tumor panel identified several alternative transcripts in both the cell lines and the primary tumors analyzed (Fig. 4b). Sequence analysis of these alternative transcripts determined that the alternative PCR products were derived from *PARK2*, but contained exonic duplications and/or deletions (Fig. 4b). The observed expression levels of *PARK2* compared to that of OSE were dependent on the particular primer set used. Nearly 55% of the primary tumors analyzed showed decreased expression of *PARK2*. The number of primary tumors with either LOE or the presence of an alternative *PARK2* transcript was 77.3%. The complete characterization of both the normal and alternative transcripts is currently ongoing in our laboratory. Additional studies will be required to determine whether *PARK2* actually plays a role both in ARJP and in the development of ovarian cancer or is merely a bystander to the observed instability in this region.

What role might *PARK2* play in the development and/or progression of ovarian cancer? *PARK2* has been linked to the ubiquitin-mediated pathway of regulated protein degradation (Imai et al., 2000; Zhang et al., 2000). *PARK2* is classified as a member of the RING finger domain E3 family of ubiquitin protein ligases because of the presence of two RING domains located at its COOH terminus (Imai et al., 2000; Weissman, 2001). Other RING finger E3s include Mdm2, which ubiquitylates p53, and BRCA1 (Weissman, 2001). Initial studies to determine ubiquitin-mediated proteins that bind to *PARK2* have identified CDCrel-1, the synaptic-vesicle–associated protein, as one protein whose degradation is mediated by *PARK2* (Zhang et al., 2000). Familial-linked mutations in both RING finger domains have been shown to disrupt the ubiquitin-protein ligase function of *PARK2* and impair both *PARK2* and CDCrel-1 degradation (Zhang et al., 2000; Weissman, 2001). This loss of function has been suggested as the cause of ARJP.

Determination of the role of the CFSs in cancer has been problematic because of the lack of observed similarities among these cloned CFSs. The data presented in this study, however, do suggest genomic similarities among the most frequently expressed human CFSs: FRA3B, FRA16D, and FRA6E. All three of the most frequently observed CFSs span at least 1.5 Mb and contain an extremely large gene that encompasses the majority of the fragile region. FRA7H (one of the top five most frequently observed CFSs) is the only high-frequency CFS that has not had any genes mapped within the region of fragility. However, Mishmar et al. (1998) did not exclude the possibility that a large gene could span the 161-kb fragile region. The three very large genes that are contained within these CFSs (*FHIT*, *WWOX*, and *PARK2*) have similar genomic structures. *FHIT*, *WWOX*, and *PARK2* span 1.4, 1.0, and 1.5 Mb, contain 10, 9, and 12 exons, and encode a 1.1, 1.1, and 2.9 kb mRNA, respectively. In contrast to these large CFS genes, dystrophin (*DMD*), the largest known gene in the genome (which is not present within a CFS region), spans 2.4 Mb, contains 79 exons, and produces an approximately 12-kb transcript. Furthermore, FRA3B, FRA16D, and now FRA6E have each been associated with a region of high LOH and LOE for genes mapping within them (Ohta et al., 1996; Druck et al., 1998; Le Beau et al., 1998; Smith et al., 1998; Bednarek et al., 2000, 2001; Krummel et al., 2000; Mangelsdorf et al., 2000; Paige et al., 2000; this study). Finally, *PARK2* is similar to both *FHIT* and *WWOX* in that alternative transcripts have been identified in both tumor-derived cell lines and primary tumors (Druck et al., 1998; Bednarek et al., 2001).

Many questions remain about *PARK2* and the highly unstable CFS region that spans it. Are the large deletions observed in some patients with ARJP attributable to instability within the CFS region? Is *PARK2* the target of 6q26 deletions in ovarian cancer? What role does *PARK2* play, if any, in the development of ovarian cancer? Is *PARK2* similar to *FHIT* and *WWOX* and, as such, is it an important tumor-suppressor target that is frequently altered during the development of ovarian and possibly other cancers? We are currently characterizing *PARK2* in greater detail to begin to address these important questions.

ACKNOWLEDGMENTS

We thank Dr. Kimberly Kalli for providing the short-term normal ovarian epithelial (OSE) cultures. This work was supported in part by grants from the National Cancer Institute (CA48031) and Department of Defense (DAMD17-99-1-9504) (both to D.I.S.).

REFERENCES

Abbas N, Lucking CB, Ricard S, Durr A, Bonifati V, De Michele G, Bouley S, Vaughan JR, Gasser T, Marconi R, Broussolle E, Brefel-Courbon C, Harhangi BS, Oostra BA, Fabrizio E, Bohme GA, Pradier L, Wood NW, Filla A, Meco G, Denefle P, Agid Y, Brice A. 1999. A wide variety of mutations in the parkin gene are responsible for autosomal recessive parkinsonism in Europe. French Parkinson's Disease Genetics Study Group and the European Consortium on Genetic Susceptibility in Parkinson's Disease. Hum Mol Genet 8:567–574.

Arlt MF, Miller DE, Beer DG, Glover TW. 2002. Molecular characterization of FRAXB and comparative common fragile site instability in cancer cells. Genes Chromosomes Cancer 33:82–92.

Becker NA, Thorland EC, Denison SR, Phillips LA, Smith DI. 2002. Evidence that instability within the FRA3B region extends four megabases. Oncogene 21:8713–8722.

Bednarek AK, Laflin KJ, Daniel RL, Liao Q, Hawkins KA, Aldaz CM. 2000. WWOX, a novel WW domain-containing protein mapping to human chromosome 16q23.3–24.1, a region frequently affected in breast cancer. Cancer Res 60:2140–2145.

Bednarek AK, Keck-Waggoner CL, Daniel RL, Laflin KJ, Bergsagel PL, Kiguchi K, Brenner AJ, Aldaz CM. 2001. WWOX, the FRA16D gene, behaves as a suppressor of tumor growth. Cancer Res 61:8068–8079.

Callahan G, Denison SR, Phillips LA, Shridhar V, Smith DI. 2003. Characterization of the common fragile site FRA9E and its potential role in ovarian cancer. Oncogene 22:590–601.

Conover CA, Hartmann LC, Bradley S, Stalboerger P, Klee GG, Kalli KR, Jenkins RB. 1998. Biological characterization of human epithelial ovarian carcinoma cells in primary culture: the insulin-like growth factor system. Exp Cell Res 238:439–449.

Coquelle A, Pipiras E, Toledo F, Buttin G, Debatisse M. 1997. Expression of fragile sites triggers intrachromosomal mammalian gene amplification and sets boundaries to early amplicons. Cell 89:215–225.

Denison SR, Becker NA, Ferber MJ, Phillips LA, Kalli KR, Lee J, Lillie J, Smith DI, Shridhar V. 2002. Transcriptional profiling reveals that several common fragile-site genes are downregulated in ovarian cancer. Genes Chromosomes Cancer 34:406–415.

de Silva HR, Khan NL, Wood NW. 2000. The genetics of Parkinson's disease. Curr Opin Genet Dev 10:292–298.

De Souza AT, Hankins GR, Washington MK, Orton TC, Jirtle RL. 1995. M6P/IGF2R gene is mutated in human hepatocellular carcinomas with loss of heterozygosity. Nat Genet 11:447–449.

Druck T, Berk L, Huebner K. 1998. FHITness and cancer. Oncol Res 10:341–345.

Hedrich K, Kann M, Lanthaler AJ, Dalski A, Eskelson C, Landt O, Schwinger E, Vieregge P, Lang AE, Breakefield XO, Ozelius LJ, Pramstaller PP, Klein C. 2001. The importance of gene dosage studies: mutational analysis of the parkin gene in early-onset parkinsonism. Hum Mol Genet 10:1649–1656.

Hellman A, Zlotorynski E, Scherer SW, Cheung J, Vincent JB, Smith DI, Trakhtenbrot L, Kerem B. 2002. A role for common fragile site induction in amplification of human oncogenes. Cancer Cell 1:89–97.

Huang H, Qian C, Jenkins RB, Smith DI. 1998a. Fish mapping of YAC clones at human chromosomal band 7q31.2: identification of YACS spanning FRA7G within the common region of LOH in breast and prostate cancer. Genes Chromosomes Cancer 21:152–159.

Huang H, Qian J, Proffit J, Wilber K, Jenkins R, Smith DI. 1998b. FRA7G extends over a broad region: coincidence of human endogenous retroviral sequences (HERV-H) and small polydispersed circular DNAs (spcDNA) and fragile sites. Oncogene 16: 2311–2319.

Imai Y, Soda M, Takahashi R. 2000. Parkin suppresses unfolded protein stress-induced cell death through its E3 ubiquitin-protein ligase activity. J Biol Chem 275:35661–35664.

Jones C, Penny L, Mattina T, Yu S, Baker E, Voullaire L, Langdon WY, Sutherland GR, Richards RI, Tunnacliffe A. 1995. Association of a chromosome deletion syndrome with a fragile site within the proto-oncogene CBL2. Nature 376:145–149.

Kitada T, Asakawa S, Hattori N, Matsumine H, Yamamura Y, Minoshima S, Yokochi M, Mizuno Y, Shimizu N. 1998. Mutations in the parkin gene cause autosomal recessive juvenile parkinsonism. Nature 392:605–608.

Knight SJL, Flannery AV, Hirst MC, Campbell L, Christodoulou Z, Phelps SR, Pointon J, Middleton-Price HR, Barnicoat A, Pembrey ME, Holland J, Oostra BA, Bobrow M, Davies KE. 1993. Trinucleotide repeat amplification and hypermethylation of a CpG island in FRAXE mental retardation. Cell 74:127–134.

Kong FM, Anscher MS, Washington MK, Killian JK, Jirtle RL. 2000. M6P/IGF2R is mutated in squamous cell carcinoma of the lung. Oncogene 19:1572–1578.

Krummel KA, Roberts LR, Kawakami M, Glover TW, Smith DI. 2000. The characterization of the common fragile site FRA16D and its involvement in multiple myeloma translocations. Genomics 69:37–46.

Le Beau MM, Rassool FV, Neilly ME, Espinosa R 3rd, Glover TW, Smith DI, McKeithan TW. 1998. Replication of a common fragile site, FRA3B, occurs late in S phase and is delayed further upon induction: implications for the mechanism of fragile site induction. Hum Mol Genet 7:755–761.

Lee SW, Reimer CL, Oh P, Campbell DB, Schnitzer JE. 1998. Tumor cell growth inhibition by caveolin re-expression in human breast cancer cells. Oncogene 16:1391–1397.

Limongi MZ, Pelliccia F, Rocchi A. 2003. Characterization of the human common fragile site FRAZE. Genomics 81:93–97.

Lucking CB, Abbas N, Durr A, Bonifati V, Bonnet AM, de Broucker T, De Michele G, Wood NW, Agid Y, Brice A. 1998. Homozygous deletions in parkin gene in European and North African families with autosomal recessive juvenile parkinsonism. The European Consortium on Genetic Susceptibility in Parkinson's Disease and the French Parkinson's Disease Genetics Study Group. Lancet 352:1355–1356.

Mangelsdorf M, Ried K, Woollatt E, Dayan S, Eyre H, Finnis M, Hobson L, Nancarrow J, Venter D, Baker E, Richards RI. 2000. Chromosomal fragile site FRA16D and DNA instability in cancer. Cancer Res 60:1683–1689.

Mao L, Fan YH, Lotan R, Hong WK. 1996. Frequent abnormalities of FHIT, a candidate tumor suppressor gene, in head and neck cancer cell lines. Cancer Res 56:5128–5131.

Mishmar D, Rahat A, Scherer SW, Nyakatura G, Hinzmann B, Kohwi Y, Mandel-Gutfroind Y, Lee JR, Drescher B, Sas DE, Margalit H, Platzer M, Weiss A, Tsui LC, Rosenthal A, Kerem B. 1998. Molecular characterization of a common fragile site (FRA7H) on human chromosome 7 by the cloning of a simian virus 40 integration site. Proc Natl Acad Sci USA 95:8141–8146.

Oates AJ, Schumaker LM, Jenkins SB, Pearce AA, DaCosta SA, Arun B, Ellis MJ. 1998. The mannose 6-phosphate/insulin-like growth factor 2 receptor (M6P/IGF2R), a putative breast tumor suppressor gene. Breast Cancer Res Treat 47:269–281.

Oberle I, Rousseau F, Heitz D, Kretz C, Devys D, Hjanauer A, Boue J, Bertheas MF, Mandel JL. 1991. Instability of a 550 base pair DNA segment and abnormal methylation in fragile X syndrome. Science 252:1097–1102.

Ohta M, Inoue H, Cotticelli MG, Kasstury K, Baffa R, Palazzo J,

Siprashvili Z, Mori M, McCue P, Druck T, Croce CM, Huebner K. 1996. The *FHIT* gene, spanning chromosome 3p14.2 fragile site and real carcinoma-associated t(3;8) breakpoint, is abnormal in digestive tract cancers. Cell 84:587–597.

Paige AJ, Taylor KJ, Stewart A, Sgouros JG, Gabra H, Sellar GC, Smyth JF, Porteous DJ, Watson JE. 2000. A 700-kb physical map of a region of 16q23.2 homozygously deleted in multiple cancers and spanning the common fragile site FRA16D. Cancer Res 60:1690–1697.

Pennington JE, Sheinis LA, editors. 1989. Human chromosomes: manual of basic techniques. New York: Pergamon Press.

Popescu NC, Zimonjic D, DiPaolo JA. 1990. Viral integration, fragile sites, and proto-oncogenes in human neoplasia. Hum Genet 84: 383–386.

Rassool FV, McKeithan TW, Neilly ME, van Melle E, Espinosa R 3rd, Le Beau MM. 1991. Preferential integration of marker DNA into the chromosomal fragile site at 3p14: an approach to cloning fragile sites. Proc Natl Acad Sci USA 88:6657–6661.

Shridhar V, Staub J, Huntley B, Cliby W, Jenkins R, Pass HI, Hartmann L, Smith DI. 1999. A novel region of deletion on chromosome 6q23.3 spanning less than 500 Kb in high grade invasive epithelial ovarian cancer. Oncogene 18:3913–3918.

Simon B, Bartsch D, Barth P, Prasnikar N, Munch K, Blum A, Arnold R, Goke B. 1998. Frequent abnormalities of the putative tumor suppressor gene FHIT at 3p14.2 in pancreatic carcinoma cell lines. Cancer Res 58:1583–1587.

Smith DI, Huang H, Wang L. 1998. Common fragile sites and cancer [review]. Int J Oncol 12:187–196.

Tatarelli C, Linnenbach A, Mimori K, Croce CM. 2000. Characterization of the human testin gene localized in the FRA7G region at 7q31.2. Genomics 68:1–12.

Terreni L, Calabrese E, Calella AM, Forloni G, Mariani C. 2001. New mutation (R42P) of the parkin gene in the ubiquitinlike domain associated with parkinsonism. Neurology 56:463–466.

Thorland EC, Myers SL, Persing DH, Sarkar G, McGovern RM, Gostout BS, Smith DI. 2000. Human papillomavirus type 16 integrations in cervical tumors frequently occur in common fragile sites. Cancer Res 60:5916–5921.

Venter JC, Adams MD, Myers EW, Li PW, Mural RJ, Sutton GG, Smith HO, Yandell M, Evans CA, Holt RA, Gocayne JD, Amanatides P, Ballew RM, Huson DH, Wortman JR, Zhang Q, Kodira CD, Zheng XH, Chen L, Skupski M, Subramanian G, Thomas PD, Zhang J, Gabor Miklos GL, Nelson C, Broder S, Clark AG, Nadeau J, McKusick VA, Zinder N, Levine AJ, Roberts RJ, Simon M, Slayman C, Hunkapiller M, Bolanos R, Delcher A, Dew I, Fasulo D, Flanigan M, Florea L, Halpern A, Hannenhalli S, Kravitz S, Levy S, Mobarry C, Reinert K, Remington K, Abu-Threideh J, Beasley E, Biddick K, Bonazzi V, Brandon R, Cargill M, Chandramouliswaran I, Charlab R, Chaturvedi K, Deng Z, Di Francesco V, Dunn P, Eilbeck K, Evangelista C, Gabrielian AE, Gan W, Ge W, Gong F, Gu Z, Guan P, Heiman TJ, Higgins ME, Ji RR, Ke Z, Ketchum KA, Lai Z, Lei Y, Li Z, Li J, Liang Y, Lin X, Lu F, Merkulov GV, Milshina N, Moore HM, Naik AK, Narayan VA, Neelam B, Nusskern D, Rusch DB, Salzberg S, Shao W, Shue B, Sun J, Wang Z, Wang A, Wang X, Wang J, Wei M, Wides R, Xiao C, Yan C, Yao A, Ye J, Zhan M, Zhang W, Zhang H, Zhao Q, Zheng L, Zhong F, Zhong W, Zhu S, Zhao S, Gilbert D, Baumhueter S, Spier G, Carter C, Cravchik A, Woodage T, Ali F, An H, Awe A, Baldwin D, Baden H, Barnstead M, Barrow I, Beeson K, Busam D, Carver A, Center A, Cheng ML, Curry L, Danaher S, Davenport L, Desilets R, Dietz S, Dodson K, Doup L, Ferriera S, Garg N, Gluecksmann A, Hart B, Haynes J, Haynes C, Heiner C, Hladun S, Hostin D, Houck J, Howland T, Ibegwam C, Johnson J, Kalush F, Kline L, Koduru S, Love A, Mann F, May D, McCawley S, McIntosh T, McMullen I, Moy M, Moy L, Murphy B, Nelson K, Pfannkoch C, Pratts E, Puri V, Qureshi H, Reardon M, Rodriguez R, Rogers YH, Romblad D, Ruhfel B, Scott R, Sitter C, Smallwood M, Stewart E, Strong R, Suh E, Thomas R, Tint NN, Tse S, Vech C, Wang G, Wetter J, Williams S, Williams M, Windsor S, Winn-Deen E, Wolfe K, Zaveri J, Zaveri K, Abril JF, Guigo R, Campbell MJ, Sjolander KV, Karlak B, Kejariwal A, Mi H, Lazareva B, Hatton T, Narechania A, Diemer K, Muruganujan A, Guo N, Sato S, Bafna V, Istrail S, Lippert R, Schwartz R, Walenz B, Yooseph S, Allen D, Basu A, Baxendale J, Blick L, Caminha M, Carnes-Stine J, Caulk P, Chiang YH, Coyne M, Dahlke C, Mays A, Dombroski M, Donnelly M, Ely D, Esparham S, Fosler C, Gire H, Glanowski S, Glasser K, Glodek A, Gorokhov M, Graham K, Gropman B, Harris M, Heil J, Henderson S, Hoover J, Jennings D, Jordan C, Jordan J, Kasha J, Kagan L, Kraft C, Levitsky A, Lewis M, Liu X, Lopez J, Ma D, Majoros W, McDaniel J, Murphy S, Newman M, Nguyen T, Nguyen N, Nodell M, Pan S, Peck J, Peterson M, Rowe W, Sanders R, Scott J, Simpson M, Smith T, Sprague A, Stockwell T, Turner R, Venter E, Wang M, Wen M, Wu D, Wu M, Xia A, Zandieh A, Zhu X. 2001. The sequence of the human genome. Science 291:1304–1351.

Weissman AM. 2001. Themes and variations on ubiquitylation. Nat Rev Mol Cell Biol 2:169–178.

Wilke CM, Hall BK, Hoge A, Paradee W, Smith DI, Glover TW. 1996. FRA3B extends over a broad region and contains a spontaneous HPV16 integration site: direct evidence for the coincidence of viral integration sites and fragile sites. Hum Mol Genet 5:187–195.

Yanagisawa K, Kondo M, Osado H, Uchida K, Takagi K, Masuda A, Takahashi T, Tahahashi T. 1996. Molecular analysis of the FHIT gene at 3p14.2 in lung cancer cell lines. Cancer Res 56:5579–5582.

Zhang Y, Gao J, Chung KKK, Huang H, Dawson VL, Dawson TM. 2000. Parkin functions as an E2-dependent ubiquitin-protein ligase and promotes the degradation of the synaptic vesicle-associated protein, CDCrel-1. Proc Natl Acad Sci USA 97:13354–13359.

MS# 14

Oncogene (2003) 00, 1–9

www.nature.com/onc

Alterations in the common fragile site gene *Parkin* in ovarian and other cancers

Stacy R Denison[1], Fang Wang[1], Nicole A Becker[1], Birgitt Müeller[2], Norman Kock[2], Leslie A Phillips[1], Christine Klein[2] and David I Smith*[,1]

[1]*Department of Laboratory Medicine and Pathology, Division of Experimental Pathology, Mayo Clinic Cancer Center, Mayo Foundation, 200 First Street SW, Rochester, MN 55905, USA;* [2]*Departments of Neurology and Human Genetics, University of Lübeck, Lübeck 23538, Germany*

The cloning and characterization of the common fragile site (CFS) FRA6E (6q26) identified *Parkin*, the gene involved in the pathogenesis of many cases of juvenile, early-onset and, rarely, late-onset Parkinson's disease, as the third large gene to be localized within a large CFS. Initial analyses of *Parkin* indicated that in addition to playing a role in Parkinson's disease, it might also be involved in the development and/or progression of ovarian cancer. These analyses also indicated striking similarities among the large CFS-locus genes: fragile histidine triad gene (*FHIT*; 3p14.2), WW domain-containing oxidoreductase gene (*WWOX*; 16q23), and *Parkin* (6q26). Analyses of *FHIT* and *WWOX* in a variety of different cancer types have identified the presence of alternative transcripts with whole exon deletions. Interestingly, various whole exon duplications and deletions have been identified for *Parkin* in juvenile and early-onset Parkinson's patients. Therefore, we performed mutational/exon rearrangement analysis of *Parkin* in ovarian cancer cell lines and primary tumors. Four (66.7%) cell lines and four (18.2%) primary tumors were identified as being heterozygous for the duplication or deletion of a *Parkin* exon. Additionally, three of 23 (13.0%) nonovarian tumor-derived cell lines were also identified as having a duplication or deletion of one or more *Parkin* exons. Analysis of *Parkin* protein expression with antibodies revealed that most of the ovarian cancer cell lines and primary tumors had diminished or absent *Parkin* expression. While functional analyses have not yet been performed for *Parkin*, these data suggest that like *FHIT* and *WWOX*, *Parkin* may represent a tumor suppressor gene.

Oncogene (2003) **0**, 000–000. doi:10.1038/sj.onc.1207072

Keywords: common fragile sites; Parkinson's disease; ovarian cancer

Introduction

Parkinson's disease is a neurodegenerative disorder characterized by tremors, rigidity, and bradykinesia. While the peak age of onset is approximately 60 years of age, there are cases of early-onset (<50 years of age) and even juvenile (<20 years of age) Parkinson's disease. Linkage studies of autosomal recessive juvenile Parkinson's (ARJP) patients and their families identified the gene *Parkin* as a potential target for mutation in these patients (Kitada *et al.*, 1998). Mutational analysis of ARJP patients has revealed the presence of various intragenic deletions/duplications and point mutations in *Parkin* (Kitada *et al.*, 1998; Lücking *et al.*, 2000; Hedrich *et al.*, 2001, 2002; Hoenicka *et al.*, 2002; Kann *et al.*, 2002; Nichols *et al.*, 2002; West *et al.*, 2002). Subsequently, these mutations have been demonstrated to be responsible for the manifestation of juvenile, early-onset, and sometimes late-onset Parkinson's disease (Imai *et al.*, 2000; Tanaka *et al.*, 2001; Kahns *et al.*, 2002).

The recent cloning and characterization of the common fragile site (CFS) FRA6E (6q26), the third most frequently observed CFS in the human population, has determined that *Parkin* localizes within the FRA6E region of instability (Denison *et al.*, 2003). CFSs are chromosomal loci that are susceptible to forming gaps and/or breaks when cultured in the presence of chemicals such as bromodeoxyuridine, 5-azacytidine, and aphidicolin. Characterization of FRA6E determined that the region of aphidicolin-induced instability extended approximately 3.6 Mb and that *Parkin* spanned the distal half of this region. The center (most unstable region) of FRA6E was determined to localize between exons 2 and 8 of *Parkin*, but was not located at the physical center of the CFS region. Loss of heterozygosity (LOH) analysis of 20 primary ovarian tumors using markers mapping to the FRA6E region identified a significantly high frequency of LOH at D6S1599 and D6S305, two markers that localize within introns 2 and 6, respectively, of *Parkin*. RT–PCR analysis of *Parkin* determined that *Parkin* expression was downregulated in over half of the primary ovarian tumors analysed. These data suggested that in addition to playing a role in Parkinson's disease, *Parkin* may also be involved in the development and/or progression of ovarian cancer (Denison *et al.*, 2003).

Parkin is the third large gene (1.5 Mb) to be identified in a region of genomic instability; fragile histidine triad

*Correspondence: DI Smith; E-mail: smith.david@mayo.edu
Received 6 June 2003; revised 28 July 2003; accepted 30 July 2003

Gml : Ver 6.0
Template: Ver 6.0

Journal: ONC ☐ Disk used Despatch Date: 30/8/2003
Article : npg_onc_6435 Pages: 1–9 Ed: Maria OP: HNM/Rajesh

(*FHIT*) and WW domain-containing oxidoreductase (*WWOX*), located within the two most active CFSs FRA3B (*FHIT*) and FRA16D (*WWOX*), have been estimated at 1.4 and 1.0 Mb, respectively. *FHIT* and *WWOX* have been shown to suppress independently tumor growth and as a result both have been classified as putative tumor suppressor genes (Ohta *et al.*, 1996; Siprashvili *et al.*, 1997; Bednarek *et al.*, 2000). Preliminary analyses of *Parkin* indicate that like *FHIT* and *WWOX*, *Parkin* may represent a tumor suppressor gene. Analyses of *FHIT* and *WWOX* in various cancer types have identified the presence of alternative transcripts in both primary tumors and tumor-derived cell lines (Druck *et al.*, 1997; Bednarek *et al.*, 2001; Roz *et al.*, 2002; Denison *et al.*, 2003). *Parkin* alternative transcripts have also been identified in both ovarian tumor-derived cell lines and primary tumors (Denison *et al.*, 2003).

The focus of this study was to investigate *Parkin* as a potential mutational target in cancer. We confirm data reported by Denison *et al.* (2003) that *Parkin* is downregulated in ovarian cancer, and analyse both ovarian tumors and cell lines for the presence of the *Parkin* protein. Western blot analysis of seven primary ovarian tumors and six ovarian tumor-derived cell lines identified five primary tumors and four cell lines as exhibiting decreased or the complete absence of *Parkin* protein expression. We also report alternative *Parkin* transcripts in both ovarian cell lines and primary tumors. Four of seven ovarian cell lines and four of 22 primary ovarian tumors were identified with a duplication/deletion of one or more *Parkin* exons. Additionally, RT–PCR of *Parkin* on a panel of cell lines derived from breast, cervical, kidney, and prostate cancers was performed to determine if *Parkin* is genetically altered in cancer types other than ovarian cancer. Heterozygous whole exon duplications and deletions were detected in both breast and cervical cancer cell lines. While in most cases a normal *Parkin* transcript is present along with the alternative transcript, we demonstrate in some instances the complete absence of *Parkin* protein in these cell lines. These data not only indicate that *Parkin* may be genetically altered in a variety of different tumor types, but also demonstrate striking similarities among the CFS genes *FHIT*, *WWOX*, and *Parkin*. As a result, these data suggest that like *FHIT* and *WWOX*, *Parkin* may represent a putative tumor suppressor gene.

Results

Homozygous duplication/deletion (HD) screening

HD analysis was performed on a genomic DNA panel consisting of six ovarian tumor-derived cell lines and 22 primary ovarian tumors for each of the 12 exons of *Parkin*. Each primer set was run individually on the panel and then run in a multiplex reaction with primers unique to one of two markers mapping to the p-arm of chromosome 6 (WI-6213 and WI-7023) for confirmation (Table 1; data not shown). Both WI-6213 and WI-7023 markers were initially tested on the DNA panel to confirm the presence of these two markers in each DNA sample examined (data not shown). None of the ovarian cell lines or primary tumors examined exhibited an HD for any of the exons analysed (data not shown).

HD screening

Hd mapping was performed using the quantitative duplex PCR technique described by Hedrich *et al.* (2001). Hedrich *et al.* (2001) used real-time PCR to determine the gene dosage ratio of the *Parkin* gene as compared to the reference gene beta globin (*HBB*) in order to identify heterozygous deletions and/or duplica-

Table 1 *Parkin* homozygous deletion and alternative transcript screening primers

Primer	*Primer sequence 5′→3′*	*Product size (bp)*
Exon 1[a]	GCGCGGCTGGCGCCGCTGCGCGCA GCGGCGCAGAGAGGCTGTAC	112
Exon 2	CTAACACATCGCCTCCT ATCACAGCGAACTGGTC	536
Exon 3	CCCAGTTCAGTGTTGTTT TTGGCATATCTAGCTTT	756
Exon 4[a]	ACAAGCTTTTAAAGAGTTTCTTGT AGGCAATGTGTTAGTACACA	261
Exon 5[a]	ACATGTCTTAAGGAGTACATTT TCTCTAATTTCCTGGCAAACAGTG	227
Exon 6	CTGACTCCGCTAAATGAC ATAAAGCAGACACTCCCC	759
Exon 7[a]	TGCCTTTCCACACTGACAGGTACT TCTGTTCTTCATTAGCATTAGAGA	239
Exon 8	AGTGGCATGACATCCTAA CCATATAGGGATCAAGAAAC	985
Exon 9	TCCCCCTACACACACA CAAAAGCAAACAAGGAC	349
Exon 10	CTGGAAACATCTTGAGGG GCTTGGAGGAATGAGTAGG	369
Exon 11	CTGACTGCCACTTATCCT TACAAAACCAAACAATCTCT	652
Exon 12	GTTTGGGAATGCGTGTTTT AGAATTAGAAAATGAAGGTAGACA	2029
Exons 1–6[b]	CCAGTGACCATGATAGTGTT TGATGTTCCGACTATTTGTTG	600
Exons 5–12[b]	TGACCCAGGGTCCATCTT TTTTCATGGACATAGTGAAG	1067
WI-6213	CATATGCTCCTTTATTTCTGTAAGG TCCTAGGACTTTTCCTCAAGAGG	260
WI-7023	TCTGAGAGAAATGACTTGTGGG ACAGTGCAAACACCACCAAA	274

[a]Primers used in a study by Hattori *et al.* (1998). [b]Primers used in a study by Denison *et al.* (2003)

tions of whole exons of *Parkin* in a subset of ARJP patients. Gene dosage analysis of the six cell lines identified four cell lines (OV202, OV177, OV207, and OVCAR5) with heterozygous *PARK2* mutations. Of the four cell lines, two (OV202 and OV107) were identified as having an HD of one or more *PARK2* exons. OV202 exhibited an HD for exon 1 (*Parkin*/*HBB* ratio of 0.8; Table 2). OV177, however, exhibited HDs for both exons 1 and 4 (*Parkin*/*HBB* ratios of 0.7 and 0.9, respectively; Table 2). Alternatively, OV207 and OVCAR5 were identified as having heterozygous duplications of *Parkin* exons. OVCAR5 was identified as having a duplication of exon 12 (*Parkin*/*HBB* ratio of 1.07; Table 2) while OV207 was identified as having a duplication of exons 5, 8, and 12 (*Parkin*/*HBB* ratios of 0.7, 0.95, and 0.74, respectively).

Alternative transcript screening

In a previous article, we screened 22 primary ovarian tumors using *Parkin*-specific primers designed to amplify exons 1–6 and 5–12 of *Parkin*. We subsequently identified eight of the 22 different ovarian tumors with possible *Parkin* alternative transcripts (Denison *et al.*, 2003). In this study, we extracted the observed alternative bands and sequenced them to demonstrate that the band was derived from *Parkin*. Sequencing of the alternative PCR products determined that four of the 22 primary ovarian tumors (354T, 526T, 103T, and 270T) did exhibit alternative transcripts. The remaining four alternative bands that were observed were not derived from *Parkin* sequence. Tumors 354T, 103T, and 270T all exhibited a heterozygous deletion of exon 4. Alternatively, 526T exhibited a heterozygous duplication of exon 2. For all four tumors, these alternative transcripts were in the presence of a normal *Parkin* transcript (Denison *et al.*, 2003). Using the same *Parkin*-specific primers, we also screened 22 nonovarian tumor-derived cell lines (nine cervical, six pancreatic, four prostate, and three renal) for the presence of *Parkin* alternative transcripts (Table 1, Figure 1). Only six of the 22 cell lines, two cervical (SW756 and SiHa) and four prostate (LNCAP, LNCAP−, DU145, and PC3), exhibited normal full-length *Parkin* transcripts (Figure 1, Table 3). The remaining 16 cell lines (72.7%) were identified as lacking a normal full-length *Parkin* transcript (i.e. did not produce a full-length PCR product when cDNA was amplified using either the 1–6 or 5–12 *Parkin* primer sets) (Figure 1, Table 3). In some instances, neither primer set produced a PCR product (C-41, CFPAC-1, BXPC-3, and CAPAN-2), indicating the complete absence of *Parkin* expression in those cell lines. The remaining 12 cell lines were identified as having truncated *Parkin* transcripts (Figure 1, Table 3). Five cell lines (HeLa, MD751, Caski, HT-3, and C-41) were identified as lacking a 5′-end normal transcript. The other seven cell lines (ME-180, ASPC-1, MIA, CAPAN-1, HTB-45, HTB-49, and CRL-1933) lacked a 3′-end normal transcript.

Four of the 22 cell lines exhibited *PARK2* alternative transcripts (Figure 1, Table 3). Two cervical (C33A and ME180) and two pancreatic cell lines (CAPAN-1 and CAPAN-2) were identified as having heterozygous

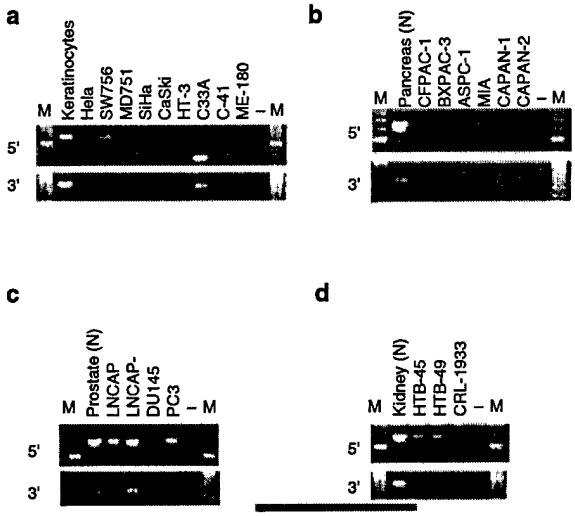

Figure 1 Alternative transcript screening of RT–PCR products obtained from cervical (**a**), pancreatic (**b**), prostatic (**c**), and renal (**d**) cell lines. Each cell line was screened for possible *Parkin* alternative transcripts using primers specifically designed to amplify exons 1–6 (5′) and exons 5–12 (3′) of *Parkin*. PCR products were gel extracted and sequenced to verify that the observed products were derived from *Parkin* sequence. A normal control (N), ladder (M), and ddH_2O negative control (−) were included in each reaction

Table 2 Real-time PCR deletion mapping in ovarian tumor-derived cell lines

Cell line	*Ratio Parkin: HBB*[a]	*Normal*[b]	*Het. del.*[c]	*Het. dup.*[d]	*Ex 1*	*Ex 2*	*Ex 3*	*Ex 4*	*Ex 5*	*Ex 6*	*Ex 7*	*Ex 8*	*Ex 9*	*Ex 10*	*Ex 11*	*Ex 12*
OV167	0.93	0.8–1.2	0.4–0.6	1.4–1.6	0. 85	0. 88	0. 94	0. 93	1. 09	1. 00	0. 94	0. 85	1. 02	0. 86	1. 07	1. 11
OV177	1.47	1.2–1.8	0.6–0.9	1.9–2.5	**0.7**[e]	1. 25	1.34	**0. 9**	1. 05	1.5	1. 12	1. 07	1.1	1. 34	1.25	1.5
OV202	1.31	1.0–1.6	0.5–0.8	1.7–2.2	**0. 8**	0. 97	1. 06	0. 99	1. 02	0. 97	1. 0	1. 05	1. 08	1. 03	1. 02	1. 02
OV207	0.54	0.4–0.6	0.2–0.3	0.7–0.9	0.51	0. 62	0. 53	0. 63	**0.7**	0.67	0.56	**0. 95**	0.63	0. 48	0.63	**0.74**
OVCAR5	0.69	0.6–0.8	0.3–0.4	0.9–1.2	0.67	0. 72	0.66	0.69	0.8	0.7	0.72	0.8	0.75	0. 66	0.75	**1. 07**
SKOV3	1.03	0.8–1.2	0.4–0.6	1.3–1.8	0.71	0.88	1.13	0.93	1.03	0.97	0.99	1.03	1.02	1.05	1.04	1.10

[a]The ratio of hybridization signals observed on interphase nuclei for BAC (RP1-179P19) containing exons 3 and 4 of the *Parkin* gene compared to that of a BAC (2643I7) containing a portion of *HBB*. [b]Normal range adjusted for differences in copy number. [c]Heterozygous deletion range based on copy number. [d]Heterozygous duplication range based on copy number. [e]Numbers in bold indicate either the duplication or deletion of that particular exon

Table 3 Alternative transcript screening of *Parkin* in 22 nonovarian tumor-derived cell lines

	Tumor type	*5'-end (exons 1–6)*	*3'-end (exons 5–12)*
Keratinocytes	Normal	+[a]	+
HeLa	Cervical	−−[b]	+
SW756	Cervical	+	+
MD751	Cervical	−−	+
SiHa	Cervical	+	+
Caski	Cervical	−−	+
HT-3	Cervical	−−	+
C33A	Cervical	alt[c]	+
C-41	Cervical	−−	−−
ME-180	Cervical	+/alt[d]	−−
Pancreas	Normal	+	+
CFPAC-1	Pancreas	−−	−−
BXPC-3	Pancreas	−−	−−
ASPC-1	Pancreas	+	−−
MIA	Pancreas	+	−−
CAPAN-1	Pancreas	+/alt	−−
CAPAN-2	Pancreas	−−	−−
Prostate	Normal	+	+
LNCAP	Prostate	+	+
LNCAP−	Prostate	+	+
DU145	Prostate	+	+
PC3	Prostate	+	+
Kidney	Normal	+	+
HTB-45	Kidney	+	−−
HTB-49	Kidney	+	−−
CRL-1933	Kidney	+	−−

[a]Presence of a normal *Parkin* transcript. [b]Absence of a normal *Parkin* transcript. [c]Presence of an alternative *Parkin* transcript. [d]Presence of both a normal and an alternative *Parkin* transcript

deletions of *Parkin* exons (Figure 1, Table 3). ME180 was identified as exhibiting a heterozygous deletion of exon 4, C33A exhibited a heterozygous deletion of both exons 3 and 4, and CAPAN-1 and CAPAN-2 both exhibited a heterozygous deletion of exon 5 (Figure 1, Table 3). None of these cell lines produced a normal full-length *Parkin* transcript.

Western blot analysis

To verify if *Parkin* expression was altered in primary ovarian tumors and tumor-derived cell lines, we performed Western blot analysis on seven primary ovarian tumors (OV111, OV270, OV465, OV470, OV491, OV714, and OV854) and six ovarian tumor-derived cell lines (OV167, OV177, OV202, OV207, SKOV3, and OVCAR5) with the AB5112 *PARK2* antibody produced by Chemicon (Temecula, CA, USA). This antibody corresponds to amino-acid residues 303–523 of *PARK2* and yields a 44–52 kDa band in normal brain tissue. However, this antibody had never been tested on any tissue other than brain. Horowitz *et al.* (2001) have shown that the size of the *Parkin* protein can vary between tissue types. Therefore, the antibody was initially tested on protein extracted from normal ovarian surface epithelium (OVSE) to determine the size of the expected protein and to confirm the expression level of *Parkin* protein in the normal surface

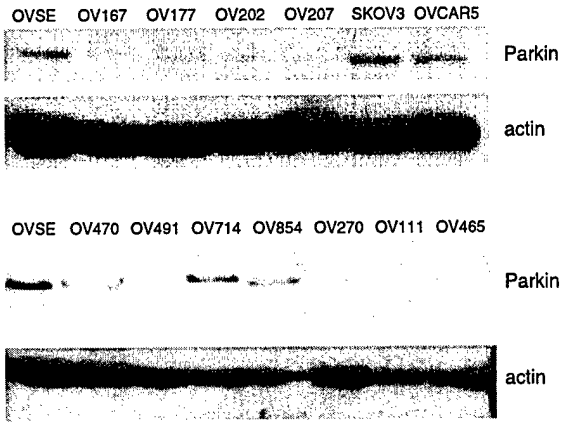

Figure 2 Western blot analysis of six ovarian tumor-derived cell lines (OV167, OV177, ON202, OV207, SKOV3, and OVCAR5) and seven primary ovarian tumors (OV470, OV491, OV854, OV270, OV111, and OV465). A *Parkin* polyclonal antibody and a corresponding control actin antibody were used to screen the tumors for the expression levels of *Parkin* protein. Normal OVSE was also analysed to determine the normal levels of *Parkin* protein expression in the OVSE

epithelium of the ovary. Contrary to what has been observed using this antibody in normal brain tissue, Western blot analysis of OVSE using the Chemicon antibody produced a single *Parkin* band at 55–60 kDa. Western blot analysis of the primary ovarian tumors revealed that four of the six cell lines (66.7%) and five of the seven tumors (71.4%) had either decreased or complete absence of *Parkin* expression. Compared to normal Parkin expression levels, the cell lines OV167, OV177, OV202, and OV207 exhibited decreased levels of Parkin expression. SKOV3 and OVCAR5 exhibited normal Parkin expression levels. As for the primary ovarian tumors, a downregulation of Parkin expression was observed for OV270, OV470, and OV491, while a complete absence of Parkin expression was observed in OV111 and OV465 (Figure 2). OV714 and OV854 exhibited normal expression levels of *Parkin* (Figure 2).

Discussion

CFSs are highly unstable genomic regions that are apparently present in all individuals. While they are characterized utilizing an *in vitro* assay of chromosomal decondensation/breakage induced by inhibitors of DNA replication, their *in vivo* significance is that they predispose chromosomes to breakage and rearrangement especially in developing cancer cells (Huebner *et al.*, 1998; Smith *et al.*, 1998; Sutherland *et al.*, 1998). CFSs have also been shown to be important in the process of gene amplification (Hellman *et al.*, 2002).

The four most active of the CFS regions are FRA3B (3p14.2), FRA16D (16q23.2), FRAXB (Xp22.31), and FRA6E (6q26). Three of these regions, FRA3B, FRA16D, and FRA6E, are consistently deleted during the development of many different cancers including

ovarian cancer. These three regions share many similarities. Instability within each CFS region extends from 2.0 to 4.5 Mb (Krummel *et al.*, 2000; Becker *et al.*, 2002; Denison *et al.*, 2003). The 'center' of each region of instability, where the majority of decondensation/breakage occurs, is only 500 kb in size and does not necessarily correspond with the physical center of the CFS region (Becker *et al.*, 2002; Denison *et al.*, 2003). Spanning the 'center' of these unstable regions are extremely large genes that encode relatively small final processed transcripts. FRA3B and FRA16D also appear to be highly conserved between humans and mice. Both FRA3B and FRA16D represent fragile regions in the mouse, Fra14A2 and Fra8E1, respectively (Shiraishi *et al.*, 2001; Krummel *et al.*, 2002). Additionally, the mouse orthologs of *FHIT* and *WWOX* (*Fhit* and *Wox1*) also appear to have been conserved together through evolution (Shiraishi *et al.*, 2001; Krummel *et al.*, 2002). The FRAXB region is distinct from the other three highly active CFS regions, as instability within this CFS region extends for only 500 kb (Arlt *et al.*, 2002). In addition, FRAXB has been shown to contain several smaller genes including the 105 and 146 kb *GSI* and *STS* genes, but not extremely large genes (Arlt *et al.*, 2002). FRAXB is also derived from a chromosomal region that is not consistently deleted in any tumor type.

An examination of multiple tumor types reveals that deletions and alterations in *FHIT* and *WWOX* are commonly observed in cancer (Druck *et al.*, 1997; Bednarek *et al.*, 2001). However, these genes rarely contain point mutations and only a single report of a point mutation within *FHIT* exons has been described (Gamma *et al.*, 1997). Corbin *et al.* (2002) examined *FHIT*/FRA3B homologues from cancer-derived cell lines using somatic cell hybrids and found that there were multiple heterozygous deletions even within one cell line, suggesting that the large deletions result in inactivation of both *FHIT* alleles. Since the genomic regions spanning these two large genes are so large and unstable, there has not been a comprehensive analysis of genomic alterations in these regions in cancer. Analysis of the proteins encoded by these CFS regions, however, has determined that expression of these genes is frequently lost in many tumor types including ovarian cancer (Druck *et al.*, 1998; Bednarek *et al.*, 2001).

While CFSs have been proposed to play a causal role in tumorigenesis and/or cancer progression, it has been unclear as to whether or not the chromosomal fragility at these loci is the consequence or cause of tumorigenicity. The development and/or progression of cancer may merely cause increased instability within the CFS regions resulting in the loss of expression (LOE) of genes localizing within the CFSs due to a bystander effect. Alternatively, these genes may in fact play an active role in cancer progression. Although the large CFS-locus genes do not appear to be traditional mutational targets like other tumor suppressor genes, there is evidence to suggest that they functionally act as tumor suppressors. Replacement of *FHIT* or *WWOX* into cancer cells that do not produce them frequently results in the inhibition of tumor growth or the induction of apoptosis (Druck *et al.*, 1998; Bednarek *et al.*, 2001). *FHIT* −/− mice are much more susceptible to tumor formation upon exposure to the mutagen NMBA, but this can be inhibited by replacement of *FHIT* into these mice (Ishii *et al.*, 2001).

Mutations in *Parkin* have been demonstrated to be responsible for the pathogenesis of juvenile, early-onset, and even late-onset Parkinson's disease. These mutations consist of point mutations, small deletions, exonic duplications and deletions, and intron–exonic deletions. All these result in amino-acid substitutions or the premature truncation of the *Parkin* protein. However, in contrast to most other disease-causing genes, the majority of *Parkin* mutations consist primarily of exonic duplications and deletions. Alterations have been documented through the *Parkin* coding sequence, but the majority of them localize between exons 2 and 8 of *Parkin* (Kitada *et al.*, 1998; Lücking *et al.*, 2000; Hedrich *et al.*, 2001, 2002; Hoenicka *et al.*, 2002; Kann *et al.*, 2002; Nichols *et al.*, 2002; West *et al.*, 2002).

To further investigate potential alterations in *Parkin* in ovarian cancer, we utilized a screening method developed by Hedrich *et al.* (2001), which they employed to search for heterozygous and homozygous deletions of the *Parkin* gene in ARJP patients. This method allows for the screening of all 12 *Parkin* exons by means of real-time quantitative PCR (Hedrich *et al.*, 2001) and for the identification of duplications and deletions that were potentially undetectable using conventional PCR. Hedrich *et al.* (2001) demonstrated that their technique was more sensitive than conventional screening at detecting mutations in *Parkin*. In the screening of 21 ARJP patients for mutations, single-strand conformational polymorphisms and sequence analysis detected only three different mutations, while the method developed by Hedrich *et al.* (2001) detected seven. We used this quantitative duplex PCR technique to analyse six ovarian cancer cell lines for *Parkin* mutations. However, due to the karyotypic variation frequently observed in both primary tumors and tumor-derived cell lines, the ratios used for the identification of alterations had to be modified to reflect accurately the changes in the gene dosage ratio of *Parkin* to *HBB* that could be attributed to aneuploidy. We therefore performed fluorescence *in situ* hybridization (FISH) on all six tumor-derived cell lines to determine the ratio of observed hybridization signals of *Parkin* to *HBB*. Based on these ratios, the normal and aberrant gene dosage values (ranges) for each individual cell line were recalculated and used for the identification of deletions, as well as duplication of *Parkin* exons (Table 2). Screening of the six ovarian cancer cell lines revealed that four were heterozygous for *Parkin* deletions. As was shown with ARJP patients, the observed large deletions identified in the ovarian cancer cell lines localized throughout the *Parkin* gene. Two cell lines (OV202 and OV177) were found to have whole exon deletions (exon 1 in OV202 and exons 1 and 4 in OV177). In the case of OV177, it is likely that both exons 1 and 4 are deleted from the same allele, as previous RT–PCR analysis of OV177 revealed the presence of a normal *Parkin* transcript (Denison *et al.*,

2003). Two other ovarian cancer cell lines, OV207 and OVCAR5, were identified as having whole exon duplications (exon 5, 8, and 12 for OV207 and exon 12 for OVCAR5). The presence of whole exon duplications/deletions in the *Parkin* gene is consistent with this gene localizing to a region of instability and indicates that instability in this region may promote the rearrangement of the *Parkin* gene in both ARJP and during cancer development.

While analyses of FRA3B, FRA16D, and FRA6E demonstrate that each has been associated with a region of high LOH and LOE for genes mapping within them, functional studies have focused primarily on *FHIT* and *WWOX* (Ohta *et al.*, 1996; Druck *et al.*, 1998; Le Beau *et al.*, 1998; Bednarek *et al.*, 2000, 2001; Krummel *et al.*, 2000; Mangelsdorf *et al.*, 2000; Paige *et al.*, 2000; Arlt *et al.*, 2002; Denison *et al.*, 2003). Alternative transcripts, typically consisting of whole exon deletions, have been identified for *FHIT* and *WWOX* in both tumor-derived cell lines and primary tumors (Druck *et al.*, 1998; Bednarek *et al.*, 2001). These types of alternative transcripts have also been identified for *Parkin* in several different cancer types (Denison *et al.*, 2003; this study). In this study, heterozygous whole exon duplications and deletions were confirmed in both primary ovarian tumors and tumor-derived cell lines (discussed previously). Of the 22 primary tumors analysed for alternative transcripts, four (18.2%) were identified as having a duplication or deletion of a *Parkin* exon. Three of the four tumors exhibited deletions for exon 4 (103T, 354T, and 270T) while the remaining tumor (526T) exhibited a duplication of exon 2. Additionally, 22 nonovarian tumor-derived cell lines (nine cervical, six pancreatic, four prostate, and three renal cell lines) were also analysed for the presence of alternative transcripts. Of the 22 cell lines analysed, 16 (72.7%) did not produce a normal full-length *Parkin* transcript (Figure 1, Table 3); two cervical (SW756 and SiHa) and four prostate cell lines (LNCAP, LNCAP–, DU145, and PC3) exhibited normal full-length *Parkin* transcripts (Figure 1, Table 3). Four of the 16 cell lines (C-41, CFPAC-1, BXPC-3, and CAPAN-2) were identified as completely lacking *Parkin* expression. The remaining 12 cell lines were identified as producing a truncated *Parkin* transcript (Figure 1, Table 3). HeLa, MD751, Caski, HT-3, and C-41 did not produce a normal 5′-end transcript when cDNA was amplified using primers specific to exons 1 and 6 of *Parkin*. ME-180, ASPC-1, MIA, CAPAN-1, HTB-45, HTB-49, and CRL-1933 did not produce a normal 3′-end transcript when cDNA was amplified using primers specific to exons 5 and 12 of *Parkin*.

A recent article by Cesari *et al.* (2003) has also identified *Parkin* alterations in ovarian and lung cancers. They performed mutational analysis of 20 ovarian tumors and identified three (15.0%) with truncating deletions. Cesari *et al.* (2003) also identified two lung adenocarcinoma cell lines with homozygous deletions of exon 2. Interestingly, the vast majority of the cell lines and primary tumors identified as having a *Parkin* mutation are the result of the duplication or deletion of an exon between exons 2 and 8, the center of the FRA6E region.

Parkin is therefore the first CFS gene that is involved in a disease other than cancer. As *Parkin* is a mutational target in ARJP patients, most of the functional studies of *Parkin* have focused on its role in neurodegeneration. *Parkin* functions as an E3 ubiquitin ligase that facilitates the degradation of misfolded and unfolded proteins through the proteasomal system. As part of the ubiquitin proteosome pathway (UPP), *Parkin* can protect neurons from diverse cellular insults, including alpha-synuclein toxicity, proteosomal dysfunction, Pael-R accumulation and kainite-induced excitotoxicitity (Zhang *et al.*, 2000; Petrucelli *et al.*, 2002; Darios *et al.*, 2003; Staropoli *et al.*, 2003). *Parkin* also plays a central role in maintaining dopaminergic neuronal integrity (Feany and Pallanck, 2003). *Parkin* has been shown to interact with actin (Huynh *et al.*, 2000), but nothing is known as to how loss of *Parkin* could contribute to cancer development.

We have therefore found that the third large CFS gene *Parkin* bears many similarities to *FHIT* and *WWOX*. Our data combined with that of Cesari *et al.* (2003) suggest that *Parkin* is a candidate tumor suppressor gene. Large structural deletions within the center of the FRA6E region are observed in ovarian cancers and also in lung and other cancers. We have demonstrated that loss of *Parkin* expression is frequently observed in ovarian and other cancers, and Cesari *et al.* (2003) also detected decreased *Parkin* protein in breast and ovarian tumors and cell lines. We are currently functionally characterizing *Parkin* to determine what role it plays in the normal cell and how loss of *Parkin* function might contribute to the development of cancer.

What role might *Parkin* play in the development and/or progression of cancer? If loss of *Parkin* promoted tumorigenesis, there would be an increased incidence of cancer in juvenile and early-onset Parkinson's patients with *Parkin* mutations. Alternatively, *Parkin* may be involved in the processes of angiogenesis and/or metastasis. Patients with *Parkin* mutations would therefore only have an increased susceptibility for cancer progression and not tumorigenesis. In that instance, one would not expect to see an increased incidence of cancer in juvenile and/or early-onset Parkinson's patients. Currently, however, there are no data of the incidence of cancer in these patients. The frequency of Parkinson's patients with *Parkin* mutations is in fact quite low; therefore, it would be difficult to determine if these patients do have a higher incidence of cancer. Therefore, functional studies of *Parkin* will be necessary to further elucidate *Parkin*'s potential role in cancer development.

Materials and methods

HD screening

Primers unique for all 12 exons were synthesized by the Mayo Foundation Molecular Core Facility (Rochester, MN, USA)

and tested on a DNA panel consisting of genomic DNA isolated from seven ovarian tumor-derived cell lines and 22 primary tumors (Table 1). Genomic DNA was isolated from the cell lines and the primary tumors using standard phenol–chloroform methods. The PCR mix (12.5 μl reaction volume) contained 20 ng of genomic DNA, 1 × PCR buffer (as supplied with enzyme), 200 μM dNTPs, 200 μM forward primer, 200 μM reverse primer, and 0.1 U *Taq* polymerase (Promega, Madison, WI, USA). The conditions for amplification were: 95°C for 3 min, then 35 cycles of 95°C for 30 s, 55–61°C for 30 s, and 72°C for 30 s with a final extension of 72°C for 10 min. All reactions were performed in duplicate to validate results. Additionally, any identified exonic HD was re-evaluated by using the exon-specific primers in a multiplex reaction, with specific primers for one of two markers localizing to the p-arm of chromosome 6 (WI-6213 and WI-7023; Table 1). These multiplex reactions were also run in duplicate to ensure reliability of the PCR results.

HD screening

Owing to the potential normal tissue contamination of the primary tumors, only the ovarian tumor-derived cell lines were analysed for possible HDs. Gene dosage analysis was performed by means of a quantitative duplex PCR assay of all 12 exons of *Parkin* on the LightCycler (Roche Diagnostics, Indianapolis, IN, USA) using the fluorescence resonance energy transfer technique in a quantitative duplex PCR assay. In brief, the *HBB* gene was coamplified with each individual *Parkin* exon and served as an internal standard. For primers, probes, and details of the method, see Hedrich *et al.* (2001). The following reagents were used for amplification in a 10 μl reaction: 1 μl Hybridization FastStart Mix (Roche Diagnostics, Indianapolis, IN, USA), 2–4.5 mM $MgCl_2$, 0.2 μM of each hybridization probes (one pair of 3′-fluorescein and 5′-LightCycler Red 640 for *Parkin*), 0.5–1.0 μM of each primer, and 1–15 ng of DNA. A standard curve was generated using human genomic DNA (Roche Diagnostics, Indianapolis, IN, USA) in concentrations of 5, 1.25, and 0.3125 ng/μl, respectively. All standards (and samples) were amplified in duplicate, followed by calculation of a regression curve, based on which sample concentrations were inferred and accepted only when within the range of the standard templates. All detected gene dosage variations were confirmed at least twice.

Hedrich *et al.* (2001) determined that the normal gene dosage ratio for any *Parkin* exon as compared to *HBB* ranged from 0.8 to 1.2. Dosage values of less than 0.4, from 0.4 to 0.6, and 1.3 to 1.7 were identified as representing a homozygous deletion, heterozygous deletion, and a heterozygous duplication, respectively, for that particular *Parkin* exon (Hedrich *et al.*, 2001). These ratios/ranges were based on the assumption that a normal ratio of *Parkin* to *HBB* would equal 1.0±20%, whereas a deletion would be reflected by a ratio of 0.5±20%. However, they did not define a heterozygous duplication as 1.2–1.8 because it would not allow for a clear differentiation between a 'high normal' and a 'low duplication' ratio. The use of a ratio of 1.3–1.7 allowed for a more conservative estimate of heterozygous duplications.

These ratios, however, specifically reflect the gene dosage levels for karyotypically normal individuals. Karyotypic analysis of primary tumors as well as tumor-derived cell lines has demonstrated that most cancers are aneuploid with variation in both chromosome number and structure (Knudson, 2001). Therefore, we modified the gene dosage ratios described by Hedrich *et al.* (2001) to reflect accurately the changes in the gene dosage ratio of *Parkin* to *HBB* that could be attributed to the observed karyotypic variation observed among the cell lines. We performed FISH using two bacterial artificial chromosomes (BACs), one containing a portion (exons 3 and 4) of *Parkin* and the other containing a portion of *HBB*, and hybridized them to interphase nuclei obtained from each cell line (Figure 3). A total of 50 interphases were analysed for each of the six different cell lines to determine the average number of *Parkin* and *HBB* hybridization signals observed per metaphase. Based on the average number of signals per metaphase, the ratio of observed hybridization signals of *Parkin* to *HBB* was determined for each individual cell line (Figure 3, Table 2). This ratio was then used to calculate the expected normal and aberrant gene dosage values (ranges) for each cell line. For example, the ratio of observed hybridization signals of *Parkin* to *HBB* for the cell line OV177 was determined to be 1.47. Therefore, the expected range values for OV177 should be 1.47 times greater than that of a karyotypically normal cell. As a result, the normal range for OV177 should be 1.2–1.8 (versus 0.8–1.2) and the ranges for a heterozygous deletion and heterozygous duplication should be 0.6–0.9 and 2.1–2.4, respectively. The modified values for each cell line are provided in Table 2.

Fluorescence in situ *hybridization*

Metaphase/interphase preparations were obtained from ovarian tumor-derived cell lines grown in a T75 tissue culture flask under the appropriate tissue culture conditions. Cultures were incubated at 37°C in 5% CO_2 until the flask reached confluency. Cell harvest and metaphase preparations followed routine cytogenetic techniques.

Three different BACs were used to determine (1) whether any of the six ovarian cell lines exhibited aneuploidy for chromosome 6 and (2) the *Parkin* dosage levels for each particular cell line. These three probes included a centromere probe specific to chromosome 6, RP-1 179P19 (a BAC containing a portion of exons 3 and 4 of *Parkin*), and CTD-2643I7 (a BAC containing a portion of *HBB*).

For clones 179P19 and 2643I7, 1 μg of purified DNA was labeled with biotin-16-dUTP (Boehringer/Roche, Indianapolis, IN, USA) by nick translation, precipitated and hybridized to the interphase chromosomes according to the protocol described by Verma and Babu (1995). The chromosome 6 centromere probe was prelabeled with a cyan fluorochrome and therefore did not require labeling with biotin-16-dUTP and could be directly hybridized to interphase chromosomes. Probe detection for the remaining BACs followed minor modifications of the manufacturer's protocols (Ventana Medical Systems, Tucson, AZ, USA). Chromosomes were counterstained with DAPI. Photomicroscopy was performed using a Zeiss Axioplan 2 fluorescence microscope and the IPLab Spectrum P software (Scanalytics Inc., Fairfax, VA, USA). A minimum of 50 interphases were analysed for each individual ovarian cell line.

Mutation analysis – RT–PCR

RT–PCR products were obtained from total RNA extracted from each sample (Table 2) using Trizol reagent (GibcoBRL, Rockville, MD, USA) following the manufacturer's instructions. For each reaction, DNA was eliminated by treating 5 μg of total RNA with RNase-free DNase for 30 min at 37°C and the DNase inactivated by incubating the reaction for 10 min at 90°C. Reverse transcription of DNase-treated RNA was performed following the manufacturer's protocol (GibcoBRL, Rockville, MD, USA).

Parkin-specific primers were designed to amplify exons 1–6 and 5–12 using the Oligo 6.4 software (Molecular Biology

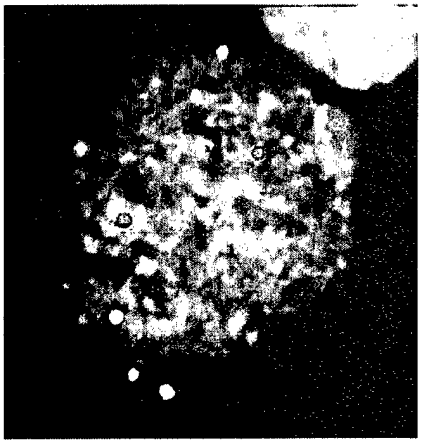

OV167

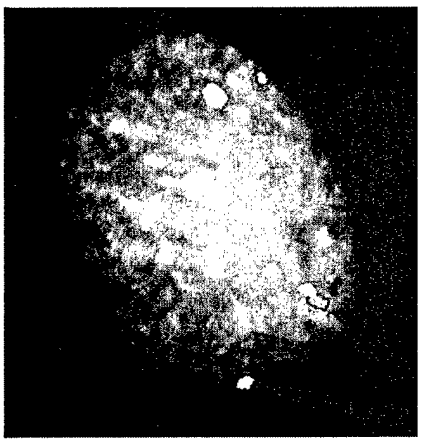

OVCAR5

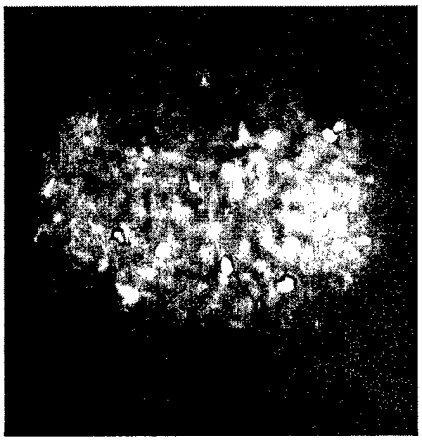

OV177

Insights) (Table 1). The PCR samples (20 μl total volume) contained 50–100 ng of reverse-transcribed cDNAs, 1 × PCR buffer (as supplied with enzyme), 0.5 mM BSA, 200 μM dNTPs, 4 mM $MgCl_2$, 750 μM forward and reverse primers for the specific genes, and 0.1 U Platinum *Taq* polymerase (Invitrogen, Carlsbad, CA, USA). The conditions for amplification were: 95°C for 3 min, then 35 cycles of 95°C for 30 s, 55–61°C for 30 s, and 72°C for 30 s with a final extension of 72°C for 10 min. PCR reactions were electrophoresed on a 2.0% agarose gel. The PCR products were gel extracted using the QIAquick gel-extraction kit (Qiagen, Valencia, CA, USA) and sequenced by the Mayo Foundation Molecular Core Facility (Rochester, MN, USA).

Western blot analysis

For immunoblotting, proteins were extracted from normal OVSE, six ovarian tumor-derived cell lines (OV167, OV177, OV202, OV207, SKOV3, and OVCAR5), and seven primary ovarian tumors (OV470, endo, 3C; OV491, endo, 4; OV714, endo, 3C; OV854, serous, 1A; OV270, serous, 3C; OV111, endo, 3C; and OV465, endo, 3C). Tissue was incubated in lysis buffer (25 mM Tris-phosphate, 2 mM DTT, 2 mM diaminocyclohexane *N,N,N′,N′*-tetraacetic acid, 10% glycerol, 1% Triton X-100, 5 mM PMSF) and homogenized using Dounce homogenizer. The supernatant was collected by centrifugation at 13 000 r.p.m., 10 min, 4°C, and the protein concentration was determined using the Bradford assay. All cells were washed three times with DPBS and then lysed in buffer (same as above) for 5 min. After centrifugation for 10 min at 13 000 r.p.m., the supernatant was collected and the protein concentration was determined using the Bradford assay. Cell lysates (containing 50 μg of protein) were resolved on 10% SDS–PAGE and processed according to standard protocols. The antibodies used were a *Parkin* polyclonal antibody and a corresponding control actin antibody. The secondary antibodies (anti-rabbit or anti-mouse) conjugated to horseradish peroxidase (dilution 1 : 5000). Signals were detected using the ECL system (Amersham Pharmacia Biotech, Piscataway, NJ, USA).

Acknowledgements

This work was supported by NIH Grant CA48031, Department of Defense Grant DAMD 17-99-1-9504, by the Minnesota Ovarian Cancer Alliance (MOCA) (all to DIS), and by the Deutsche Forschungsgemeinschaft Kl-1134/2-1 and 2-2 (to CK).

References

Arlt MF, Miller DE, Beer DG and Glover TW. (2002). *Genes Chromosomes Cancer*, **33**, 82–92.

Becker NA, Thorland EC, Denison SR, Phillips LA and Smith DI. (2002). *Oncogene*, **21**, 8713–8722.

Bednarek A., Keck-Waggoner CL, Daniel RL, Laflin KJ, Bergsagel PL, Kiguchi K, Brenner AJ and Aldaz CM. (2001). *Cancer Res.*, **61**, 8068–8073.

Figure 3 FISH analysis of ovarian cell lines to determine the ratio of *PARK2* to *HBB*. Probes for *PARK2* (yellow), *HBB* (red), and the centromere of chromosome 6 (aqua) were hybridized to interphase chromosomes obtained from each cell line. Chromosomal interphases were counterstained with DAPI. All three possible ratios are represented in the figure: (**a**) 1 : 1 ratio of *PARK2* to *HBB* (three yellow : three red); (**b**) < 1 : 1 ratio of *PARK2* to *HBB* (three yellow : two red); and (**c**) > 1 : 1 ratio of *PARK2* to *HBB* (three yellow : two red)

Bednarek AK, Laflin KJ, Daniel RL, Liao Q, Hawkins KA and Aldaz CM. (2000). *Cancer Res.*, **60,** 2140–2145.

Cesari R, Martin ES, Calin GA, Pentimalli F, Bichi R, McAdams H, Trapasso F, Drusco A, Shimizu M, Masciullo V, D'Andrilli G, Scambia, Picchio MC, Alder H, Godwin AK and Croce CM. (2003). *Proc. Natl. Acad. Sci. USA.* (in press).

Corbin S, Neilly ME, Espinosa R, Davis EM, McKeithan TW and LeBeau MM. (2002). *Cancer Res.*, **62,** 3477–3484.

Darios F, Corti O, Lücking CB, Hampe C, Muriel MP, Abbas N and Gu WJ. (2003). *Hum. Mol. Genet.*, **12,** 517–526.

Denison SR, Callahan G, Becker NA, Phillips LA and Smith DI. (2003). *Genes Chromosomes Cancer.* (in press).

Druck T, Berk L and Huebner K. (1998). *Oncol. Res.*, **10,** 341–345.

Druck T, Hadaczek P, Fu TB, Ohta M, Siprashvili Z, Baffa R, Negrini M, Kastury K, Veronese ML, Rosen D, Rothstein J, McCue P, Cotticelli MG, Inoue H, Croce CM and Huebner K. (1997). *Cancer Res.*, **57,** 504–512.

Feany MB and Pallanck LJ. (2003). *Neuron,* **38,** 13–16.

Gamma A, Hagiwara K, Ke Y, Burke LM, Khan MA, Nahashima M, Bennett WP and Harris CC. (1997). *Cancer Res.*, **57,** 1435–1437.

Hattori N, Kitada T, Matsumine H, Asakawa S, Yamamura Y, Yoshino H, Kobayashi T, Yokochi M, Wang M, Yoritaka A, Konda T, Kuzuhara S, Naamura S, Shimizu M and Mizuno Y. (1998). *Ann. Neurol.*, **4,** 935–941.

Hedrich K, Kann M, Lanthaler AJ, Dalski A, Eskelson C, Landt O, Schwinger E, Vieregge P, Lang AE, Breakefiend XO, Ozelius LJ, Pramstaller PP and Klein C. (2001). *Hum. Mol. Genet.*, **10,** 1649–1656.

Hedrich K, Marder K, Harris J, Kann M, Lynch T, Meijia-Santana H, Pramstaller PP, Schwinger E, Bressman SB, Fahn S and Klein C. (2002). *Neurology,* **58,** 1239–1246.

Hellman A, Zlotorynski E, Scherer SW, Cheung J, Vincent JB, Smith DI, Trakhtenbrot L and Kerem B. (2002). *Cancer Cell,* **1,** 89–97.

Hoenicka J, Vidal L, Morales B, Ampuero I, Jimenez-Jimenez FJ, Berciano J, del Ser T, Jimenez Z, Ruiz PG and de Yebenes JG. (2002). *Arch. Neurol.*, **59,** 966–970.

Horowitz JM, Vernace VV, Myers J, Stachowiak MK, Hanlon DW, Fraley GS and Torres G. (2001). *J. Chem. Neuroanat.*, **21,** 75–93.

Huebner K, Garrison PN, Barnes LD and Croce CM. (1998). *Ann. Rev. Genet.*, **32,** 7–31.

Huynh DP, Scoles DR, Ho TH, Del Bigio MR and Pulst SM. (2000). *Ann. Neurol.*, **48,** 737–744.

Imai Y, Soda M and Takahashi R. (2000). *J. Biol. Chem.*, **275,** 35661–35664.

Ishii H, Damon KR, Vecchione A, Gong LY, Baffa R, Huebner K and Croce CM. (2001). *JAMA,* **286,** 2441–2449.

Kahns S, Lykkebo S, Jakobsen LD, Nielson MS and Jensen PH. (2002). *J. Biol. Chem.*, **8,** 15303–15308.

Kann M, Jacobs H, Mohrmann K, Schumacher K, Hedrich K, Garrels J, Wiegers K, Schwinger E, Pramstaller PP, Breakefield XO, Ozelius LJ, Vieregge P and Klein C. (2002). *Ann. Neurol.*, **51,** 621–625.

Kitada T, Asakawa S, Hattori N, Matsumine H, Yamamura Y, Minoshima S, Yokochi M, Mizumo Y and Shimizu N. (1998). *Nature,* **392,** 605–608.

Knudson AG. (2001). *Nat. Rev. Cancer,* **1,** 157–162.

Krummel KA, Denison SR, Calhoun E, Phillips LA and Smith DI. (2002). *Genes Chromosomes Cancer,* **34,** 154–167.

Krummel KA, Roberts LR, Kawakami M, Glover TW and Smith DI. (2000). *Genomics,* **69,** 37–46.

Le Beau MM, Drabkin H, Glover TW, Gemmill R, Rassool FV, McKeithan TW and Smith DI. (1998). *Genes Chromosomes Cancer,* **21,** 281–289.

Lücking CB, Durr A, Bonifati V, Vaughan J, De Michele G, Gasser T, Harhangi BS, Meco G, Denefle P, Wood NW, Agid Y and Brice A. (2000). *N. Engl. J. Med.*, **342,** 1560–1567.

Mangelsdorf M, Ried K, Woollatt E, Dayan S, Eyre H, Finnis M, Hobson L, Nancarrow J, Venter D, Baker E and Richards RI. (2000). *Cancer Res.*, **60,** 1683–1689.

Nichols WC, Pankratz N, Uniacke SK, Pauciulo MW, Halter C, Rudolph A, Conneally PM and Foroud T. (2002). *J. Med. Genet.*, **39,** 489–492.

Ohta M, Inoue H, Cotticelli MG, Kastury K, Baffa R, Palazzo J, Siprashvili Z, Mori M, McCue P, Druck T, Croce CM and Huebner K. (1996). *Cell,* **84,** 587–597.

Paige AJ, Taylor KJ, Stewart A, Sgouros JG, Gabra H, Sellar GC, Smyth JF, Porteous DJ and Watson JE. (2000). *Cancer Res.*, **60,** 1690–1697.

Petrucelli L, O'Farrell C, Lockhart PJ, Baptista M, Kehoe K, Vink L, Choi P, Wolozin B, Farrer M, Hardy J and Cookson MR. (2002). *Neuron,* **36,** 1007–1019.

Roz L, Gramegna M, Ishii H, Croce CM and Sozzi G. (2002). *Proc. Natl. Acad. Sci. USA,* **99,** 3615–3620.

Shiraishi T, Druck T, Mimori K, Flomenberg J, Berk L, Alder H, Miller W, Huebner K and Croce CM. (2001). *Proc. Natl. Acad. Sci. USA,* **98,** 5722–5727.

Siprashvili Z, Sozzi G, Barnes LD, McCue P, Robinson AK, Eryomin V, Sard L, Tagliabue E, Greco A, Fusetti L, Schwartz G, Pierotti MA, Croce CM and Huebner K. (1997). *Proc. Natl. Acad. Sci. USA,* **94,** 13771–13776.

Smith DI, Huang H and Wang L. (1998). *Int. J. Oncol.*, **12,** 187–196.

Staropoli JF, McDermott C, Marinat C, Schulman B, Demireva E and Abeliovich A. (2003). *Neuron,* **37,** 735–749.

Sutherland GR, Baker E and Richards RI. (1998). *Trends Genet.*, **14,** 501–506.

Tanaka K, Suzuki T, Chiba T, Shimura H, Hattori N and Mizuno Y. (2001). *J. Mol. Med.*, **79,** 482–494.

Verma R and Babu A (eds). (1995). *Human Chromosomes: Principles and Techniques, 2nd edn.* McGraw-Hill: New York.

West A, Periquet M, Lincoln S, Lucking CB, Nicholl D, Bonifati V, Rawal N, Gasser T, Lohmann E, Deleuze JF, Maraganore D, Levey A, Wood N, Durr A, Hardy J, Brice A and Farrer M. (2002). *Am. J. Med. Genet.*, **114,** 584–591.

Zhang Y, Gao J, Chung KK, Huang H, Dawson VL and Dawson TM. (2000). *Proc. Natl. Acad. Sci. USA,* **97,** 13354–13359.